Ein-Elektronen-Reduktionen von Doppelbindungen

Kumulative Dissertationsschrift

zur Erlangung des akademischen Grades eines

Doktors der Naturwissenschaften

(Dr. rer. Nat.)

dem Fachbereich Chemie

der Philipps-Universität Marburg

vorgelegt von

Grégoire Horst Robert Sieg, M. Sc.

(geb. am 05.02.1990 in Berlin)

Erstgutachter: Dr. Gunnar Werncke

Zweitgutachter: Prof. Dr. Stefanie Dehnen

Marburg (Lahn) 2022

Hochschulkennziffer 1180

Ein-Elektronen-Reduktionen von Doppelbindungen

Kumulative Dissertationsschrift

zur Erlangung des akademischen Grades eines

Doktors der Naturwissenschaften

(Dr. rer. Nat.)

dem Fachbereich Chemie

der Philipps-Universität Marburg

vorgelegt von

Grégoire Horst Robert Sieg, M. Sc.

(geb. am 05.02.1990 in Berlin)

Erstgutachter: Dr. Gunnar Werncke

Zweitgutachter: Prof. Dr. Stefanie Dehnen

Marburg (Lahn) 2022

Hochschulkennziffer 1180

Tag der Einreichung: Tag der mündlichen Prüfung:

Erklärung

Ich erkläre, dass eine Promotion noch an keiner anderen Hochschule als der Philipps-Universität Marburg, Fachbereich Chemie, versucht wurde.

Ich versichere, dass ich meine vorgelegte Dissertation

„**Ein-Elektronen-Reduktionen von Doppelbindungen**“

selbst und ohne fremde Hilfe verfasst, nicht andere als die in ihr angegebenen Quellen oder Hilfsmittel benutzt, alle vollständig oder sinngemäß übernommenen Zitate als solche gekennzeichnet, sowie die Dissertation in der vorliegenden oder einer ähnlichen Form noch bei keiner anderen in- oder ausländischen Hochschule anlässlich eines Promotionsgesuchs oder zu anderen Prüfungszwecken eingereicht habe.

Ort/Datum Unterschrift

Die vorliegende Arbeit wurde im Zeitraum zwischen September 2018 und Juli 2022 am Fachbereich Chemie der Philipps-Universität Marburg unter der Leitung von Dr. Gunnar Werncke angefertigt.

Inhalt

Abkürzungsverzeichnis VI
1. Einleitung 1
1.1 Einleitende Worte 1
1.2 Organische Radikale und Radikalanionen 2
1.2.1 Stabilität organischer Radikale[11] 3
1.2.2 Vorkommen und Anwendung von Radikalanionen 4
1.2.3 Anionische Polymerisation 6
1.2.4 Isolierte Radikalanionen 7
1.2.5 Metallstabilisierte Radikalanionen 11
1.2.6 Radikalanionen in organischen Reduktionen 15
1.3 Niedrig-koordinierte 3d-Metallkomplexe 18
1.3.1 Allgemeines 18
1.3.2 Eigenschaften und Reaktivität niedrig-koordinierter 3d-Metall(I)komplexe 19
2. Motivation und Zielsetzung 24
3. Kumulativer Teil 25
3.1 Cobalt and Iron Stabilized Ketyl, Ketiminyl and Aldiminyl Radical Anions 25
3.2 A Diarsene Radical Anion 139
3.3 Taming the Stilbene Radical Anion 182
3.4 Bond activation by bent, formally manganese(I), iron(I) and cobalt(I) di(silylamides) 226
4. Zusammenfassung 274
5. English Summary 278
6. Anhang 282
6.1 Wissenschaftlicher Werdegang 282
6.2 Publikationsliste 283
6.3 Dewar-Chatt-Duncanson-Modell 284
6.4 Molekularer Magnetismus 284
6.4.1 Magnetische Suszeptibilität 284
6.4.2 Paramagnetismus 285
7. Danksagung 288
8. Literaturverzeichnis 290

Abkürzungsverzeichnis

18c6	18-Krone-6
bama	Benzaldehydmethylamin, (*Z*)-*N*-Methyl-1-phenylmethanimin
bp	Benzophenon
bpi	Benzophenonimin, Diphenylmethanimin
CHD	Cyclohexadien
DFT	Dichtefunktionaltheorie
Dipp	2,6-Di*iso*propylphenyl
DME	1,2-Dimethoxyethan
EPR	*electron paramagnetic resonance*
HAT	*hydrogen atom transfer*
HOMO	*highest occupied molecular orbital*
IR	Infrarot
ISET	*inner sphere electron transfer*
LOHC	*liquid organic hydrogen carrier*
LUMO	*lowest occupied molecular orbital*
Me	Methyl
Mes	2,4,6-Trimethylphenyl
NacNac	β-Diketiminat (von *N*-Acetyl-*N*-acetonat)
NMR	*nuclear magnetic resonance*
*n*Bu	*n*-butyl
PB	Polybutadien
PDI	Pyridindiimin
phpy	2-Phenylpyridin
PS	Polystyrol
PUM	Philipps-Universität Marburg
ROS	*reactive oxygen species*
SET	*single electron transfer*
SOMO	*singly occupied molecular orbital*
TEMPO	(2,2,6,6-Tetramethylpiperdin-1-yl)oxyl

THF	Tetrahydrofuran
^{Me}THF	2-Methyltetrahydrofuran
XAS	*x-ray absorption spectroscopy*

1. Einleitung

1.1 Einleitende Worte

Im Zuge einer Vielzahl an organischen Reaktionsmechanismen, vor allem Reduktionen, und Katalysen kommt es im entscheidenden Teilschritt oft zur Bildung von Radikalverbindungen. Dabei spielt auch die Koordination dieser an Metallionen eine wichtige Rolle. Die moderne Koordinationschemie liefert mit den bisher nur wenig erforschten niedrig-koordinierten 3d-Metall(I)komplexen ein mächtiges Werkzeug zur Untersuchung von (teilweise bisher nur postulierten) Zwischenstufen und zum allgemeinen Verständnis der Chemie von Radikalverbindungen. Verantwortlich dafür ist vor allem die ungewöhnlichen Koordinationsumgebung, sowie von die hohe Reduktionskraft solcher Komplexe.

Die vorliegende Arbeit beschäftigt sich mit Beiträgen zum Verständnis von Ein-Elektronen-Reduktionsprozessen verschiedener Substrate mit C=C-, C=O-, C=N-, N=N- und As=As-Doppelbindungen mittels niedrig-koordinierter 3d-Metall(I)komplexe. Die radikalischen, Reaktionsprodukte wurden weiter auf ihre Bindungssituation, ihre spektroskopischen und magnetischen Eigenschaften, sowie ihre weiterführende Reaktivität untersucht.

In Kapitel 1.2 wird auf die grundlegenden Eigenschaften, die Reaktivität und die Verwendung von Radikalverbindungen, besonders von Radikalanionen, eingegangen. Kapitel 1.3 stellt die Entwicklung, die Reaktivität und die Eigenschaften von niedrig-koordinierten Metall(I)komplexen dar. Zum besseren Verständnis der Bindungssituation zwischen Metallionen und organischen Mehrfachbindungen, ist in Kapitel 6.3 das CHATT-DEWAR-DUNCANSON Modell erläutert. Kapitel 6.4 liefert eine Übersicht über den molekularen Magnetismus, der die Grundlage für das Verständnis der elektronischen Eigenschaften der in dieser Arbeit verwendeten Komplexe und deren Untersuchungsmethoden darstellt.

1.2 Organische Radikale und Radikalanionen

Radikale gehören seit ihrer ursprünglichen Entdeckung durch GOMBERG im Jahr 1900 zu einer faszinierenden Verbindungsklasse, die auch in der modernen Forschung viel Beachtung findet.[1] Sie spielen eine besondere Rolle bei verschiedensten organischen Reaktionsmechanismen,[2,3] und finden sich als kurzlebige Intermediate in der Photoredox-Katalyse, welche in der modernen Chemie eine prominente Rolle einnimmt (siehe Kapitel 1.2.6).[4–6]

Radikale sind definiert als Moleküle, welche ein ungepaartes Elektron besitzen, beispielsweise •CH_3, •SnH_3 oder Cl•.[7] Das erste bekannte Radikal (Triphenylmethyl, GOMBERGS Radikal) wurde als Reaktionsprodukt von Triphenylchloromethan und elementarem Zink oder Silber erhalten (Schema 1).[1] Dabei steht das Radikal im Gleichgewicht mit seinem asymmetrischen Dimerisierungsprodukt.[8]

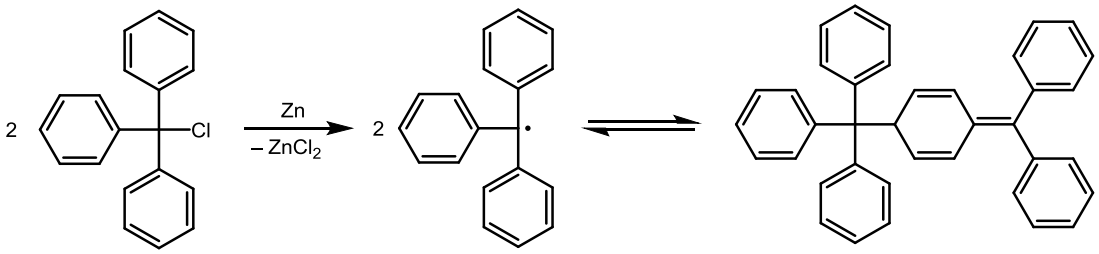

Schema 1. Reduktion von Triphenylchloromethan zum Triphenylmethylradikal (Mitte) und dessen Gleichgewicht mit GOMBERGS-Dimer (rechts).[8]

Zwei etablierte Wege um Radikale darzustellen sind die homolytische Bindungsspaltung und die Ein-Elektronen-Reduktion von Molekülen. Bei der homolytischen Bindungsspaltung können vergleichsweise schwache Bindungen thermisch oder photolytisch in zwei Radikale gespalten werden (Schema 2).[9,10] Alternativ können Radikale durch Elektrontransfer von oder auf geeignete Molekülen dargestellt werden.

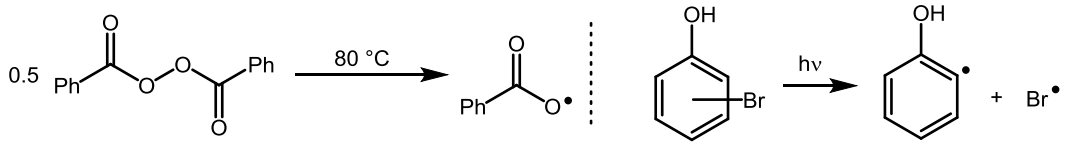

Schema 2. Thermische (links) und photolytische (rechts) Erzeugung von Radikalen.[9,10]

Je nach Gesamtladung der Teilchen wird zwischen neutralen Radikalen, Radikalkationen und Radikalanionen unterschieden. Dadurch, dass Radikale stets einen Elektronenspin besitzen, der größer als Null ist, eröffnet sich die Möglichkeit zur genaueren Untersuchung solcher Verbindungen, besonders durch die Elektronenspinresonanzspektroskopie (engl.: *electron paramagnetic resonance spectroscopy*, EPR *spectroscopy*).

1.2.1 Stabilität organischer Radikale[11]

Die Stabilität von Radikalen wird stark von der Struktur der Verbindungen diktiert: Bei Alkylverbindungen hängt die Stabilität von der Zahl der Substituenten am Kohlenstoffatom ab. Hier nimmt die Stabilität vom Methylradikal hin zu tertiären Radikalen mit zunehmender Möglichkeit zur Hyperkonjugation zu (Schema 3).

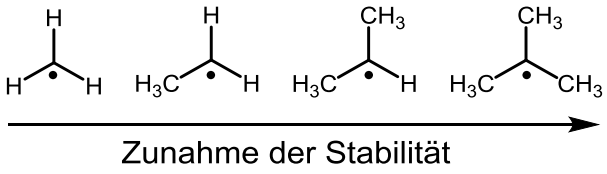

Schema 3. Stabilitätstrend von Alkylradikalen.

Radikale mit konjugierten π-Systemen, etwa Allyl- oder Benzylgruppen sind durch die Mesomeriestabilisierung vergleichsweise unreaktiv. Im Gegensatz hierzu sind Vinyl-, Alkinyl- und Phenylradikale durch das Fehlen von Mesomeriestabilisierung und Hyperkonjugation deutlich reaktiver als Alkylradikale (Schema 4).

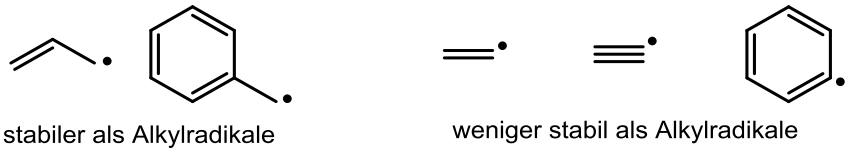

Schema 4. Stabilität verschiedener Radikale im Vergleich zu Alkylradikalen.

Auch benachbarte funktionelle Gruppen, elektronenziehende wie auch elektronenschiebende, tragen erheblich zu Stabilität von Radikalen bei (Schema 5).

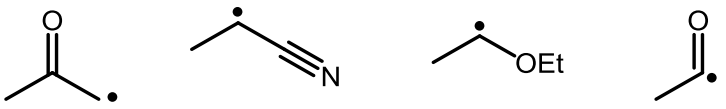

Schema 5. Durch funktionelle Gruppen stabilisierte Radikale.

Die Stabilität kann durch die Lage der Molekülorbitale erklärt werden. Im Falle von elektronenziehenden funktionellen Gruppen existiert ein energetisch niedrig liegendes π*-Orbital, welches mit dem einfach besetzten Molekülorbital (engl.: *singly occupied molecular orbital*, SOMO) des hypothetischen unfunktionalisierten Radikals wechselwirken kann (Schema 6 links). Hierbei wird die Gesamtenergie des SOMOs abgesenkt und damit die Stabilität des Moleküls erhöht. Im Falle von elektronenschiebenden Gruppen kann das SOMO des Radikals mit einem energetisch niedrig liegenden Orbital des freien Elektronenpaars (engl.: *lone pair*) wechselwirken (Schema 6 rechts). Dabei

wird zwar das SOMO energetisch angehoben, dies wird allerdings durch die Absenkung des zweifach-besetzten HOMO überkompensiert, was insgesamt ebenso die Stabilität erhöht.

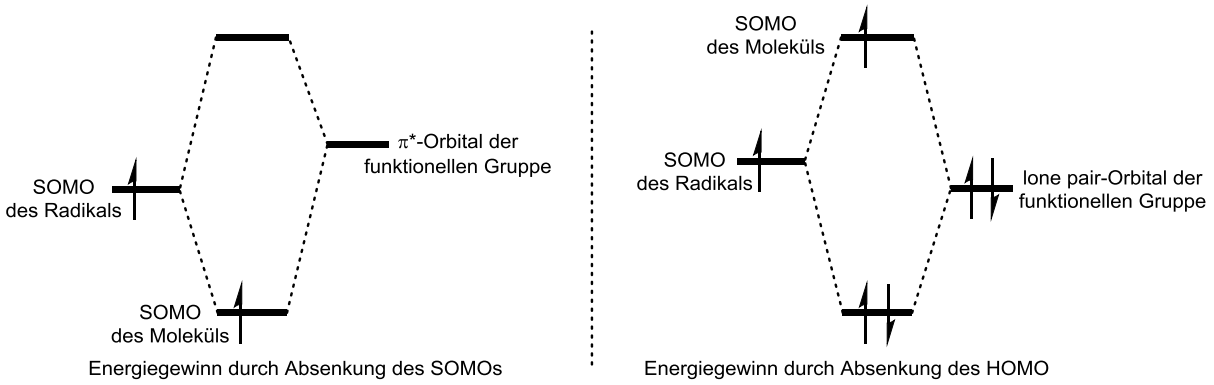

Schema 6. Schematische Abbildung der Molekülorbitale für Radikale mit elektronenziehenden (links) und elektronenschiebenden (rechts) funktionellen Gruppen.

Zusätzlich zur elektronischen Stabilisierung von Radikalen kommen sterische Effekte hinzu: Je größer der sterische Anspruch der Substituenten um das freie Elektron herum ist, desto stabiler das Radikal. Der Einfluss der elektronischen und sterischen Stabilisierung kann am Beispiel substituierter Triphenylmethylradikale gezeigt werden: Hier kann die Anbringung von Substituenten in zwei von drei *para*-Positionen die Neigung zur Dimerisierung deutlich verringern (Schema 7).[12] Zudem existieren sterisch und elektronisch stark modifizierte, stabile Derivate von GOMBERGS Radikal, welche im Bereich der Bioanalytik eingesetzt werden.[13,14] Im Umkehrschluss findet eine Destabilisierung statt, wenn die Möglichkeit zu Hyperkonjugation, der Delokalisierung oder funktionelle Gruppen fehlen.

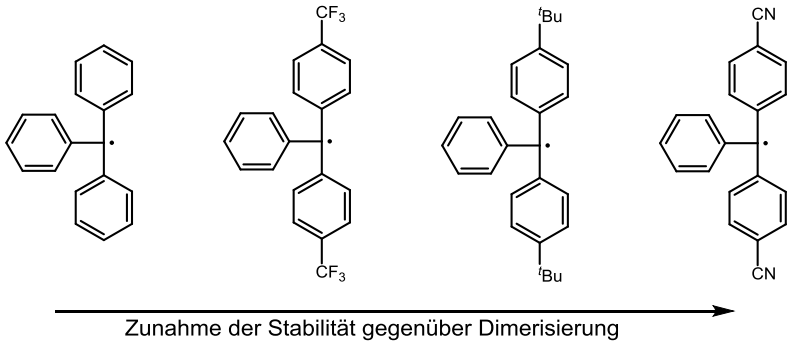

Schema 7. Stabilität verschiedener Derivate von GOMBERGS Radikal.[12]

1.2.2 Vorkommen und Anwendung von Radikalanionen

Radikale lassen sich in Abhängigkeit ihrer Ladung in neutrale Radikale, Radikalkationen und Radikalanionen unterteilen. Ein bekanntes Beispiel für Radikalkationen ist das Thianthrenium-Radikalkation, welches durch die Ein-Elektronen-Oxidation von Thianthren erhalten wird (Schema 8 links).[15] Ein bekanntes Beispiel für ein Radikalanion entsteht bei der Reduktion von Benzophenon mit Natrium, wodurch ein tiefblaues Ketylradikal erzeugt wird, welches unter anderem zur Indikation von trockenen Lösungsmitteln verwendet wird (Schema 8 rechts).[16,17]

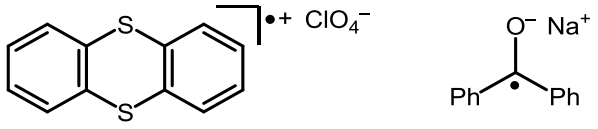

Schema 8. Thianthrenium-Radikalkation (links) und Diphenylketyl-Radikalanion (rechts).[15,16]

Letztere beiden besitzen zusätzlich zu den in Kapitel 1.2.1 gezeigten Eigenschaften auch die Möglichkeit der Redoxchemie. Im Folgenden sollen die natürlichen Vorkommen und die Anwendung von Radikalanionen erläutert werden.

Aufgrund ihrer intrinsischen Reaktivität zeigen Radikalanionen unübliche Eigenschaften, weswegen sie in der Natur und neuerdings auch bei technischen Anwendungen oft eine Schlüsselposition einnehmen.

In der Natur finden sich verschiedene Beispiele für das Vorkommen von Radikalen. Im Mineral Lapislazuli (lateinisch für *blauer Stein*) (Abbildung 1) konnten unter anderem mittels EPR-Spektroskopie $S_3^{\bullet-}$-Radikalanionen als hauptsächlich farbgebende Substanz identifiziert werden.[18]

Abbildung 1. Lapislazuli-Gesteinsblock.[19]

Doch auch in biologischen Prozessen spielen radikalische Spezies eine essenzielle Rolle.[20–22] So können beispielsweise sogenannte reaktive Sauerstoffspezies (engl.: *reactive oxygen species*, ROS) den Alterungsprozess von Säugetieren beeinflussen.[23] Diese entstehen durch die unvollständige Aufnahme von Sauerstoff in mitochondrialen Prozessen, wobei bis zu 2% des Sauerstoffs in Gegenwart der Cytochrom-Oxidase zu $O_2^{\bullet-}$-Radikalen reduziert wird, welche weiter zu hochreaktiven Hydroxylradikalen reagieren können (Schema 9).[24,25] In ähnlicher Weise können ROS auch in FENTON-artigen Reaktionen durch Reduktion von H_2O_2 durch Fe(II)-Spezies generiert werden, etwa in Wolken, Gewässern oder im menschlichen Körper.[26–28]

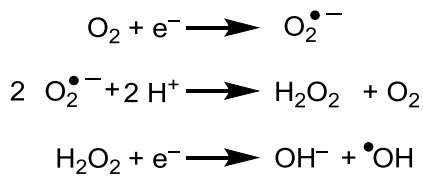

Schema 9. Schrittweise Reduktion von Sauerstoff unter Bildung von Hydroxylradikalen.[25]

Ferner nehmen radikalische Verbindungen oder Intermediate eine Schlüsselposition in modernen Anwendungen auf dem Gebiet der organischen Elektronik ein. Zu den bekannten Anwendungen zählen unter anderem Materialien zur Energiespeicherung,[29] als Leitermaterialien,[30] Transistoren[31] oder Photoschaltungen.[32] Für letztere können funktionalisierte N=N-Doppelbindungen beispielsweise als Bausteine eingesetzt werden, indem eine *E*- nach *Z*-Isomerisierung hervorgerufen wird (Schema 10). Dabei werden auch unter sehr milden Bedingungen stabile Radikalanionen als Zwischenstufe gebildet.

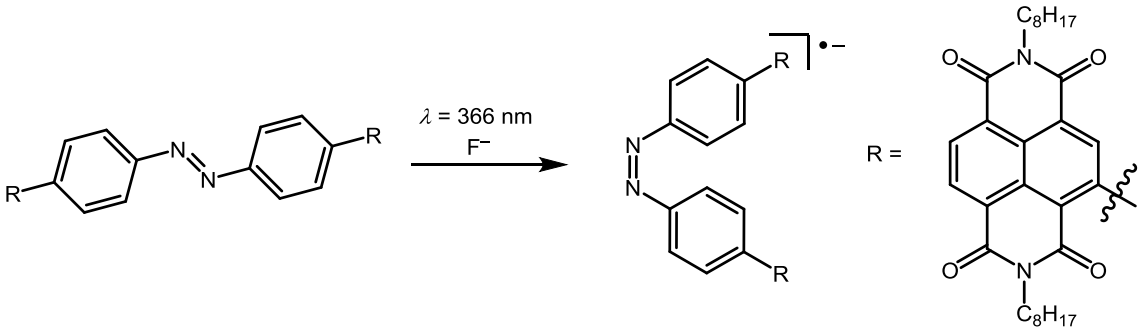

Schema 10. Lichtinduzierte Erzeugung eines Radikalanions durch als Zwischenstufe der photochemischen *E*- nach *Z*-Isomerisierung eines substituierten Diazobenzols.[32]

1.2.3 Anionische Polymerisation

Neben den bereits erwähnten Anwendungen, treten organische Radikale bei der anionischen Polymerisation auf, welche zu den industriell wichtigsten Verfahren zur Herstellung von breit eingesetzten Materialien gehört.[33] Hierbei werden monomere Einheiten durch die Induzierung mit (Radikal)anionen zur Polymerisation gebracht. Auf diese Weise können unter anderem die vielverwendeten Polymere Polybutadien (PB) und Polystyrol (PS) gewonnen werden.[11]

Zum Starten der Reaktion werden oft Moleküle wie Ammoniak oder Naphtalin durch Alkalimetalle reduziert.[34] Diese können anschließend mit Monomeren, welche über passende funktionellen Gruppen verfügen (i. d. R. C=C-Doppelbindungen) zur Reaktion gebracht werden (Schema 11). Je nach genauen Reaktionsbedingungen kann darauf folgend einer Dimerisierung stattfinden.

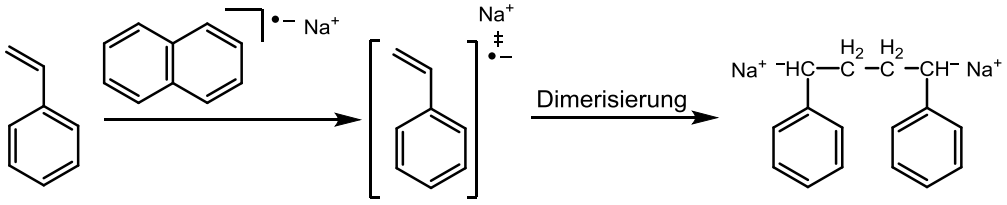

Schema 11. Erzeugung von Radikalanionen zur Initiierung von anionischen Polymerisationen am Beispiel von Styrol.[34]

In einem zweiten Schritt können die erzeugten Anionen mit Doppelbindungen von Monomeren reagieren, wodurch sich die Kettenlänge um eine monomere Einheit vergrößert (Schema 12).

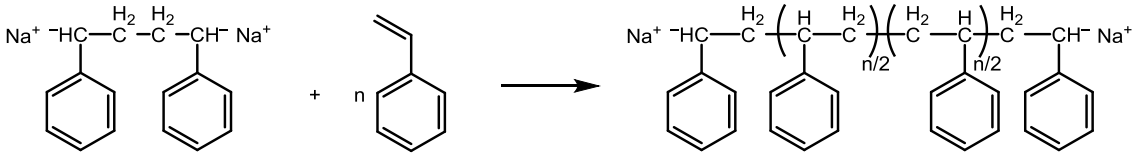

Schema 12. Kettenwachstumsreaktion in radikalischen Polymerisationen.

Dieser Schritt wiederholt sich solange, bis die Polymerisation durch eine Kettenabbruchsreaktion zum Erliegen kommt. Dies kann durch Protonierung, z. B. mit dem Lösungsmittel, erfolgen (Schema 13) oder ganz ausbleiben. Für den Fall, dass keine Kettenabbruchreaktion möglich ist, spricht man von einer *lebenden Polymerisation*.[35]

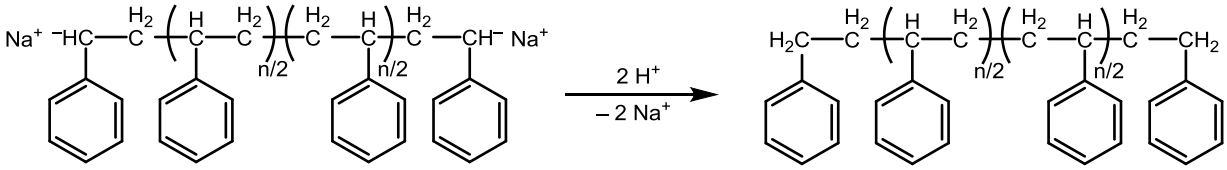

Schema 13. Kettenabbruch durch Protonentransfer.

1.2.4 Isolierte Radikalanionen

Während eine Vielzahl an bekannten, stabilen Radikalverbindungen existieren[36], ist diese Zahl für stabile Radikalanionen deutlich geringer, da sowohl Dimerisierungen, als auch sich direkt anschließende Elektronen-Transferreaktionen beobachtet werden. Im Falle von Kohlenstoff-zentrierten Radikalanionen handelt es sich hierbei in der Regel um Verbindungen mit ausgedehnten aromatischen Systemen und/oder stabilisierenden funktionellen Gruppen (Schema 14).[37–39] Ein entscheidendes Kriterium für die Stabilität solcher Radikalanionen ist die energetische Lage des π^*-Orbitals, in welchem sich das ungepaarte Elektron befindet. Je energetisch niedriger dieses Orbital liegt, desto geringer ist Tendenz zur Abgabe des freien Elektrons. Da ausgedehnte aromatische Systeme die Energie des π^*-Orbitals absenken, trägt dies in großem Maße zur Stabilität der Radikalanionen bei.

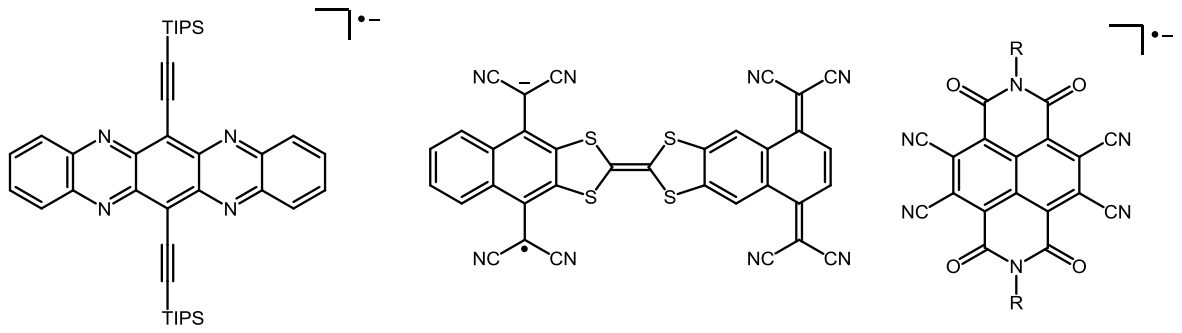

Schema 14. Auswahl an stabilen, Kohlenstoff-zentrierten Radikalanionen.[37–39]

Im Falle von reinen Kohlenwasserstoffen sind die einfachsten Vertreter von Radikalanionen die aromatischen Toluol-, Naphtalin- und Anthracen-Radikalanionen, welche durch Reduktion ihrer neutralen Vorläufer mit Alkalimetallen gewonnen und isoliert werden können (Schema 15).[40–42] Der Einfluss der Mesomeriestabilisierung zeigt sich im Redoxpotential (in Ethylenglycoldimethylether): Dieses ist für das Naphtalenid-Radikalanion (E = –3.05 V vs. Fc/Fc^+) etwa ein halbes Volt höher, als für das Anthracenid-Radikalanion (E = –2.47 V vs. Fc/Fc^+).[43] In Gegenwart von Protonenquellen reagieren diese Radikalanionen in einer BIRCH-Reduktion weiter zu den entsprechenden cyclischen Olefinen.[44]

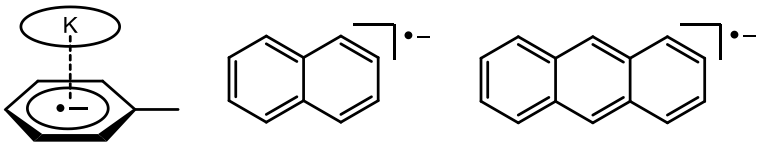

Schema 15. Radikalanionen ausgehend von Toluol, Naphtalin und Anthracen.[40–42]

Im Gegensatz zu diesen Verbindungen konnte das Benzol-Radikalanion bisher nur spektroskopisch nachgewiesen werden. Für nicht-aromatische Kohlenwasserstoffe existieren ebenso nur spektroskopische Nachweise. Besonders gut untersucht ist das 1,2-Diphenylethen, welches in *Z*- und *E*-Konformation existiert. Durch Reduktion von *Z*-Stilben in THF mit Natrium-Anthracenid ($Na^+A^{\bullet-}$) konnte mittels EPR-Spektroskopie das Stilben-Radikalanion in Lösung detektiert werden.[45] Dieses Radikalanion kann allerdings durch Überschuss an Anthracenid (alternativ durch Disproportionierung) weiter zum Dianion reduziert werden, welches höchstwahrscheinlich eine *Z*- nach *E*-Isomerisierung eingeht (Schema 16).[46]

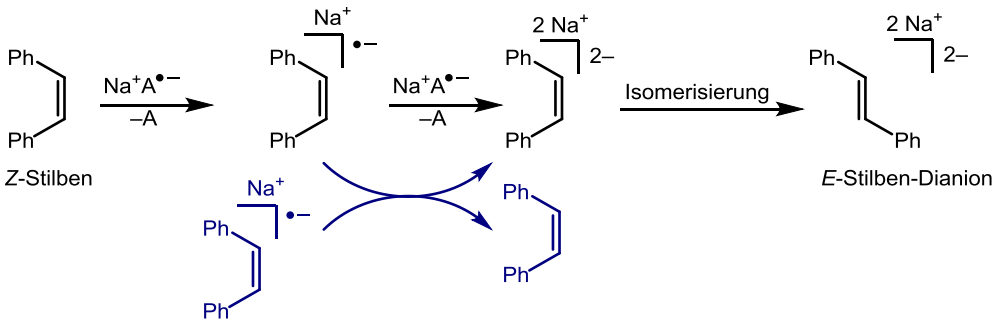

Schema 16. Reduktion von *Z*-Stilben zum Radikalanion und weiter zum Dianion mit abschließender Isomerisierung. Die Disproportionierungs-Reaktion ist in blau dargestellt.[46]

Für das verwandte System 2,2,4,4-Tetramethyl-3,4-diphenyl-3-hexen wurde berechnet, dass die Rotation um die C-C-Achse bei Radikalanionen Vergleich zu Neutralverbindungen energetisch begünstigt ist (Abbildung 2).[47] Für Dianionen hingegen ist ein Torsionswinkel von etwa 90° um die zentrale C-C-Bindung bevorzugt.

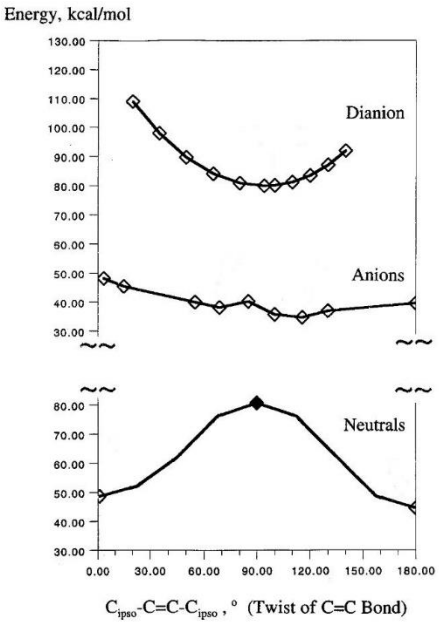

Abbildung 2. Energieprofil der Bindungsrotation um die zentrale C-C-Bindung bei 2,2,4,4-Tetramethyl-3,4-diphenyl-3-hexen im neutralen (unten), radikalanionischen (Mitte) und dianionischen Zustand.[47]

Das *E*-Stilben-Dianion kann photolytisch wiederum zum *E*-Radikalanion gespalten werden.[48] Trotz der intensiven Untersuchungen konnte bisher das Stilben-Radikalanion nicht als stabile Verbindung isoliert werden.

Das Radikalanion des 1,1-Diphenylethen konnte durch Reduktion mit Natrium-Naphtalenid ($Na^+Naph^{\bullet-}$) *in situ* erzeugt werden, dieses dimerisiert jedoch zum 1,1,4,4-Tetraphenylbutyl-Dianion (Schema 17).[49]

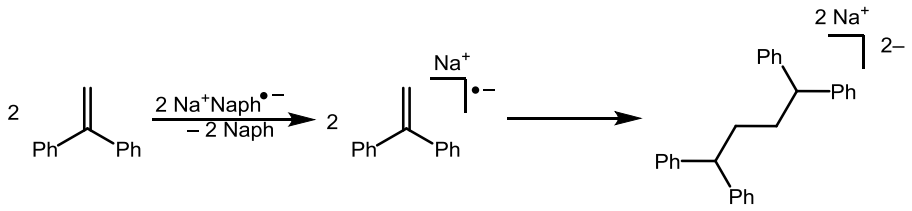

Schema 17. Generierung des 1,1-Diphenylethen-Radikalanions und anschließende Dimerisierung.[49]

Das vermutlich prominenteste Radikalanion, das aus Benzophenon generierte Ketylradikal, konnte im Jahr 2009 mit Kalium als Gegenion kristallisiert und erstmal strukturell charakterisiert werden.[17] Dessen Struktur im Festkörper beinhaltet ein kubanartiges Grundgerüst aus Sauerstoff- und Kaliumatomen. Das Radikalanion zeigt durch einen $\pi \rightarrow \pi^*$-Übergang mit λ_{max} = 656 nm eine charakteristische Photoabsorption, die in einer tiefblauen Farbe resultiert. Andere, kohlenstoffzentrierte Radikalanionen ohne ausgeprägte Delokalisierung konnten bis heute nicht frei isoliert werden. Zuvor konnte bereits das Fluorenyl-Radikalanion durch Reduktion von Fluorenon mit Natrium im Dimethoxyethan (DME) erzeugt werden.[50]

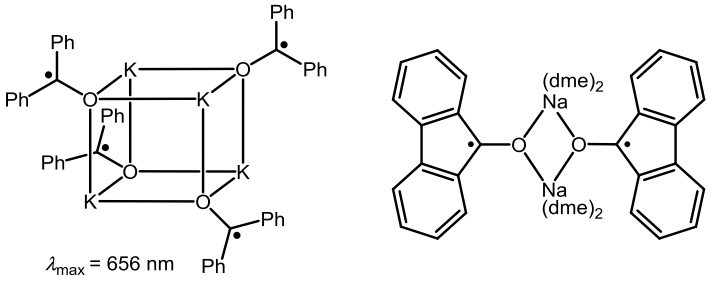

Schema 18. Molekülstruktur im Festkörper von K(Ph_2CO) und Na$(dme)_2$(fluorenon).[17,50]

Neben den bekannten Kohlenstoff-zentrierten Radikalanionen existieren auch Verbindungen, bei denen sich das ungepaarte Elektron an anderen Hauptgruppenelementen befindet. So finden sich Beispiele mit Elementen der Gruppen 13 – 15, bei denen sich das radikalische Zentralatom durch die Wahl passender Substituenten sterisch und elektronisch stabilisieren lässt (Schema 19).[51–54]

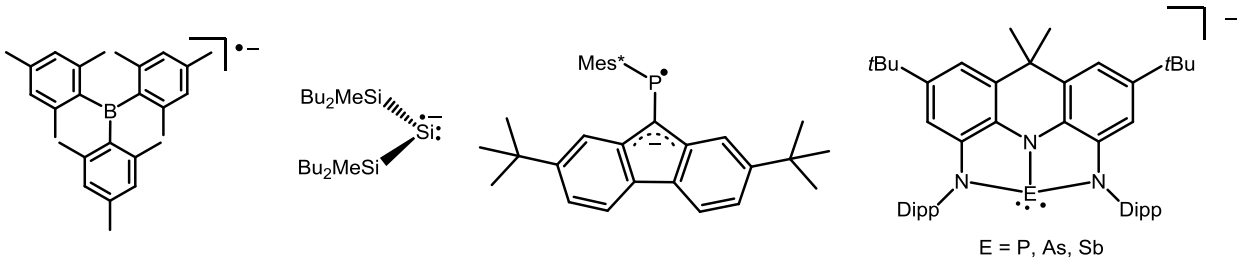

Schema 19. Beispiele für stabile Radikalanionen der Gruppen 13 – 15.[51–54]

Ferner existieren für die Elemente der Gruppe 15 eine Reihe von E=E-Doppelbindungen (E = N, P, Sb, Bi), welche zu Radikalanionen reduziert werden konnten.[55–58] In all diesen Verbindungen wird durch die Besetzung des π^*-Orbitals die Bindungsordnung reduziert, was sich in einer verlängerten E-E-

Doppelbindung wiederspiegelt. Lediglich für eine Spezies mit analogem Arsen-Bindungsmotiv gibt es bis heute keinen strukturellen Nachweis. Die Reaktivität solcher Radikalanionen mit Gruppe 15 E-E-Bindungen ist bis heute vollkommen unerforscht.

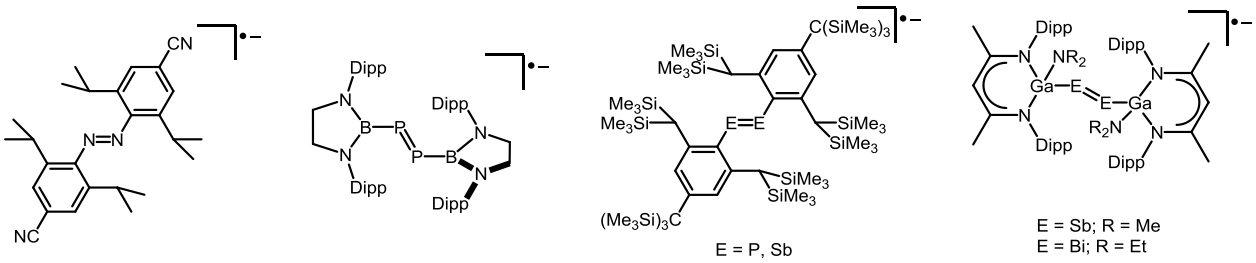

Schema 20. Radikalanionen mit E=E-Doppelbindungen der Gruppe 15.[55–58]

1.2.5 Metallstabilisierte Radikalanionen

Wie bereits gezeigt, können sterisch anspruchsvolle Substituenten verschiedene Radikalanionen stabilisieren. Ein weiterer Ansatz hierfür ist die Koordination an Metallionen zu Radikalanion-Komplexen.[59,60] Durch die Überlappung mit den Orbitalen der Metallionen wird das π^*-Orbitals energetisch abgesenkt, was zur Stabilisierung solcher Verbindungen beiträgt. Ausgewählte Beispiele werden im folgenden Kapitel vorgestellt.

Bereits vor 40 Jahren wurden im Kontext der sogenannten *nicht unschuldigen Liganden* (engl.: *non-innocent ligands*) verschiedene Komplexe mit Radikalanionen beschrieben.[61,62] Hier werden Liganden genutzt, welche Elektronen aufnehmen können und bei Anbringung an ein Metallion zum Radikalanion reduziert werden. Vor allem als Modellkomplexe für biochemische Vorgänge konnten solche Verbindungen an Interesse gewinnen.[63–65]

Zur Generierung von Radikalanionen-Komplexen bieten sich klassischerweise entweder die Reduktion von Vorläuferkomplexen reduktionsinerter Metalle an, welche durch einen Ein-Elektronen-Transfer (engl.: *single electron transfer*, SET) in die entsprechenden Radikalkomplexe überführt werden (Schema 21 links), oder die Übertragung von bereits generierten Radikalen auf Übergangsmetallionen (Schema 21 rechts). Neben der EPR-Spektroskopie bieten sich für den Nachweis der Radikalanionen auch die UV-Vis-Spektroskopie an. Die $\pi \rightarrow \pi^*$-Übergänge sorgen in den meisten Fällen für eine starke Photoabsorption im sichtbaren Bereich, welche als Nachweis für das Vorliegen des ungepaarten Elektrons dient.

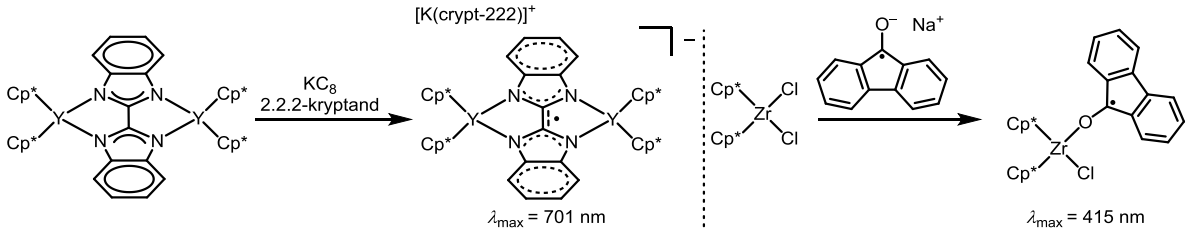

Schema 21. Darstellung von Radikalkomplexen durch Reduktion von Vorläuferkomplexen (links) und Radikaltransfer (rechts).[59,60]

Alternativ konnten verschiedene Radikalkomplexe durch Koordination von Substraten an reduzierende Metallionen generiert werden, wobei die resultierende Koordinationsbindung zur Stabilisierung der erhaltenen Verbindungen beiträgt. So wurde ausgehend von Fluorenon und einem Samarium(II)-Vorläuferkomplex ein entsprechender Samarium(III)-Radikalkomplex dargestellt, welcher in Abhängigkeit des verwendeten Lösungsmittels eine reversible Dimerisierung der Fluorenyleinheit zeigt (Schema 22).[66]

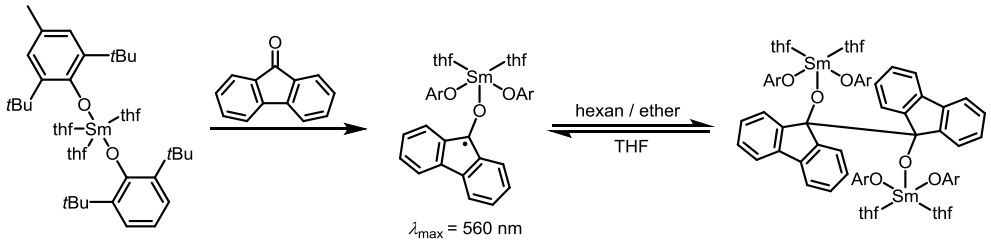

Schema 22. Synthese eines Samarium(III)-Fluorenylkomplexes mit lösungsmittelabhängiger Dimerisierung.[66]

In ähnlicher Weise konnte auch die Reduktion der C=O-Doppelbindung in 4,4‘-*tert*-Butylbenzophenon durch Reaktion mit einem Uran(III)-Komplex realisiert werden (Schema 23).[67]

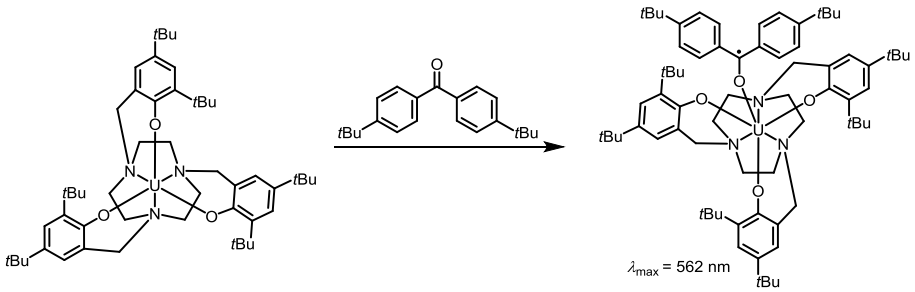

Schema 23. Darstellung eines Uran(IV)-Komplexes mit radikalischem Ketylliganden.[67]

In den letzten Jahren gelang es auch für 3d-Metallionen (allem voran Eisen) C=O Doppelbindungen in SET Prozessen zu reduzieren. Beispielsweise konnte der Elektronentransfer eines Eisen(I)-Pincerkomplexes auf Benzophenon beobachtet werden, was in einem Eisen(II)-Radikalkomplex mit gebundene Ketylliganden in endständiger (engl.: *end-on*) Koordination resultiert (Schema 24).[68]

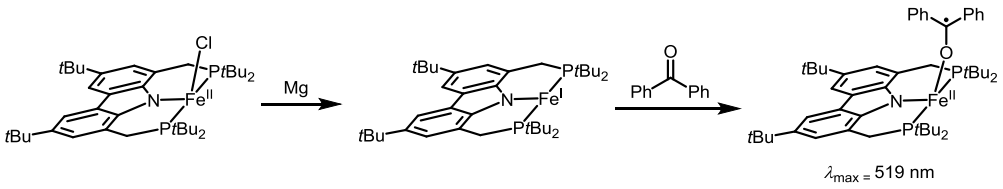

Schema 24. Darstellung eines Eisen(I)-Pincerkomplexes und anschließender oxidativer Addition an Benzophenon.[68]

Wird hingegen ein dimerer Eisen(I)-β-Diketiminatkomplex („Fe-NacNac“) verwendet, so bildet sich bei der Reaktion mit Benzophenon ein Komplex mit einer *side-on*-Koordination (deut.: seitlich koordiniert) (Schema 25).[69] Bei der Reaktion mit GOMBERGS-Dimer konnte die Bildung des Triphenylmethylkomplexes beobachtet werden. In beiden Fäll wurde zwar die Oxidationsstufe des Eisenions durch spektroskopische Untersuchungen als +II bestimmt, was einen radikalischen Charakter der Liganden impliziert. Jedoch konnte weder eine, für Radikale typische Reaktivität beobachtet werden, noch konnte der Radikalcharakter spektroskopisch nachgewiesen werden. Durch quantenchemische Rechnungen wurde eine starke Überlappung der Metall- und Ligandenorbitale ermittelt, wodurch das freie Elektron sich primär in den zwischen dem Metallion und dem Benzophenon-Liganden befindet. Aus diesem Grunde wurde diese Verbindung als sogenanntes „maskierte Radikale“ beschrieben.

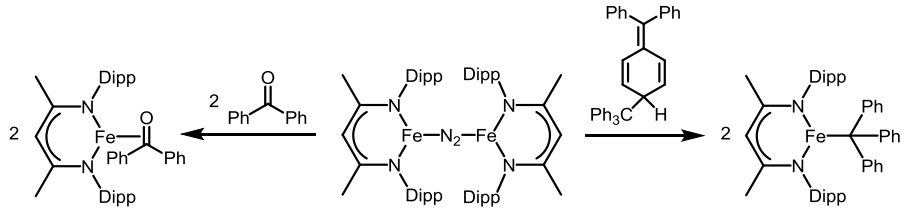

Schema 25. Darstellung von „maskierten“ Radikalkomplexen ausgehend von einem dimeren Fe-NacNac-Distickstoffkomplexes.[69]

In der Literatur sind verschiedene Komplexe beschrieben, in denen die Aktivierung einer R-N=N-R Bindung stattfindet. Neben der Zwei-Elektronen-Reduktion zu Hydrazinderivaten[70,71] ist auch Bildung von Radikalkomplexen mit N-N-Bindung bekannt (Schema 26).[72–75]

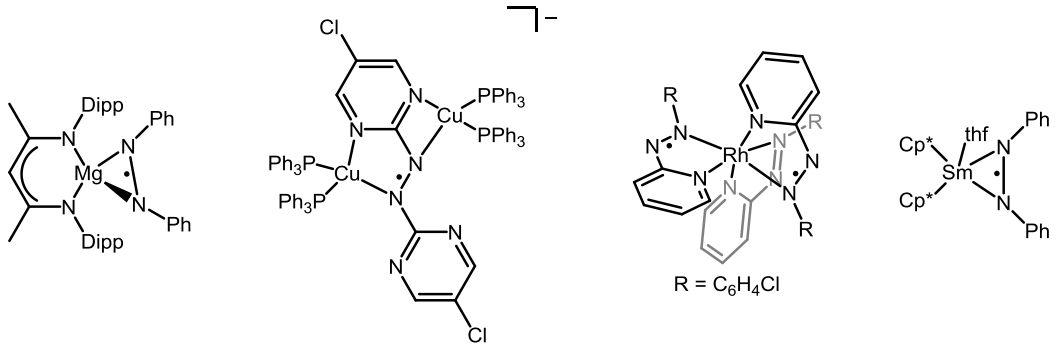

Schema 26. Ausgewählte Beispiele von Komplexen mit radikalanionischen R-N-N-R-Liganden.[72–75]

Die Generierung von Radikalanionen aus C=N-Doppelbindungen ist vor allem im Kontext der Diimine, speziell der Pyridindiimine (PDI) erforscht.[76–81] Diese sind vor allem im Bereich der Olefinpolymerisation wichtige Katalysatoren.[82,83] Der Einsatz reduktionsfähiger Liganden führt wahlweise zur Bildung von Mono- oder Diradikalanionen (Schema 27).

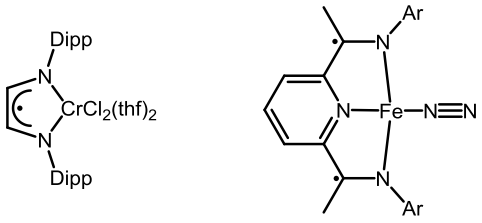

Schema 27. 3d-Metallkomplexe mit Diiminyl-Monoradikalanion (links) du Diiminyl-Diradikalanion (rechts).[76,81]

1.2.6 Radikalanionen in organischen Reduktionen

Radikalanionen treten in einer Vielzahl an organischen Reduktionen als instabile Intermediate auf. Ihre Erzeugung durch Ein-Elektronen-Reduktion der Doppelbindung ist in der Regel der entscheidende Schritt zu Bindungsaktivierung, weswegen das Verständnis ihrer Bildung und Reaktivität von besonderem Interesse ist. Im Folgenden sollen exemplarisch wichtige organische Reduktionsmechanismen unter Bildung von Radikalanionen gezeigt werden.

Im Fall der CLEMMENSEN-Reduktion können Moleküle mit C=O-Doppelbindungen durch den Einsatz von Zink unter sauren Bedingungen zu Alkanen umgewandelt werden (Schema 28).[84]

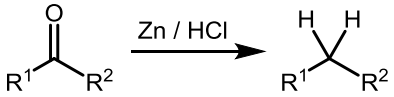

Schema 28. Reduktion von Carbonylen im Zuge der CLEMMENSEN-Reduktion.[84]

Hierbei handelt es sich um eine heterogen durchgeführte Reaktion unter Zugabe von stöchiometrischen Mengen Salzsäure. Hierbei findet an der Metalloberfläche ein SET statt (die Zinkoberfläche liefert die hier abgebildeten Elektronen), bei dem das Keton zu einem Radikalanion reduziert und gleichzeitig von entstehenden Zinkionen koordiniert wird (Schema 29).[3]

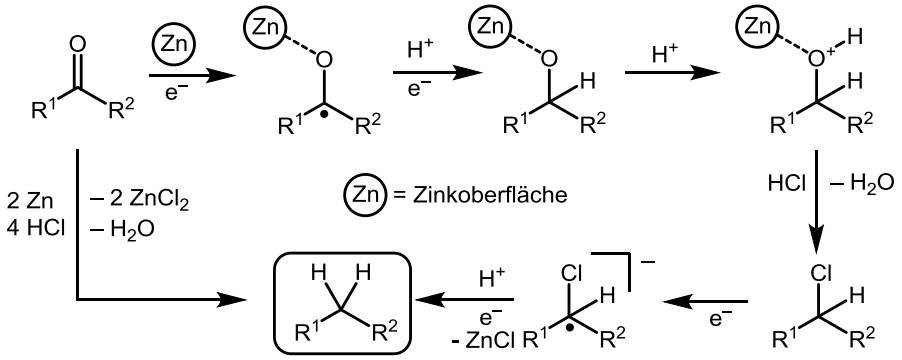

Schema 29. Schematischer Reaktionsmechanismus der CLEMMENSEN-Reduktion.[3]

Neben den (deoxygenierenden) Reduktionen der C=O-Doppelbindung existiert auch eine Vielzahl an Beispielen für reduktive Kupplungen, welche entweder zu Diolen oder zu Alkenen führen. Beispielsweise können Aldehyde oder Ketone durch Reduktion mit Magnesium zu Diolen am Carbonylkohlenstoffatom gekuppelt werden.[85] Dabei wird zunächst die Carbonylfunktion durch einen SET zu einem Radikalanion reduziert, welches anschließend, vermittelt durch ein koordinierendes Magnesiumion mit einem weiteren Radikalanion durch eine Radikalrekombination zum Diolatkomplex und nach saurer Aufarbeitung zum Diol gekuppelt (Schema 30).[2] Ähnliche Reaktionen können auch mit Aluminiumamalgam oder Samariumiodid herbeigeführt werden.[86,87]

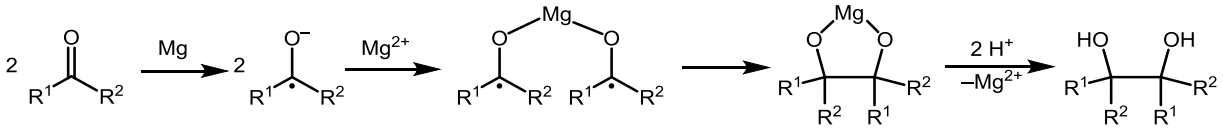

Schema 30. Reaktionsmechanismus der Pinakolkupplung.[2]

Alternativ zu den bereits beschriebenen Reagenzien zur Pinakolkupplung können auch niedervalente Titanreagenzien (bspw. $TiCl_3/LiAlH_4$ oder $TiCl_4/Li(Hg)$) verwendet werden.[88] Der genaue Reaktionsverlauf dieser sogenannten McMURRY-Reaktion ist abhängig von den eingesetzten Substraten und kann über zwei grundlegende Pfade verlaufen (Schema 31).[89] Unabhängig der eingesetzten Substrate kann der erste Schritt ein SET auf das Carbonyl unter Bildung eines Titan-koordinierten Radikalanions beschrieben werden. Im zweiten Schritt findet bei kleinen Substituenten eine Radikalrekombination zum Metallopinakolat statt, die bei wässriger Aufarbeitung zum Pinakol oder bei weiterer Reduktion zum Alken führt. Bei sterisch anspruchsvolleren Substituenten hingegen bildet sich unter reduktiven Bedingungen aus dem Radikalanion ein carbenoides Intermediat, welches mit einem Äquivalent Keton in einer Bindungsmetathese unter Abspaltung einer Titan-Oxo-Spezies das Alken bildet.

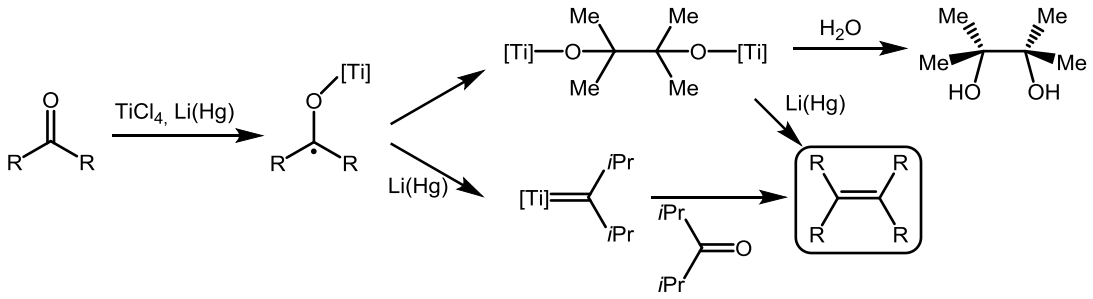

Schema 31. Verlauf der McMurry-Reaktion mit Aceton und Di(isopropyl)keton unter Verwendung von $TiCl_4/Li(Hg)$.[89]

Analog zu C=O-Doppelbindungen lassen sich auch C=N-Doppelbindungen durch Einsatz von passender Reagenzien zu den entsprechenden Aminen reduzieren. Bei der Verwendung von $NbCl_4(thf)_2$ als Reduktionsmittel wird, wie auch bei der klassischen Pinakolkupplung mit Magnesium oder der McMURRY-Reaktion, ein metallkoordiniertes Radikalanion als Intermediat gebildet, welches nach Radikalrekombination zum Diamin überführt werden kann (Schema 32).[90]

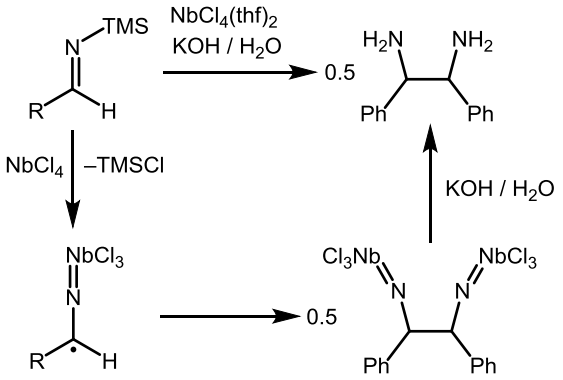

Schema 32. Radikalischer Mechanismus der reduktiven Kupplung von Aldiminen mit $NbCl_4(thf)_2$.[90]

Als (metallfreie) Alternative konnten auch photoredox-katalysierte Synthesewege etabliert werden, um Aldimine zu Diaminen zu kuppeln (Schema 33).[91,92]

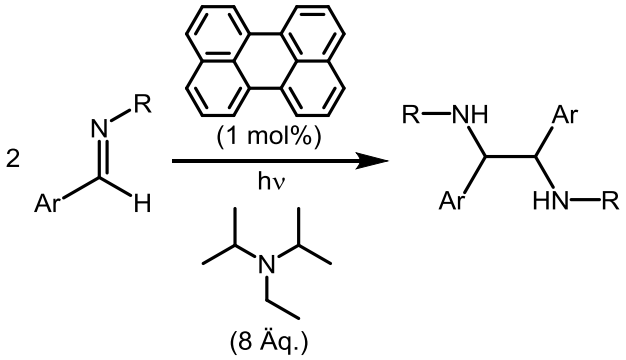

Schema 33. Reduktive Kupplung von Aldiminen durch Photoredoxkatalyse.[92]

Dabei wird eine radikalische Zwischenstufe postuliert, die durch einen SET von einem tertiären Amin indirekt auf das Aldimin entsteht (Schema 34).[93] Der optisch angeregte Katalysator (hier Perylen, P*) wird zunächst vom Amin reduziert und überträgt dann ein Elektron weiter auf das Substrat. Im letzten (hier nicht abgebildeten Schritt) wird ein Proton des Radikalkations auf das Radikalanion übertragen, welches zum Diamin dimerisieren kann.

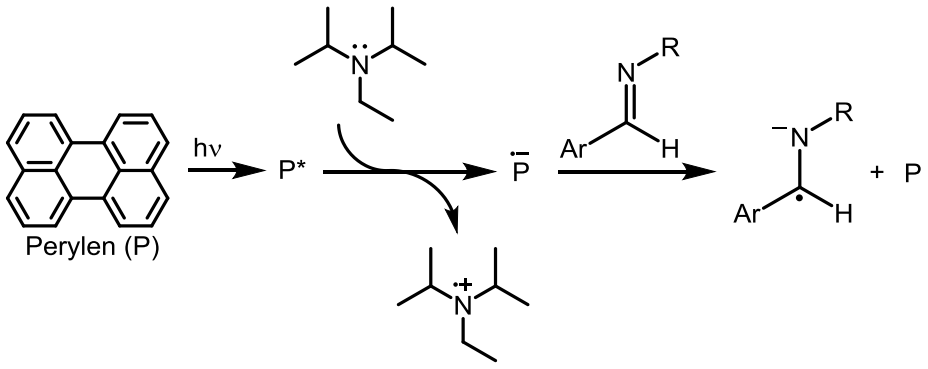

Schema 34. Postulierter Mechanismus zur photoinduzierten Generierung von Aldiminyl-Radikalanionen.[93]

1.3 Niedrig-koordinierte 3d-Metallkomplexe

Wie in Kapitel 1.2.5 gezeigt, eignen sich Koordinationsverbindungen in vielfältiger Weise um organische Reduktionen mit hoher Chemo- und Regioselektivität zu ermöglichen, sowie ansonsten labile Moleküle zu stabilisieren. Die bisher nur wenig erforschten niedrig-koordinierten 3d-Metall(I)komplexe zeichnen sich durch ihre ungewöhnliche Koordinationsumgebung und ihrer oft hohen Reduktionskraft aus. Daher öffnen sie neue Möglichkeiten, die Aktivierung von organischen Doppel- und Dreifachbindungen, sowie reduktive C-C-Knüpfungen zu untersuchen. Gleichzeitig können unter Verwendung von vergleichsweise wenig toxischen[94–96] und besser verfügbaren[97,98] Metallen wie Eisen, Mangan und Cobalt die üblichen, teils toxischen, Metalle wie Rhodium, Ruthenium und Palladium umgangen werden. Im Folgenden soll deshalb eine knappe historische Einordnung, sowie die Beschreibung grundlegender Eigenschaften und Reaktivität dieser Verbindungen erfolgen.

1.3.1 Allgemeines

Die Chemie der niedrig-koordinierten 3d-Metallkomplexe mit der Oxidationsstufe +II begann in den 1960er Jahren auf Grundlage der Arbeiten von BÜRGER und WANNAGAT[99] und wurde im Verlauf der 1980er Jahre durch strukturelle Charakterisierung solcher Verbindungen weiter etabliert.[100–103] Diese Verbindungen zeichnen sich aufgrund ihres Elektronenmangels durch ihre Neigung zur Reaktion mit LEWIS-Basen oder Oxidationsmitteln aus. Dies zeigt sich besonders in ihrer hohen Sensibilität gegenüber Wasser und Sauerstoff.

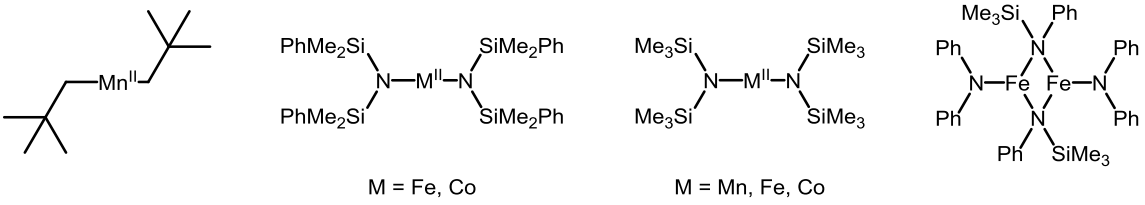

Schema 35. Ausgewählt Beispiele für niedrig koordinierte 3d-Metall(II)komplexe.[100–102,104]

Im Gegensatz hierzu wurden niedrig-koordinierte 3d-Metallkomplexe in der ungewöhnlichen Oxidationsstufe +I erst ab dem Jahr 2007 (mit Ausnahme von Kupfer) für verschiedene Metalle beschrieben (Schema 36).[105–108] An dieser Stelle ist zwischen homo- und heteroleptischen Komplexen zu unterscheiden.

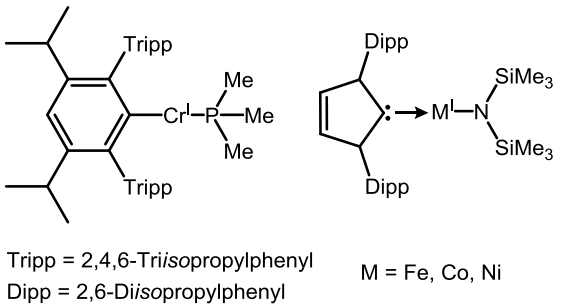

Schema 36. Heteroleptische Metall(I)komplexe der Metalle Chrom, Eisen, Cobalt und Nickel.[105–108]

Neben den oben gezeigten heteroleptischen Komplexen konnten auch verschiedene homoleptische Metall(I)komplexe, sowohl kationischer wie auch anionischer Natur, dargestellt werden. Üblicherweise werden schwach koordinierende und redoxinerte Gegenionen eingesetzt, um die geringe Koordinationszahl beizubehalten (Schema 37).[109–112] Zusätzlich sind auch solche Komplexe bekannt, bei denen das Gegenion nicht separiert ist und durch die Koordination an die Liganden einen insgesamt neutral geladenen Komplex ergibt (Schema 37 rechts).[113,114]

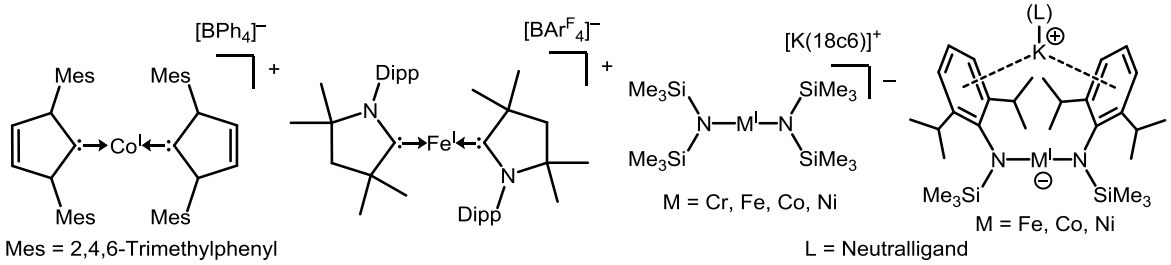

Schema 37. Auswahl an ionischen homoleptischen 3d-Metall(I)komplexen.[109–114]

1.3.2 Eigenschaften und Reaktivität niedrig-koordinierter 3d-Metall(I)komplexe

Während niedrig-koordinierte Metall(II)komplexe elektronisch ungesättigt sind und dadurch bereitwillig ihre Koordinationszahl von zwei auf drei erhöhen (bspw. mit LEWIS-Basen oder in Form von Dimeren),[103,115] ist dieses Verhalten bei den anionischen Metall(I)verbindungen nicht zu beobachten. So kann der Komplex $[Fe(N(SiMe_3)_2)_2]$ mit Tricyclohexylphosphan (PCy_3) zur Reaktion gebracht werden, während dieses nach der Reduktion mit Kaliumgraphit (KC_8) nicht mehr koordiniert (Schema 38).[111]

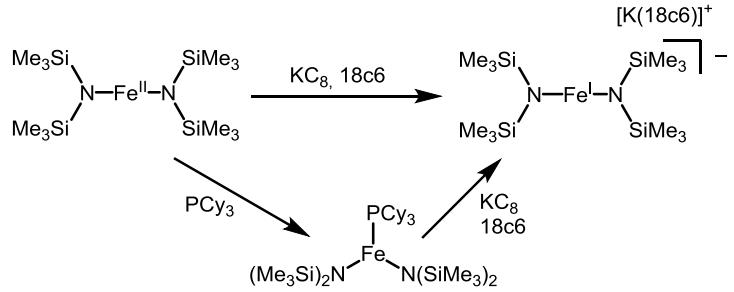

Schema 38. Reduktion von $[Fe(N(SiMe_3)_2)_2]$ mit Kaliumgraphit mit der alternativen Synthese über die Zugabe von Tricyclohexylphosphan.[111]

Durch die höhere Elektronendichte am Metallion werden dative Hinbindungen von LEWIS-basischen Positionen unterbunden, was auch durch die Abwesenheit von intramolekularen Metall-Ligand-Wechselwirkungen zu beobachten ist (Schema 39).[116,117]

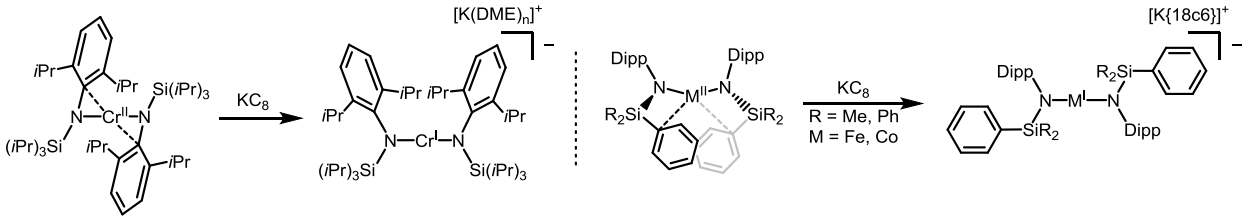

Schema 39. Aufhebung von intramolekularen Wechselwirkungen (gestrichelte Bindung) bei der Reduktion von Metall(II)- zu Metall(I)komplexen.[116,117]

Die ungewöhnliche Oxidationsstufe äußert sich auch im Redoxverhalten der Metall(I)komplexe gegenüber verschiedenen reduzierbaren Substraten. Die Redoxpotentiale der Silylamidokomplexe $[K\{18c6\}][M^I(N(SiMe_3)_2)_2]$ (M = Fe, Co; im Folgenden $[M^I]$ genannt) liegen in THF bei –1.98 V für Eisen und bei –1.47 V für Cobalt gegenüber dem Ferrocen / Ferrocenium-Redoxpaar. Dies lässt sich am Beispiel der Reaktion von $[M^I]$ (M = Cr –Co) mit 2,2'-Bipyridin demonstrieren, welches im Zusammenspiel mit der Koordination an ein Metallion durch einen SET zum Radikalanion reduziert wird (Schema 40).[118]

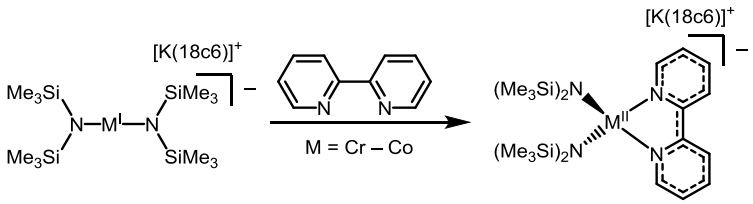

Schema 40. Reduktion von 2,2'-Bipyridin mit $[M^I]$ (M = Cr – Co).[118]

In ähnlicher Weise kann auch Pyridin durch Metall(I)komplexe aktiviert werden, wodurch sich zunächst ebenfalls ein Metall(II)-Radikalkomplex bildet. Dieser kann in *para*-Position des Pyridyl-Liganden zum 4,4'-Dihydrobipyridyl-Komplex kuppeln (Schema 41).[119,120]

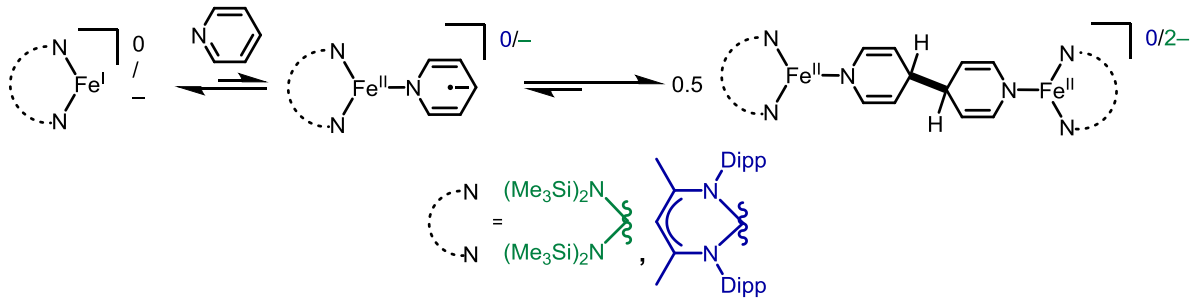

Schema 41. Reduktion und anschließende Kupplung von Pyridin durch Koordination an niedrig-koordinierte Metall(I)komplexe.[119,120]

Wird hingegen Pentafluoropyridin als Substrat eingesetzt, bildet sich unter Übertragung eines Fluorid-Ions in einer reduktiven Kupplung das 4,4'-Octafluorobipyridin (Schema 42).

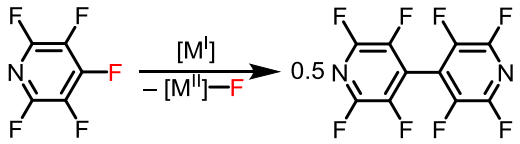

Schema 42. Reduktive Kupplung von Pentafluoropyridin durch [M^{I}] (M = Mn – Fe).

Bei der Reaktion von Phenylpyridin (phpy) mit [Mn^{I}] konnte die Bildung des Radikalkomplexes [(K{18c6})$_2$(phpy)][Mn(N(SiMe$_3$)$_2$)$_3$] als vermeintliches Zersetzungsprodukt beobachtet werden. Die Synthese konnte bei der gezielten Reduktion von Phenylpyridin mit KC_8 in Gegenwart von 18c6 und [K{18c6}][Mn(N(SiMe$_3$)$_2$)$_3$] verifiziert werden (Schema 43). Der Radikalcharakter der Verbindung konnte durch die erhöhte Länge der zentralen C-C-Bindung (1.429(4) Å) belegt werden.

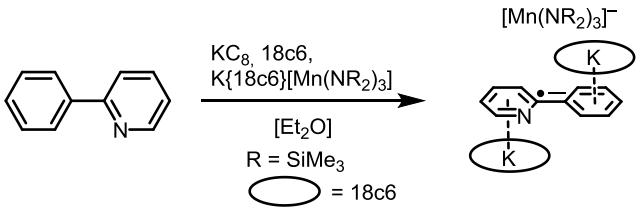

Schema 43. Darstellung des Radikalkomplexes [(K{18c6})$_2$(phpy)][Mn(N(SiMe$_3$)$_2$)$_3$].

Organoazide konnten durch die Reaktion mit niedrig-koordinierten 3d-Metallkomplexen (auf für die Oxidationszahl +I) unter Abspaltung von Stickstoff zu einer Reihe von metallstabilisierten Imidylradikalanionen reduziert werden (Schema 44). Die komplizierte Bindungssituation dieser Verbindungen wurde durch den Einsatz von ^{57}Mößbauer-Spektroskopie (für Eisen), EPR- und Röntgenabsorptions-Spektroskopie (engl. *X-ray absorption spectroscopy*, XAS) aufgeklärt.[121–123]

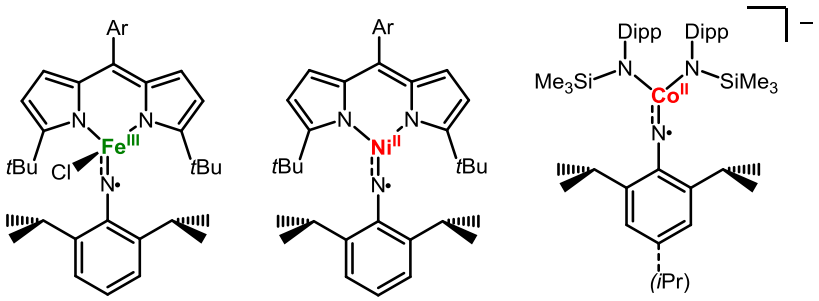

Schema 44. Niedrig-koordinierte 3d-Metallkomplexe mit Imidylradikalanionen als Liganden.[121–123]

Neben den bereits gezeigten Reduktionen von Substraten können niedrig-koordinierte 3d-Metallkomplexe auch die nicht-klassische Aktivierung von C-C-Mehrfachbindungen vollführen. Die *side-on* Koordination von C-C-Dreifachbindungen an frühe Übergangsmetallkomplexe kann als Metallacyclopropen mit kovalenten Metall-Kohlenstoffbindungen beschrieben werden,[124,125] während bei späten Übergangsmetallen die d → π*-Rückbindung mit zusätzlichem elektrostatischem Anteil dominiert.[126,127] Während die meisten Beispiele mit dieser Bindungsart aus *low-spin*-Komplexen bestehen, konnten durch den Einsatz niedrig-koordinierter Komplexe verschiedene *high-spin*-Verbindungen mit *side-on*-koordinierten Alkinen dargestellt werden (Schema 45).[128–135]

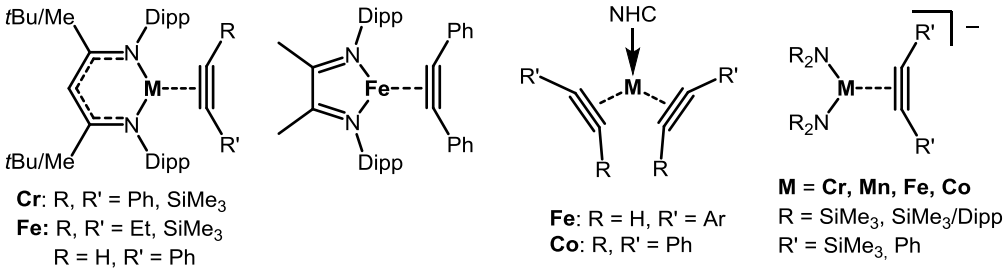

Schema 45. Niedrig-koordinierte Metall-Alkin-Komplexe der Metalle Chrom bis Cobalt.[128–135]

Im Falle der Amidkomplexe (Schema 45 rechts) konnte durch quantenchemische Rechnungen ermittelt werden, dass die Koordination als Resonanzstrukturen mit einem drei-Elektronen-drei-Zentren-Charakter beschrieben werden können (Schema 46): Entweder koordiniert das Alkin als Neutralligand an das Metall(I)ion, als Alkinylradikalanion an ein Metall(II)ion oder der Komplex liegt als Metallacyclopropen vor. Je nach Metall unterscheiden sich die vorliegenden Anteile zwischen diesen Zuständen.

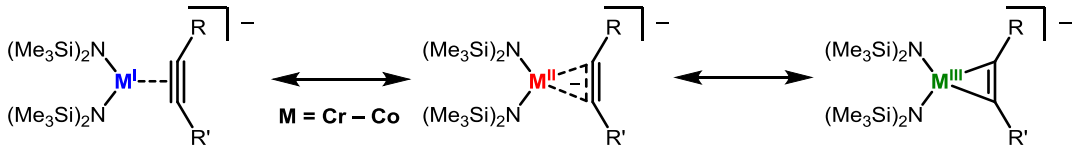

Schema 46. Resonanzstrukturen für Metall-Alkin-Komplexe: Alkin als Neutralligand (links), als Radikalanion (Mitte) oder Metallacyclopropen (rechts).[135]

Analog zu oben gezeigten Alkinkomplexen existieren auch Beispiele für die Aktivierung von Olefinen durch niedrig-koordinierte 3d-Metallkomplexe. Auch hier kann die elektronische Situation als Grenzfall zwischen klassischem π-Komplex und Metallacyclopropan beschrieben werden (Schema 47).[130,132,136] Für den Eisen-Trimethylsilylethen-Komplex (Schema 47 links) konnte anhand von ^{57}Mößbauer-Spektroskopie eine formale Oxidationszahl zwischen +I und +II für das Eisenion bestimmt werden, was für eine partielle Reduktion der Doppelbindungen der Liganden spricht.

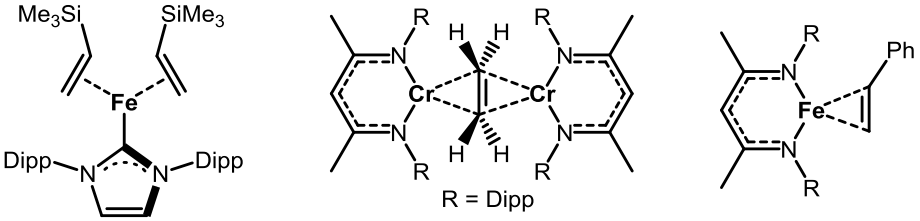

Schema 47. Niedrig-koordinierte Metall-Alken-Komplexe der Metalle Chrom und Eisen.[130,132,136]

2. Motivation und Zielsetzung

Wie in Kapitel 1 beschrieben, ist das Verständnis der Ein-Elektronen-Reduktion von (organischen) Doppelbindungen von hohem Wert. Aufbauend auf ersten Arbeiten der Arbeitsgruppe zur Stabilisierung von Radikalanionen soll dies konzeptionell auf bis reaktivere, bislang nur in-situ beobachtbare Radikalanionen ausgeweitet werden. Die Redox- und Koordinationseigenschaften von niedrig-koordinierten Metall(I)komplexen bietet sich hierbei besonders an, um eine gleichzeitige Reduktion, wie auch eine Stabilisierung der entstehenden Spezies zu ermöglichen. Das primäre Ziel der Arbeit war deswegen, neue Radikalanionen darzustellen und zu isolieren, die bisher höchstens *in situ* nachgewiesen wurden. Darauf aufbauend sollte das Reaktionsverhalten dieser Verbindungen zu untersuchen. Dazu wurden im Rahmen dieser Arbeit verschiedene Teilprojekte bearbeitet, welche verschiedene Bindungstypen abdecken (Schema 48).

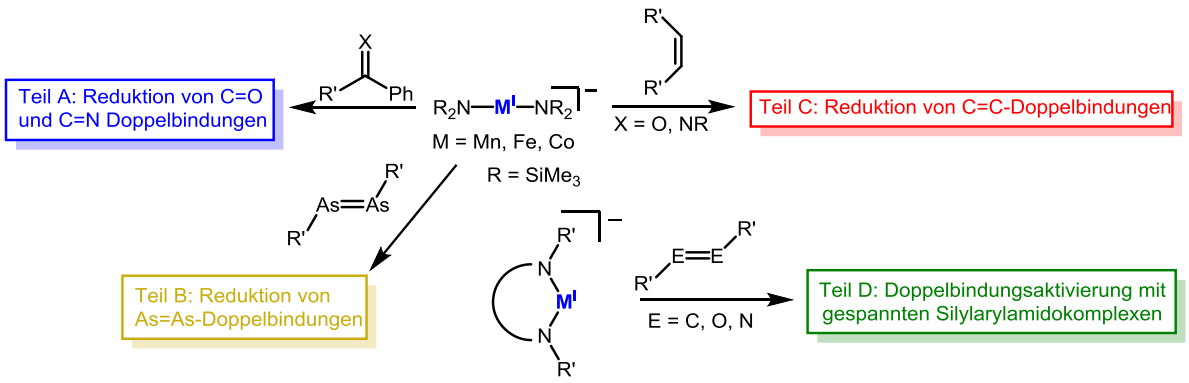

Schema 48. Übersicht über die im Rahmen dieser Arbeit behandelten Teilprojekte A – D.

Im ersten Teilprojekt A sollte zunächst die Reaktivität niedrig-koordinierter Metall(I)komplexe gegenüber C=O-Doppelbindungen untersucht werden, aufbauend auf den prinzipiell bekannten Ketylradikalen. Der Einsatz niedrig-koordinierter, linearer Vorläuferkomplexe zielte auf die zusätzliche Ausweitung auf C=N-Doppelbindungen ab. Die erhaltenen Radikalkomplexe sollten hinsichtlich ihrer spektroskopischen Eigenschaften und ihrer Reaktivität untersucht werden. Teilprojekt B widmete sich der Untersuchung zu der Reduktion einer As=As-Doppelbindung. In Teilprojekt C sollte die Reduktion verschiedener, nicht-aromatischer C=C-Doppelbindungen untersucht werden. In Teilprojekt D wurde den Einsatz von neuen, niedrig-koordinierten Metall(I)komplexen mit gespanntem Ligandenrückgrad behandelt, bei denen, ähnlich zu den NacNac-Komplexen, ein nichtlinearer N-M-N-Bindungswinkel vorliegt. Hierbei sollte die Reaktivität gegenüber verschiedenen Substraten untersucht werden, um Verständnis für den Einfluss der Abwinkelung des Liganden zu gewinnen.

3. Kumulativer Teil

3.1 Cobalt and Iron Stabilized Ketyl, Ketiminyl and Aldiminyl Radical Anions

G. Sieg, Q. Pessemesse, S. Reith, S. Yelin, C. Limberg, D. Munz, C. G. Werncke, *Chem. Eur. J.* **2021**, *27*, 16760 – 16767.

Abstract

Carbonyl and iminyl based radical anions are reactive intermediates in a variety of transformations in organic synthesis. Herein, the isolation of ketyl, and more importantly unprecedented ketiminyl and aldiminyl radical anions coordinated to cobalt and iron complexes is presented. Insights into the electronic structure of these unusual metal bound radical anions is provided by X-Ray diffraction analysis, NMR, IR, UV/Vis and Mössbauer spectroscopy, solid and solution state magnetometry, as well as a by a detailed computational analysis. The metal bound radical anions are very reactive and facilitate the activation of intra- and intermolecular C–H bonds.

Zusammenfassung

Im Zuge dieser Publikation wurden verschiedene Radikalanionen ausgehend von Ketonen, Ket- und Aldiminen dargestellt, welche durch die Koordination an niedrig-koordiniert Metallkomplexe von Eisen und Cobalt stabilisiert wurden. Dafür wurden Benzophenon (bp), Benzophenonimin (bpi) und Benzaldehydmethylamin (bama) mit den Komplexen $[K\{18c6\}][M^{I}(N(SiMe_3)_2)_2]$ (M = Fe, Co) zur Reaktion gebracht (Schema 49). Dabei werden die organischen Substrate bp, bpi und bama in einem SET reduziert und koordinieren terminal als Radikalanionen über ihr Sauerstoff- bzw. Stickstoffatom an das Metallion. Komplexe von Ketylradikalanionen wurden bereits an verschiedenen Stellen in der Literatur beschrieben.[17,60,137] Analoge Verbindungen mit Ket- oder Aldiminylradikalanionen waren bislang nicht bekannt.

Während die Ketyl- und Ketiminylkomplexe $[\mathbf{1}]^{-}$, $[\mathbf{2}]^{-}$ und $[\mathbf{5}]^{-}$ stabil und vergleichsweise gut isolierbar sind, zerfallen die Ketiminylkomplexe $[\mathbf{3}]^{-}$ und $[\mathbf{4}]^{-}$ nach wenigen Minuten. Zum Vergleich wurde die Bildung der divalenten Adduktverbindungen verfolgt. Hierbei konnten bei der Umsetzung der Neutralkomplexe $[M^{II}(N(SiMe_3)_2)_2]$ (M = Fe, Co) mit bp, bpi und bama die Adduktkomplexe **1**, **2**, **5** und **6** erhalten werden, während bei der Umsetzung mit bpi unter Abspaltung eines protonierten Liganden $HN(SiMe_3)_2$ die dimeren Komplexe **7** und **8** entstanden. Diese wurden nicht weiter auf ihre Reaktivität untersucht. **1**, **2** und **5** lassen sich durch Reduktion in $[\mathbf{1}]^{-}$, $[\mathbf{2}]^{-}$ und $[\mathbf{5}]^{-}$ überführen, für **6** ist eine Reduktion nicht möglich. Im letzteren Fall wird $[Co^{I}(N(SiMe_3)_2)_2]^{-}$ gebildet, was die höhere Reduktionskraft des Aldiminylradikalanions im Vergleich zum Cobalt(I)ion zeigt.

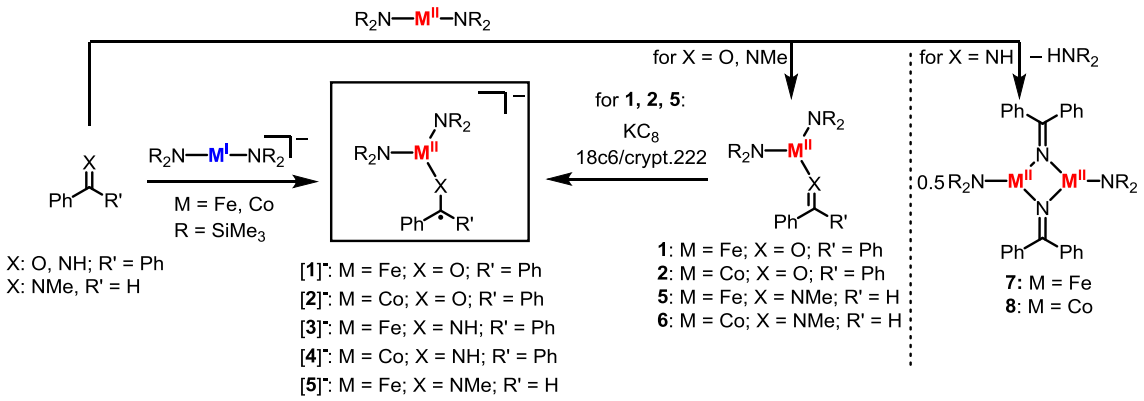

Schema 49. Synthese der Radikalanionen-Komplexe [**1**]$^-$ – [**5**]$^-$, sowie der Neutralkomplexe **1**, **2**, **5** – **8**.

Die reduzierten Komplexe [**1**]$^-$ – [**5**]$^-$ wurden weitergehend durch spektroskopische Methoden und quantenchemische Rechnungen untersucht. Die Komplexe [**1**]$^-$ – [**4**]$^-$ zeigen in Lösung im UV-Vis Spektrum eine starke Photoabsorption zwischen 550 und 600 nm, was im Einklang mit bereits beobachteten Ketylradikalkomplexen steht.[17,66,137] [**5**]$^-$ zeigt aufgrund seines kleineren aromatischen Systems eine Absorption bei λ_{max} = 486 nm. Die Absorptionen kommen durch $\pi \rightarrow \pi^*$- Übergänge zustande, was auch durch quantenchemische Rechnungen für Radikalanionen gezeigt werden konnte. Anhand von UV-Vis, ^{1}H-NMR-, ^{57}Mößbauer und EPR-Spektroskopie, sowie durch Messungen des magnetischen Momentes im Festkörper und in Lösung wurde für [**1**]$^-$, [**2**]$^-$ und [**5**]$^-$ zweifelsfrei die Oxidationsstufe +II für die Metallionen bestimmt. Dies impliziert die Reduktion der Substrate und untermauert weiter den radikalischen Charakter der Verbindungen.

Als Zerfallsweg für [**3**]$^-$ konnte die Bildung eines dinuklearen Komplexanions $[Fe_2(NCPh_2)_4(\mu\text{-}NCPh_2)_2]^{2-}$ ([**10**]$^{2-}$) mit vier terminalen und zwei verbrückenden Ketimidatoliganden gezeigt werden, welcher sich unter Abspaltung aller $N(SiMe_3)_2^-$-Liganden bildet. [**4**]$^-$ zerfällt unter Bildung des dinuklearen Komplexanions $[Co_2(N(SiMe_3)_2)(NC(Ph)(C_6H_5))_2]^{2-}$. Hier findet an beiden Liganden in *ortho*-Position von jeweils einer Phenylgruppe eine C–H-Aktivierung mit anschließender Koordination zu einem Cobaltion statt.

Für [**2**]$^-$ und [**5**]$^-$ konnte bei stöchiometrischer Zugabe von 1,4-Cyclohexadien (1,4-CHD) ein HAT unter Bildung von Benzol beobachtet werden. Bei Zugabe eines Überschusses 1,4-CHD auf [**2**]$^-$ bildet sich der ungewöhnliche Sandwichkomplex $[Co^{-I}(\eta^4\text{-}1,3\text{-}CHD)_2]^-$ ([**9**]$^-$), verbunden mit einer 1,3-H-Umlagerung innerhalb der Cyclohexadienmoleküle.

Eigener Anteil

[**2**]$^-$, **1**, **2**, **7** und **8** wurden von *Sascha Reith* unter meiner Aufsicht erstmalig dargestellt und durch Röntgenbeugung identifiziert. Alle übrigen Verbindungen wurden von mir vollständig anhand von Röntgenbeugung, ^{1}H-NMR-, UV-Vis- (sofern angegeben) und IR-Spektroskopie charakterisiert.
Die Röntgenbeugungsexperiemente wurden durch *Dr. Gunnar Werncke* oder durch die Serviceabteilung für Kristallographie der Philipps-Universität-Marburg durchgeführt, die Sturkturlösung und -verfeinerung wurde von mir durchgeführt. Die Elementaranalyse wurde durch die Serviceabteilung Massenspektrometrie und Elementaranalytik der PUM durchgeführt und von mir ausgewertet. Die cyclovoltammetrischen Messungen wurden von mir unter Beaufsichtigung von *Dr. Christian Schneider* durgeführt. Die Messungen des magnetischen Momentes im Festkörper wurden von *Clemens Pietzonka* durchgeführt und von mir nach dem CURIE-WEISS-Gesetz angepasst. Die ^{57}Fe-Mössbauer Messungen wurden von *Dr. Stefan Yelin* aus der Arbeitsgruppe von *Prof. Dr. Christian Limberg* (Humbold-Universität zu Berlin) durchgeführt und ausgewertet. Die EPR Messungen wurden von *Jurek Lange* aus der Arbeitsgruppe von *Prof. Dr. Detlev Hofmann* (Justus-Liebig Universität Gießen) durchgeführt und von mir ausgewertet. Die quantenchemischen Berechnungen wurden von *Quentin Pessemesse* und *Prof. Dr. Dominik Munz* durchgeführt. Das Manuskript wurde in Zusammenarbeit mit *Dr. Gunnar Werncke* von mir verfasst und von den übrigen Autoren überarbeitet.

Check for updates

Chemistry Europe
European Chemical Societies Publishing

Cobalt and Iron Stabilized Ketyl, Ketiminyl and Aldiminyl Radical Anions

Grégoire Sieg,[a] Quentin Pessemesse,[b, c] Sascha Reith,[a] Stefan Yelin,[e] Christian Limberg,[e] Dominik Munz,[c, d] and C. Gunnar Werncke*[a]

Abstract: Carbonyl and iminyl based radical anions are reactive intermediates in a variety of transformations in organic synthesis. Herein, the isolation of ketyl, and more importantly unprecedented ketiminyl and aldiminyl radical anions coordinated to cobalt and iron complexes is presented. Insights into the electronic structure of these unusual metal bound radical anions is provided by X-Ray diffraction analysis, NMR, IR, UV/Vis and Mössbauer spectroscopy, solid and solution state magnetometry, as well as a by a detailed computational analysis. The metal bound radical anions are very reactive and facilitate the activation of intra- and intermolecular C–H bonds.

Introduction

The metal-mediated reduction of ketones and aldehydes is a well-known synthetic methodology. It can be employed for substrate deoxygenation (Clemmensen reduction, Zn) or for the construction of 1,2-diols (pinacol coupling; Mg, SmI_2 or low valent early transition metal complexes) and olefins (McMurray-Coupling, Ti).[1,2,3] Similarly, ketimines and aldimines may be reduced leading to 1,2-diamines.[2] In these, and in other reactions such as the amide reduction to alcohols,[4] the initial substrate reduction via the formation of metal-bound radical anions supposedly is the key step, which concurs with the umpolung of the electrophilic carbonyl carbon atom. In recent years, the importance of these and other radical anions further emerged due to their role as crucial intermediates in photoredox catalysis.[3,5] Hitherto, experimental insights into those radical anions is essentially restricted to in situ EPR- and UV/Vis spectroscopic data.[6] Another way to expand the knowledge of these radical anions is by isolation of their metal complexes. However, examples for metal-bound carbonyl or iminyl radical anions are scarce and mostly restricted to diaryl ketones as illustrated for the isolation of the alkali metal salts the benzophenone or fluorenone radical anion.[7,8]

Few additional examples of other metal complexes bearing simple diaryl ketyl or fluorenyl radical anions were authenticated in case of transition- (Fe, Zr)[9–11] and rare earth metals (Sm, Eur, Yb, La)[12,13–16] as well as uranium[17] and alkali (earth) metals.[18,19] Here, the intermolecular coupling of the substrate occurs in the absence of sufficient steric protection or blocking of susceptible substrate positions, which in rare cases is found to be reversible. The coupling occurs under pinacol coupling or Gomberg-type dimerization, as expected from the behaviour of free radical anions.[11,13–17,20,21] Recently, these endeavours were extended to organic amides using a highly reducing U^{III} complex.[21] In contrast, complexes with aldehyde radical anions or related "simple" imine derivatives such as aldimines (R(H)NH) and ketimines (R_2NH) are absent in the literature. This is surprising given the reversible redox chemistry (*viz.* redox activity) of ubiquitous imino containing ligands including α-diimines, α-iminopyridines or pyridino diimines (PDIs).[22]

Herein, we present the isolation of rare examples of metal*stabilized ketyl radical anions as well as unique ketiminyl and aldiminyl radical anions using the quasilinear cobalt(I) and iron(I) complexes K{m}[M(N(SiMe$_3$)$_2$)$_2$] (m = 18c6, crypt.222) as reductants and coordination site (Figure 1). The radical anionic nature of the substrates L in the K{m}[M(L$^{\bullet-}$)(N(SiMe$_3$)$_2$)$_2$] complexes was proven via thorough characterization using X-Ray diffraction (XRD) analysis, ^{1}H-, IR-, EPR- (for cobalt), Mössbauer (for iron) and UV/Vis spectroscopy, cyclic voltammetry as well as magnetic measurements in comparison to the neutral metal(II) adducts. Quantum chemical calculations at the

[a] G. Sieg, S. Reith, Dr. C. G. Werncke
Fachbereich Chemie
Philipps-Universität Marburg
Hans-Meerwein-Straße 4, 35043 Marburg (Germany)
E-mail: gunnar.werncke@chemie.uni-marburg.de

[b] Q. Pessemesse
Univ. Lyon, ENS de Lyon, CNRS UMR 5182
Université Claude Bernard Lyon 1, Laboratoire de Chimie
69342, Lyon (France)

[c] Q. Pessemesse, Prof. Dr. D. Munz
Anorganische Chemie: Koordinationschemie
Campus C4.1
Universität des Saarlandes 66123 Saarbrücken (Germany)

[d] Prof. Dr. D. Munz
Department Chemie und Pharmazie
Friedrich-Alexander Universität (FAU) Erlangen-Nürnberg
Egerlandstr. 1, D-91058 Erlangen (Germany)

[e] S. Yelin, Prof. Dr. C. Limberg
Institut für Chemie
Humboldt-Universität zu Berlin
Brook-Taylor-Str. 2, 12489 Berlin (Germany)

Supporting information for this article is available on the WWW under https://doi.org/10.1002/chem.202103096

© 2021 The Authors. Chemistry - A European Journal published by Wiley-VCH GmbH. This is an open access article under the terms of the Creative Commons Attribution Non-Commercial NoDerivs License, which permits use and distribution in any medium, provided the original work is properly cited, the use is non-commercial and no modifications or adaptations are made.

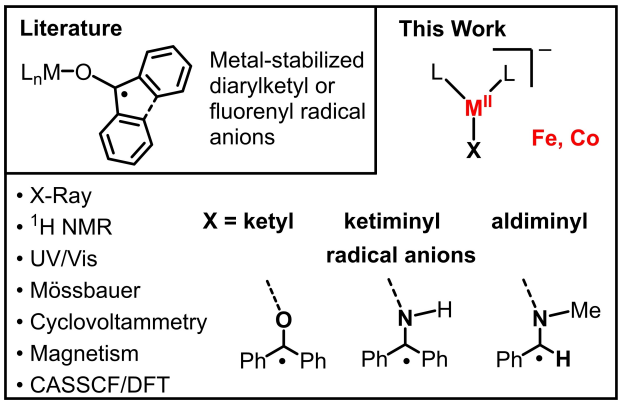

Figure 1. Metal-stabilized ketyl, ketiminyl and aldiminyl radical anions in the literature and in this report.

density functional theory (DFT) as well as NEVPT2/CASSCF level of theory further corroborate this picture. The radical anion complexes undergo varied bond activation chemistry.

Results and Discussion

Synthesis and structure

Addition of benzophenone (bp) to the quasilinear iron(I) and cobalt(I) complexes K{m}[M^{I}(N(SiMe$_3$)$_2$)$_2$] (m = 18-crown-6 or crypt.222)[23–25] resulted immediately in intensely blue and violet colored solutions from which K{m}[Fe(bp)(N(SiMe$_3$)$_2$)$_2$], K{m}[**1**], and K{m}[Co(bp)(N(SiMe$_3$)$_2$)$_2$], K{m}[**2**] were isolated (Scheme 1). The analogous, yet more challenging, reduction of aldehydes and the related ketimines and aldimines was attempted as well. Whereas only colorless unidentifiable products were obtained for acetaldehyde, which arguably indicates substrate coupling, ketimine benzophenone imine (bpi) allowed to isolate turquois K{m}[Fe(bpi)(N(SiMe$_3$)$_2$)$_2$], [**3**]$^-$, and K{m}[Co(bpi)(N(SiMe$_3$)$_2$)$_2$], [**4**]$^-$. Both bpi-complexes decompose rapidly ($t_{1/2} \approx 5$ min.) at room temperature and could therefore only be analysed via XRD and in situ UV/VIS spectroscopy. The analogous reaction of the aldimine benzaldehyde methylamine (bama) with the metal (I) precursors led in case of iron to the formation of dark yellow K{m}[Fe(bama)(N(SiMe$_3$)$_2$)$_2$], **5**. In contrast, no reaction was observed for the reaction of the cobalt(I) complex with bama.

For comparison, the synthesis of the neutral metal(II) substrate adducts was pursued as well. [M(N(SiMe$_3$)$_2$)$_2$] readily formed adducts with bama and bp, whereas for bpi unproductive substrate deprotonation and formation of dimeric complexes [(M(N(SiMe$_3$)$_2$))$_2$(μ-NCPh$_2$)$_2$] (Fe: **7**, Co: **8**) was observed. The metal(II) adducts **1, 2** and **5** could also be used for the

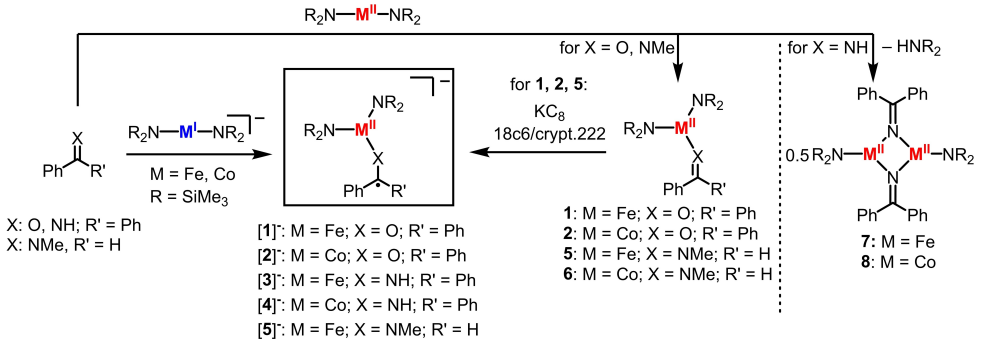

Scheme 1. Synthesis of iron and cobalt ketyl-, ketiminyl- and aldiminyl radical anion complexes [**1**]$^-$–[**5**]$^-$ and neutral complexes **1**, **2**, **5** and **6**.

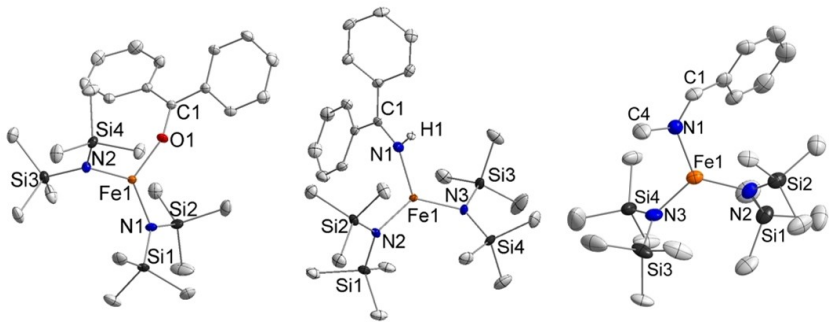

Figure 2. Molecular structures of the complex anions of compounds K{m}[**1**], K{m}[**3**] and K{m}[**5**]. H atoms (except H1) and [K{18c6}]$^+$ cations are omitted for clarity and ellipsoids are shown at 50% probability.

© 2021 The Authors. Chemistry - A European Journal published by Wiley-VCH GmbH

formation of their reduced counterparts, with the exception of **6**. There, the reduction with KC_8 led to the formation of the adduct free $[Co^{I}(N(SiMe_3)_2)_2]^-$. This indicates that the aldiminyl radical anion is more reducing than the cobalt ion which is in line with indifference of bama towards the cobalt(I) complex.

X-ray diffraction analysis of the anionic, trigonal planar iron and cobalt benzophenone complexes revealed C–O bond lengths of 1.310(2) Å ($[\mathbf{1}]^-$) and 1.324(2) Å ($[\mathbf{2}]^-$) (Figure 1). In comparison to those found for their respective, neutral counterparts (1.248(9) Å (**1**) and 1.244(2) Å (**2**)) as well as for other authenticated ketyl radical anion complexes,[9–11,17,18] this hints at the presence of a ketyl radical anion.

Accordingly, the M–O bonds of 1.869(1) Å ($[\mathbf{1}]^-$), 1.903(1) Å ($[\mathbf{2}]^-$) are considerably shorter than those of their neutral counterparts (**1** (bp): 2.025(5) Å, **5** (bama): 2.119(2) Å). This is similar to the only other late 3*d*-metal ketyl complex. (Fe(II)–O 1.8565(10) Å)[9] and in the general range found for anionic O-donor ligands. The iron benzophenone imine complex $[\mathbf{3}]^-$ exhibits an Fe–N_{bpi} bond length of 1.917(2) Å with N_{bpi}–C distance of 1.299(3) Å. For $[\mathbf{4}]^-$ both the Co–N_{bpi} (1.946(2) Å) and the N_{bpi}–C bonds are longer (1.350(4) Å) (Table 1). While the value of N_{bpi}–C of $[\mathbf{4}]^-$ is comparable to cobalt(II) complexes of monoreduced aryliminopyridines (approx. 1.34 Å),[26] the N_{bpi}–C distance of the iron complex $[\mathbf{3}]^-$ is surprisingly short.[27] However, the very short Fe–N_{bpi} bond implicated an anionic amide ligand which gave overall an ambiguous picture for $[\mathbf{3}]^-$ on a structural level. The comparison of the structural metrics for the iron aldimine complexes $[\mathbf{5}]^-$ and **5** show clearly longer N_{bama}–C bond (1.331(6) Å) and shorter Fe–N_{bama} bond (1.978(4) Å) for the reduced complex $[\mathbf{5}]^-$ (**5**: Fe–N_{bama} 2.0119(2) Å; N_{bama}–C 1.275(3) Å). The average M–N_{SiMe3} bond lengths of all reduced complexes are slightly elongated (Fe: 1.95–1.97 Å; Co: 1.93–1.97 Å) in comparison to the neutral counterparts (Fe: 1.91–1.94 Å; Co: 1.90–1.92 Å)).

The electrochemical behaviour of all isolable mononuclear compounds was investigated by cyclic voltammetry (Figures S41–S44). The anionic compounds exhibited no meaningful redox events, a phenomenon already observed for other anionic, low-valent 3*d*-metal silylamides with radical anionic ligands.[28] In contrast, for the neutral compounds **1** and **2** a reversible reduction at $E_{1/2} = -2.06$ V (**1**) and $E_{1/2} = -2.10$ V (**2**) was observed (200 mVs^{-1}, vs. Fc/Fc^+ propylene carbonate). For **5** the reduction is irreversible ($E_{p/2} = -2.83$ V (**5**)). These reduction potentials are suspiciously similar to those of the free substrates, which is indicative for a substrate-centred reduction although we cannot fully rule out substrate dissociation under the CV conditions.

Table 1. Selected structural metrics of complexes $[\mathbf{1}]^-$–$[\mathbf{5}]^-$, [**1**], [**2**], [**5**] and [**6**].

Compound	M–X/Å	C–X/Å	M–N1/Å	M–N2/Å
Fe(bp$^\bullet$) ($[\mathbf{1}]^-$)	1.869(1)	1.310(2)	1.951(1)	1.953(1)
Co(bp$^\bullet$) ($[\mathbf{2}]^-$)	1.903(1)	1.324(2)	1.960(1)	1.934(1)
Fe(bpi$^\bullet$) ($[\mathbf{3}]^-$)	1.917(2)	1.299(3)	1.965(2)	1.966(2)
Co(bpi$^\bullet$) ($[\mathbf{4}]^-$)	1.946(2)	1.350(4)	1.954(2)	1.971(2)
Fe(bama$^\bullet$) ($[\mathbf{5}]^-$)	1.978(4)	1.331(6)	1.971(4)	1.968(4)
Fe(bp) (**1**)	2.025(5)	1.248(9)	1.937(6)	1.912(6)
Co(bp) (**2**)	2.025(1)	1.244(2)	1.899(1)	1.903(2)
Fe(bama) (**5**)	2.119(2)	1.275(3)	1.934(2)	1.930(2)
Co(bama) (**6**)	2.061(2)	1.276(4)	1.905(2)	1.916(2)

Spectroscopy

UV/Vis spectroscopic examination of the anionic iron ketyl and ketiminyl complexes show distinct absorption maxima at 581 nm ($[\mathbf{1}]^-$) and 567 nm ($[\mathbf{3}]^-$) (Figure 3 and Table 2), which is consistent with previously reported ketyl-radical anions.[7,9,11,17] We attribute these features on the basis of TD-DFT (Table S11, Figure S60–S70) and state averaged CASSCF/NEVPT2 (Table S12–S15, Figure S76–78) calculations to the π-π* transitions, which share considerable metal-to-ligand charge-transfer (MLCT) character. Similarly, the analogous cobalt compounds exhibit absorption maxima at 567 nm ($[\mathbf{2}]^-$) and 594 nm ($[\mathbf{4}]^-$). The aldiminyl radical iron complex $[\mathbf{5}]^-$ lacks any absorption in this region, but exhibits a pronounced absorption at 486 cm^{-1}. The blue-shift is likely due to the absence of the second aryl substituent and thus overall smaller aromatic system. For comparison, the neutral metal substrate adducts exhibit no such absorption bands.

^{1}H NMR spectroscopic examination of the reduced, stable complexes $[\mathbf{1}]^-$, $[\mathbf{2}]^-$, and $[\mathbf{5}]^-$ revealed extensive paramagnetic features. The position of the respective $SiMe_3$ signals (Fe: $[\mathbf{1}]^-$: −2.56 ppm, $[\mathbf{5}]^-$: −3.02 ppm; Co: $[\mathbf{2}]^-$: −12.47 ppm) resembles those of comparable trigonal metal(II) complexes (e.g. $[Fe(N(SiMe_3)_2)_2(F)]^-$: −2.29 ppm);[29] ($[Co(NH^tBu)(N(SiMe_3)_2)_2]^-$: −15.45 ppm[23]). As the $SiMe_3$ signal is highly sensitive to the coordination environment and oxidation state, it would support the notion of three-coordinate metal(II) ions in all these compounds. Interestingly, upon dissolution of otherwise analytical pure $[\mathbf{2}]^-$ the presence of precursor complex $[K(18c6)][Co(N(SiMe_3)_2)_2]$ could be detected. Addition of further amounts of benzophenone did not fully suppress the signal belonging to the cobalt(I) starting compound (and also initiated partial

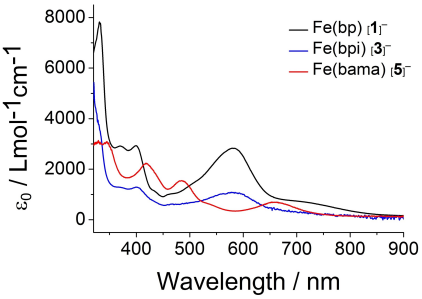

Figure 3. UV-Vis spectra of complexes $[\mathbf{1}]^-$, $[\mathbf{3}]^-$ and $[\mathbf{5}]^-$ in Et_2O.

Table 2. UV/Vis-spectroscopic characteristics of $[\mathbf{1}]^-$–$[\mathbf{5}]^-$.

	Fe(bp$^\bullet$) [1]-	Fe(bpi$^\bullet$) [3]-	Fe(bama$^\bullet$) [5]-	Co(bp$^\bullet$) [2]-	Co(bpi$^\bullet$) [4]-
λ_{max} /nm	581	584	486	567	594
ε_0 / L $mol^{-1}cm^{-1}$	2830	1080	1550	3720	n.a.

© 2021 The Authors. Chemistry - A European Journal published by Wiley-VCH GmbH

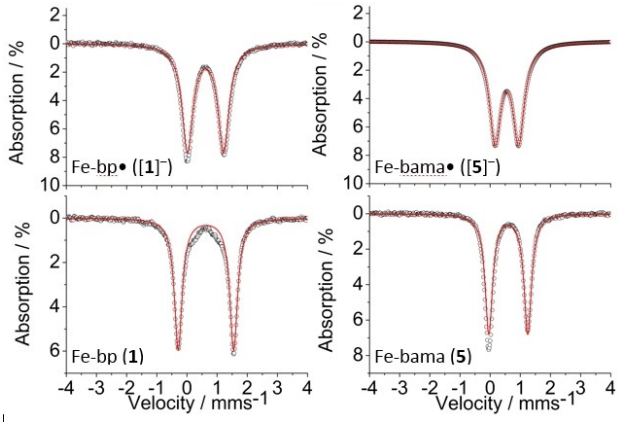

Figure 4. ^{57}Fe-Mössbauer spectra of K(18c6)[**1**] (top left), **1** (bottom left), [K(18c6)][**5**] (top right) and **5** (bottom right) at 15 K. Isomer shifts δ and quadrupole splittings ΔQ are as following: [**1**]$^-$: $\delta = 0.62$ mms^{-1}, $\Delta Q = 1.20$ mms^{-1}; **1**: $\delta = 0.62$ mms^{-1}, $\Delta Q = 1.83$ mms^{-1}; [**5**]$^-$: $\delta = 0.56$ mms^{-1}, $\Delta Q = 0.78$ mms^{-1}; **5**: $\delta = 0.58$ mms^{-1}, $\Delta Q = 1.31$ mms^{-1}.

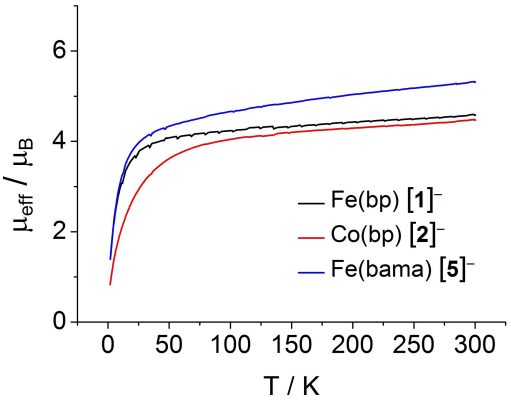

Figure 5. Temperature dependent magnetic susceptibility (χT vs. T) for 1,2 and 5 from 3 K to 300 K

decomposition via detection of [Co(N(SiMe$_3$)$_2$)$_3$]$^-$), which points to an equilibrium between [**2**]$^-$ and starting complex/free benzophenone. A similar observation was already made by us for the cobalt alkyne complex [Co(η^2-PhCCPh)(N(SiMe$_3$)$_2$)$_2$][30] which we attribute in the present case also to the low reduction potential of [Co(N(SiMe$_3$)$_2$)$_2$] ($E_{red} = -1.47$ V).[25]

For more intimate insights into the electronic situation, ^{57}Fe Mössbauer (for iron) and EPR spectroscopy (for cobalt) was performed. All iron compounds **1**, [**1**]$^-$, **5** and [**5**]$^-$ (Figure 4, S53–56), show doublets with similar isomer shifts (0.56–0.62 mms^{-1}) in the Mössbauer spectra. These values correspond well with those observed for related trigonal planar high-spin iron(II) complexes ([Fe(NR$_2$)$_2$I]$^-$: $\delta = 0.63$ mm s^{-1}; [Fe(NR$_2$)$_3$]$^-$: $\delta = 0.59$ mm s^{-1})[24,31] which speaks to a divalent metal ion in all compounds presented herein. The measured quadrupole splittings are smaller for the reduced complexes (0.78–1.20 mm s^{-1}) than for the neutral counterparts (1.31–1.83 mm s^{-1}). This can be reasoned by the more pseudo-C_3-symmetric geometry of the reduced compounds.

For the cobalt complex [**2**]$^-$ X-Band EPR-spectroscopy showed at 4 K broad absorptions at $g \approx 10$ and 3.84 and as well as a very sharp signal at $g = 2.00$ (Figure S57). The broad features are indicative of an axial signal corresponding to a high-spin cobalt(II) ion.[32] This becomes more evident as these signals disappear above 80 K (Figure S58). The signal at $g = 2.00$ likely belongs to the ketyl centred radical whereas its sharp, isotropic form suggests rather weak delocalisation of the electron over the cobalt ion.[21,33]

Magnetism

For further insights into the electronic structure of the anionic complexes, namely the iron complexes [**1**]$^-$, [**5**]$^-$ as well as the cobalt complex [**2**]$^-$, their magnetic features in the solid state and solution (Evans method) were probed (Figure 5). The effective magnetic moments of the iron complexes amount to $\mu_{eff} = 4.92\ \mu_B$ ([**1**]$^-$) and $\mu_{eff} = 4.65\ \mu_B$ ([**5**]$^-$) in solution, which is in good agreement to the values found in the solid state at 300 K ([**1**]$^-$: $\mu_{eff} = 4.40\ \mu_B$; [**5**]$^-$: $\mu_{eff} = 4.67\ \mu_B$. The $\chi_m T$ vs. T slopes of these compounds decrease steadily down to 50 K where a sharper drop is observed (Figure 5). Under the premise of an iron(II) ion interacting with an organic radical the observed values for both compounds lie between the theoretical spin-only values expected for a ferromagnetically coupled (5.19 μ_B) system and for strong antiferromagnetic coupling (3.87 μ_B). Further, these values are higher than those of low-coordinate high-spin iron(I) complexes, which would be the hypothetical case of a non-reduced substrate.[34] The presence of antiferromagnetic coupling also explains that the curves do not plateau at higher temperatures. Similar conclusions can be drawn for the cobalt complex [**2**]$^-$ (solution: $\mu_{eff} = 4.43\ \mu_B$; solid state, 300 K: $\mu_{eff} = 4.75\ \mu_B$). Its values are higher than the one of the cobalt(I) precursor ($\mu_{eff} = 4.21\ \mu_B$)[25] and the spin-only value of a cobalt(II) ion with antiferromagnetic coupling to the radical anion ($S = 1$; 2.83 μ_B) but lower than the alternative of ferromagnetic coupling ($S = 2$; 4.90 μ_B). Considering the general presence of significant spin-orbit contributions for cobalt(II) ions this speaks for an antiferromagnetically coupled system in [**2**]$^-$.

Quantum chemical calculations

In order to further pinpoint the electronic structure of the anionic complexes [**1**]$^-$–[**5**]$^-$ as well as the neutral congeners **1**, **2**, and **5**, scalar relativistic (ZORA) quantum chemical calculations were performed.[35] Various methods (CASSCF/NEVPT2; PBE, BP86, PBE0, TPSS, TPSSh, B3LYP, M06, PBEh-3c, B97-3c) were applied, which all gave qualitatively consistent results. Overall, all complexes [**1**]$^-$–[**5**]$^-$ contain a high-spin metal ion anti-ferromagnetically coupled to a ligand centred radical (Table S8–16). For instance, the benzophenone coordinated iron

© 2021 The Authors. Chemistry - A European Journal published by Wiley-VCH GmbH

complex $[\mathbf{1}]^-$ features a d^6 configured iron centre in the oxidation state +II with overall $S=3/2$ (Figure 6).[1]

Thereof, the $d(z^2)$ orbital is doubly occupied. The ligand centred radical is mainly located at the carbonyl carbon atom in the p(y) orbital (Table S10). It is moderately delocalized over the two phenyl substituents, and mixes with the d(xy) orbital. The NEVPT2/CASSCF (Table S15) calculations[36] predict a vertical quartet–sextet gap $\Delta E^{q/sex}$ of 0.16 eV, which is well reproduced by both vertical as well as adiabatic values from the DFT calculations ($PBE^{adiabatic}$: $\Delta E^{quart/sex}=24\ kJ\,mol^{-1}$; $PBE^{vertical}$: $\Delta E^{quart/sex}=25\ kJ\,mol^{-1}$). Accordingly, the cobalt complex $[\mathbf{2}]^-$ can be understood as a d^7 configured cobalt centre with doubly occupied $d(z^2)$ and d(xz) orbitals, and an anti-ferromagnetically coupled radical ligand, leading to a $S=1$ spin system (Figure S80). The triplet-quintet gap $\Delta E^{t/quin}$ is predicted to be 0.12 eV ($PBE^{adiabatic}$: $\Delta E^{t/quint}=21\ kJ\,mol^{-1}$; $PBE^{vertical}$: $\Delta E^{t/quint}=30\ kJ\,mol^{-1}$). While anionic complexes $[\mathbf{1}]^-$ to $[\mathbf{5}]^-$ display ligand-centered radicals, the iminyl and aldiminyl ligands bear slightly reduced spin-density on the carbon atom (Table S10).

Contrarily, the carbonyl- and imine ligand in the neutral metal complexes are all redox-innocent and coordinate the high-spin metal centres (Table S19). This picture is not only consistent with the experimental (see above) and computed C=X bond lengths, but manifests as well in the C–X stretches (Table 3). Whereas their intensity is too low to allow for an unambiguous identification experimentally (Figure S82), they were extracted from the computational data (Table S16). The stretches in $[\mathbf{1}]^-$–$[\mathbf{5}]^-$ occur at lower wave numbers in reference

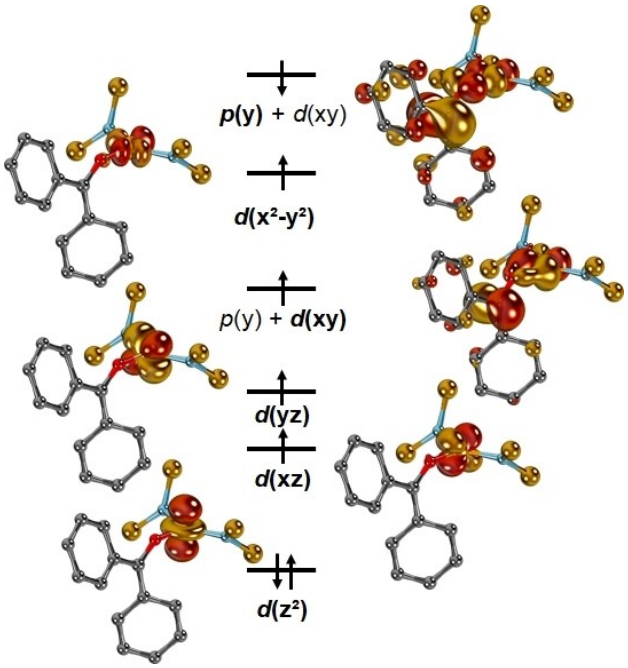

Figure 6. Molecular frontier orbitals[1] of $[\mathbf{1}]^-$ as obtained at the CASSCF (11,10) level of theory. Two doubly occupied and the related unoccupied, ligand-centred orbitals are omitted for clarity.

[1] For a thorough benchmark regarding structural parameters and absorption spectra, see Table S2–S9, S11 and Figure S61–S71.

Table 3. Calculated C–X resonances and bond lengths for benzophenone-coordinate complexes and comparison with free benzophenone (bp) and the anionic ketyl radical (bp^-).

Compound	$\tilde{\nu}$ in cm^{-1}	*C–O bond length* in [Å]
$Fe(bp^{\bullet-})$ ($[\mathbf{1}]^-$)	1563	1.31
$Co(bp^{\bullet-})$ ($[\mathbf{2}]^-$)	1565	1.31
Fe(bp) (**1**)	1615	1.28
Co(bp) (**2**)	1590	1.27
bp^-	1536	1.27
bp	1701	1.23

to **1**–**3** and **6**, thus corroborating a substantially reduced bond order and bond strength. For example, the C–O stretch is computed to resonate at 1563 cm^{-1} in $[\mathbf{1}]^-$ (C–O: 1.31 Å), at 1565 cm^{-1} in $[\mathbf{2}]^-$ (C–O: 1.31 Å), and at 1536 cm^{-1} for the "free" anionic benzophenone radical (C–O: 1.27 Å). In contrast, these stretches occur at considerably higher energies for the neutral congeners **1** ($\tilde{\nu}=1615\ cm^{-1}$; C–O: 1.28 Å) and **2** ($\tilde{\nu}=1590\ cm^{-1}$; C–O: 1.27 Å) as well as free benzophenone ($\tilde{\nu}=1701\ cm^{-1}$; C–O: 1.23 Å).

Reactivity

Having established the substrate based radical character of the anionic compounds we were interested in how this would translate into radical-like reactivity, namely H atom abstraction (HAA) capability. The iron ketyl complex $[\mathbf{1}]^-$ showed no reaction with 1,4-cyclohexadiene (CHD). In contrast, CHD was dehydrogenated to benzene using the cobalt ketyl complex $[\mathbf{2}]^-$ and the iron aldimine complex $[\mathbf{5}]^-$ (Scheme 2).

This is accompanied by the appearance of new paramagnetic signals in the ^{1}H NMR spectroscopic analysis; unfortunately, the composition of the metal containing products (e.g. a metal(II) benzhydrolate) remained so far elusive. The presence of the radical anion in $[\mathbf{2}]^-$ and $[\mathbf{5}]^-$ is crucial as neither the metal(I) precursors nor the neutral complexes **2** and **3** facilitate the HAA of 1,4-CHD. Interestingly, using an excess of 1,4-CHD in

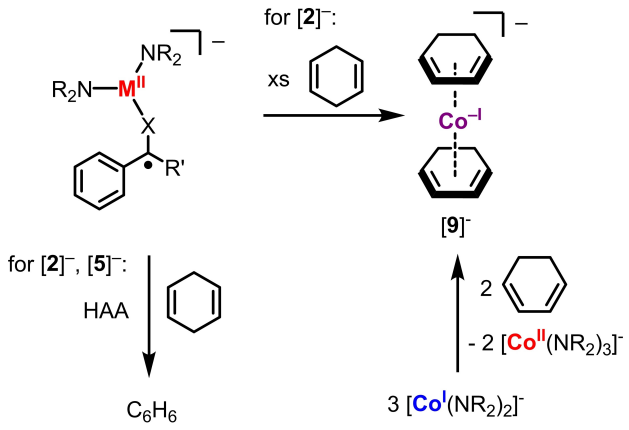

Scheme 2. Reactivity of $[\mathbf{2}]^-$ and $[\mathbf{5}]^-$ with 1,4-CHD and independent synthesis of $[\mathbf{9}]^-$.

 © 2021 The Authors. Chemistry - A European Journal published by Wiley-VCH GmbH

the presence of $[\mathbf{2}]^-$ led, besides some C_6H_6, to the formation of the anionic sandwich complex $[Co^{-I}(1,3\text{-CHD})_2]^-$, $[\mathbf{9}]^-$, and concomitantly $[Co(NR_2)_3]^-$ which speaks to redox and ligand rearrangement. $[\mathbf{9}]^-$ resembles the related anthracenide or butadiene cobaltates(–I) from Ellis and co-workers (Scheme 2).[37] The presence of the ketyl ligand is thereby not necessary for the formation of $[\mathbf{9}]^-$ as it can be directly obtained via reaction of either 1,3- *or* 1,4-CHD and $[Co(N(SiMe_3)_2)_2]^-$. The formation of the 1,3-CHD complex $[\mathbf{9}]^-$ is accompanied by a sigmatropic H-atom shift of 1,4-CHD. The metal bound radical anions thus intriguingly act in two roles: a) as a facilitator for HAA abstraction and b) as an electron reservoir that reversibly masks a metal(I) ion. Next, we turned to the highly labile ketiminyl complexes $[\mathbf{3}]^-$ and $[\mathbf{4}]^-$. Analysis of the decomposition of $[\mathbf{3}]^-$ revealed the formation of the homoleptic dinuclear iron(II) ketiminato complex $[(L_2Fe)_2(\mu\text{-}L)_2]^{2-}$, $[\mathbf{10}]^{2-}$ (Scheme 3, Figure S95), which is likely the product of intermediate $[Fe(NR_2)_3]^-$ followed by deprotonation of the liberated ketimine ($L = -N{=}CPh_2$).

No HAA abstraction was observed when treating $[\mathbf{3}]^-$ with 1,4-CHD. More intriguingly, the cobalt ketiminyl complex $[\mathbf{4}]^-$ transformed slowly into the dinuclear compound $[\mathbf{11}]^{2-}$ with deprotonation of the NH function as well as orthometallation of the ketimine ligand (Scheme 4, Figure S96). *In-situ* ^{1}H NMR spectroscopy showed the further formation of $HN(SiMe_3)_2$ and $[Co(N(SiMe_3)_2)_3]^-$ which indicated an interplay of redox disproportionation and intramolecular deprotonation for the formation of $[\mathbf{11}]^{2-}$. In contrast, in the presence of 1,4-CHD $[\mathbf{4}]^-$ slowly converts into the binuclear cobalt compound $[\mathbf{12}]^-$ (Figure S97) which forms as the result of a multitude of bond formation and cleavage processes. A now bridging ketimine was deprotonated at the nitrogen atom with additional C–C bond formation in *ortho*-C_{aryl}-H position with the employed 1,4-CHD, that binds as a rearranged 1,3-cyclohexadienyl unit to one of the cobalt ions via the butadiene moiety. The coordination sphere of this cobalt ion is completed by a second ketimine that binds in a η_2-κ^2-N:κ^1-C fashion, whereas the C–N bond lengths of 1.396(5) Å speaks for a partially reduced state. The second cobalt ion is ligated by a 1,3-CHD ligand in addition to the two ketimine ligands. It is interesting to note that $[\mathbf{12}]^-$ is not a subsequent product of $[\mathbf{11}]^{2-}$ but of an unknown intermediate. The observed orthometallation of a ketone or imine linked arene is reminiscent of directing group assisted C–H bond functionalisation.[38,39] This is catalysed by a variety of metals, including cobalt. In these instances the directing group acts as a donor ligand and the C–H bond is broken either via deprotonation for high-valent[40] or oxidative addition and metal hydride formation for low-valent[39] cobalt species. In the presented case of $[\mathbf{11}]^{2-}$ and $[\mathbf{12}]^-$ the mechanism is not fully understood, but resembles imine activation by a Zr/Co-complex involving a cobalt hydride.[11] Eventually, the highly basic $N(SiMe_3)_2$ ligands likely assists in a concerted metalation-deprotonation type pathway.

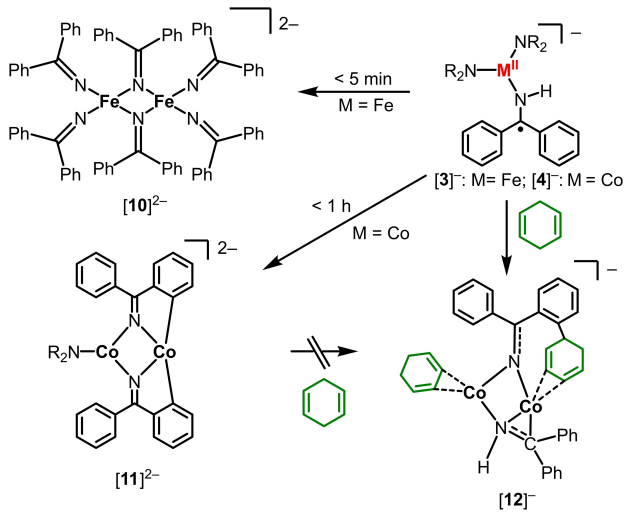

Scheme 3. Further conversion of $[\mathbf{3}]^-$ and $[\mathbf{4}]^-$ and its reactivity towards 1,4-CHD.

Conclusion

We reported on the reduction of a diarylketone (benzophenone), a ketimine (ketimine benzophenone imine), as well as of a phenylaldimine (aldimine benzaldehyde methylamine) by anionic linear metal(I) complexes of iron and cobalt. Besides rare examples of ketyl radical anion complexes, this leads to the first structurally authenticated ketiminyl and aldiminyl radical metal compounds. The electronic description of a metal(II) bound radical anion is supported by comprehensive analysis of the structural, spectroscopic and physical properties of these compounds, and corroborated by quantum chemical calculations. We further revealed the multifaceted chemical behaviour of the high-spin complexes, which show H atom abstraction capability, reversible substrate reduction and coordination as well as, in case of cobalt, intramolecular C–H bond activation and dehydrogenative C–C bond formation via double C–H bond activation.

Experimental Section

Details concerning the syntheses of all complexe, the spectroscopic and physical properties, in situ spectroscopic data and X-ray diffraction data are given in the Supporting Information. Deposition Numbers 2093093 ([K{18c6}][**1**]), 2093094 ([K{18c6}][**2**]), 2093095 (K{18c6}[**3**]), 2093096 (K{18c6}[**4**]), 2093097 (K{18c6}[**5**]), 2093086 (**1**), 2093087 (**2**), 2093088 (**5**), 2093089 (**6**), 2093090 (**7**), 2093091 (**8**), 2093098 (K{18c6}[**9**]), 2093099 ([K{18c6}]$_2$[**10**]), 2093100 ([K{18c6}]$_2$[**11**]), 2093092 (K{18c6}[**12**]) contain the supplementary crystallographic data for this paper. These data are provided free of charge by the joint Cambridge Crystallographic Data Centre and Fachinformationszentrum Karlsruhe Access Structures service.[2]

[2] Molecular orbitals were plotted with IBOView *J. Chem. Theory Comput.* **2013**, *9*, 4834.

© 2021 The Authors. Chemistry - A European Journal published by Wiley-VCH GmbH

Acknowledgements

C.G.W. thanks the Deutsche Forschungsgemeinschaft (WE 5627/4-1), the Fond der Chemischen Industrie and the Philipps-University for financial support. D.M. thanks the RRZ Erlangen for computational resources. We thank J. Lange (I. Physikalisches Institut, Univ. Gießen) for the acquisition of the EPR data. Open Access funding enabled and organized by Projekt DEAL.

Conflict of Interest

The authors declare no conflict of interest.

Keywords: cobalt · iron · radical anions · quantum chemical calculation · spectroscopy

[1] a) E. Clemmensen, *Ber. Dtsch. Chem. Ges.* **1913**, *46*, 1837; b) M. L. Di Vona, V. Rosnati, *J. Org. Chem.* **1991**, *56*, 4269; c) J. G. C. St. Buchanan, P. D. Woodgate, *Q. Rev. Chem. Soc.* **1969**, *23*, 522; d) E. Vedejs in *Organomet. React.*, Wiley Online Library, [Hoboken, N. J.], **2004**, pp. 401–422; e) J. H. Brewster, *J. Am. Chem. Soc.* **1954**, *76*, 6364; f) T. Wirth, *Angew. Chem. Int. Ed.* **1996**, *35*, 61; g) M. Ephritikhine, *Chem. Commun.* **1998**, 2549; h) M. Ephritikhine, C. Villiers in *Modern Carbonyl Olefination* (Ed.: T. Takeda), Wiley-VCH, Weinheim, **2004**, pp. 223–285.

[2] R. D. Rieke, S.-H. Kim, *J. Org. Chem.* **1998**, *63*, 5235.

[3] Á. Péter, S. Agasti, O. Knowles, E. Pye, D. J. Procter, *Chem. Soc. Rev.* **2021**, *50*, 5349.

[4] a) M. Szostak, M. Spain, A. J. Eberhart, D. J. Procter, *J. Am. Chem. Soc.* **2014**, *136*, 2268; b) D. Parmar, L. A. Duffy, D. V. Sadasivam, H. Matsubara, P. A. Bradley, R. A. Flowers, D. J. Procter, *J. Am. Chem. Soc.* **2009**, *131*, 15467; c) M. Szostak, B. Sautier, M. Spain, M. Behlendorf, D. J. Procter, *Angew. Chem. Int. Ed.* **2013**, *52*, 12559.

[5] a) O. Ishitani, C. Pac, H. Sakurai, *J. Org. Chem.* **1983**, *48*, 2941; b) K. T. Tarantino, P. Liu, R. R. Knowles, *J. Am. Chem. Soc.* **2013**, *135*, 10022; c) L. J. Rono, H. G. Yayla, D. Y. Wang, M. F. Armstrong, R. R. Knowles, *J. Am. Chem. Soc.* **2013**, *135*, 17735; d) M. Nakajima, E. Fava, S. Loescher, Z. Jiang, M. Rueping, *Angew. Chem. Int. Ed.* **2015**, *54*, 8828; e) S. Wang, N. Lokesh, J. Hioe, R. M. Gschwind, B. König, *Chem. Sci.* **2019**, *10*, 4580; f) D. Hager, D. W. C. MacMillan, *J. Am. Chem. Soc.* **2014**, *136*, 16986; g) M. Li, S. Berritt, L. Matuszewski, G. Deng, A. Pascual-Escudero, G. B. Panetti, M. Poznik, X. Yang, J. J. Chruma, P. J. Walsh, *J. Am. Chem. Soc.* **2017**, *139*, 16327; h) C. K. Prier, D. A. Rankic, D. W. C. MacMillan, *Chem. Rev.* **2013**, *113*, 5322; i) S. Wang, B. König, *Angew. Chem. Int. Ed.* **2021**, 10.1002/anie.202105469.

[6] a) E. J. Enholm, M. A. Battiste, M. Gallagher, K. M. Moran, A. Alberti, M. Guerra, D. Macciantelli, *J. Org. Chem.* **2002**, *67*, 6579; b) J. E. Bennett, B. Mile, A. Thomas, *J. Chem. Soc. A* **1968**, *0*, 298; c) A. G. Davies, A. G. Neville, *J. Chem. Soc. Perkin Trans. 2* **1992**, 163; d) R. Koeppe, P. H. Kasai, *J. Phys. Chem.* **1994**, *98*, 12904; e) A. G. Evans, J. C. Evans, P. J. Emes, S. I. Haider, *J. Chem. Soc. Perkin Trans. 2* **1974**, 1121; f) K. J. Covert, P. T. Wolczanski, S. A. Hill, P. J. Krusic, *Inorg. Chem.* **1992**, *31*, 66; g) H. Zhang, B. Wu, S. L. Marquard, E. D. Litle, D. A. Dickie, M. W. Bezpalko, B. M. Foxman, C. M. Thomas, *Organometallics* **2017**, *36*, 3498; h) M. Shit, S. Bera, S. Maity, T. Weyhermüller, P. Ghosh, *New J. Chem.* **2017**, *41*, 4564; i) N. Hirota, S. I. Weissman, *J. Am. Chem. Soc.* **1964**, *86*, 2538.

[7] T. A. Scott, B. A. Ooro, D. J. Collins, M. Shatruk, A. Yakovenko, K. R. Dunbar, H.-C. Zhou, *Chem. Commun.* **2009**, 65.

[8] H. Bock, H.-F. Herrmann, D. Fenske, H. Goesmann, *Angew. Chem. Int. Ed.* **1988**, *27*, 1067.

[9] J. C. Ott, H. Wadepohl, L. H. Gade, *Angew. Chem.* **2020**, *132*, 9535.

[10] Z. Hou, A. Fujita, T. Koizumi, H. Yamazaki, Y. Wakatsuki, *Organometallics* **1999**, *18*, 1979.

[11] S. L. Marquard, M. W. Bezpalko, B. M. Foxman, C. M. Thomas, *Organometallics* **2014**, *33*, 2071.

[12] a) G. A. Molander, C. R. Harris, *Chem. Rev.* **1996**, *96*, 307; b) Z. Hou, A. Fujita, H. Yamazaki, Y. Wakatsuki, *J. Am. Chem. Soc.* **1996**, *118*, 2503; c) A. Domingos, I. Lopes, J. C. Waerenborgh, N. Marques, G. Y. Lin, X. W. Zhang, J. Takats, R. McDonald, A. C. Hillier, A. Sella et al., *Inorg. Chem.* **2007**, *46*, 9415.

[13] Z. Hou, T. Koizumi, M. Nishiura, Y. Wakatsuki, *Organometallics* **2001**, *20*, 3323.

[14] Z. Hou, A. Fujita, H. Yamazaki, Y. Wakatsuki, *J. Am. Chem. Soc.* **1996**, *118*, 7843.

[15] Z. Hou, T. Miyano, H. Yamazaki, Y. Wakatsuki, *J. Am. Chem. Soc.* **1995**, *117*, 4421.

[16] Z. Hou, A. Fujita, Y. Zhang, T. Miyano, H. Yamazaki, Y. Wakatsuki, *J. Am. Chem. Soc.* **1998**, *120*, 754.

[17] O. P. Lam, C. Anthon, F. W. Heinemann, J. M. O'Connor, K. Meyer, *J. Am. Chem. Soc.* **2008**, *130*, 6567.

[18] C. Jones, L. McDyre, D. M. Murphy, A. Stasch, *Chem. Commun.* **2010**, *46*, 1511.

[19] Z. Hou, X. Jia, A. Fujita, H. Tezuka, H. Yamazaki, Y. Wakatsuki, *Chem. Eur. J.* **2000**, *6*, 2994.

[20] a) K. J. Covert, P. T. Wolczanski, *Inorg. Chem.* **1989**, *28*, 4565; b) S. L. Marquard, M. W. Bezpalko, B. M. Foxman, C. M. Thomas, *J. Am. Chem. Soc.* **2013**, *135*, 6018; c) W. Zhou, S. L. Marquard, M. W. Bezpalko, B. M. Foxman, C. M. Thomas, *Organometallics* **2013**, *32*, 1766; d) F. Ortu, J. Liu, M. Burton, J. M. Fowler, A. Formanuik, M.-E. Boulon, N. F. Chilton, D. P. Mills, *Inorg. Chem.* **2017**, *56*, 2496; e) C. A. P. Goodwin, N. F. Chilton, G. F. Vettese, E. Moreno Pineda, I. F. Crowe, J. W. Ziller, R. E. P. Winpenny, W. J. Evans, D. P. Mills, *Inorg. Chem.* **2016**, *55*, 10057; f) G. B. Deacon, P. C. Junk, J. Wang, D. Werner, *Inorg. Chem.* **2014**, *53*, 12553; g) I. L. Fedushkin, A. A. Skatova, V. K. Cherkasov, V. A. Chudakova, S. Dechert, M. Hummert, H. Schumann, *Chem. Eur. J.* **2003**, *9*, 5778; h) G. B. Deacon, C. M. Forsyth, D. L. Wilkinson, *Chem. Eur. J.* **2001**, *7*, 1784.

[21] K. C. Mullane, T. Cheisson, E. Nakamaru-Ogiso, B. C. Manor, P. J. Carroll, E. J. Schelter, *Chem. Eur. J.* **2018**, *24*, 826.

[22] a) Z. Flisak, W.-H. Sun, *ACS Catal.* **2015**, *5*, 4713; b) V. C. Gibson, C. Redshaw, G. A. Solan, *Chem. Rev.* **2007**, *107*, 1745; c) K. G. Caulton, *Eur. J. Inorg. Chem.* **2012**, *2012*, 435; d) S. Blanchard, E. Derat, M. Desage-El Murr, L. Fensterbank, M. Malacria, V. Mouriès-Mansuy, *Eur. J. Inorg. Chem.* **2012**, *2012*, 376; e) N. J. Hill, I. Vargas-Baca, A. H. Cowley, *Dalton Trans.* **2009**, 240; f) I. L. Fedushkin, A. A. Skatova, V. A. Chudakova, G. K. Fukin, *Angew. Chem. Int. Ed.* **2003**, *42*, 3294; g) T. M. Maier, M. Gawron, P. Coburger, M. Bodensteiner, R. Wolf, N. P. van Leest, B. de Bruin, S. Demeshko, F. Meyer, *Inorg. Chem.* **2020**, *59*, 16035; h) T. M. Maier, S. Sandl, I. G. Shenderovich, A. Jacobi von Wangelin, J. J. Weigand, R. Wolf, *Chem. Eur. J.* **2019**, *25*, 238; i) C. C. Lu, T. Weyhermüller, E. Bill, K. Wieghardt, *Inorg. Chem.* **2009**, *48*, 6055; j) W. N. Palmer, T. Diao, I. Pappas, P. J. Chirik, *ACS Catal.* **2015**, *5*, 622; k) C. C. Lu, E. Bill, T. Weyhermüller, E. Bothe, K. Wieghardt, *J. Am. Chem. Soc.* **2008**, *130*, 3181.

[23] A. Reckziegel, C. Pietzonka, F. Kraus, C. G. Werncke, *Angew. Chem. Int. Ed.* **2020**, *59*, 8527.

[24] C. G. Werncke, P. C. Bunting, C. Duhayon, J. R. Long, S. Bontemps, S. Sabo-Etienne, *Angew. Chem.* **2015**, *127*, 247.

[25] C. G. Werncke, E. Suturina, P. C. Bunting, L. Vendier, J. R. Long, M. Atanasov, F. Neese, S. Sabo-Etienne, S. Bontemps, *Chem. Eur. J.* **2016**, *22*, 1668.

[26] S. Yao, C. Milsmann, E. Bill, K. Wieghardt, M. Driess, *J. Am. Chem. Soc.* **2008**, *130*, 13536.

[27] a) S. Camadanli, R. Beck, U. Flörke, H.-F. Klein, *Organometallics* **2009**, *28*, 2300; b) S. Yogendra, T. Weyhermüller, A. W. Hahn, S. DeBeer, *Inorg. Chem.* **2019**, *58*, 9358.

[28] I. Müller, C. Schneider, C. Pietzonka, F. Kraus, C. G. Werncke, *Inorganics* **2019**, *7*, 117.

[29] a) I. Müller, C. G. Werncke, *Chem. Eur. J.* **2021**, *27*, 4932; b) C. G. Werncke, I. Müller, *Chem. Commun.* **2020**, *56*, 2268; c) C. G. Werncke, J. Pfeiffer, I. Müller, L. Vendier, S. Sabo-Etienne, S. Bontemps, *Dalton Trans.* **2019**, *48*, 1757.

[30] I. Müller, D. Munz, C. G. Werncke, *Inorg. Chem.* **2020**, *59*, 9521.

[31] A. Eichhöfer, Y. Lan, V. Mereacre, T. Bodenstein, F. Weigend, *Inorg. Chem.* **2014**, *53*, 1962.

[32] a) K. Ding, T. R. Dugan, W. W. Brennessel, E. Bill, P. L. Holland, *Organometallics* **2009**, *28*, 6650; b) A. Reckziegel, M. Kour, B. Battistella, S. Mebs, K. Beuthert, R. Berger, C. G. Werncke, *Angew. Chem. Int. Ed.* **2021**, *60*, 15376; c) P. Pietrzyk, M. Srebro, M. Radoń, Z. Sojka, A. Michalak, *J. Phys. Chem. A* **2011**, *115*, 2316.

[33] V. Lyaskovskyy, A. I. O. Suarez, H. Lu, H. Jiang, X. P. Zhang, B. de Bruin, *J. Am. Chem. Soc.* **2011**, *133*, 12264.

[34] a) J. C. Ott, H. Wadepohl, L. H. Gade, *Angew. Chem. Int. Ed.* **2020**, *59*, 9448; b) K. P. Chiang, S. M. Bellows, W. W. Brennessel, P. L. Holland,

 © 2021 The Authors. Chemistry - A European Journal published by Wiley-VCH GmbH

Chem. Sci. **2014**, *5*; c) J. M. Smith, A. R. Sadique, T. R. Cundari, K. R. Rodgers, G. Lukat-Rodgers, R. J. Lachicotte, C. J. Flaschenriem, J. Vela, P. L. Holland, *J. Am. Chem. Soc.* **2006**, *128*, 756; d) J. J. Kiernicki, J. P. Shanahan, M. Zeller, N. K. Szymczak, *Chem. Sci.* **2019**, *10*, 5539; e) K. P. Chiang, C. C. Scarborough, M. Horitani, N. S. Lees, K. Ding, T. R. Dugan, W. W. Brennessel, E. Bill, B. M. Hoffman, P. L. Holland, *Angew. Chem. Int. Ed.* **2012**, *51*, 3658.

[35] a) F. Neese, *WIREs Comput. Mol. Sci.* **2012**, *2*, 73; b) F. Neese, *WIREs Comput. Mol. Sci.* **2018**, *8*.

[36] a) B. O. Roos, P. R. Taylor, P. E. Sigbahn, *Chem. Phys.* **1980**, *48*, 157; b) C. Angeli, R. Cimiraglia, S. Evangelisti, T. Leininger, J.-P. Malrieu, *J. Chem. Phys.* **2001**, *114*, 10252.

[37] W. W. Brennessel, J. V. G. Young, J. E. Ellis, *Angew. Chem. Int. Ed.* **2002**, *41*, 1211.

[38] a) K. Gao, N. Yoshikai, *Acc. Chem. Res.* **2014**, *47*, 1208; b) P.-S. Lee, N. Yoshikai, *Org. Lett.* **2015**, *17*, 22; c) S. M. Ujwaldev, N. A. Harry, M. A. Divakar, G. Anilkumar, *Catal. Sci. Technol.* **2018**, *8*, 5983; d) Y. Lian, T. Huber, K. D. Hesp, R. G. Bergman, J. A. Ellman, *Angew. Chem. Int. Ed.* **2013**, *52*, 629; e) Y. Lian, R. G. Bergman, L. D. Lavis, J. A. Ellman, *J. Am. Chem. Soc.* **2013**, *135*, 7122; f) E. Nakamura, N. Yoshikai, *J. Org. Chem.* **2010**, *75*, 6061; g) K. Gao, P.-S. Lee, T. Fujita, N. Yoshikai, *J. Am. Chem. Soc.* **2010**, *132*, 12249; h) S. Murahashi, *J. Am. Chem. Soc.* **1955**, *77*, 6403.

[39] B. J. Fallon, J.-B. Garsi, E. Derat, M. Amatore, C. Aubert, M. Petit, *ACS Catal.* **2015**, *5*, 7493.

[40] a) J. R. Hummel, J. A. Ellman, *J. Am. Chem. Soc.* **2015**, *137*, 490; b) T. Yoshino, H. Ikemoto, S. Matsunaga, M. Kanai, *Angew. Chem. Int. Ed.* **2013**, *52*, 2207.

Manuscript received: August 25, 2021
Accepted manuscript online: September 27, 2021
Version of record online: October 22, 2021

 © 2021 The Authors. Chemistry - A European Journal published by Wiley-VCH GmbH

Chemistry–A European Journal

Supporting Information

Cobalt and Iron Stabilized Ketyl, Ketiminyl and Aldiminyl Radical Anions

Grégoire Sieg, Quentin Pessemesse, Sascha Reith, Stefan Yelin, Christian Limberg, Dominik Munz, and C. Gunnar Werncke*

Table of content

Table of content 1
Materials and Methods 2
Synthesis of K{18c6}[Fe(bp)(N(SiMe$_3$)$_2$)$_2$] (K{18c6}[1]) 3
Synthesis of K{18c6}[Co(bp)(N(SiMe$_3$)$_2$)$_2$] (K{18c6}[2]) 3
Synthesis of K{18c6}[Fe(bpi)(N(SiMe$_3$)$_2$)$_2$] (K{18c6}[3]) 4
Synthesis of K{18c6}[Co(bpi)(N(SiMe$_3$)$_2$)$_2$] (K{18c6}[4]) 5
Synthesis of K{18c6}[Fe(bama)(N(SiMe$_3$)$_2$)$_2$] (K{18c6}[5]) 5
Synthesis of [Fe(bp)(N(SiMe$_3$)$_2$)$_2$] (1) 7
Synthesis of [Co(bp)(N(SiMe$_3$)$_2$)$_2$] (2) 8
Synthesis of [Fe(bama)(N(SiMe$_3$)$_2$)$_2$] (5) 8
Synthesis of [Co(bama)(N(SiMe$_3$)$_2$)$_2$] (6) 9
Synthesis of [Fe(bpi)(N(SiMe$_3$)$_2$)$_2$] (7) 9
Synthesis of [Co(bpi)(N(SiMe$_3$)$_2$)$_2$] (8) 10
Synthesis of K{18c6}[Co(1,3-CHD)$_2$] (K{18c6}[9]) 11
Synthesis of [K{18c6}]$_2$(Fe$_2$(NCPh$_2$)$_6$] ([K{18c6}]$_2$[10]) 11
Synthesis of [K{18c6}]$_2$[Co$_2$(N(SiMe$_3$)$_2$)(CPh(C$_5$H$_4$)] ([K{18c6}]$_2$[11]) 11
Reaction of K{18c6}[4] with excess 1,4-cyclohexadiene ([K{18c6}]$_2$[12]) 12
Reaction of K{18c6}[2] with 1,4-cyclohexadiene 13
Reaction of K{18c6}[5] with 1,4-cyclohexadiene 15
IR Spectra 17
UV Vis Spectra 23
Cyclic voltammetry 29
Magnetic measurements 32
^{57}Mößbauer Spectra 35
EPR spectroscopy 37
Computational Details 38
XYZ coordinates 55
X-Ray diffraction analysis and molecular structures 86
References 102

Materials and Methods

All manipulations were carried out in a glovebox under a dry argon atmosphere, unless indicated otherwise. Used solvents were dried by continuous distillation over sodium metal for several days, degassed via three freeze-pump cycles and stored over molecular sieves 4 Å. Deuterated solvents were used as received, degassed via three freeze-pump cycles and stored over molecular sieves 4 Å.
The ^{1}H-NMR spectra were recorded on a BRUKER AV 500, a BRUKER AV 300 or a Bruker HD 500 NMR spectrometer (Bruker Corporation, Billerica, MA, USA). Chemical shifts are reported in ppm relative to the residual proton signals of the solvent. $w_{1/2}$ is the line width of a signal at half its maximum intensity. Integrals of the broad signals of the hmds units were obtained directly or by peak fitting (in case of overlapping signals) using the MestreNova software package (Mestrelab, Santiago de Compostela, Spain).
IR measurements were conducted on a Bruker Alpha ATR-IR spectrometer (Bruker Corporation, Billerica, MA, USA).
Elemental analyses were performed by the "in-house" service of the Chemistry Department of the Philipps University Marburg, Germany using a CHN(S) analyzer vario MICRO Cube (Elementar Analysensysteme GmbH, Langenselbold, Germany).
UV/Vis-spectra were recorded on an AnalytikJena Specord S600 diode array spectrometer (AnalytikJena, Jena, Germany). All UV/Vis-spectra were measured in Et_2O if not stated otherwise.
The dc susceptibility data was obtained in a range of 3 K to 300 K on a physical properties measurement system from LQT/QD (Quantum Design, San Diego, CA, USA). The samples were mounted in a plastic sample holder. The Curie-Weiss Law was used for fitting the magnetic data, whereas the diamagnetic correction was obtained using tabulated pascal constants as well as experimental data for the sample holder. Magnetic moments in solution were determinated by using Evans' method.[1,2]
EPR measurements were conducted on a BRUKER ESP 900 spectrometer. ^{57}Mößbauer spectra were recorded on a SeeCo MS6 spectrometer, which comprises the following instruments: A Janis CCS-850 cryostat, including a CTI-Cryogenics closed cycle 10 K refrigerator and a CTI-Cryogenics 8200 helium compressor. Temperature was controlled by a LakeShore 335 temperature controller. Spectra were recorded using a LND45431 Kr gas proportional counter with a beryllium window connected to the CeeCo W204 gamma-ray spectrometer. The W204 includes high voltage supply, a 10 bit and 5 µs ADC and two single channel analyzers. Motor control and recording of spectra was taken care of by the W304 resonant gamma-ray spectrometer. For the reported spectra a Rivertec MCo7.114 source (^{57}Co in Rh matrix) with an activity of about 1 GBq was used. Spectra were recorded in plastic sample holders with about 30 mg of sample at 13 K and data was accumulated for about 48 hours each. Mößbauer data was processed and simulated using the WMOSS4 program ver. F (www.wmoss.org). Isomeric shifts are referenced to alpha-iron at room temperature.
Benzophenone (bp), benzophenone imine (bpi), benzaldehyde methylamine (bama), 1,4-cyclohexadiene (1,4-CHD), tetrametylsilane (TMS) and 18-crown-6 (18c6) were purchased from commercial sources (Sigma Aldrich, Fluorochem, Acros Organics, Alfa Aesar and TCI Chemicals).
$[Fe(N(SiMe_3)_2)_2]$, $[Co(N(SiMe_3)_2)_2]$, K{18c6}$[M(N(SiMe_3)_2)_2]$ (Fe and Co), were prepared according to literature procedures.[3–5]
KC_8 was prepared by mixing respective amounts of graphite (previously dried in vacuo via heatgun) with freshly cut potassium metal. The mixture was heated *in vacuo* via heat gun until all potassium metal had reacted.

Synthesis of K{18c6}[Fe(bp)(N(SiMe$_3$)$_2$)$_2$] (K{18c6}[1])

[K(18c6)][Fe((N(SiMe$_3$)$_2$)$_2$] (680 mg, 1.0 mmol, 1.0 eq.) and bp (182 mg, 1.0 mmol, 1.0 eq.) were dissolved in 4 mL of Et$_2$O and filtered after 2 min. The solution was slowly added to 50 mL of *n*-pentane to afford K{18c6}[**1**] as a deep purple micocrystalline solid (590 mg, 0.68 mmol, 68%).

^{1}H-NMR ([D8]THF, 300 MHz, 300 K, ppm): 15.95 (br, 3H, $w_{1/2}$ = 188 Hz), 3.49 (br, 24H, $w_{1/2}$ = 130 Hz, O-C**H**$_2$-), –2.56 (br, 36H, $w_{1/2}$ = 897 Hz, SiMe$_3$), –4.11 (br, 4H, $w_{1/2}$ = 175 Hz), –67,74 (br, $w_{1/2}$ = 50 Hz).

IR (ATR, cm^{-1}): ν = 2944 (m), 2889 (m), 1657 (w), 1562 (w), 1472 (w), 1451 (w), 1389 (w), 1350 (m), 1280 (w), 1233 (m), 1103 (s), 980 (s), 959 (s), 866 (m), 823 (s), 780 (m), 749 (m), 704 (m), 663 (s), 609 (m), 588 (w), 529 (w), 473 (w).

Elemental analysis: calculated ($C_{37}H_{70}FeKN_2O_7Si_4$ 861.32 g/mol) C 51.54 H 8.18 N 4.53; experimental C 52.02 H 8.23 N 3.65.

μ_{eff} = 4.92 μ_B (Evans, [D8]THF + 1%TMS, 500 MHz, 298K, $\mu_{S.O.}$ = 4.89 μ_B)

Crystals, suitable for X-ray diffraction analysis were obtained by layering a solution of K{18c6}[**1**] in Et$_2$O with *n*-pentane at –40 °C.

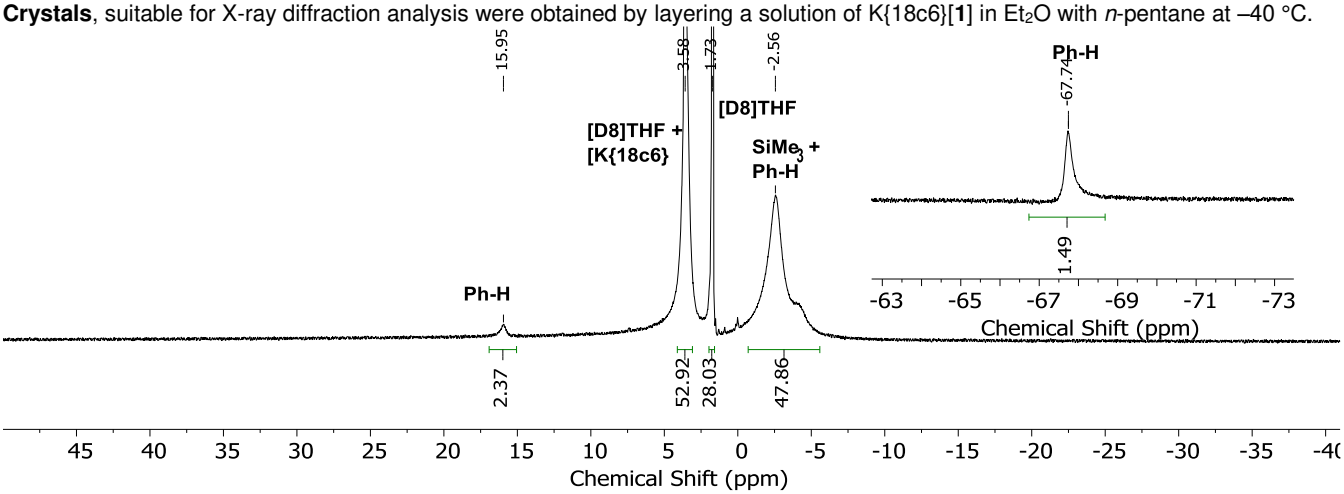

Figure S1. ^{1}H-NMR spectrum of K{18c6}[**1**] in [D8]THF at 300 K, 300 MHz. Integral of [K{18c6}]$^+$ overlaps with the solvent residue signal at 3.58 ppm, thus the integral was determined by substracting the integral of the solvent residue signal at 1.73 ppm from the integral of the signal at 3.58 ppm.

Synthesis of K{18c6}[Co(bp)(N(SiMe$_3$)$_2$)$_2$] (K{18c6}[2])

[K(18c6)][Co(N(SiMe$_3$)$_2$)$_2$] (205 mg, 0.3 mmol, 1.0 eq.) and bp (55 mg, 0.3 mmol, 1.0 eq.) were dissolved in 2 mL of Et$_2$O and stirred for 2 min. The resulting deep-violet solution was layered with 2 mL of *n*-pentane and stored overnight at –40 °C. This afforded a violet crystalline solid of K{18c6}[**2**] (199 mg, 0.23 mmol, 77%).

Alternative synthesis: A solution of **2** (60 mg, 0.11 mmol, 1.00 eq.) in 2 mL of Et$_2$O was added to a mixture of KC$_8$ (15 mg, 0.11 mmol, 1.0 eq.) and 18c6 (25 mg, 0.11 mmol, 1.0 eq.) and filtered immediately. The solution was layered with 2 mL of *n*-pentane, which afforded a violet crystalline solid. (67 mg, 0.08 mmol, 73%). The ^{1}H-NMR signature of the reaction product is identical to the one of K{18c6}[**2**].

^{1}H-NMR ([D8]THF, 300 MHz, 300 K, ppm): 7.63 (br, 1H, $w_{1/2}$ = 289 Hz, Ph-**H**), 4.64 (br, 24H, $w_{1/2}$ = 9 Hz, OC**H**$_2$), –15.30 (br, 36H, $w_{1/2}$ = 23 Hz, SiMe$_3$), –57.91 (br, 3H, $w_{1/2}$ = 22 Hz, Ph-**H**). Not all phenyl-protons could be detected.

IR (ATR, cm^{-1}): ν = 2948 (w), 2889 (m), 2825 (w), 1562 (w), 1472 (m), 1449 (w), 1365 (w), 1350 (m), 1274 (w), 1235 (m), 1103 (s), 1006 (s), 961 (s), 862 (m), 819 (s), 778 (m), 749 (m), 687 (m), 663 (s), 623 (m), 597 (m), 529 (m), 473 (m), 409 (m).

Elemental analysis calculated ($C_{37}H_{70}CoKN_2O_7Si_4$ 865.34 g/mol) C 51.36 H 8.15 N 3.24; experimental C 50.84 H 7.49 N 3.60.

μ_{eff} = 4.43 μ_B (Evans, [D8]THF + 1%TMS, 500 MHz, 298K, $\mu_{S.O.}$ = 3.87 μ_B)

Crystals, suitable for X-ray diffraction analysis, were obtained from a *n*-pentane layered solution of K{18c6}[**2**] in Et$_2$O at –40 °C.

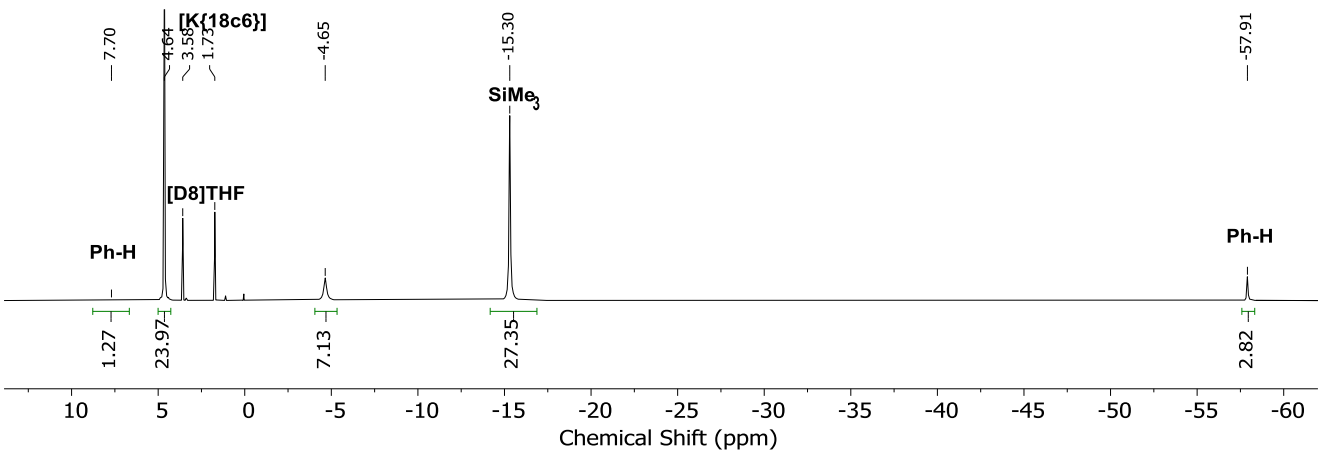

Figure S2. ^{1}H-NMR spectrum of K{18c6}[**2**] in [D8]THF at 300 K, 300 MHz.

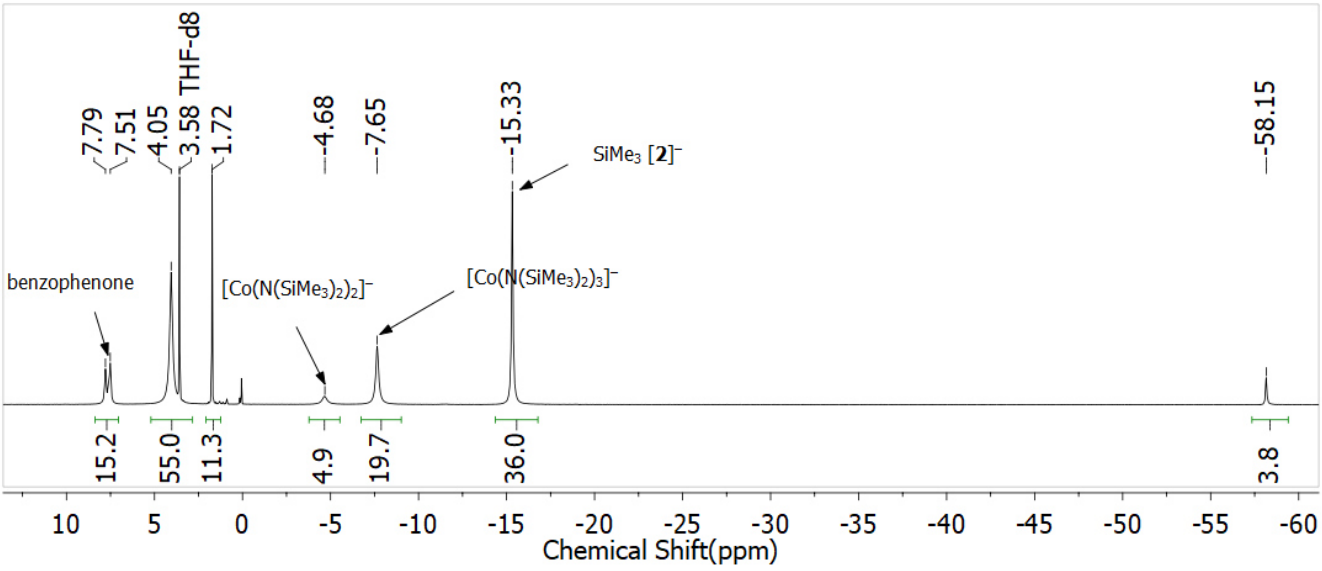

Figure S3. ^{1}H-NMR spectrum of K{18c6}[**2**] in [D8]THF with additional 1 eq. benzophenone at 300 K, 300 MHz.

Synthesis of K{18c6}[Fe(bpi)(N(SiMe$_3$)$_2$)$_2$] (K{18c6}[3])

[K(18c6)][Fe((N(SiMe$_3$)$_2$)$_2$] (680 mg, 1.00 mmol, 1.0 eq.) and bpi (182 mg, 1.00 mmol, 1.0 eq.) were dissolved in 3 mL of THF. After 2 minutes the mixture was slowly added to 50 mL of *n*-pentane to afford K{18c6}[**3**] as dark blue solid. Crystals, suitable for X-ray diffraction analysis were obtained by cooling a saturated solution of K{18c6}[**3**] in THF to –40 °C (525 mg, 0.61 mmol, 61%).
K{18c6}[**3**] decomposes rapidly in solution, yielding no conclusive ^{1}H-NMR signature, prohibited the determination of UV/Vis extinction coefficients as well as solution magnetic susceptibility.
Elemental analysis calculated ($C_{37}H_{71}FeKN_3O_6Si_4$ 861.27 g/mol) C 51.60 H 8.31 N 4.88; experimental C 51.68 H 8.23 N 4.41.

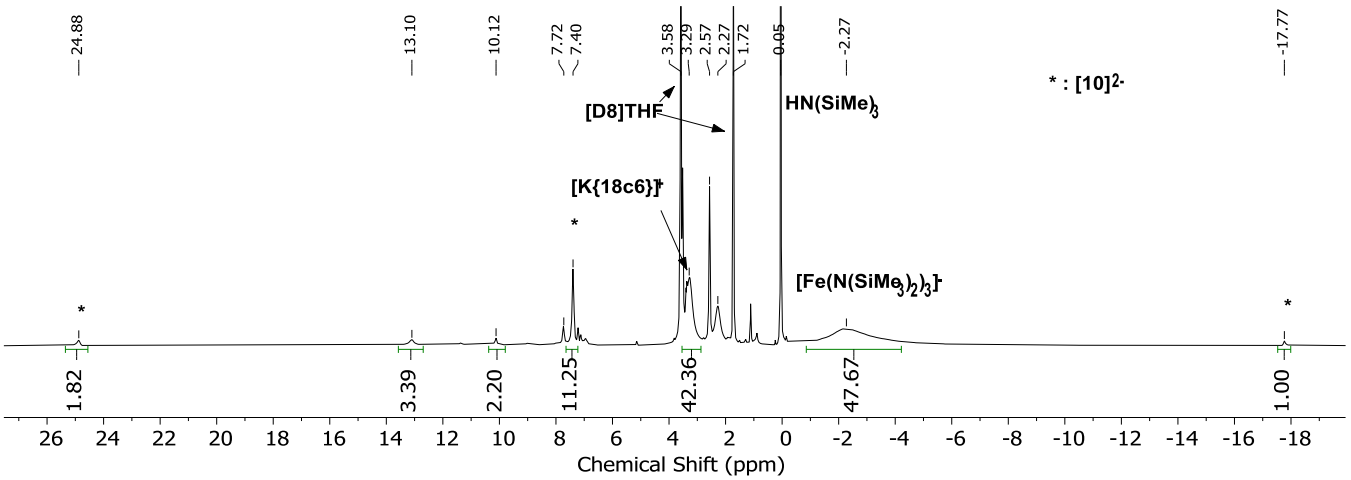

Figure S4. ^{1}H-NMR spectrum of K{18c6}[**3**] in [D8]THF 2 min after synthesis at 300 K, 300 MHz.

Synthesis of K{18c6}[Co(bpi)(N(SiMe$_3$)$_2$)$_2$] (K{18c6}[4])

[K(18c6)][Co((N(SiMe$_3$)$_2$)$_2$] (74 mg, 0.11 mmol, 1.0 eq.) and bpi (20 mg, 0.11 mmol, 1.0 eq.) were dissolved in 1.5 mL of Et_2O. The mixture was stirred for 2 min before being filtered and then layered with *n*-pentane. Cooling the solution to –40 °C afforded K{18c6}[**4**] as crystalline violet solid.

K{18c6}[**4**] decomposes rapidly in solution, yielding no useful ^{1}H-NMR signature and prohibited the determination of UV/Vis extinction coefficients as well as solution magnetic susceptibility.

Elemental analysis calculated ($C_{37}H_{71}CoKN_3O_6Si_4$ 861.27 g/mol) C 51.41 H 8.28 N 4.86; experimental C 52.49 H 7.51 N 3.62. Several attempts did not lead to improved purity, which can be attributed to high sensitivity to the compound.

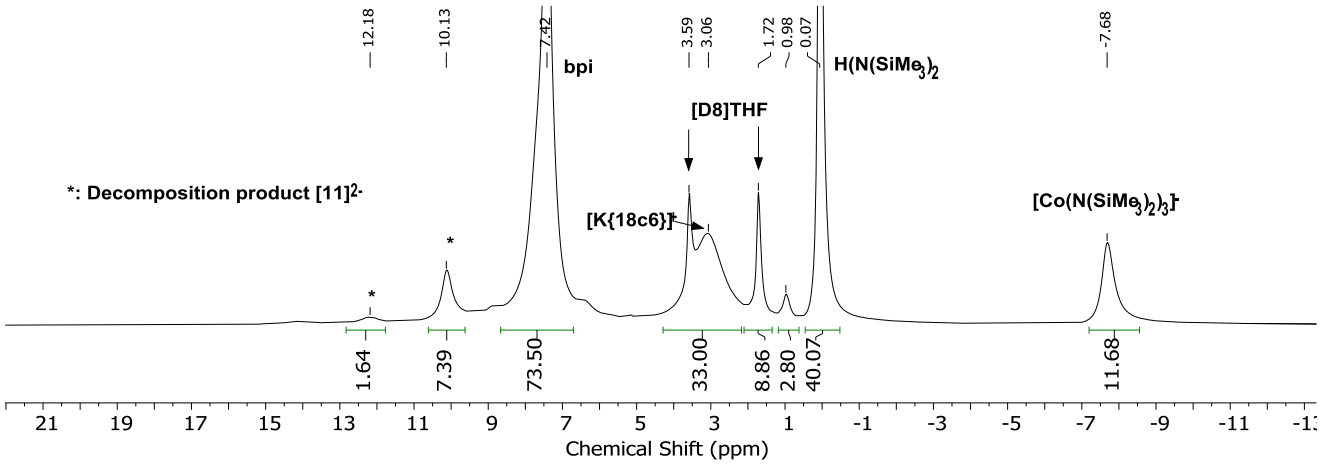

Figure S5. ^{1}H-NMR spectrum of the reaction mixture of K{18c6}[**4**] with bpi after 20 min in [D8]THF at 300 K, 300 MHz.

Synthesis of K{18c6}[Fe(bama)(N(SiMe$_3$)$_2$)$_2$] (K{18c6}[5])

[Fe(bama)] (**5**) (128 mg, 0.26 mmol, 1.0 eq.) was dissolved in 2 mL of Et_2O and added to KC_8 (35 mg, 0.26 mmol, 1.0 eq.) and 18c6 (60 mg, 0.26 mmol, 1.0 eq.). The mixture was filtered and the resulting dark yellow solution was layered with 1.5 mL of *n*-pentane and then stored at -40 °C. K{18c6}[**5**] could be obtained as dark yellow single crystals (81 mg, 0.1 mmol, 40%).

^{1}H-NMR ([D8]THF, 300 MHz, 300 K, ppm): 3.44 (s, 24H, -OC**H**$_2$-), –3.02 (br, 32H, $w_{1/2}$ = 333 Hz, $SiMe_3$). Signals belonging to the bama-ligand could not be identified unambiguously.

IR (ATR, cm^{-1}): ν = 2940 (m), 2882 (m), 2823 (w), 1569 (w), 1476 (w), 1445 (w), 1352 (m), 1295 (m), 1231 (s), 1167 (w), 1132 (m), 1101 (s), 1076 (s), 988 (s), 951 (s), 932 (m), 885 (m), 864 (s), 817 (s), 778 (s), 747 (s), 708 (m), 661 (s), 609 (m), 566 (w), 523 (m), 481 (m)

Elemental analysis calculated ($C_{32}H_{69}FeKN_3O_6Si_4$ 799.20 g/mol) C 48.09 H 8.70 N 5.26; experimental C 47.65 H 8.29 N 5.53.

μ_{eff} = 4.65 μ_B (Evans, [D8]THF + 1%TMS, 500 MHz, 298K, $\mu_{S.O.}$ = 4.89 μ_B)

Crystals suitable for x-ray diffraction were obtained by layering a solution of K{18c6}[**5**] in Et_2O with *n*-pentane at –40 °C.

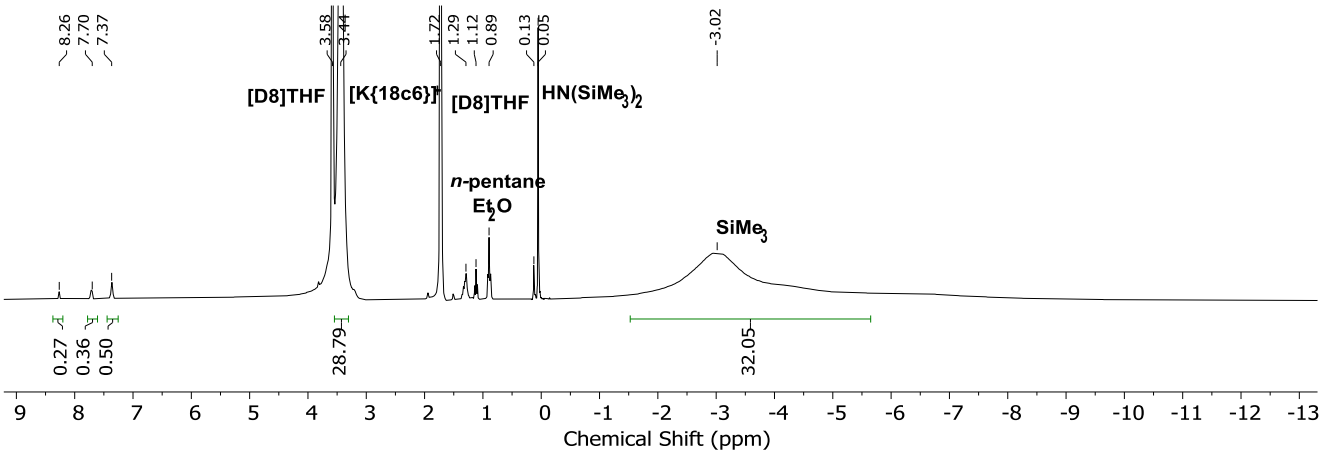

Figure S6. ^{1}H-NMR spectrum of K{18c6}[**5**] in [D8]THF at 300 K, 300 MHz.

Synthesis of [Fe(bp)(N(SiMe$_3$)$_2$)$_2$] (1)

[Fe(bp)] (6): [Fe(N(SiMe$_3$)$_2$)$_2$] (113 mg, 0.3 mmol, 1.0 eq.) and bp (55 mg, 0.3 mmol, 1.0 eq.) were dissolved in 1 mL of *n*-pentane and filtered after 2 min. The resulting brown solution was cooled to –40 °C to afford **1** as a brown crystalline solid (122 mg, 0.22 mmol, 74%).
^{1}H-NMR ([D6]Benzene, 300 MHz, 300 K, ppm): 12.70 (br, 36H, $w_{1/2}$ = 398 Hz, SiMe$_3$), 5.83 (br, 4H, $w_{1/2}$ = 32 Hz, Ph-**H**), –5.62 (s, 2H, Ph-**H**), –6.47 (br, 4H, $w_{1/2}$ = 803 Hz, Ph-**H**)
IR (ATR, cm^{-1}): ν = 2946 (m), 2891 (w), 1612 (m), 1593 (m), 1567 (m), 1449 (w), 1394 (w), 1328 (m), 1291 (m), 1239 (s), 1182 (w), 1161 (w), 971 (s), 926 (m), 887 (m), 815 (s), 763 (m), 747 (m), 700 (s), 667 (s), 634 (m), 611 (m), 584 (m), 448 (w), 422 (w).
Elemental analysis calculated ($C_{25}H_{46}FeN_2OSi_4$ 558.84 g/mol) C 53.79 H 8.30 N 5.01; experimental C 54.12 H 8.06 N 5.48.
μ_{eff} = 4.82 μ_B (Evans, [D8]THF + 1%TMS, 500 MHz, 298K, $\mu_{S.O.}$ = 4.89 μ_B)

Crystals suitable for X-ray diffraction analysis were obtained from a saturated solution of **1** in *n*-pentane at –40 °C.

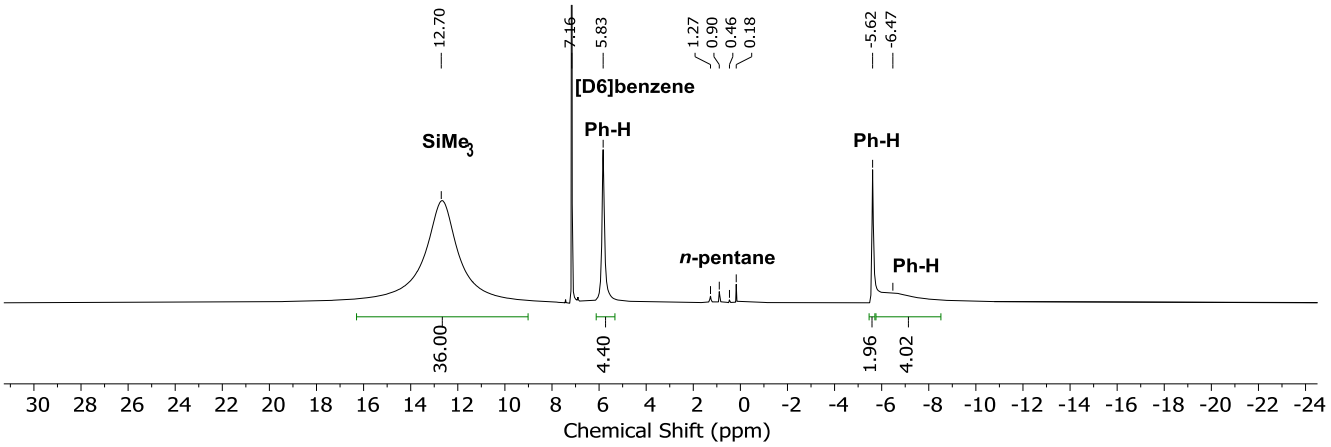

Figure S7. ^{1}H-NMR-spectrum of **1** in [D6]benzene at 300 K, 300 MHz.

Synthesis of [Co(bp)(N(SiMe$_3$)$_2$)$_2$] (2)

[Co(N(SiMe$_3$)$_2$)$_2$] (152 mg, 0.40 mmol, 1.0 eq.) and bp (73 mg, 0.4 mmol, 1.0 eq.) were dissolved in 4 mL of Et$_2$O and stirred for 1 min. The solvent was removed from the resulting brown solution to afford **2** as an orange solid (218 mg, 0.39 mmol, 97%).
^{1}H-NMR ([D6]Benzene, 300 MHz, 300 K, ppm): 56.14 (br, 4H, $w_{1/2}$ = 565 Hz, Ph-**H**), 15.34 (br, 4H, $w_{1/2}$ = 25 Hz, Ph-**H**), 8.35 (s, 2h, Ph-**H**), -12.47 (36H, $w_{1/2}$ = 49 Hz, Si Me$_3$).
IR (ATR, cm^{-1}): ν = 2946 (m), 2893 (w), 1614 (m), 1595 (m), 1569 (m), 1447 (w), 1326 (m), 1313 (w), 1289 (m), 1237 (s), 1182 (w), 1159 (w), 994 (s), 924 (m), 817 (s), 782 (s), 761 (s), 747 (s), 698 (s), 665 (s), 634 (m), 609 (m), 446 (w), 420 (w)
Elemental analysis calculated ($C_{25}H_{46}CoN_2OSi_4$ 561.93 g/mol) C 53.44 H 8.25 N 4.99; experimental C 52.38 H 8.09 N 5.08. Slightly lower C-values were consistently observed despite several attempts using crystalline samples. This can in part be attributed to high sensitivity to the compound.
μ_{eff} = 4.73 μ_B (Evans, [D8]THF + 1%TMS, 500 MHz, 298K, $\mu_{S.O.}$ = 3.87 μ_B)

Crystals suitable for X-ray diffraction analysis were obtained from a saturated solution of **2** in Et$_2$O at –40 °C.

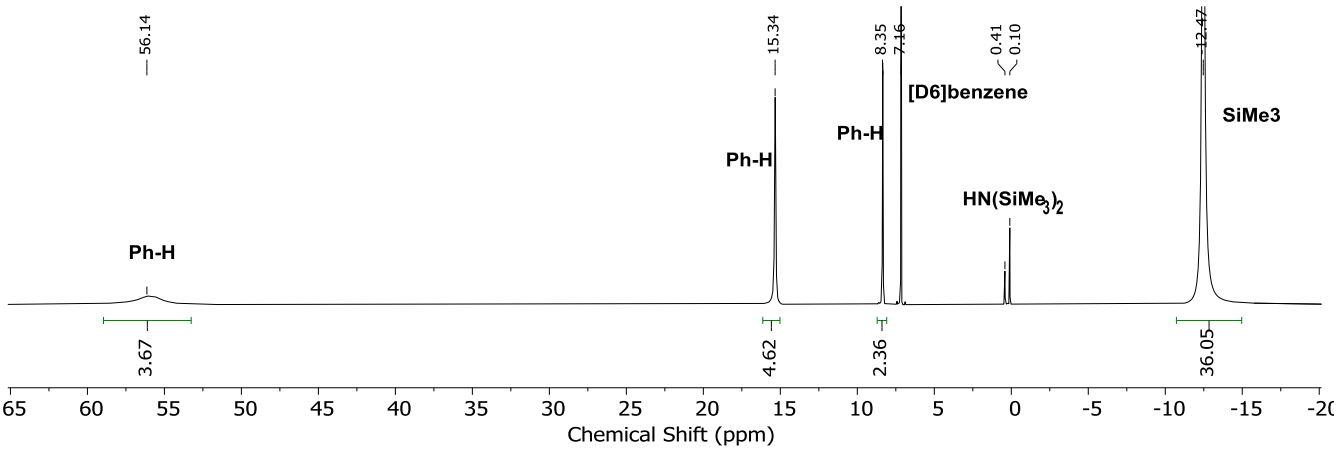

Figure S8. ^{1}H-NMR-spectrum of **2** in [D6]benzene at 300 K, 300 MHz.

Synthesis of [Fe(bama)(N(SiMe$_3$)$_2$)$_2$] (5)

[Fe(N(SiMe$_3$)$_2$)$_2$] (259 mg, 0.68 mmol, 1.0 eq.) and bama (81 mg, 0.68 mmol, 1.0 eq.) were dissolved in 1 mL of *n*-pentane and filtered after 2 min. The resulting brown solution was cooled to –40 °C to afford **5** as a yellow crystalline solid (237 mg, 0.48 mmol, 70%).
^{1}H-NMR ([D6]Benzene, 300 MHz)**:** Due to strong signal-broadening, only solvent residue signals can be assigned.
IR (ATR, cm^{-1}): ν = 3006 (m), 2952 (w), 1667 (m), 1635 (w), 1616 (w), 1480 (w), 1431 (w), 1266 (s), 971 (s), 906 (m), 831 (s), 798 (s), 763 (s), 679 (s), 623 (m), 502 (s), 422 (w)
Elemental analysis calculated ($C_{20}H_{45}FeN_3Si_4$ 495.78 g/mol) C 48.45 H 9.15 N 8.48; experimental C 48.25 H 8.59 N 8.85.
μ_{eff} = 4.78 μ_B (Evans, [D8]THF + 1%TMS, 500 MHz, 298K, $\mu_{S.O.}$ = 4.89 μ_B)

Crystals suitable for X-ray diffraction analysis were obtained from a saturated solution of **5** in *n*-pentane at –40 °C.

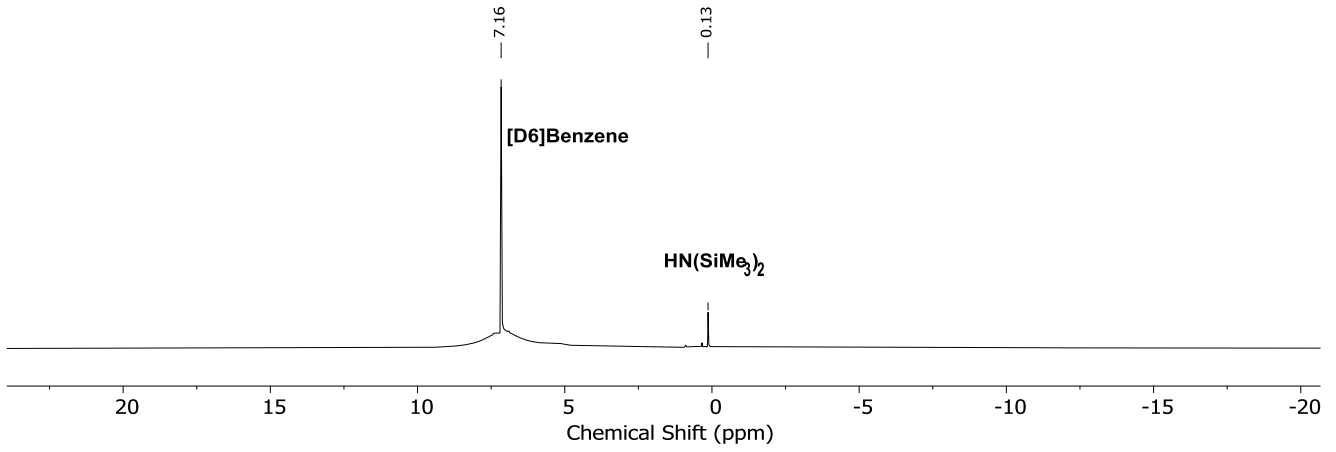

Figure S9. ^{1}H-NMR spectrum of **5** in [D6]benzene at 300 K, 300 MHz.

Synthesis of [Co(bama)(N(SiMe$_3$)$_2$)$_2$] (6)

[Co(N(SiMe$_3$)$_2$)$_2$] (270 mg, 0.71 mmol, 1.0 eq.) and bama (84 mg, 0.71 mmol, 1.0 eq.) were dissolved in 1 mL of *n*-pentane. The solvent was removed from the resulting green solution to afford **6** as a green crystalline solid (308 mg, 0.62 mmol, 87%).
^{1}H-NMR ([D6]benzene, 300 MHz, 300 K, ppm): 105.52 (br, 2H, $w_{1/2}$ = 299.7 Hz, Ph-**H**), 20.55 (br, 1H, $w_{1/2}$ = 428.4 Hz, N=C-**H**), 0.25 (br, 3H, $w_{1/2}$ = 4250.3 Hz, N-Me), -2.36 (br, 1H, $w_{1/2}$ = 42.6 Hz, Ph-**H**), -11.95 (br, 36H, $w_{1/2}$ = 139.5 Hz, SiMe$_3$), -15.12 (br, 2H, $w_{1/2}$ = 167.3 Hz, Ph-**H**).
IR (ATR, cm^{-1}): ν = 3006 (m), 2955 (w), 1665 (m), 1637 (w), 1614 (w), 1480 (w), 1433 (w), 1266 (s), 974 (s), 829 (s), 801 (s), 766 (s), 722 (m), 679 (s), 623 (m), 502 (w), 422 (w).
Elemental analysis calculated ($C_{20}H_{45}CoN_3Si_4$ 498.87 g/mol) C 48.15 H 9.09 N 8.42; experimental C 48.00 H 8.65 N 8.76.
μ_{eff} = 4.92 μ_B (Evans, [D8]THF + 1%TMS, 500 MHz, 298K, $\mu_{S.O.}$ = 3.87 μ_B)

Crystals suitable for X-ray diffraction analysis were obtained from a saturated solution of **6** in *n*-pentane at –40 °C.

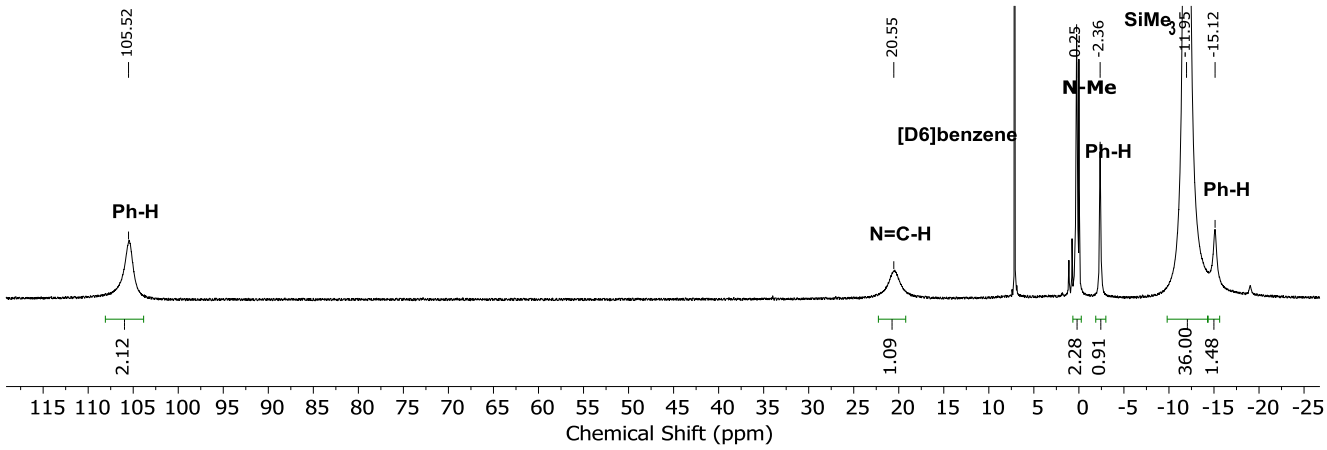

Figure S10. ^{1}H-NMR-spectrum of **6** in [D6]benzene at 300 K, 300 MHz.

Synthesis of [Fe(bpi)(N(SiMe$_3$)$_2$)$_2$] (7)

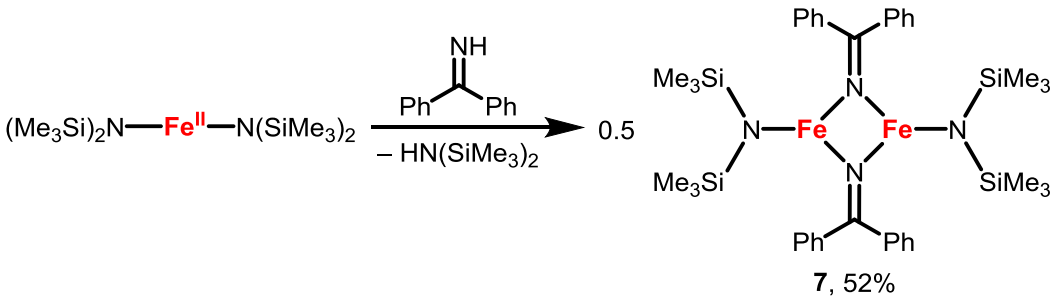

[Fe(bpi)] (7) : [Fe(N(SiMe$_3$)$_2$)$_2$] (113 mg, 0.3 mmol, 1.0 eq.) and bpi (54 mg, 0.3 mmol, 1.0 eq.) were dissolved in 1 mL of *n*-pentane. The deep brown solution was filtered after 2 min and then cooled to –40 °C to afford **7** as a yellow crystalline solid (104 mg, 0.13 mmol, 52%).
^{1}H-NMR ([D6]benzene, 300 MHz, 300 K, ppm): 12.13 s, 8H, $w_{1/2}$ = 22.3 Hz, Ph-**H**), –0.21 (br, 8H, $w_{1/2}$ = 73.5 Hz, Ph-**H**), –0.51 (br, 4H, $w_{1/2}$ = 37.6 Hz, Ph-**H**), –0.91 (br, 36H, $w_{1/2}$ = 35 Hz, SiMe$_3$).
IR (ATR, cm^{-1}): ν = 3057 (w), 2944 (w), 2891 (w), 1587 (m), 1560 (m), 1486 (w), 1441 (w), 1311 (w), 1239 (m), 1179 (w), 1072 (w), 1027 (w), 967 (m), 936 (m), 864 (m), 823 (s), 776 (m), 693 (s), 669 (m), 646 (s), 611 (m), 500 (m), 461 (m).
Elemental analysis calculated ($C_{38}H_{56}Fe_2N_4Si_4$ 792.92 g/mol) C 57.56 H 7.12 N 7.07; experimental C 57.57 H 6.43 N 6.51. Slightly lower N/H-values were consistently observed despite several attempts using crystalline samples. This can in part be attributed to high sensitivity to the compound.
μ_{eff} = 3.83 μ_B (Evans, [D6]Benzene + 1%TMS, 300 MHz, 298K, $\mu_{S.O.}$ = 6.93 μ_B)

Crystals suitable for X-ray diffraction analysis were obtained from a saturated solution of **7** in *n*-pentane at –40 °C.

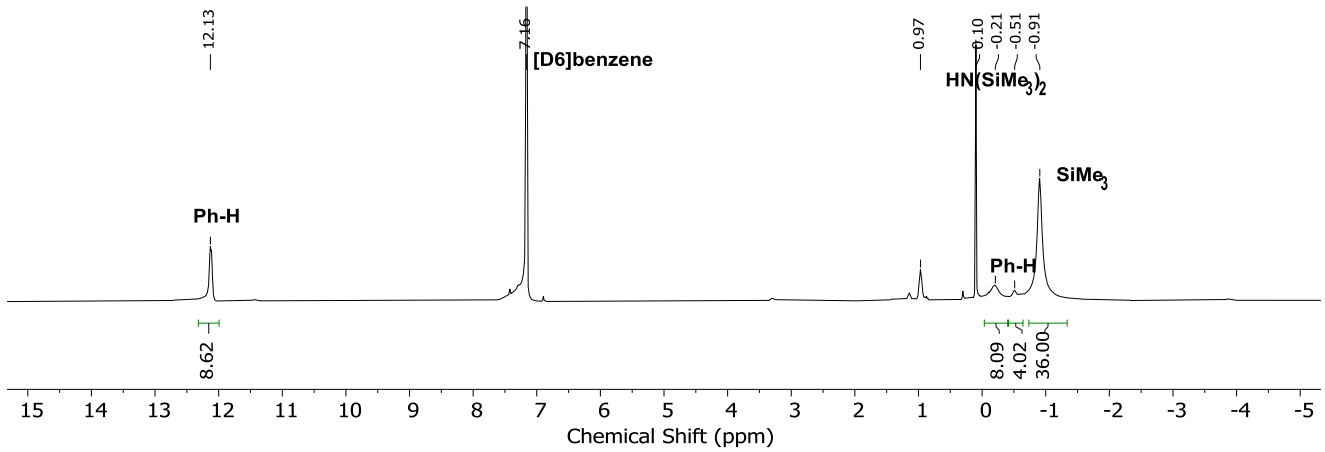

Figure S11. ^{1}H-NMR-spectrum of **7** in [D6]benzene at 300 K, 300 MHz.

Synthesis of [Co(bpi)(N(SiMe$_3$)$_2$)$_2$] (8)

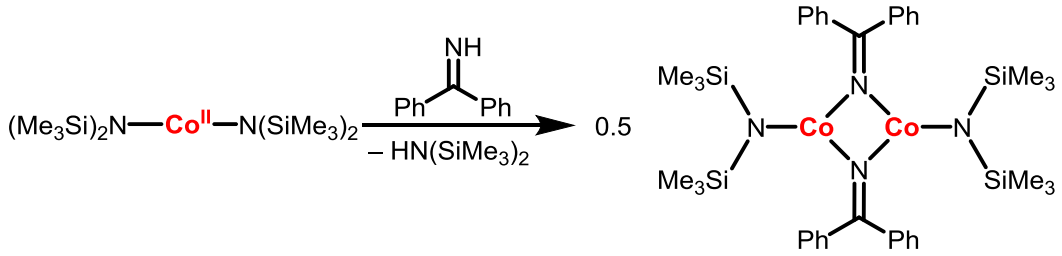

8, 98%

[Co(bpi)] (11): [Co(N(SiMe$_3$)$_2$)$_2$] (114 mg, 0.3 mmol, 1.0 eq.) and bpi (54 mg, 0.3 mmol, 1.0 eq.) were dissolved in 1.5 mL of *n*-pentane and filtered after 2 min. The deep brown solution was cooled to –40 °C to afford **8** as a dark yellow crystalline solid (196 mg, 0.24 mmol, 98%).
^{1}H-NMR ([D6]benzene, 300 MHz, 300 K, ppm): 27.43 (br, 8H, $w_{1/2}$ = 31.5 Hz, Ph-H), 12.69 (br, 8H, $w_{1/2}$ = 30.2 Hz, Ph-H), 11.79 (br, 4H, $w_{1/2}$ = 28.6 Hz, Ph-H), –5.06 (s, 36H, $w_{1/2}$ = 26.7 Hz, SiMe$_3$).
IR (ATR, cm^{-1}): ν = 2942 (w), 2893 (w), 1591 (w), 1569 (w), 1486 (w), 1443 (w), 1241 (m), 1072 (w), 1011 (m), 936 (w), 856 (m), 840 (m), 815 (s), 778 (s), 747 (m), 691 (s), 669 (m), 650 (s), 609 (m), 504 (w), 465 (w).
Elemental analysis calculated ($C_{38}H_{56}CoN_4Si_4$ 799.10 g/mol) C 57.12 H 7.06 N 7.01; experimental C 59.53 H 6.81 N 7.07. Slightly higher C-values were consistently observed despite several attempts using crystalline samples. This can in part be attributed to high sensitivity to the compound.
μ_{eff} = 2.89 μ_B (Evans, [D6]benzene + 1%TMS, 500 MHz, 298K, $\mu_{S.O.}$ = 5.48 μ_B)
Crystals suitable for X-ray diffraction analysis were obtained from a saturated solution of **8** in *n*-pentane at –40 °C.

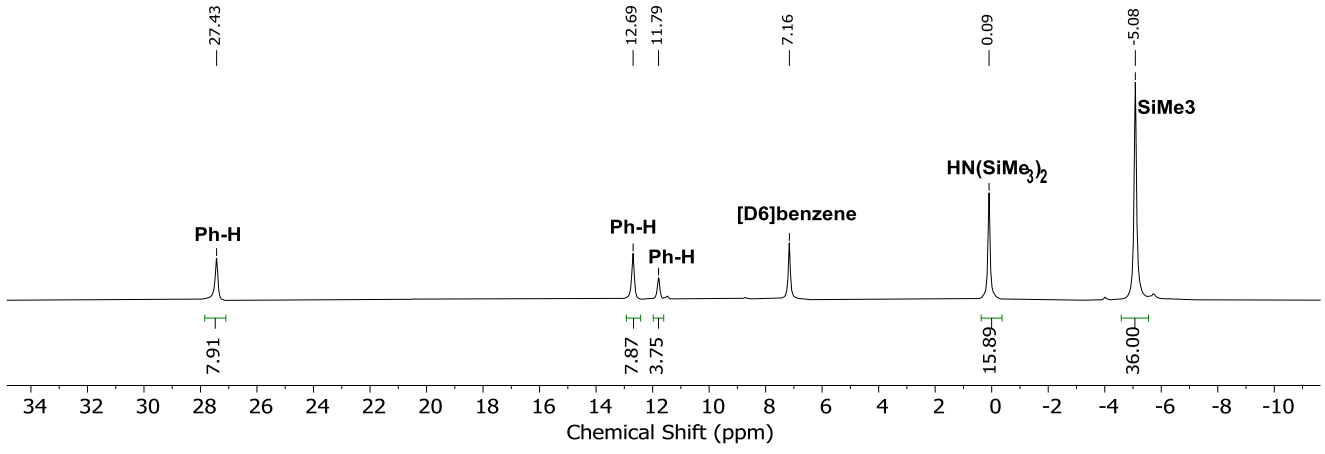

Figure S12. ^{1}H-NMR-spectrum of **8** in [D6]benzene at 300 K, 300 MHz.

Synthesis of K{18c6}[Co(1,3-CHD)$_2$] (K{18c6}[9])

1,3-CHD (39.6 μL, 0.42 mmol, 2.00 eq.) were added to a solution of K{18c6}[Co(N(SiMe$_3$)$_2$)$_2$] (143 mg, 0.21 mmol, 1.00 eq.) in 2 mL of Et$_2$O and stirred for 2 h. After resting overnight, orange single crystals formed at the bottom of the reaction vial. The liquid phase was filtered off and the solid was dried under vacuum. K{18c6}[**9**] could be identified as by X-ray diffraction but could not be further isolated due to unseperable decontaminations of K{18c6}[Co(N(SiMe$_3$)$_2$)$_3$] which is a by-product of the reaction. The latter was identified via X-Ray diffraction analysis.
Crystals suitable for X-ray diffraction analysis were obtained by layering the reaction solution with *n*-pentane at ambient temperature.

Synthesis of [K{18c6}]$_2$(Fe$_2$(NCPh$_2$)$_6$] ([K{18c6}]$_2$[10])

K{18c6}[Fe(N(SiMe$_3$)$_2$)$_2$] (90 mg, 0.13 mmol, 1.00 eq.) and bpi (24 mg, 0.13 mmol, 1.00 eq.) were dissolved in 2 mL of Et$_2$O and stirred for 1 h. The green solution was dried under vacuum and the remaining solid was dissolved in 1.5 mL of 1,2-difluorobenzene. The solution was layered in 1.5 mL of *n*-pentane, which afforded [K{18c6}]$_2$[**10**]·(1,2-dfb)$_4$ (dfb: difluorobenzene) as a black crystalline solid (32 mg, 0.014 mmol, 32%).
^{1}H-NMR ([D8]THF, 300 MHz): Due to strong signal-broadening, signals could not be assigned usefully.
IR (ATR, cm^{-1}): ν = 2942 (w), 2889 (w), 1470 (w), 1433 (w), 1350 (w), 1254 (w), 1233 (m), 1103 (s), 980 (s), 959 (s), 864 (m), 825 (s), 778 (m), 749 (m), 969 (m), 661 (m), 609 (w), 527 (w), 467 (w), 438 (w).
elemental analysis calculated (C$_{126}$H$_{124}$F$_8$Fe$_2$K$_2$N$_6$Si$_{12}$ 2256.28 g/mol) C 67.07 H 5.54 N 3.72; experimental C 65.77 H 5.52 N 3.91
Crystals suitable for X-ray diffraction analysis were obtained by layering a solution of [K{18c6}]$_2$[**10**] in 1,2-difluorobenzene with *n*-pentane at –40 °C.

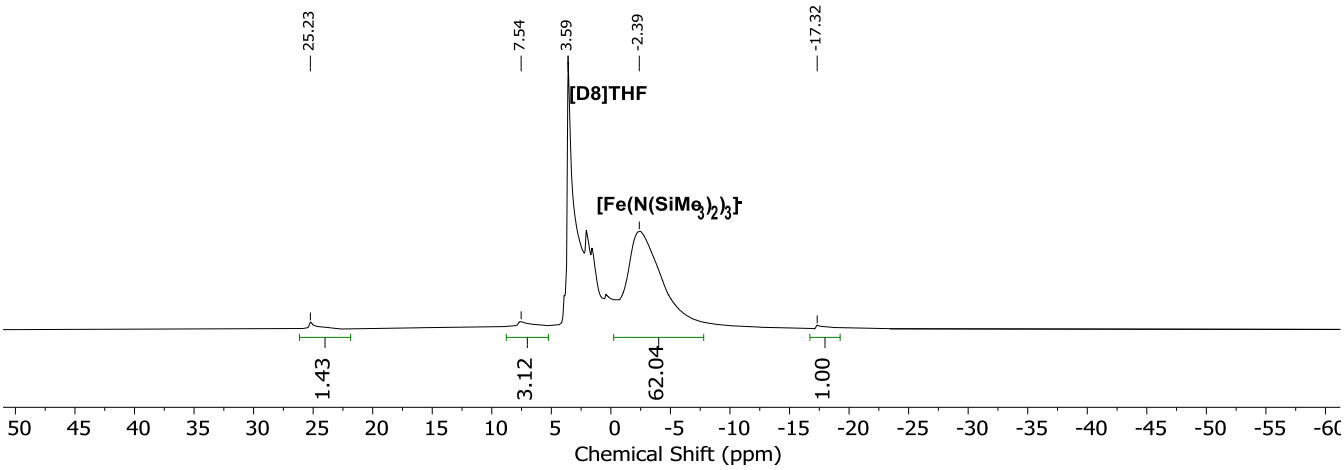

Figure S13. ^{1}H-NMR-spectrum of [K{18c6}]$_2$[**10**] in [D8]THF at 300 K, 300 MHz.

Synthesis of [K{18c6}]$_2$[Co$_2$(N(SiMe$_3$)$_2$)(CPh(C$_5$H$_4$)] ([K{18c6}]$_2$[11])

K{18c6}[Co(N(SiMe$_3$)$_2$)$_2$] (293 mg, 0.43 mmol, 1.00 eq.) and bpi (78 mg, 0.43 mmol, 1.00 eq.) were dissolved in 3 mL of Et$_2$O and stirred for 30 min. The initially violet solution quickly turned black and was layered with 4 mL of *n*-pentane. The black precipitate was filtered off and dried under vacuum to obtain [K{18c6}]$_2$[**11**] as a crystalline black solid (145 mg, 0.11 mmol, 51%).
IR (ATR, cm^{-1}): ν =3105 (w), 3000 (w), 2944 (w), 1616 (w), 1501 (w), 1482 (w), 1377 (m), 1307 (w), 1258 (m), 1124 (s), 1013 (m), 980 (s), 883 (m), 840 (s), 782 (m), 710 (m), 675 (m), 621 (w), 539 (w).
Elemental analysis calculated (C$_{56}$H$_{86}$Co$_2$K$_2$N$_3$Si$_2$ 1245.55 g/mol) C 54.00 H 6.96 N 3.37; experimental C 53.92 H 6.62 N 3.36.
μ_{eff} = 2.27 μ_B (Evanst, [D8]THF + 1%TMS, 500 MHz, 298K)
Crystals suitable for X-ray diffraction analysis were obtained by layering a saturated solution of [K{18c6}]$_2$[**11**] in THF with *n*-pentane at –40 °C.

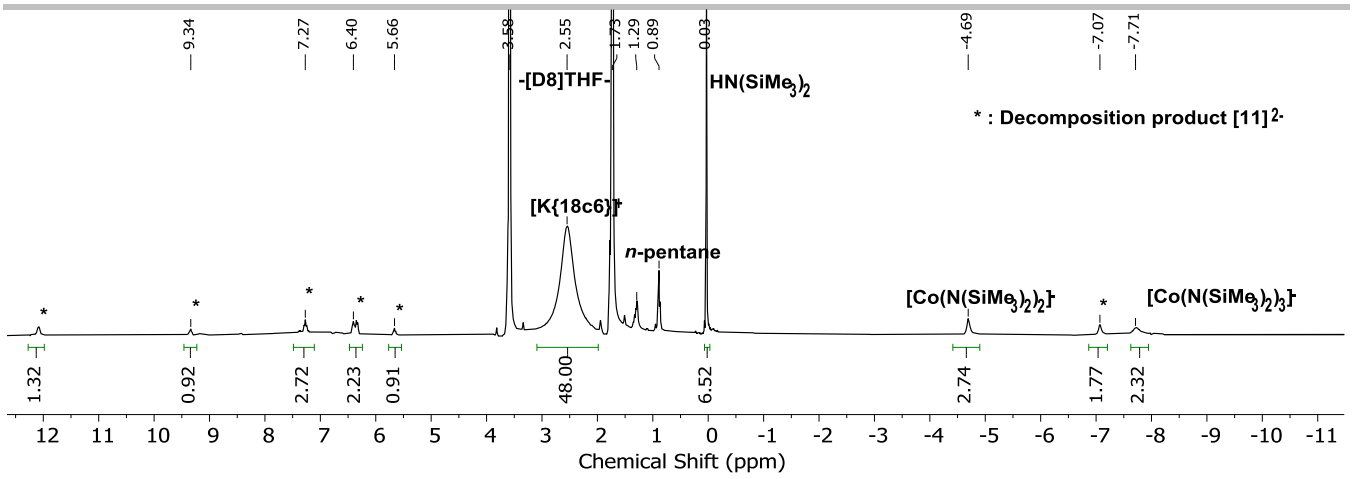

Figure S14. ^{1}H-NMR-spectrum of [K{18c6}]$_2$[**11**] in [D8]THF at 300 K, 300 MHz.

Reaction of K{18c6}[4] with excess 1,4-cyclohexadiene ([K{18c6}]$_2$[12])

K{18c6}[Co(N(SiMe$_3$)$_2$)$_2$] (135 mg, 0.21 mmol, 1.00 eq.) and bpi (36 mg, 0.21 mmol, 1.00 eq.) were dissolved in 1 mL of THF. The reaction mixture was quickly added to a solution of 1,4-CHD (excess) in1 mL of Et_2O and stirred of 2 h. The solvent was removed from the resulting dark brown solution to obtain [K{18c6}]$_2$[**12**] as a dark brown solid (48 mg, 0.041 mmol, 39%).
^{1}H-NMR ([D8]THF, 300 MHz): Due to strong signal-broadening, only residual solvent signals can be detected.
IR (ATR, cm^{-1}): ν = 3080 (w), 2944 (m), 1610 (w), 1515 (w), 1501 (w), 1480 (w), 1377 (m), 1309 (w), 1272 (m), 1124 (s), 1046 (w), 1011 (m), 980 (m), 885 (m), 852 (m), 766 (m), 710 (m).
Elemental analysis calculated ($C_{62}H_{77}Co_2KN_2O_9$ 1151.24 g/mol) C 64.68 H 6.74 N 2.43; experimental C 61.57 H 6.93 N 3.16. Slightly lower N/H-values were consistently observed despite several attempts using crystalline samples. This can in part be attributed to high sensitivity to the compound.
μ_{eff} = 3.78 μ_B (Evans, [D8]THF + 1%TMS, 500 MHz, 298K)

Crystals suitable for X-ray diffraction analysis were obtained by layering a saturated solution of [K{18c6}]$_2$[**12**] in Et_2O with *n*-pentane at –40 °C.

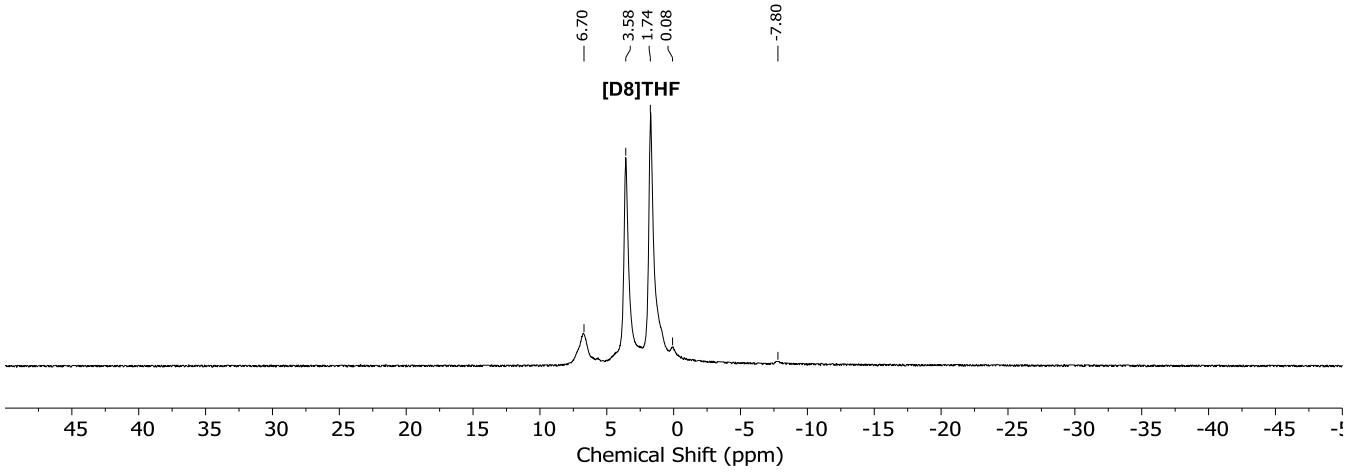

Figure S15. ^{1}H-NMR-spectrum of [K{18c6}]$_2$[**12**] in [D8]THF at 300 K, 300 MHz.

Reaction of K{18c6}[2] with 1,4-cyclohexadiene

1,4-cyclohexadiene (4.3 mg, 0.053 mmol, 1.00 eq.) was added to a solution of K{18c6}[**2**] (93 mg, 0.017 mmol, 2.00 eq.) in 2 mL of [D8]THF. The reaction was monitored via ^{1}H-NMR-spectroscopy. The formation of benzene (δ = 7.30 ppm) was amounted to 90% relative to 1,4-CHD (δ = 5.62, 2.62 ppm) after 72 h.

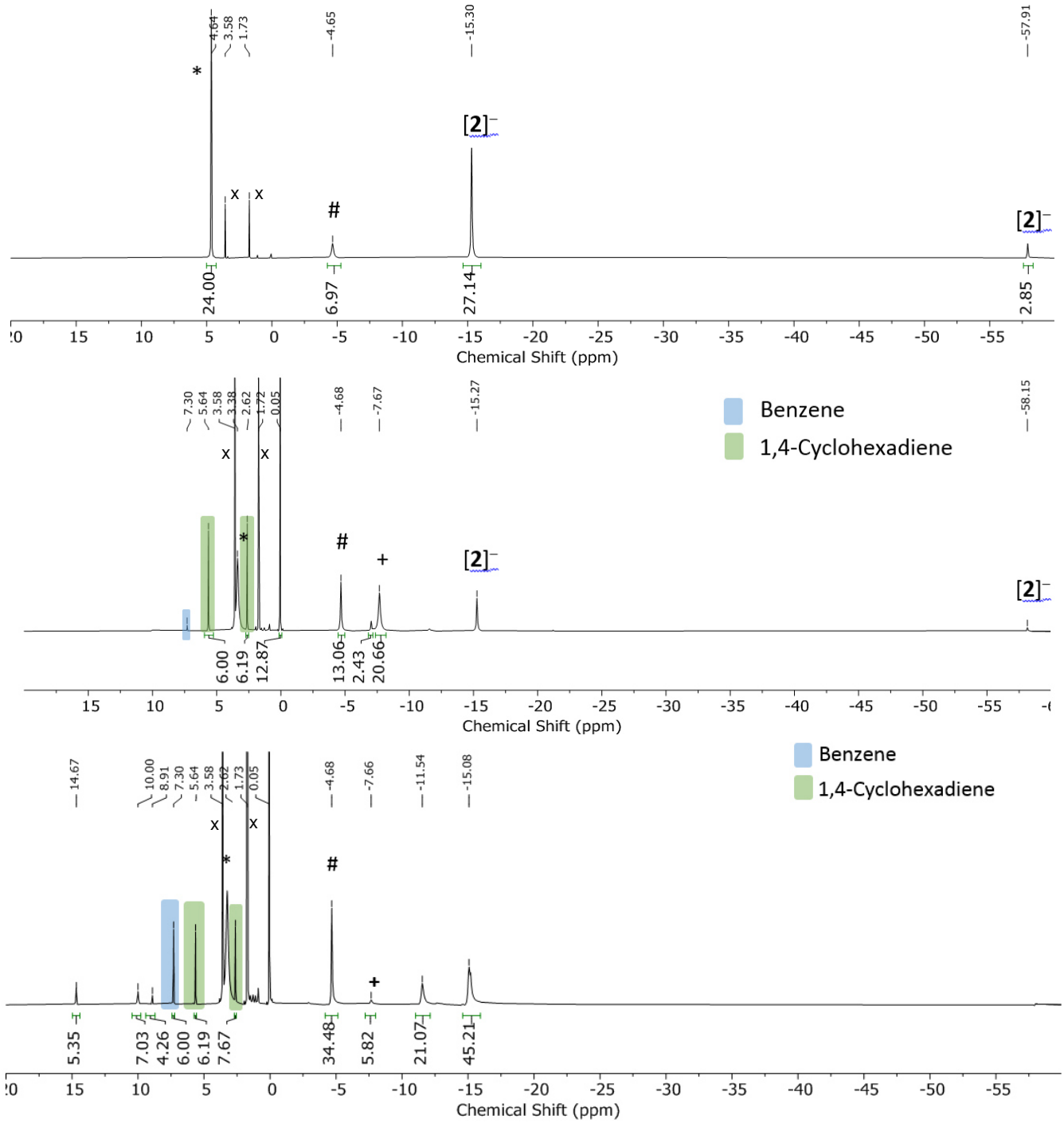

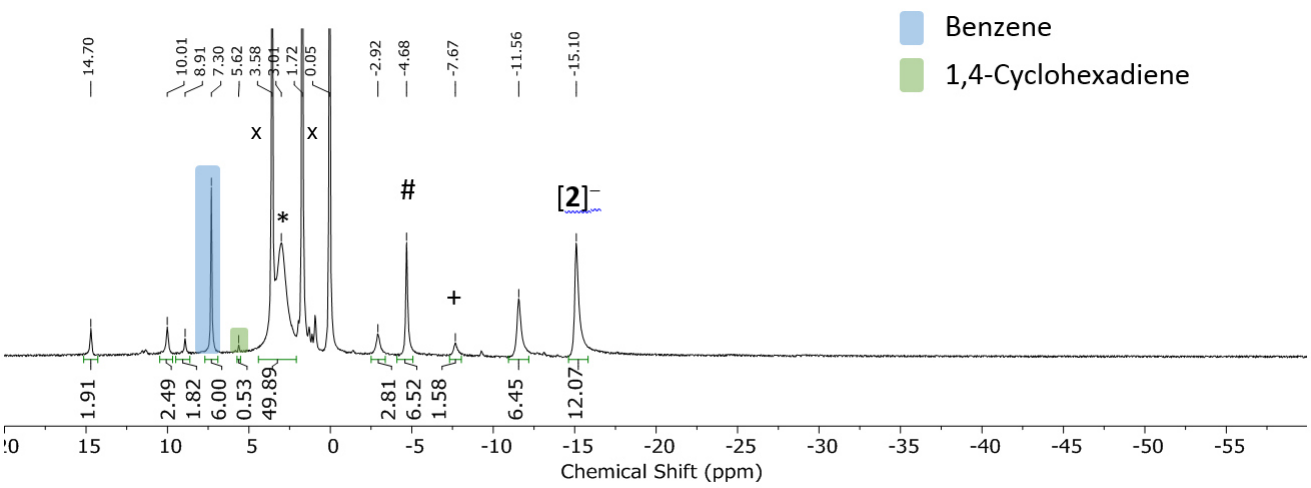

Figure S16. ^{1}H-NMR-spectra of K{18c6}[**2**] (top), the reaction mixture after 20 min (second from top), 24 h (third from top) and 72 h (bottom) in [D8]THF at 300 K, 300 MHz. Benzene is highlighted in blue, 1,4-cyclohexadiene is highlighted in green. Marked signals are labelled as following: x: [D8]THF; *: $[K\{18c6\}]^{+}$; **#**: $[Co(N(SiMe_3)_2)_2]^{-}$; **+**: $[Co(N(SiMe_3)_2)_3]^{-}$

Reaction of K{18c6}[5] with 1,4-cyclohexadiene

1,4-cyclohexadiene (0.95 mg, 0.012 mmol, 1.00 eq.) was added to a solution of K{18c6}[**5**] (19 mg, 0.023 mmol, 2.00 eq.) in 0.5 mL of [D8]THF. The reaction was monitored via ^{1}H-NMR-spectroscopy. The formation of benzene (δ = 7.30 ppm) was completed to a degree of 72% (relative to 1,4-CHD (δ = 5.64, 2.62 ppm)) after 10 d.

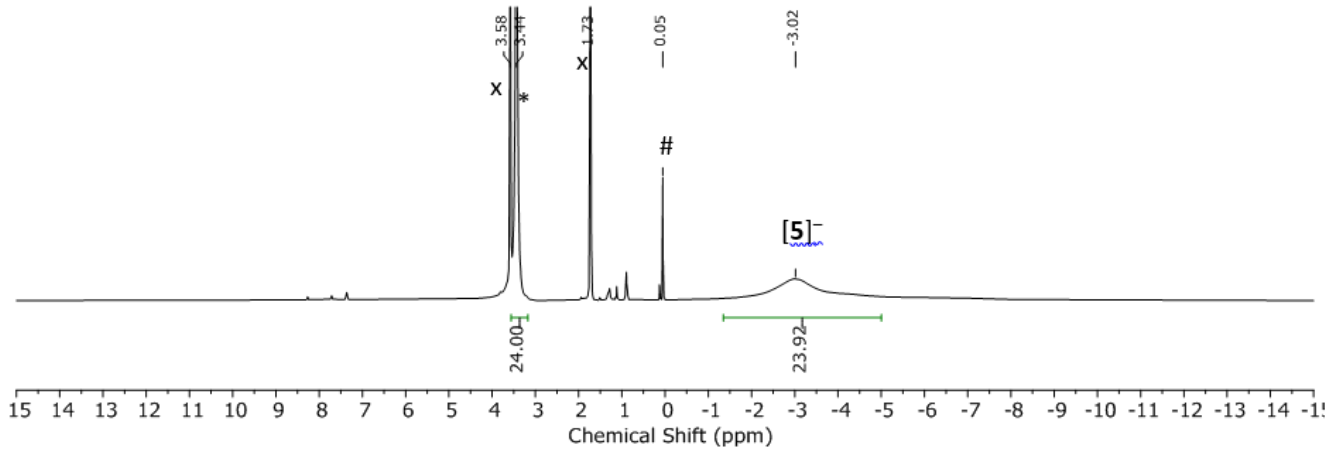

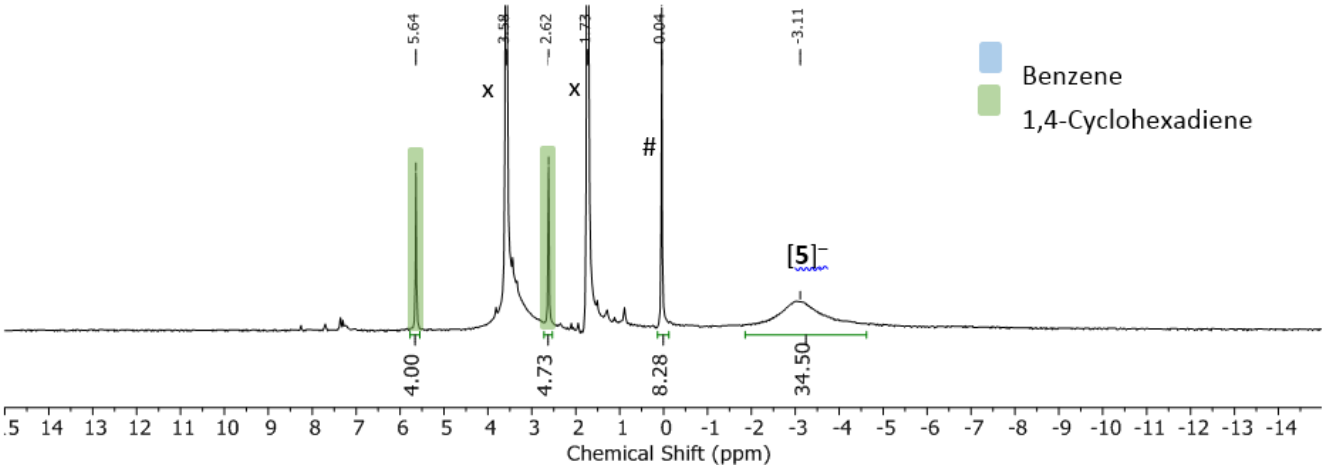

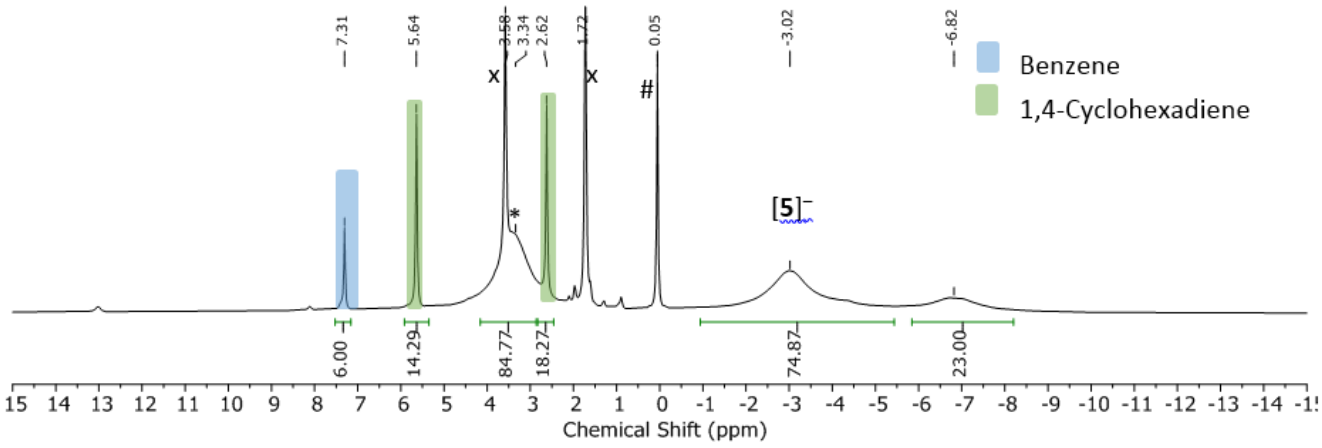

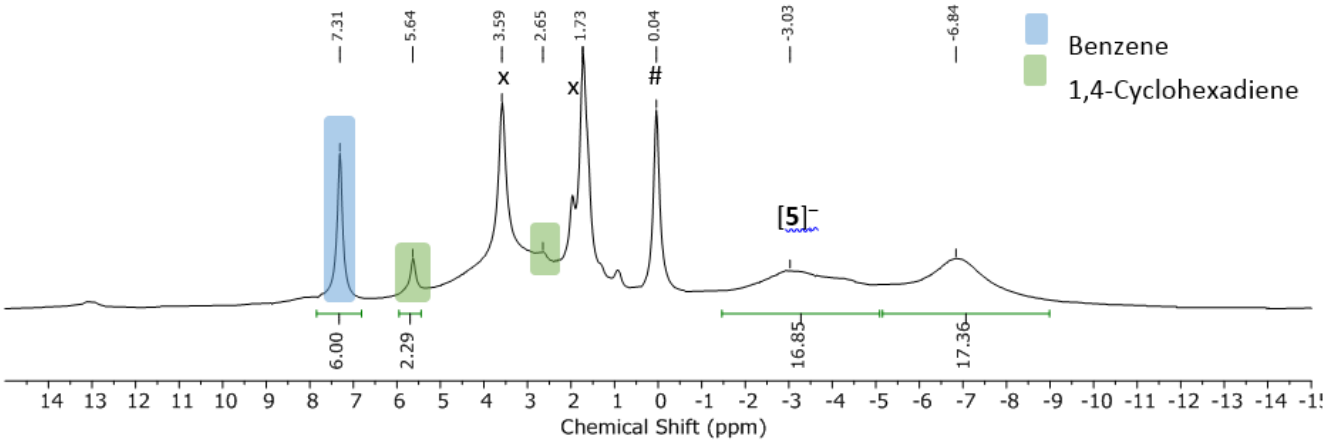

Figure S17. ^{1}H-NMR-spectrum of K{18c6}[**5**] (top), the reaction mixture after 1 h (second from top), 72 h (third from top) and 10 d (bottom) in [D8]THF at 300 K, 300 MHz. Benzene is highlighted in blue, 1,4-cyclohexadiene is highlighted in green. Marked signals are labelled as following: x: [D8]THF; *: $[K\{18c6\}]^{+}$; **#**: $HN(SiMe_3)_2$.

IR Spectra

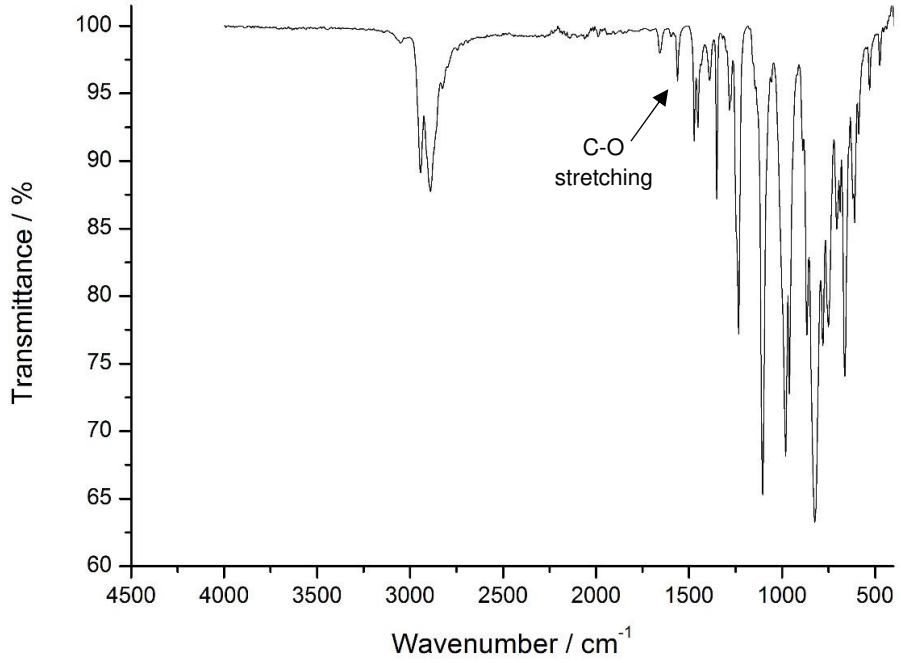

Figure S18. IR-spectrum of K{18c6}[**1**].

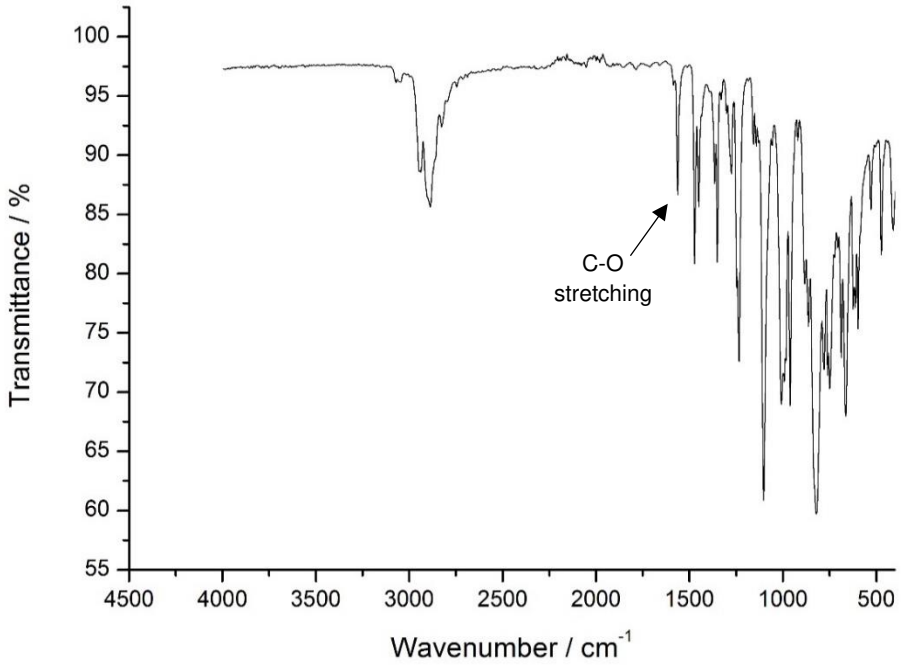

Figure S19. IR-spectrum of K{18c6}[**2**].

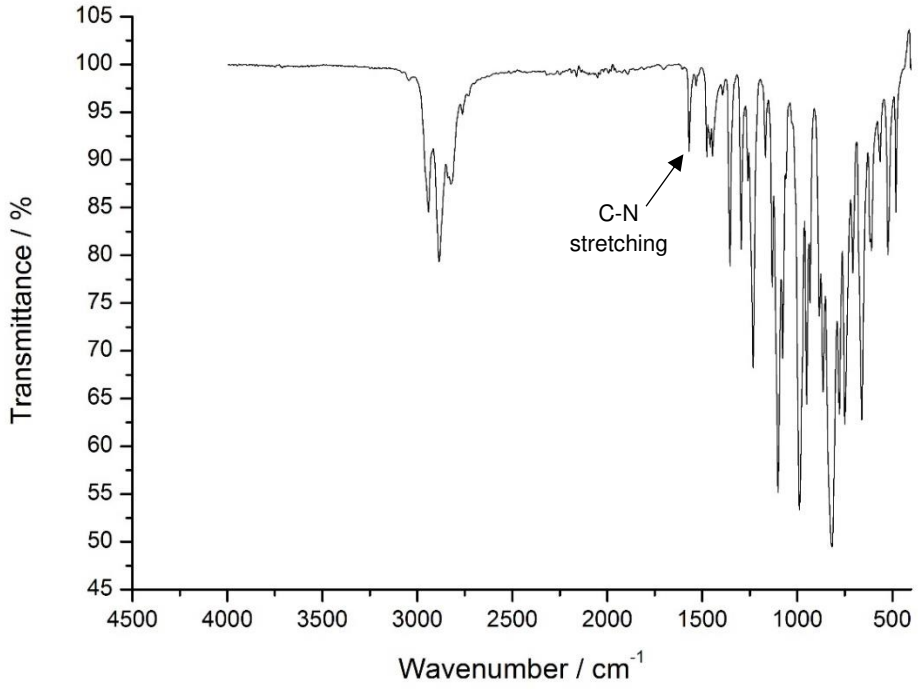

Figure S20. IR-spectrum of K{18c6}[**5**].

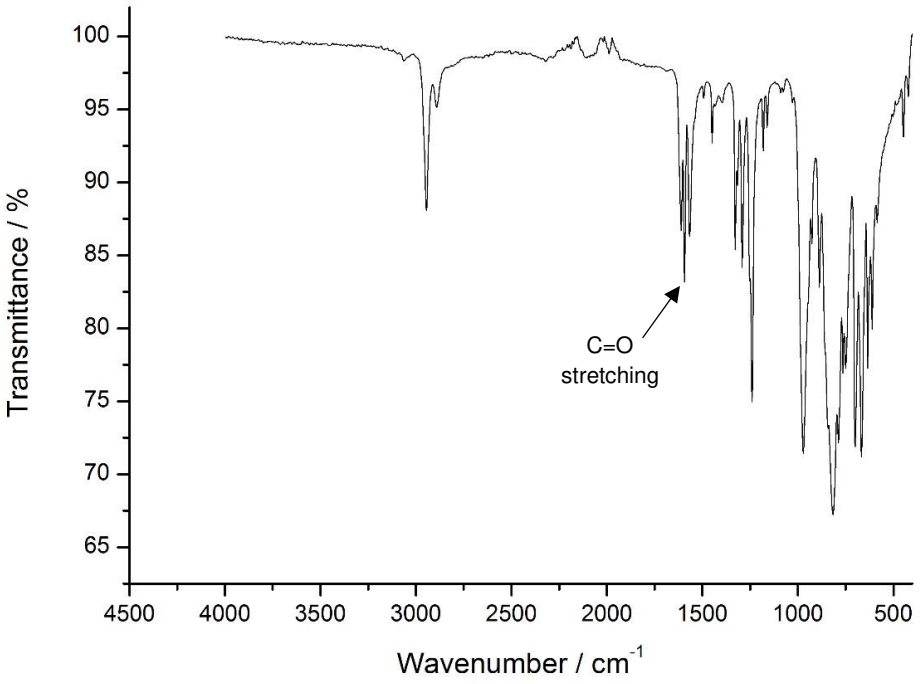

Figure S21. IR-spectrum of **1**.

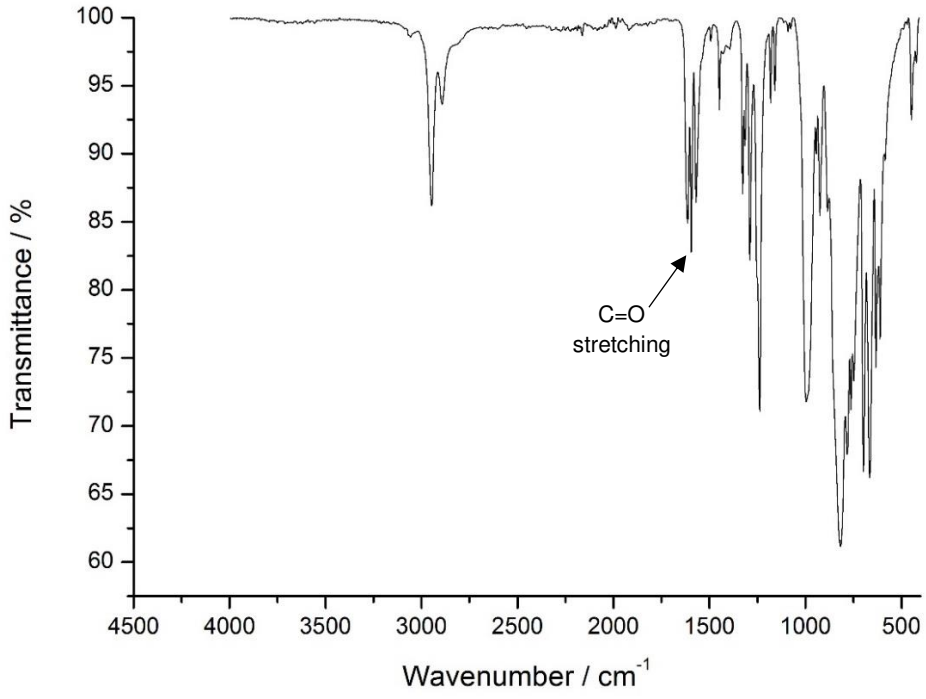

Figure S22. IR-spectrum of **2**.

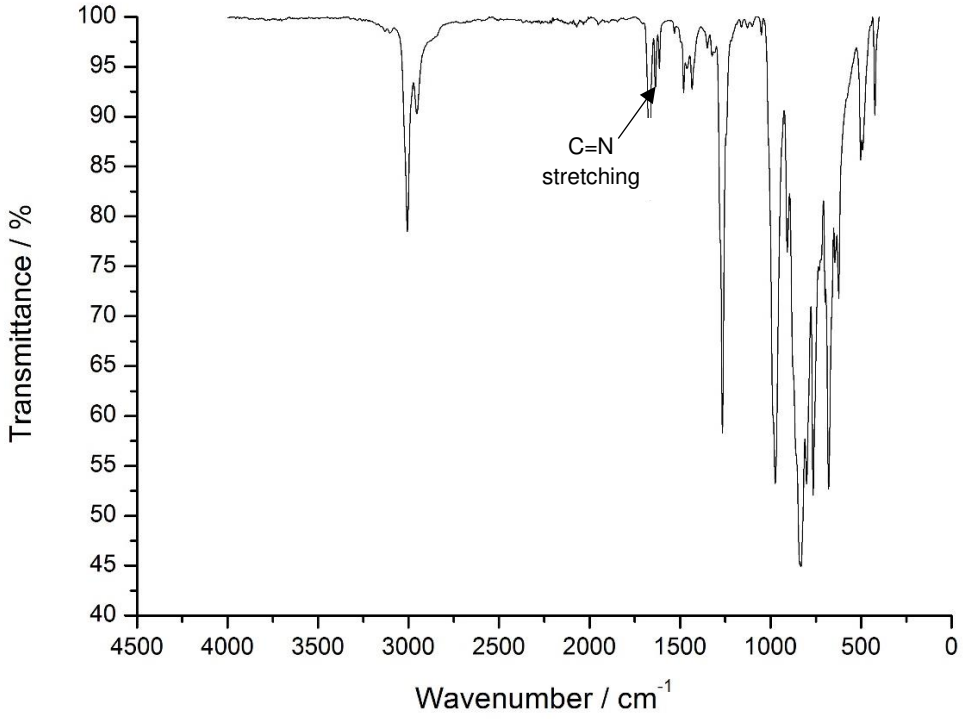

Figure S23. IR-spectrum of **5**.

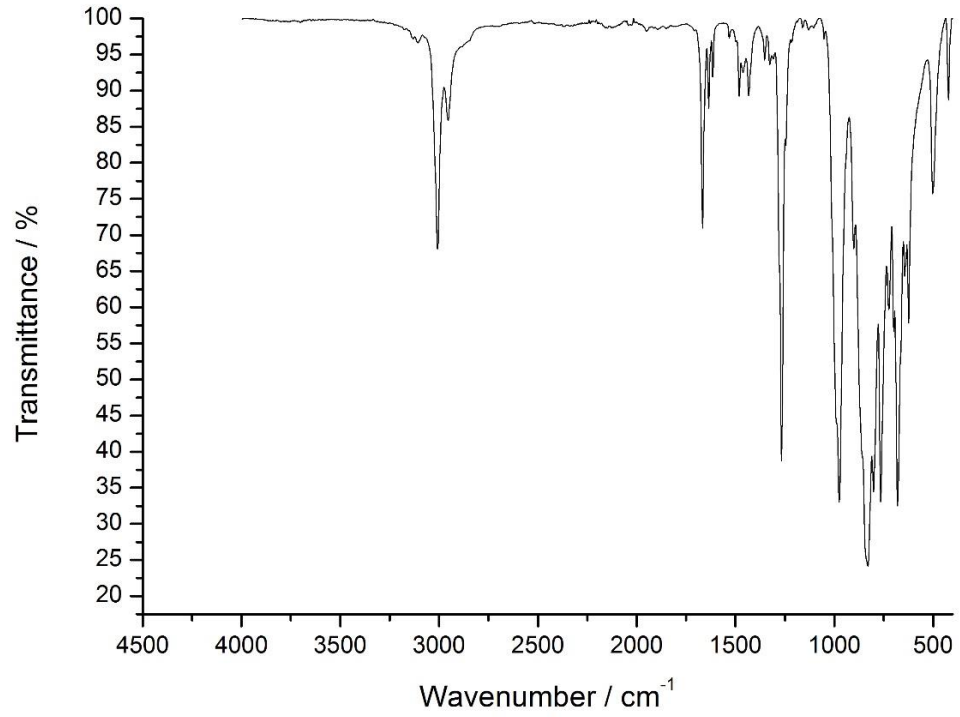

Figure S24. IR-spectrum of **6**.

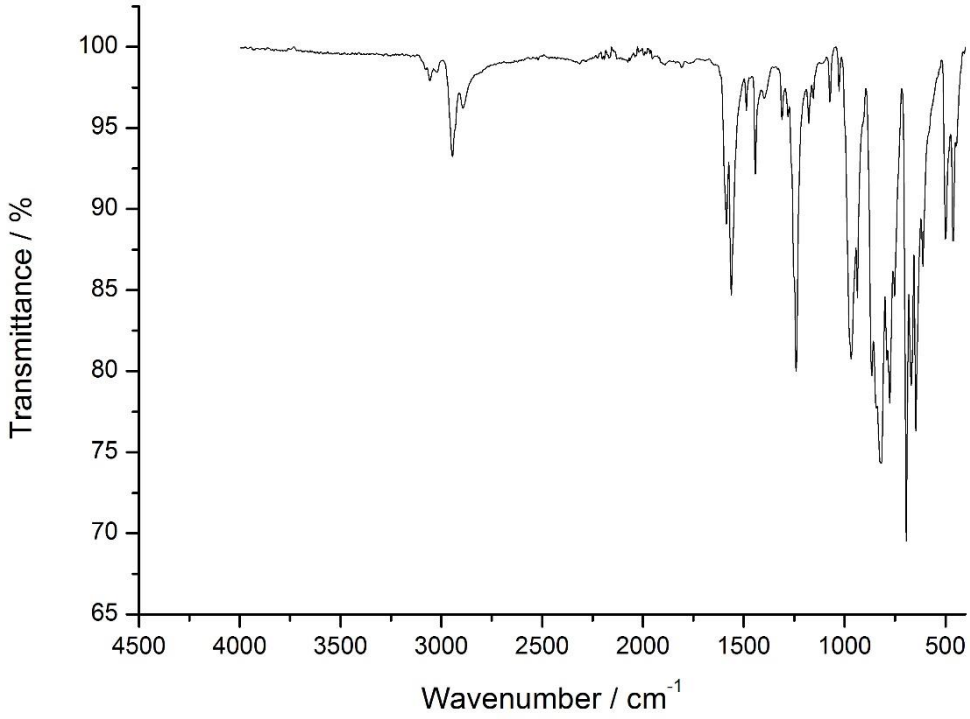

Figure S25. IR-spectrum of **7**.

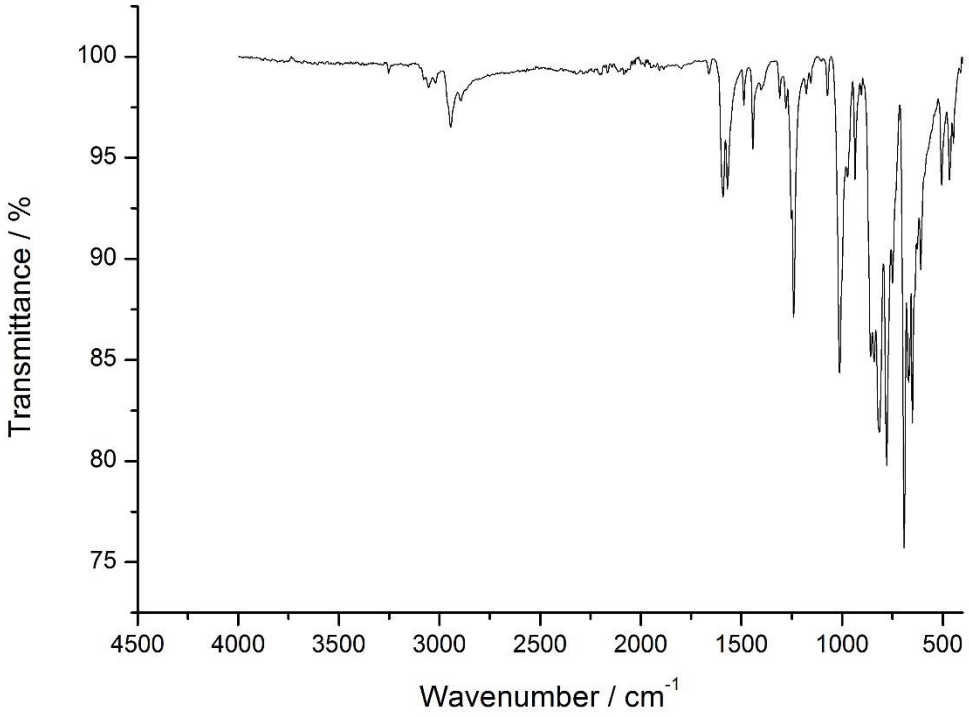

Figure S26. IR-spectrum of **8**.

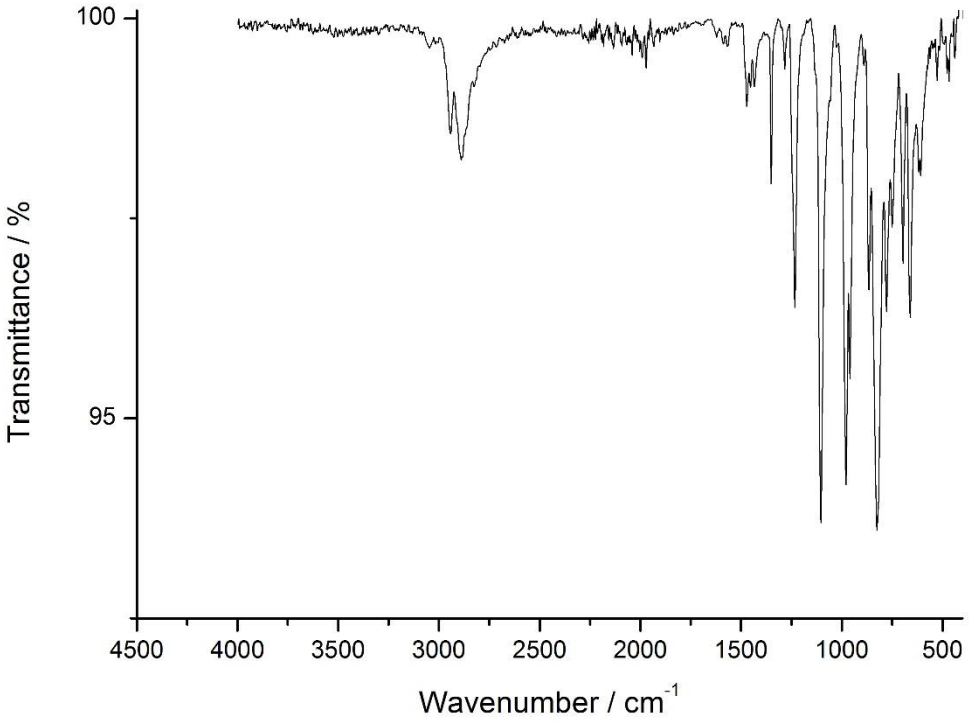

Figure S27. IR-spectrum of [K{18c6}]$_2$[**10**].

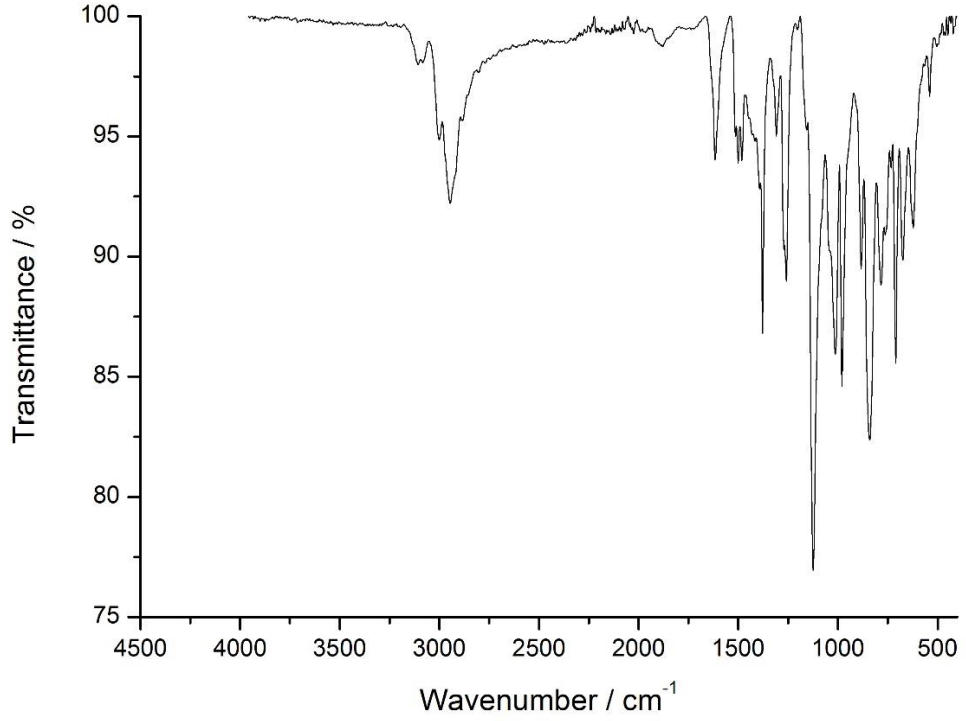

Figure S28. IR-spectrum of [K{18c6}]$_2$[**11**].

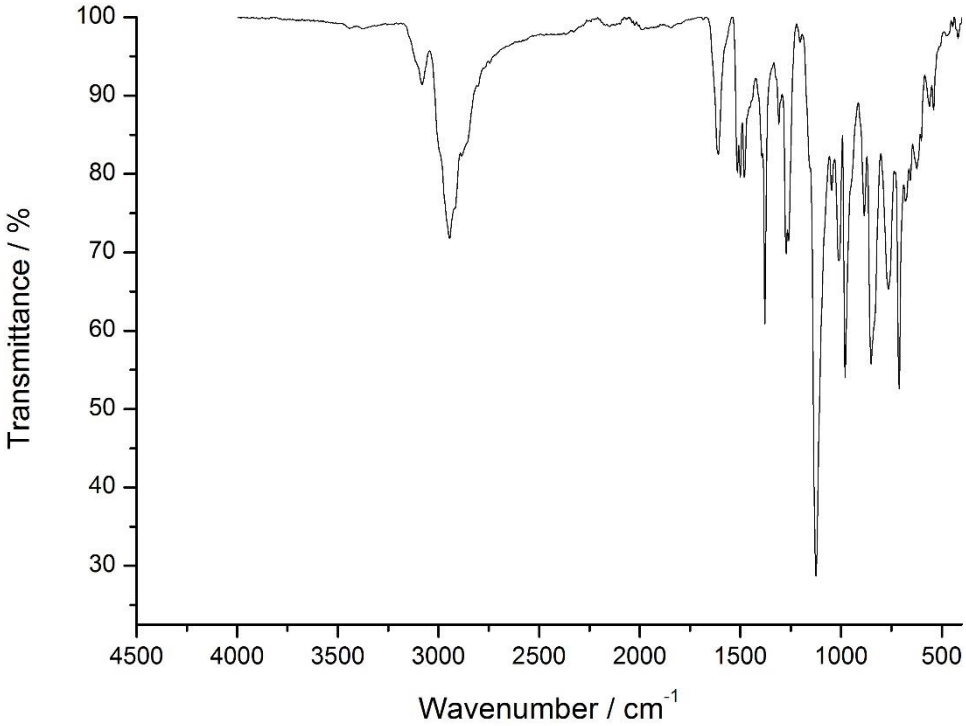

Figure S29. IR-spectrum of K{18c6}[**12**].

UV Vis Spectra

Table S1. UV-Vis-absorption maxima λ_{max} and molar extinction coefficients ε_0 for compounds $[\mathbf{1}]^-$ – $[\mathbf{5}]^-$, **1**, **2**, **5** and **6**.

Compound	λ_{max} (ε_0) / nm ($Lmol^{-1}cm^{-1}$)
Fe(bp•) $[\mathbf{1}]^-$	370 (3590), 400 (3680), 581 (3270)
Co(bp•) $[\mathbf{2}]^-$	417 (2960), 567 (3730)
Fe(bpi•) $[\mathbf{3}]^-$	400 (1290), 584 (1080)
Co(bpi•) $[\mathbf{4}]^-$	594 (n.a.)
Fe(bama•) $[\mathbf{5}]^-$	418 (1430), 482 (1070), 654 (600)
Fe(bp) (**1**)	–
Co(bp) (**2**)	685 (130)
Fe(bama) (**5**)	–
Co(bama) (**6**)	–

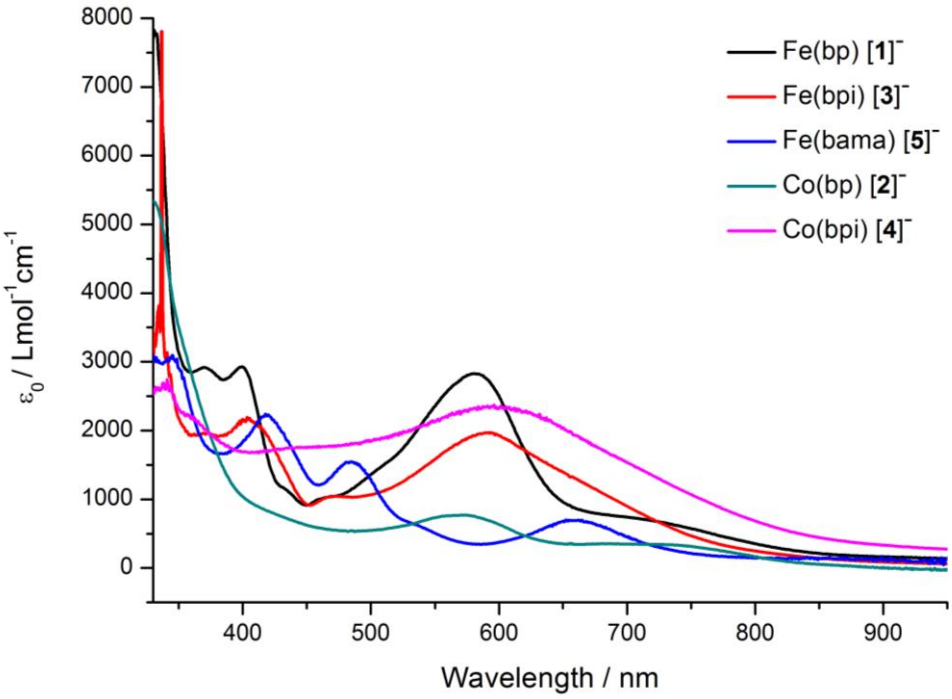

Figure S30. Comparison of UV-Vis spectra of $[\mathbf{1}]^-$ – $[\mathbf{5}]^-$ in Et2O. Extinction coefficients of [**2**]– and [**4**]– could not be determined an have thus been arbitrarily scaled for better comparison.

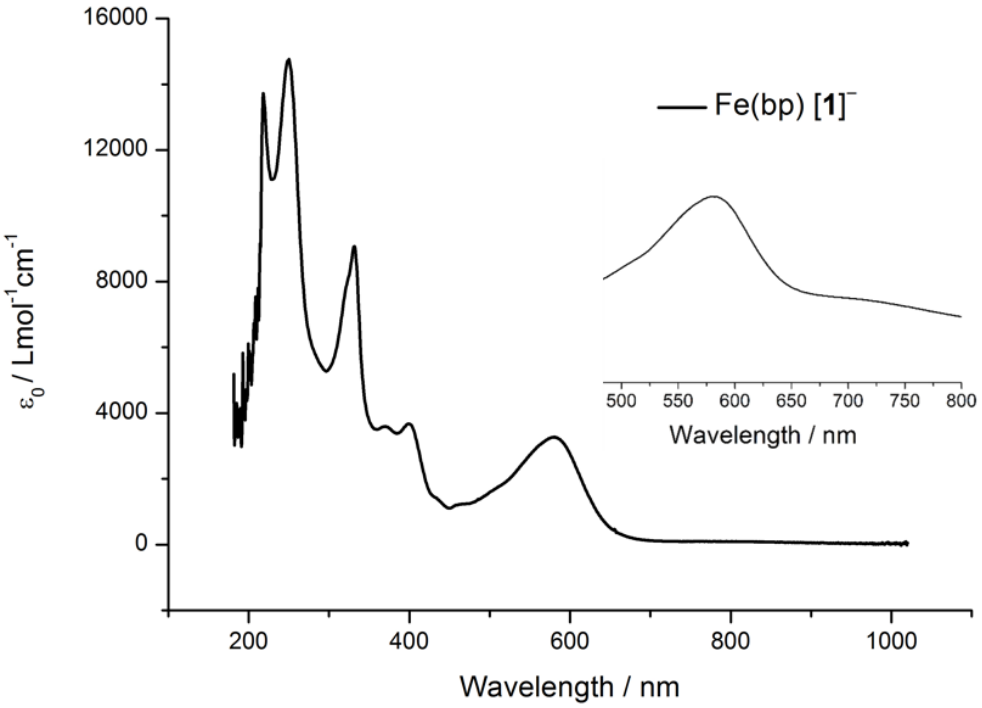

Figure S31. UV-Vis-spectrum of K{18c6}[**1**] in Et_2O with inset for better visibility of the weak absorption at 700 – 750 nm.

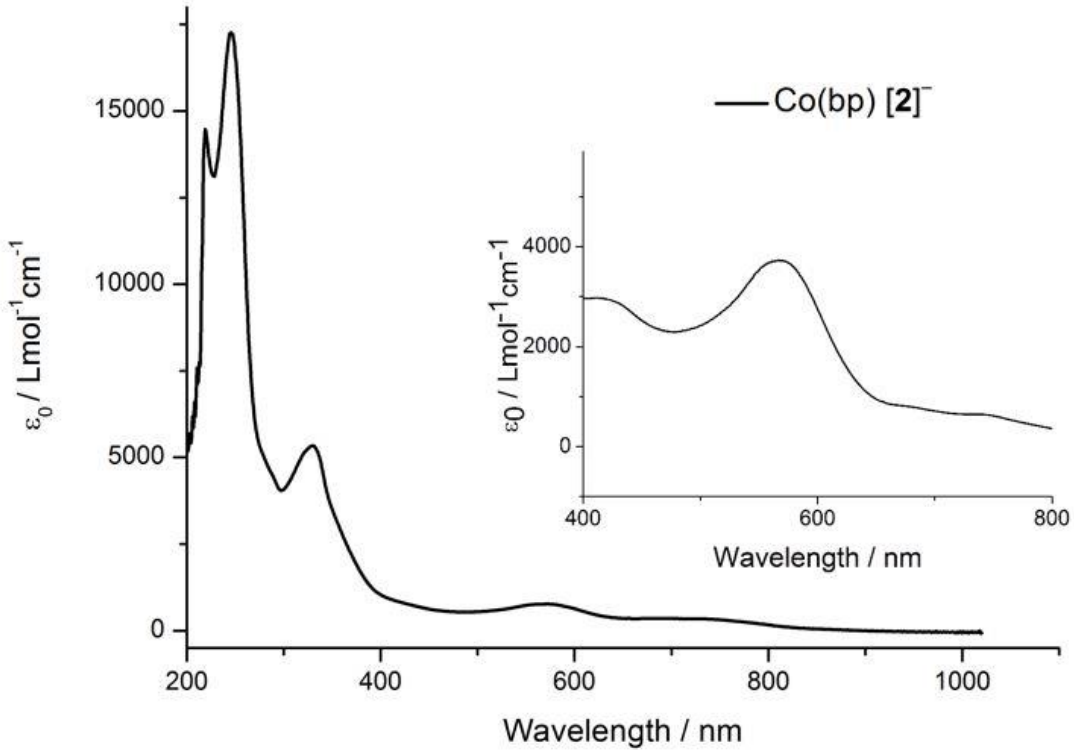

Figure S32. UV-Vis-spectrum of K{18c6}[**2**] in Et_2O with inset from another measurement.

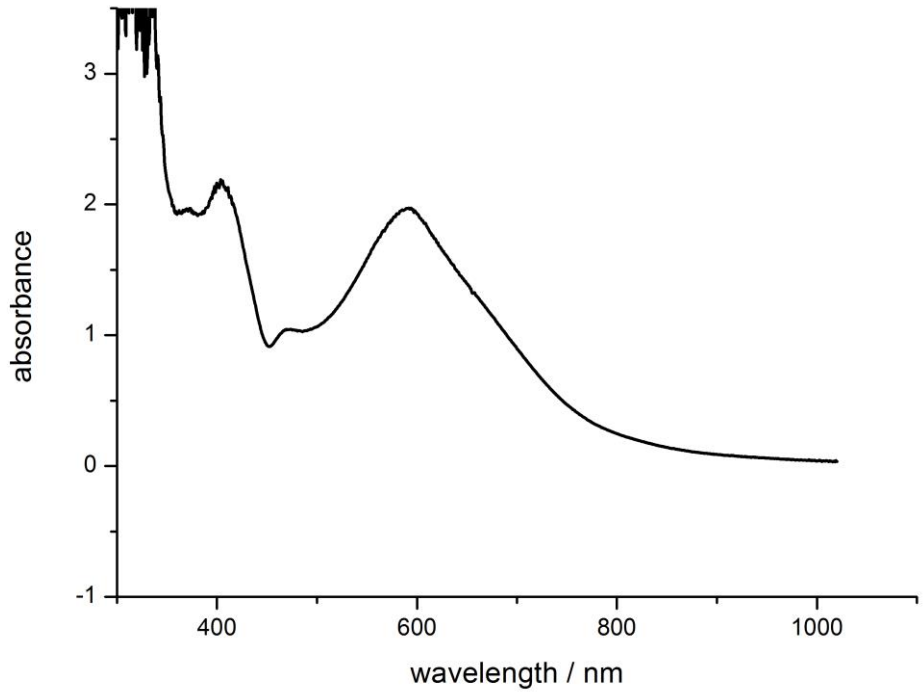

Figure S33. *In situ* UV-Vis-spectrum of K{18c6}[**3**] in Et_2O.

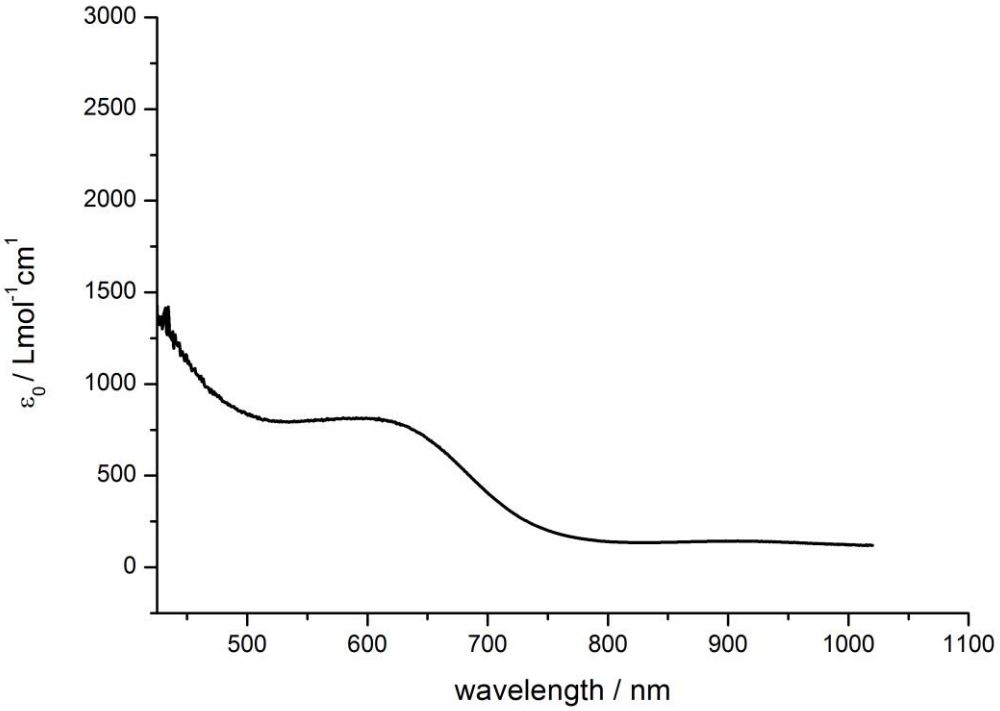

Figure S34. UV-Vis-spectrum of K{18c6}[**3**] after 30 seconds in Et_2O.

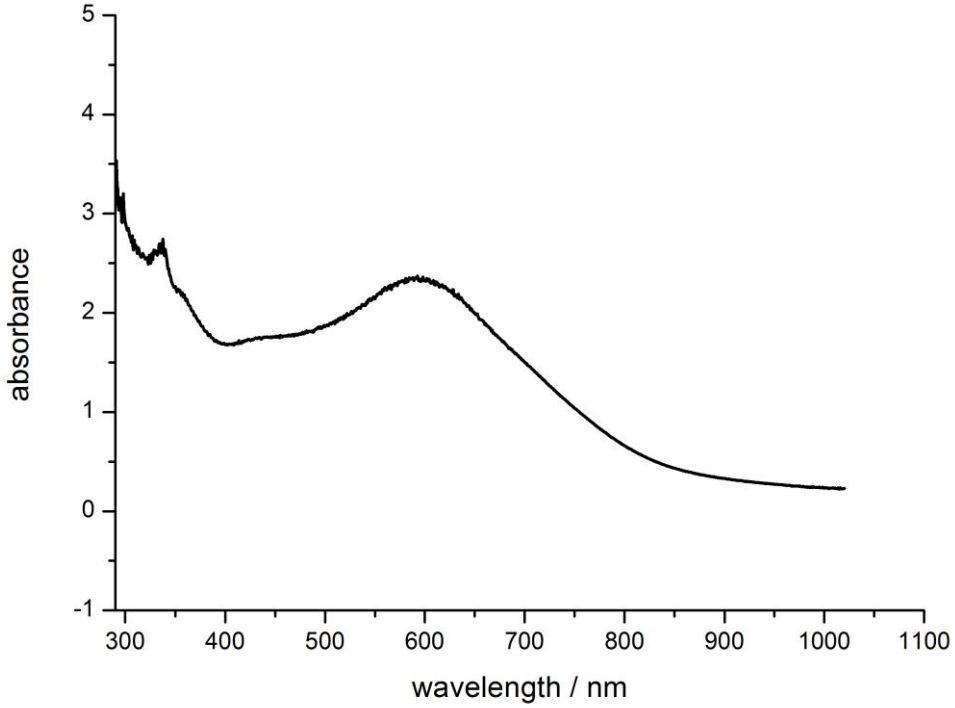

Figure *S*35. In-situ UV-Vis spectrum of K{18c6}[**4**] in Et_2O.

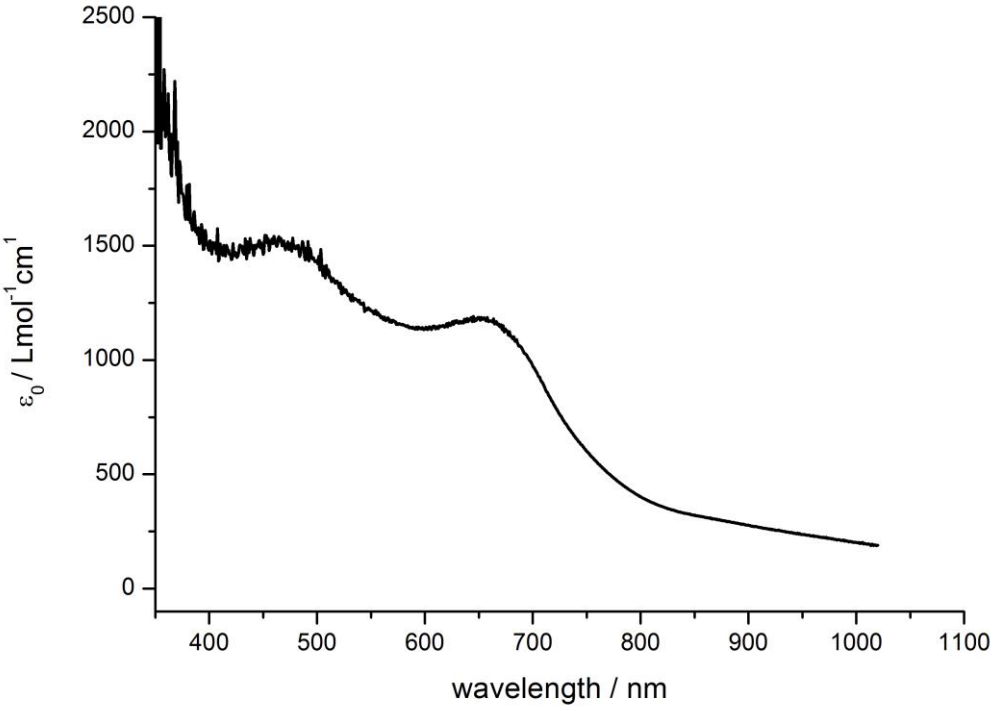

Figure S36. UV-Vis-spectrum of K{18c6}[**4**] after 30 seconds in Et_2O.

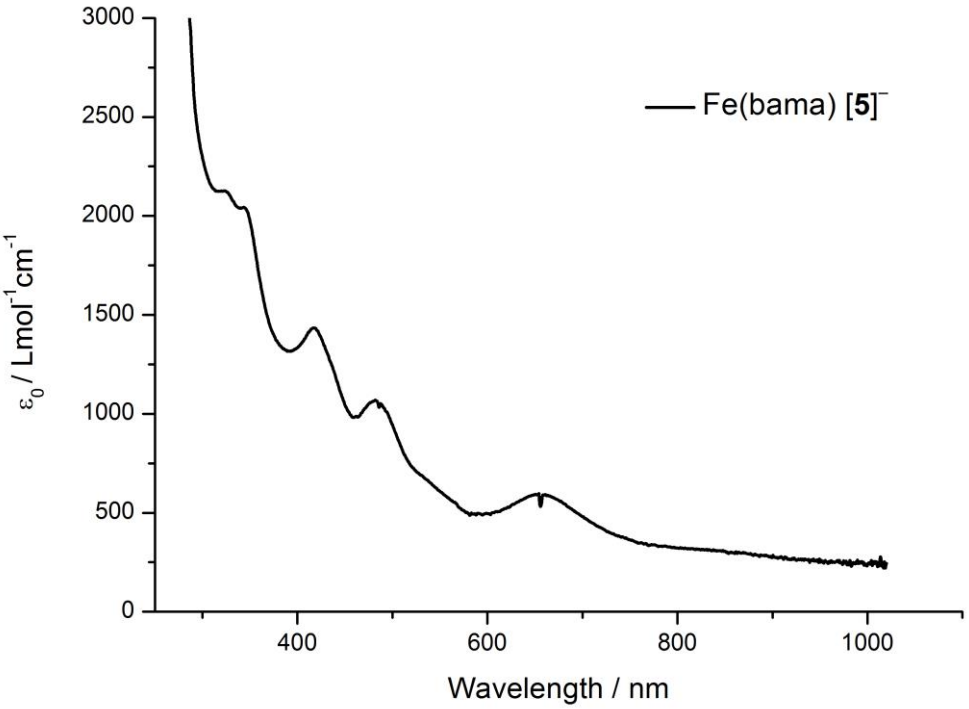

Figure S37. UV-Vis-spectrum of K{18c6}[**5**] in Et_2O.

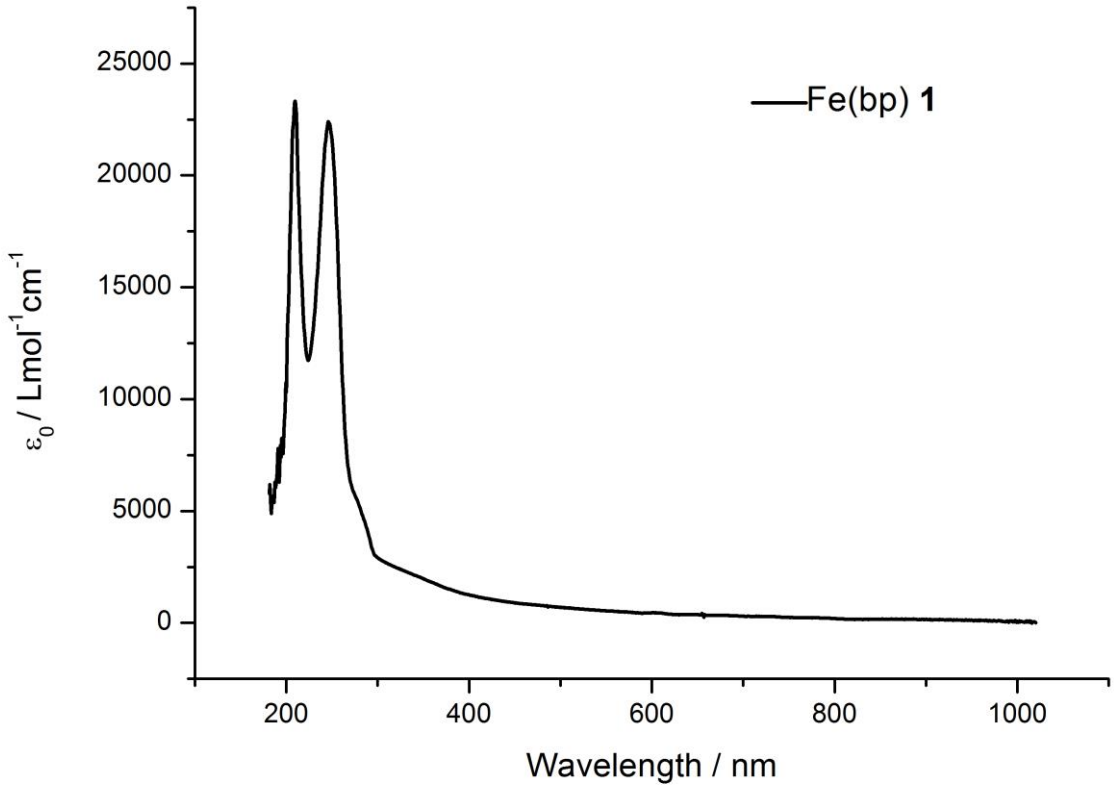

Figure S38. UV-Vis-spectrum of **1** in *n*-pentane.

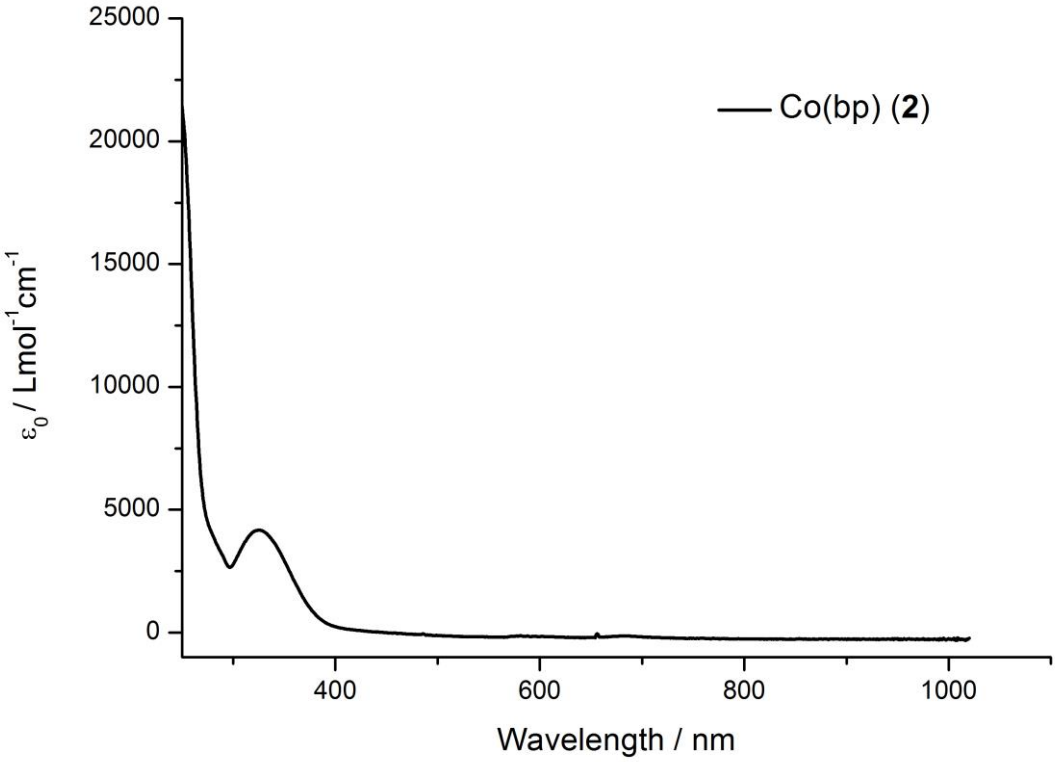

Figure *S*39. UV-Vis-spectrum of **2** in Et_2O.

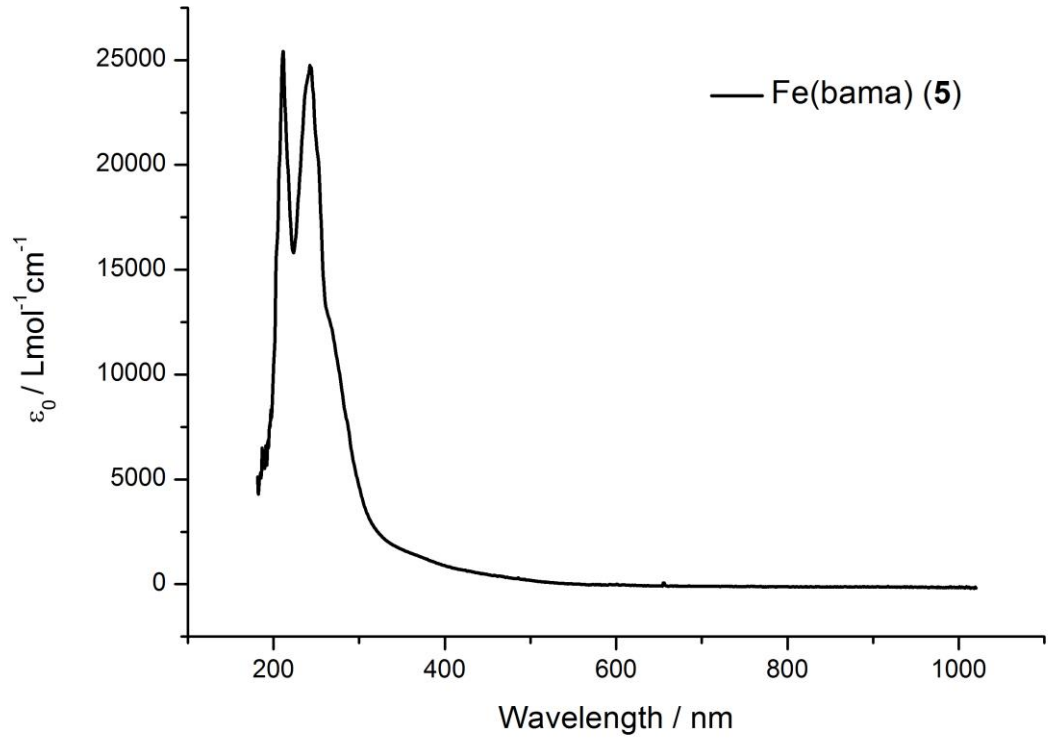

Figure S40. UV-Vis spectrum of **5** in *n*-pentane.

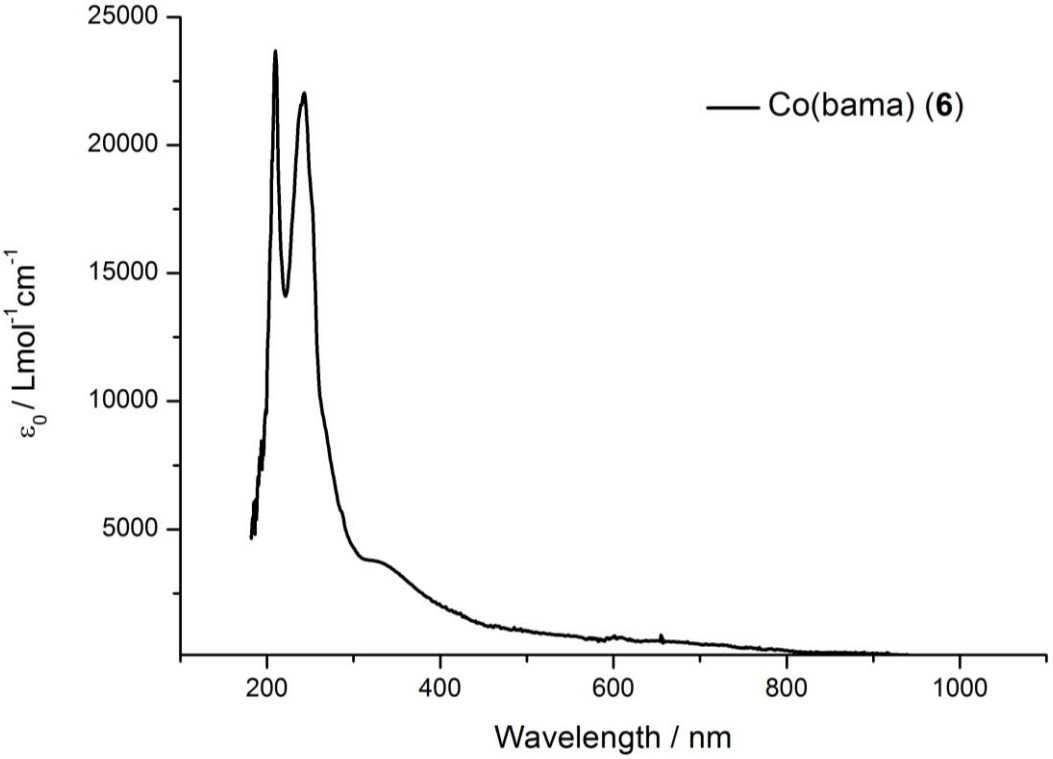

Figure S41. UV-Vis spectrum of **6** in *n*-pentane.

Cyclic voltammetry

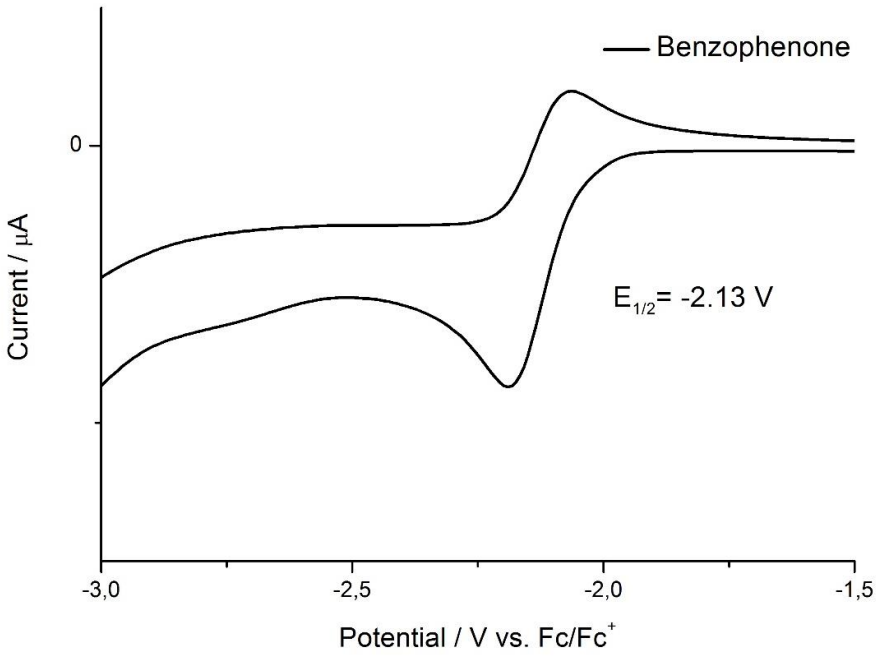

Figure S42. Cyclic voltammogram of benzophenone in propylene carbonate (1 mM, 200 mV·s^{-1}, 0.1 M [NnBu$_4$][PF$_6$]).

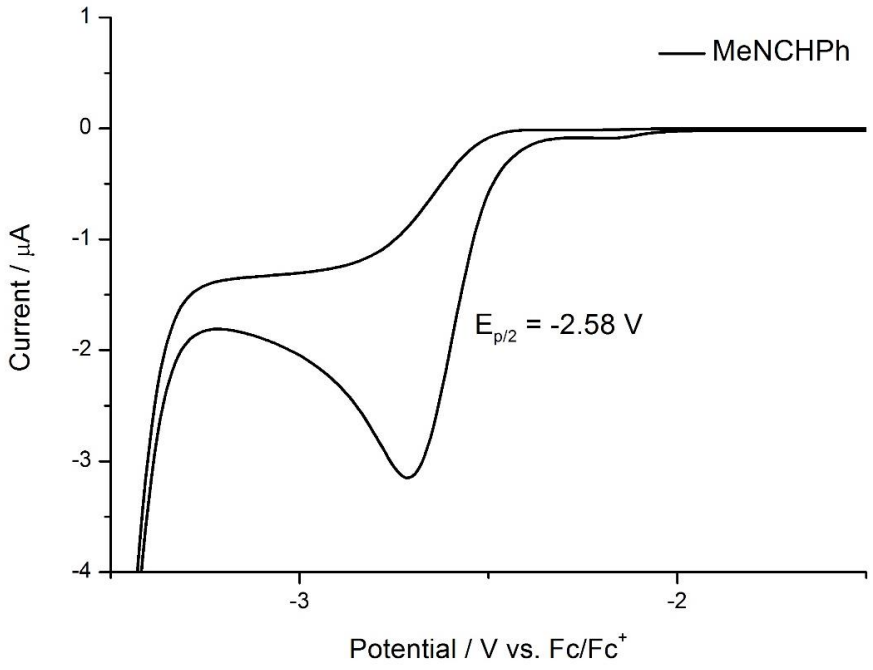

Figure S43. Cyclic voltammogram of benzaldehyde methylamine in propylene carbonate (1 mM, 200 mV·s^{-1}, 0.1 M [NnBu$_4$][PF$_6$]).

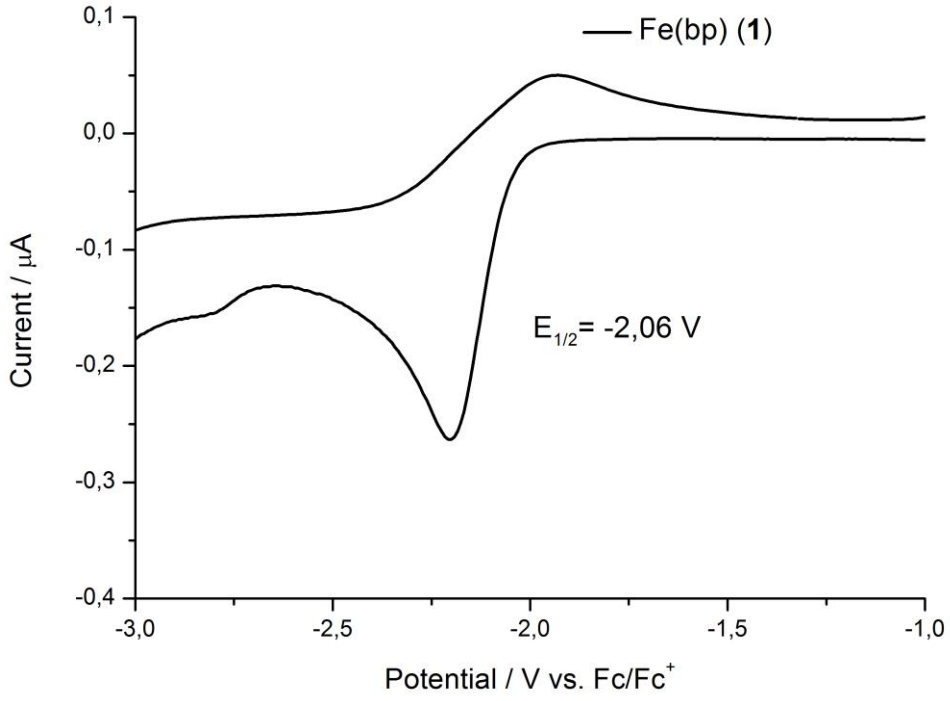

Figure S44. Cyclic voltammogram of **1** in propylene carbonate (1 mM, 200 mV·s^{-1}, 0.1 M [NnBu$_4$][PF$_6$]).

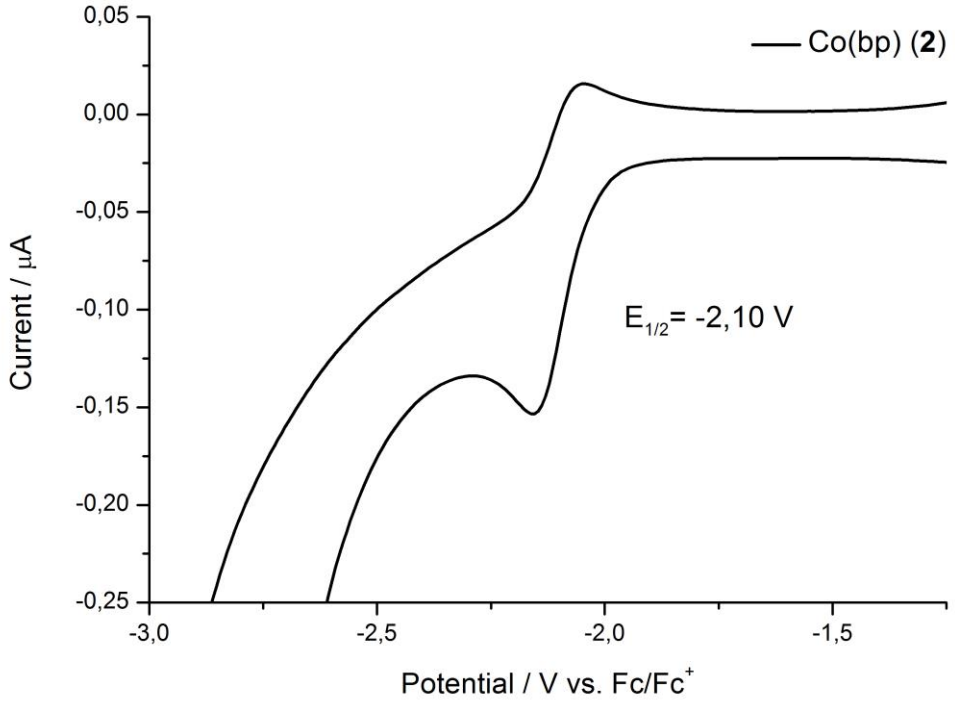

Figure S45. Cyclic voltammogram of **2** in propylene carbonate (1 mM, 200 mV·s^{-1}, 0.1 M [NnBu$_4$][PF$_6$]).

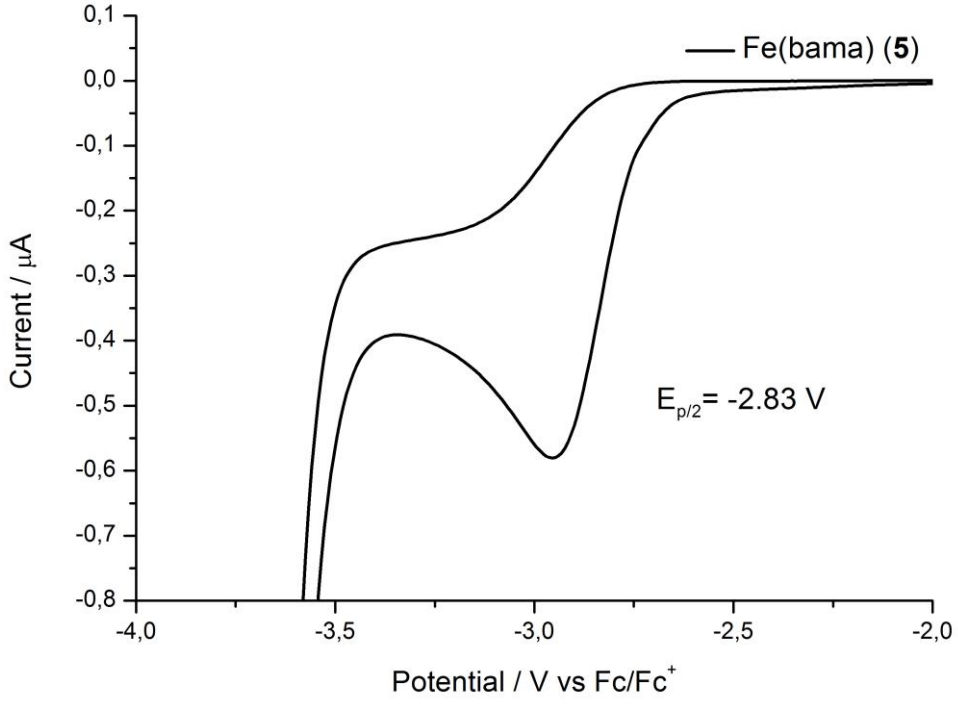

Figure S46. Cyclic voltammogram of **5** in propylene carbonate (1 mM, 200 mV·s^{-1}, 0.1 M [NnBu$_4$][PF$_6$]).

Magnetic measurements

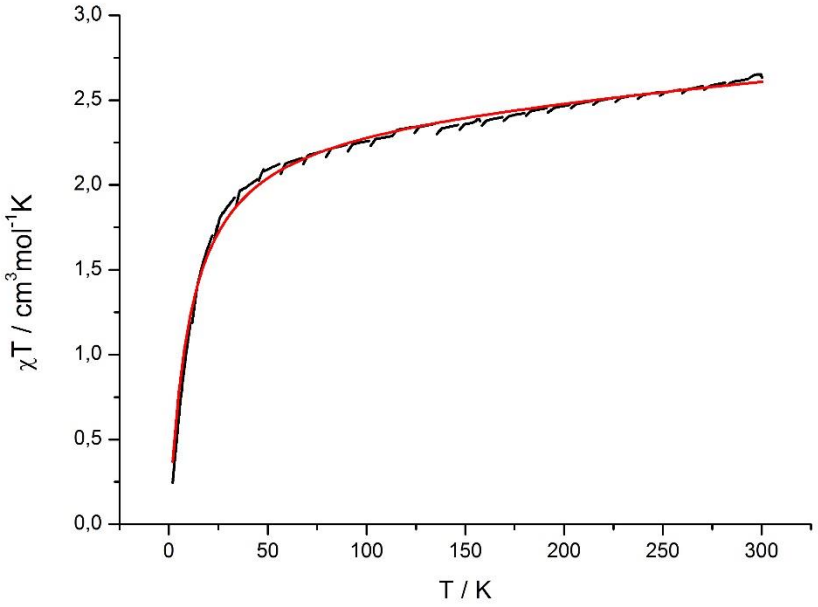

Figure S47. Temperature dependence of the molar magnetic susceptibility times temperature product (χT vs T) for compound K{18c6}[**1**]. Data were collected under an applied dc field of 7.16 ·10^6 A/m in a temperature range of 1 to 300 K. Molar diamagnetic correction = −5.22 x 10^{-4} emu mol^{-1}, χ_{TIP} = 9.08 (3) x 10^{-4} emu mol^{-1}, μ_{eff} = 4.398 (7) μ_B f.u.$^{-1}$ (f.u. = formula unit), χ_MT = 2.64 cm^3 mol^{-1} K (300K), Θ = –10.64(14) K.

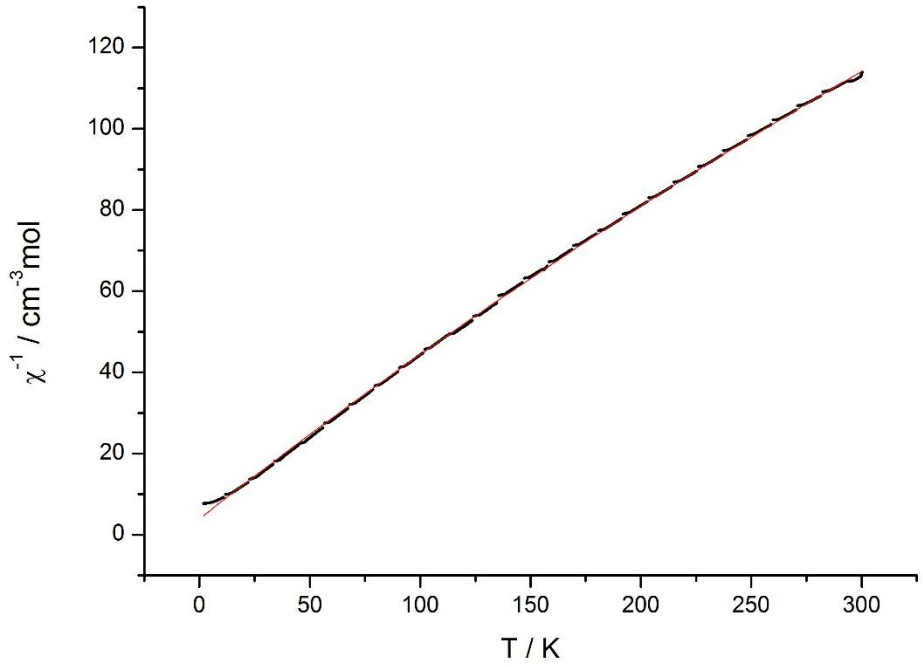

Figure S48. Reciprocal molar magnetic susceptibilities (χ^{-1}) for compound K{18c6}[**1**]. Data were collected under an applied dc field of 7.16 ·10^6 A/m in a temperature range of 3 to 300 K.

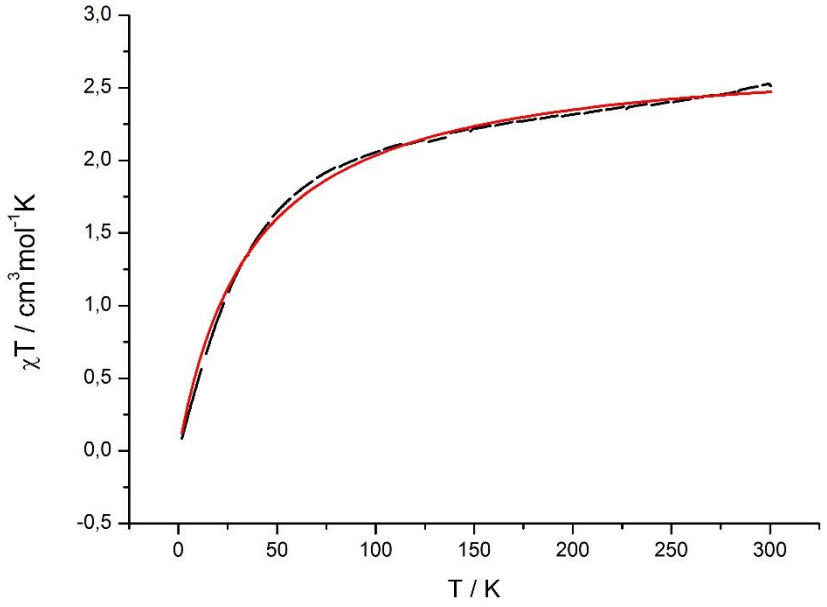

Figure S49. Temperature dependence of the molar magnetic susceptibility times temperature product (χT vs T) for compound K{18c6}[**2**]. Data were collected under an applied dc field of 7.16 ·10^6 A/m in a temperature range of 1 to 300 K. Molar diamagnetic correction = −5.22 x 10^{-4} emu mol^{-1}, χ_{TIP} = 9.72 (528) x 10^{-5} emu mol^{-1}, μ_{eff} = 4.745 (16) μ_B f.u.$^{-1}$ (f.u. = formula unit), χ_MT = 2.53 cm^3 mol^{-1} K (300K), Θ = – 7.72(53) K.

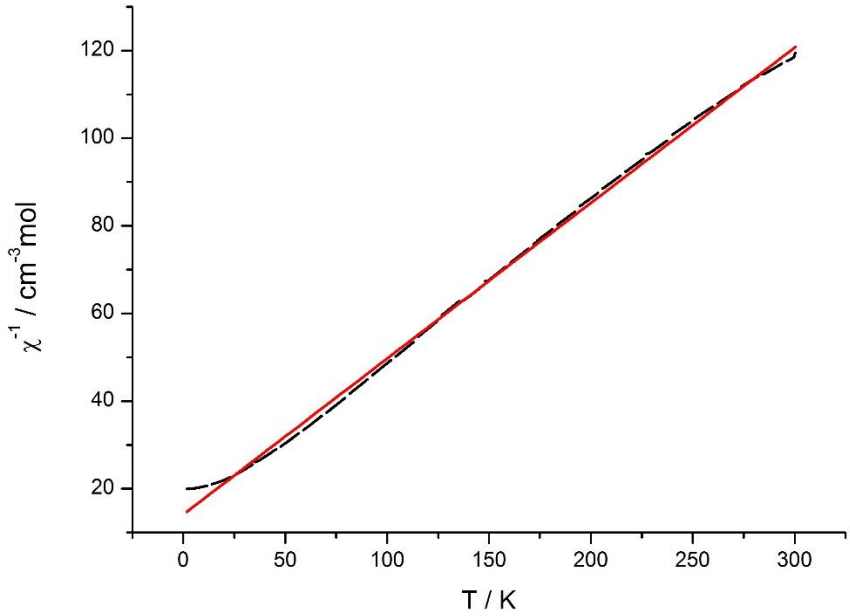

Figure S50. Reciprocal molar magnetic susceptibilities (χ^{-1}) for compound K{18c6}[**2**]. Data were collected under an applied dc field of 7.16 ·10^6 A/m in a temperature range of 3 to 300 K.

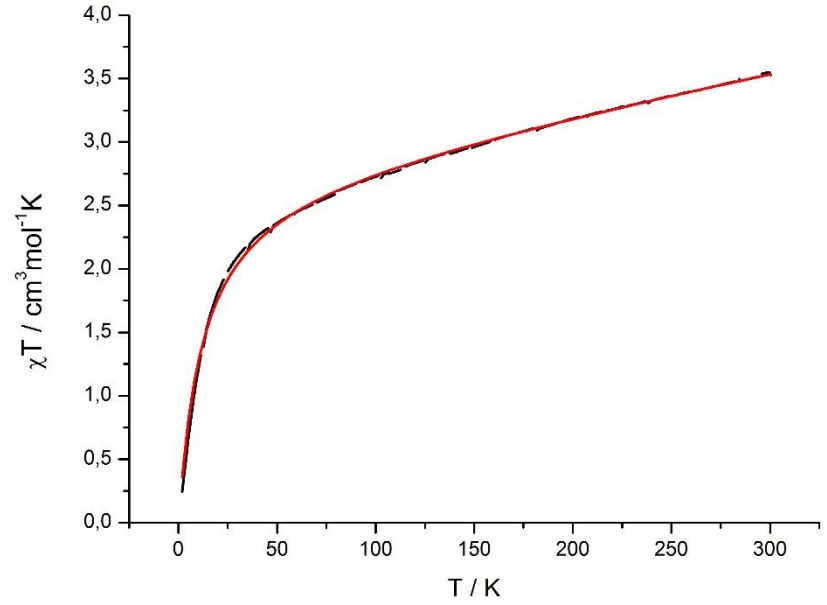

Figure S51. Temperature dependence of the molar magnetic susceptibility times temperature product (χT vs T) for compound K{18c6}[**5**]. Data were collected under an applied dc field of 7.16 ·10^6 A/m in a temperature range of 1 to 300 K. Molar diamagnetic correction = −5.03 x 10^{-4} emu mol^{-1}, χ_{TIP} = 3.05 (2) x 10^{-3} emu mol^{-1}, μ_{eff} = 4.667 (6) μ_B $f.u.^{-1}$ (f.u. = formula unit), χ_MT = 3.53 cm^3 mol^{-1} K (300K), Θ = – 1.99(11) K.

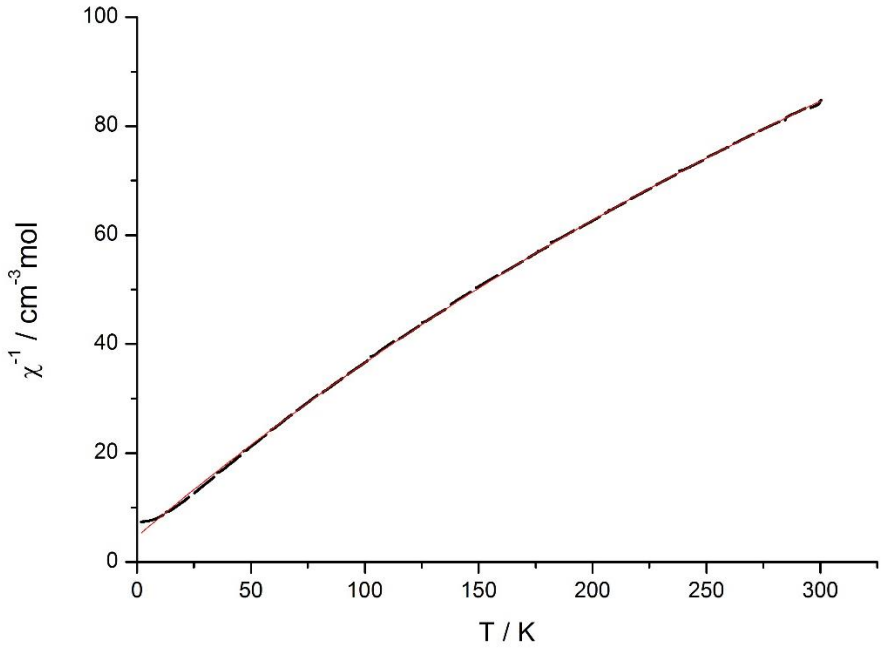

Figure S52. Reciprocal molar magnetic susceptibilities (χ^{-1}) for compound K{18c6}[**5**]. Data were collected under an applied dc field of 7.16 ·106 A/m in a temperature range of 3 to 300 K.

^{57}Mößbauer Spectra

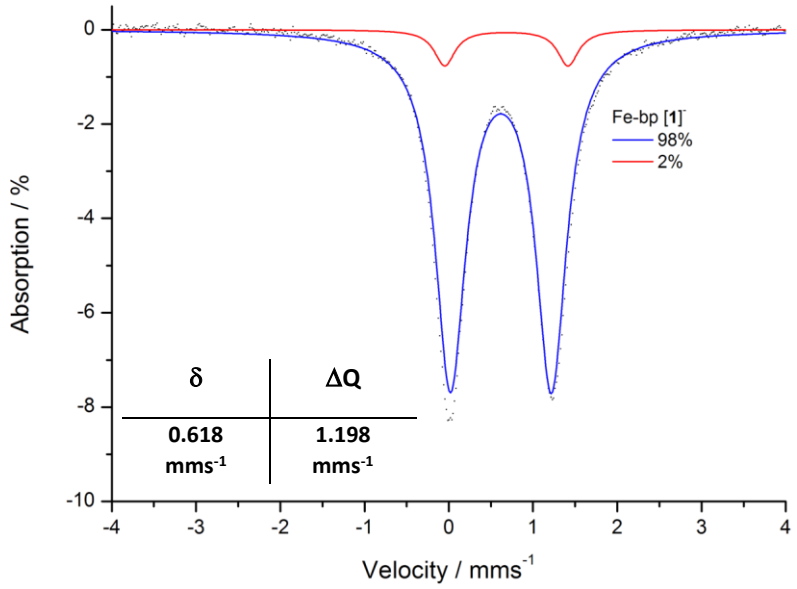

Figure S53. Zero field ^{57}Mössbauer spectrum of K{18c6}[**1**] at 15 K. The blue line represents a fit with $\delta = 0.618$ mms^{-1}, $\Delta Q = 1.198$ mms^{-1}, which can be assigned to K{18c6}[**1**] (98%). The red line represents a fit with $\delta = 0.684$ mms^{-1}, $\Delta Q = 1.468$ mms^{-1} which can be assigned to an unknown decomposition product (2%).

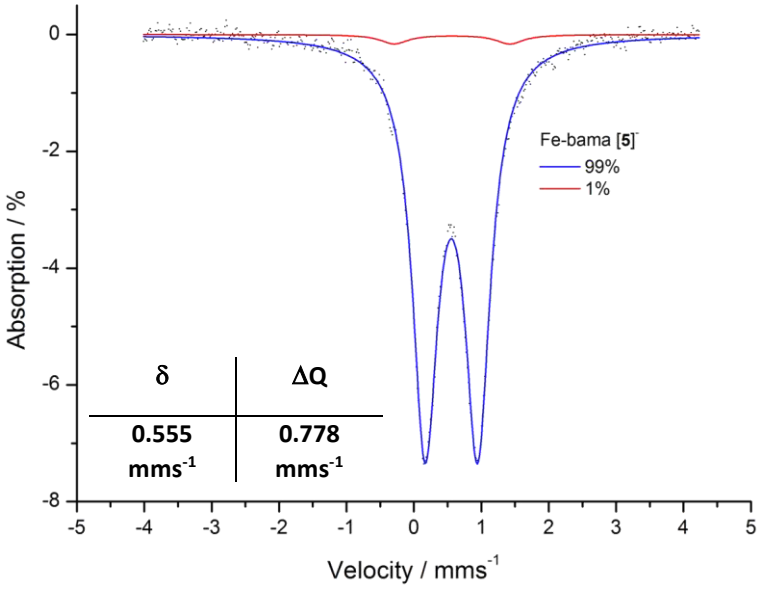

Figure S54. Zero field ^{57}Mössbauer spectrum of K{18c6}[**5**] at 15 K. The blue line represents a fit with $\delta = 0.555$ mms^{-1}, $\Delta Q = 0.778$ mms^{-1}, which can be assigned to K{18c6}[**5**] (99%). The red line represents a fit with $\delta = 0.558$ mms^{-1}, $\Delta Q = 1.763$ mms^{-1} which can be assigned to an unknown decomposition product (1%).

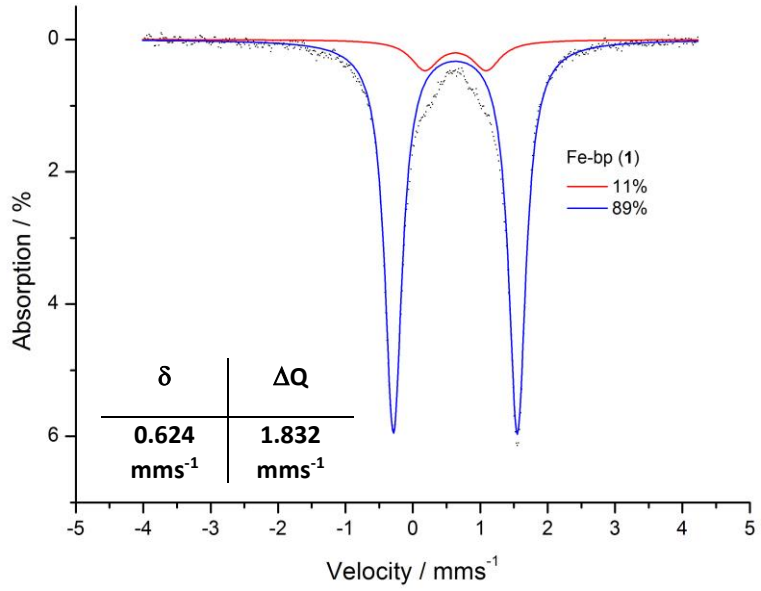

Figure S55. Zero field ^{57}Mössbauer spectrum of **1** at 15 K. The blue line represents a fit with $\delta = 0.624$ mms^{-1}, $\Delta Q = 1.832$ mms^{-1}, which can be assigned to **1** (89%). The red line represents a fit with $\delta = 0.627$ mms^{-1}, $\Delta Q = 0.912$ mms^{-1} which can be assigned to an unknown decomposition product (11%).

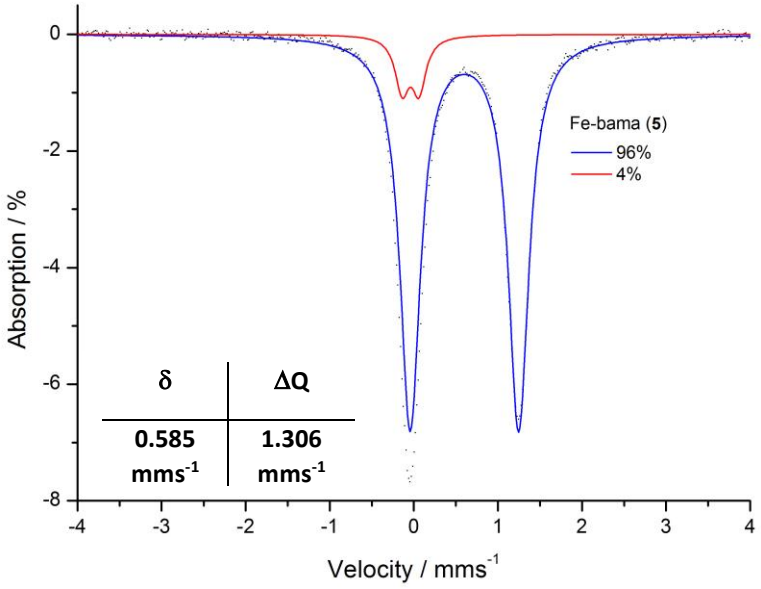

Figure S56. Zero field ^{57}Mössbauer spectrum of **5** at 15 K. The blue line represents a fit with $\delta = 0.585$ mms^{-1}, $\Delta Q = 1.306$ mms^{-1}, which can be assigned to **8** (96%). The red line represents a fit with $\delta = 0.036$ mms^{-1}, $\Delta Q = 0.117$ mms^{-1} which can be assigned to an unknown decomposition product (4%).

EPR spectroscopy

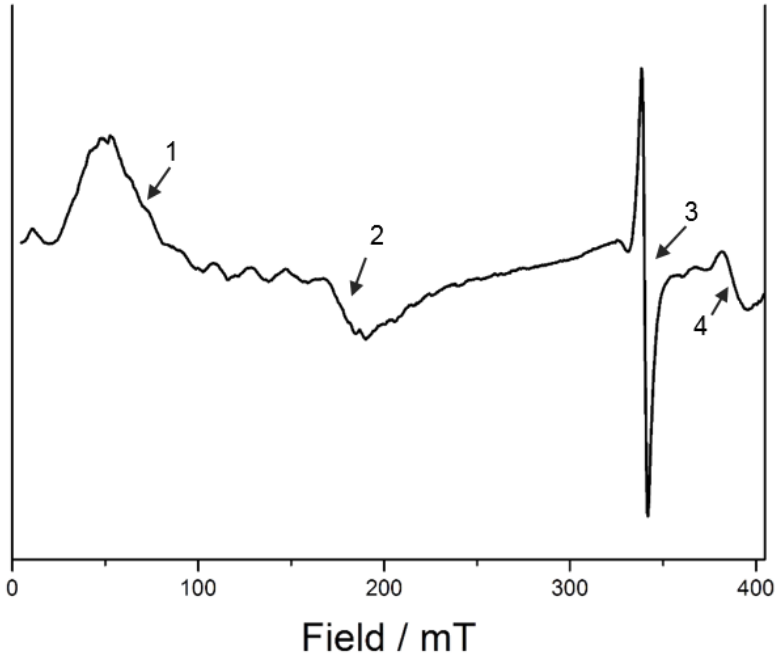

Figure S57. X-band EPR measurement of K(18c6)[**2**] in frozen toluene solution (9.514075 GHz) collected at 4.0 K. g-values at positions 1 – 4 are as following: 1: g = 10.0; 2: g = 3.84; 3: g = 2.00; 4: g= 1.75.

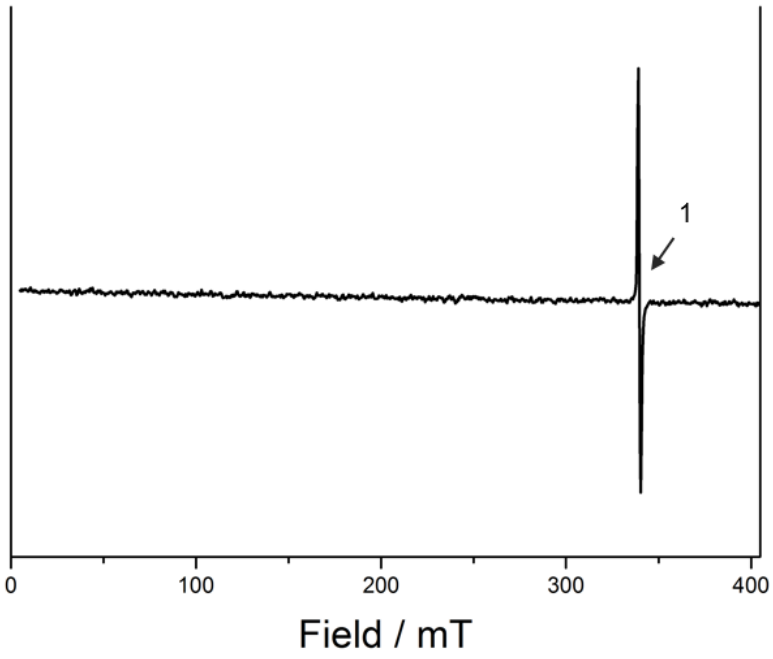

Figure S58. X-band EPR measurement of K(18c6)[**2**] in frozen toluene solution (9.514075 GHz) collected at 80 K. g-values at position 1: g = 2.03.

Computational Details

All calculations were performed with ORCA v4.2.1.[6,7] Two computational strategies were applied, relying either (1.) on the structural parameters from the solid-state structures, or (2.) optimized structural parameters. Both methods gave consistent results.

1. The positions of all hydrogen atoms were optimized (*optimizehydrogens true*) using the structural parameters from the solid-state structures and thus constraining the positions of all other atoms. Single point calculations were performed using the PBE,[8] BP86,[9] TPSS,[10] PBE0,[11] B3LYP,[12–15] TPSSh,[16,17] and M06[18] functionals (Table S6). Significant spin-contamination was observed for the hybrid functionals (Table S9). Scalar relativistic effects were modeled using the Zeroth Order Regular Approximation (ZORA) and the ZORA-def2-TZVPPbasis set and the segmented relativistically recontracted all-electrons basis set SARC for Fe, Co and the def2-TZVPP[19] basis set for all other elements.[20][21–23][8,19,24,25] The D3[25] dispersion correction with Becke-Johnson[24] damping was used for all functionals except M06, in which case the D3 zero-damped correction was used. The RI[26] approximations with the related auxiliary basis sets (*SARC/J*)[27] were used to reduce computation time. For meta-GGA and hybrid functionals, the RIJCOSX approximation was used with the same auxiliary basis set.[28,29] Tighter-than-default scf (*tightscf*) criteria was applied, in addition to finer-than-default grid values (*grid6*, *nofinalgrid*, gridx6). For benchmarking (Fig. S65 – S75 and Table S11), absorption spectra were modeled by time-dependent DFT calculations (TD-DFT) using as well the ZORA-def2-TZVPP basis set and the same set of functionals (PBE, BP86, TPSS, PBE0, M06, TPSSh). 70 roots were computed and solvation effects were considered with the SMD solvation model using the parameters for the experimentally used solvent (diethyl ether).[30] The Tamm-Dancoff approximation[31] was used; for the PBE and PBE0 functionals spectra were also computed without the Tamm-Dancoff approximation (Fig. S66 – S67 and S69 – 70; 25 roots). Broken-symmetry DFT calculations were carried out. The effective exchange integral J_{AB} was calculated from the broken-symmetry DFT wavefunction by using $J_{AB} = (E^{LS} - E^{HS}) / (\langle S^2 \rangle^{HS} - \langle S^2 \rangle^{LS})$, with E and $\langle S^2 \rangle$ the total energy and total spin angular momentum for the high- and low-spin states, respectively (Table S20).[32] Further, CASSCF/NEVPT2 calculations were carried out at the triple-ζ level of theory (ZORA-def2-TZVPP), with active spaces of (11,10) and (12,10) for Fe and Co, respectively (Table S15).[33,34] The active space was chosen as to include the 3d-orbitals, and a set of two ligand-centred π and π* orbitals (Fig. S76 – S80). Quasi-restricted orbitals (QROs, Fig. 63)[35] and intrinsic bond orbitals (IBOs, Fig. 64)[36] were calculated, and were visualized using Chemcraft[37] and IBOview.[38]

2. The structural parameters of the ground- (S = 3/2 for Fe, S = 5/2 for Co) and excited spin states (S = 5/2 for Fe, S = 7/2 for Co) were optimized at the ZORA-PBE-D3(BJ)/def2-SVP level of theory with the def2-TZVP basis for the metal atoms (Table S2-S6). The RI (for GGA functionals) and RIJCOSX (for meta-GGA and hybrid functionals) approximations with the auxiliary basis set SARC/J were used to reduce computation time. Tighter-than-default scf (*tightscf*) and optimization (*tightopt*) criteria were applied, in addition to finer-than-default grid values (*grid6*, *nofinalgrid*, gridx6). Single-point calculations at ZORA-PBE-D3(BJ)/def2-TZVPP level of theory gave adiabatic triplet-quintet and quartet-sextet gaps that were consistent with those obtained with strategy 1 (Table S8). The structural parameters of neutral complexes **1**, **2**, and **5** were as well optimized, along with that of the neutral and anionic forms of the ligand (benzophenone and the related ketyl radical, benzimine and the iminyl radical, and *N*-methylbenzaldimine and the benzaldiminyl radical). For benchmarking, the ground state of [**1**]$^-$ was as well optimized with BP86[9] and PBE0[39] as well as using the composite methods PBEh-3c[40] and BP97-3c[41] (Table S17 – S18). Default convergence criteria were used for the composite methods. The PBE functional gave an accurate prediction of the C–O and C–N bond lengths, and overall good agreement with the experimental parameters. All optimized structures were verified as true minima by the absence (*Nimag* = 0) of negative eigenvalues in the harmonic vibrational frequency analysis. In one case (PBEh-3c), a minor imaginary frequency is attributed to the loose default convergence criteria of the method.

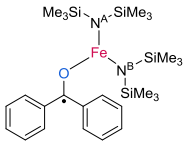

[**1**]$^-$

	B97-3c	PBEh-3c	PBE	PBE0	BP86
Fe–N^A in [Å]	0.025	0.007	0.033	0.017	0.049
Fe–N^B in [Å]	0.031	0.001	0.049	0.025	0.058
Fe–O in [Å]	0.072	0.039	0.087	0.053	0.083
C–O in [Å]	0.045	0.053	0.042	0.053	0.036
Mean Deviation	0.043	0.025	0.053	0.037	0.057

Table S2. The PBE functional gives a good fit for the structural parameters in [**1**]$^-$ in reference to the solid-state structure. This is especially true for the C–O bond length (strategy 1).

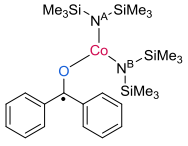

[**2**]$^-$

	B97-3c	PBEh-3c	PBE	PBE0	BP86
Co–N^A in [Å]	0.026	0.011	0.042	0.017	0.052
Co–N^B in [Å]	0.042	0.006	0.066	0.029	0.074

Co–O in [Å]	0.003	0.003	0.000	0.005	0.014
C–O in [Å]	0.024	0.021	0.015	0.021	0.011
Mean Deviation	0.024	0.010	0.031	0.018	0.038

Table S3. The PBE functional gives a good fit for the structural parameters in [**2**]$^-$ in reference to the solid-state structure. This is especially true for the C–O bond length (strategy 1).

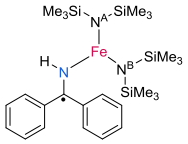

[**3**]$^-$

	B97-3c	**PBEh-3c**	**PBE**	**PBE0**	**BP86**
Fe–N^A in [Å]	0.025	0.005	0.038	0.018	0.050
Fe–N^B in [Å]	0.009	0.014	0.020	0.004	0.030
Fe–N in [Å]	0.020	0.088	0.001	0.047	0.009
C–N in [Å]	0.046	0.054	0.060	0.053	0.061
Mean Deviation	0.025	0.040	0.030	0.031	0.037

Table S4. The PBE functional gives a good fit for the structural parameters in [**3**]$^-$ in reference to the solid-state structure. This is especially true for the C–N bond (strategy 1).

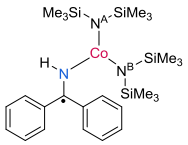

[**4**]$^-$

	B97-3c	**PBEh-3c**	**PBE**	**PBE0**	**BP86**
Co–N^A in [Å]	0.048	0.013	0.063	0.027	0.075
Co–N^B in [Å]	0.028	0.005	0.041	0.008	0.059
Co–N in [Å]	0.027	0.023	0.041	0.021	0.050
C–N in [Å]	0.016	0.001	0.002	0.000	0.003
Mean Deviation	0.030	0.010	0.037	0.014	0.047

Table S5. The PBE functional gives a good fit for the structural parameters in [**4**]$^-$ in reference to the solid-state structure. This is especially true for the C–N bond (strategy 1).

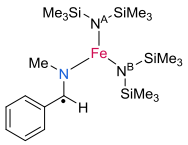

[**5**]$^-$

	B97-3c	**PBEh-3c**	**PBE**	**PBE0**	**BP86**
Fe–N^A in [Å]	0.030	0.005	0.031	0.016	0.042
Fe–N^B in [Å]	0.018	0.003	0.022	0.013	0.033
Fe–Y in [Å]	0.003	0.034	0.018	0.003	0.029
C–N in [Å]	0.012	0.001	0.000	0.001	0.001
Mean Deviation	0.016	0.011	0.018	0.008	0.026

Table S6. The PBE functional gives a good fit for the structural parameters in [**5**]$^-$ in reference to the solid state structure. This is especially true for the C–N bond (strategy 1).

	PBE	**BP86**	**TPSS**	**PBE0**	**B3LYP**	**TPSSh**	**M06**	**CASSCF/NEVPT2**
***S* = 1/2**	1.04	1.03	0.95	-	-	-	1.79	2.09
***S* = 3/2**	0	0	0	0	0	0	0	0
***S* = 5/2**	0.26	0.28	0.27	0.15	0.18	0.20	0.16	0.16
***S* = 7/2**	3.57	3.61	3.77	4.12	4.14	3.98	3.93	-

Table S7. Computed vertical energy gaps in [eV] using strategy 1. All functionals as well as CASSCF/NEVPT2 give consistent results (strategy 2).

	[**1**]$^{-}$	[**2**]$^{-}$	[**3**]$^{-}$	[**4**]$^{-}$	[**5**]$^{-}$
E^{vert} **in [eV]**	0.26	0.31	0.50	0.33	0.41
E^{adia} **in [eV]**	0.25	0.22	0.36	0.08	0.31
***Deviation* in [eV]**	0.01	0.09	0.14	0.25	0.10

Table S8. The energy difference between the adiabatic and vertical quartet-sextet or triplet-quintet gaps of the anionic complexes [**1**]$^{-}$ to [**5**]$^{-}$ is small, at the ZORA-PBE-D3(BJ)/def2-TZVPP//ZORA-PBE-D3(BJ)/def2-TZVPP level of theory. This indicates the results obtained using strategy 1 are consistent with those obtained using strategy 2.

	PBE	**BP86**	**TPSS**	**PBE0**	**B3LYP**	**TPSSh**	**M06**
***S* = 1/2**	1.43	1.45	1.60	-	-	-	1.74
***S* = 3/2**	0.69	0.69	0.72	0.95	0.91	0.86	0.98
***S* = 5/2**	0.02	0.02	0.02	0.05	0.04	0.03	0.08
***S* = 7/2**	0.02	0.02	0.02	0.04	0.03	0.03	0.04

Table S9. The DFT calculations for [**1**]$^{-}$ show significant spin-contamination for $S = 1/2$ and moderate-to-high spin contamination for $S = 3/2$.

Spin Density	[**1**]$^{-}$	[**2**]$^{-}$	[**3**]$^{-}$	[**4**]$^{-}$	[**5**]$^{-}$
Carbon	-0.22	-0.21	-0.16	-0.17	-0.19
Metal	3.29	2.27	3.20	2.24	3.24

Table S 10. Hirshfeld spin density on the metal and the carbonyl/iminyl/aldiminyl carbon atom indicate a ligand-centred radical computed using strategy 1.

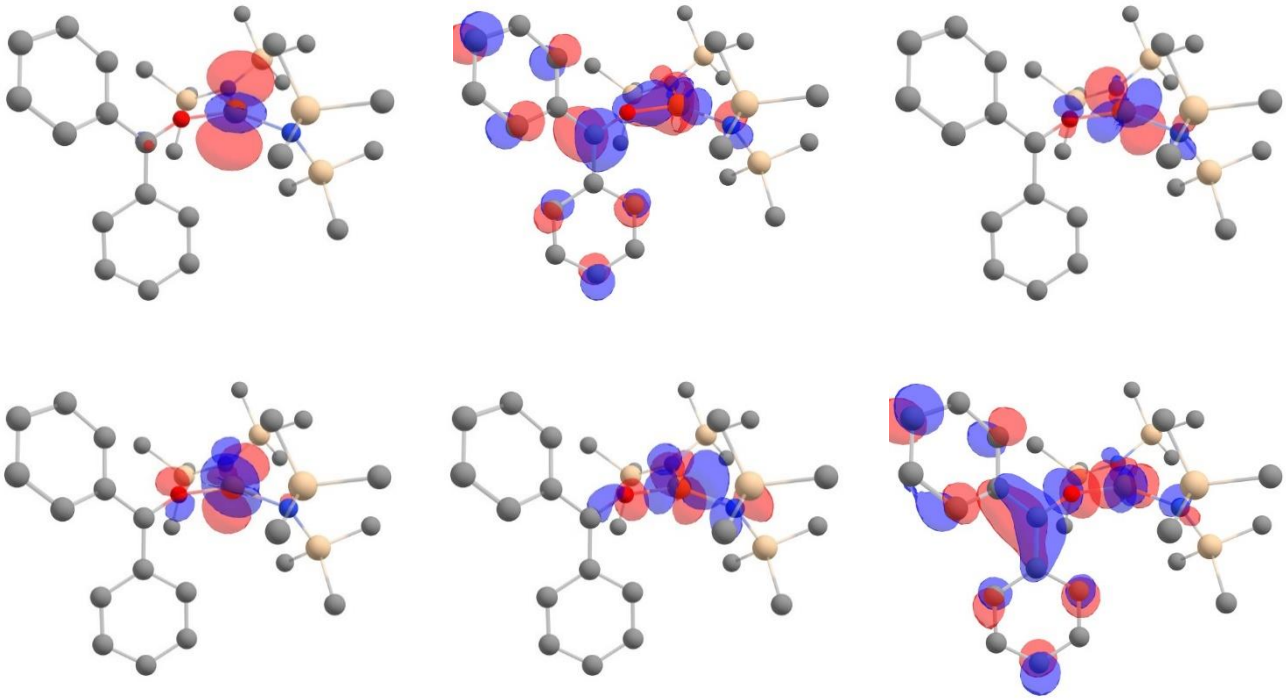

Figure S59. Quasi-restricted orbitals (QROs) associated with the metal in [**1**]$^{-}$ (S = 3/2) as obtained by the using strategy 1, with the PBE functional. The shape of the QROs is consistent with the CASSCF/NEVPT(2) results, indicating an antiferromagnetically coupled radical ligand. Analysis of the QROs of the respective high-spin states reveals the corresponding ferromagnetically coupled pair.

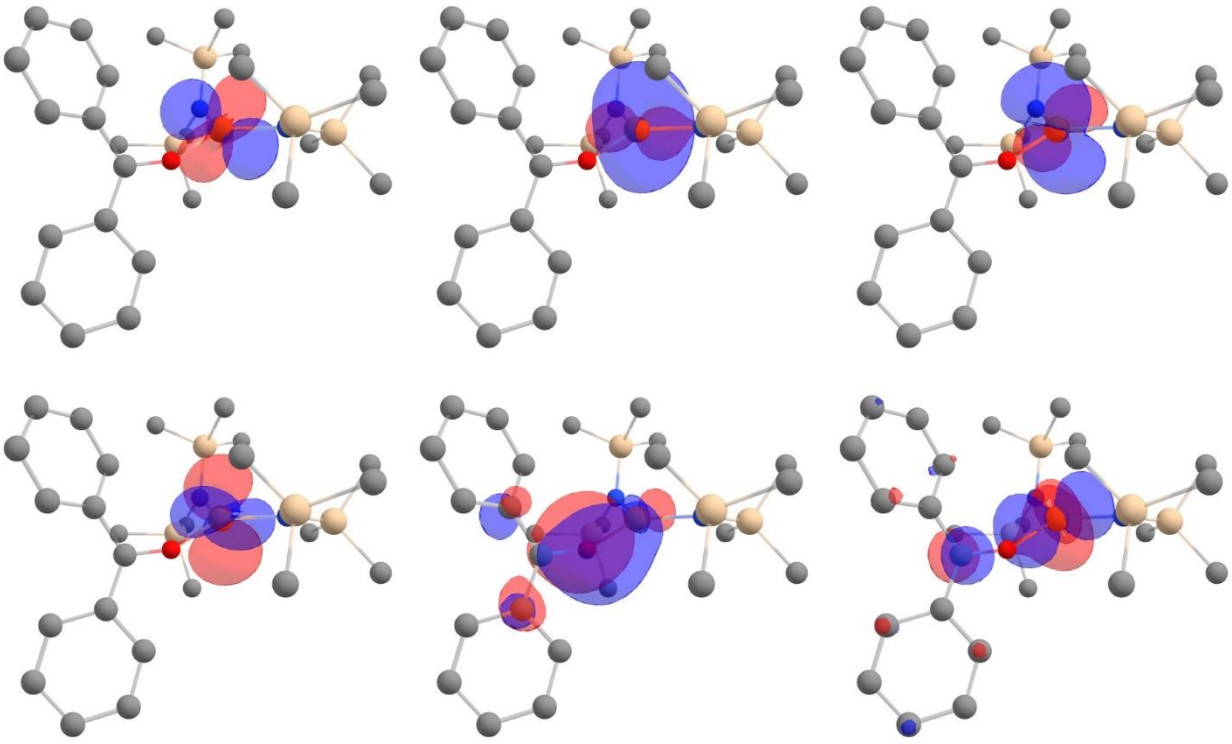

Figure S60. Intrinsic bond orbitals (IBOs) associated with the metal in [**1**]$^{-}$ (S = 3/2) as obtained by the using strategy 1, with the PBE functional. The shape of the IBOs is consistent with the CASSCF/NEVPT(2) results, indicating an antiferromagnetically coupled radical ligand. Analysis of the IBOs of the respective high-spin states reveals the corresponding ferromagnetically coupled pair.

	PBE	BP86	TPSS	PBE0	B3LYP	TPSSh	M06	Experimental
$\tilde{\nu}^1$ **in [cm-1] (*f*^{osc})**	18948 (0.16)	18431 (0.16)	19249 (0.11)	20906 (0.10)	23570 (0.1)	21841 (0.15)	23227 (0.09)	-
$\tilde{\nu}^2$ **in [cm-1] (*f*^{osc})**	18491 (0.13)	526 (0.11)	18115 (0.08)	19873 (0.08)	19093 (0.07)	20735 (0.05)	21218 (0.06)	-
$\tilde{\nu}^{max}$ **with broadening in [cm^{-1}] (f^{osc})**	18657	18622	18450	20367	20161	20964	21413	17123
Vertical energy gap in [eV]	2.313	2.309	2.288	2.525	2.500	2.599	2.655	2.123
Deviation from experiment in [eV]	0.190	0.186	0.165	0.402	0.377	0.476	0.532	-

Table S 11. Computed absorption wavenumbers $\tilde{\nu}^1$ and $\tilde{\nu}^2$ under the Tamm-Dancoff approximation, according to strategy 1 and intensities *f*^{osc}. The spectra were visualized with Gaussian broadening to better match the experimental maximal absorption frequency $\tilde{\nu}^{max}$. The PBE functional gives the best match with the experimental maximal absorption wavelength.

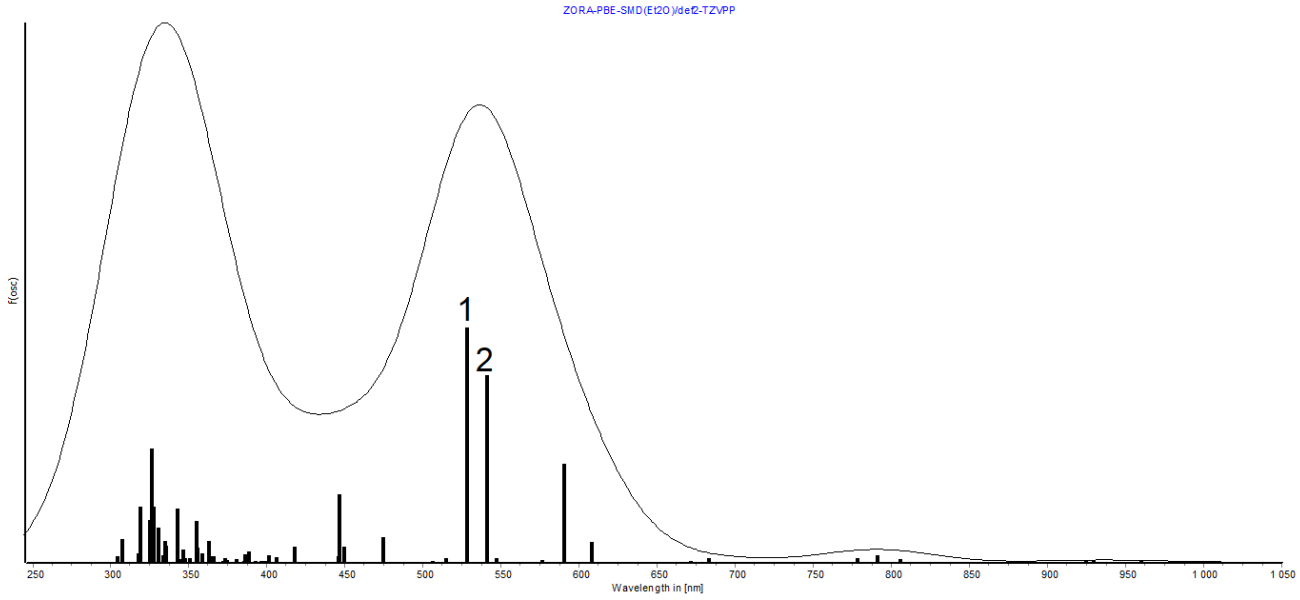

Figure S61. The computed UV-Visible spectrum at the ZORA-PBE-SMD(Et_2O)/def2-TZVPP level of theory (strategy 1). A Gaussian broadening of the spectral lines of 80 was applied to better match the experimental data. The PBE functional gives the best match to the experimental maximal absorption wavelength.

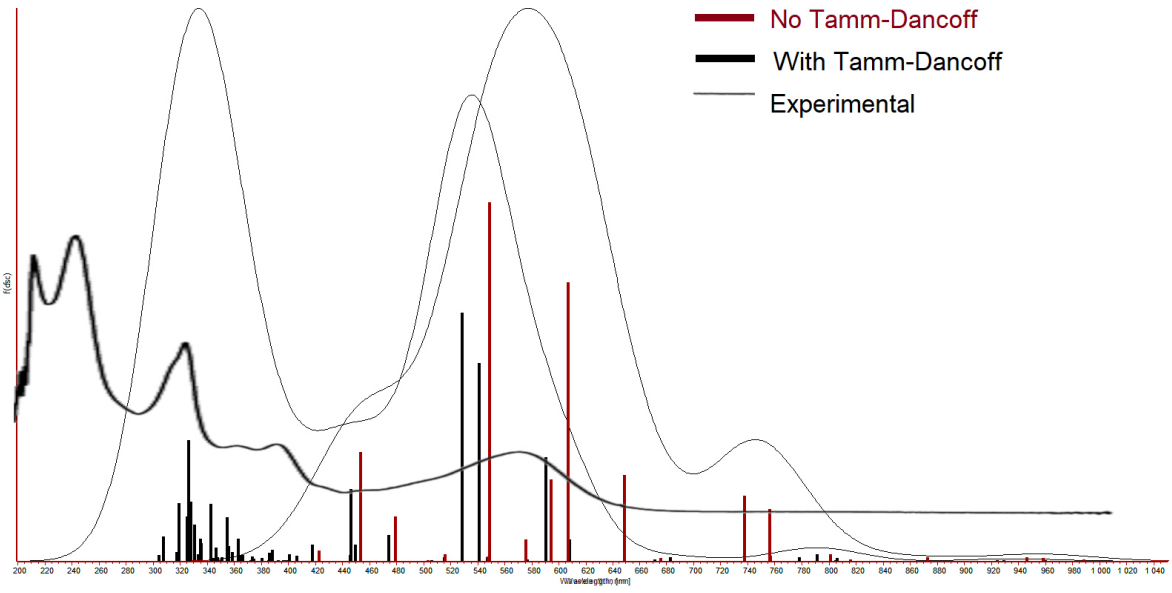

Figure S62. Computed UV-Visible spectrum at the ZORA-PBE-SMD(Et_2O)/def2-TZVPP level of theory (strategy 1), without applying the Tamm-Dancoff approximation (in red), compared to the Tamm-Dancoff spectrum (in black). A Gaussian broadening of the spectral lines of 80 was applied. The experimental spectrum is given for comparison. The two intense bands between 400 and 450 nm correspond to the π–π* transitions with MLCT character.

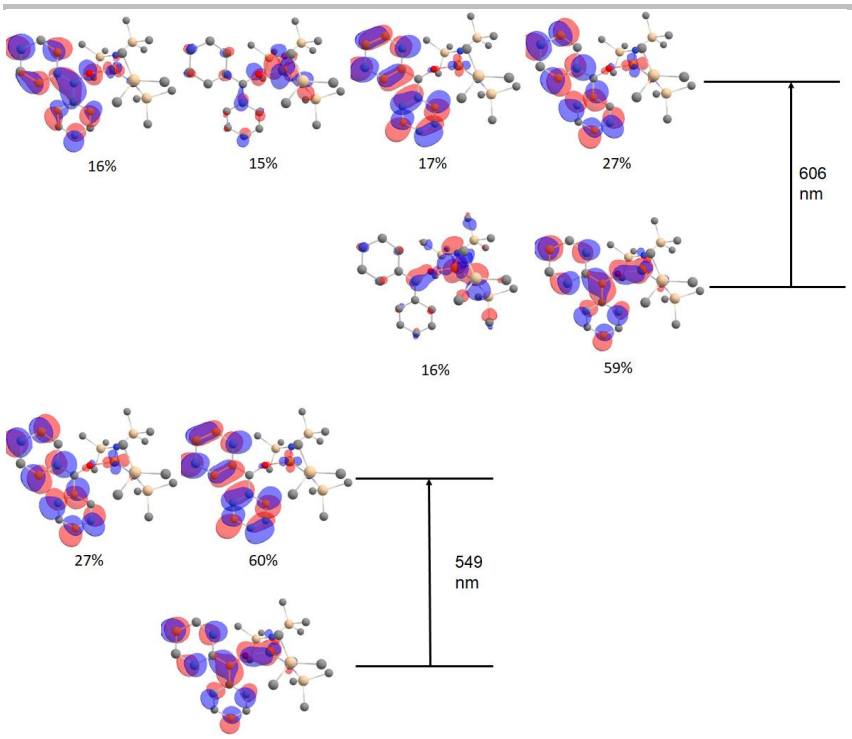

Figure S63. The two main absorption rays in the computed UV-Vis spectrum at the ZORA-PBE-SMD(Et_2O)/def2-TZVPP level of theory without the Tamm-Dancoff approximation correspond to the π–π* transitions with MLCT character. The Kohn-Sham orbitals composing each state are plotted.

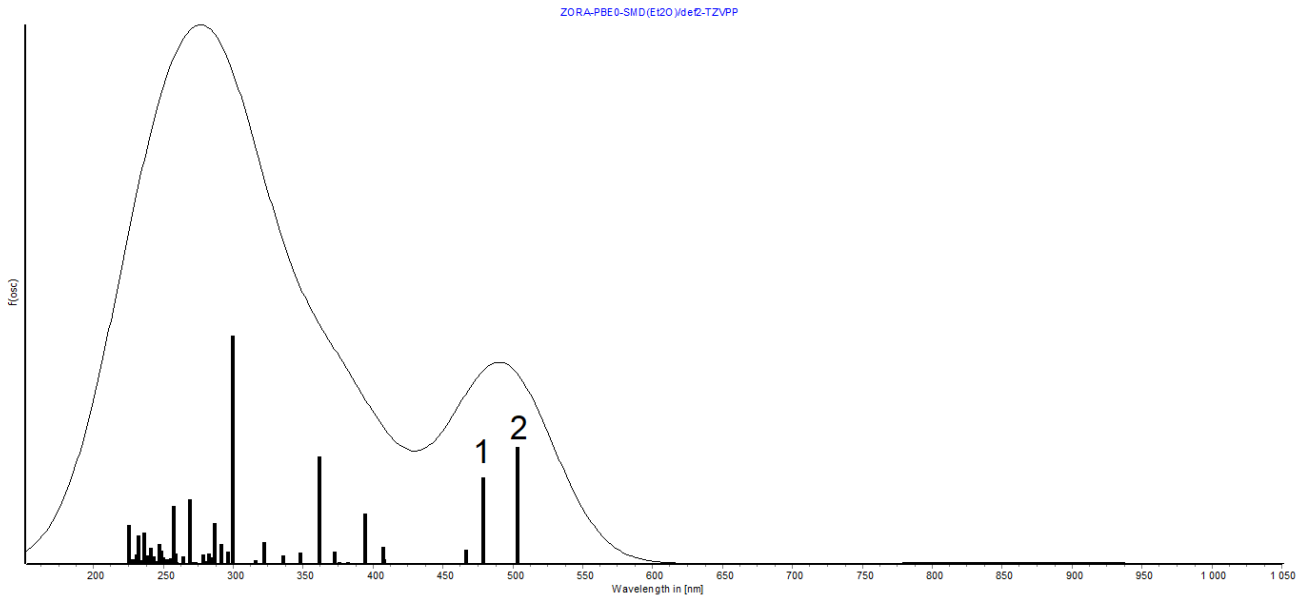

Figure S64. Computed UV-Visible spectrum at the ZORA-PBE0-SMD(Et_2O)/def2-TZVPP level of theory (strategy 1). A Gaussian broadening of the spectral lines of 80 was applied.

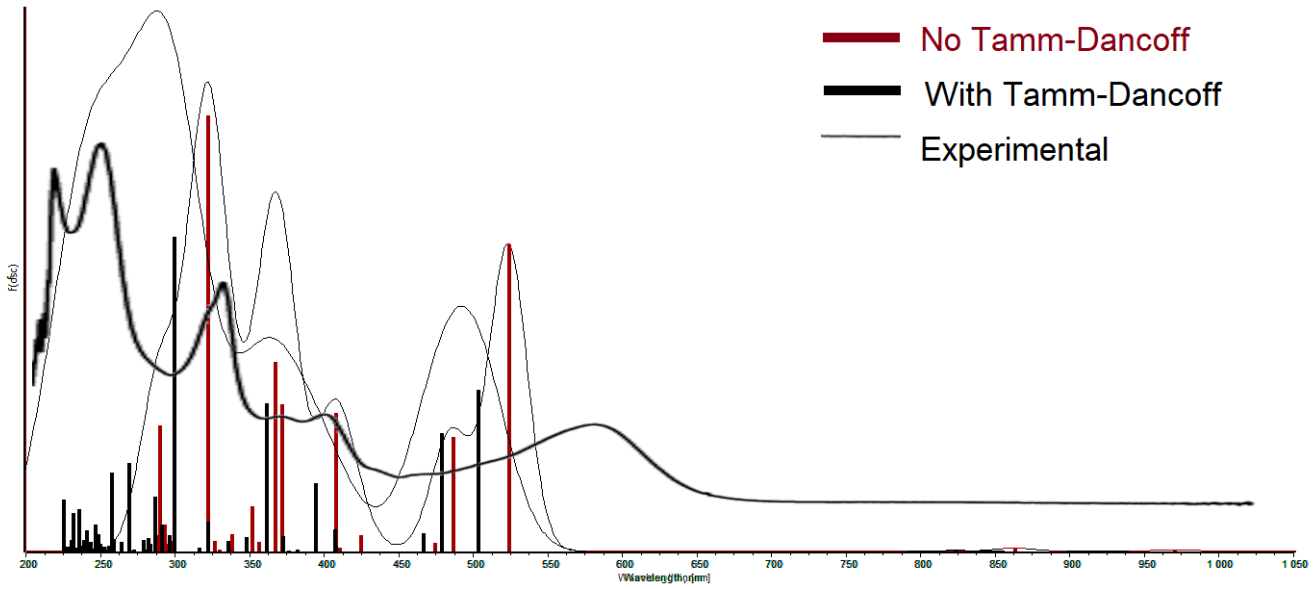

Figure S65. Computed UV-Visible spectrum at the ZORA-PBE0-SMD(Et_2O)/def2-TZVPP level of theory (strategy 1), without applying the Tamm-Dancoff approximation (in red), compared to the Tamm-Dancoff spectrum. A Gaussian broadening of the spectral lines of 50 was applied. The experimental spectrum is given for comparison. The two intense bands at 485 and 523 nm in the spectrum without Tamm-Dancoff approximation correspond to the π–π* transitions with MLCT character.

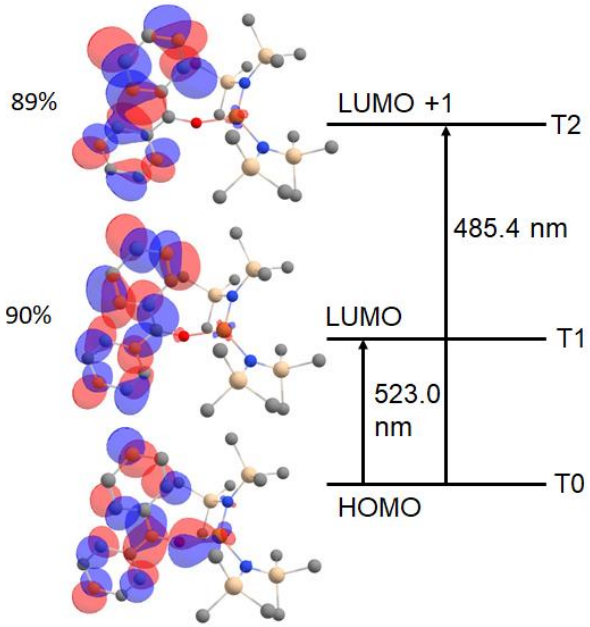

Figure 66. The two main absorption bands in the computed UV-Vis spectrum at the ZORA-PBE0-SMD(Et_2O)/def2-TZVPP level of theory without the Tamm-Dancoff approximation correspond to the π–π* transitions with MLCT character. The excited states T1 and T2 are mainly (~90%) composed of a single π* orbital.

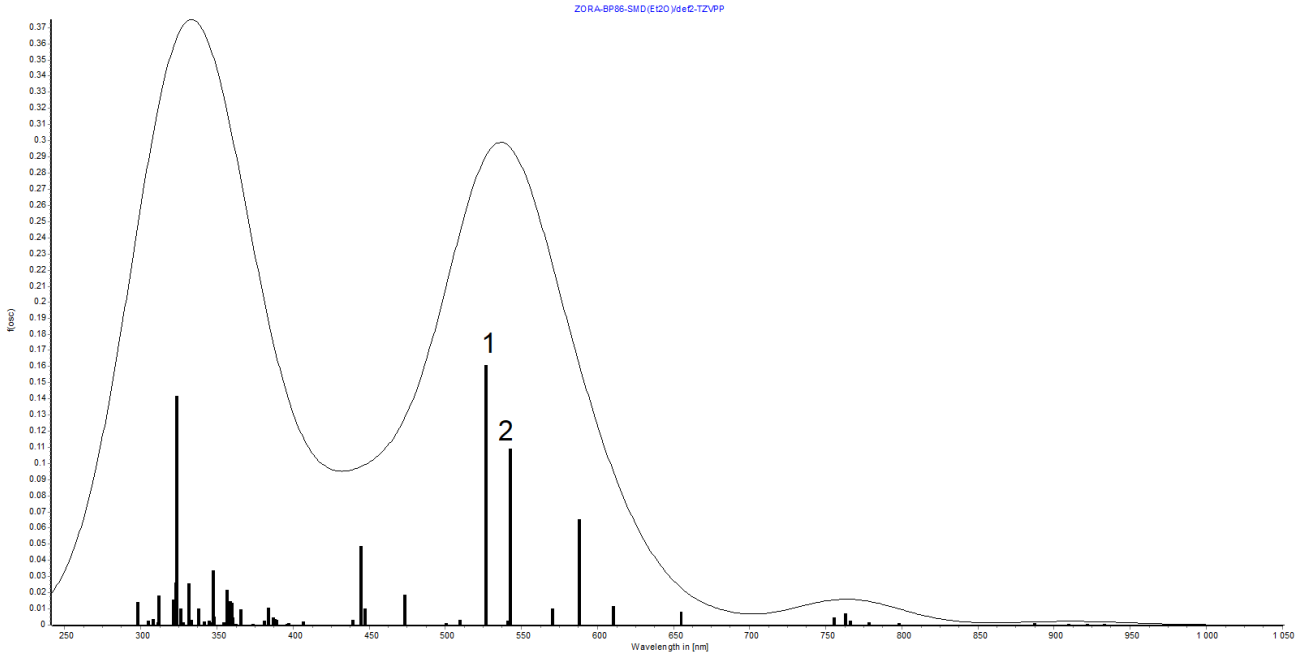

Figure S67. Computed UV-Visible spectrum at the ZORA-BP86-SMD(Et_2O)/def2-TZVPP level of theory (strategy 1). A Gaussian broadening of the spectral lines of 80 was applied.

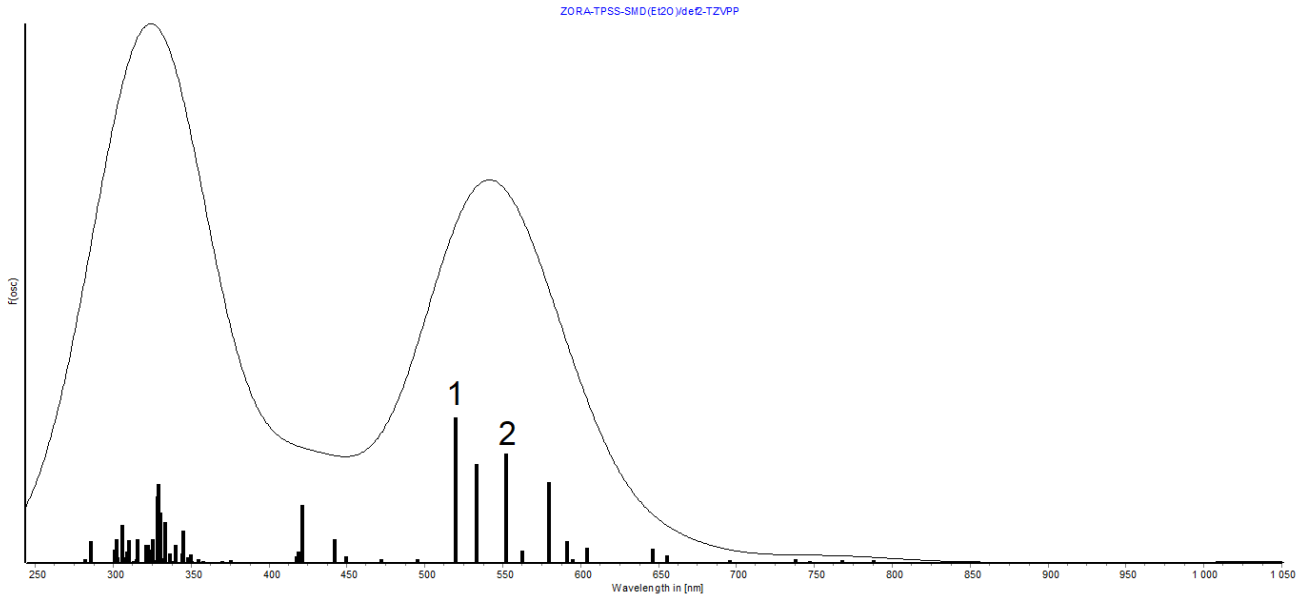

Figure S68. Computed UV-Visible spectrum at the ZORA-TPSS-SMD(Et_2O)/def2-TZVPP level of theory (strategy 1). A Gaussian broadening of the spectral lines of 80 was applied.

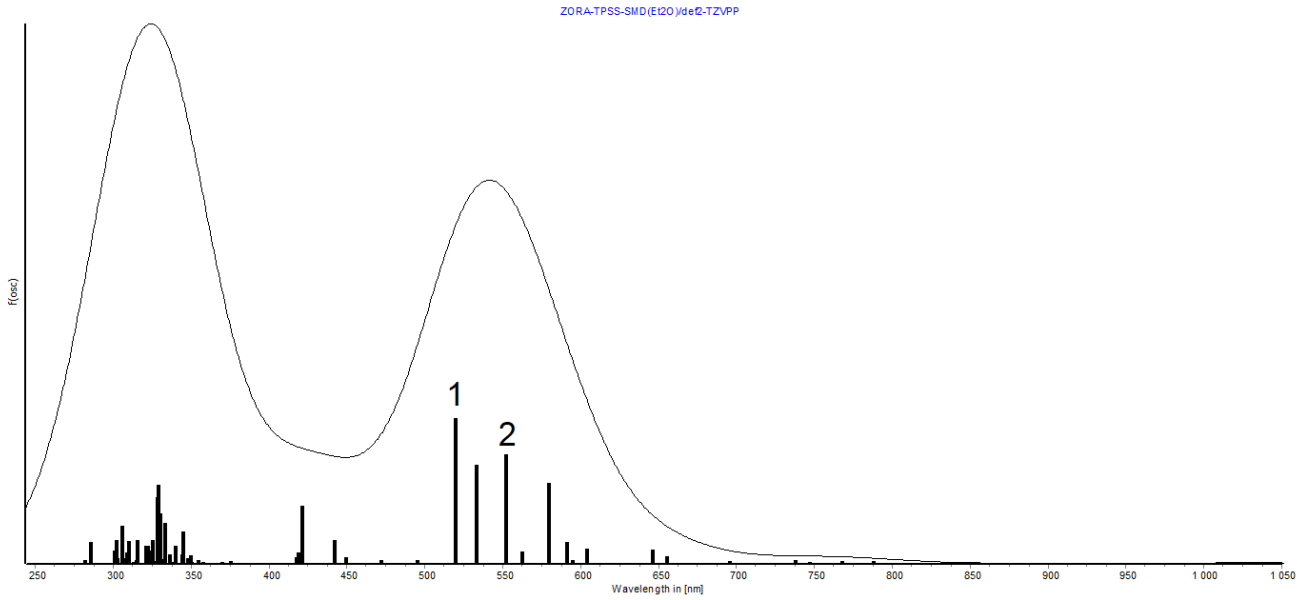

Figure S69. Computed UV-Visible spectrum at the ZORA-B3LYP-SMD(Et_2O)/def2-TZVPP level of theory (strategy 1). A Gaussian broadening of the spectral lines of 80 was applied.

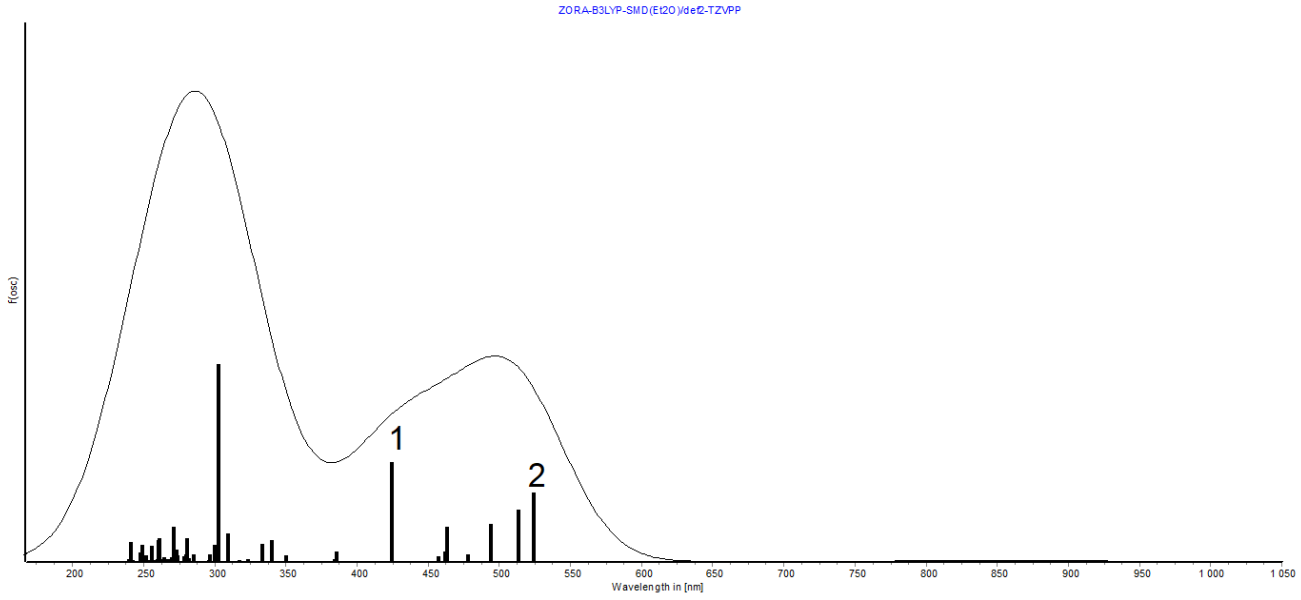

Figure S70. Computed UV-Visible spectrum at the ZORA-TPSSh-SMD(Et_2O)/def2-TZVPP level of theory (strategy 1). A Gaussian broadening of the spectral lines of 80 was applied.

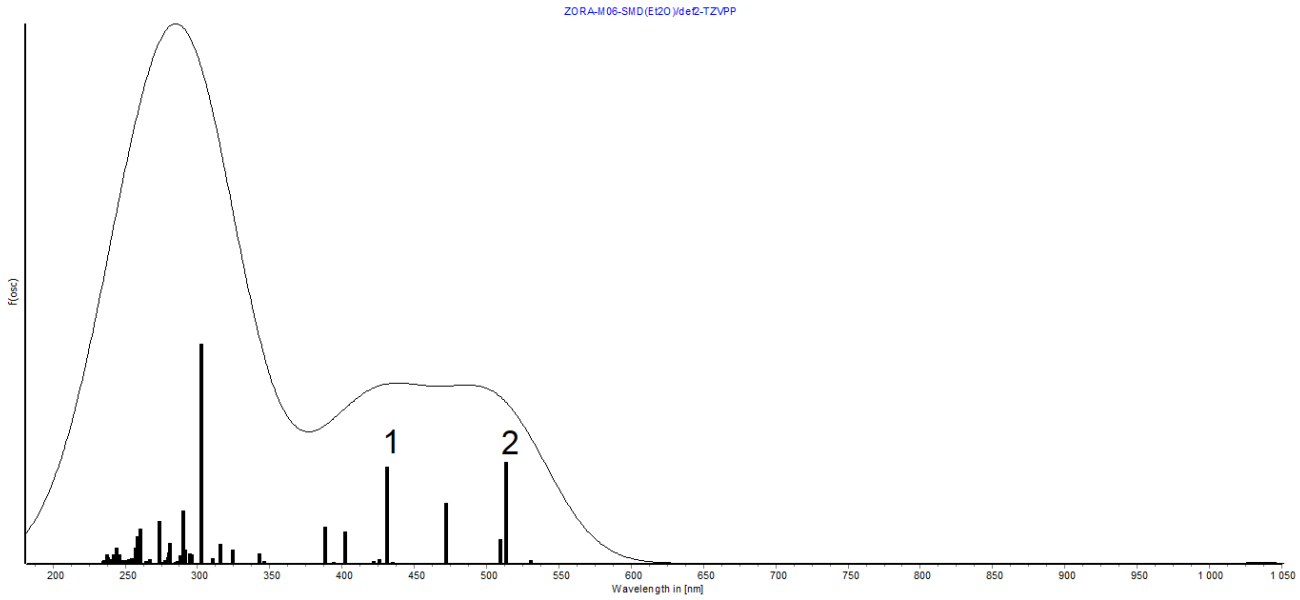

Figure S71. Computed UV-Visible spectrum at the ZORA-M06-SMD(Et_2O)/def2-TZVPP level of theory (strategy 1). A Gaussian broadening of the spectral lines of 80 was applied.

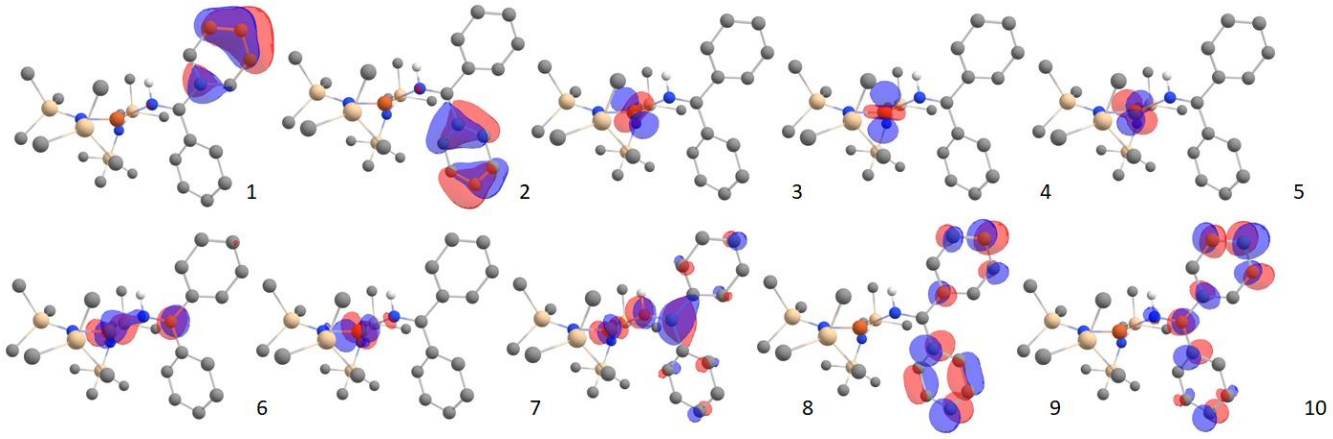

Figure S72. CASSCF/NEVPT2 active space orbitals of [**1**]$^-$.

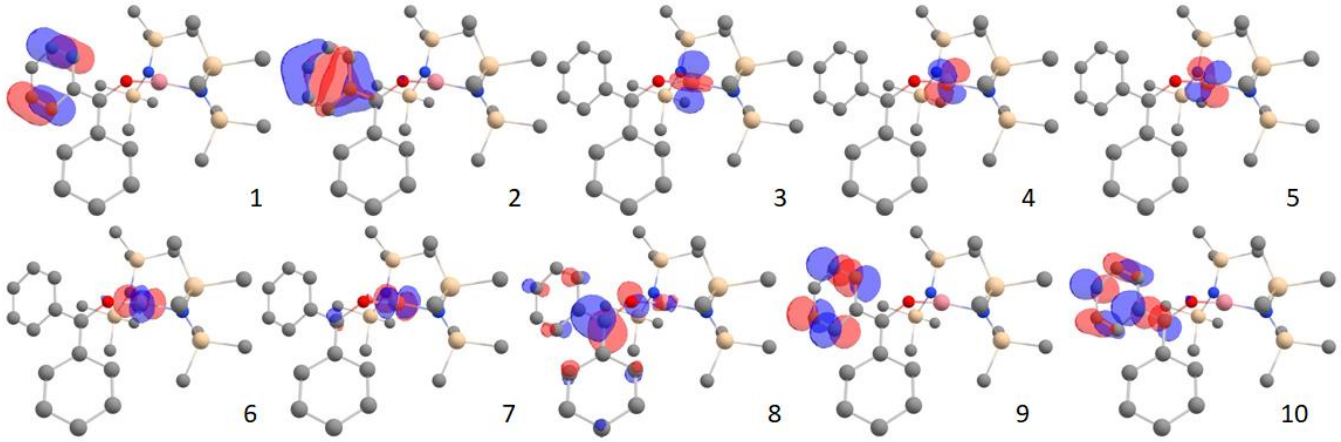

Figure S73. CASSCF/NEVPT2 active space orbitals of [**2**]$^-$.

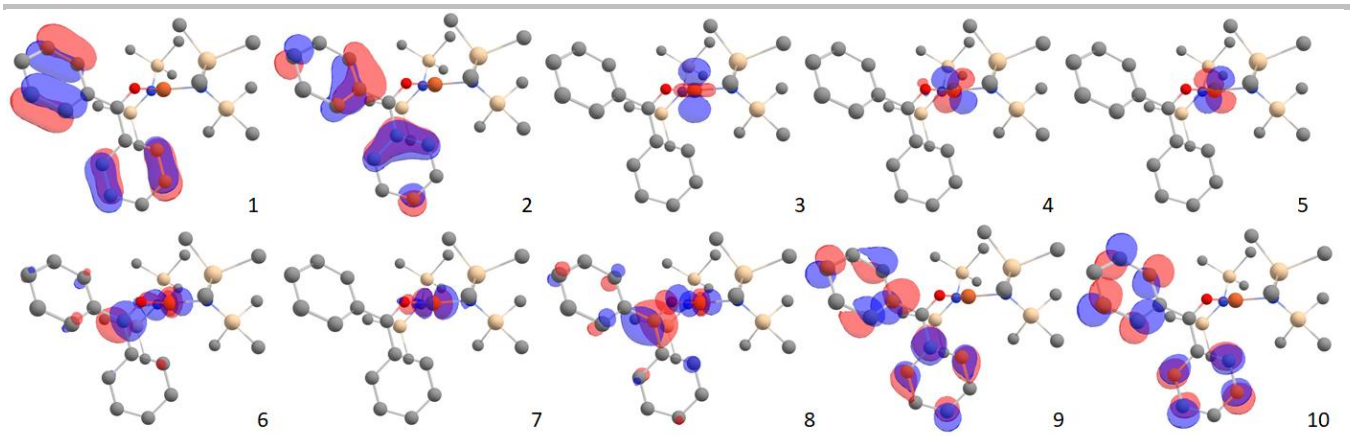

Figure S74. CASSCF/NEVPT2 active space orbitals of [**3**]$^{-}$.

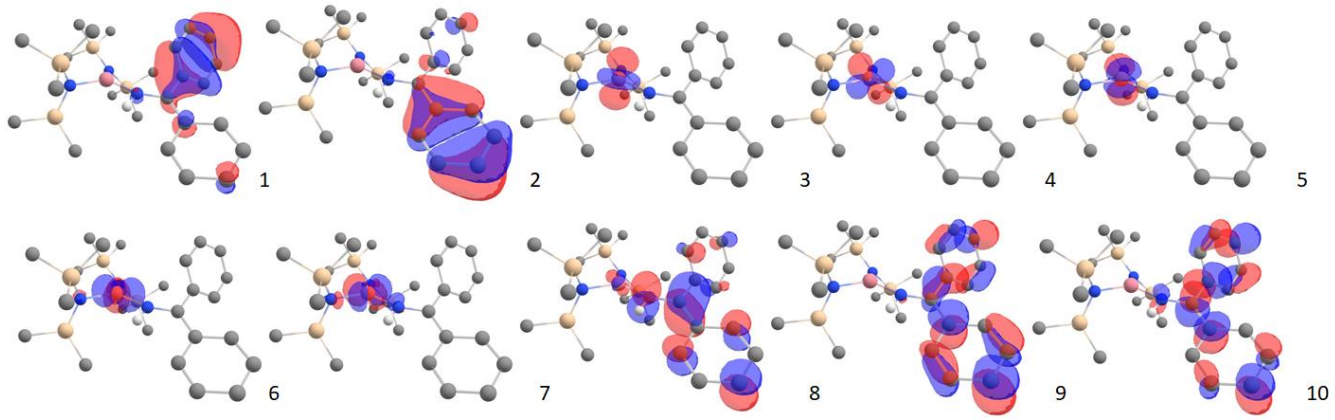

Figure S75. CASSCF/NEVPT2 active space orbitals of [**4**]$^{-}$.

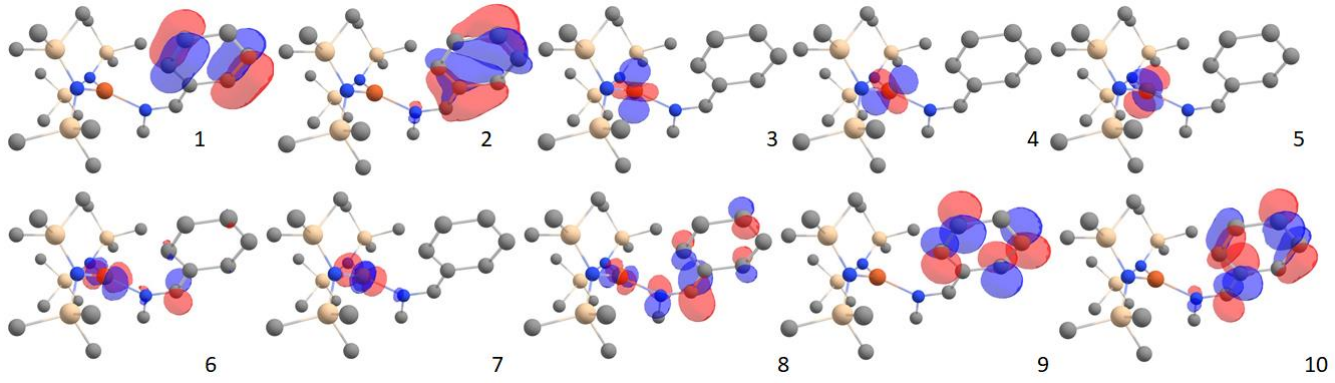

Figure S76. CASSCF/NEVPT2 active space orbitals of [**5**]$^{-}$.

	S	***E* in [Eh]**	C_i	**Configuration**	***Energy Gap* in [eV]**	**Attribution**
Ground state	***S* = 3/2**	-3601.00914			-	
			0.47	22**21111**100		
			0.23	22**21121**000		
			0.13	22**21101**200		
			0.08	22**12111**100		
Excited state 1	***S* = 3/2**	-3600.94893			1.568	$d(z^2)$ -> d(xy) + p(y)
			0.82	22**11121**100		
			0.15	22**11111**200		
Excited state 2	***S* = 3/2**	-3600.93681			1.884	$d(z^2)$ -> $d(x^2\text{-}y^2)$
			0.57	22**11112**100		
			0.26	22**11122**000		
			0.14	22**11102**200		

Table S12. Excited state configurations obtained at the CASSCF/NEVPT2(11,10) of [**1**]$^{-}$. The lowest energy transition has partial MLCT character due to mixing of the d(xy) orbital with the p(y) orbital of the ligand. The d orbitals of the active space are written in bold in the configuration. The active space orbitals of [**1**]$^{-}$ are plotted above (Figure S72).

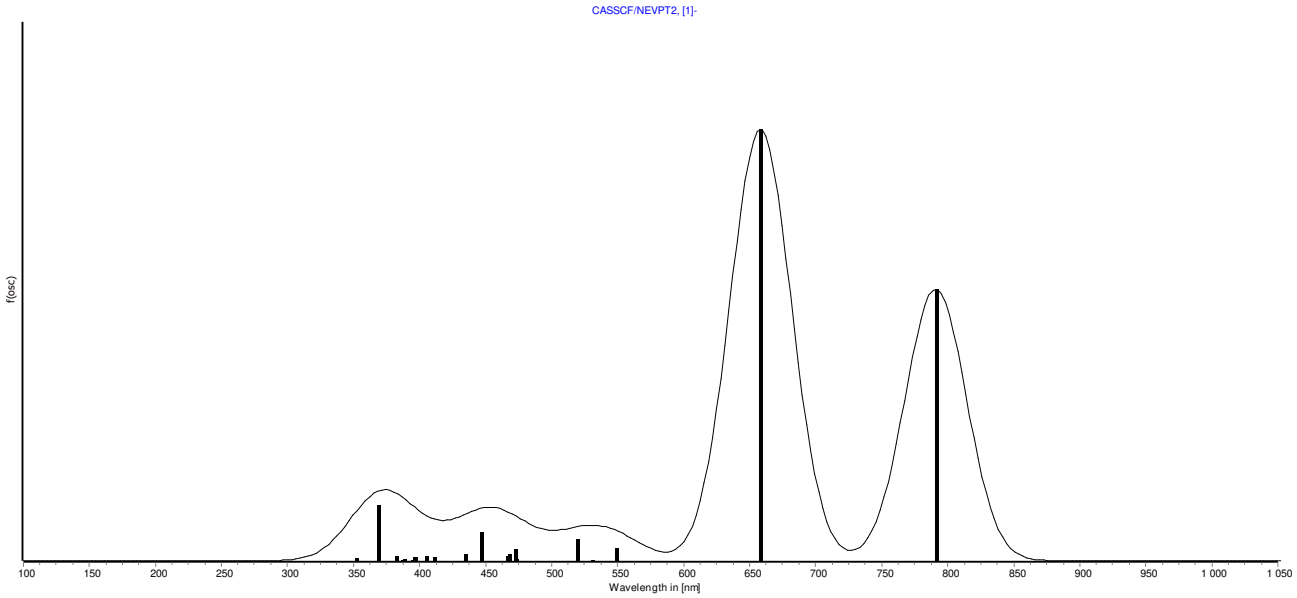

Figure S77. The spectrum computed at the CASSCF/NEVPT2(11,12) level of theory shows two main bands in the visible region of [**1**]$^-$ (Table S12).

	S	***E* in [Eh]**	C_I	**Configuration**	***Energy Gap* in [eV]**	**Attribution**
Ground state	***S* = 3/2**	-3581.073567			-	
			0.20	22**12111**100		
			0.19	22**12121**000		
			0.19	22**21111**100		
			0.18	22**21121**000		
			0.09	22**12101**200		
Excited state 1	***S* = 3/2**	-3581.015215			1.588	$d(z^2)$ -> d(xy) + p(y)
			0.44	22**11121**100		
			0.15	22**11122**000		
			0.14	22**11112**100		
			0.13	22**11111**200		
			0.06	22**11102**200		
Excited state 2	***S* = 3/2**	-3581.014018			1.620	$d(z^2)$ -> $d(x^2-y^2)$
			0.28	22**11121**100		
			0.26	22**11112**100		
			0.21	22**11122**000		
			0.11	22**11102**200		
			0.08	22**11111**200		
Excited state 3	***S* = 3/2**	-3580.975198			2.677	MLCT
			0.43	22**12111**100		
			0.18	22**21111**100		
			0.08	22**12121**000		

Table S13. The excited state configurations obtained at the CASSCF/NEVPT2(11,10) level of theory for the most intense transitions in the visible region of the UV-Vis spectrum of [3]$^-$. The lowest energy *d-d* transition has partial MLCT character due to mixing of the d(xy) orbital with the p(y) orbital of the ligand. The *d* orbitals of the active space are written in bold in the configuration. The active space orbitals of [**3**]$^-$ are plotted above (Figure S74).

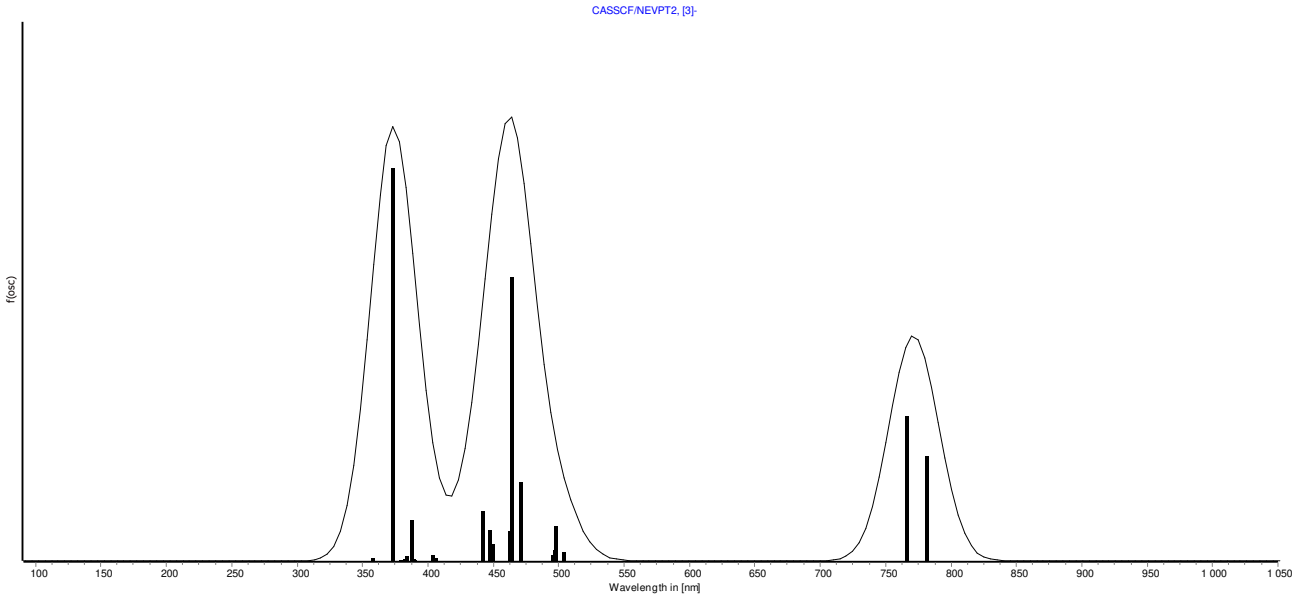

Figure S78. The computed CASSCF shows two main bands in the visible region of [**3**]$^-$ (*cf.* Table S13).

	S	***E* in [Eh]**	C_i	**Configuration**	***Energy Gap* in [eV]**	**Attribution**
Ground State	***S* = 3/2**	-3389.59870			-	
			0.28	22**21111**100		
			0.20	22**21121**000		
			0.13	22**12111**100		
			0.11	22**21101**200		
			0.09	22**12121**000		
Excited state 1	***S* = 3/2**	-3389.543287			1.508	$d(z^2)$ -> d(xy) + p(y)
			0.41	22**11121**100		
			0.16	22**11112**100		
			0.15	22**11122**000		
			0.12	22**11111**200		
			0.06	22**11102**200		
Excited state 2	***S* = 3/2**	-3389.542175			1.538	$d(z^2)$ -> $d(x^2-y^2)$
			0.29	22**11121**100		
			0.27	22**11112**100		
			0.15	22**11122**000		
			0.11	22**11102**200		
			0.07	22**11111**200		

Table S14. Excited state configurations obtained at the CASSCF/NEVPT2(11,10) level of theory for the most intense transitions in the visible region of the UV-Vis spectrum of [**5**]$^-$. The lowest energy transition has partial MLCT character due to mixing of the d(xy) orbital with the p(y) orbital of the ligand. The *d* orbitals of the active space are written in bold in the configuration. The active space orbitals of [**5**]$^-$ are plotted below (Figure S76).

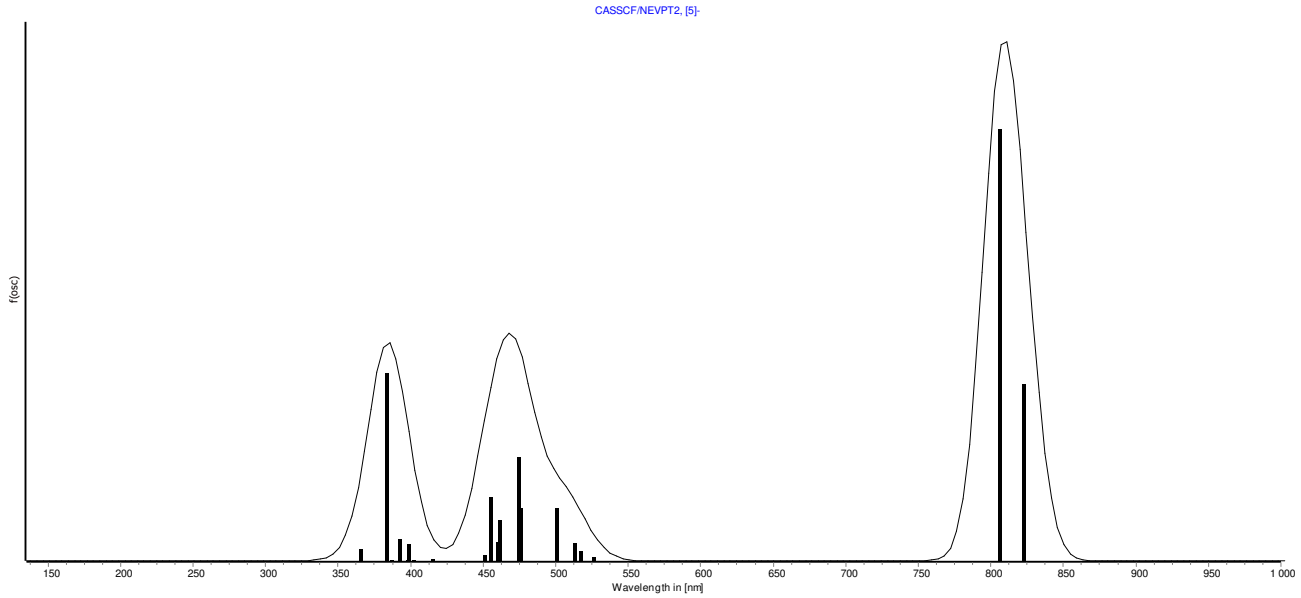

Figure S79. The computed CASSCF shows two main bands in the visible/near infrared region of [**5**]$^{-}$ (*cf.* Table S14). As this spectrum is in poor agreement with the experimental one, the main bands of the experimental spectrum are likely due to transitions to π* orbitals outside of the active space.

State		*E* in [Eh]	C_i	Configurations	*E* of gap in [eV]
1	[**1**]$^{-}$				
	***S* = 3/2**	-3601.00914			-
			0.47	22**21111**100	
			0.23	22**21121**000	
			0.13	22**21101**200	
			0.08	221**2111**100	
2	***S* = 5/2**	-3601.00329			0.159
			0.85	22**21111**100	
			0.14	221**2111**100	
	[**2**]$^{-}$				
1	***S* = 2/2**	-3722.46834			-
			0.72	221**2211**100	
			0.08	221**2212**000	
			0.05	221**1122**100	
2	***S* = 2/2**	-3722.46384			0.122
			0.49	22**2211**100	
			0.14	221**1221**100	
			0.11	221**2112**100	
			0.7	22**2211**2000	
3	***S* = 4/2**	-3722.46349			0.132
			0.85	221**2211**100	
			0.5	221**1122**100	
	[**3**]$^{-}$				
1	***S* = 3/2**	-3581.07371			-
			0.20	221**2111**100	
			0.19	221**2121**000	
			0.19	22**21111**100	
			0.18	22**21121**000	
			0.09	221**2101**200	
			0.9	22**21101**200	
2	***S* = 3/2**	-3581.06575			0.216
			0.21	22**21111**100	
			0.19	221**2111**100	
			0.19	22**21121**000	
			0.18	221**2121**000	

			0.09	222**11101**200	
			0.09	221**12101**200	
3	***S* = 5/2**	-3581.06111			0.343
			0.49	221**12111**100	
			0.45	222**11111**100	
	[**4**]$^{-}$				
1	***S* = 2/2**	-3702.54901			-
			0.67	221**22111**100	
			0.8	222**11211**100	
			0.5	222**22111**100	
2	***S* = 2/2**	-3702.54737			0.045
			0.37	222**22111**100	
			0.15	221**22111**100	
			0.10	221**11221**100	
			0.09	222**11211**100	
			0.06	221**21121**100	
			0.05	221**21121**00	
3	***S* = 4/2**	-3702.54726			0.048
			0.78	221**22111**100	
			0.11	222**11211**100	
			0.05	221**11122**100	

	[**5**]$^{-}$				
1	***S* = 3/2**	-3389.59870			-
			0.28	222**11111**100	
			0.20	222**11121**000	
			0.13	221**21111**100	
			0.11	222**11101**200	
			0.09	221**21121**000	
			0.05	221**21101**200	
2	***S* = 5/2**	-3389.59225			0.175
			0.64	222**11111**100	
			0.26	221**21111**100	

Table S 15. CASSCF/NEVPT2 energies of the ground state and first excited states. The weight of the main configurations (>4%) for each state is given, and the *d* orbitals are highlighted in bold in each configuration. For [**1**]$^{-}$ to [**5**]$^{-}$. The HOMO corresponds to the ligand centred radical. The active spaces are plotted above (Fig. S65 – S79).

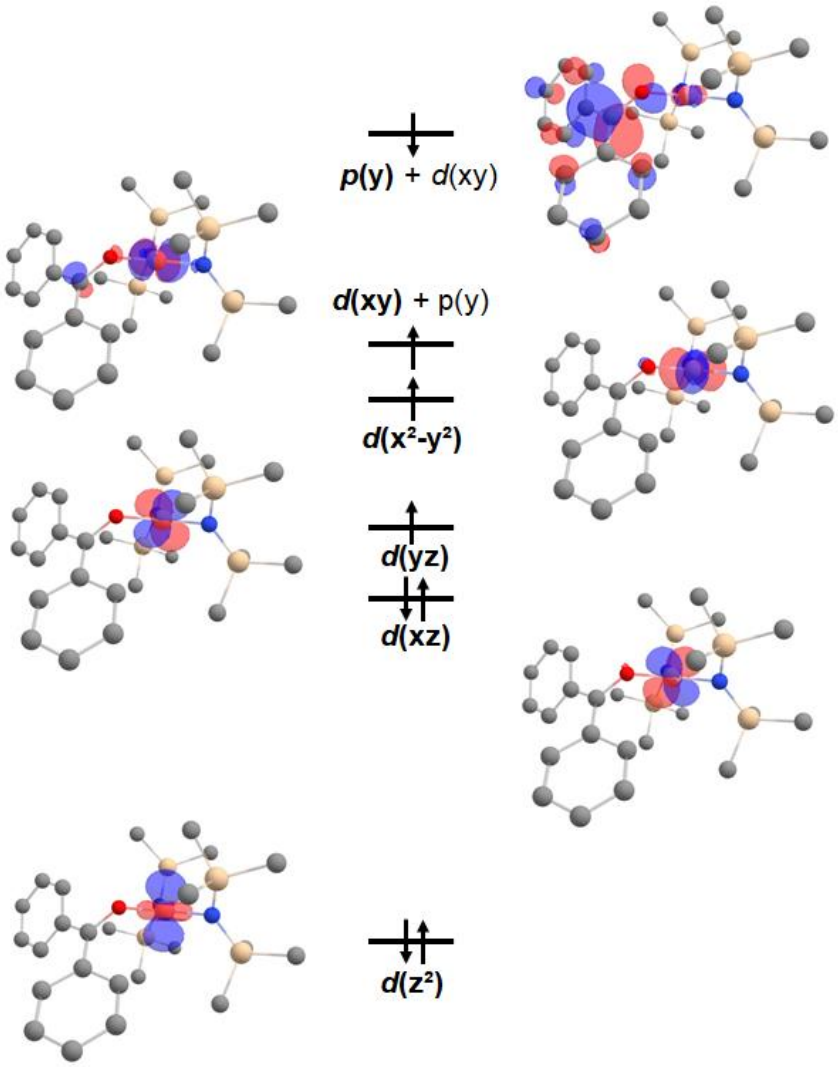

Figure 80. The molecular orbital diagram of the cobalt-benzophenone complex [**2**]$^-$ at the CASSCF(12,10) level of theory reveals an antiferromagnetically coupled ligand-centred radical, with two doubly occupied d-orbitals.

Bond	IR stretching frequencies in [cm^{-1}]	Bond Length
Benzophenone C=O	1701	1.23060
Ketyl Radical C–O	1536	1.27398
1 C=O	1585	1.27898
[**1**]$^-$ C–O	1563	1.30746
2 C=O	1590	1.26779
[**2**]$^-$ C–O	1565	1.30918
Benzimine C=N	1633	1.29364
Benzimyl Radical C–N	1454	1.34239
[**3**]$^-$ C–N	1451	1.35802
[4]$^-$ C–N	1455	1.35128
N-Methybenzaldimine C=N	1697	1.28173
Benzaldimyl radical C–N	1554	1.33228
5 C=N	1622	1.30522
[**5**]$^-$ C–N	1545	1.34623

Table S16. Computed IR stretching frequencies (strategy 2) and bond lengths at the ZORA-PBE-D3(BJ)/def2-SVP level of theory suggest that the ligands have strong radical character in the anionic complex, and negligible radical character in the neutral complexes.

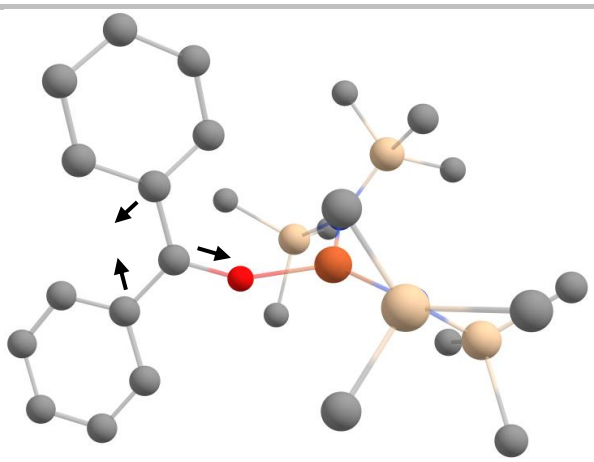

Figure S81. C–O stretching mode of complex [**1**]$^{-}$.

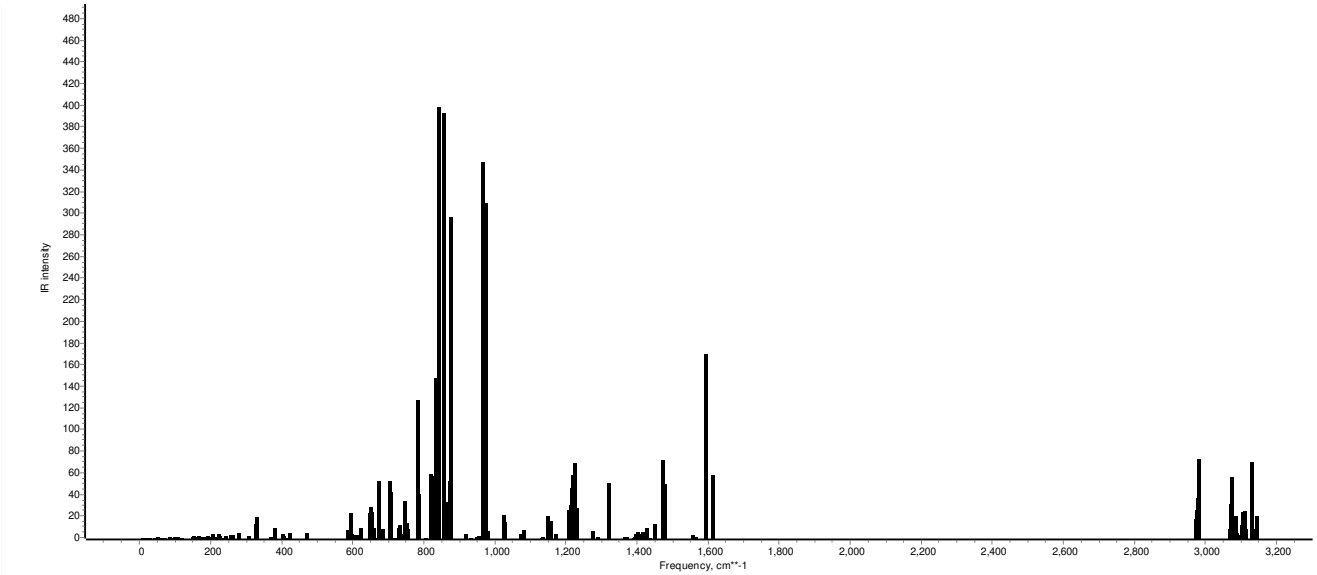

Figure S82. Computed IR spectra of [**1**]$^{-}$. The stretching mode of the C–O bond depicted in the previous figure is not prominent in the IR spectrum due to low intensity relative to the neighbouring modes.

	$E^{\text{B97-3c}}$	$G^{\text{B97-3c}}$	$E^{\text{PBEh-3c}}$	$G^{\text{PBEh-3c}}$
[**1**]$^{-}$ *S* = 3/2	-3586.70023	-3586.10430	-3582.464137	-3581.86831
[**2**]$^{-}$ *S* = 2/2	-3705.81123	-3705.24137	-3701.456118	-3700.86029
[**3**]$^{-}$ *S* = 3/2	-3566.82184	-3566.11576	-3562.609025	-3561.99635
[**4**]$^{-}$ *S* = 2/2	-3685.93701	-3685.35151	-3681.604253	3680.99669
[**5**]$^{-}$ *S* = 3/2	-3375.15715	-3374.50009	-3371.265357	-3370.70995

Table S 17. Calculated electronic energies (*E*) and Gibbs free energies (*G*) in [Eh] as obtained with strategy 2, using composite methods B97-3c and PBEh-3c.

	E^{BP86}	G^{BP86}	E^{PBE0}	G^{PBE0}
[**1**]$^{-}$ *S* = 3/2	-3605.35855	-3604.80255	-3604.42027	-3602.26576
[**2**]$^{-}$ *S* = 2/2	-3725.95467	-3726.07680	-3724.08729	-3723.49581
[**3**]$^{-}$ *S* = 3/2	-3584.76715	-3584.89059	-3582.95681	-3582.36551
[**4**]$^{-}$ *S* = 2/2	-3706.04503	-3706.16769	-3704.20340	-3703.37598
[**5**]$^{-}$ *S* = 3/2	-3393.04401	-3393.16104	-3391.41188	-3390.87152

Table S 18. Calculated electronic energies (*E*) and Gibbs free energies (*G*) in [Eh] as obtained with strategy 2 using GGA functional BP86 and meta-GGA functional PBE0

.

PBE	*E*	*G*	E^{TZVPP}
[**1**]$^-$ *S* = 3/2	-3602.58071	-3602.02421	-3604.21226
[**1**]$^-$ *S* = 5/2	-3602.57157	-3602.01548	-3604.20306
[**2**]$^-$ *S* = 2/2	-3723.83272	-3723.27422	-3723.83272
[**2**]$^-$ *S* = 4/2	-3723.82480	-3723.26804	-3723.8248
[**3**]$^-$ *S* = 3/2	-3582.69165	-3582.12231	-3582.69165
[**3**]$^-$ *S* = 5/2	-3582.67859	-3582.10975	-3582.67859
[**4**]$^-$ *S* = 2/2	-3703.94583	-3703.37598	-3705.80218
[**4**]$^-$ *S* = 4/2	-3703.93635	-3703.36725	-3705.79933
[**5**]$^-$ *S* = 3/2	-3391.15919	-3390.63912	-3392.56414
[**5**]$^-$ *S* = 5/2	-3391.14545	-3390.62540	-3392.55275
1 *S* = 4/2	-3602.50927	-3601.94856	-
1 *S* = 6/2	-3602.48022	-3601.92179	-
2 *S* = 3/2	-3724.01138	-3723.45135	-
2 *S* = 5/2	-3723.96215	-3723.40397	-
5 *S* = 4/2	-3391.10364	-3390.57909	-
5 *S* = 6/2	-3391.06143	-3390.53827	-

Table S19 . Calculated electronic energies (*E*), Gibbs free energies (*G*) and single-point electronic energies (E^{TZVPP}) in [Eh] as obtained with strategy 2 (PBE).

PBE - BS	E^{HS} in [Eh]	E^{LS} in [Eh]	Δ*E* in [eV]	*J* in [cm^{-1}]
[**1**]$^-$	-3604.075459	-3604.085974	0.286	-531.85
[**2**]$^-$	-3725.573532	-3725.585062	0.314	-736.77
[**3**]$^-$	-3584.143179	-3584.161466	0.498	-887.34
[**4**]$^-$	-3705.654640	-3705.666891	0.333	-781.25
[**5**]$^-$	-3392.435618	-3392.450846	0.414	-750.13

Table S 20. Broken-symmetry DFT calculations support the picture painted by strategies 1 and 2: All complexes have antiferromagnetically coupled spin systems in their ground states, with a low-lying ferromagnetically coupled excited state.

XYZ coordinates

[**1**]$^-$, strategy 1, positions of hydrogen atoms optimized at the PBE/def2-SVP level of theory using the structural parameters in the solid state.

Fe	4.39445366620451	11.21157997910518	7.25823859217453
Si	2.45246833805722	8.92617990380223	6.25782745972293
Si	1.49162614222496	11.77725762737289	6.16608669644868
Si	5.66699149208387	14.08647415489950	7.32589820851227
Si	6.05511889286020	12.40644860171629	4.84380024880261
N	5.32871441153870	10.35381440530688	8.76173435035702
N	2.65384432769538	10.59012729405805	6.55872917010526
N	5.39548635891604	12.67904270841207	6.39683516595467
C	5.08630042490120	10.13768568921869	10.06784877986529
C	3.85800258578691	10.31997228837408	10.75637721390883
C	2.63468484621213	10.65814970325013	10.12735965680865
H	2.60179843712707	10.78028415845817	9.03568097847309
C	6.68255961463663	9.94404484410340	8.35872930063162
H	6.75228726611251	8.84859245664243	8.17330982052139
H	7.43519005967253	10.20083468884878	9.13812744139574
H	6.97987745632799	10.45963728903901	7.42745048187614
C	5.23163443910725	13.80639164383730	9.12846147911520
H	4.17748348332524	13.50255143709881	9.26295128005031
H	5.38938328649747	14.73359386564823	9.71303384758788
H	5.84639178719762	13.00591988266177	9.57635378961361
C	1.15642719665381	8.14798593622733	7.36742657860195
H	1.38035972296908	8.36619918764661	8.42912954804670
H	1.12883266809879	7.04784831120946	7.24233737817313
H	0.14371995050108	8.53507858389751	7.15594319587212
C	-0.28627709891304	11.17287252930792	6.29005062781834
H	-0.52242985337737	10.34024213465425	5.60231173560947
H	-0.97405041240753	12.00670214957588	6.05116974865220
H	-0.51583244068688	10.83408601993914	7.31707455224960
C	1.90743930058248	8.58082756329666	4.48918176627915
H	0.96073179750285	9.09779286954143	4.24723613655993
H	1.74766440459509	7.49747912938871	4.32740046213000
H	2.66898689838652	8.92406509967956	3.76464342130766
C	4.03454430147280	7.95898918921273	6.55503348869773
H	4.85373074648292	8.29058670543895	5.89148690539599
H	3.86472117643115	6.87953530136401	6.37726736287435
H	4.37341233269247	8.09053439383921	7.59867603558746
C	3.80577499666677	10.14156952740472	12.16581464429238
H	4.73596880203270	9.87372313677764	12.68966968319520
C	1.71707448160506	12.44148270462838	4.42928442893222
H	2.70964764449557	12.91794021904019	4.33443563207633
H	0.95189848256936	13.20050471982060	4.17818751789867
H	1.65794105311076	11.63430254836854	3.67579612849347
C	2.64586921206592	10.29517796164677	12.88070035134868
H	2.65791325325956	10.14615708750902	13.97021592977772
C	1.45157209309215	10.63026541450608	12.23663700243310
H	0.52080379370223	10.75224509536464	12.80576879573693
C	1.47125804066178	10.80444130434624	10.85683631736178
H	0.54359990965298	11.05969627291002	10.32351832793620
C	5.30813528126453	10.90154211604840	4.01906119887652

H	5.61353880252674	9.97151354915720	4.53228692978487
H	5.64310299290422	10.83097240778749	2.96638654902855
H	4.20522457823375	10.93776269126452	4.03627054557277
C	1.55720333995282	13.22481551268507	7.34711178002459
H	1.36860691986022	12.89446588586647	8.38560273590290
H	0.80267237855321	13.99125208531570	7.08547300186433
H	2.54972600002880	13.70482995225488	7.33113331792684
C	7.91702574932744	12.10480436422994	4.87133133854579
H	8.48169851510253	12.97798332404407	5.24127303942161
H	8.29058713967756	11.86417613515741	3.85749724587490
H	8.16035473093713	11.25079042015251	5.53057923176677
C	5.75667971072513	13.85006803209319	3.67739856956792
H	4.67561883059009	14.05837274486731	3.58102766758809
H	6.15218288762032	13.63414068003494	2.66660920350753
H	6.24345401022784	14.77725856728146	4.03227824060042
C	7.45125374907513	14.66569091108874	7.27783367898215
H	8.14463988552617	13.87029021419975	7.60702967495416
H	7.58814193707369	15.53506232448336	7.94872731759873
H	7.75804450002469	14.97976674630439	6.26263928176995
C	4.67619055775312	15.58842868641562	6.76404675664668
H	4.91192146713164	15.86289498120328	5.71981333346690
H	4.91287450440687	16.45898010434587	7.40542645163321
H	3.58623070959464	15.41648636855069	6.82037262641227
H	5.94394205149696	9.81083847677093	10.68540961741702

[**1**]$^{-}$, (S = 3/2), strategy 2, B97-3c

Fe	10.76469805790072	8.01476064188939	21.13831289685189
Si	12.46012409066451	10.58291559034104	20.65128925764066
Si	12.83607833984627	9.00394788313759	23.24225699343673
Si	9.36387126878484	5.28427775089492	21.59546988968009
Si	12.21491048564055	5.31091793415468	20.49038399154633
O	9.10225752856354	8.75666345505408	20.69623435903398
N	12.14329164577589	9.24638414066008	21.69008295569604
N	10.81600265117438	6.07530903618242	21.12140247417123
C	8.14951877802441	10.39205104308631	19.30279827554070
C	8.20225700952620	9.51274111621846	18.20085041939703
H	8.43858353905100	8.47521222223915	18.38716565481807
C	8.45502853845239	9.88651969245873	20.62336712376939
C	8.08316031338789	10.55052639732789	21.85685955310820
C	7.88926612200380	11.74979055999992	19.02887622893390
H	7.91773207165020	12.47047099207345	19.83258934931643
C	8.82173822822865	10.30567944759692	23.03070387371621
H	9.68602904769440	9.66217667256598	22.96995806485990
C	8.44730261678523	6.23798576181726	22.93598815714054
H	9.07434353683004	6.37540523895369	23.81626895507355
H	7.54876837977931	5.69924205067151	23.24536860322269
H	8.14623166090370	7.22400636628939	22.58971699037411
C	6.96090350996286	11.39520100699140	21.96759357572689
H	6.32662837229606	11.55004704996774	21.10687762952387
C	7.96955324679751	9.95886225807824	16.91541282758574
H	8.00920387390906	9.25444583103594	16.09293890945674
C	11.96568100294468	10.21848005593238	18.87234545618555
H	12.50231130784441	9.35367877833646	18.48518365820269
H	12.19690653121095	11.07220154531867	18.23102899247298
H	10.90094443712158	10.01950080847137	18.77352129567086
C	13.36042090681627	6.53440098592646	19.62954861765556
H	12.87799085428402	6.96162390129266	18.75066574734094
H	14.27696780905359	6.03877721641117	19.30111553447693
H	13.63378207109231	7.36232585810350	20.27983867915702
C	7.38070806507562	11.74594546317046	24.31630980756834
H	7.11216122614700	12.20620791214072	25.25893558649938
C	14.61917003273755	8.37707674026571	23.14685650636400
H	14.66988291185861	7.43039642421679	22.61050665459930
H	15.03715847042846	8.21484460643635	24.14264400484769
H	15.26511264250083	9.08209868349107	22.62565519521535
C	7.66371728335531	12.18896608724014	17.73832960049880
H	7.48496097862134	13.24303986694088	17.56040664841643
C	7.68753586881626	11.29939393147948	16.66760587740424
H	7.51136463091768	11.64835112426628	15.65786028191382
C	14.30486741558690	11.01774089106592	20.61014410328133
H	14.68744017678595	11.30359117151662	21.58989583875220
H	14.48795523782819	11.85267120443182	19.93091038866598
H	14.89459537488800	10.16987640898201	20.26096654549308
C	8.48206610418768	10.89942182067279	24.22948462932501
H	9.08468519861849	10.70237041866856	25.10792338277751
C	11.53351373771799	12.14012850930563	21.17759328697193
H	10.45897697663701	11.96802649321116	21.16757335743610
H	11.74446811968053	12.97317524902940	20.50392081738771
H	11.80224148851280	12.44725230465689	22.18747382427046
C	12.86485811767420	10.59486927238077	24.26925467660948
H	13.49474837012435	11.36366652788152	23.82151212033078
H	13.24314084784600	10.40499325809950	25.27572735983781
H	11.86114223904507	11.00988462454207	24.36031809623606
C	6.61897339871181	11.97656382470640	23.17430523708569
H	5.74056894309926	12.60912925632068	23.22923697145079
C	11.87992183716210	7.73379820871601	24.25563547462062
H	10.86503779938388	8.06804986853917	24.46684865301287
H	12.37855894504500	7.55625469626978	25.21168198036101
H	11.79938856977151	6.78320118115995	23.73189081844831
C	13.23152591748966	4.46046500961808	21.84076452180419
H	13.54559451530117	5.18376532489307	22.59277413997535
H	14.13047595385456	3.99118009425372	21.43551311052714
H	12.65332901621034	3.69049103052683	22.35004998339859
C	8.18295081527303	5.08728879804532	20.13503647558118
H	7.96388985019976	6.06735309275156	19.71146382991618
H	7.23643371070799	4.62850956040466	20.42810981373444
H	8.62305049783719	4.47615845985009	19.34677260615162
C	11.79487503835152	3.99663248360514	19.19072857770447
H	11.18413444811887	3.19058951007932	19.59562851081229
H	12.70030432347591	3.54758061331455	18.77706068709683
H	11.23905741704601	4.44399918656145	18.36615392590945
C	9.67460722244579	3.55865250068031	22.32042868053092
H	10.15279706880530	2.87907028550561	21.61586116585040
H	8.73127745870039	3.10117407027069	22.62520865075981
H	10.31111790341279	3.62017466035392	23.20332260377538

[**1**]$^{-}$, (S = 3/2), strategy 2, PBEh-3c

Fe	11.00543589331850	8.32333767514133	21.02557639753338
Si	13.19289788088974	10.59232812696404	20.78687900638640
Si	12.97247252583261	9.02930580569106	23.38929184362641
Si	9.26623030345088	5.71654002692068	21.30711146687433
Si	12.18165961415562	5.42564542092292	20.52761528044978
O	9.61881617249546	9.37078342003724	20.24153412222900
N	12.50653532358187	9.36294494915594	21.77169700053966
N	10.82903621817545	6.37030710460393	20.99933398233498
C	7.69863318225950	10.23856122736045	19.20825072137911
C	7.91206309290857	9.43540567335624	18.06816371577440
H	8.66814620094640	8.66360815517022	18.10608530551299
C	8.51307697074794	10.03290541424592	20.38459490107974
C	8.14779420966172	10.52656472178767	21.70479279723007
C	6.72811307879259	11.25495805442053	19.09745271978933
H	6.57723696060253	11.94517107929810	19.91677247959716
C	9.14770786156249	10.80914889050594	22.65328186161983
H	10.19068725803927	10.72306209737108	22.37970742200246

C	8.27544956906131	6.78709516394802	22.50904712314736
H	8.82378990778664	6.96481540278064	23.43577648117839
H	7.33725501101225	6.29351887303814	22.77463412812267
H	8.01310004009345	7.76279065442828	22.09915762623097
C	6.81221519165839	10.66129340462706	22.12533152844211
H	6.00982310072583	10.39263768384213	21.45095852726947
C	7.16788855997034	9.60852601214223	16.91755280592617
H	7.34970074747569	8.96158869017019	16.06767770991436
C	12.84480885225484	10.29306289212597	18.95067373289675
H	13.24238962438322	9.33346713733186	18.61527782370884
H	13.31169257449636	11.07076309516120	18.34076560180903
H	11.77609655694212	10.30785353285091	18.72908191327940
C	13.57163721238186	6.48635142355965	19.80209906986919
H	13.25001290690198	6.98010098118848	18.88246843593922
H	14.43220347870126	5.86155342400507	19.54980642078523
H	13.91759107358328	7.26612274501516	20.48226028873247
C	7.50223503342448	11.36815999650568	24.32380059160571
H	7.25387956688905	11.68979284862997	25.32698257414355
C	14.59451283470777	8.05222551920771	23.50748401953344
H	14.49121756745162	7.07553622454382	23.03027664673499
H	14.88778780714737	7.87765428676222	24.54555872530510
H	15.42079841404862	8.56566608524145	23.01313680341823
C	5.99259508715617	11.42483588240534	17.93999442890900
H	5.26169165014555	12.22301834282123	17.89086871227790
C	6.19372053927972	10.59885969394371	16.83883271461771
H	5.61310813263756	10.73246059052195	15.93505868503802
C	15.08333336030136	10.68745728792794	20.95919130258194
H	15.40263037984708	10.93035113435315	21.97486800607690
H	15.49970103606872	11.45192656699320	20.29909130185494
H	15.54515403431952	9.73469141167035	20.69149098196038
C	8.82781703465082	11.22583657030376	23.93242382451103
H	9.62687990077167	11.44365740456445	24.63136441336210
C	12.51315358087027	12.31865080653529	21.17677757595429
H	11.43969145428336	12.36608266348807	20.98215897114247
H	12.98945310872143	13.08743787927535	20.56317484031584
H	12.66452833664270	12.59322652624998	22.22237650359583
C	13.19808153927896	10.61494649952456	24.41176397858726
H	13.97684619671966	11.26235534873721	24.00397203136589
H	13.46555190239983	10.39541610410133	25.44793419216606
H	12.27267182333671	11.19594107834867	24.42449991255110
C	6.49913595403962	11.07601182250595	23.40690130873145
H	5.45907782337308	11.15304445405298	23.70007711453601
C	11.65992799961909	8.00640857887152	24.28984978056846
H	10.70897158117916	8.54136567283089	24.34844602791402
H	11.97801019305736	7.78975204210804	25.31276586049276
H	11.46377867010502	7.05133610727090	23.79804057732958
C	12.93600135342738	4.45272810850330	21.97369173100629
H	13.07856790406495	5.10233324100496	22.83978351809643
H	13.90907441162472	4.02775250670881	21.71569145086275
H	12.29603298690949	3.62832242721896	22.29398148792750
C	8.24362195632895	5.54649035484536	19.72198679454202
H	8.07536008410425	6.52498740135047	19.26729385699247
H	7.26393062601199	5.09949541203442	19.90714164346490
H	8.75726426800122	4.92679620299024	18.98399899640789
C	11.76446696931547	4.16579631200118	19.16695446431149
H	11.01739361394317	3.43368352981419	19.47923590360304
H	12.65277488619228	3.61024425895469	18.85666383308533
H	11.36991512544603	4.67315255204299	18.28409043362602
C	9.34546829016045	3.99289960437411	22.10665580671778
H	9.83408076311724	3.25009837464031	21.47313331165977
H	8.34114796732600	3.62149235846145	22.32379392116181
H	9.89358909670027	4.02810296558730	23.05033019813639

[**1**]$^{-}$, (S = 3/2), strategy 2, BP86

Fe	10.72551904518821	7.97421664548032	21.07345838394649
Si	12.37004058475649	10.58426134036191	20.56823088595560
Si	12.77869005681382	8.97610223179344	23.18448466429756
Si	9.34231875116943	5.25092942424410	21.59212844418506
Si	12.27596322753838	5.29666596553668	20.57493287297504
O	9.09194623024771	8.74219964774949	20.61484989129342
N	12.07810704835637	9.20661534281402	21.60477113442982
N	10.81726944208010	6.06381655683388	21.13356782983479
C	8.16763510204456	10.46820433424610	19.28841250263558
C	8.24436743428612	9.62757350901181	18.13696428502492
H	8.47507627072715	8.56779840675310	18.29272025862246
C	8.45363265699618	9.88973505031267	20.59852948859345
C	8.11721962187684	10.51294494907452	21.87796818097154
C	7.90941489388660	11.85313091184115	19.06720232105379
H	7.92034634945348	12.54534370129814	19.91613733935804
C	8.86373902867262	10.16363515457511	23.04170234142011
H	9.69921119820791	9.46253013614606	22.92993217651517
C	8.36224879747623	6.26168917052146	22.86583908038965
H	8.95813763184306	6.41956391896118	23.78272661635447
H	7.42518892102632	5.74163929357456	23.14340012641388
H	8.10570552306779	7.25394117879432	22.45472968903055
C	7.03885410571035	11.42989227027387	22.04821388736720
H	6.39870230659779	11.67147084565067	21.19229014754099
C	8.03892876354069	10.13598710957872	16.85128455529522
H	8.09959255371099	9.45927339681796	15.98817768657460
C	11.92028800339290	10.18839646346308	18.76801299415213
H	12.50905422943131	9.32958841633265	18.39891897374672
H	12.12188819810269	11.06001109648878	18.11603421203033
H	10.84967090948821	9.93728288620232	18.67153987484812
C	13.41662306841797	6.53402653470269	19.69286680988833
H	12.95945225418592	6.86527968461452	18.74248061636066
H	14.39819186583709	6.07441999580254	19.46711748407609
H	13.57177942317185	7.43485983838363	20.31279604133683
C	7.51969543856404	11.64920438966909	24.43310507856392
H	7.29324449896085	12.09029723405785	25.41219449995126
C	14.58302312424820	8.36449368413314	23.07186313228830
H	14.62735952221603	7.40556212572846	22.52449307887098
H	15.01859137090968	8.20694565010551	24.07715634350849
H	15.21658694364861	9.08928888703334	22.53015428401512
C	7.71014372398161	12.35527161523190	17.77594428922394
H	7.53268862988894	13.43084632508361	17.64007270232510
C	7.76136934172584	11.50412046161040	16.65372854191737
H	7.60493182281276	11.90266157228005	15.64326459116526
C	14.21816747112050	11.07434771619666	20.58783429859691
H	14.55638900333497	11.36316106308398	21.59994552637415
H	14.39997611583847	11.93216165145539	19.91255130490137
H	14.84487295809402	10.22944143768270	20.24767655431280
C	8.57582059060756	10.72713382048840	24.28766058701331
H	9.18614840555290	10.44640725873885	25.15654472804858
C	11.36155166369361	12.10773376434968	21.09585996561353
H	10.28444192362157	11.86852493892665	21.07011411816942
H	11.54218256685152	12.96130594319479	20.41523857105841
H	11.60976504569813	12.42054212594562	22.12556149176909
C	12.77540090202313	10.59316245675168	24.19949892206911
H	13.39285572255162	11.37759671741166	23.72486206394486
H	13.16744779852220	10.42182345583595	25.22022920618235
H	11.74379708795200	10.98151794644557	24.28316965240519
C	6.75027722467921	11.98479082955336	23.30105713572192
H	5.90402417441281	12.67838292882002	23.39977856678275
C	11.81906666870916	7.68293450794737	24.19555988630887
H	10.81177445121853	8.05272989200862	24.46008248050908

H	12.35782201183089	7.44409280537656	25.13301961609411
H	11.68452894743766	6.75627640193127	23.60938225950022
C	13.26273318829418	4.52983301309697	22.01814909206940
H	13.51793565328011	5.30820673886810	22.76008753963603
H	14.20464606114481	4.06581413442645	21.66802763970260
H	12.66803580214371	3.75557160900301	22.53573416374601
C	8.22227575317736	4.99054955818705	20.07362692092897
H	7.99306855922745	5.97702816840051	19.63047736568253
H	7.26726138251864	4.49643115308552	20.33545289718089
H	8.73327007721134	4.38104677259893	19.30606113985044
C	11.91400846838670	3.90014497630340	19.32026431979305
H	11.29665474160494	3.09599729275047	19.76025739375871
H	12.85307008261999	3.44495829704839	18.95108178394662
H	11.36556708169392	4.30990832792088	18.45196279807929
C	9.67681362758964	3.54528465533980	22.39057971141711
H	10.22135442671036	2.86220704849056	21.71388958774884
H	8.72267503512201	3.05798590551519	22.66820520375935
H	10.27871141126172	3.66384733364883	23.31041716897013

[**1**]$^{-}$, (S = 3/2), strategy 2, PBE

Fe	10.87930345121861	8.06475523489579	21.08440230217307
Si	12.66047249044598	10.57871952712157	20.59770725322830
Si	12.95568443381075	8.99586587928634	23.25273004282910
Si	9.29268429266639	5.44274941946186	21.54036131909071
Si	12.24766676888552	5.26176673947668	20.60390797718480
O	9.36120840705068	8.96193194408055	20.49607708311764
N	12.29859278753701	9.22905021952648	21.65278720041153
N	10.84717331393559	6.14504181921000	21.15060273230106
C	8.02889759320659	10.44923602867329	19.23476047972016
C	8.22744232752240	9.64911107552677	18.06976082732505
H	8.70719497353235	8.67169820913890	18.19544135811607
C	8.50728399548832	9.95167295783402	20.52244317454688
C	8.10539329178986	10.49166002627522	21.82491832854230
C	7.43752451528504	11.73289404123623	19.04651429296419
H	7.33431550224015	12.40820097914298	19.90304191643737
C	8.98001978545237	10.34720895340010	22.94037323509046
H	9.95957170718331	9.87955929354421	22.77827522551737
C	8.35862188499137	6.48795813830257	22.82195716222355
H	8.93960506025876	6.56847301133395	23.75817446526748
H	7.37883264047296	6.03033668343710	23.05771957213148
H	8.18346951867783	7.51184143897536	22.44807403697228
C	6.84176680318337	11.10347335014932	22.06460273855420
H	6.11538548937128	11.17445925272207	21.24709439828121
C	7.82299267087260	10.09035375676897	16.80747941790296
H	7.98327201478776	9.44354804287257	15.93439346367711
C	12.27511902640656	10.16023743017112	18.78504687040951
H	12.85273617500987	9.27889216517543	18.45373311002370
H	12.52942233971794	11.01442104817124	18.12862975868837
H	11.20120417552070	9.93545959309365	18.65655883987994
C	13.51710181617339	6.40794517994002	19.77438732197344
H	13.12245783776975	6.78558433577223	18.81361648062263
H	14.46118935572807	5.86577715675593	19.57506687017814
H	13.73075283725653	7.28612799420611	20.40921975874031
C	7.37670620837406	11.43081980721161	24.42343594190151
H	7.09655335908543	11.79306048185902	25.42064385813677
C	14.73187494571087	8.29719502376194	23.20477085744658
H	14.74399361534926	7.31625743468860	22.69586190446984
H	15.13476192887554	8.15936598799697	24.22609920548738
H	15.41114120603228	8.97135204113507	22.65316592884550
C	7.03886362792837	12.16858755554438	17.77844315914805
H	6.59907442778478	13.16916188213336	17.66864507349939
C	7.21557188555197	11.35114539332390	16.64523687414750
H	6.89966817118967	11.69633889876416	15.65276108172813
C	14.51345028607203	11.04756389222314	20.67349604177365
H	14.82299186731135	11.35381633907470	21.68924322845045
H	14.72647614846692	11.88830005886495	19.98659937637714
H	15.14092212894127	10.18926941573549	20.37095847926159
C	8.62423905305025	10.81427667850325	24.20855802434801
H	9.33206787756368	10.69732770940879	25.04032985878327
C	11.64961660328012	12.13065864654929	21.04101081042404
H	10.57088794861427	11.92793856557912	20.91380284156121
H	11.91880070873477	12.98062680094470	20.38571605567250
H	11.81254631759253	12.43439770239320	22.09037601599523
C	13.01018184330239	10.62778097084102	24.24677249164890
H	13.65830497950474	11.38367611683711	23.76746582798114
H	13.39266439943156	10.45092327267920	25.26985021404267
H	11.99503262892053	11.05800775705392	24.32723783594846
C	6.48847557900391	11.56210191702242	23.33909670081720
H	5.49895749873340	12.01346011226066	23.49286286748064
C	11.90254761404453	7.77682833582706	24.26310518520054
H	10.90720397372761	8.20458625788295	24.48175252404437
H	12.39798249149889	7.53755593061976	25.22362349584620
H	11.74015953589059	6.84134110197476	23.69802604059304
C	13.13572887299381	4.37771726906668	22.04569220977431
H	13.45527803214511	5.11400845615019	22.80559250149966
H	14.03295334090359	3.83331990895669	21.69494412227393
H	12.46442215063091	3.65342607838733	22.54095669440847
C	8.19632297415251	5.31138416719703	19.98761239399663
H	8.05550382349166	6.32138025846634	19.56105870023602
H	7.19972601626994	4.88979113833210	20.21762610733755
H	8.67477965670941	4.67861359929341	19.21817469317534
C	11.80369125474137	3.92962041796015	19.30539408587956
H	11.11869453823248	3.16219093790556	19.70823041837930
H	12.71516318867869	3.41632611804241	18.94444155310583
H	11.30897548199817	4.40227274453690	18.43715228663332
C	9.45512705290481	3.69411183177020	22.30019223028794
H	9.95235433541112	2.97965990303146	21.62010182034564
H	8.45290457259472	3.29170963564983	22.54051888710530
H	10.03912656512234	3.73533452087898	23.23780448037381

[**1**]$^{-}$, (*S* = 3/2), strategy 2, PBE0

Fe	10.97023864449493	8.17724804358502	21.06048401694388
Si	12.90267012297540	10.61564451608768	20.70714360254410
Si	12.98560013311110	9.01960488620113	23.32933174142310
Si	9.27289997370270	5.60661998648123	21.41553680373044
Si	12.22415039217313	5.31574619771605	20.61416458714853
O	9.50993529787787	9.12691220394012	20.31874307587319
N	12.39773918567310	9.31644858027660	21.73361216035668
N	10.85211794133776	6.24348344595496	21.09708602759936
C	7.85225125725438	10.33993765509719	19.18682281612972
C	8.09770608261147	9.57625582076618	18.01849211061924
H	8.75671306782835	8.71513362080291	18.10528489844260
C	8.51819828432357	9.95671911618756	20.41822227958777
C	8.14284505043493	10.45263317488942	21.73916817488996
C	7.02595981111839	11.48185087903144	19.04859333531204
H	6.86941544851320	12.13672034624868	19.90292683311766
C	9.11632331215005	10.50669432396622	22.76367646029095
H	10.14342308467505	10.22511730585344	22.53253912225735
C	8.32564424927506	6.69551799451405	22.63244397605739
H	8.85024236614736	6.75146504450831	23.59453249061979
H	7.32112890884928	6.28778110246032	22.81124163081916
H	8.21080304025846	7.71894247310813	22.25634556740927
C	6.82059850096981	10.81518532099553	22.08341004422257

H	6.03081238718890	10.71985712072492	21.34101530318916
C	7.51955512804953	9.91048170619648	16.80221794086448
H	7.72334355866764	9.29383992132593	15.92636903150336
C	12.45850803883878	10.26009794252171	18.90586069536055
H	12.95316447929221	9.34548542572200	18.55485137722623
H	12.77177612130160	11.09092891184755	18.25880015824897
H	11.37457092992074	10.12744708499887	18.79442780607683
C	13.53974206226922	6.41096023304443	19.81021489129807
H	13.17918774835778	6.79031949600432	18.84506906553114
H	14.46258370387399	5.84229580192307	19.63055656984627
H	13.77704280693168	7.27889985295978	20.43849412479072
C	7.48065374922446	11.30208536529239	24.36326909065395
H	7.22580190963917	11.62805340165649	25.37095119232773
C	14.69680152565898	8.20024095521621	23.33615293290038
H	14.66488337547717	7.24570442249564	22.79565276077613
H	15.03962287377722	8.00185054043712	24.36094644764616
H	15.44119569952544	8.83770148821104	22.84330813665165
C	6.45356854846144	11.81117834921030	17.82628186129855
H	5.83140277528475	12.70370510220863	17.75275083215326
C	6.68349140299487	11.02687560767120	16.69105357522166
H	6.23081294109887	11.28884459699827	15.73545867926180
C	14.78321882860522	10.87884272540119	20.77306938485800
H	15.12505952149637	11.14330874833662	21.78211975999742
H	15.08601047265184	11.68600241408530	20.09225815670519
H	15.30533498472863	9.96189422876992	20.46990098730604
C	8.79008445221095	10.93038683762660	24.04565519457957
H	9.56959007982973	10.97043971692980	24.80686691502690
C	12.08354375708239	12.26136363142354	21.16568490927291
H	10.99297931979517	12.17964419370086	21.07242364116928
H	12.42351197487806	13.06981865945921	20.50399266039634
H	12.30920963067585	12.54660420927970	22.20065037004421
C	13.13561772055273	10.61645636995769	24.34769785935665
H	13.85243938411643	11.31806418242029	23.90192886905133
H	13.46986879770832	10.39807229545056	25.37114891076949
H	12.16435051822582	11.12468967532438	24.40504825600211
C	6.49945377032550	11.23182921024811	23.37033997653957
H	5.46601934487826	11.48642420328567	23.60698754168166
C	11.80894287012387	7.87613777163945	24.26666750059311
H	10.83206866872228	8.35684341022214	24.40853681082070
H	12.21490888655265	7.62129882435169	25.25522310136594
H	11.63962883166798	6.94812910669715	23.70521928751660
C	13.04398451705901	4.42690790936248	22.07715120647602
H	13.36945284341309	5.15319173505213	22.83283393270469
H	13.92278707026864	3.85198083227522	21.75436555353514
H	12.34161950587924	3.73582514225581	22.55988501087891
C	8.24083894120656	5.49094183276534	19.83169024981860
H	8.13572513661298	6.49289069195541	19.39583526317723
H	7.23493728917357	5.09394487240019	20.02439971646944
H	8.73014325800663	4.84780557765302	19.08903613073743
C	11.79626447738081	3.98517591135710	19.32673161536866
H	11.09161002826549	3.23960484973572	19.71527228063351
H	12.70317250462697	3.45566916347050	19.00364241508569
H	11.33994471682184	4.45033950482973	18.44323378644143
C	9.33358224029594	3.87595027685356	22.20041339177873
H	9.83672244342725	3.13876387785960	21.56270012582099
H	8.31404173831142	3.51423743366005	22.39187028791775
H	9.86503555283042	3.91260460856388	23.16031471187667

[**1**]$^{-}$, (*S* = 5/2), strategy 2, PBE

Fe	10.83577763545779	8.01028402574945	21.10628009749667
Si	12.51123096425771	10.60707661156031	20.63216859288489
Si	12.89642977695199	9.00607781873478	23.26525125282575
Si	9.32169670675218	5.33067271910177	21.58393374491519
Si	12.25343766518607	5.26114627079942	20.55854216924977
O	9.16075481522421	8.77349958261500	20.54487870148267
N	12.18751005190369	9.24447928162451	21.68701551517865
N	10.83982245562202	6.09335423671423	21.15375050402519
C	8.08183697054425	10.43076579554056	19.24147248335840
C	8.17094992062192	9.58248586825913	18.09425526374395
H	8.49311881707746	8.54680196383175	18.25077088430181
C	8.46798434345711	9.89533955350767	20.54080681137964
C	8.11327775411634	10.51110580047966	21.81856435933490
C	7.70459713835554	11.78935770996069	19.01423129110759
H	7.70286743325881	12.49414276103998	19.85313854747410
C	8.91020893206022	10.25362422063610	22.97405219609844
H	9.81743703212076	9.64858426076587	22.85537907528728
C	8.38315710911998	6.34169558352965	22.88689933601982
H	8.98375272414495	6.45302702537052	23.80742553417618
H	7.42889309733833	5.84685900917967	23.14998183333607
H	8.16072210511477	7.35258934903081	22.50242597734284
C	6.94881936301931	11.31510813466336	22.00495494387998
H	6.26855686361956	11.47685389880516	21.16118957372262
C	7.85739870199439	10.05209942675113	16.81708867496167
H	7.92624561846693	9.36837876642488	15.96006214406219
C	12.03508954338653	10.19442981678850	18.84060872085108
H	12.61872841825309	9.33456131427489	18.46599536692575
H	12.22919733624045	11.06240731748020	18.18215561531107
H	10.96209024599848	9.94407891302614	18.75903045318899
C	13.45720558064282	6.46327756901819	19.70887896894815
H	13.02356690240484	6.83770470697359	18.76375277918129
H	14.41409904662241	5.95808140201716	19.47638040539830
H	13.66081912408852	7.34062565987668	20.34852922911229
C	7.44319425320644	11.60331375209950	24.37865070150870
H	7.18919324645219	12.02784282900762	25.35806653672141
C	14.68185105363469	8.33849282762646	23.15930794288747
H	14.69655450301126	7.36613071344690	22.63425799812095
H	15.11308094882100	8.19081923703860	24.16758112098942
H	15.33612984061947	9.03198550743402	22.60168668582628
C	7.40021345150089	12.25221150886458	17.73119545684619
H	7.13090487929541	13.30802335404028	17.59176995519078
C	7.45966005670291	11.38945096016848	16.61725446732356
H	7.21929061703154	11.75772415222998	15.61199338924822
C	14.36852092600289	11.06114170842576	20.62809117120510
H	14.72157777085999	11.36159657359105	21.63145279326693
H	14.55804080932776	11.90340897190148	19.93624326171689
H	14.97688246674045	10.19980488486092	20.29671281734078
C	8.58478612859249	10.79292197602548	24.22054421442407
H	9.23580524128668	10.58417200142446	25.08040030901194
C	11.53836906207879	12.16269438354805	21.13631872541714
H	10.45370857898550	11.95860977271541	21.09408724897008
H	11.75856680666519	13.00350199062768	20.45176320762364
H	11.78144514677873	12.47785996808015	22.16646443738902
C	12.94596076629527	10.62644469476673	24.27483893622228
H	13.57559224868795	11.39507436980248	23.79094963375053
H	13.34872279037986	10.44566617307954	25.28933054187713
H	11.92586564104379	11.04048926325840	24.37424401194261
C	6.62642671128060	11.84879137634275	23.25678657015623
H	5.71384525878966	12.45062433761441	23.36506113396675
C	11.89476198817835	7.74801465805713	24.28058463730335
H	10.89645407866215	8.14832213179553	24.53465595029655
H	12.42071726900318	7.50229763943959	25.22288712857512
H	11.73975571301178	6.81829181802979	23.70356853738863
C	13.21025494125432	4.39750031424168	21.96720415643396
H	13.51547835204200	5.13716255439989	22.72969365020146
H	14.12141040456996	3.89651519465813	21.58898803377005

H	12.58164213978725	3.63917829595455	22.46734266415660
C	8.19456834478231	5.16299885221809	20.05848185260610
H	7.99787218856413	6.17375138751293	19.65647685467285
H	7.22536579007229	4.69107188141679	20.30700731504188
H	8.68205275512647	4.56612325787469	19.26646310062518
C	11.81952407949826	3.92856929515590	19.25861594346531
H	11.16868918548344	3.13735434632297	19.67185364085694
H	12.73706142907076	3.44682599815239	18.87080570902732
H	11.28853155864484	4.39254599541067	18.40736860208532
C	9.57875297039036	3.58937798361407	22.33380406353666
H	10.08724185878245	2.89747444544274	21.63882172667637
H	8.60060423208046	3.14529027211330	22.59856690436243
H	10.18462132349755	3.65256001603416	23.25620521340452

[**2**]$^{-}$, strategy 1, positions of hydrogen atoms optimized using the structural parameters from the solid state, PBE

Fe	4.39445366620451	11.21157997910518	7.25823859217453
Si	2.45246833805722	8.92617990380223	6.25782745972293
Si	1.49162614222496	11.77725762737289	6.16608669644868
Si	5.66699149208387	14.08647415489950	7.32589820851227
Si	6.05511889286020	12.40644860171629	4.84380024880261
N	5.32871441153870	10.35381440530688	8.76173435035702
N	2.65384432769538	10.59012729405805	6.55872917010526
N	5.39548635891604	12.67904270841207	6.39683516595467
C	5.08630042490120	10.13768568921869	10.06784877986529
C	3.85800258578691	10.31997228837408	10.75637721390883
C	2.63468484621213	10.65814970325013	10.12735965680865
H	2.60179843712707	10.78028415845817	9.03568097847309
C	6.68255961463663	9.94404484410340	8.35872930063162
H	6.75228726611251	8.84859245664243	8.17330982052139
H	7.43519005967253	10.20083468884878	9.13812744139574
H	6.97987745632799	10.45963728903901	7.42745048187614
C	5.23163443910725	13.80639164383730	9.12846147911520
H	4.17748348332524	13.50255143709881	9.26295128005031
H	5.38938328649747	14.73359386564823	9.71303384758788
H	5.84639178719762	13.00591988266177	9.57635378961361
C	1.15642719665381	8.14798593622733	7.36742657860195
H	1.38035972296908	8.36619918764661	8.42912954804670
H	1.12883266809879	7.04784831120946	7.24233737817313
H	0.14371995050108	8.53507858389751	7.15594319587212
C	-0.28627709891304	11.17287252930792	6.29005062781834
H	-0.52242985337737	10.34024213465425	5.60231173560947
H	-0.97405041240753	12.00670214957588	6.05116974865220
H	-0.51583244068688	10.83408601993914	7.31707455224960
C	1.90743930058248	8.58082756329666	4.48918176627915
H	0.96073179750285	9.09779286954143	4.24723613655993
H	1.74766440459509	7.49747912938871	4.32740046213000
H	2.66898689838652	8.92406509967956	3.76464342130766
C	4.03454430147280	7.95898918921273	6.55503348869773
H	4.85373074648292	8.29058670543895	5.89148690539599
H	3.86472117643115	6.87953530136401	6.37726736287435
H	4.37341233269247	8.09053439383921	7.59867603558746
C	3.80577499666677	10.14156952740472	12.16581464429238
H	4.73596880203270	9.87372313677764	12.68966968319520
C	1.71707448160506	12.44148270462838	4.42928442893222
H	2.70964764449557	12.91794021904019	4.33443563207633
H	0.95189848256936	13.20050471982060	4.17818751789867
H	1.65794105311076	11.63430254836854	3.67579612849347
C	2.64586921206592	10.29517796164677	12.88070035134868
H	2.65791325325956	10.14615708750902	13.97021592977772
C	1.45157209309215	10.63026541450608	12.23663700243310
H	0.52080379370223	10.75224509536464	12.80576879573693
C	1.47125804066178	10.80444130434624	10.85683631736178
H	0.54359990965298	11.05969627291002	10.32351832793620
C	5.30813528126453	10.90154211604840	4.01906119887652
H	5.61353880252674	9.97151354915720	4.53228692978487
H	5.64310299290422	10.83097240778749	2.96638654902855
H	4.20522457823375	10.93776269126452	4.03627054557277
C	1.55720333995282	13.22481551268507	7.34711178002459
H	1.36860691986022	12.89446588586647	8.38560273590290
H	0.80267237855321	13.99125208531570	7.08547300186433
H	2.54972600002880	13.70482995225488	7.33113331792684
C	7.91702574932744	12.10480436422994	4.87133133854579
H	8.48169851510253	12.97798332404407	5.24127303942161
H	8.29058713967756	11.86417613515741	3.85749724587490
H	8.16035473093713	11.25079042015251	5.53057923176677
C	5.75667971072513	13.85006803209319	3.67739856956792
H	4.67561883059009	14.05837274486731	3.58102766758809
H	6.15218288762032	13.63414068003494	2.66660920350753
H	6.24345401022784	14.77725856728146	4.03227824060042
C	7.45125374907513	14.66569091108874	7.27783367898215
H	8.14463988552617	13.87029021419975	7.60702967495416
H	7.58814193707369	15.53506232448336	7.94872731759873
H	7.75804450002469	14.97976674630439	6.26263928176995
C	4.67619055775312	15.58842868641562	6.76404675664668
H	4.91192146713164	15.86289498120328	5.71981333346690
H	4.91287450440687	16.45898010434587	7.40542645163321
H	3.58623070959464	15.41648636855069	6.82037262641227
H	5.94394205149696	9.81083847677093	10.68540961741702

[**2**]$^{-}$, (S = 2/2), strategy 2, B97-3c

Co	10.77099327609002	5.93040380866068	4.84982130749371
Si	7.83439185862678	6.73207675392600	5.53641342976628
Si	11.22073589934194	6.90313802421749	1.98124716410429
Si	13.64493554865779	6.01942109205664	3.68103722903794
Si	10.29024752471660	8.15672393875087	6.78520226664966
O	11.09396631264386	4.25439560261841	5.68235130610891
N	11.97528448900506	6.32100605387140	3.40839355694037
N	9.50807550086064	7.04975546936827	5.73669677943466
C	10.25965458508229	3.25714239038968	5.65334947968548
C	10.30990509528218	2.33396492200892	4.53326335458339
C	9.89054606729486	0.99154396517222	4.61888298912332
H	9.50278773540168	0.61198954587661	5.55256063847161
C	9.38187757150072	3.08643211946959	6.79982010695134
C	11.02282837533680	1.88339860675931	2.25444610601517
H	11.47020121108125	2.24057689608815	1.33515772032585
C	10.89675651359168	2.74877949086137	3.32224187403066
H	11.24231088611975	3.76805648406721	3.23574543192621
C	9.74787985627717	3.66691138208698	8.02827774637845
H	10.67711157339887	4.21280544935969	8.07592820271975
C	8.94586700570407	3.54400707522222	9.14539495485179
H	9.25942829276447	3.99604777602125	10.07856387254977
C	8.14136685121134	2.42597043004150	6.74107623188182
H	7.78593797138663	2.04220136197142	5.79609497747574
C	10.58398763261013	0.56596084599793	2.34911592283200
H	10.68690379841121	-0.11109348349113	1.51034260988187
C	7.56543637774851	5.40837869250038	4.21973729022369
H	7.80312302619105	5.78986050672326	3.22802223671418
H	6.52218260164124	5.08668692435640	4.20704309175885
H	8.17542111853049	4.52261192653758	4.38893453874350
C	10.02742832296721	0.12875035636936	3.54686575123619
H	9.70611278971690	-0.90122270363281	3.64998323215297
C	6.87215833518501	8.25714797888639	4.95318278801786
H	6.85737119776434	9.03561577535398	5.71481338134518

H	5.83547803956785	7.99878036413305	4.72583376442303
H	7.31308516548526	8.68416223631551	4.05279714389656
C	10.09029056601232	8.36526502535617	2.34553387858667
C	11.58749120907345	9.17098154276062	5.86220715652349
H	12.22821839373769	8.52942334659576	5.26106536359397
H	12.21465386330959	9.74778039373304	6.54454670817004
H	11.10272377023623	9.86837934377513	5.17842214968213
C	12.43983231977553	7.50981274668104	0.65979935887676
H	12.96596880865165	8.40776754056430	0.98003931792504
H	11.89861912827126	7.75517339882243	-0.25628750873969
H	13.18754072223852	6.75843001649425	0.40577802961344
C	7.33657249177179	2.31706090809590	7.86057353764940
H	6.37624505749539	1.82210586527871	7.77912624654332
C	14.00955431597388	5.63748985696374	5.48956765705894
H	13.76199861034707	6.48199015502643	6.13263664172879
H	15.07396165563686	5.42786421535921	5.61869718371306
H	13.44590811879216	4.77717240084395	5.84097099383974
C	14.27223647678418	4.55351417872632	2.66219681016081
H	13.75633941355060	3.63771254583208	2.94897510135283
H	15.34312647843867	4.39204286602936	2.80240823947499
H	14.09716331543473	4.70653404202363	1.59651957080743
C	10.20199758337157	5.56301854369817	1.12356066484322
H	10.84450693330599	4.76101060282122	0.75883779704690
H	9.66272151007232	5.97097256446341	0.26583374396314
H	9.47331237868371	5.10977311499879	1.79127364161750
C	6.98949746264919	6.15756830115720	7.12254772899795
H	7.41227514004250	5.22367558189510	7.48288371136018
H	5.92013714236498	6.00119005762321	6.96438055534804
H	7.09852118888623	6.89530792697219	7.91781375064823
C	14.74907769004373	7.50143435825560	3.25835278294963
H	14.82003934140547	7.68680565024885	2.18861798905562
H	15.76182903149130	7.33191791577103	3.63061810801625
H	14.37392960773268	8.41043278989820	3.72930066520722
C	7.73583872684973	2.85980619114400	9.07740160576384
H	7.10075597724212	2.77706183635999	9.95013567391484
C	11.13926854643800	7.27718807630535	8.22512461033666
H	10.40579834862233	6.73213492872325	8.81979804050425
H	11.65634130330139	7.97832813926330	8.88385329334901
H	11.86804913083804	6.55116423693262	7.86704399178426
C	9.11786535142012	9.42471709417816	7.57140620842342
H	8.66536132927727	10.07104178850945	6.81991135123639
H	9.67261721272097	10.06391482507185	8.26147189146322
H	8.31171121364388	8.95824400934591	8.13726552585316
H	9.49127353160183	8.64610890445295	1.47722299571674
H	10.67823435061600	9.23274336214980	2.64629785391381
H	9.42096784464936	8.13722875188136	3.17091290439233

[**2**]$^{-}$ (*S* = 2/2), strategy 2, PBEh-3c

Co	10.71199429324436	5.91357591154648	4.89177910557436
Si	7.87550918772719	6.98507180603518	5.67038733382174
Si	11.13755973877037	6.82874050016357	1.92888925454507
Si	13.57186507868536	6.14033945806761	3.65491244181392
Si	10.39911734489630	8.21310755733722	6.92472754560026
O	10.98458689039466	4.14899845165171	5.54027042022432
N	11.88819531293442	6.34499573019622	3.39238528829733
N	9.57041584287923	7.14873206198829	5.86859880623278
C	10.21520972308119	3.09817343574908	5.53027066270657
C	10.39963575160418	2.11698336029749	4.48102982366745
C	10.02253791375113	0.76462152091836	4.60467532732794
H	9.57714209477750	0.41473444983998	5.52593056551811
C	9.27328819201247	2.93964099463873	6.62535872311213
C	11.29242779433546	1.57038791354641	2.28387014357757
H	11.79459229815266	1.89790343496569	1.38114430156674
C	11.06469255927810	2.48582602243175	3.29318469182676
H	11.39326760578811	3.50755767476475	3.15925288633190
C	9.51724634720039	3.60324454599390	7.84301382045183
H	10.41014362067835	4.20435741852686	7.94403645517167
C	8.64529067849061	3.48866903253874	8.90881081078123
H	8.87088520880967	4.00290595372432	9.83527664936199
C	8.07623565869584	2.20705116056295	6.52437987278930
H	7.80883128213647	1.74709033421604	5.58201734836712
C	10.88889275327052	0.24579000885987	2.41507359129750
H	11.07210332778277	-0.46949107868829	1.62352616228551
C	7.49772193288076	5.62868472230786	4.40142277846630
H	7.89862388351001	5.85385292023408	3.41024095943608
H	6.41710100572088	5.51982607500924	4.28161755726593
H	7.87669648648613	4.65153590131823	4.70838886414271
C	10.25945919600778	-0.14569260787653	3.59172879228002
H	9.96418762819609	-1.17916608531196	3.72926020881722
C	7.02849114296543	8.56273476162519	5.02675819105754
H	7.04630435003376	9.36211557881434	5.77018630563123
H	5.97963744584243	8.37451359033919	4.78340308694967
H	7.51073236170765	8.94706875006871	4.12611762348426
C	10.02168906090482	8.33344323444535	2.19789056434207
C	11.66471110187092	9.25972025440427	5.97930224972280
H	12.33455586043029	8.64151216620477	5.38010000083193
H	12.27835159879374	9.87311177003843	6.64269899401777
H	11.15359884882112	9.92517632910651	5.28020704567434
C	12.35089699137257	7.31457086143319	0.54938318898295
H	12.88240626388600	8.23813498882890	0.78179640509710
H	11.80922149650504	7.47535110109777	-0.38565287132018
H	13.09866978687862	6.54189716608248	0.36061767255280
C	7.20204580940902	2.10673427954316	7.59165393332350
H	6.28267526367837	1.54573999553716	7.47346385317195
C	13.94819485408304	5.77544267221249	5.47574372939665
H	13.67722309433124	6.60344571887387	6.13584843737142
H	15.02144892105106	5.61200656482819	5.60361891186961
H	13.44051142203935	4.87789217598270	5.83051946436310
C	14.30282212690252	4.69869332507603	2.66041459676939
H	13.88419472303978	3.74811371756615	2.99632401434427
H	15.38844560184053	4.63670174439157	2.76794437208647
H	14.08629657568964	4.78928629650494	1.59355133397762
C	10.06913590031965	5.45031580814264	1.18354228921963
H	10.67068399562015	4.56960749302918	0.94800166676441
H	9.58851042785499	5.77636144655562	0.25746831585002
H	9.27637659033525	5.11034339903807	1.85289533499065
C	6.94950354419984	6.51647620329046	7.25416794067357
H	7.31742286947612	5.57351134781483	7.66034548624789
H	5.87850094265866	6.40116263480658	7.06935097238838
H	7.06204223505351	7.27844816326692	8.02825376864079
C	14.60231162954525	7.68108134224468	3.23227282274042
H	14.66496961667737	7.86795001867686	2.15965658354331
H	15.62540582429411	7.57537921325016	3.60154786379531
H	14.17583614192206	8.57394014273007	3.69424169176966
C	7.48190832208035	2.73427698545468	8.79986288646982
H	6.79636148033828	2.65520412479867	9.63367471958553
C	11.32421632679545	7.25763646957937	8.27809010728562
H	10.61616655872949	6.71728227207226	8.91014217568125
H	11.91024031696047	7.91722197193555	8.92241135089686
H	12.00805415422249	6.51446299111704	7.86312334602966
C	9.27526359651117	9.44584330367628	7.83235388899624
H	8.69698690628217	10.05779162996493	7.13858161888753
H	9.87423740200323	10.12505857547364	8.44362907098973
H	8.56965192000158	8.94673660148737	8.49842015075694
H	9.55410274312656	8.67358630037287	1.27105181109803

H	10.59883139386628	9.16515389834873	2.60763075296368
H	9.22684882686739	8.12539003431200	2.91521308737631

[**2**]$^{-}$, (S = 2/2), strategy 2, BP86

Co	10.81746925876892	5.91615542408971	4.85464745936478
Si	7.81843503942352	6.59196420501803	5.49000742408354
Si	11.25206975530636	6.97355667792953	2.02793630059782
Si	13.69837574187907	5.96247865874847	3.71610905690532
Si	10.26239642166648	8.12845387435928	6.75607114309806
O	11.18323020516930	4.26664950098682	5.69748242051369
N	12.01688086530314	6.35825485694332	3.46828008798241
N	9.50651348751617	6.94795640788960	5.72517670920511
C	10.30997177282988	3.28652875884502	5.68812121478417
C	10.29538469504686	2.38167253809971	4.53594623175312
C	9.82940447305122	1.03580978973720	4.58732050189666
H	9.45852675064359	0.62939052319497	5.53474124589841
C	9.43827846020357	3.15689047938474	6.85639309059772
C	10.90669863545020	1.99980920760965	2.18355415127015
H	11.32943372939308	2.38854446347547	1.24773747067685
C	10.85183252114043	2.83349031890503	3.30383138858639
H	11.22242794959707	3.86448148821873	3.24863540355958
C	9.80548850531956	3.84257424924616	8.05055764721406
H	10.73186222761516	4.42450135383862	8.03562105069701
C	9.01229041316838	3.77617306824083	9.19921777109651
H	9.32818297658267	4.31160591846573	10.10454975957655
C	8.20049245573970	2.45143212285248	6.86223933391460
H	7.83983856365069	1.98686392659633	5.93811216645610
C	10.42239882339454	0.67744417662832	2.24526910958387
H	10.46548246045226	0.02458641733237	1.36405233449150
C	7.63108004467071	5.19765618573658	4.21229783557247
H	7.96236450459790	5.54104595613092	3.21591338499560
H	6.57348746705580	4.88194331691967	4.13048167606709
H	8.22827100902461	4.30912697676981	4.48229949921421
C	9.89255020630089	0.20430201654530	3.46162046606940
H	9.53596266796258	-0.83209016414538	3.53805169877683
C	6.86106493300704	8.09418190360370	4.79536509938437
H	6.83628554305394	8.92563941559760	5.52289356550116
H	5.81504275300298	7.81680436681461	4.56111325389256
H	7.33510328811368	8.46646721835845	3.86921023873340
C	10.08377354954612	8.40708479746676	2.45980853845524
C	11.50368818010455	9.18478971962547	5.77142193126148
H	12.09481904684767	8.52595773963545	5.10961557508695
H	12.18793182544970	9.74614151875979	6.43506027657616
H	10.96960189949999	9.90636683642932	5.12631487209597
C	12.49268590957184	7.63748335579171	0.73206046575676
H	13.05169260591038	8.50937536773275	1.11618464531199
H	11.94350998290260	7.95705184066565	-0.17446537213697
H	13.22453801758016	6.86612635719759	0.42840314737034
C	7.40588100176180	2.39548488215728	8.01422964193634
H	6.44780197084813	1.85955983792797	7.98135442721329
C	14.05180105193300	5.55406072319957	5.53550339430794
H	13.84768745857653	6.43207522510198	6.17615905241577
H	15.11434279006214	5.27275927325520	5.66769714124533
H	13.41072782787898	4.72335564740635	5.87800192769755
C	14.21527603550641	4.46388831365203	2.65772747608611
H	13.63014417297132	3.57389371625640	2.95276439199456
H	15.29019375482368	4.22686084200546	2.77314489766685
H	14.01908982370015	4.65592594411049	1.58616875325830
C	10.25895421743746	5.62385187784277	1.12160590683834
H	10.93574089061841	4.83197236803308	0.75120812774360
H	9.71623660753690	6.04537826492307	0.25384627791599
H	9.52487649592739	5.14071032414080	1.78961104657341
C	6.93515216584144	6.07649468859120	7.09132114015809
H	7.40708074577778	5.18066517790142	7.52666413000147
H	5.86899747242481	5.84891375035397	6.89991884672826
H	6.98046375733466	6.88415711483768	7.84489548213137
C	14.85145056713736	7.42175521806250	3.27754768025100
H	14.88339181889892	7.62702089442093	2.19360555994393
H	15.88312515734606	7.20577536816248	3.61594264367268
H	14.50806315695690	8.33947053228860	3.79016974980404
C	7.80834395852856	3.04242043810070	9.19918174398322
H	7.18047924804024	2.99949609760823	10.09801161042414
C	11.19743195863787	7.29775260551334	8.19244192515722
H	10.49066114304783	6.71435357085012	8.81032571160050
H	11.70404274034637	8.03898712859768	8.83991825693561
H	11.95762839618144	6.59748795258713	7.80129208408082
C	9.00839183966234	9.33328305802634	7.55106344756597
H	8.47564449775732	9.91999025552661	6.78079218385652
H	9.53400624786298	10.04451881442436	8.21670604375373
H	8.25434167884328	8.79702593495519	8.15566527257553
H	9.37441283727363	8.62852645922792	1.64071362879930
H	10.66355449826596	9.32224991968956	2.67931532530860
H	9.51991339173514	8.14883264798851	3.37350579858473

[**2**]$^{-}$, (S = 2/2), strategy 2, PBE

Co	10.80140610729650	5.96098463898868	4.82951005693971
Si	7.79396758447606	6.63521403611909	5.47790806948854
Si	11.30003847704932	7.02369628439720	1.99558457473040
Si	13.70246847071899	5.93369758238391	3.67985523171422
Si	10.22782080758759	8.18254390225813	6.74637265078691
O	11.09078192439345	4.29019442331917	5.69242094655696
N	12.02829813254946	6.38710511304597	3.45099727501972
N	9.48451529360090	7.00844703944504	5.69296894259113
C	10.26957930811722	3.27075866270895	5.71032139741270
C	10.26222345854442	2.35618117976529	4.56549371025993
C	9.85550409305646	0.99248509181579	4.63945118757932
H	9.52434956578157	0.57999717268601	5.59893868947859
C	9.43909031674235	3.10141553776198	6.90607371318265
C	10.83132561951638	1.97445665674168	2.20230220963735
H	11.21415671626898	2.37148436091031	1.25275481156225
C	10.76966897262589	2.81589390511961	3.31583638256533
H	11.10204697028938	3.85921053062912	3.24331255935284
C	9.82004773033309	3.78437305272771	8.09655577228961
H	10.73335001390272	4.38691639895423	8.06534166748649
C	9.05425802951049	3.69710458898943	9.26166669881526
H	9.38101526069482	4.23312887182295	10.16280281576014
C	8.22072976741761	2.36510179155942	6.93921162615506
H	7.85026848441553	1.89361859112365	6.02222063710973
C	10.40478210288672	0.63477497836578	2.28807130926216
H	10.45340118868013	-0.02473408671197	1.41236180679083
C	7.59835554003613	5.24032737943610	4.20058704941700
H	7.96231063724525	5.56413077033721	3.20905268662890
H	6.53313945902048	4.95885678174727	4.09801754699478
H	8.15946375154777	4.33469544422464	4.49146726190674
C	9.92641825007084	0.15328208520074	3.52133002209968
H	9.61623615234913	-0.89620827024842	3.61678805772529
C	6.80888567867369	8.12734512231006	4.79997474091594
H	6.78134669621769	8.95787437379022	5.52787544425960
H	5.76486893827142	7.83535414774043	4.57705515584289
H	7.26804781316794	8.50555411027050	3.86868689647759
C	10.11853395481335	8.45494732377643	2.40237608994632
C	11.48385489856546	9.24951471665354	5.79186028155804
H	12.09998747327519	8.59784242374162	5.14597916190981
H	12.14360611444836	9.81624660595050	6.47497031158071

H	10.96009058029288	9.96670815047893	5.13383053123778
C	12.56993350982048	7.70821749195845	0.73850183132639
H	13.11861259150162	8.57397919970304	1.15001040431550
H	12.03756967207428	8.04352138414326	-0.17186936990194
H	13.30939801055981	6.94470018044419	0.43495940863285
C	7.45287872122802	2.28862024797539	8.10739734556181
H	6.50746955273271	1.72999323037818	8.09375810000060
C	14.04589562853975	5.40783840668280	5.47120751329604
H	13.87866638977818	6.25363296078887	6.16368717908236
H	15.09793254812662	5.08104517225468	5.57608246362785
H	13.37596265990074	4.58450592202783	5.77334648585538
C	14.19374010065697	4.48630180771805	2.53891292786816
H	13.57770757055979	3.59755019392467	2.76706536031994
H	15.25815961371175	4.21160171397620	2.66404129670835
H	14.03021666066089	4.74736726684365	1.47682464851745
C	10.32977494209563	5.68608969673677	1.04406764067142
H	11.01136003872396	4.88384685265167	0.70604972157878
H	9.83582434400194	6.11585560609396	0.15198941360058
H	9.55633350924523	5.21649956562687	1.67674707937322
C	6.93435936620296	6.08984204919588	7.08550622788500
H	7.42035345348523	5.19233317604653	7.50412509178637
H	5.86957731707292	5.85266569620873	6.89969255035708
H	6.97583482263961	6.88704265039463	7.84999864023184
C	14.89546327169485	7.38657159956364	3.33398439117678
H	14.93131149535052	7.66453234981895	2.26677570662717
H	15.92073617514653	7.11952105867442	3.65363635861756
H	14.57846176249237	8.27611141987379	3.90917583112730
C	7.86545876045039	2.94138196165873	9.28428769581768
H	7.25876061533107	2.88167914422123	10.19648368759291
C	11.14622290569925	7.34642252666261	8.19212002996360
H	10.43872451035462	6.74332155877545	8.78977595844421
H	11.62627695968078	8.08956565275001	8.85688672694645
H	11.92670743529619	6.66406991481072	7.80926687820886
C	8.96789676285304	9.38689917142536	7.53388527710543
H	8.45089841095395	9.98503805760247	6.76207259571145
H	9.49172020431315	10.08695264773005	8.21202557546452
H	8.20196781556605	8.85253098032092	8.12454530120436
H	9.44553097043404	8.68559885765223	1.55588717205206
H	10.69245320352842	9.36571314919029	2.65257010333745
H	9.51575838308243	8.19219600715691	3.28961476887749

[**2**]$^{-}$, (S = 2/2), strategy 2, PBE0

Co	10.77516147784086	5.92482688791692	4.86865472347677
Si	7.85909281654098	6.74560251101507	5.53924836763860
Si	11.24869223770466	6.92262657034277	1.95135490300067
Si	13.63643113580413	6.04362807449636	3.72438232238540
Si	10.29582443879434	8.22725844901636	6.79784313511662
O	11.05502422681202	4.17950664899341	5.58594693725906
N	11.96795693661360	6.35589084883377	3.41233711179279
N	9.53504137462122	7.08914191125707	5.75274815508603
C	10.23766362058196	3.16552258821433	5.61486032423705
C	10.24859644692157	2.24316398968721	4.49190950958691
C	9.78082132684664	0.90785408500042	4.54744402861131
H	9.39120170361105	0.51373339104598	5.48332499326951
C	9.40099614432360	3.01917009995818	6.79828748049709
C	10.90342081688148	1.83249955137083	2.17262420139232
H	11.34620090188362	2.20445291373732	1.24861495540821
C	10.83247923140385	2.67289337239079	3.27467307607856
H	11.22355438197439	3.68724741913490	3.21608607916133
C	9.79440839499892	3.69017270611681	7.98035181206584
H	10.71407413482032	4.26888012535787	7.95095483881172
C	9.03273706789266	3.62038440530742	9.13811454058227
H	9.36912887751317	4.14527341513014	10.03241990050993
C	8.17302936584407	2.31886548329259	6.83069067182327
H	7.79289315155873	1.86017399686416	5.92055531601416
C	10.41486922970415	0.52353897094183	2.23869740074963
H	10.47455168948340	-0.13535725055862	1.37318112713240
C	7.67810739146957	5.41957881778315	4.19735266950043
H	7.98334957917722	5.80702675360563	3.21684107260891
H	6.63290247035770	5.09263313869082	4.11428839695389
H	8.27961897287994	4.52710606662816	4.41853290287487
C	9.86413132991195	0.07019930419292	3.44149674464594
H	9.50661161036643	-0.95671503518103	3.52273127486248
C	6.86895020256130	8.25641973324181	4.94916820109293
H	6.82715013628877	9.03162471808460	5.72443266787377
H	5.83663278755010	7.97078700584513	4.70363441706782
H	7.32550041972647	8.69648742503750	4.05346463373267
C	10.04980218776456	8.33721735006511	2.31896013758927
C	11.56623569510915	9.24411833201272	5.82907995673498
H	12.16914204005737	8.57791951200582	5.19854361765001
H	12.23394251546504	9.82009066394215	6.48354824369662
H	11.05162178527118	9.94118340463497	5.15490446103692
C	12.49974664078198	7.58566057225206	0.68429831204028
H	13.01230699484829	8.47868435441011	1.06254867355540
H	11.97312021149806	7.86344500051478	-0.23918408043484
H	13.26144384453664	6.83872992541599	0.42503510778220
C	7.40897287251985	2.26175984813929	7.99122939954910
H	6.45740023612034	1.73001078565211	7.97773255835119
C	13.89015567630682	5.69275897289886	5.56481195488746
H	13.63607031786405	6.57259533579352	6.17126825598872
H	14.94226145414001	5.44724297371467	5.76339921302308
H	13.26599883922601	4.85096899807546	5.89142769976765
C	14.27458072445509	4.54305939736413	2.75898173401645
H	13.70834890659230	3.64748346605663	3.04519014143575
H	15.33954981093663	4.35564659641455	2.95296477844708
H	14.14751908932915	4.68949076531431	1.67794074401866
C	10.29196524147510	5.55544477517091	1.05119470733609
H	10.97979568313073	4.76689002088539	0.71908372113851
H	9.77443087716943	5.95140256574187	0.16655212010042
H	9.54484463435467	5.08040833428047	1.69837450840205
C	7.00321808640137	6.12076653068626	7.10503350762469
H	7.45438793266569	5.18283065264790	7.44813603314460
H	5.93366180572149	5.94408800999017	6.92651678641725
H	7.09272125131332	6.85373793464892	7.91756881855054
C	14.77575807027430	7.50837508800009	3.31773504117470
H	14.84215638308402	7.70094095201613	2.24091729749615
H	15.79073235935279	7.31003894292430	3.68909675838909
H	14.40786053346526	8.42094471411938	3.80497127915030
C	7.83489056153876	2.89817945911407	9.16040324484946
H	7.23114941898075	2.85348999191101	10.06588968551391
C	11.19870234389221	7.34317164432683	8.21101071821479
H	10.47553650684520	6.78177393325625	8.81704162095862
H	11.73259576998874	8.04580234955790	8.86539255753069
H	11.92644588026193	6.62212287754842	7.81708513119179
C	9.09515194066758	9.45169785391921	7.61352881761178
H	8.58899013010635	10.07518960228595	6.86609369656705
H	9.64534999079620	10.11790327232633	8.29213394813054
H	8.32747295502080	8.93268257799604	8.20173079671261
H	9.39342782462763	8.56340893621354	1.46842283303349
H	10.61076527924414	9.24478173324005	2.57784790544598
H	9.43511366553265	8.08543989972168	3.19159066327706

[**2**]$^{-}$, (S = 4/2), strategy 2, PBE

Co	10.72201578200459	5.99835472707567	4.78224409568597

Si	7.80185347792550	6.69270846684939	5.46110029235640
Si	11.37949032904790	7.26293021091611	2.05697314686887
Si	13.63573836303746	6.01762285578089	3.83003120931875
Si	10.18331418626063	8.28511688320140	6.77026130848210
O	10.90180986048401	4.14167557402193	5.02213011720538
N	12.02805439186498	6.64700103491976	3.55385104780752
N	9.48697338015722	7.10322300436287	5.69007370341726
C	10.18404932313029	3.08200277181380	5.34164656897396
C	10.12010583639776	2.01718313724795	4.34944528183417
C	9.76635221364675	0.66300542281856	4.63168715702651
H	9.54420454667206	0.36813029937745	5.66319146385737
C	9.54246271427394	3.04486703751239	6.65104538150074
C	10.47407815253053	1.34514284268788	2.00406662951916
H	10.75472161065615	1.62239086972007	0.97880140397778
C	10.49506789583229	2.32020454427191	3.00338353573560
H	10.79050500719392	3.34981468567613	2.77506369579981
C	10.04841913492338	3.87985358500275	7.69250799179048
H	10.91090415180444	4.51640707440207	7.47021965775539
C	9.46994946588409	3.89205365065092	8.96337998605100
H	9.89787981619788	4.53876448155905	9.74115872644086
C	8.38527279761243	2.26594752127450	6.95390149506447
H	7.91288964998225	1.67612416835646	6.16061426313952
C	10.09526618208780	0.01953486716693	2.29733005553038
H	10.07917643754566	-0.74585915062956	1.51119034709809
C	7.64336323014613	5.33374709793954	4.13903363745245
H	8.01407967470169	5.68106337416946	3.15759263906037
H	6.57857667223262	5.05838676336048	4.01722328928953
H	8.19353456583387	4.41588073655416	4.41430023393325
C	9.75330273301777	-0.30771131933168	3.62535766045655
H	9.48729372541970	-1.34234833959224	3.88221464209396
C	6.77820713086794	8.17709229378280	4.82831125496564
H	6.72221855646379	8.98355432749907	5.58074242074131
H	5.74479135142143	7.86025514047120	4.59127906793551
H	7.22886806068218	8.59714967455511	3.91082805824726
C	10.11423914452944	8.63756587522849	2.40147946355801
C	11.44784734535842	9.36509667443084	5.84936540427570
H	12.08008130030206	8.72253367462603	5.20937626208538
H	12.08834634825396	9.93385899133659	6.54877507093503
H	10.93057047262237	10.08190765169759	5.18582362342257
C	12.70996558900639	8.00050847086685	0.89977309430833
H	13.24100872236906	8.83972811058647	1.38367716714216
H	12.23075683195565	8.38335957975679	-0.02116362659214
H	13.46017213020128	7.24552056033230	0.60113465795844
C	7.80358995719009	2.29354698572517	8.22557087805594
H	6.90084847191327	1.69725712209615	8.41550649931989
C	13.83141801143998	5.47428355397654	5.64121798262528
H	13.65114588101058	6.32145117772686	6.32828869287689
H	14.85686868156453	5.10037225946246	5.82326881008282
H	13.11505484304368	4.66821671090856	5.87888319251641
C	14.01204531248969	4.51355626450248	2.72482346028330
H	13.27799599924394	3.71443572866398	2.93480648964970
H	15.02675819715158	4.11172736352738	2.90590137612910
H	13.93410985750750	4.77671745390175	1.65353533802593
C	10.52295705746307	5.88548008560858	1.05226238054509
H	11.24724583835056	5.08590848170467	0.80991737464637
H	10.10489185452569	6.27332498806586	0.10393764201062
H	9.70108961854923	5.42122255942612	1.62637423023856
C	6.97174237483192	6.05962245511518	7.04970325180998
H	7.48006372216187	5.15177336973013	7.41781479886600
H	5.90892055776335	5.81295695215122	6.86593792476651
H	7.01050316774990	6.81901021711379	7.85194831486404
C	14.97903490608459	7.34153880046698	3.52675958705796
H	15.05039497694527	7.63317847881719	2.46480912833655
H	15.96827406242002	6.96189948564188	3.84577917499205
H	14.75268963206468	8.24955232336265	4.11546461132183
C	8.34474797732238	3.09380153240805	9.25161392462316
H	7.88511884510247	3.11260716631761	10.24749241931687
C	11.07604260961746	7.44620900543883	8.22986074493975
H	10.37182836488046	6.80052294245677	8.78451210465708
H	11.49559143661694	8.19389503771104	8.92927002087237
H	11.90450567543776	6.80856845995378	7.87166835419413
C	8.88469133544968	9.45880661124152	7.53718614927659
H	8.38516036492344	10.06421627157078	6.75975233610529
H	9.37831281880680	10.15295668553439	8.24332623114517
H	8.10711656328570	8.90529639693069	8.09413063667993
H	9.48696597799885	8.85233430106634	1.51672577514627
H	10.62971872090100	9.56808240377901	2.70099368035060
H	9.46692903565052	8.33599846358728	3.24381590016414

[**3**]$^{-}$

[**3**]$^{-}$, strategy 1, positions of hydrogen atoms optimized using the structural parameters from the solid state, PBE

Fe	2.08858742348189	8.13917023511926	12.77901699408715
Si	0.04997635869044	9.13176682484680	10.56447435066267
Si	0.05229357699939	10.42870205679580	13.29233000126506
Si	3.79826667507470	5.59691013114882	12.35494823686697
Si	0.88856898790789	5.20016537783818	13.03145222210832
N	2.22609140770663	6.18120128857118	12.66062473172584
N	0.58899797593497	9.25685933024045	12.17596323291296
N	3.53126079366782	9.09426457718118	13.60429348165590
H	3.31613719132122	8.96956209160787	14.60391044862163
C	5.31302795395991	10.35376624622968	14.65034892392073
C	5.34512183104188	9.52919390961395	15.78424446844410
H	4.86728996005041	8.54071790932149	15.74744172910558
C	4.52797125473889	9.91345093571693	13.45756079579792
C	4.93063257667460	10.37383658301332	12.09881446416548
C	3.96959155783571	10.45651255658624	11.08472324379524
H	2.92146476438732	10.23814096422848	11.32980906263674
C	5.98218796918158	11.57489549550979	14.73687474388373
H	5.94590986254449	12.26388935697253	13.88357777958890
C	-0.59882830747155	6.18041164183285	13.57863453197908
H	-0.42919745273426	6.64184753662720	14.56943495845965
H	-1.48699608086293	5.52482239938694	13.65751787552976
H	-0.82542205981367	7.00399820515670	12.88022305860291
C	-1.67723870772250	8.39589020699391	10.43190268339875
H	-1.69241512521048	7.36815994795240	10.83729858750017
H	-2.00488881511652	8.34301675392003	9.37585578907698
H	-2.42388674855022	8.98648205218931	10.99038871575272
C	0.01420884608323	10.79186690058255	9.68052485870726
H	-0.70295727268161	11.50028805440473	10.13458459027153
H	-0.26863126593056	10.66351986121075	8.61844999479075
H	1.01276654341265	11.26617244118258	9.71091212525971
C	5.62530092283090	11.07774728012630	9.46342719624257
H	5.89636047672650	11.34631605739741	8.43378757746114
C	6.25560926928652	10.66465658808022	11.74434168839766
H	7.04451992750108	10.57229447835836	12.50141074232318
C	-1.78633387512835	10.79522732448354	13.11983079391357
H	-2.04271147787891	11.18231144325879	12.11673064124443
H	-2.09563930027411	11.55890618721311	13.85877436725818
H	-2.39665241787587	9.88968935153907	13.29398719696353
C	4.67270280467826	6.62686607498290	11.07324122410906
H	4.12282964963803	6.60301217200122	10.11464139481712
H	5.69473246376790	6.24399203625633	10.88901438120592

H	4.76038625621331	7.68717982256996	11.37009301151264
C	6.02691115505883	9.89329417709093	16.92681445225645
H	6.05127787065180	9.20827536247948	17.78588630622329
C	4.31161191791453	10.79467220796165	9.79296686204134
H	3.52601049270281	10.84790104149712	9.02571608592363
C	6.69895280280624	11.10438552078709	16.98132181891096
H	7.23923642035914	11.39988868748665	17.89031998134311
C	0.93891530152914	12.06990922610206	13.12366176287701
H	2.02624907851368	11.93104428382324	13.27260101590816
H	0.58051043856536	12.80053092777299	13.87382860776445
H	0.79879699787943	12.51527911521529	12.12102884877422
C	1.18793041054469	8.02325378061798	9.56886647866218
H	2.19110302178879	8.47593329044377	9.46250153503540
H	0.78231542281127	7.84236411698835	8.55547534682710
H	1.32711638766401	7.04726796545854	10.06879737977818
C	6.59374970677825	11.00850566889438	10.44787302796405
H	7.64542642615608	11.21308606768724	10.20349568058874
C	6.65870627372809	11.94205338227871	15.88416613367007
H	7.16178561487677	12.91818131954757	15.91832789859884
C	4.84558130505522	5.59403389680083	13.90582042998405
H	4.95354757389360	6.62772260267280	14.28279378741312
H	5.86099477149766	5.19613733975756	13.71949606051796
H	4.38177121136042	4.98786065908069	14.70581896050737
C	0.31379618050854	9.88549566371991	15.06114362204012
H	-0.14098472484093	8.89724678474752	15.25476349067003
H	-0.14156587660131	10.61331042135802	15.75992640560201
H	1.38798830240254	9.81818619692607	15.31141174349372
C	0.31074710207601	4.18881545248113	11.56321644500917
H	0.03613239599922	4.85596804708862	10.72428475316192
H	-0.58041030620672	3.58356266831313	11.81803074546628
H	1.09072082406881	3.49960563667780	11.19463559561873
C	1.24418469263692	3.98408512358183	14.42370663989895
H	2.07003656764371	3.29322743252146	14.17429849037217
H	0.35227184442637	3.37175628603111	14.65684489713086
H	1.53302146217990	4.52506440292608	15.34406123706996
C	3.85876060042318	3.85483894305089	11.66999770722205
H	3.39193117074771	3.09666534847030	12.32517691346840
H	4.91700447513584	3.56278430544142	11.53071237501074
H	3.36784431317765	3.79387695797027	10.68148858117133

[**3**]$^{-}$, (S = 3/2), strategy 2, B97-3c

Fe	2.09218834075654	8.20710876054045	12.80642051778689
Si	0.09520023700322	8.98961675099807	10.50857777082476
Si	-0.04185329375939	10.46809386770262	13.17339487224797
Si	3.82388593322972	5.67742980308669	12.35473608557387
Si	0.88781915765000	5.30407367179590	13.08195038339663
N	2.24136341250751	6.27283665601096	12.67030029448368
N	0.56544307437235	9.24256070442967	12.13827794345452
N	3.44504688086816	9.19430874436001	13.78787623710070
H	3.29206890333372	9.05920121637815	14.78204597893198
C	5.40236467080537	10.28018690864021	14.70353628521842
C	5.50944761972813	9.42686419284234	15.82167303729914
H	5.02036198701561	8.46147086628050	15.80140886956930
C	4.54075867377125	9.94598336302078	13.58366998053793
C	4.84581419941997	10.38795101973158	12.23462671995952
C	3.83022144985653	10.52691474066819	11.27045151717683
H	2.80106123775769	10.37253845109921	11.55814837987978
C	6.11208984861710	11.49676575843037	14.76679578930092
H	6.02662355892276	12.19596387066214	13.94704394685542
C	-0.48350467415279	6.29917039448619	13.90518998632924
H	-0.16057376033917	6.66426910986381	14.88027746035254
H	-1.36933358206914	5.67838391881490	14.05762923707687
H	-0.76761814215799	7.16669989230886	13.31406446513628
C	-1.58891151749991	8.13931347553098	10.36264208769776
H	-1.58353701875006	7.18197693192214	10.88209276798507
H	-1.85282064483167	7.94905077989132	9.32019201527564
H	-2.38091997545637	8.74400064461435	10.80276616504787
C	-0.02782599962931	10.61140912495848	9.53138843463022
H	-0.80489497826447	11.27356227633011	9.91245549608981
H	-0.25001178029814	10.41623022427651	8.48010865512160
H	0.91315313974228	11.15990618436866	9.57354261991868
C	5.43683200099818	11.09656738010125	9.56476363152761
H	5.66382991117498	11.35982351182683	8.53928139921724
C	6.16919120459784	10.60916700121661	11.80869058941047
H	6.98057678362893	10.46164552465743	12.50720262957511
C	-1.89083402406690	10.79068718045696	12.89989900195355
H	-2.11432421002783	11.10346909876322	11.88041618990529
H	-2.24952046408827	11.57545267612994	13.56895813395620
H	-2.47392299024301	9.89170177577362	13.10175504429181
C	4.81627410666405	6.82550945164200	11.24412353420655
H	4.31964173639687	6.97220727223485	10.28629529612291
H	5.80526469061444	6.40525327338150	11.04681106102312
H	4.96088879954819	7.80802392595236	11.68527571791931
C	6.27479127647825	9.76713419530437	16.92186916405518
H	6.34550475421721	9.07520818058356	17.75289891478663
C	4.12406526087510	10.87632413751001	9.96553762242208
H	3.31559468661846	10.97858769513195	9.25247150830535
C	6.96792017859974	10.97183048445678	16.96105905456184
H	7.56551631083001	11.23747575994184	17.82359697392401
C	0.85733621277075	12.11580730390419	12.95628648883460
H	1.90721519089477	12.01268369990307	13.22906130815827
H	0.42479490064266	12.89391434179909	13.58891601877724
H	0.82116581403898	12.46435089498710	11.92454697319668
C	1.33705273937769	7.91872574506148	9.58214223910783
H	2.31175312873045	8.40175836376812	9.53053560881295
H	0.99765364038805	7.73401508437871	8.56021022112624
H	1.48238073694784	6.95892750839713	10.07306191358080
C	6.45654619824372	10.95476763270133	10.50175271124880
H	7.48884092230685	11.09891251087306	10.20500329243581
C	6.87313581879026	11.83261874642652	15.86884271884387
H	7.39062962428766	12.78470451706565	15.88548088418930
C	4.81930099726704	5.44533997575387	13.94551224016824
H	4.90521867925225	6.39739277322066	14.46852274574933
H	5.83065959753884	5.08749811314623	13.74245871496080
H	4.34109922130859	4.73721459598017	14.62174092560777
C	0.12210331173864	10.02043331204187	15.00022769637737
H	-0.32780773038639	9.05282147099768	15.21454461198928
H	-0.37283284119302	10.76849129233913	15.62372399685107
H	1.16641972067007	9.97911275742404	15.30489821870257
C	0.12955084391862	4.45301814253627	11.57141967990744
H	-0.20241268723609	5.18580693016832	10.83735870444902
H	-0.73342060566283	3.84222127469372	11.84503400791536
H	0.85424414341326	3.80529504310241	11.07988224943980
C	1.31875519898169	3.93359477161057	14.32078634902814
H	2.04993391732784	3.22654425293705	13.93053368094908
H	0.42745939815260	3.36539292271260	14.59538732722981
H	1.73132552231263	4.36277714843513	15.23439383017168
C	3.80772922407485	4.00607211960900	11.45577033586835
H	3.30486449281402	3.21895890662452	12.01620663928726
H	4.83005587652064	3.67117145580318	11.26849277999089
H	3.30982782080086	4.09349656248747	10.48977041961798

[**3**]$^{-}$, (S = 3/2), strategy 2, PBEh-3c

Fe	2.10188868301468	8.20785066528431	12.80245303578523

Si	0.09105327306715	8.98026562102293	10.52046693145315
Si	-0.03156530877857	10.46678432994779	13.17985912425685
Si	3.82612611053375	5.67224997332625	12.36160755307352
Si	0.88483209380863	5.31330276283900	13.06377694480613
N	2.24601007836077	6.27779561754627	12.66674445731092
N	0.57239510873348	9.23866410180930	12.14573306637839
N	3.45910119909641	9.18442451794894	13.77945308678764
H	3.31300899991584	9.03934681304891	14.77260903298101
C	5.41027474469696	10.27889891071416	14.69751036419192
C	5.53004931854761	9.41813874607340	15.80832811403110
H	5.05343564203331	8.44774320927258	15.77880167033038
C	4.55040566532716	9.94256793558096	13.57646425140196
C	4.85232900463740	10.39098701188535	12.22929078850943
C	3.83856593857792	10.51677652555647	11.26118257864476
H	2.81169835357282	10.34508379904522	11.54482029583160
C	6.10190836288738	11.50482209384799	14.77060312945665
H	6.00527477356589	12.20733898607707	13.95596892395458
C	-0.49999256331271	6.31942642107746	13.84933088416347
H	-0.20032566246455	6.68530789589605	14.83101454427671
H	-1.39430670037883	5.70671887806750	13.98083491075290
H	-0.76067898614625	7.18749493610445	13.24924347405216
C	-1.58988945035882	8.12196439570309	10.37982641719809
H	-1.57865312541984	7.15488179937431	10.88010470203996
H	-1.86216420450020	7.95098235038281	9.33643457826317
H	-2.38101737564213	8.71486320910534	10.83649742601342
C	-0.05211877728510	10.60183748528186	9.54816787293647
H	-0.81883516588757	11.26176417471237	9.95272715501530
H	-0.30219317490471	10.41084868180416	8.50285930762929
H	0.88916449766805	11.14987605574926	9.56885419835906
C	5.44315666974211	11.11295213706131	9.56230175573601
H	5.66934880639864	11.38253465559623	8.53908024176520
C	6.17388830261967	10.63110220631379	11.80760516134614
H	6.98350980050790	10.49462216511322	12.50925863030208
C	-1.88634564619732	10.77365903719344	12.92992970684891
H	-2.12831327718674	11.08581197562702	11.91490203141467
H	-2.24230109660376	11.55372972312880	13.60538668569235
H	-2.45733537692562	9.86916726566079	13.13971131216966
C	4.84189990509477	6.81785808382682	11.27055482008060
H	4.34414252603753	7.00466047612499	10.32050748322690
H	5.81590384762918	6.37336238527432	11.05448272710582
H	5.02012513219553	7.78385664138672	11.73431650581253
C	6.29057357221049	9.76031740901682	16.91141782204463
H	6.37135933234073	9.06333608806371	17.73646650593667
C	4.13231910111978	10.87259311864747	9.95789434396065
H	3.32667965159926	10.96523443994681	9.24114844597472
C	6.96574938059944	10.97485961841694	16.96031950061899
H	7.55900475044503	11.24216326140202	17.82448846356811
C	0.84998297379900	12.11893871977196	12.93387037245138
H	1.90932867573264	12.02490015376685	13.16872326901071
H	0.43401387063467	12.89573280889718	13.57846672558208
H	0.77494551906568	12.46443163237223	11.90341915938547
C	1.33096619627085	7.91438404723537	9.58631512149100
H	2.29548282564770	8.41252889087375	9.50259973170998
H	0.97243878629808	7.70364155469856	8.57641177772448
H	1.50426241480031	6.96757669981245	10.09277790184412
C	6.46149580933386	10.98399807622512	10.50270822938457
H	7.49211392219259	11.14317562591671	10.21012655570805
C	6.85845239438950	11.84305676671313	15.87522764691650
H	7.36149747129906	12.80201256217702	15.89986009111978
C	4.79827626792368	5.41953848416251	13.96271313005943
H	4.89780132876348	6.36947263274454	14.48662902861162
H	5.80390972818697	5.03811690891621	13.77670453164371
H	4.29237165593805	4.72389725809632	14.63141859268143
C	0.15208883861583	10.03508426694744	15.00820677619569
H	-0.30740437600496	9.07602990354461	15.23947618547890
H	-0.32767505590523	10.79521841508739	15.62867381972316
H	1.19798338969801	9.98450478527266	15.30404746495250
C	0.15002406356456	4.44639983336005	11.55061039437070
H	-0.13343373211773	5.17037606893004	10.78807650059549
H	-0.74208679303807	3.87391804694819	11.81193590758681
H	0.86410800709710	3.76050092359940	11.09743108302887
C	1.29598766794551	3.95787620181278	14.32535770628370
H	2.04932509590568	3.25883624775445	13.96483307733974
H	0.40568064929141	3.37901230684880	14.57883983874131
H	1.67597377543192	4.40023708515314	15.24648772353851
C	3.79875661461074	4.00758844518487	11.45267650543934
H	3.27323746967152	3.22777486728425	12.00172983088274
H	4.81695469835142	3.65523417770833	11.27775732041852
H	3.31496911201325	4.10892801029572	10.48124203660801

[**3**]$^{-}$, (S = 3/2), strategy 2, BP86

Fe	2.09746885953662	8.20442708192118	12.86964357727485
Si	0.09900447871931	8.93768829836410	10.54463958752473
Si	-0.01568287688699	10.45545255641438	13.24210780634647
Si	3.85344033496896	5.71682662185308	12.36736752547126
Si	0.85221352803119	5.30915816134138	13.00592363583240
N	2.23488016180404	6.30661376180646	12.65287678598887
N	0.56494677291848	9.18362887823463	12.20387658784973
N	3.42965639415185	9.18475636705410	13.82113499537817
H	3.29289194058131	9.06118082363762	14.83193959459813
C	5.40309454095822	10.30640547894414	14.70346168171506
C	5.49392638793715	9.46752882642470	15.85592942346044
H	4.97358981288975	8.50071825480610	15.85518037227162
C	4.52616285958931	9.95232229900504	13.58571898144322
C	4.80776683492753	10.37371643741191	12.21066585503594
C	3.76567228288692	10.43996227976240	11.24055742281297
H	2.73338280705869	10.23340940158213	11.54893345953300
C	6.14528005728778	11.52499965011886	14.73933271904034
H	6.06957728562998	12.21434410984068	13.89031077751921
C	-0.56017609176117	6.30792830967084	13.79015720445457
H	-0.27945411865631	6.62804247537151	14.81034463365610
H	-1.48228796937939	5.69899717268780	13.85658007278070
H	-0.76386313600265	7.22076573872022	13.20336724207229
C	-1.60911865911393	8.09736209264237	10.39897564365760
H	-1.59842265396863	7.11357726138163	10.90193007142980
H	-1.89248369657761	7.93959515458661	9.34061830485647
H	-2.39298864168455	8.71139580520466	10.87826801828055
C	-0.00301538690152	10.59021365062558	9.58632804986778
H	-0.79127986487489	11.25432878680395	9.98483103228049
H	-0.21762001444680	10.41293451763623	8.51499465718556
H	0.95773424819574	11.13193405175693	9.65855418857951
C	5.35008262589764	11.03592629856966	9.48040723861364
H	5.55821943092271	11.28286493821536	8.43153259337807
C	6.13204468565577	10.64258102766980	11.75886336632549
H	6.96545197409506	10.54989685834133	12.46497285574500
C	-1.84462382967579	10.89296324655133	12.88796334360442
H	-1.99854543243000	11.23641773234652	11.84917257226081
H	-2.18955822762714	11.69739354649521	13.56538299760201
H	-2.48822275898078	10.00885869175481	13.05157526622328
C	4.84488291734372	6.87094153709226	11.23645854793140
H	4.32402653408692	7.01664319020878	10.27347557251812
H	5.84572345463147	6.44449531247695	11.03071542603251
H	4.98598551818872	7.86685454883728	11.68899534775767
C	6.27275148033857	9.82321854251351	16.96357040984090
H	6.32715655154883	9.14154540344753	17.82326183447929

C	4.03541783153677	10.76655653520711	9.90662048913444
H	3.20564120105594	10.80969383685332	9.18886901655095
C	6.99933453054330	11.02933840358068	16.97491071449580
H	7.61096796664788	11.30667566283834	17.84262837435632
C	1.01901481180388	12.04444885007161	13.06909964801929
H	2.06758530687896	11.83899746888011	13.35162036482082
H	0.63567427022053	12.85308268454772	13.72043109336479
H	1.01803353838108	12.40850662479019	12.02571121368769
C	1.35649046580023	7.85290226461649	9.62458781206459
H	2.32571195738992	8.37583599860124	9.53519486167197
H	0.99320200950101	7.60725351081912	8.60808477676922
H	1.54205670865741	6.91821640464299	10.18221673389121
C	6.39550526449599	10.96738140632517	10.42278446620934
H	7.43206992004496	11.14868046905138	10.10750350841345
C	6.92326968257985	11.87484337003704	15.84746882230038
H	7.46646463934744	12.82977484320506	15.84207280703399
C	4.81764025308081	5.53744433930927	14.00198175899633
H	4.90454872467611	6.53123511122372	14.47791257049004
H	5.83944868033375	5.14420406192389	13.84147912291420
H	4.28897361854158	4.86546579834731	14.70237287028483
C	0.03905224894841	9.94780628711341	15.07660879052255
H	-0.53636413742242	9.01969970384152	15.24211544796878
H	-0.38736814763009	10.74522870552604	15.71564662839526
H	1.07872234515545	9.76710957011909	15.40211704841024
C	0.16155535973145	4.47527978134734	11.43370819624767
H	-0.13284676028292	5.24107871336188	10.69358271253201
H	-0.72725860065108	3.85591948634025	11.66094069327886
H	0.92225685510785	3.82768618704003	10.96188192327617
C	1.27084070827080	3.92060667036377	14.25409348063626
H	2.04557351641258	3.23095577055793	13.87341889512506
H	0.37077683830332	3.32239862044634	14.49410457777771
H	1.64757129185321	4.36522256404630	15.19391604118789
C	3.84612521060672	4.01194688648624	11.49726853087639
H	3.31760660652644	3.23628867424225	12.07993523616557
H	4.88399009767506	3.66456877975256	11.33263858025018
H	3.35401978406336	4.09060177441043	10.51026991136727

[**3**]$^{-}$, (S = 3/2), strategy 2, PBE

Fe	2.09624162467333	8.20325433927509	12.82853264709844
Si	0.06943299005723	8.96021255280790	10.51272684609356
Si	-0.02830995439924	10.48018375795028	13.20346732845630
Si	3.84889044860026	5.67696986167703	12.35719118870078
Si	0.86573090989266	5.28873669588795	13.06232089584465
N	2.23777446982346	6.28915949700396	12.66052571337696
N	0.56451871027270	9.20566058783909	12.16802709269463
N	3.45446554929735	9.17720334013820	13.76897518855690
H	3.30994991389155	9.03377278455465	14.77617148341145
C	5.41249449621302	10.28126253506218	14.70430793812932
C	5.48968608426337	9.41986902953981	15.84013753888888
H	4.97631798993872	8.44969101235650	15.81145171000352
C	4.55465794511231	9.94647646666345	13.56400818511064
C	4.85758059777311	10.40102644007817	12.20370006563159
C	3.83207207445748	10.48666067538335	11.21830057743147
H	2.79670193197704	10.26045767517707	11.50392466151407
C	6.14474189222399	11.50299978259679	14.78105253125876
H	6.08007297810771	12.21074720803646	13.94641347904684
C	-0.53855073122923	6.29425173913551	13.85476984335121
H	-0.24393673100529	6.63467803862088	14.86418468026734
H	-1.45349082652149	5.67858880292397	13.94793623577963
H	-0.76267734647212	7.19377510546524	13.25468522958593
C	-1.63809844801369	8.11355953745084	10.38397090724859
H	-1.61827107751212	7.12812487884801	10.88345190649252
H	-1.92717234729129	7.95748926995641	9.32726536254426
H	-2.42202488559264	8.72158996488753	10.86990932165764
C	-0.04988059721540	10.60810013319810	9.54701384095466
H	-0.81717259748396	11.28412498005953	9.96543335750775
H	-0.30395835451880	10.42077152059135	8.48643497244834
H	0.91855135396368	11.14001687142760	9.57891303094111
C	5.43629708431318	11.15682918030818	9.50505130867565
H	5.65835253128150	11.44220644865623	8.46903712227645
C	6.18561223828993	10.69462907070916	11.78021965838671
H	7.00950053649658	10.58899108867864	12.49562395446268
C	-1.87990912023869	10.85754847073864	12.89860004385789
H	-2.07772091758014	11.17775538047293	11.86000961484158
H	-2.22317260054025	11.66446440512721	13.57330386984059
H	-2.49274847174193	9.95967262525227	13.09940611827715
C	4.84264789959547	6.81566611029934	11.21101782186917
H	4.31988260143888	6.95181117082075	10.24758353934434
H	5.83963568507032	6.37990595579358	11.00764506620720
H	4.99048470616106	7.81614544935306	11.65192731347768
C	6.24571918204970	9.75668012573798	16.96825612136707
H	6.28951230799404	9.05687280291832	17.81364549310339
C	4.11913311570046	10.85987755734203	9.90078479071354
H	3.29980770185196	10.91893653052731	9.17187073998028
C	6.96205941598518	10.96642636710698	17.01909684852059
H	7.55559151049039	11.22942405527250	17.90345092086772
C	0.94212294221712	12.10419216542938	12.97786535899426
H	2.00651766605811	11.94164526185284	13.22670868644774
H	0.54986430826052	12.90289681156125	13.63547919647297
H	0.89203502155760	12.45869135725327	11.93259812120618
C	1.31272378366231	7.87513662700299	9.57146088961286
H	2.28143615439420	8.39629777394534	9.46596065582368
H	0.93134639713877	7.63313693718559	8.56103923498049
H	1.50380188024453	6.93675793209631	10.12164320825072
C	6.46648120148190	11.06550072923177	10.46063778781862
H	7.50590536548002	11.26722750786732	10.16853867231181
C	6.89932067127001	11.83461640660059	15.90985398188669
H	7.43458283860668	12.79351577388628	15.93452163892148
C	4.83910893321529	5.47950226366178	13.97543339935857
H	4.95554799777739	6.46838476085394	14.45486043810837
H	5.84934596942243	5.06840165370274	13.79043642613606
H	4.31433605911490	4.81296620685200	14.68351675620651
C	0.09555422043391	10.01674471603416	15.04664382274969
H	-0.43244813983089	9.06866565057085	15.25121490997021
H	-0.35204646216090	10.81106270816154	15.67439566754590
H	1.15023826450514	9.89500543003767	15.35003416312057
C	0.13927689638678	4.41884480420116	11.52463039849279
H	-0.17205913888345	5.16693356069443	10.77332095255750
H	-0.74483800187149	3.80847388378183	11.78974150859850
H	0.88587954036404	3.75708521645644	11.05063028375715
C	1.30655358752504	3.92288020417059	14.32869820740029
H	2.07389249504586	3.22478615468969	13.94914275158253
H	0.40834042532587	3.33176042445646	14.59044026315676
H	1.69657737314558	4.38184765592906	15.25577475555696
C	3.81905880103980	3.97053027047388	11.48919768141496
H	3.29719322259954	3.19677952633904	12.07991110669826
H	4.85390406392284	3.62148545610804	11.31180494859443
H	3.31439819264881	4.04873728920249	10.50882502016712

[**3**]$^{-}$, (S = 3/2), strategy 2, PBE0

Fe	2.07383774174959	8.32356080695922	12.80890702387861
Si	0.07505583980452	8.96662359763149	10.43856383682264
Si	-0.18697574251122	10.53218106188154	13.03904804372675
Si	3.85283371658438	5.78884041922336	12.33846949822324

Si	0.93697129675479	5.39189237939495	13.15129563529070
N	2.26707665207648	6.38979905122048	12.69076071495201
N	0.54971605912132	9.31021449232264	12.06468015957952
N	3.40025246694043	9.28531527053459	13.89102708708564
H	3.24197972090065	9.14658239809687	14.88423885090014
C	5.48986949274622	10.12735855058624	14.79180099763720
C	5.47488513643824	9.24494038919926	15.90182379374191
H	4.82457976065222	8.37114847546226	15.87485586522865
C	4.56543500015361	9.93901177861605	13.68399206229671
C	4.86868929499464	10.41083504454139	12.33850029843433
C	3.82678519416825	10.66731446612851	11.41640746900705
H	2.79052184940499	10.57264925773759	11.73802106182664
C	6.39067994697628	11.21959381603498	14.86509599298533
H	6.40414597713548	11.94609839623494	14.05478837195792
C	-0.43428670308072	6.40444939449132	13.97156944720152
H	-0.09411017892234	6.78899708840241	14.94214983538259
H	-1.32543458689683	5.78535282543042	14.14410515437489
H	-0.71411623307704	7.26587571293109	13.35231077301672
C	-1.53729109543534	7.96871979334036	10.34223400412755
H	-1.45441853123331	7.04625120043830	10.92960133571382
H	-1.77022644840237	7.69371776861911	9.30426121978787
H	-2.38295054471136	8.54216971714571	10.74102579600888
C	-0.21951889372825	10.54302092635282	9.41570536787358
H	-1.02126640258023	11.16138063091130	9.83930284232913
H	-0.50143209290997	10.28690656687261	8.38514925695478
H	0.69072922100617	11.15537071422142	9.37812719655985
C	5.41310391221929	11.17332953289984	9.65541625515253
H	5.62207951200321	11.45936026727975	8.62541420394117
C	6.19422043458262	10.53973868370095	11.86003897548978
H	7.02308788615723	10.29631284271110	12.52213335876583
C	-2.07817558563705	10.56273583917052	12.84728112015427
H	-2.38383979337602	10.77839627092479	11.81550312153836
H	-2.51987851668761	11.33111818647047	13.49628808777387
H	-2.50474277336224	9.59099174564486	13.12816670763174
C	4.79400701215527	6.93031439146026	11.16905225448695
H	4.27976622496585	7.01014133416546	10.20350883515812
H	5.80463819531153	6.53816284521492	10.98939669473494
H	4.89898726709449	7.94338005976360	11.57390624699680
C	6.30688224178005	9.43598012483472	16.99835463599155
H	6.27376230964882	8.72266013662245	17.82249588816522
C	4.09732759881629	11.04241160020844	10.10563434249827
H	3.26571967811040	11.23465522713952	9.42755647106414
C	7.19216376887948	10.51550495444822	17.04400394177361
H	7.84422659359742	10.66468571393206	17.90364903264749
C	0.44728024318956	12.27201580071362	12.62962659040107
H	1.52966275881534	12.33025091237095	12.80206258880659
H	-0.04001305159611	13.03162989496633	13.25634039803526
H	0.26393431515680	12.52571405653703	11.57823143298659
C	1.40666393694465	7.97453271296337	9.54173408222153
H	2.33894946048961	8.55046691881448	9.47590140192616
H	1.08314488868887	7.71930335490675	8.52333908299249
H	1.62868655683916	7.04815388842849	10.08660089346235
C	6.45779606415835	10.91387580125318	10.54858696301453
H	7.49245916083110	10.98269853021814	10.21129013611041
C	7.21933465339801	11.40538475300956	15.96268312649224
H	7.88753549472860	12.26695328682261	15.98519575890793
C	4.90635237663949	5.59444568109883	13.90279645032730
H	5.07331550513962	6.57960562373179	14.35620179305591
H	5.88786360311300	5.15524570596055	13.67837314772328
H	4.40422377354940	4.95839670110748	14.64272293484335
C	0.15348777939254	10.25834380947573	14.87939383652811
H	-0.17081448825691	9.25963429398360	15.19667103617283
H	-0.38114059859267	11.00380746972644	15.48387293453814
H	1.22634189271103	10.35620393483498	15.08478278103012
C	0.16592098642181	4.48846443204988	11.67110205774674
H	-0.12719800140049	5.20837922530314	10.89693567565169
H	-0.72710306858396	3.92180824784064	11.96847458575223
H	0.88067796710709	3.78866570234849	11.22083615293434
C	1.42165643647255	4.06143260131229	14.42015540793050
H	2.17491801894263	3.36610582628908	14.02964305980674
H	0.54220153665536	3.47380412255518	14.71783324509115
H	1.83629329427761	4.53390543722405	15.32023394723006
C	3.80684421007656	4.09583893650112	11.47163250305821
H	3.31344625568695	3.32142264861175	12.07171377526796
H	4.83016371155634	3.75637753832651	11.26039728923009
H	3.27273744706932	4.17483140315732	10.51571076385096

[**3**]$^{-}$, (S = 5/2), strategy 2, PBE

Fe	2.05947838216945	8.28218901122218	12.78201436504557
Si	0.08743150262223	8.98233449291902	10.42438784630373
Si	-0.15946969378798	10.51649900940475	13.09330100359350
Si	3.85381995241705	5.75696684687464	12.35299463285479
Si	0.88671152499257	5.35454181962492	13.11269583975245
N	2.24170792240127	6.36350461251305	12.67642105905323
N	0.56305516075346	9.28843570896648	12.07934266344211
N	3.43736095397495	9.22811224337704	13.90483194422761
H	3.28931559030511	9.08401020818753	14.90759271621464
C	5.51551619264223	10.15914602254241	14.78255652177202
C	5.52326783083940	9.29844278201363	15.92607814594988
H	4.89490051781561	8.39852457335018	15.92157740078153
C	4.58711042587519	9.92549552521979	13.67830977031790
C	4.86627708615587	10.40201323765212	12.32420003582185
C	3.80387787587052	10.62095850315504	11.39582277222005
H	2.76549459500936	10.50074975759608	11.72788417695817
C	6.38664030463026	11.29090646719250	14.83434507025623
H	6.37373107931810	12.00521849147123	14.00297387882486
C	-0.52899169323232	6.37300690401415	13.87088756296047
H	-0.23585998335178	6.75773801682719	14.86470798350550
H	-1.43569281349268	5.75039706961595	13.99330119146155
H	-0.77118916835591	7.24368137416262	13.23636121570782
C	-1.54892563112011	8.00433374884315	10.30768880287166
H	-1.46057440312980	7.03947518779008	10.83814202049465
H	-1.80789676524848	7.79287990963254	9.25281483346529
H	-2.38603239373679	8.56291708596082	10.76270505656513
C	-0.17051395504175	10.60355503854960	9.44419381875454
H	-0.98378122703650	11.21826655957298	9.87104996596838
H	-0.42767789189957	10.38389505173955	8.39078253828439
H	0.75205284981521	11.21205155433150	9.45362036439423
C	5.37766450872627	11.16275955645373	9.60942782909823
H	5.57405855217360	11.44929747617996	8.56870095942191
C	6.19542504333507	10.56728849188865	11.83129340521342
H	7.03990165853659	10.34837151204374	12.49505296146020
C	-2.05794481019484	10.59563633338572	12.88067907473206
H	-2.34952382967762	10.85179382292416	11.84599447975319
H	-2.48842615496525	11.36137325170172	13.55333219880647
H	-2.51524308043445	9.62106474410867	13.13128475388974
C	4.80892760474900	6.89051965191407	11.17061703936412
H	4.28927762346156	6.97142411293710	10.19950821056760
H	5.82264218077233	6.48486599252524	10.98964787715991
H	4.92083819296532	7.91135599809776	11.57442885998459
C	6.35356726221447	9.54376931836872	17.02407675592007
H	6.34168271020669	8.84508496865131	17.87175138374347
C	4.05927739232993	10.99326617493148	10.07173638918133
H	3.21282750206309	11.15672269386882	9.39116723728173
C	7.21000727220232	10.66065998003659	17.04693398186553

H	7.85754569669994	10.85370446111629	17.91117844726147
C	0.52732558302947	12.25725643144387	12.72692483818663
H	1.61798680683748	12.27956605039130	12.90309561047217
H	0.05699028779231	13.01598407321136	13.38086577735861
H	0.35046273217854	12.54884343311459	11.67636950155805
C	1.40962370027832	7.97616359839674	9.50697647582774
H	2.35894654317582	8.53877129686427	9.45107340725686
H	1.07681125152643	7.73970260679614	8.47826478559063
H	1.61449113556847	7.03265011264237	10.04415464139345
C	6.44280263452106	10.94107817274315	10.50778224065363
H	7.48083663677037	11.03871214861875	10.16223469186754
C	7.21044400496981	11.53249721504641	15.93506704550731
H	7.85227754959488	12.42400349133375	15.93925216789326
C	4.87060602831079	5.59546980996284	13.95613370650725
H	4.99554485099787	6.59571364818804	14.40870086986844
H	5.87667002183456	5.17741090096302	13.76407258827004
H	4.35680018156540	4.94714325775164	14.68880826899428
C	0.16694224171484	10.18176826051521	14.93604917886552
H	-0.20667161370113	9.18603267662795	15.23302199550682
H	-0.33318166498360	10.94621417767070	15.56071814269578
H	1.25124000591884	10.22247853323397	15.14180246922781
C	0.17130657394579	4.42442676576715	11.60545834028871
H	-0.10871232402943	5.14026255423011	10.81166293025911
H	-0.73038181825596	3.84532626957214	11.88113577832003
H	0.91316032608482	3.72552769702711	11.18005528624013
C	1.34776305560643	4.03850772343282	14.42210571720293
H	2.12623242319442	3.34240314351811	14.06175236509094
H	0.46007680391766	3.44043387558147	14.70309487790423
H	1.73201910663540	4.53172350667379	15.33377040781373
C	3.82244522631033	4.03622849788571	11.51505138938812
H	3.32281815492651	3.26896392175312	12.13312739652539
H	4.85738821766584	3.69503934480791	11.32331721804363
H	3.29626188275882	4.08824244877597	10.54439784688937

[**4**]$^{-}$

[**4**]$^{-}$, strategy 1, positions of hydrogen atoms optimized using the structural parameters from the solid state, PBE

Co	16.34626018371783	5.51437926064209	15.50575892121336
Si	14.82031271632521	6.21394011922626	18.06077630923309
Si	18.40678620992485	7.69975101087653	14.62938710513008
Si	19.40420266877385	5.36493867944292	16.24247157592798
Si	14.77703089987751	3.31292180285622	17.10786848085752
N	15.37345341170731	4.91072774635493	17.11047663873962
N	18.16338641063758	6.23231225899597	15.45999778616731
N	14.97627503142460	5.51490735456871	14.12393791954751
C	13.48293897435454	6.18947560642149	12.31297414467829
C	14.79118307219549	5.81097556347170	12.82026445403229
C	15.93076566703060	5.56470951672884	11.92052749327996
C	12.40907087990632	6.47015053383690	13.19272698404317
H	12.59513281344538	6.57380052079411	14.26946086026823
C	16.26813694955973	6.40621398725603	10.85382216318011
H	15.71451372786643	7.34313484965544	10.71484072057607
C	13.16964868008047	6.17063701277794	10.93505785383340
H	13.95904951081584	5.93861870522916	10.21191864286411
C	14.15562399162364	5.67513882629517	19.72739463256894
H	13.29795583337003	4.98265210515941	19.64086933014861
H	13.81625157514465	6.55460135609204	20.30674995989085
H	14.94059238126066	5.16684680104907	20.31782420527498
C	16.72339124838536	4.42397016270389	12.09344084868454
H	16.49247988747286	3.75530946233861	12.93231040769134
C	16.77194758496013	8.52615930733211	14.23758301721524
H	16.15769836879933	7.91785099511295	13.55013242745693
H	16.94846563464130	9.50688725047183	13.75628320533403
H	16.17066857266646	8.70493443399977	15.14908584755433
C	16.19256863382256	7.43806508343986	18.42947881579242
H	16.94753607250012	6.99174100869876	19.10259357321503
H	15.79477096200063	8.34862504126805	18.91490815795662
H	16.72314910395977	7.73339649486964	17.50708698352248
C	15.35726825166472	2.34720606390081	15.62427981725911
H	15.03384090907961	2.82801908905957	14.68269607912486
H	14.93760168108127	1.32422543246285	15.64880976531722
H	16.45850781324821	2.25685050682326	15.59700805222227
C	13.45198107648618	7.17610581026580	17.18798752786405
H	13.83036294566331	7.59448706504730	16.23681811239409
H	13.07428406539950	8.01556629577721	17.80183929312442
H	12.59587773809032	6.52044903786568	16.94247219130333
C	11.88236194805408	6.35669173122731	10.48421802163456
H	11.68334506188483	6.30900155785015	9.40369959635370
C	19.41237491874853	8.94079123864426	15.62427156471384
H	18.94191938804429	9.15252167633253	16.60210602892273
H	19.49341705677111	9.89516391646616	15.07040462038877
H	20.43953322289214	8.58187156459508	15.81947397235708
C	17.31954796687767	6.09388842628839	9.99060747767651
H	17.56855172938061	6.78777145580323	9.17630385262214
C	11.11581458791915	6.62750573153572	12.71910424566674
H	10.30949161053110	6.82444610693920	13.44016743715515
C	17.74782575829868	4.10386784343955	11.21596312308642
H	18.32321357567331	3.18218200382981	11.37676164907185
C	18.04409029704759	4.93232710925621	10.16396737918356
H	18.86611069163965	4.68908106962677	9.47684852741105
C	19.29684149484741	7.49036973087891	12.99197009715519
H	20.34681797728684	7.17328671997486	13.11565200189788
H	19.29427199480354	8.44276384354777	12.42811004035399
H	18.78448827284861	6.73194066266429	12.37312966931542
C	10.83297908506033	6.56231431915949	11.37289235737257
H	9.80625579833216	6.69308992597504	11.00686652656606
C	19.90465472038316	6.07454990282226	17.89630692395105
H	20.24925622173270	7.12155013435212	17.82383759283970
H	20.72083412919221	5.47698508502738	18.34563357116861
H	19.04693591963403	6.05766094720405	18.59326546486757
C	12.90878263853357	3.20643175328184	17.05374951966151
H	12.42046496017907	3.68910720081865	17.92035578232479
H	12.58422542990763	2.14893498156119	17.03483327225845
H	12.51368525823486	3.69151829873868	16.14118082851062
C	15.34207407155859	2.31101020129357	18.59300276684129
H	16.44605082024783	2.25639633657118	18.62630177080116
H	14.95337175535303	1.27660915253830	18.53772324861629
H	15.00007573522916	2.74818514138571	19.54886749949929
C	18.87430960829636	3.61699859927805	16.64219561000317
H	17.94774467566958	3.63213164398893	17.24337467915549
H	19.65740346713256	3.08925520099121	17.21920705957018
H	18.67473707557106	3.03076523483485	15.72635422240842
C	20.94796085447847	5.29101180902782	15.20096073210654
H	20.72953402161584	4.88638410559475	14.19603134103861
H	21.71509596288316	4.64548922767057	15.67025266702782
H	21.39810909656607	6.29172184068909	15.06586762701108
H	14.08386000169447	5.45806640912588	14.62708132694460

[**4**]$^{-}$, (S = 2/2), strategy 2, B97-3c

Co	16.26212893898519	5.48122958313772	15.49409109635733
Si	14.89364234063221	6.17552727700062	18.08729453526721
Si	18.11102268577411	7.81001836897843	14.63192439860812
Si	19.31577485071817	5.33377267729580	15.94087320032938

Si	14.74196889894981	3.26183935343759	17.15974919932427
N	15.35979560884496	4.85721725491470	17.09744134007745
N	18.00118452695434	6.24212890500640	15.32261591831282
N	14.90537877256521	5.24944373728466	14.15661847416976
C	13.61117653960006	6.06320382744257	12.28311157246332
C	14.84245674974688	5.53325715157915	12.85493929809232
C	16.02227692310764	5.29582230170501	12.03731232250085
C	12.77018856662641	6.89643430644008	13.04474662193224
H	13.09232357091414	7.21831726315451	14.02572233722997
C	16.25724613848249	5.99508183087236	10.84125975664789
H	15.54835173802732	6.74322939937649	10.51705332012576
C	13.17029322168529	5.71179942980509	10.99379246211755
H	13.77666490451886	5.04673841340077	10.39520189131220
C	14.18918110159189	5.65339985579026	19.77260174608737
H	13.33977252446749	4.97703086548927	19.68411544119549
H	13.85290547715655	6.53100719676333	20.32861895226752
H	14.94676419943195	5.15390519204230	20.37652808239612
C	17.00628504454392	4.38210409492799	12.45592639506416
H	16.85541357545961	3.84646147495543	13.38016519635611
C	16.41810861327643	8.59663696665274	14.36402951551129
H	15.81821595063321	8.02764771407722	13.65666393426401
H	16.53126234930489	9.60724324896069	13.96380904713701
H	15.85361289494425	8.66815788678256	15.29267108035367
C	16.33021639964835	7.32714952632163	18.48502817634462
H	17.05009340454377	6.83907329377813	19.14164329338569
H	15.98359727093658	8.23478314010505	18.98334601058917
H	16.86526185982348	7.61019527358811	17.58289170062710
C	15.30367516888567	2.18707744702008	15.71523453677710
H	14.98498748105310	2.60515090884905	14.76276849820243
H	14.87593890430849	1.18584856081092	15.80838391656801
H	16.38608728871981	2.08265882355834	15.68230257199320
C	13.54487977996379	7.22030756644275	17.26054224307642
H	13.93087584533745	7.68332200625034	16.35250978650118
H	13.17656137329435	8.01773689880416	17.90972794914942
H	12.69316421724470	6.60047571385163	16.97583950652703
C	11.96068288932776	6.16384585689804	10.50102168858690
H	11.64382682843505	5.86119558657463	9.50988528256438
C	19.08466252192164	8.99871238542344	15.74542126424122
H	18.63415182058735	9.07199229539893	16.73512768847575
H	19.11627829670641	10.00226583736926	15.31574256892985
H	20.11551948436455	8.66855545978971	15.87932038740480
C	17.39966867483234	5.77368440562588	10.09333308145776
H	17.55935195695315	6.34155852190689	9.18485393064783
C	11.56405644461694	7.35142768521799	12.54433559349666
H	10.94965997376572	8.00437594735231	13.15243194694656
C	18.14919188587596	4.17086954865508	11.70971717910791
H	18.89035605721638	3.46490315875916	12.06319224466526
C	18.35575639641511	4.85718558814985	10.51780435263298
H	19.25733275890378	4.69777039226049	9.94016409071797
C	18.98077624458881	7.83343027352035	12.95605531408071
H	20.02963663162199	7.55405176098358	13.04246397637563
H	18.93759425366134	8.82822128960154	12.50683705406883
H	18.51341520874607	7.13560851043489	12.26591666408608
C	11.14521682032420	6.99171679199240	11.26793824477912
H	10.19938135597287	7.34630756387811	10.87847682111805
C	19.83049572652754	5.88033896711432	17.67643228882681
H	20.09904673857696	6.93564548760963	17.70466955313156
H	20.68457900785969	5.30495432785210	18.04035709815667
H	19.00614514964045	5.73495597365100	18.37297994996397
C	12.84331295862625	3.22202658640239	17.10204671009893
H	12.39259238151243	3.78379853969329	17.92011996522070
H	12.46415282688526	2.19919393035204	17.15514611956409
H	12.47944885704467	3.65820743456620	16.17062749918146
C	15.26734108695476	2.34167500537693	18.73056963346650
H	16.35481814557371	2.32427193165335	18.81228306136024
H	14.91792015226358	1.30680299830308	18.72271148233737
H	14.87925542253731	2.81693839212201	19.63050094797506
C	18.90280007171079	3.50051915103538	16.08402591038347
H	18.05031735882656	3.35099683501277	16.74403006830690
H	19.74820656409794	2.94067228952270	16.49037192048501
H	18.65132256389278	3.06960461934924	15.11565723547667
C	20.86302875476320	5.44429192445419	14.85078567588018
H	20.63193250685185	5.15818314749562	13.82485886711484
H	21.64374071424638	4.77613369384520	15.22032050354262
H	21.27974870459132	6.45128595844171	14.82480192404830
H	13.99393310147343	5.32171120969921	14.59639088584896

[**4**]$^-$ (S = 2/2), strategy 2, PBEh-3c

Co	16.18127944246304	5.48427871679238	15.51394989333802
Si	14.99815040095299	6.02601557988104	18.33615617908219
Si	17.89280670485336	8.03132219178443	14.78411463887824
Si	19.27307423206631	5.53200537937406	15.81029538293875
Si	14.68622388257521	3.24305769107431	17.18496830496130
N	15.37655852205079	4.80950709799524	17.18795645666162
N	17.87240879433020	6.43176113703751	15.40519955190161
N	14.82116831393815	5.50865575141711	14.09115083290857
C	13.73185612515203	6.13353148363550	12.01256641600189
C	14.84816868412518	5.56924932617476	12.74224645716372
C	16.03231631349582	5.09085987574375	12.05231599446043
C	12.86111623718975	7.06094424058392	12.62363921183919
H	13.08160061756119	7.42175040850061	13.62095536475914
C	16.48692333620459	5.66938532097442	10.85188733477103
H	15.92721675652728	6.48583654200632	10.41421678113160
C	13.40785095973841	5.74342746577627	10.69551609560055
H	14.02133690164590	5.00341376155314	10.19822022692280
C	14.38421844873628	5.36240729155015	20.00908782911768
H	13.48466225365140	4.74947757753606	19.92539682161319
H	14.14505437203389	6.19415461921849	20.67644011587023
H	15.14645960775648	4.75732541453418	20.50311349555803
C	16.82774949209397	4.06996851889901	12.60147657075078
H	16.48703450676735	3.54906339865944	13.48568924849144
C	16.17325425669561	8.81999354502454	14.88707925538781
H	15.44433849570455	8.28189036066534	14.27803707921943
H	16.20159170298862	9.85066574072528	14.52600069815033
H	15.79604422645223	8.84872761513180	15.91194983881703
C	16.49727229103070	7.10353821485939	18.74661916160935
H	17.27368710864089	6.50683153271432	19.22956868846721
H	16.23401542707243	7.91701450592718	19.42662045456782
H	16.95258104944335	7.53902140559951	17.85724308941354
C	15.17863399314059	2.25485039206686	15.64645892080040
H	14.80799181545888	2.71608702322422	14.72970545639260
H	14.76158673924161	1.24626422327189	15.69756234580313
H	16.26138245122060	2.14392356493760	15.55587097886725
C	13.62224965492585	7.17084576239580	17.69571108347764
H	13.89407007937914	7.63757251519984	16.74567380247922
H	13.38426041283566	7.97743554751315	18.39339301224036
H	12.70457179395506	6.60438730296554	17.52019391055170
C	12.30493172745043	6.25249559065843	10.04034197392780
H	12.08710786174536	5.91682462451324	9.03344113330774
C	19.06642480147191	9.16613886784691	15.76054009593148
H	18.81502812509695	9.17081950183139	16.82321429725967
H	19.01907128218783	10.19705071359163	15.40148365101177
H	20.10690594349816	8.84302779237518	15.67624173568108
C	17.65829984900932	5.25559759038791	10.24768685912981
H	17.98361212361942	5.74080717587803	9.33542112558500

C	11.75740861709557	7.56633368026933	11.96189321452347
H	11.12498015887218	8.28796410964731	12.46509620027117
C	18.00139609862545	3.65983178472814	11.99510676778160
H	18.58272025041335	2.86594120842424	12.44878804728349
C	18.43410000775042	4.24925575492606	10.81468444151543
H	19.35727968225018	3.93363364565102	10.34603224861921
C	18.43666076246902	8.13276803425788	12.97438732146580
H	19.47520916843105	7.82220870512875	12.84502809540778
H	18.34547281301032	9.14916551590999	12.58316690935588
H	17.82924739937701	7.47665074203706	12.34960802786203
C	11.46299217638320	7.17190273543281	10.66248901885127
H	10.59887183519577	7.56870883441549	10.14568372401338
C	20.08379879967259	6.08175220680678	17.43685295613509
H	20.41979889094707	7.11919988927761	17.39254592283980
H	20.95084527156469	5.46645616685210	17.69009178304935
H	19.37498805270691	6.01230638726266	18.26388936377310
C	12.78488753296087	3.26730409315420	17.19030165928928
H	12.38220663687186	3.79300696837973	18.05864205069998
H	12.36246436496954	2.25980163258794	17.19433105085650
H	12.40877766220300	3.77702406137883	16.30046912192831
C	15.23645000713874	2.18367593639016	18.66358799062905
H	16.32626414625390	2.16170640820585	18.73100108411599
H	14.89230729151907	1.15105138168794	18.56639032784289
H	14.86060390909362	2.56533810121549	19.61387911437672
C	18.85464567453057	3.69623865574066	16.04476227978329
H	18.12359860833200	3.54175345251625	16.84123369159476
H	19.75175856856129	3.13520279144127	16.31850588070457
H	18.46248783551381	3.24155510613865	15.13172832091173
C	20.62042259280401	5.61083341148722	14.47568865977779
H	20.22006250791306	5.29306472819724	13.51075796244091
H	21.46714728989128	4.96530290279779	14.72166239423591
H	21.01200826621776	6.62282862960172	14.34759757641686
H	13.88338000228337	5.67334443804372	14.44032093884343

[**4**]$^{-}$, (S = 2/2), strategy 2, BP86

Co	16.25062145813341	5.42786557948511	15.52641795992797
Si	14.94873468050464	6.12889740657706	18.10890623261105
Si	17.96012449838348	7.85851103442192	14.55999371543411
Si	19.29207572432937	5.38328909735832	15.85152140519211
Si	14.70788830436183	3.18790826513767	17.15036989581793
N	15.40733797690413	4.77827973066582	17.11501030043131
N	17.91068181843552	6.27564654535693	15.28545116392691
N	14.91205688095973	5.09273266459698	14.22620984836993
C	13.69671846489837	6.08085961199946	12.35802132275143
C	14.89826676899379	5.45271349215713	12.92204769353789
C	16.10757651571276	5.20919565375688	12.12992782904171
C	12.86170741650672	6.89360279607911	13.18011979167465
H	13.17901288999031	7.11367745057245	14.20702541825308
C	16.37843380371309	5.88286507325656	10.90593381948403
H	15.66555772645954	6.62778071181652	10.53471096354942
C	13.26090339977687	5.85086559040559	11.02053818318769
H	13.85655436935432	5.19625345073827	10.37368761863006
C	14.21580209905780	5.60479072761418	19.79846598836479
H	13.30823523110010	4.98385087582815	19.68295795546788
H	13.93989228912812	6.49941018289958	20.38929530917621
H	14.95263427662005	5.02429094067397	20.38339756847734
C	17.10640324364894	4.31598786883203	12.61552305451775
H	16.92999866561982	3.81639360931713	13.57352945715999
C	16.20923181099249	8.54349790978014	14.28902602837868
H	15.63635375323927	7.90409639010245	13.59473892213986
H	16.25560008865075	9.56122084811388	13.85539369216306
H	15.65428956624414	8.60029246776789	15.24242504588019
C	16.43370252157936	7.25289798395021	18.48078677926527
H	17.09804073359224	6.78709298097105	19.23167003562044
H	16.11623953033532	8.24174081025703	18.86126813229940
H	17.01954399855867	7.38858370492753	17.55480927535879
C	15.36286102203775	2.09097310972787	15.74470794616056
H	15.16700907033617	2.57294299762396	14.77092937956671
H	14.86656354150232	1.10159307478017	15.76394735951591
H	16.45204447346097	1.93299663449760	15.83437170023793
C	13.60095421855879	7.18721202321938	17.26027686699575
H	14.00140119019051	7.63469070129460	16.33210656227406
H	13.23386211004082	8.00748381354803	17.90709366596303
H	12.73762687723081	6.55417585728119	16.98143725588749
C	12.06893874203576	6.40435989842790	10.53835709157959
H	11.75638061869719	6.19306475098491	9.50659731528706
C	18.88514348322092	9.09754836330983	15.68669820213314
H	18.42654515905175	9.13025643971681	16.69192116318345
H	18.86330573436215	10.11889788681988	15.26033915447641
H	19.94509793633702	8.80563838935529	15.80903912013533
C	17.56098159695469	5.64764036789853	10.19169434048361
H	17.74370680540800	6.19571086926817	9.25788437591088
C	11.67240402332267	7.44702597513122	12.69220971559206
H	11.06512635191208	8.08136784845374	13.35168746828960
C	18.28654837669485	4.08791864439935	11.90186022864335
H	19.03211322135365	3.39117553472580	12.30704814494045
C	18.52582339070687	4.74435395024732	10.67843344861667
H	19.45714582622139	4.57121189407267	10.12469907777094
C	18.83837446215776	7.89400978886304	12.87289138297692
H	19.91730978537904	7.67942713729721	12.96842252335500
H	18.72675777495765	8.88846285560021	12.39913972267584
H	18.40139655142011	7.13941656566988	12.19757371467847
C	11.26184709986761	7.21141997186331	11.36551256510198
H	10.32937533506639	7.64577209128359	10.98340531999905
C	19.91063650778234	6.00338263273744	17.54664902326191
H	20.15694307296365	7.07995303271790	17.52025455759052
H	20.81146836176384	5.44835475437595	17.87267538337663
H	19.12099579515026	5.85931374974007	18.30560262439541
C	12.80532794504703	3.25448970157912	16.94570925842591
H	12.33655421358049	3.86968913563457	17.73598590848951
H	12.35174232791389	2.24532872243790	16.98474926846664
H	12.54090338699101	3.70472888602254	15.97041640817787
C	15.07559621540815	2.26637691951823	18.78381501117888
H	16.16743325307269	2.23473136692315	18.95696322863474
H	14.70295651371108	1.22453491524770	18.74565606848809
H	14.61046472970760	2.76624283326488	19.65178884921490
C	18.87063325993466	3.54647960723084	16.10072604214821
H	18.04813370127464	3.45063026354070	16.83239345090880
H	19.74848642796488	2.98958492210313	16.48277777605436
H	18.54518309001364	3.07377485069432	15.15688278811936
C	20.76265791151569	5.47860789250860	14.63767951393762
H	20.43311011395446	5.20139691746864	13.62012780374816
H	21.57477060653122	4.79278052663766	14.94643223206323
H	21.18209667766959	6.50060175206801	14.59070782145930
H	13.97643160377588	5.17949972676919	14.64136376333539

[**4**]$^{-}$, (S = 2/2), strategy 2, PBE

Co	16.27530402241236	5.46881675023942	15.52799111052303
Si	14.93931150510906	6.10927097062813	18.14869643878167
Si	18.02899724945680	7.89835381391601	14.61231958591476
Si	19.33366292145003	5.42126740875708	15.92951085278311
Si	14.68581105375809	3.19993258597947	17.10362295777204
N	15.38951749888211	4.79132244518853	17.10368342720037
N	17.95498845683925	6.32228847394734	15.35865674612050

N	14.92904839841125	5.22305064106356	14.20374668101162
C	13.65787335454891	6.07569480150962	12.30660448645295
C	14.88135414973692	5.50166868241092	12.88236524595516
C	16.07209613124835	5.21980583479091	12.07366473033155
C	12.81705726186159	6.91525978109397	13.09451791932976
H	13.14298745007655	7.20060705125081	14.10296233257036
C	16.32384075089702	5.85198840203174	10.82416472506758
H	15.60675975647248	6.58752612181277	10.44191608188255
C	13.20673281879431	5.76479590084051	10.99131870079673
H	13.80754185714048	5.08972553789388	10.37075465804176
C	14.18573683173085	5.54236858160067	19.81569081438768
H	13.27409830295157	4.93278759045687	19.67734400043865
H	13.91268688518961	6.42543443714546	20.42426748046804
H	14.91233650305306	4.94249494173065	20.39325654948069
C	17.07130537055534	4.33131746355073	12.56466059833338
H	16.90873652014474	3.85771628766764	13.53874803315363
C	16.29214668550849	8.64459592003933	14.40807671045409
H	15.66988677125800	8.02765439588903	13.73609773483506
H	16.36105354875254	9.66051325531282	13.97367939267174
H	15.77788821288928	8.72065085162703	15.38261751578490
C	16.43325064477640	7.20209150104809	18.58047879363821
H	17.09102449608920	6.68962791443378	19.30627393695489
H	16.11923602212887	8.16842639288498	19.01691486649768
H	17.02456046811766	7.38774940263512	17.66643971738263
C	15.34200710928873	2.13161139545946	15.67480078123725
H	15.13891424595490	2.62235809819330	14.70714732881819
H	14.85175000579063	1.13943060378609	15.68315610829812
H	16.43229704743442	1.97817428771005	15.75891322987623
C	13.61394890952131	7.22321306311343	17.33349162578979
H	14.01896652278183	7.68766105090581	16.41580949842712
H	13.27295925942560	8.03283590145687	18.00689724274665
H	12.73209942075007	6.62132374060734	17.04382280874764
C	11.99668004415856	6.26460387692727	10.49887210549161
H	11.67413119197071	5.99008431007992	9.48542768258841
C	19.03657760029618	9.12469526104713	15.68145160270436
H	18.62251939008833	9.18059435949775	16.70478193629343
H	19.01739220370520	10.14006067886977	15.24204881417327
H	20.09408595600850	8.81139297729723	15.76099253277373
C	17.49112610584729	5.58853858898954	10.09683902382920
H	17.65934356145534	6.10588332683584	9.14308998438240
C	11.60920114284483	7.41482794961336	12.59626290095653
H	10.99760709588587	8.07116690597619	13.22952365812877
C	18.23563910488146	4.07269062647933	11.83553963123177
H	18.98223231903166	3.37964289014159	12.24545332539428
C	18.45769255530634	4.69275255307246	10.59162630514743
H	19.37636318084515	4.49500688033804	10.02532065905356
C	18.83077889672964	7.88902662175062	12.88523575001712
H	19.89827376025986	7.61105209617524	12.93244639872258
H	18.75676316548022	8.89036296913083	12.41951429751333
H	18.32185556959082	7.16345825714218	12.22764932669531
C	11.18403170109512	7.09745416326981	11.29270321988723
H	10.23615535613676	7.48901327711056	10.90292382350021
C	20.00475503042473	6.07296022740433	17.59385111600519
H	20.29729983176350	7.13583162161936	17.52657985000503
H	20.88794377432094	5.49019425486098	17.91840510107289
H	19.22737678885615	5.98801280078730	18.37378797062365
C	12.78267841771791	3.26134945941952	16.89795009299499
H	12.30706305783293	3.84903065488257	17.70458613993498
H	12.33891863011028	2.24753477541025	16.90705681923528
H	12.51725871449649	3.73705746570120	15.93530771223386
C	15.05245963612008	2.22819487560962	18.70918520474403
H	16.14468169491055	2.17963881072412	18.87469630277049
H	14.66916229064418	1.19226481949737	18.63952336428758
H	14.59689478769032	2.70475915941292	19.59475345153057
C	18.88253405054609	3.59868907523652	16.23272583834348
H	18.04328367654041	3.53390786407604	16.94892156932399
H	19.74672176245090	3.04634392843396	16.64964188860909
H	18.57254620891610	3.09979203579210	15.29693111603753
C	20.78833099339949	5.44993336653919	14.69148648114192
H	20.44334128062971	5.13663084510260	13.68965147274006
H	21.59427517976019	4.76576074219649	15.01828931230924
H	21.22108788018919	6.46299779588527	14.59862065465596
H	14.00255298987071	5.32771657105342	14.63408611395563

[**4**]$^{-}$ (*S* = 2/2), strategy 2, PBE0

Co	16.25093214531560	5.56046713967151	15.51478949434082
Si	15.04818334732079	6.03138291817325	18.29000041542933
Si	18.00962344045776	8.05492649645788	14.79186506178623
Si	19.32895019248859	5.52317270709489	15.88687184960414
Si	14.63762483631479	3.28267614153319	17.02596311513593
N	15.41654938744912	4.81342474232797	17.12714061399976
N	17.95250758152841	6.46348875185861	15.45378873143509
N	14.88321986800064	5.67968706865022	14.16516671149546
C	13.63460142002926	6.04446272420521	12.11343140689342
C	14.83642182294950	5.63008790803153	12.81776719874835
C	16.02855009291353	5.18219272069193	12.11112608680803
C	12.70811546569758	6.93123487551999	12.71899528449937
H	12.94786329417793	7.37249246534627	13.68602069137039
C	16.38005578228048	5.66418480684274	10.82843077257141
H	15.72197027494714	6.37517125746749	10.33221370459078
C	13.28528417054994	5.53687146830226	10.83695317502365
H	13.94843973894515	4.81972632823037	10.35673597792453
C	14.36832234848622	5.36046230659067	19.93285198327494
H	13.45035291848300	4.77414273434455	19.79929530103516
H	14.13793242207980	6.19717692410790	20.60662077764085
H	15.11016356404899	4.72156749609723	20.42890617162960
C	16.94604524931190	4.31028049695375	12.73975208348574
H	16.68498987900171	3.88659492179294	13.70666243171828
C	16.32243327826387	8.89327958440742	14.95713963679451
H	15.55992843192411	8.32523417379203	14.40930256242802
H	16.35267360437119	9.91248657774337	14.54882316785053
H	16.01606452750445	8.95681505549137	16.00927551118062
C	16.57814085043828	7.05339773758379	18.71973827740308
H	17.26675347017776	6.46361756407914	19.33857043271375
H	16.31540156360145	7.96653256139660	19.27006656333456
H	17.11591873148662	7.32466415035598	17.80257740951020
C	15.14736052330711	2.34839818409738	15.46248230677637
H	14.83978080268996	2.89927315849496	14.56540292568342
H	14.66558041695002	1.36130552579587	15.44003048402699
H	16.23277169973979	2.19067104870013	15.42070565116472
C	13.73673758299068	7.22836032036442	17.60956232196913
H	14.08561919820100	7.68698205115500	16.67473849752425
H	13.50141751936954	8.03848206542289	18.31348234548505
H	12.80808821553792	6.68590728397444	17.38646418290910
C	12.10083382107943	5.89777145845699	10.21128815759478
H	11.86401534759494	5.47374371637562	9.23510438105023
C	19.26507303828955	9.16024076506415	15.69718339001140
H	19.03458066981742	9.20331273476412	16.76966476247344
H	19.24494049987842	10.18403176947457	15.29932087166548
H	20.28957987015245	8.78013825753655	15.58920498356756
C	17.57131792705540	5.29416026640167	10.21864587485731
H	17.81861449285372	5.70274582590070	9.23888965621049
C	11.52289119995810	7.28774252609275	12.08768320991061
H	10.84361977566112	7.98251255637824	12.58241592401061
C	18.13765083015154	3.94164271597119	12.12683404699933

H	18.81668650496078	3.26269923627848	12.64287953340852
C	18.46544296363402	4.42986713604359	10.86074284633937
H	19.40349036171730	4.14873989629481	10.38401347631187
C	18.46829770306127	8.07051354124590	12.95736836796508
H	19.48830393171479	7.69708284584352	12.80230560784147
H	18.40444555343555	9.08190289602942	12.53296098306423
H	17.79121689548129	7.41404497055361	12.39730566831121
C	11.20252998708181	6.77888528681612	10.82624838972053
H	10.27212920795164	7.05771655390095	10.33359073030111
C	20.12724758852034	6.08007260885033	17.51576257637680
H	20.48719749072524	7.11416109180191	17.45027620658090
H	20.97886269580927	5.43746332818302	17.77949035963234
H	19.39377305507680	6.03330657092448	18.32979253555993
C	12.74253653343262	3.42134063551101	16.95174067153540
H	12.33472454726133	3.90870150596846	17.84686485841092
H	12.26901099817187	2.43424350460372	16.85992559643042
H	12.44710321469432	4.02111139100868	16.08056234214227
C	15.05819619256203	2.14020407206283	18.48442967841683
H	16.14632039339319	2.01024851182090	18.55455826072382
H	14.60277925530206	1.14906467896579	18.35117845873893
H	14.70704063456030	2.54985469616939	19.43898430265432
C	18.81351154220445	3.71855102846146	16.14693149031257
H	17.98180328561175	3.66433535517851	16.86291476335341
H	19.64977626719027	3.12755675285081	16.54444533741438
H	18.49024423046198	3.25031529580356	15.20839195315506
C	20.69582615191374	5.55727190534657	14.56922301310868
H	20.28998461691217	5.26517927694694	13.59259549311630
H	21.51364916177588	4.87082558354664	14.82866682932438
H	21.12299271572638	6.56369552583005	14.46648806673405
H	13.96978018782915	5.87404128159386	14.56223702746560

[**4**]$^{-}$, (S = 4/2), strategy 2, PBE

Co	16.21691604859823	5.51930648060473	15.53610886360894
Si	14.96370324047998	6.22225552951603	18.20680077240980
Si	18.06378290597972	7.85495513715253	14.68139317393197
Si	19.31086709287453	5.30027125148579	15.91507360808851
Si	14.73077112937986	3.30063132860405	17.17865367192201
N	15.42506117150863	4.90245388263470	17.16217386850407
N	17.95396606499576	6.24266624025190	15.35891317939084
N	14.87142394499657	5.44052618732074	14.14334367865163
C	13.60322738500042	6.05583168671074	12.16074271482447
C	14.84155779831155	5.60235770074761	12.78651498417360
C	16.05054839748764	5.31296810625582	12.02109998505524
C	12.63694425566941	6.79216479906046	12.91938549101915
H	12.88901401252547	7.10431161744951	13.94118376976146
C	16.33949435252789	5.91868439881888	10.76057659909342
H	15.63415767030677	6.64885231788347	10.34715154057694
C	13.23511832009412	5.72539290628735	10.81929557825309
H	13.92214396798998	5.12011535155467	10.21655747260729
C	14.32353872836743	5.64628344888821	19.91450288370230
H	13.42755571781318	5.00466501167132	19.83471897686260
H	14.05622269885013	6.52437368193823	20.53239898245898
H	15.10404417173002	5.07772738590675	20.45224659666870
C	17.04604926600491	4.43512860576071	12.54716356325721
H	16.86355565153542	3.97080391662397	13.52228303218847
C	16.33876931847010	8.65067414776832	14.57719501604461
H	15.66080767599866	8.05196752041824	13.94281639919408
H	16.41948087299671	9.66126958292017	14.13383149652980
H	15.87838655590826	8.75426723895829	15.57638008497425
C	16.44284155752128	7.36562370909747	18.54210666537018
H	17.13226888302211	6.90724062847392	19.27407253267268
H	16.12049242969503	8.34801943568115	18.93363968039821
H	17.00954693847791	7.51406401432471	17.60668887188861
C	15.22761526308280	2.31271388540663	15.63303940921602
H	14.95774244589437	2.87326231058577	14.71963989585595
H	14.69943039374263	1.34067448795209	15.61841389859885
H	16.31257344655786	2.11053958107789	15.60284300473794
C	13.57039272948707	7.25530290953556	17.41037178192415
H	13.90048221576032	7.64801277508637	16.43122591907370
H	13.26964087312641	8.11151093355589	18.04324819782036
H	12.67887749274327	6.62553585829605	17.23340643872598
C	12.00509602355754	6.10763209385072	10.28073445838864
H	11.75779630178148	5.81657316254521	9.25046622037447
C	19.14138368463201	8.99128465557568	15.77943481476660
H	18.72905712547941	9.04990368515031	16.80317220488538
H	19.18257595958080	10.01549806758056	15.36282454012412
H	20.17826272152537	8.61462363452772	15.85294943126101
C	17.52300312064348	5.64105695186938	10.06891474544046
H	17.71288676759625	6.14136038689192	9.10961358751323
C	11.40685319980267	7.17200940541019	12.37299825794029
H	10.70351509090521	7.75061340105010	12.98768800765096
C	18.22768520756342	4.16328346277813	11.85443974391111
H	18.96316780694351	3.47799689071699	12.29770401013667
C	18.48286776161673	4.75626989732424	10.60188378959977
H	19.41509457359777	4.54882539805976	10.06212931820493
C	18.80507256016969	7.88171091561690	12.93329265862636
H	19.85235296765685	7.53282509326662	12.92977305193821
H	18.78242490894681	8.90838303411732	12.52087669836765
H	18.22792200597445	7.22391490567175	12.26066828460133
C	11.07085139216916	6.83924604313614	11.04728053715823
H	10.10510597931633	7.13726990466617	10.62043044609713
C	19.82167929763251	5.75703988221984	17.69445641966403
H	20.07746747153465	6.82832265959494	17.77911783110775
H	20.69204172806161	5.16239874445088	18.03104740413964
H	18.97750560763660	5.55715031235490	18.37858180239251
C	12.82044382785841	3.35839907685076	17.17732122767233
H	12.42185839976793	3.89869955556594	18.05490383872862
H	12.38984709268975	2.33918381237897	17.18011667046621
H	12.45978501002459	3.87706229161604	16.26974532798774
C	15.29032203044764	2.29664949508239	18.70152760086549
H	16.39415471304583	2.24201502913113	18.72905782943057
H	14.89437543460200	1.26410535142341	18.66566381553698
H	14.95097108829072	2.76371705702254	19.64298008454287
C	18.88020251669586	3.44942387317320	15.95488721930552
H	18.05450990622753	3.26910329760273	16.66593953964009
H	19.75415305596992	2.85525732903115	16.28268047731106
H	18.56810895074481	3.08415024211280	14.96034112274632
C	20.84332884581375	5.50181914795886	14.79500646852215
H	20.58679191542264	5.24011792721344	13.75245072730690
H	21.66376129845708	4.84047925492473	15.13188853989896
H	21.22146631453440	6.54036945565552	14.80066768050074
H	13.92462824956789	5.44317122256241	14.53596328520862

[**5**]$^{-}$

[**5**]$^{-}$, strategy 1, positions of hydrogen atoms optimized using the structural parameters from the solid state, PBE

Fe	4.39445366620451	11.21157997910518	7.25823859217453
Si	2.45246833805722	8.92617990380223	6.25782745972293
Si	1.49162614222496	11.77725762737289	6.16608669644868
Si	5.66699149208387	14.08647415489950	7.32589820851227
Si	6.05511889286020	12.40644860171629	4.84380024880261
N	5.32871441153870	10.35381440530688	8.76173435035702
N	2.65384432769538	10.59012729405805	6.55872917010526

N	5.39548635891604	12.67904270841207	6.39683516595467
C	5.08630042490120	10.13768568921869	10.06784877986529
C	3.85800258578691	10.31997228837408	10.75637721390883
C	2.63468484621213	10.65814970325013	10.12735965680865
H	2.60179843712707	10.78028415845817	9.03568097847309
C	6.68255961463663	9.94404484410340	8.35872930063162
H	6.75228726611251	8.84859245664243	8.17330982052139
H	7.43519005967253	10.20083468884878	9.13812744139574
H	6.97987745632799	10.45963728903901	7.42745048187614
C	5.23163443910725	13.80639164383730	9.12846147911520
H	4.17748348332524	13.50255143709881	9.26295128005031
H	5.38938328649747	14.73359386564823	9.71303384758788
H	5.84639178719762	13.00591988266177	9.57635378961361
C	1.15642719665381	8.14798593622733	7.36742657860195
H	1.38035972296908	8.36619918764661	8.42912954804670
H	1.12883266809879	7.04784831120946	7.24233737817313
H	0.14371995050108	8.53507858389751	7.15594319587212
C	-0.28627709891304	11.17287252930792	6.29005062781834
H	-0.52242985337737	10.34024213465425	5.60231173560947
H	-0.97405041240753	12.00670214957588	6.05116974865220
H	-0.51583244068688	10.83408601993914	7.31707455224960
C	1.90743930058248	8.58082756329666	4.48918176627915
H	0.96073179750285	9.09779286954143	4.24723613655993
H	1.74766440459509	7.49747912938871	4.32740046213000
H	2.66898689838652	8.92406509967956	3.76464342130766
C	4.03454430147280	7.95898918921273	6.55503348869773
H	4.85373074648292	8.29058670543895	5.89148690539599
H	3.86472117643115	6.87953530136401	6.37726736287435
H	4.37341233269247	8.09053439383921	7.59867603558746
C	3.80577499666677	10.14156952740472	12.16581464429238
H	4.73596880203270	9.87372313677764	12.68966968319520
C	1.71707448160506	12.44148270462838	4.42928442893222
H	2.70964764449557	12.91794021904019	4.33443563207633
H	0.95189848256936	13.20050471982060	4.17818751789867
H	1.65794105311076	11.63430254836854	3.67579612849347
C	2.64586921206592	10.29517796164677	12.88070035134868
H	2.65791325325956	10.14615708750902	13.97021592977772
C	1.45157209309215	10.63026541450608	12.23663700243310
H	0.52080379370223	10.75224509536464	12.80576879573693
C	1.47125804066178	10.80444130434624	10.85683631736178
H	0.54359990965298	11.05969627291002	10.32351832793620
C	5.30813528126453	10.90154211604840	4.01906119887652
H	5.61353880252674	9.97151354915720	4.53228692978487
H	5.64310299290422	10.83097240778749	2.96638654902855
H	4.20522457823375	10.93776269126452	4.03627054557277
C	1.55720333995282	13.22481551268507	7.34711178002459
H	1.36860691986022	12.89446588586647	8.38560273590290
H	0.80267237855321	13.99125208531570	7.08547300186433
H	2.54972600002880	13.70482995225488	7.33113331792684
C	7.91702574932744	12.10480436422994	4.87133133854579
H	8.48169851510253	12.97798332404407	5.24127303942161
H	8.29058713967756	11.86417613515741	3.85749724587490
H	8.16035473093713	11.25079042015251	5.53057923176677
C	5.75667971072513	13.85006803209319	3.67739856956792
H	4.67561883059009	14.05837274486731	3.58102766758809
H	6.15218288762032	13.63414068003494	2.66660920350753
H	6.24345401022784	14.77725856728146	4.03227824060042
C	7.45125374907513	14.66569091108874	7.27783367898215
H	8.14463988552617	13.87029021419975	7.60702967495416
H	7.58814193707369	15.53506232448336	7.94872731759873
H	7.75804450002469	14.97976674630439	6.26263928176995
C	4.67619055775312	15.58842868641562	6.76404675664668
H	4.91192146713164	15.86289498120328	5.71981333346690
H	4.91287450440687	16.45898010434587	7.40542645163321
H	3.58623070959464	15.41648636855069	6.82037262641227
H	5.94394205149696	9.81083847677093	10.68540961741702

[**5**]$^{-}$, (S = 3/2), strategy 2, B97-3c

Fe	4.41336284197750	11.41108290566423	7.34296795790412
Si	2.46567013439156	9.04174143024169	6.67305086567282
Si	1.52365895379032	11.94213507292941	6.38922148609556
Si	5.66771864549675	14.27691548827233	7.02874494969921
Si	6.05709059437077	12.24518118322570	4.80379682904804
N	5.43124422335855	10.75955383691732	8.89068893477847
N	2.66827688371055	10.73993300803919	6.80923283907153
N	5.41511098873555	12.74125010729527	6.31221548645357
C	5.05592293224611	9.98814479330011	9.91169872783634
C	3.76492028759887	9.94167166839404	10.50107566399323
C	2.73620603917939	10.86204276894728	10.19872887686408
H	2.92756213485676	11.63799065080189	9.47294891248787
C	6.86900673378342	10.76833959140509	8.65278466528302
H	7.24740951696019	9.76823007462367	8.41123820362648
H	7.41318315874654	11.12542101201792	9.53397886847631
H	7.09969825989318	11.42644531772201	7.82096346047072
C	5.34047794454501	14.28459847479934	8.88709658084178
H	4.30630841254155	14.04798482506980	9.13055600438055
H	5.56264510665553	15.27211830965236	9.29967001368493
H	5.95919488332377	13.55442429594350	9.40528199933433
C	1.13707049759877	8.35191558758866	7.82582678890208
H	1.33920032852473	8.64302955438255	8.85520973199777
H	1.11190733875043	7.26060749368705	7.78365469491767
H	0.14245532749786	8.71406643702323	7.56931753145667
C	-0.25843733993027	11.29861912733132	6.29411814895912
H	-0.37999464320031	10.48248687509135	5.58261607153306
H	-0.92799256677350	12.10444089933276	5.98589697062247
H	-0.59760789637438	10.94115715989322	7.26621054515918
C	2.00195194833274	8.52086562332112	4.90878954160521
H	1.09540129680672	9.01761458000245	4.56287399113927
H	1.83296931341095	7.44360437500425	4.84295653739767
H	2.79987382231417	8.77742875857561	4.21264454084634
C	4.04508515283543	8.09861454310649	7.09362342714545
H	4.87867604754380	8.38351324365393	6.45309699120683
H	3.88019016872439	7.02553977986031	6.97021814255995
H	4.34640414474978	8.27419607441069	8.12438476019970
C	3.46761199401291	8.93975693264821	11.45467059041422
H	4.23591272702273	8.21734477452194	11.70805353805726
C	1.91138152580497	12.73692607267675	4.72029938113495
H	2.91392796174820	13.16108625618221	4.74240680504023
H	1.21043076928831	13.53736568988819	4.47526957727072
H	1.87896707181529	12.00306179760198	3.91432841485851
C	2.22642744565856	8.85512420881167	12.04964036120576
H	2.03056026259434	8.06627095257527	12.76702729845091
C	1.22247822277412	9.76985143822990	11.73086558956980
H	0.24450460131416	9.69751011000073	12.18912231582389
C	1.50131669578049	10.77348258335569	10.80388671694363
H	0.73286220419969	11.49139317700407	10.54247382105052
C	5.14603894640317	10.77081575255303	4.06794928889260
H	5.28014167491948	9.87738291453364	4.67485098228214
H	5.51667738955480	10.55285531207161	3.06357006195931
H	4.07741152434561	10.95588069441413	4.00601751102361
C	1.44974525680889	13.35313700347339	7.64394101358433
H	1.08875786629459	13.00277856460810	8.60977648040797
H	0.77634618688687	14.14264470824583	7.30311723941833
H	2.42819706496006	13.79945176232770	7.80412047069637
C	7.87403860124548	11.71757461265705	4.93047697565997

H	8.49484724073825	12.50318506679438	5.35994299179701
H	8.28532239801726	11.46504043267028	3.95053060100192
H	7.97400477541436	10.83630113601253	5.56484297113850
C	5.99278356502837	13.61646631800894	3.49387480075164
H	4.96411061512660	13.91510328099538	3.29255763962000
H	6.42975259268482	13.27599967170124	2.55289281636282
H	6.53797180551122	14.50805282401141	3.80369482517458
C	7.45738704602609	14.88328878436578	6.83903389419390
H	8.15112621010659	14.20722471723856	7.34000387883015
H	7.58184728556704	15.87277963804439	7.28420954096636
H	7.76448371137742	14.95291263221920	5.79564248943889
C	4.56956097419543	15.61948023528439	6.27199632230669
H	4.78105034757163	15.75557646344331	5.21173373719565
H	4.71633034993270	16.58140563203575	6.76831004617436
H	3.51661672319610	15.35689260697814	6.36025219033719
H	5.80189774909922	9.31579131428514	10.34192407931211

[**5**]$^{-}$, (S = 3/2), strategy 2, PBEh-3c

Fe	4.36531061891920	11.22530499484731	7.26068249093435
Si	2.41996054517461	8.92286478452457	6.25071533642582
Si	1.46167646078890	11.81990330261200	6.23155933719287
Si	5.62683174872186	14.11755011886815	7.26162014071782
Si	6.05104264575245	12.36895159404510	4.82119129051230
N	5.36795045241826	10.37424699020891	8.76813551036526
N	2.61903420835779	10.59764743425287	6.57215900512130
N	5.36135165461588	12.67922450695889	6.35978767163055
C	5.12143773523898	10.21601951494319	10.08118911629193
C	3.89283800947578	10.32301558445747	10.76721334743124
C	2.62076744133124	10.45388914313802	10.15158363862607
H	2.52613679355548	10.44265058408260	9.07455926985359
C	6.69974515564610	9.96512782053183	8.37300819571243
H	6.74050799477465	8.90617771084939	8.08813297429130
H	7.43205750385135	10.11090553579507	9.17745094173059
H	7.05996020075478	10.54303930731424	7.51956334668809
C	5.12982200383648	13.91346881461855	9.07496255242235
H	4.07266370655673	13.67397497236142	9.21013355502481
H	5.31771424669934	14.83930605138937	9.62502062074010
H	5.69462534582622	13.11851859555236	9.56421173775574
C	1.08787006041866	8.09835260361223	7.32166961524478
H	1.25794882171960	8.30396508065432	8.38052587779580
H	1.09659235596416	7.01308341865070	7.19306215010179
H	0.08288053724334	8.44603391125542	7.07787793906807
C	-0.32505171291908	11.17614236898672	6.16360058636210
H	-0.47269702332950	10.39496873014365	5.41615905295339
H	-1.00885045450435	11.99214848845357	5.91701925961455
H	-0.63624821721667	10.77043931366841	7.12772669790633
C	1.95902209296734	8.58228243629318	4.43794190439282
H	1.01934021517428	9.06315688391219	4.15737299666306
H	1.84580141167821	7.51306792020353	4.24324328727738
H	2.73075044846064	8.96297354613454	3.76573659533640
C	4.01131841336870	7.95398422660642	6.59465546641294
H	4.85203771842004	8.29501690217631	5.98650033540421
H	3.86072882768782	6.89477228404756	6.37055770209555
H	4.30783527476133	8.03190149514934	7.64209506573431
C	3.89798361628112	10.28199160136711	12.18793450449470
H	4.84837503033143	10.17481420007753	12.70032536057551
C	1.80068872368355	12.70205760460320	4.58958867840217
H	2.78992538881129	13.16395539186602	4.61926194194257
H	1.07258450216825	13.49119383721395	4.38703731570198
H	1.78744198177458	12.01158894562393	3.74356206353012
C	2.74134883667946	10.38003548044220	12.92546540381668
H	2.79756118789862	10.34852467120918	14.00761345059871
C	1.50042357276668	10.52263733459042	12.29737204508093
H	0.59100478214039	10.60446848494631	12.87810439593538
C	1.46752497450116	10.55148308624198	10.90501723570185
H	0.51780097951573	10.64545787892611	10.38979343155227
C	5.23582989989896	10.88859961600907	3.96794611950546
H	5.47233918675158	9.94588488723113	4.46651233836941
H	5.58461228658051	10.79951341079321	2.93591176518327
H	4.14940702304454	10.97623538246533	3.94902304973739
C	1.45700936019999	13.16479421226459	7.56541262203748
H	1.39915767364691	12.73937407620486	8.56917967535966
H	0.60335256034606	13.83599208995592	7.44100203659202
H	2.35470038999867	13.78401041815468	7.52755560822934
C	7.90415160201512	11.94926058207220	4.90411687603550
H	8.50051216122037	12.79236207010206	5.25694497022817
H	8.29407200889564	11.65616034223669	3.92607669277637
H	8.08610573279281	11.11985494342627	5.59073926313434
C	5.91188339550565	13.83817458191358	3.62573984001804
H	4.87196500588252	14.12905690887601	3.46569181033255
H	6.33859040322696	13.59118504657749	2.65061297708882
H	6.44300743421242	14.71726530526659	3.99791976376018
C	7.45012366925485	14.65918195115536	7.26693525068161
H	8.09362564494751	13.85870359001806	7.63703982435532
H	7.60248605874052	15.53029122256501	7.90862599912998
H	7.80393137217631	14.92684446653613	6.26865312067404
C	4.65387998267435	15.60536403004108	6.59051505155951
H	4.92322746992834	15.83538553179188	5.55817488274280
H	4.84274408787721	16.50147024339292	7.18699341168544
H	3.57797322776840	15.42193921254500	6.60787919074795
H	5.98658654367023	10.01091138999544	10.71578442086939

[**5**]$^{-}$, (S = 3/2), strategy 2, BP86

Fe	4.39822434413972	11.25478645538691	7.28581729830039
Si	2.39264766908037	8.98286768736600	6.51756653802826
Si	1.56355121181250	11.98125806897944	6.24060353168608
Si	5.60122309850695	14.15471340077968	7.17739009733305
Si	6.00296907376177	12.25119102416880	4.77435760839740
N	5.45715347657981	10.57424247370314	8.75893334000838
N	2.66509580087598	10.69671951361006	6.63845648871529
N	5.37002518044526	12.64812493109436	6.34232879088852
C	5.18027388293602	10.11947789259994	9.99597961583333
C	3.90612660059347	10.11240546360966	10.65289604590248
C	2.69670668939365	10.58583928433070	10.05318355806057
H	2.71514541270324	10.95686328024621	9.02016774515000
C	6.86286903070827	10.44941609328127	8.36755577675369
H	7.06067490675419	9.47239044651471	7.87897611597670
H	7.53837784392266	10.53336693321001	9.24600551558275
H	7.12026334168373	11.24381565970865	7.64596766137432
C	5.28275763368592	13.98616273845903	9.04429156392670
H	4.25312665732902	13.64303405821344	9.25163765018205
H	5.43674839580679	14.95762356436466	9.55346306441382
H	5.96063268810947	13.23953845717332	9.49417309047718
C	0.93403030009702	8.37453122920706	7.58646775458715
H	1.09124869805018	8.67413764045246	8.63832151893739
H	0.85220783756066	7.27114129890160	7.54822436658103
H	-0.02715754881229	8.79939020877800	7.24620425387512
C	-0.20741995842017	11.36626532567703	5.85659592083481
H	-0.22181428149230	10.62667975363701	5.03543475665463
H	-0.83987682817150	12.22216996630064	5.55196764515251
H	-0.67189321123217	10.89994391702188	6.74416814634276
C	2.04253280373515	8.44385984058343	4.71710447140106
H	1.14773058954956	8.95243917050393	4.31338750402349
H	1.87247768774738	7.35186946008108	4.64996176712583

H	2.89899720967936	8.70339726247429	4.06881985605455
C	3.92005822171935	8.00837484846025	7.09989790145086
H	4.81276528382306	8.27164278579540	6.50339944927604
H	3.74061310832241	6.92024982508744	6.99790154371672
H	4.14658773368152	8.22734087968835	8.15906111983042
C	3.81079376585059	9.61149727698468	11.99155129572295
H	4.72358122448113	9.24091977101390	12.48029617621575
C	2.14534758953037	12.97289792467193	4.72516143332279
H	3.17464145013978	13.32433607647408	4.91281183118551
H	1.49914093425952	13.85067592586563	4.53479360726041
H	2.15632901789374	12.34342284796618	3.81641562718078
C	2.59644021747350	9.58451993068937	12.67954630312636
H	2.56447240925684	9.19146834121602	13.70542513587723
C	1.41208297039882	10.05601323789713	12.06819623214396
H	0.45597405192479	10.03137305682478	12.60624549144503
C	1.48576286065351	10.55360472952158	10.75021906133663
H	0.57727055076686	10.91808831859905	10.25094491996760
C	5.12037877674707	10.74883836222300	4.01604228420447
H	5.36869259190714	9.82992385060100	4.57723536696419
H	5.41986960641827	10.60571055389621	2.95964512508186
H	4.02627985093498	10.87454211513448	4.06922530857217
C	1.38294458497265	13.21516564368481	7.68093508859288
H	0.96845348335785	12.72020975394614	8.57763051779184
H	0.71915837773003	14.05863335274794	7.40959033266123
H	2.36910091523575	13.62620878424002	7.96006082733901
C	7.86371308527600	11.80738659730567	4.82845608839149
H	8.46445050057292	12.63570033805611	5.24572956965922
H	8.24742782565467	11.58013842978251	3.81480737176419
H	8.02885260580451	10.91624084550052	5.46142400064857
C	5.84394406252358	13.69766286603767	3.53117015278922
H	4.78291081105784	13.96491806949931	3.37643010927365
H	6.27613982273020	13.42224574021952	2.54998620497305
H	6.37188710962894	14.59971952894576	3.89213980312529
C	7.39155616099986	14.80970188555275	6.99188300589072
H	8.11298407270461	14.07805973982338	7.40066148981213
H	7.52419802041459	15.76394184420278	7.53709886558228
H	7.65394393307318	14.98616887345906	5.93229692497862
C	4.45096250840008	15.52858901717477	6.51907926013971
H	4.63136580075846	15.71300818553809	5.44453063905095
H	4.60662762923664	16.47931347815287	7.06459521742740
H	3.39267045791466	15.23434899051168	6.63430361406713
H	6.02862077864937	9.72763587658785	10.58745364359737

[**5**]$^{-}$, (S = 3/2), strategy 2, PBE

Fe	4.38529545295278	11.25060109505622	7.27753617355970
Si	2.39097567048453	8.96247302759165	6.45301808651641
Si	1.51547316262259	11.94957037623270	6.24668104810473
Si	5.63224182525683	14.15375878200674	7.18541014289961
Si	6.04053169223741	12.27143424077560	4.77593162286300
N	5.41897675950623	10.55126571197009	8.77421774907590
N	2.64202246029772	10.67809198652586	6.63705162522878
N	5.38866878044993	12.64527433298223	6.34669396806772
C	5.15131542997145	10.15264299802769	10.03191555742276
C	3.88609319686427	10.15436638390281	10.70538655456020
C	2.65186012492224	10.53678402204977	10.09248007459459
H	2.64234343321080	10.82967475550738	9.03414884118052
C	6.81832518280742	10.38672828453814	8.37942596999845
H	6.99690343398017	9.38567908868738	7.93378418042763
H	7.50196140628276	10.49693732656219	9.24880258966997
H	7.08633915553798	11.14480455082806	7.62321910392639
C	5.30283365147350	13.99478638808981	9.05164096012103
H	4.26967770125548	13.66183496762763	9.25739775734866
H	5.46236413042713	14.96880914714895	9.55326385392508
H	5.97436943827118	13.24756562048451	9.50981404802088
C	0.94509152737779	8.29388333753209	7.50579029647572
H	1.09499483052867	8.56308825358145	8.56701226094357
H	0.88916202284085	7.19099996163465	7.43273146288506
H	-0.02549295314526	8.70651950156006	7.17855823384039
C	-0.26224564392593	11.32151058573342	5.91637887927053
H	-0.29859362859098	10.56902622546084	5.10813335659010
H	-0.90119744701046	12.17310882696078	5.61459790082552
H	-0.70326151397836	10.87101229277771	6.82363172843383
C	2.03885123010748	8.47146176354356	4.63834528733982
H	1.13778133444274	8.98012363072753	4.24967142550605
H	1.87935342086826	7.38007939716301	4.54636521912842
H	2.89069414079580	8.75378436630512	3.99384104037275
C	3.93041098740892	7.98195436683171	6.99567524608452
H	4.81471755427266	8.25819346515860	6.39294408482390
H	3.75083708037329	6.89625549351112	6.87393649097491
H	4.16945397491914	8.18133072753955	8.05577137737421
C	3.82710234660188	9.75166249956799	12.07805749400694
H	4.75954369059480	9.45168374349243	12.57765332354027
C	2.04696753468410	12.92565294475002	4.70012124739454
H	3.07503504959342	13.29874567504586	4.85132442068176
H	1.38029222560141	13.78846002842655	4.51321954980753
H	2.04296056649493	12.28118226506813	3.80192983138089
C	2.62574453714667	9.73493644911912	12.78698119281432
H	2.62343771444740	9.42034942805716	13.83986037508454
C	1.41735308745314	10.11748467024321	12.16344660795180
H	0.47113294230982	10.10183548851041	12.71866895364775
C	1.45367852520229	10.51441172546705	10.81123930098324
H	0.52501106436195	10.80724424540187	10.30166400895481
C	5.17217256268683	10.77993615818402	3.97903346597425
H	5.39259240189466	9.85417092151559	4.54016444606965
H	5.51145101987143	10.64458458489007	2.93404942372819
H	4.07785685243154	10.91520082527067	3.98841963893221
C	1.35739694213264	13.20595806035801	7.67045085644850
H	0.97761731526256	12.72188130338457	8.58803743361427
H	0.67085661738829	14.03086618712313	7.39979432030005
H	2.34310696959908	13.64061949583087	7.91243974756126
C	7.90203401113698	11.82751062002867	4.83305255961447
H	8.50331733438098	12.64870474353005	5.26245340382539
H	8.28549739508783	11.61437962233115	3.81670630627927
H	8.06540920159268	10.92699206444809	5.45289793635241
C	5.88561180328612	13.72881683953957	3.54388252275990
H	4.82475396164335	13.99740595106929	3.39025495121808
H	6.31674742473314	13.45545091412056	2.56209573708664
H	6.41461052845060	14.62885505540102	3.90712924705449
C	7.42886470593804	14.79845522505058	7.01782797314868
H	8.14352484362021	14.06236384116296	7.42976478325501
H	7.55602436813017	15.74764247718189	7.57232099551963
H	7.70386565509905	14.98336376263522	5.96325439310672
C	4.50261656353697	15.54516734666461	6.52453137524106
H	4.69216654310676	15.73360132965385	5.45254225306033
H	4.66979280843868	16.48960264145074	7.07678814472747
H	3.43929619037793	15.26660301976662	6.63249611194230
H	6.01007868958405	9.80290356363995	10.63492846854895

[**5**]$^{-}$, (S = 3/2), strategy 2, PBE0

Fe	4.37993548444523	11.22199995171083	7.22873219701782
Si	2.45191455561212	8.87188748203669	6.36122785418837
Si	1.49245513318199	11.75717159865576	6.06513444287953
Si	5.69368826333462	14.07728983792916	7.45159577990532
Si	5.95630441045469	12.50612636141079	4.82592715409155

N	5.38529556109150	10.36911744601335	8.69227618137393
N	2.67430119173987	10.57993265455950	6.51328046513118
N	5.35590074986992	12.72494333839670	6.42762407654118
C	5.11083963081482	10.10351240963047	9.98223002615412
C	3.87558710062190	10.28829880840953	10.65664179825105
C	2.67444981769122	10.71318449797508	10.02017329436447
H	2.65732025870383	10.87697282005971	8.94327765665924
C	6.72955966337746	10.02297562002608	8.28308616666564
H	6.84143725534646	8.94094365127374	8.09387512329266
H	7.47443927504877	10.30452100378124	9.04780660960401
H	6.99549179508536	10.55255339242260	7.35995291766916
C	5.04412206490328	13.80100402920533	9.20213358917670
H	3.95524943073976	13.66723465574686	9.21816805274683
H	5.28704419051363	14.66621636054865	9.83482054548531
H	5.48555928023251	12.90424698006719	9.65394660152138
C	1.19989402044858	8.16973535719300	7.59832297366900
H	1.49165316193272	8.44604713871650	8.61981980784660
H	1.16092151940022	7.07348910703057	7.53432332445579
H	0.18944805122506	8.55743904781389	7.42239800740229
C	-0.29324051816711	11.15160762082785	6.30603810614578
H	-0.51925709532893	10.26112963442703	5.70598930190630
H	-0.99633862452786	11.94253559115497	6.01068732501136
H	-0.47922542544452	10.90556168069471	7.35927237403929
C	1.87248444934594	8.38742159688288	4.61627150472232
H	0.90647475652497	8.84369013421402	4.36386320533346
H	1.76407893612749	7.29781594157004	4.52536395307955
H	2.60677021264126	8.72217471930620	3.87172324760053
C	4.07024938858275	7.94111365257684	6.66540144130632
H	4.84583880520883	8.24720349036588	5.95134925373021
H	3.91149982037255	6.85924459731243	6.55684965220148
H	4.44285733672480	8.14052938991715	7.67765759905908
C	3.79720058451701	10.04086158259134	12.05804251002844
H	4.69695472912661	9.70910143090933	12.57923591649060
C	1.63928149329218	12.29603859258355	4.25170189746057
H	2.61067875909448	12.77542900135953	4.07854819898684
H	0.85276593684895	13.01636819939637	3.98753391427462
H	1.56138086562770	11.43704347720951	3.57280702417810
C	2.62100741098173	10.21643635973293	12.76561027740282
H	2.60765082856537	10.01902692535226	13.83850048466509
C	1.44995619077411	10.64530312458294	12.11895758203301
H	0.52449788506898	10.78521481178970	12.67588074043746
C	1.50052545927262	10.88344829969544	10.74011799185460
H	0.60192293732070	11.20261057189091	10.20993139691916
C	5.21485164776636	10.96594976864813	4.01488021266042
H	5.63181501930617	10.05531206034997	4.46512108100047
H	5.44850671852381	10.94939464015248	2.94124179256728
H	4.12799461365393	10.92356723590472	4.14376051457333
C	1.66826811766530	13.32227474329397	7.10654702576636
H	1.54405819978265	13.10689641151406	8.17548157732620
H	0.92574172775178	14.07686170204224	6.81320879446714
H	2.66703568035681	13.74942847894845	6.96085007169453
C	7.84054336488359	12.25174538371538	4.75222673915241
H	8.38926362155124	13.12551051459879	5.12308933846812
H	8.16221111425127	12.06110147184621	3.71869841401875
H	8.13694418682461	11.38887135626645	5.36301126028322
C	5.59366087707009	13.98837939344969	3.69222173690560
H	4.53504792468716	14.27249270515636	3.74262115519304
H	5.83789894413395	13.75142382898291	2.64782032591093
H	6.18922298853055	14.86299697817703	3.98475715602727
C	7.55537235077254	14.43298742593043	7.61240575975619
H	8.09602359103322	13.52732882389859	7.91640557696136
H	7.73528862164491	15.21005139629504	8.36801738495339
H	7.98545244907975	14.78111998517648	6.66432033232626
C	4.92416858284799	15.69796392407159	6.82230305970755
H	5.32134944566696	15.97709328504147	5.83881587604217
H	5.14042766058585	16.51706730422849	7.52216210391303
H	3.83466774903661	15.60983590029880	6.73012659252730
H	5.94000881422606	9.73069230505332	10.59648357283638

[**5**]$^{-}$, (S = 5/2), strategy 2, PBE

Fe	4.36245753770073	11.30056319452148	7.27368955140317
Si	2.39475075889879	8.97722297890500	6.48794833818298
Si	1.49882265811606	11.95930336315707	6.22812672841261
Si	5.61464052210234	14.17456818340100	7.18051951471731
Si	6.04183745538157	12.28348897663258	4.76854392954933
N	5.47768858561305	10.53691498640111	8.76820564447148
N	2.64415547769464	10.70318057003272	6.63431918701766
N	5.37267776124104	12.66635810039911	6.33307517314347
C	5.16228242840073	10.09219618484303	10.01388440720538
C	3.90511673751394	10.11077428194224	10.67991994552929
C	2.68136461365175	10.59916486400905	10.10284617962592
H	2.67787378604307	10.96150605074737	9.06680702007189
C	6.86612730551245	10.34845011884679	8.38589176945947
H	7.05813505365347	9.33407012402517	7.96393292052121
H	7.55598845161244	10.47580053857198	9.25099304506899
H	7.15053558241354	11.08558264007421	7.61444665801624
C	5.22846430957979	14.00405779513011	9.03308325582207
H	4.17205377694364	13.73474162723481	9.21345923649129
H	5.43477773564752	14.95794112243744	9.55550636496340
H	5.84079539660772	13.20680300825901	9.48984133986387
C	0.96148712873878	8.33339745032923	7.56682497806171
H	1.12239084665818	8.63759786251428	8.61702902054824
H	0.91280707632650	7.22857882038583	7.52688353617260
H	-0.01477264873520	8.72997561782937	7.23714891709061
C	-0.27178731425881	11.30603758391814	5.92087999979665
H	-0.30550179510118	10.53241489296715	5.13309134472797
H	-0.91865504319565	12.14447530584511	5.60013565088985
H	-0.70411058255768	10.87643891210544	6.84210593876734
C	2.03297497517626	8.46840262469253	4.68071301036446
H	1.12841441226561	8.96887867209468	4.28997198242676
H	1.87687787944211	7.37555007375748	4.60287146546763
H	2.88107075580300	8.74491391973775	4.02870748300261
C	3.94226824320480	8.01484824981481	7.03163024041051
H	4.82328440742643	8.27944392413954	6.41917269831933
H	3.75956351776572	6.92824242524831	6.92564845611818
H	4.18882914800238	8.22890965625047	8.08690126738655
C	3.81825490665840	9.62244852193422	12.03140718281610
H	4.73312868000799	9.24131309568033	12.50823748374784
C	2.02022935181286	12.90682656485514	4.66123923174566
H	3.04375318248942	13.29608477937501	4.80260628899079
H	1.34306816127177	13.75749242963741	4.45746529093961
H	2.02263061858241	12.24395090564840	3.77664262468728
C	2.61994449151167	9.62138753450051	12.73918362607738
H	2.60287672379621	9.23738250665073	13.76903735532246
C	1.42652260411451	10.10741665772285	12.14877573195469
H	0.48119409743212	10.10408609287036	12.70524247496013
C	1.48661387807061	10.59173348581432	10.82300922503360
H	0.57442678564847	10.96775802727687	10.33772981958680
C	5.18158579432997	10.77715728220547	3.99301952430474
H	5.38775300834229	9.86463978822543	4.58085885757786
H	5.54177918614598	10.61395417301768	2.95941488155125
H	4.08773602152877	10.91555796598263	3.97514986914860
C	1.33844310595882	13.23926566683534	7.62854193852930
H	1.01267000920190	12.76040355701166	8.56938186644598
H	0.60640805507229	14.02607215862807	7.36415661509237

H	2.31008600570236	13.72487727533414	7.82560368961075
C	7.90346922543418	11.85297345071976	4.84237233454374
H	8.49649006962335	12.67883162764246	5.27375124655585
H	8.29358279940070	11.64116688482537	3.82845400806285
H	8.06896548470100	10.95497279723008	5.46480660643788
C	5.88095079407149	13.73106006474470	3.52855192622763
H	4.82036432374529	14.00298416556033	3.37977984011615
H	6.30529871315178	13.44955093532488	2.54624848189070
H	6.41628269636827	14.63088563099275	3.88303509217650
C	7.42373770238706	14.78664352219695	7.05661407523388
H	8.11528225596880	14.03452260332304	7.47841394006350
H	7.55554222781081	15.72934491955243	7.62070446997496
H	7.72367173949103	14.97422649007930	6.00932969978197
C	4.52155787610454	15.57658195337684	6.48443819139731
H	4.75261808469685	15.77029129511859	5.42166031533029
H	4.67527312550158	16.51601942130289	7.04870088217296
H	3.45261508115102	15.30647545997695	6.55110803905661
H	6.00415719142305	9.69296660762214	10.61125807376446

1

1, (S = 2/2), strategy 2, PBE

Fe	11.10542646747626	8.22497063136881	21.17909496139194
Si	12.96875184888062	10.68948471628246	20.66070307926494
Si	13.06502891998469	9.11553929982061	23.37950558599832
Si	9.16699863632379	5.87834416433802	21.90408650605746
Si	11.91082262539073	5.38934271402659	20.44175440191915
O	10.07363180707476	9.30743853628479	20.19525755871716
N	12.45919586361151	9.35466603350512	21.72729695615731
N	10.76288727944270	6.44028292435689	21.31869996218392
C	8.24876946888569	10.20635387504689	19.01823679414222
C	8.63545647821783	9.51338366321962	17.83845049494867
H	9.40326201272872	8.73542885700238	17.91575653056226
C	8.91241288976683	9.89655675260884	20.28397391498310
C	8.34112734063394	10.17985417273363	21.60672222563326
C	7.25682427520960	11.21779922217170	18.90737108854512
H	6.97770176940608	11.80028447219311	19.79249357109572
C	9.19813305192105	10.44513907838371	22.70808016519788
H	10.28041655467711	10.48068111293207	22.54342625294436
C	8.57181871839074	6.83485591481127	23.41990849046797
H	9.22015890283214	6.64411613958293	24.29239267889172
H	7.54797079498209	6.50352965925107	23.67473936095004
H	8.54095985253013	7.92249142503991	23.24220878302977
C	6.94282671282209	10.12446972856696	21.84343443354994
H	6.26652905438851	9.87377994581437	21.01823033649979
C	8.03830118906961	9.80522054391096	16.60898110490828
H	8.34393366391131	9.25103609822831	15.71287278691327
C	12.86600875907524	10.19347645915574	18.83648494322820
H	13.51872310555528	9.32869267121422	18.62442934782571
H	13.20247330339374	11.03884159721577	18.20803998307765
H	11.83353035061992	9.93818966742262	18.54499927402133
C	13.26596605359229	6.41372384699239	19.60296261374606
H	12.85285762190725	7.03996577122638	18.79275670094135
H	14.01797202013254	5.73331307019451	19.16016886906241
H	13.77680265610580	7.08233417819908	20.31792493495566
C	7.28571980883854	10.61176155963014	24.20551226141190
H	6.87714903867789	10.77645634531528	25.20965551713316
C	14.81452026104824	8.38115766461463	23.34536948031188
H	14.80889489391556	7.41970063533320	22.80029625249215
H	15.17206184757371	8.18906771656941	24.37371539010158
H	15.53764324146679	9.05055265409088	22.84989177473800
C	6.66607462060918	11.50530200434990	17.67193362293213
H	5.90942172300383	12.29692139496641	17.60655848109507
C	7.04674277850593	10.79933478046571	16.51669082331442
H	6.57964509449276	11.02681753156745	15.55101683611849
C	14.78699806008345	11.13647739633646	20.99797986430275
H	14.97397464794951	11.46326139181870	22.03517414929448
H	15.07719838368378	11.96626387735301	20.32718820573484
H	15.44927846004045	10.28003892834335	20.77972236115789
C	8.67341489675817	10.66613198660266	23.98648595907832
H	9.35415813172595	10.87991421072056	24.82008134389104
C	11.89975034825860	12.23301081554344	20.93633343263292
H	10.85237195137693	12.04851162928536	20.64016443448624
H	12.28176124125923	13.07121349097151	20.32469166129860
H	11.90846149697968	12.55096144225108	21.99387299013894
C	13.05705651973528	10.75449400617560	24.34320174093646
H	13.70488793618862	11.52148858841152	23.88500873722845
H	13.40873053568876	10.58892741497346	25.37820022487456
H	12.03204715892061	11.16449135202877	24.39466649875004
C	6.42597474897398	10.33386561754942	23.12795106057570
H	5.34369053381342	10.26590602938564	23.29290761845901
C	11.95585366434371	7.90883012108144	24.33075553967110
H	10.93194383896160	8.30585347883889	24.44050219284787
H	12.37855525399173	7.76004500949778	25.34210643428645
H	11.88868225883107	6.92777523097196	23.83000420788700
C	12.75015803430541	4.23530960272143	21.69090669005004
H	13.25532074985685	4.82894256377995	22.47421524629886
H	13.51435291703064	3.61831008757841	21.18360896944722
H	12.03176272058888	3.55833193401740	22.18260119199811
C	7.93614270412061	6.14093156788317	20.48505162633802
H	7.87150896872027	7.21244819746113	20.22407065331804
H	6.92685556290213	5.79793871799859	20.77764632645368
H	8.24129075597111	5.58730487634467	19.58009821135506
C	11.02807327741723	4.39304393611678	19.08809733000754
H	10.25283477189585	3.71825953193927	19.48954339511612
H	11.76154228283965	3.77724707024252	18.53579137310026
H	10.54666839988295	5.07604987537707	18.36517642784451
C	9.20284362666616	4.04380822683659	22.39695335285977
H	9.50668054845110	3.37447570080411	21.57417078685689
H	8.18858474401503	3.74267214010749	22.71828435843346
H	9.88586651269709	3.87740472164491	23.24900027152567

1, (S = 4/2), strategy 2, PBE

Fe	11.12995793688557	8.53591458278168	21.60089485880901
Si	13.18418254891335	10.85404688221125	21.12590013147123
Si	13.79832521531948	8.57101322694065	23.18002482455284
Si	9.11184075574827	6.22714034541472	22.05491237261583
Si	11.55703680412091	5.79752574300347	20.13875789739400
O	9.74480958253752	9.84505606022532	21.29353030483911
N	12.79405270299606	9.33296706800926	21.94240385603917
N	10.56818497064477	6.78509235949527	21.22102561966640
C	8.41467528163812	9.80953993966118	19.32435384966461
C	9.18531472349388	8.81259211263376	18.67436555630817
H	9.82598128980718	8.16105974584656	19.28150755282353
C	8.59488774864063	10.03902254390916	20.76832065695605
C	7.50215090557833	10.49749572502457	21.64240991554736
C	7.54805084212014	10.61728520877958	18.54410947649501
H	6.97852784264707	11.42149955466326	19.02391410530847
C	7.82475595283482	11.11231187686658	22.87958714028592
H	8.88118378073439	11.27062342868106	23.12538790387507
C	8.79769859871329	7.32221674023743	23.57568756279584
H	9.62714916095108	7.24197112288478	24.30063635310542
H	7.87078229494595	6.99567954882538	24.08308659764091
H	8.66597273074821	8.38700180274613	23.31225639007625

C	6.13751339029707	10.27438141568529	21.32836082996617
H	5.87250722325049	9.75394756212448	20.40116766532942
C	9.08316792405531	8.62326224419950	17.29229233054954
H	9.67604168301431	7.83699570244775	16.80864550667548
C	12.41997697771685	10.89780369707364	19.39027801054615
H	12.80430729293312	10.06874953918519	18.76981341160429
H	12.67825206139880	11.84873436173010	18.88826351081070
H	11.32020434062040	10.81611202079229	19.42550571028961
C	12.69582990214864	6.92564774326619	19.12155695650560
H	12.12146077731674	7.56831565933360	18.43023055920645
H	13.39433022080895	6.31599356735016	18.51905159092998
H	13.28921043833292	7.58685006708204	19.77870865130108
C	5.46397806109973	11.29578936386704	23.43155441298475
H	4.67324526102088	11.60573196943184	24.12537499291641
C	15.28526186708260	7.68043146900581	22.40394332482455
H	14.94906463327891	6.92827972213506	21.66796246563025
H	15.88025337603747	7.16080242694946	23.17749336598966
H	15.94932688786669	8.39093261322421	21.88151705985235
C	7.45974205217550	10.42990726957961	17.15976377878451
H	6.80067249909272	11.07477264845148	16.56601124104212
C	8.22179363176915	9.43010308243776	16.52888413342022
H	8.14507268958990	9.28289841832769	15.44481188396669
C	15.06071630982105	11.07274408360520	20.90568162460332
H	15.60681778879491	11.08682431875167	21.86478520849390
H	15.26291948309138	12.02968607336259	20.38997189941836
H	15.47839425117456	10.26003054636749	20.28466380246967
C	6.81545944633820	11.51417143747542	23.75849586346731
H	7.07943455748442	11.99945505823962	24.70589898396300
C	12.49392859189967	12.31012105505877	22.13063936845957
H	11.39878046708628	12.20382049208924	22.23386282846108
H	12.70147527983099	13.27775503117593	21.63802238815322
H	12.93289763883721	12.33574139432604	23.14384520788748
C	14.42238747125750	9.84351174388759	24.44776170238654
H	15.07781482579890	10.60655909546993	23.99306327740270
H	14.99743243649949	9.33684536109740	25.24479029606872
H	13.57013828236929	10.36423734375257	24.92038112642375
C	5.13118260217341	10.66935190789121	22.21835257827229
H	4.08064434028535	10.47617969027166	21.96984447746977
C	12.76943269107094	7.29377889231463	24.14149100548327
H	11.98837895129079	7.79355202893912	24.74321554617006
H	13.41986795592826	6.72963704473518	24.83567314141910
H	12.27258450965801	6.56986022558155	23.47110974128524
C	12.64346609586023	4.56752575013914	21.09252416758662
H	13.32238481449033	5.09723429423416	21.78420032122783
H	13.26346017971865	3.97623032538572	20.39356813568447
H	12.03431071506156	3.86500968854035	21.68719599908947
C	7.58680790157554	6.33076241731959	20.92752323623556
H	7.39372922492152	7.37309797531953	20.61911758819242
H	6.68937071142303	5.96062560753299	21.45686110423114
H	7.72041945303989	5.72820670186052	20.01205795419679
C	10.44818542081682	4.83141973732189	18.93272546809771
H	9.78929443452350	4.11845313700385	19.45963299774145
H	11.06638117302436	4.25482501995275	18.22019536656163
H	9.80629046454487	5.51854938151694	18.35235694151730
C	9.30089001768090	4.43799868412652	22.66468350398979
H	9.45369868773497	3.72823813486049	21.83247574300424
H	8.39093383875477	4.12631672360861	23.20976190222486
H	10.15978412721144	4.34874541336225	23.35360518326254

1, (*S* = 6/2), strategy 2, PBE

Fe	10.78060112857667	8.02007936946665	21.11644418466636
Si	12.38286263234265	10.61781747307353	20.61711158812180
Si	12.87573145513780	8.96692999228846	23.25960501782686
Si	9.31946805511338	5.29750474642213	21.53367534511885
Si	12.30824055007887	5.33634621222979	20.54342812195402
O	9.08203139227035	8.69878318153802	20.75514899364988
N	12.09008658562585	9.22397690289230	21.68874458408290
N	10.83160200620621	6.15216722452894	21.10593240477322
C	8.12922539074446	10.34523568670999	19.33620570473422
C	8.13424847434473	9.41461198447345	18.25321591982734
H	8.31137225718962	8.35646591585240	18.47547395670207
C	8.44332653039556	9.87828685916330	20.67429636531389
C	8.10672281146469	10.55308843296540	21.91558230925475
C	7.91240095271827	11.71986890970094	19.02078541670864
H	7.97457582672401	12.47245693295772	19.81425748738809
C	8.82966120441331	10.26278278125024	23.11102105733313
H	9.67030245119950	9.56264332674026	23.06477378059597
C	8.40252630783384	6.26819223571618	22.87599006258214
H	9.01928261273054	6.37299566133180	23.78646279391931
H	7.47942202524554	5.72704643889250	23.15431113547748
H	8.11654818503981	7.27471004556891	22.52559376355523
C	7.02798520978933	11.48217716839534	22.01832417605083
H	6.39922550943432	11.67459317341295	21.14250563613443
C	7.90225678062844	9.83255107469961	16.94058824506099
H	7.89801476128749	9.09214472304790	16.13066299899862
C	11.82545986353411	10.12880469001873	18.87059654611187
H	12.43407377462288	9.29735905657485	18.47256530135963
H	11.95321534534165	10.99212977870963	18.19142892182433
H	10.75750980442207	9.84884655731486	18.81843595970571
C	13.43936531569684	6.60031787130406	19.69289360650999
H	12.97826256050864	6.97090576631249	18.75903379652369
H	14.39722059160458	6.11867533325819	19.42255541242459
H	13.65808798499779	7.46994923875327	20.33608430704763
C	7.47479228195380	11.82829916120422	24.39163969739491
H	7.23408505421206	12.32205735297452	25.34043779050312
C	14.64738327133010	8.31862775575348	23.06875300341672
H	14.66565113942984	7.35343897084446	22.53321798506120
H	15.10542090495926	8.16431775521846	24.06314217745282
H	15.27887644347986	9.03001891957001	22.50915309158492
C	7.68792912951480	12.12771424048504	17.70355888003844
H	7.54092551395500	13.19372523307902	17.48890384962538
C	7.67195523915902	11.19071563655175	16.65174381569263
H	7.49403303187136	11.51731187200664	15.62031610470900
C	14.23805239290820	11.01609996488158	20.55450048237773
H	14.63010497024461	11.32398756359735	21.53996007232801
H	14.41626022648392	11.84758000437044	19.84796019890767
H	14.81934617601706	10.14307394854137	20.20823288469861
C	8.52531375970471	10.89400187121731	24.31857339567945
H	9.11514691323469	10.65859297264070	25.21389724387162
C	11.42576812114381	12.14895785228970	21.17791693460778
H	10.34361910214664	11.93795438644451	21.21671587577957
H	11.59238845355651	12.97915666815526	20.46722316395299
H	11.74345265119241	12.48234908980242	22.18073789709391
C	12.89811829355986	10.59217586005045	24.23772869720990
H	13.51703282690504	11.36340256369657	23.74627994796995
H	13.31221897029111	10.41997833122022	25.24822734968061
H	11.87414717185506	10.99230812964700	24.34565518781915
C	6.72640851358228	12.10654489649060	23.23149068268824
H	5.88367785732833	12.80759270074688	23.27941030169127
C	11.86599306061337	7.69600156311632	24.24498873711482
H	10.86213238393220	8.08357210493915	24.49795681589857
H	12.38192875165711	7.46220754551908	25.19448731845056
H	11.73627743234913	6.75292657420147	23.68468421989697
C	13.24281738623158	4.52721633776263	21.98094074033980
H	13.50542333259208	5.27040308539450	22.75421655044171

H	14.18006082453061	4.06636504479880	21.61858406771481
H	12.63747836730186	3.73818062340905	22.45935361743955
C	8.22757895200551	5.15176858324647	19.99461820294199
H	7.97479998224621	6.16311051496523	19.62947765188877
H	7.28498422186274	4.62221049211966	20.22384377063829
H	8.74365498879600	4.60651313956154	19.18499609014904
C	11.87405920792810	4.02646207290946	19.23891332663420
H	11.24730470948824	3.21189173911365	19.63969304439684
H	12.80258854328159	3.57545093989409	18.84272068980326
H	11.33413907103268	4.49118461645328	18.39465296013944
C	9.68714096352663	3.57656548894075	22.24917544050238
H	10.21859554191388	2.91228497106967	21.54690548782141
H	8.72973329231421	3.08968062547703	22.51181834559524
H	10.28711424111222	3.65617548906274	23.17316130901661

2

2, (S = 1/2), strategy 2, PBE

Co	10.67737246523616	5.95457689202432	4.92684005120664
Si	7.93109005869560	7.03421747892707	5.58640980020133
Si	10.93783297824049	6.84172093907132	1.98711259063072
Si	13.46450412020183	6.08370490269759	3.75397600321831
Si	10.56507142120399	8.35770615184984	6.76967867473668
O	10.75717524685597	4.25542878460407	5.55009186278185
N	11.71782799213832	6.32375806086625	3.49681028338144
N	9.69920070763336	7.25140020702621	5.67998896077164
C	10.17344991210044	3.11028303335082	5.56110441613879
C	10.47958759182354	2.14331811161266	4.50136933246722
C	10.27747847136087	0.74689749075279	4.65551727602154
H	9.88754389372712	0.35508365595618	5.60144591311230
C	9.22427532041316	2.85444513027334	6.66063855439107
C	11.37345631338066	1.72778030709280	2.26147703770911
H	11.80296625114533	2.11439540440099	1.32886210307241
C	11.04740923993768	2.61623458801804	3.29006982345852
H	11.21607186372894	3.69273123255447	3.17237453936969
C	9.42985088439505	3.50382430153643	7.90428056804446
H	10.30649221388470	4.15117313467262	8.02084471101125
C	8.53471005351404	3.31739872961000	8.96278585695269
H	8.71638512423429	3.81719180556725	9.92206899172424
C	8.07658368343062	2.03820850634423	6.50380050193895
H	7.87348278116006	1.57005729422822	5.53391749450549
C	11.15708581030496	0.34683461548332	2.42039507463582
H	11.41843486485419	-0.34950129185035	1.61447357699259
C	7.47118964039624	5.64060884199410	4.38583449560406
H	7.78858351473558	5.86736785204690	3.35390453720844
H	6.37155910523630	5.51804675076009	4.38388930824508
H	7.91651439323024	4.67563259276006	4.68408869466431
C	10.61500628995501	-0.13747172726457	3.62400127129487
H	10.46419990678800	-1.21492173038159	3.76355038037682
C	7.03172879658537	8.61180128879247	5.02726185764771
H	7.13577539303862	9.42152719058388	5.76893252132007
H	5.95382950943312	8.39114180819381	4.91528450324271
H	7.40384126543458	8.98593344637940	4.05805213603861
C	9.82761200348956	8.34064375915039	2.29880829504473
C	11.99523729344816	9.19467371169302	5.85905286598613
H	12.76185066210448	8.46406039285835	5.55792603187929
H	12.47113152490015	9.95611373934751	6.50351888027193
H	11.62559551269463	9.69194493620432	4.94486690648943
C	12.21488474690932	7.37264486748400	0.68037004762687
H	12.74504708089615	8.29283940783649	0.98010929445052
H	11.67504100433515	7.58568074773646	-0.26102196733212
H	12.96538726879705	6.59252262568208	0.46486139349724
C	7.17497155192772	1.86830071120489	7.56274384983073
H	6.28182709912642	1.24799256360412	7.41943656170833
C	13.83293696984834	5.60776091118617	5.55319509622757
H	13.57762642115722	6.41496005106007	6.26128887720114
H	14.91566667144604	5.40206053057941	5.65019192970501
H	13.27904051326743	4.70105456486918	5.85000588624464
C	14.07555696334875	4.65369140289375	2.65828706425849
H	13.64665927924766	3.69129861622155	2.98742778270223
H	15.17691330018770	4.57669501565927	2.72064766310339
H	13.80746078784951	4.80456241654694	1.59777846814072
C	9.92703388411094	5.42699358138448	1.22308000645402
H	10.59324582386047	4.62170044920173	0.86447892553129
H	9.34275542535091	5.79269279980714	0.35840587887390
H	9.22613662748314	4.98032467483074	1.94914785307200
C	7.27664769868246	6.56066187749340	7.30436965230599
H	7.68840917969760	5.58634509781869	7.61811351700253
H	6.17426307719002	6.47868107776318	7.27871289705759
H	7.54221515509421	7.31040955557643	8.07009049874584
C	14.49609383061553	7.62368249165820	3.32942747921183
H	14.57365357717896	7.77276252641991	2.23930553998005
H	15.52058292106521	7.49512368762005	3.72562426069389
H	14.07248461651379	8.54149197842400	3.77222297096321
C	7.40352305759289	2.49766825314944	8.79811392531153
H	6.69890950251936	2.35751559929499	9.62660371692497
C	11.20343965351169	7.37334998651604	8.26219362824628
H	10.35543953344337	6.90680823275313	8.79592762281679
H	11.74534483181494	8.02234118531423	8.97438839475227
H	11.88545906977382	6.56703833937964	7.93881664408374
C	9.43639482444271	9.74518134072590	7.41574751448460
H	9.10053092130592	10.40192011524097	6.59407967432952
H	10.00896749240444	10.36518935977936	8.13029555843474
H	8.54421791010102	9.36550374401123	7.94318256914083
H	9.34109146037778	8.66988132595281	1.36269795297248
H	10.42805143803978	9.17873154874481	2.69527626372598
H	9.04924575441045	8.11164241878488	3.04235042372920

2, (S = 3/2), strategy 2, PBE

Co	10.74313917000332	6.11822172036931	4.78629779984096
Si	7.78644240153600	6.76921351254804	5.49258020307671
Si	11.31275700310341	7.18063797900893	1.95303237277720
Si	13.63054323456270	6.04249217804687	3.75513609912963
Si	10.23601227000350	8.23045131258786	6.88764465617326
O	10.82012974870247	4.20519186736321	4.98417171598385
N	11.96688488859860	6.56963362779763	3.47332696029780
N	9.50567000103337	7.04953645164391	5.79057620427049
C	10.18334373851700	3.16119168497171	5.31861420775493
C	10.20279618261646	2.02071710439865	4.38154994619092
C	9.99719027513088	0.68127846811552	4.79386753649391
H	9.81809172432952	0.45850671076984	5.85167805628964
C	9.46839690070803	3.11691277890039	6.61248731801560
C	10.55245845358367	1.23556814820619	2.09312848376982
H	10.76613037473190	1.45361448488592	1.03973844208725
C	10.49633896858067	2.28110643047586	3.01894746723865
H	10.66903125948158	3.31779911156056	2.70898498200305
C	9.97996091120588	3.87234081954472	7.69423011922247
H	10.88920860621869	4.46382448432978	7.54360620652204
C	9.34150183450913	3.85164917877443	8.93837639512623
H	9.75843357628981	4.42830328586040	9.77272090481586
C	8.27705740088041	2.37443650993058	6.79727405103688
H	7.84188053561921	1.82773189546046	5.95295085815616
C	10.33637869779469	-0.09059440749476	2.51102054394835
H	10.38548283776518	-0.91108475480442	1.78488567095345

C	7.57456029626325	5.45424058728569	4.13567745062053
H	8.04951143001868	5.76977101447581	3.18946780669676
H	6.49812733953647	5.29763387119735	3.93596394204527
H	8.00196205800899	4.47986568105230	4.42917862282174
C	10.06727618515387	-0.36335520978540	3.86317271986084
H	9.92000302436083	-1.39796735245624	4.19576653590190
C	6.89083852084427	8.33719642461844	4.89771698667860
H	6.84101312101246	9.10270846293399	5.69080288863078
H	5.85422230995419	8.08499892850441	4.60640347327584
H	7.39179030776867	8.78479141690570	4.02140743887301
C	10.03142303662826	8.53292355871229	2.29521988226498
C	11.46691335571054	9.32238505920376	5.94445723576070
H	12.21045870939743	8.70845895920129	5.40615333830073
H	11.99717903980713	10.00664573359467	6.63190599776285
H	10.93413095077114	9.93064526734837	5.19154751523961
C	12.64669768164211	7.92536813743628	0.82180155654002
H	13.13033070146963	8.80016008631941	1.29079641582688
H	12.17535917161438	8.26305831035685	-0.11979772702771
H	13.43252092014017	7.19483878343725	0.55930931476588
C	7.62913408790827	2.37449058355254	8.03952545098861
H	6.69629152705613	1.81233672033855	8.16649847887705
C	13.83705310483111	5.41968250085031	5.53862206511831
H	13.59500249718694	6.21408157771294	6.26792382153074
H	14.88793227410669	5.11874417040800	5.70704684679072
H	13.19396977045112	4.54683397773596	5.74421559309079
C	14.07195370399394	4.62185707628767	2.57249103562932
H	13.38774955154308	3.76948918464078	2.73546837835793
H	15.10677732170496	4.27028540003520	2.73911885945547
H	13.98480322326056	4.93360699523789	1.51612074079348
C	10.48813251684962	5.75830267729219	0.99419790284838
H	11.22513091817299	4.96206352622885	0.78228310205577
H	10.07638153870769	6.10944457304785	0.02998435426729
H	9.66193224465489	5.31222928548148	1.57656065199511
C	6.90938775585333	6.14786713082722	7.05666283711371
H	7.34966324589705	5.19942908004287	7.40639891022403
H	5.83664402069177	5.97669216826334	6.85004878246226
H	6.98251784782176	6.88164297982640	7.87860184223281
C	14.86393496881510	7.47010858214539	3.53421875125293
H	14.93060849009204	7.80870123040441	2.48688841666236
H	15.87225961247034	7.14868886829853	3.85479721819816
H	14.56749341620940	8.33467413652493	4.15532453652157
C	8.16564020157456	3.10119895178010	9.11620642465589
H	7.66031105902748	3.09376869033051	10.08937787661865
C	11.15075331350884	7.33785324665420	8.29471508099709
H	10.44752464497691	6.71578411293742	8.87662144201387
H	11.61799949969472	8.06597476453748	8.98307469996250
H	11.94822119165237	6.68193382795542	7.90154036871956
C	8.95124227602296	9.37771988104871	7.69344112411380
H	8.46480328215460	10.03064793039756	6.94808551768958
H	9.46241722574563	10.02863133727365	8.42677651278756
H	8.16501186974724	8.81967573035805	8.23169046952852
H	9.53573206737129	8.85630971254205	1.36184887544617
H	10.51762267062541	9.41207606070372	2.75441917574308
H	9.26053890400716	8.17580302470192	2.99870725924094

2, (*S* = 5/2), strategy 2, PBE

Co	10.93839535291546	5.92570242811380	4.88711031962104
Si	7.81678629125456	6.40263758800299	5.25058867543631
Si	11.31760777680058	7.52485634533854	2.24349924352858
Si	13.73399420388038	5.93839068900463	3.57687246557195
Si	10.00937896983762	8.11533187129504	6.74405185203368
O	11.18631348687741	4.15291797805101	5.30181374973875
N	12.05436428878909	6.56052445715716	3.55414313797039
N	9.51442573137749	6.85553704744339	5.57297623910303
C	10.38501821755891	3.10422219845396	5.56932274879933
C	10.22927970392481	2.13535000532268	4.50126408416132
C	9.82994812105287	0.78389644650443	4.72379249396285
H	9.66198564593392	0.43281826701993	5.74747020356001
C	9.76646352619890	3.04985084738138	6.88043418842092
C	10.41324552543857	1.61061698478409	2.10404449188035
H	10.64517252051976	1.93769863145500	1.08238864863411
C	10.53855745025864	2.51592502368211	3.15979185899102
H	10.86322455458878	3.54433301941603	2.96743830735030
C	10.32069199613145	3.81294186534616	7.95065648435355
H	11.24630464940433	4.36984965969562	7.76741871741885
C	9.71606987174652	3.83977473885902	9.20945717156952
H	10.17298575629744	4.42613796024241	10.01657040866818
C	8.55661473625637	2.33771333631701	7.14131468775008
H	8.06367442516801	1.79344640107876	6.32852480755630
C	9.99062858544203	0.28853564740153	2.34076104189978
H	9.89393838358521	-0.42141026093316	1.51081865437893
C	7.70523436575039	4.77444651732296	4.29980755977502
H	8.33397896540414	4.74845186700825	3.39335508441897
H	6.65665678061729	4.62253032084808	3.98346638322031
H	7.99542262143501	3.92240378804765	4.93480851820777
C	9.71108056220535	-0.11527217188193	3.66073123266473
H	9.41404496083243	-1.15179371274047	3.86429880320291
C	6.99209272558805	7.74941970060358	4.19518229315016
H	6.98835265533791	8.73350141539375	4.69281194917656
H	5.94319899541469	7.46522458662248	3.99070306600737
H	7.50781712339157	7.85869045496198	3.22458474826717
C	10.52629846365891	9.10170670628458	2.92548011800830
C	11.82118789827096	8.60270767339245	6.45299039957979
H	12.50559665222613	7.76030576711445	6.66086319954419
H	12.08598010274805	9.42500522769434	7.14360830532690
H	12.00410684648352	8.94132670688952	5.42015258822143
C	12.56306089593150	8.02674713702381	0.90281964459892
H	13.28519440111476	8.77711640558396	1.26675486524419
H	11.99932777927695	8.48028221510809	0.06651667409111
H	13.12509491632770	7.16678039578394	0.49869747041743
C	7.95226893748933	2.38155619965804	8.40040800514596
H	7.01084213340478	1.84205137881543	8.56339928099640
C	14.15114091650188	5.24050660248009	5.28569965110972
H	14.08274979734138	6.01986413325639	6.06639885830763
H	15.19318817023118	4.87079213367800	5.27384026122955
H	13.48447414990384	4.40555385288421	5.55885167855372
C	13.91578530326541	4.57061781926504	2.27809756197190
H	13.26497846651608	3.71556545975546	2.53365648541106
H	14.96004853456717	4.20987664395823	2.24203247585509
H	13.64192717709219	4.92524680906993	1.26879811362197
C	9.98216708513166	6.46118251509931	1.41934775702153
H	10.40267705950053	5.50240699293561	1.06683616205431
H	9.54682055850305	6.98818795548689	0.55057875798562
H	9.16598480001536	6.23493198201748	2.12616092540121
C	6.88103998349616	6.19272571316861	6.88507130728147
H	7.36898874125066	5.42082606054531	7.50757048373938
H	5.84619176311281	5.86271502768419	6.67901529817900
H	6.82672685770102	7.13094043233925	7.46483716223360
C	14.96700504524498	7.34539357127135	3.24882899056572
H	14.99704266743142	7.65738070305507	2.19251977144198
H	15.97925192588572	7.00197679235588	3.53165450227208
H	14.72469116989181	8.22752686741696	3.86831091413029
C	8.52677583980938	3.12561021561409	9.44930302509197
H	8.04987774947348	3.15493514655192	10.43604510822970
C	9.88878581140258	7.47404550851712	8.52199781616483

H	8.87723565865204	7.11385498505146	8.77171052672985
H	10.15511882167129	8.28622867257949	9.22366395907290
H	10.58991285031063	6.63723490802098	8.67769121061037
C	8.92354804954418	9.66249137375021	6.57946821848750
H	8.97001013297961	10.09123683272621	5.56348705330216
H	9.27962290301767	10.42957401126905	7.29164492335634
H	7.86742546945129	9.44666912597569	6.81857880439582
H	9.99191294608696	9.63312740690816	2.11691896442753
H	11.28493682737847	9.78773702340083	3.34173526245857
H	9.80219921348588	8.85392696594098	3.71896513767910

5

5, (S = 2/2), strategy 2, PBE

Fe	4.34856290349556	11.46398415993094	7.21592992900426
Si	2.71061498233299	8.92063282018159	6.54244782545459
Si	1.35623084874812	11.74520686046232	6.47483148260445
Si	5.77041985355617	14.23868906720124	7.26236634837491
Si	6.08216562248384	12.28958689549534	4.82194328515989
N	5.33225166225329	10.80129193711771	8.65167846772847
N	2.75795671727206	10.68792279377650	6.76180993349700
N	5.40974255727241	12.72236029114651	6.40693393107847
C	4.89741812679711	10.20205918495081	9.75790375232507
C	3.57387009757319	10.26264782816030	10.34142041821948
C	2.62745231781068	11.27335698878007	10.03230804870759
H	2.90779776310684	12.04898186028077	9.31160004687684
C	6.77181237709947	10.67486732816247	8.38337250821444
H	6.94725258220019	10.00214275860247	7.52643025456303
H	7.30300029063971	10.27818669287359	9.26796936409822
H	7.18832215956640	11.65985210727522	8.11937954756285
C	5.21094949402340	14.16139100737801	9.07325302199437
H	4.11360810851952	14.07241457350264	9.15506643834053
H	5.51137986128883	15.09574247165667	9.58353084178186
H	5.65959884441001	13.31261224172216	9.61673529980078
C	1.65374622890563	8.10822224104646	7.89269472846291
H	1.96891451500644	8.45039114054269	8.89385707283350
H	1.77301749576703	7.00969724801250	7.84914235242788
H	0.58196375329705	8.33964845956350	7.77605353598886
C	-0.26601180198066	10.96827726853875	7.08117507992251
H	-0.52788431977487	10.05889272851682	6.51202427671835
H	-1.09204337161398	11.69265640042299	6.95684411529229
H	-0.19856684051071	10.69963667148972	8.14999580454069
C	1.99183832831394	8.48330347456634	4.84020259297768
H	0.94777078850450	8.82877810520012	4.73767790867184
H	1.99834624654086	7.38662543088813	4.70067110369184
H	2.58669369842080	8.93799872574992	4.02853720253286
C	4.44506169440503	8.15710033209334	6.67208644529670
H	5.16032712030579	8.60849393191115	5.96274775625284
H	4.38235330441606	7.07499603730533	6.45148516645272
H	4.84886565912902	8.27045043473690	7.69319494490958
C	3.20972936922107	9.28009578183045	11.30201606549241
H	3.93284802968791	8.49658951333124	11.56434999651219
C	1.21676785283212	12.09936962561765	4.61399361182042
H	2.08362965769166	12.69495221374935	4.27579838856115
H	0.30087957592781	12.68237380565614	4.40461274373029
H	1.18063407761217	11.17423685739712	4.01418998228273
C	1.94082174087183	9.28354790985402	11.89143521019042
H	1.67598394011312	8.50434615200180	12.61649843075571
C	1.00669264671817	10.27950473253013	11.55492240519727
H	0.01149757191670	10.28273930842196	12.01512068688239
C	1.36586898272991	11.28007797045651	10.63144832089715
H	0.65206159153144	12.07525044390714	10.38150492049508
C	4.98846990170688	11.05608852054727	3.88774074516139
H	4.96299533198532	10.07032795285596	4.38069925752733
H	5.38828895011249	10.91905359473318	2.86548148683753
H	3.94982230112868	11.41866701108565	3.81020536183922
C	1.55244374534657	13.43549715391234	7.31487491377486
H	1.45432537817265	13.38897624218368	8.41247617294775
H	0.76718686868773	14.11609525658373	6.93565495742828
H	2.53313355326379	13.87927099977023	7.07197622857213
C	7.81839666152046	11.53010754518673	4.97799265755263
H	8.49747965823366	12.17993366035241	5.55756952907518
H	8.25889414453216	11.38525108685653	3.97417221349962
H	7.78315303255189	10.54320276959677	5.47214348479914
C	6.22024330216219	13.83569987059780	3.72144736499953
H	5.22974792160221	14.29835871812708	3.56445333023856
H	6.61867795897582	13.54116407384517	2.73310235597228
H	6.89604479987061	14.60130086853296	4.14075719155868
C	7.64225606862461	14.58671893178838	7.25083684525667
H	8.20547992472117	13.78887268465328	7.76789224392879
H	7.85414203724317	15.53906504356751	7.77109049776746
H	8.03980031816898	14.66904300382402	6.22388848859487
C	4.88880086532335	15.71349220458193	6.45494409349764
H	5.24079630907730	15.89252842848522	5.42533426296505
H	5.07862621330105	16.62873278913419	7.04577935510155
H	3.79693755381002	15.55310847454511	6.41936641820053
H	5.62629349344032	9.56736130065361	10.28961594772359

5, (S = 4/2), strategy 2, PBE

Fe	4.29874756583485	11.31576654577742	7.20929332905035
Si	2.36930711489430	8.93247323305262	6.38807299003703
Si	1.44376985551883	11.91998984570383	6.23519807140480
Si	5.60404215362384	14.11267615683873	7.27665709507891
Si	6.11804536619433	12.28110730425651	4.80400121223099
N	5.41744193592904	10.40487133328756	8.67465581080699
N	2.60415466923637	10.65834013548694	6.67052840621800
N	5.43605385433706	12.59883537171644	6.39613461517308
C	5.18400989362437	10.14219409691336	9.93167634860728
C	3.92396116379886	10.26523269359789	10.65647837256411
C	2.67955804072207	10.55145070954481	10.04333922196232
H	2.61069710393418	10.67350444399792	8.95148313067971
C	6.78024845071185	10.17374433070476	8.19852589102706
H	6.77579560165364	9.36985537984493	7.44005445019182
H	7.46522792363709	9.88645435081103	9.02007641188580
H	7.14617140634766	11.08935399510076	7.70219419601374
C	5.15530121678431	13.82364025283319	9.10595204695577
H	4.15169657020065	13.37742829010874	9.24131729988683
H	5.15599611452341	14.78736489276089	9.64824422895661
H	5.88819797486420	13.15854522387641	9.59629377238913
C	0.95703793092584	8.23162014522190	7.45300822466116
H	1.13411121540618	8.43905696235241	8.52383011998964
H	0.89385571798412	7.13496563203759	7.32545665795548
H	-0.02119184283979	8.66061504633381	7.17682278529892
C	-0.32173890697486	11.25774257449828	5.98051573179487
H	-0.38330871101860	10.48344863887802	5.19625104483248
H	-0.97378326843844	12.09670660211980	5.67410346112889
H	-0.73387052799530	10.83588276663293	6.91418296909096
C	2.00181471424694	8.56666497275553	4.55938135261378
H	1.10118789225888	9.09758941860578	4.20422425849975
H	1.83761450140596	7.48389504810920	4.40666372070219
H	2.85116980370843	8.87771379353751	3.92563590199832
C	3.93013062029459	7.95291400612614	6.85649410076931
H	4.80468674493551	8.26394706029336	6.25725461285858
H	3.75801770754941	6.87686171734465	6.66805281476806

H	4.17963295840002	8.07635651608082	7.92475940638377
C	3.95817524760279	10.06896373286476	12.06056000747984
H	4.91588386996160	9.83833923021739	12.54561381788001
C	1.98004515974949	12.81451865817449	4.65110337461352
H	2.99903903011744	13.21939227842584	4.77952131577220
H	1.29860698205310	13.65108201261291	4.41105435758361
H	1.99131065690419	12.12147501084863	3.79051006982288
C	2.79362746948996	10.17092582473277	12.83001637169119
H	2.84083497330064	10.02187527124640	13.91536437420090
C	1.56643902620170	10.45908436280655	12.20926582162409
H	0.65085118599246	10.53531765166761	12.80808564125419
C	1.51703944006949	10.64275337966438	10.81508041489313
H	0.56010573029465	10.85358034941994	10.32177120725974
C	5.27317508504234	10.76260723061613	4.04146015530729
H	5.44715221383189	9.85550579846273	4.64852649644514
H	5.67316993266794	10.57090853284069	3.02869966822760
H	4.18306272205587	10.91231619539508	3.96441400383024
C	1.32926411448268	13.19848004183832	7.63876770552746
H	0.95649276518978	12.73711018923102	8.57074212249783
H	0.63611419475598	14.01457515748277	7.36249640669040
H	2.31097917112333	13.65301415994088	7.85827985009998
C	7.98227946260934	11.90536954991091	4.90256930938607
H	8.54073749306415	12.73284531321126	5.37417104202205
H	8.39496718557608	11.75169751300313	3.88806642310547
H	8.17612416370949	10.98670409905577	5.48493742198302
C	5.89584103061778	13.75237795839399	3.62018667881951
H	4.82861794048797	14.00874052299079	3.49748929197129
H	6.30481895196095	13.50490870669781	2.62321581126399
H	6.42388987133860	14.65196366259701	3.98459669164767
C	7.39425356867397	14.75596501477766	7.23222403785663
H	8.09684247546003	14.00840826894710	7.64257462577974
H	7.48627697708954	15.67886078202959	7.83417720189285
H	7.71513478122457	14.99478286230435	6.20231339594780
C	4.48010086571475	15.48030408093929	6.58798738689899
H	4.75624821187846	15.73033461833303	5.54861245583084
H	4.56829285609076	16.40023575334938	7.19523655555431
H	3.42082215624733	15.16995707639799	6.58803769502544
H	6.03424351114814	9.78601066142642	10.54614372784488

5, (S = 6/2), strategy 2, PBE

Fe	4.34450255144299	11.42064416549906	7.45567072225608
Si	2.72392455131040	8.78202659304194	6.66101959010756
Si	1.54403923963306	11.61901561857892	6.12801024726923
Si	6.01756458588516	14.09475297355704	7.54446420178072
Si	5.62918986465062	12.66872475088966	4.81806149383520
N	5.50205154718664	10.57043645955415	8.79692518228735
N	2.86458031285885	10.56022094042634	6.67763132128188
N	5.34983400055631	12.76096826220771	6.57185064191983
C	4.93396137642656	9.91526401717642	9.86086299167532
C	3.63818623155320	10.21410046505504	10.34953984545898
C	2.90154606404785	11.36943077707098	9.90773632205449
H	3.43163188448786	12.17481113348211	9.36972950496595
C	6.90941625328793	10.32628658787566	8.54920636008825
H	7.11920843066629	9.24421263148753	8.39617890768584
H	7.54677115057474	10.66922807187241	9.39241952013259
H	7.23070208474492	10.86377735845649	7.64141052621614
C	5.12892669976501	14.20791599492166	9.21595921800861
H	4.04333298008765	14.38027109854353	9.10328125015792
H	5.54113267168291	15.06625425383498	9.77831885239702
H	5.28602632522011	13.30225595393224	9.82796184062718
C	1.61162123948765	8.13183991719416	8.04586787887211
H	1.94448801657779	8.50395664853829	9.02924123999395
H	1.64939616433339	7.02667164350706	8.06121500354384
H	0.56072115236783	8.43531567797275	7.90450467043697
C	-0.11797863239845	11.05030165027287	6.84355466474956
H	-0.43694832388550	10.08094243784941	6.42180698521444
H	-0.89899887297730	11.79545491931299	6.60387125074845
H	-0.05630625023053	10.94718376809776	7.94113514032137
C	2.00696117166964	8.21316002716338	4.99422230621804
H	0.96688382452076	8.55610893875567	4.85255163665052
H	2.00152629155957	7.10800085215163	4.95902997914027
H	2.61080125692879	8.57942165824505	4.14514825323447
C	4.44246815146551	8.00169096222383	6.84441327023895
H	5.16765382343030	8.42319185231505	6.12605146887132
H	4.36747480100806	6.91575997120535	6.65103656439723
H	4.83444185265273	8.14319598032310	7.86560661321430
C	2.97165535446497	9.35086488012243	11.28466045366444
H	3.51258327167850	8.47719489512314	11.67122616563733
C	1.39487175003212	11.65412881327638	4.23529081687569
H	2.36192577229492	11.85891746890700	3.74663396945434
H	0.68373976077634	12.44406866297781	3.93026188335138
H	1.01825286988420	10.69217314158172	3.84805537633622
C	1.65407149011538	9.58078900214649	11.66769286642660
H	1.16841133121030	8.88845869586024	12.36690451461321
C	0.92764832912302	10.68766012410622	11.16092978326827
H	-0.11199934168524	10.85757405460552	11.46200002317486
C	1.57795260992148	11.58690391689257	10.29274651572664
H	1.05211523047758	12.48454763543666	9.94255072047610
C	5.32718542011375	10.89638106235931	4.21842775720397
H	6.04318100129949	10.19913042670718	4.69088499131682
H	5.47345416820226	10.83869623232474	3.12423977588107
H	4.30742988421556	10.55107834442946	4.45711691519141
C	1.86471538471526	13.38718813007566	6.75111835912823
H	1.80103357306364	13.44128048483060	7.85291986780988
H	1.09257942565766	14.06512636263884	6.34256626350090
H	2.85349265950261	13.76820242342327	6.44175188606443
C	7.43536271897565	13.08955563923229	4.40033280253165
H	7.70381236364609	14.12727068217870	4.66448563163277
H	7.59071402320352	12.97015559920998	3.31198636929511
H	8.13372603321062	12.40914270392847	4.91922107800366
C	4.51985029520721	13.86791796547831	3.84999731969012
H	3.45567927448824	13.75210379094961	4.11434685568508
H	4.62285240923534	13.68459354725804	2.76444080356607
H	4.80423681528460	14.91621405943373	4.04466282745355
C	7.86803555412731	13.88041036264068	7.90638614552431
H	8.04955927809977	12.99096930897323	8.53349363653652
H	8.23791009487467	14.76479291004704	8.45771894506245
H	8.46458990396168	13.78053773469462	6.98411779634343
C	5.76276029106981	15.75761366007083	6.66017252427274
H	6.32820840693026	15.82395297918243	5.71431823315131
H	6.10774991493651	16.57864346813972	7.31545553077169
H	4.69473931914269	15.92672787045388	6.43492092475470
H	5.50982988596151	9.10633894770648	10.34115520456831

Benzophenone, optimized at the PBE-D3(BJ)/def2-SVP level of theory

C	-2.17200248903266	4.98131855968824	-0.60746471284589
C	-2.24211555387205	3.65241826314946	-1.06336253713360
C	-1.07899019871572	2.99902834615533	-1.50110894664700
C	0.15734715928251	3.66154519278011	-1.46228665556197
C	0.23798546560267	4.99178455882047	-0.99590938148445
C	-0.94296275935033	5.64972588304803	-0.58818691478903
C	1.51292679829311	5.78785839006703	-1.00122338459876
C	2.83492426476665	5.08734942271534	-0.85683744596157
C	3.97502836654417	5.72324153674759	-1.39495816098539

C	2.99541921487975	3.88379504528358	-0.13623955788941
C	4.27030503662236	3.32023924082806	0.02510706244793
C	5.24309731086860	5.14953198493734	-1.25163857846171
C	5.39306400880828	3.94459373885639	-0.54145278973379
H	3.83307731556181	6.67601803573658	-1.91883568194551
H	6.12048214534796	5.64322247995381	-1.68707451301511
H	4.38786967281031	2.39294049052628	0.59897064292463
H	6.38766739377632	3.49741985868235	-0.42230015503796
H	2.12455341740277	3.40391839703519	0.32524616848411
H	1.05936484147727	3.15472505351778	-1.82442334637020
H	-3.20622560842125	3.12954466646046	-1.08561580211116
H	-1.13493825216417	1.97076352377512	-1.87869004219722
H	-0.86388180395567	6.69449801726618	-0.26479372081742
H	-3.08124100679219	5.49614619859817	-0.27373356526386
O	1.47445526025950	7.01174311537106	-1.12369798100565

Ketyl radical (S = 2/2), optimized at the PBE-D3(BJ)/def2-SVP level of theory

C	-2.21314905613823	5.09002292674658	-0.77460463901045
C	-2.35142113601353	3.70314475292149	-1.00976014045511
C	-1.18439520400238	2.94969304915289	-1.26478801317427
C	0.08012844142434	3.54960929002783	-1.25139069277233
C	0.24516122871643	4.94216290913168	-0.97798524416849
C	-0.95526096310203	5.69331451477179	-0.77213179803889
C	1.51570012959015	5.70066536510154	-0.99299793655638
C	2.83102548032103	5.03478150861997	-0.86513822395635
C	3.98369687872600	5.80329833059937	-1.22337329614403
C	3.08052840909579	3.73724012476027	-0.32179613854497
C	4.37976988487238	3.23163777871306	-0.19749657468599
C	5.27660441201925	5.29184715968976	-1.10902415042569
C	5.49929073809641	3.99052812097114	-0.60423029096425
H	3.78930564549780	6.82098474097372	-1.58437133979788
H	6.13324226351999	5.91263717891102	-1.41166423832785
H	4.52672476827447	2.23335157170212	0.24039655217308
H	6.51637954912814	3.58737324764949	-0.51088153761288
H	2.24335556303517	3.14022266985046	0.05694834527864
H	0.95513847612548	2.94239280344388	-1.50912634828585
H	-3.34089212609227	3.22708138840528	-1.01492699591472
H	-1.26629911890233	1.87720012393298	-1.49494878901399
H	-0.82674110147898	6.77245512909893	-0.62138775381994
H	-3.10856148208818	5.70406211067267	-0.59574221984632
O	1.47587831937510	6.96766320415204	-1.12008853593507

Benzophenone imine, optimized at the PBE-D3(BJ)/def2-SVP level of theory

C	-4.45562004906012	3.04062892060705	-1.70728125031147
C	-4.66915568074857	1.66858993490335	-1.49738912175333
C	-3.27085878117003	3.64337829402049	-1.26295229528999
C	-2.27470831386787	2.88207898033768	-0.61392964383736
C	-2.49491982901134	1.50085918098219	-0.41796351944660
C	-3.68797971564653	0.90242016586701	-0.84773646592566
C	-1.04857401859343	3.55909981394951	-0.08044484630230
C	0.28657442578036	2.93759983830345	-0.33218901765746
C	1.38258916555591	3.31875665352545	0.47407348561044
C	2.65300062396565	2.77899488529809	0.24882576718360
C	0.49918912625460	2.01427435709154	-1.37888629572343
C	1.77590172483525	1.47934209442842	-1.60793410684194
C	2.85415086923879	1.85527678893617	-0.79267879215091
H	1.19959444178216	4.05079618371696	1.27407455982998
H	-0.33871185794078	1.72510944685091	-2.03005238434700
H	1.92914614964062	0.76582231787710	-2.43188305057593
H	3.85413996388891	1.43009475426269	-0.96897654141453
H	3.49682483657300	3.07794135859509	0.88952911588653
H	-3.85325348328022	-0.17182100676671	-0.67363227337932
H	-1.72796571858572	0.89862656148649	0.09187570310226
H	-5.21607677954643	3.64485487941779	-2.22507179531972
H	-5.60078117977597	1.19524375013283	-1.84279477602295
H	-3.09900472797836	4.71767013270151	-1.43398037330551
N	-1.09718966350256	4.65762176204449	0.60101599427690
H	-2.08402152880728	4.94579995143043	0.72103192371571

Benzimyl radical (S = 2/2), optimized at the PBE-D3(BJ)/def2-SVP level of theory

C	-4.60734492890292	3.11119108291464	-1.44628761908706
C	-4.78011492575709	1.71120675416211	-1.47562262042981
C	-3.39051799703933	3.67905594848086	-1.06202682451126
C	-2.25757852821905	2.87912254158416	-0.69235214352133
C	-2.46143905259911	1.46323195865106	-0.72575738049194
C	-3.68221883273300	0.89844056649162	-1.10228233703098
C	-1.03242338862992	3.53146210185609	-0.19976824914954
C	0.28469638584442	2.89083218871459	-0.36202847616495
C	1.39041508000447	3.40152902922928	0.39097329241913
C	2.67639715586233	2.87599767709083	0.25483316104380
C	0.58093109627337	1.85105272295230	-1.29357228667520
C	1.87157053847536	1.32798499225329	-1.42666314869103
C	2.94144906962410	1.82302940538077	-0.64743062624244
H	1.16741250464248	4.23287197311226	1.07616138966910
H	-0.21762255415931	1.47287961155983	-1.94892958709709
H	2.05414235875304	0.52755373336451	-2.16420816609226
H	3.95697661843232	1.40882714019574	-0.75343205354103
H	3.49837592456516	3.29199131618193	0.86389343558296
H	-3.79318888640972	-0.19952578922149	-1.08942995991166
H	-1.64433506727102	0.80281475834781	-0.39922830711145
H	-5.44159355041730	3.77174703758557	-1.74095801787609
H	-5.74221573607604	1.26394332153117	-1.77118586662136
H	-3.26939862505266	4.77435599630877	-1.07181556086366
N	-1.04976269388299	4.73360138965744	0.39736388261014
H	-2.04032196532757	4.99386254161484	0.54440406978500

N-Methylbenzaldimine, optimized at the PBE-D3(BJ)/def2-SVP level of theory

C	-2.34995351840566	1.63651192350896	-0.14242435280511
C	-2.56442721873802	0.24574334949216	-0.19767759377400
C	-1.07366652752341	2.14157594203494	0.12402493070874
C	0.01060055615155	1.26063012802573	0.33987046256093
C	-0.21312282272296	-0.13140095952186	0.28266106998861
C	-1.49382417943983	-0.63729515843447	0.01531420368856
H	-1.65758113119460	-1.72101458159618	-0.02707092083132
H	-3.56692786992750	-0.14749108763914	-0.40693058534132
H	-3.18706053538230	2.32582163564383	-0.30898329017624
H	-0.87415183463512	3.21874214070386	0.17373056843464
H	0.62771554767443	-0.81818742652925	0.44999003121657
C	1.36127682643659	1.77823344263075	0.62187980471368
N	1.62207273061722	3.03151724429839	0.68589759931738
H	2.14423757191804	0.99591129642318	0.77643885091140
C	2.98605082433445	3.43701339974988	0.96977517050689
H	3.69611574748793	3.06821441286922	0.20110345229955
H	3.33643794189709	3.05361516058212	1.95023458258886
H	3.06133789145209	4.53763913775785	0.99444601599218

N-Methylbenzaldimyl radical (S = 2/2), optimized at the PBE-D3(BJ)/def2-SVP level of theory

C	-2.36531440597624	1.62157943042901	-0.14563034323366
C	-2.59646101377390	0.22135649724466	-0.20448022195481

C	-1.10238886092895	2.14413162633146	0.11825374438264
C	0.03707918696526	1.28343642896485	0.34557493172485
C	-0.21866899024935	-0.13123276868385	0.28147637101697
C	-1.48745554557657	-0.64220566043460	0.01649012014445
H	-1.63107036345443	-1.73336810076811	-0.02192233495007
H	-3.59631154167772	-0.18153796250772	-0.41332087843190
H	-3.20643606397448	2.31356332061439	-0.31296359222118
H	-0.92199811154396	3.22582513130694	0.16410730085523
H	0.62363398131109	-0.82136969522994	0.44901174375327
C	1.33784817928991	1.81329015331164	0.61743662883219
N	1.62414398271580	3.11258754649852	0.68694601892752
H	2.13841445026277	1.04514645382862	0.77581882416061
C	2.99002685865487	3.42548055402051	0.97044430997909
H	3.72359872569751	3.03431077486946	0.20945970475641
H	3.36488818723417	3.02042399389773	1.95312283504227
H	3.15160134502422	4.52436227630643	1.01245483721613

X-Ray diffraction analysis and molecular structures

Data for K{18c6}[**1**] (CCDC 2093093), K{18c6}[**2**] (CCDC 2093094), K{18c6}[**3**] (CCDC 2093095), K{18c6}[**4**] (CCDC 2093096), K{18c6}[**5**] (CCDC 2093097), **1** (CCDC 2093086), **2** (CCDC 2093087), **5** (CCDC 2093088), **6** (CCDC 2093089), **7** (CCDC 2093090), **8** (CCDC 2093091), K{18c6}[**9**] (CCDC 2093098), [K{18c6}]$_2$[**10**] (CCDC 2093099), and K{18c6}[**12**] (CCDC 2093092) were collected on a Bruker Quest D8 diffractometer using a graphite-monochromated Mo-Kα radiation and equipped with an *Oxford Instrument Cooler Device*. Data for [K{18c6}]$_2$[**11**] (CCDC 2093100) was collected on a STOE StadiVari diffractometer, using Cu-Kα radiation from an X-ray micro source with X-ray optics and a Pilatus 300K Si hybrid pixel array detector. The structures have been solved using OXEX SHELXT V2014/1[42] and refinded by means of least-squares procedures on a F^2 with the aid of the program SHELXL-2016/6, included in the software package WinGX version 1.63[43] or using CRYSTALS.[44] The Atomic Scattering Factors were taken from *International Tables for X-Ray Crystallography*.[45] All non-hydrogen atoms were refinded anisotropically. All hydrogen atoms were refinded by using a riding model. Absorption corrections were introduced by using the MULTISCAN[46] and X-Red program[47]. Drawings of molecules were performed with the program DIAMOND with 50% probability displacement ellipsoids for non-H atoms. H atoms are generally omitted for clarity with the exception of N-H functionalities.

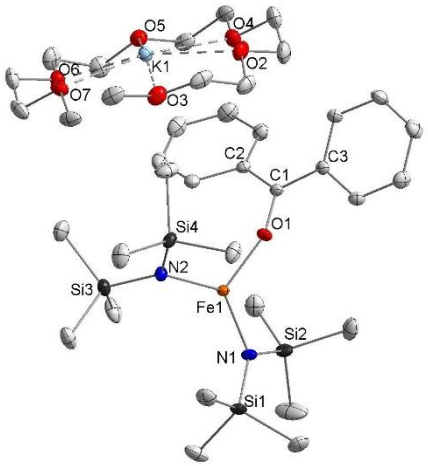

Figure S83. Molecular structure of K{18c6}[**1**] within the crystal. Hydrogen atoms are omitted for clarity, thermal ellipsoids are shown with 50% probability.

Table S21. Crystal data and structure refinement for K{18c6}[**1**].

Identification code	K_18c6_1
Empirical formula	$C_{37}H_{70}FeKN_2O_7Si_4$
Formula weight	862.26
Temperature/K	100.01
Crystal system	monoclinic
Space group	C2/c
a/Å	19.7321(17)
b/Å	14.5258(14)
c/Å	34.550(3)
α/°	90
β/°	101.197(4)
γ/°	90
Volume/Å^3	9714.4(16)
Z	8
ρ_{calc}g/cm^3	1.179
μ/mm^{-1}	0.537
F(000)	3704.0
Crystal size/mm^3	0.363 × 0.355 × 0.288
Radiation	MoKα (λ = 0.71073)
2Θ range for data collection/°	4.422 to 58.444
Index ranges	-25 ≤ h ≤ 27, -19 ≤ k ≤ 19, -47 ≤ l ≤ 47
Reflections collected	126875
Independent reflections	13138 [R_{int} = 0.0365, R_{sigma} = 0.0206]
Data/restraints/parameters	13138/0/481
Goodness-of-fit on F^2	1.062
Final R indexes [I>=2σ (I)]	R_1 = 0.0311, wR_2 = 0.0669
Final R indexes [all data]	R_1 = 0.0412, wR_2 = 0.0702
Largest diff. peak/hole / e Å^{-3}	0.36/-0.33

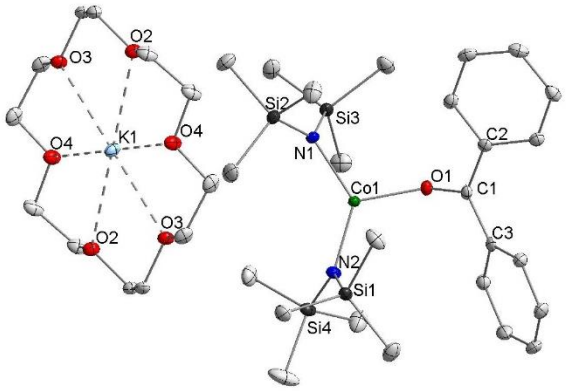

Figure S84. Molecular structure of K{18c6}[**2**] within the crystal. Hydrogen atoms are omitted for clarity, thermal ellipsoids are shown with 50% probability.

Table S22. Crystal data and structure refinement for K{18c6}[**2**].

Identification code	K_18c6_2
Empirical formula	$C_{37}H_{70}CoKN_2O_7Si_4$
Formula weight	865.34
Temperature/K	99.99
Crystal system	triclinic
Space group	P-1
a/Å	11.1083(7)
b/Å	11.3941(8)
c/Å	20.2368(14)
α/°	77.246(2)
β/°	85.093(2)
γ/°	70.902(2)
Volume/Å^3	2360.4(3)
Z	2
ρ_{calc}g/cm^3	1.218
μ/mm^{-1}	0.596
F(000)	928.0
Crystal size/mm^3	0.517 × 0.199 × 0.194
Radiation	MoKα (λ = 0.71073)
2Θ range for data collection/°	4.37 to 51.998
Index ranges	-13 ≤ h ≤ 13, -14 ≤ k ≤ 13, -24 ≤ l ≤ 24
Reflections collected	51701
Independent reflections	9262 [R_{int} = 0.0459, R_{sigma} = 0.0311]
Data/restraints/parameters	9262/0/495
Goodness-of-fit on F^2	1.046
Final R indexes [I>=2σ (I)]	R_1 = 0.0272, wR_2 = 0.0648
Final R indexes [all data]	R_1 = 0.0334, wR_2 = 0.0666
Largest diff. peak/hole / e Å^{-3}	0.35/-0.28

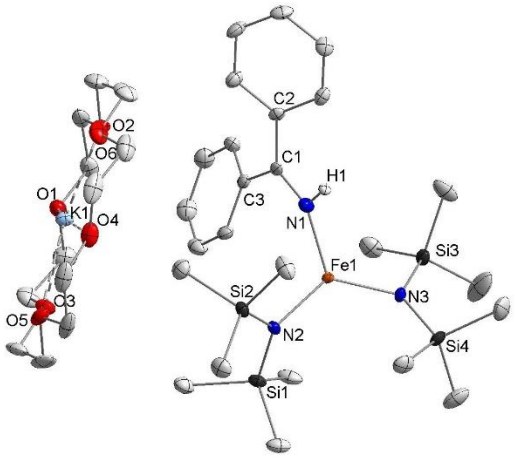

Figure S85. Molecular structure of K{18c6}[**3**] within the crystal. Hydrogen atoms (except H1) are omitted for clarity, thermal ellipsoids are shown with 50% probability.

Table S23. Crystal data and structure refinement for K{18c6}[**3**].

Identification code	K_18c6_3
Empirical formula	$C_{37}H_{71}FeKN_3O_6Si_4$
Formula weight	861.27
Temperature/K	100
Crystal system	monoclinic
Space group	C2/c
a/Å	19.8906(9)
b/Å	14.5797(6)
c/Å	34.2968(15)
α/°	90
β/°	100.751(2)
γ/°	90
Volume/Å^3	9771.5(7)
Z	8
ρ_{calc}g/cm^3	1.171
μ/mm^{-1}	0.532
F(000)	3704.0
Crystal size/mm^3	0.169 × 0.133 × 0.077
Radiation	MoKα (λ = 0.71073)
2Θ range for data collection/°	4.412 to 49.998
Index ranges	-23 ≤ h ≤ 23, -17 ≤ k ≤ 16, -40 ≤ l ≤ 40
Reflections collected	80662
Independent reflections	8615 [R_{int} = 0.1063, R_{sigma} = 0.0465]
Data/restraints/parameters	8615/0/481
Goodness-of-fit on F^2	1.066
Final R indexes [I>=2σ (I)]	R_1 = 0.0452, wR_2 = 0.0791
Final R indexes [all data]	R_1 = 0.0686, wR_2 = 0.0839
Largest diff. peak/hole / e Å^{-3}	0.28/-0.39

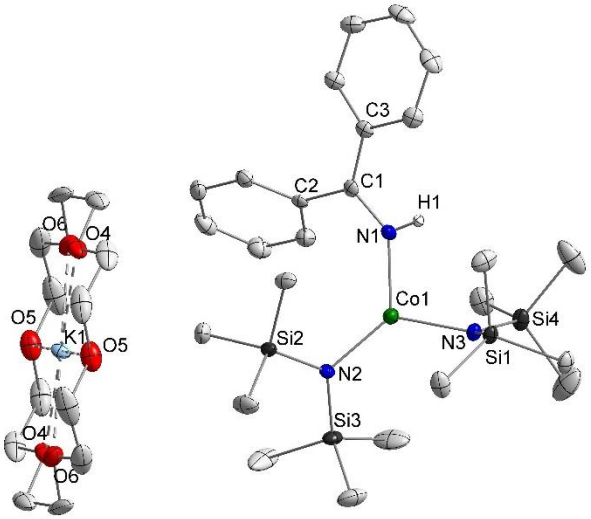

Figure S86. Molecular structure of K{18c6}[**4**] within the crystal. Hydrogen atoms (except H1) are omitted for clarity, thermal ellipsoids are shown with 50% probability.

Table S24. Crystal data and structure refinement for K{18c6}[**4**].

Identification code	K_18c6_4
Empirical formula	$C_{37}H_{71}CoKN_3O_6Si_4$
Formula weight	864.35
Temperature/K	99.99
Crystal system	orthorhombic
Space group	Pbca
a/Å	21.4162(12)
b/Å	19.3981(11)
c/Å	22.9957(15)
α/°	90
β/°	90
γ/°	90
Volume/Å^3	9553.2(10)
Z	8
ρ_{calc}g/cm^3	1.202
μ/mm^{-1}	0.588
F(000)	3712.0
Crystal size/mm^3	0.348 × 0.204 × 0.164
Radiation	MoKα (λ = 0.71073)
2Θ range for data collection/°	4.2 to 52.182
Index ranges	-26 ≤ h ≤ 26, -23 ≤ k ≤ 23, -28 ≤ l ≤ 28
Reflections collected	96966
Independent reflections	9456 [R_{int} = 0.0962, R_{sigma} = 0.0437]
Data/restraints/parameters	9456/0/488
Goodness-of-fit on F^2	1.093
Final R indexes [I>=2σ (I)]	R_1 = 0.0496, wR_2 = 0.0983
Final R indexes [all data]	R_1 = 0.0743, wR_2 = 0.1065
Largest diff. peak/hole / e Å^{-3}	0.50/-0.64

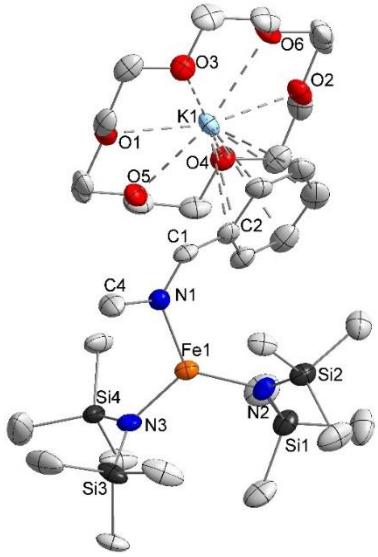

Figure S87. Molecular structure of K{18c6}[**5**] within the crystal. Hydrogen atoms are omitted for clarity, thermal ellipsoids are shown with 50% probability. Disorders were found for the $SiMe_3$ groups of Si3 (67% / 33%) and Si4 (80% / 20%).

Table S 25. Crystal data and structure refinement for K{18c6}[**5**].

Identification code	K_18c6_5
Empirical formula	$C_{32}H_{69}FeKN_3O_6Si_4$
Formula weight	799.21
Temperature/K	99.99
Crystal system	orthorhombic
Space group	Pbca
a/Å	13.0204(4)
b/Å	20.9396(7)
c/Å	32.8983(10)
α/°	90
β/°	90
γ/°	90
Volume/Å^3	8969.5(5)
Z	8
ρ_{calc}g/cm^3	1.184
μ/mm^{-1}	0.575
F(000)	3448.0
Crystal size/mm^3	0.27 × 0.239 × 0.103
Radiation	MoKα (λ = 0.71073)
2Θ range for data collection/°	4.438 to 49.996
Index ranges	-15 ≤ h ≤ 15, -24 ≤ k ≤ 24, -39 ≤ l ≤ 39
Reflections collected	105625
Independent reflections	7900 [R_{int} = 0.1500, R_{sigma} = 0.0602]
Data/restraints/parameters	7900/38/515
Goodness-of-fit on F^2	1.075
Final R indexes [I>=2σ (I)]	R_1 = 0.0730, wR_2 = 0.1476
Final R indexes [all data]	R_1 = 0.1153, wR_2 = 0.1604
Largest diff. peak/hole / e Å^{-3}	0.97/-0.39

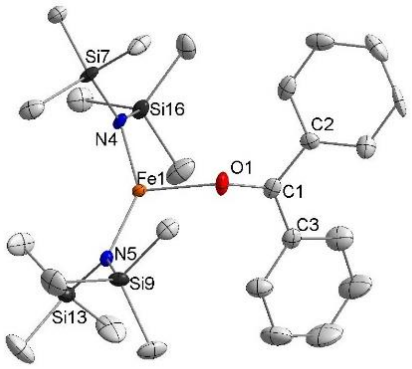

Figure 88. Molecular structure of **1** within the crystal. Hydrogen atoms are omitted for clarity, thermal ellipsoids are shown with 50% probability. The structure was refined as an inversion twin, twin ratio refined to 0.1742(12). Residual electron density of 2.6 eA^{-3} could not be attributed and is probably due to twinning.

Table S26. Crystal data and structure refinement for **1**.

Identification code	1
Empirical formula	$C_{100}H_{184}Fe_4N_8O_4Si_{16}$
Formula weight	2235.38
Temperature/K	100.0
Crystal system	monoclinic
Space group	$P2_1/c$
a/Å	44.079(3)
b/Å	12.6283(9)
c/Å	23.4472(17)
α/°	90
β/°	90.469(2)
γ/°	90
Volume/$Å^3$	13051.3(16)
Z	4
$\rho_{calc}g/cm^3$	1.138
μ/mm^{-1}	0.627
F(000)	4800.0
Crystal size/mm^3	0.254 × 0.226 × 0.198
Radiation	MoKα (λ = 0.71073)
2Θ range for data collection/°	4.254 to 49.998
Index ranges	-52 ≤ h ≤ 52, -14 ≤ k ≤ 15, -27 ≤ l ≤ 27
Reflections collected	87885
Independent reflections	22811 [R_{int} = 0.0583, R_{sigma} = 0.0570]
Data/restraints/parameters	22811/633/1220
Goodness-of-fit on F^2	1.097
Final R indexes [I>=2σ (I)]	R_1 = 0.0968, wR_2 = 0.2384
Final R indexes [all data]	R_1 = 0.1073, wR_2 = 0.2444
Largest diff. peak/hole / e $Å^{-3}$	2.63/-0.89

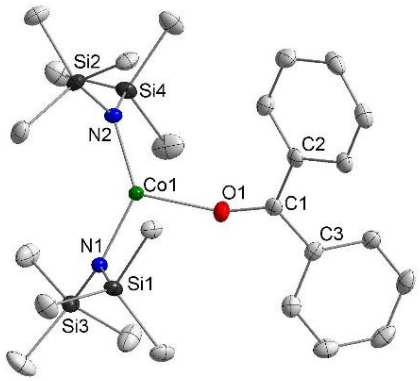

Figure S89. Molecular structure of **2** within the crystal. Hydrogen atoms are omitted for clarity, thermal ellipsoids are shown with 50% probability.

Table S27. Crystal data and structure refinement for **2**.

Identification code	2
Empirical formula	$C_{25}H_{46}CoN_2OSi_4$
Formula weight	561.93
Temperature/K	100.02
Crystal system	monoclinic
Space group	$P2_1/n$
a/Å	15.6864(7)
b/Å	12.5188(5)
c/Å	16.4231(7)
α/°	90
β/°	94.131(2)
γ/°	90
Volume/Å^3	3216.7(2)
Z	4
ρ_{calc}g/cm^3	1.160
μ/mm^{-1}	0.701
F(000)	1204.0
Crystal size/mm^3	0.288 × 0.24 × 0.156
Radiation	MoKα (λ = 0.71073)
2Θ range for data collection/°	4.756 to 49.998
Index ranges	-18 ≤ h ≤ 18, -14 ≤ k ≤ 14, -19 ≤ l ≤ 19
Reflections collected	66087
Independent reflections	5658 [R_{int} = 0.0652, R_{sigma} = 0.0262]
Data/restraints/parameters	5658/0/310
Goodness-of-fit on F^2	1.048
Final R indexes [I>=2σ (I)]	R_1 = 0.0291, wR_2 = 0.0629
Final R indexes [all data]	R_1 = 0.0399, wR_2 = 0.0654
Largest diff. peak/hole / e Å^{-3}	0.31/-0.28

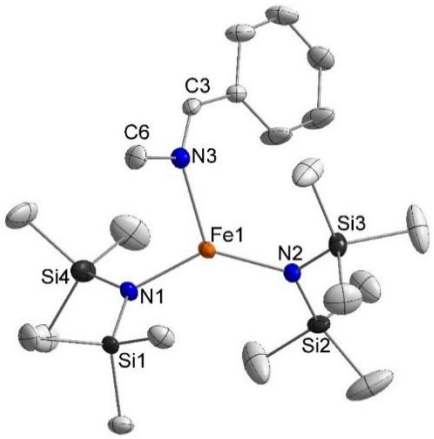

Figure S90. Molecular structure of **5** within the crystal. Hydrogen atoms are omitted for clarity, thermal ellipsoids are shown with 50% probability.

Table S28. Crystal data and structure refinement for **5**.

Identification code	5
Empirical formula	$C_{20}H_{45}FeN_3Si_4$
Formula weight	495.80
Temperature/K	100.0
Crystal system	orthorhombic
Space group	$Pna2_1$
a/Å	19.4610(8)
b/Å	16.8526(7)
c/Å	8.9032(3)
α/°	90
β/°	90
γ/°	90
Volume/Å^3	2920.0(2)
Z	4
ρ_{calc}g/cm^3	1.128
μ/mm^{-1}	0.691
F(000)	1072.0
Crystal size/mm^3	0.455 × 0.227 × 0.162
Radiation	MoKα (λ = 0.71073)
2Θ range for data collection/°	4.834 to 59.99
Index ranges	-27 ≤ h ≤ 27, -22 ≤ k ≤ 23, -12 ≤ l ≤ 12
Reflections collected	63788
Independent reflections	8514 [R_{int} = 0.0272, R_{sigma} = 0.0233]
Data/restraints/parameters	8514/13/266
Goodness-of-fit on F^2	1.059
Final R indexes [I>=2σ (I)]	R_1 = 0.0298, wR_2 = 0.0744
Final R indexes [all data]	R_1 = 0.0321, wR_2 = 0.0753
Largest diff. peak/hole / e Å^{-3}	0.75/-0.46
Flack parameter	0.010(3)

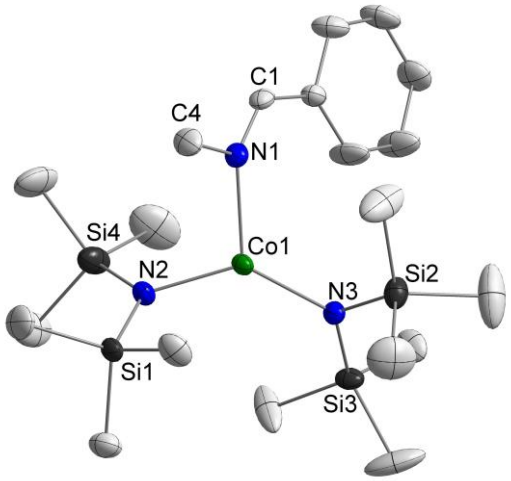

Figure S91. Molecular structure of **6** within the crystal. Hydrogen atoms are omitted for clarity, thermal ellipsoids are shown with 50% probability. Disorder of the methyl groups of Si3 (75% / 25%) are not depicted.

Table S29. Crystal data and structure refinement for **6**.

Identification code	6
Empirical formula	$C_{20}H_{45}CoN_3Si_4$
Formula weight	498.88
Temperature/K	100.0
Crystal system	monoclinic
Space group	$Pna2_1$
a/Å	19.4140(18)
b/Å	16.8685(15)
c/Å	8.9303(8)
α/°	90
β/°	90
γ/°	90
Volume/Å^3	2924.5(5)
Z	4
ρ_{calc}g/cm^3	1.133
μ/mm^{-1}	0.761
F(000)	1076.0
Crystal size/mm^3	0.293 × 0.278 × 0.264
Radiation	MoKα (λ = 0.71073)
2Θ range for data collection/°	4.83 to 60.32
Index ranges	-23 ≤ h ≤ 27, -23 ≤ k ≤ 23, -12 ≤ l ≤ 12
Reflections collected	40296
Independent reflections	8606 [R_{int} = 0.0430, R_{sigma} = 0.0466]
Data/restraints/parameters	8606/10/296
Goodness-of-fit on F^2	1.038
Final R indexes [I>=2σ (I)]	R_1 = 0.0363, wR_2 = 0.0724
Final R indexes [all data]	R_1 = 0.0509, wR_2 = 0.0772
Largest diff. peak/hole / e Å^{-3}	0.52/-0.39
Flack parameter	0.009(5)

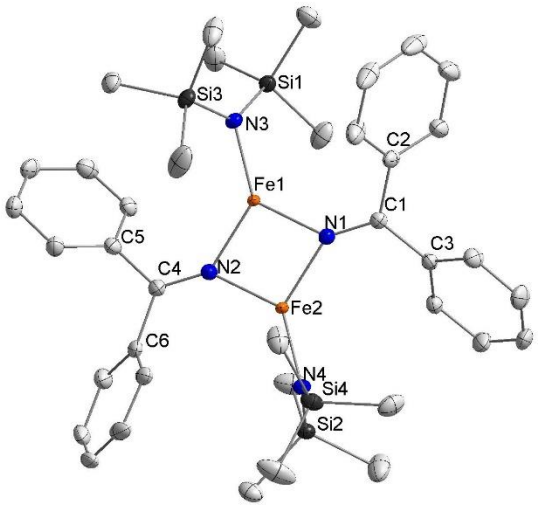

Figure S92. Molecular structure of **7** within the crystal. Hydrogen atoms are omitted for clarity, thermal ellipsoids are shown with 50% probability.

Table S30. Crystal data and structure refinement for **7**.

Identification code	7
Empirical formula	$C_{38}H_{56}Fe_2N_4Si_4$
Formula weight	792.92
Temperature/K	100.01
Crystal system	monoclinic
Space group	$P2_1/c$
a/Å	14.0711(7)
b/Å	12.2861(6)
c/Å	25.1541(13)
α/°	90
β/°	96.632(2)
γ/°	90
Volume/Å^3	4319.5(4)
Z	4
ρ_{calc}g/cm^3	1.219
μ/mm^{-1}	0.812
F(000)	1680.0
Crystal size/mm^3	0.318 × 0.196 × 0.168
Radiation	MoKα (λ = 0.71073)
2Θ range for data collection/°	4.414 to 51.996
Index ranges	-17 ≤ h ≤ 17, -15 ≤ k ≤ 15, -31 ≤ l ≤ 31
Reflections collected	94739
Independent reflections	8477 [R_{int} = 0.0703, R_{sigma} = 0.0306]
Data/restraints/parameters	8477/0/445
Goodness-of-fit on F^2	1.042
Final R indexes [I>=2σ (I)]	R_1 = 0.0317, wR_2 = 0.0648
Final R indexes [all data]	R_1 = 0.0457, wR_2 = 0.0680
Largest diff. peak/hole / e Å^{-3}	0.24/-0.36

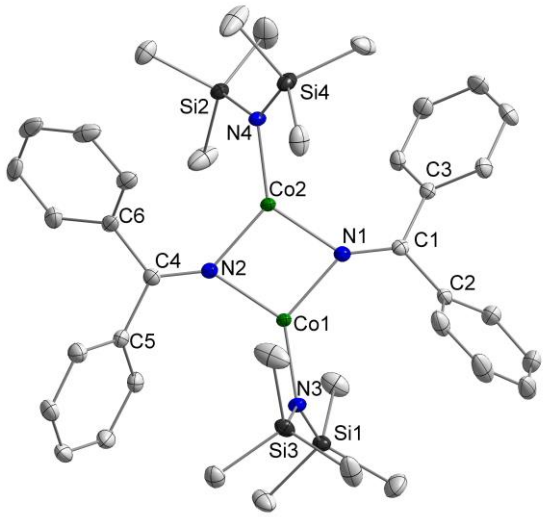

Figure S93. Molecular structure of **8** within the crystal. Hydrogen atoms are omitted for clarity, thermal ellipsoids are shown with 50% probability.

Table S31. Crystal data and structure refinement for **8**.

Identification code	8
Empirical formula	$C_{38}H_{56}Co_2N_4Si_4$
Formula weight	799.08
Temperature/K	99.99
Crystal system	monoclinic
Space group	$P2_1/c$
a/Å	14.0892(6)
b/Å	12.2772(6)
c/Å	25.1152(12)
α/°	90
β/°	96.631(2)
γ/°	90
Volume/Å^3	4315.3(3)
Z	4
ρ_{calc}g/cm^3	1.230
μ/mm^{-1}	0.909
F(000)	1688.0
Crystal size/mm^3	0.358 × 0.231 × 0.181
Radiation	MoKα (λ = 0.71073)
2Θ range for data collection/°	4.414 to 49.998
Index ranges	-16 ≤ h ≤ 16, -14 ≤ k ≤ 14, -29 ≤ l ≤ 29
Reflections collected	160538
Independent reflections	7613 [R_{int} = 0.0579, R_{sigma} = 0.0170]
Data/restraints/parameters	7613/0/445
Goodness-of-fit on F^2	1.051
Final R indexes [I>=2σ (I)]	R_1 = 0.0249, wR_2 = 0.0579
Final R indexes [all data]	R_1 = 0.0313, wR_2 = 0.0597
Largest diff. peak/hole / e Å^{-3}	0.27/-0.27

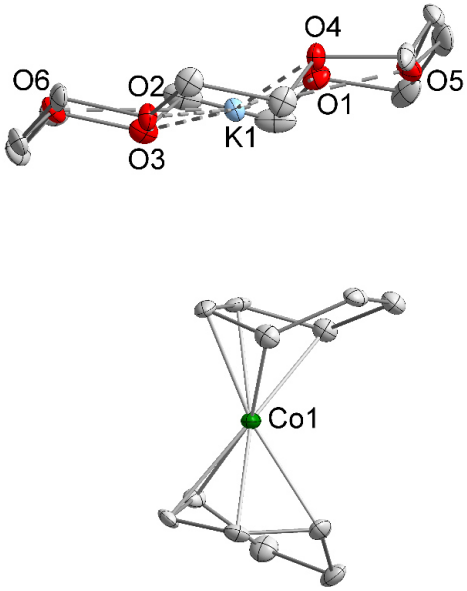

Figure S94. Molecular structure of K(18c6)[**9**] within the crystal. Hydrogen atoms are omitted for clarity, thermal ellipsoids are shown with 50% probability.

Table S32. Crystal data and structure refinement for K(18c6)[**9**].

Identification code	K_18c6_9
Empirical formula	$C_{24}H_{40}CoKO_6$
Formula weight	522.59
Temperature/K	100.0
Crystal system	monoclinic
Space group	$P2_1/n$
a/Å	9.154(12)
b/Å	18.66(2)
c/Å	14.720(15)
α/°	90
β/°	97.68(3)
γ/°	90
Volume/Å^3	2492(5)
Z	4
ρ_{calc}g/cm^3	1.393
μ/mm^{-1}	0.892
F(000)	1112.0
Crystal size/mm^3	0.166 × 0.143 × 0.091
Radiation	MoKα (λ = 0.71073)
2Θ range for data collection/°	4.364 to 52.216
Index ranges	-11 ≤ h ≤ 11, -23 ≤ k ≤ 23, -18 ≤ l ≤ 18
Reflections collected	30368
Independent reflections	4932 [R_{int} = 0.0785, R_{sigma} = 0.0496]
Data/restraints/parameters	4932/0/309
Goodness-of-fit on F^2	1.019
Final R indexes [I>=2σ (I)]	R_1 = 0.0441, wR_2 = 0.0885
Final R indexes [all data]	R_1 = 0.0674, wR_2 = 0.0943
Largest diff. peak/hole / e Å^{-3}	1.77/-0.60

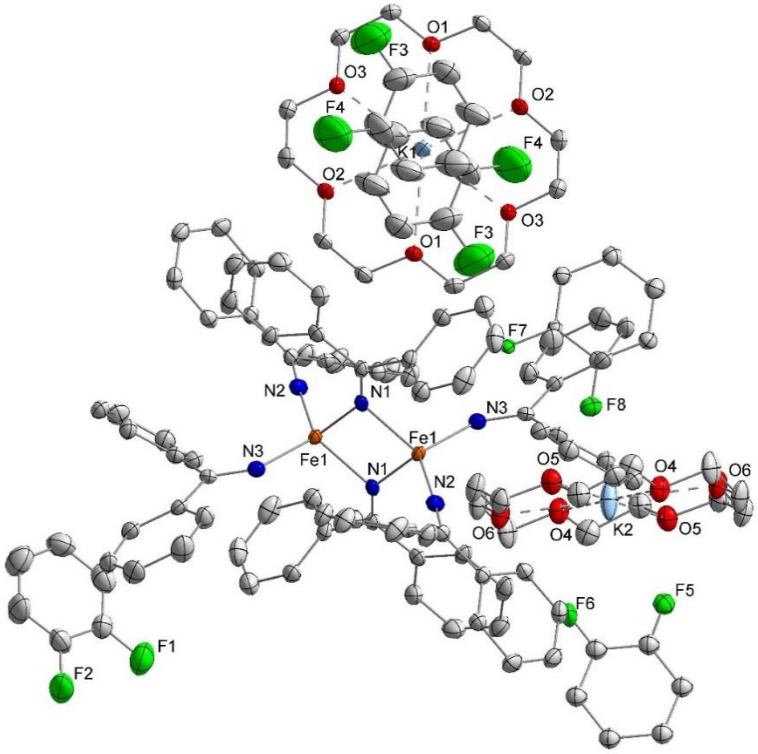

Figure S95. Molecular structure of [K{18c6}]$_2$[**10**]•4.4(1,2-difluorobenzene) within the crystal. Hydrogen atoms are omitted for clarity, thermal ellipsoids are shown with 50% probability. One molecule of 1,2-difluorobenzene (F5, F6) is disordered and only partially occupied (both 10%).

Table S33. Crystal data and structure refinement for [K{18c6}]$_2$[**10**]•4.4(1,2-difluorobenzene).

Identification code	K_18c6_2_10
Empirical formula	$C_{128.4}H_{122.6}F_{8.8}Fe_2K_2N_6O_{12}$
Formula weight	2298.82
Temperature/K	100.0
Crystal system	triclinic
Space group	P-1
a/Å	14.7202(9)
b/Å	15.4279(9)
c/Å	15.7275(9)
α/°	84.050(2)
β/°	76.272(2)
γ/°	77.910(2)
Volume/Å^3	3387.3(3)
Z	1
ρ_{calc}g/cm^3	1.127
μ/mm^{-1}	0.342
F(000)	1200.0
Crystal size/mm^3	0.267 × 0.252 × 0.13
Radiation	MoKα (λ = 0.71073)
2Θ range for data collection/°	3.906 to 50
Index ranges	-17 ≤ h ≤ 17, -18 ≤ k ≤ 18, -18 ≤ l ≤ 18
Reflections collected	86321
Independent reflections	11924 [R_{int} = 0.1345, R_{sigma} = 0.0673]
Data/restraints/parameters	11924/360/826
Goodness-of-fit on F^2	1.093
Final R indexes [I>=2σ (I)]	R_1 = 0.0712, wR_2 = 0.2330
Final R indexes [all data]	R_1 = 0.0967, wR_2 = 0.2442
Largest diff. peak/hole / e Å^{-3}	1.48/-0.48

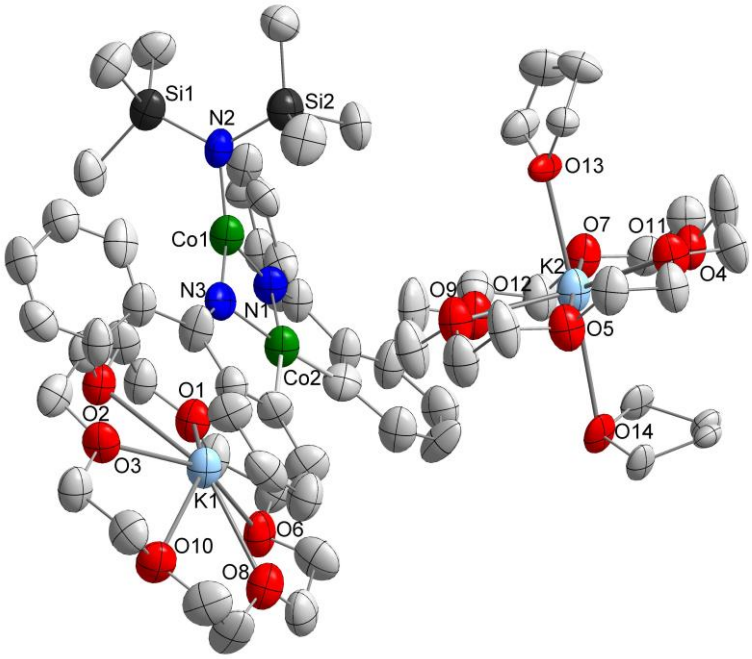

Figure S96. Molecular structure of [K{18c6}]$_2$[**11**]•2thf within the crystal. Hydrogen atoms are omitted for clarity, thermal ellipsoids are shown with 30% probability. Hydrogen atoms are omitted for clarity, thermal ellipsoids are shown with 30% probability. Dataset is of poor quality due to weak scattering of the crystal. Various attempts of recrystallizing and measurements on different diffractometers did not result in better data quality. Both THF molecules are only partially occupied (50%, top; 33%, bottom). Two molecules of *n*-pentane are heavily disordered and were thus squeezed.

Table S34. Crystal data and structure refinement for [K{18c6}]$_2$[**11**]•2thf.

Identification code	K_18c6_2_10
Empirical formula	$C_{59.33}H_{90.67}Co_2K_2N_3O_{12.84}Si_2$
Formula weight	1303.63
Temperature/K	293(2)
Crystal system	triclinic
Space group	P-1
a/Å	14.516(6)
b/Å	14.719(6)
c/Å	20.997(7)
α/°	88.32(3)
β/°	82.00(3)
γ/°	66.64(3)
Volume/Å^3	4077(3)
Z	2
ρ_{calc}g/cm^3	1.062
μ/mm^{-1}	4.776
F(000)	1381.0
Crystal size/mm^3	0.3 × 0.2 × 0.1
Radiation	CuKα (λ = 1.54186)
2Θ range for data collection/°	6.698 to 87.116
Index ranges	-10 ≤ h ≤ 12, -13 ≤ k ≤ 13, -18 ≤ l ≤ 18
Reflections collected	23055
Independent reflections	5904 [R_{int} = 0.1447, R_{sigma} = 0.1202]
Data/restraints/parameters	5904/144/781
Goodness-of-fit on F^2	0.942
Final R indexes [I>=2σ (I)]	R_1 = 0.1052, wR_2 = 0.2672
Final R indexes [all data]	R_1 = 0.1656, wR_2 = 0.2960
Largest diff. peak/hole / e Å^{-3}	0.71/-0.42

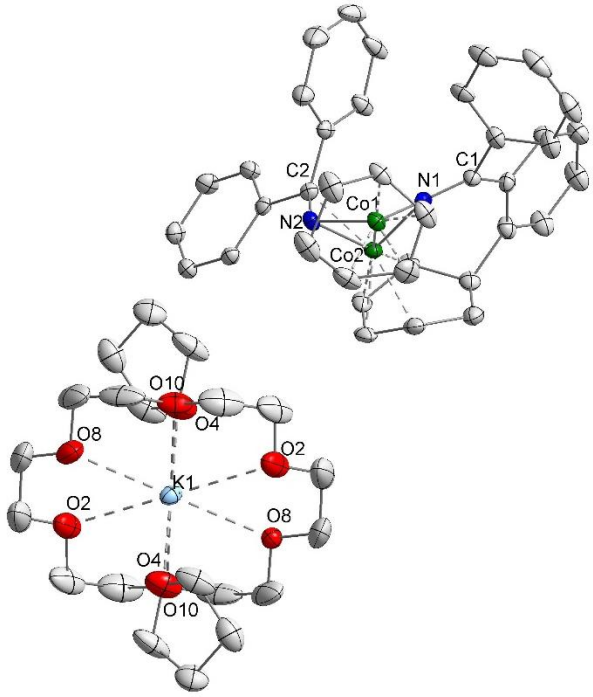

Figure S97. Molecular structure of K{18c6}[**12**]•2thf within the crystal. Hydrogen atoms are omitted for clarity, thermal ellipsoids are shown with 50% probability. Only half of the here shown [K{18c6}(thf)$_2$] unit is present in the asymmetric unit but doubled by symmetry generation for better visibility. Another half fragment is not depicted here and contains disorder of the coordination THF molecule over three positions (50% / 25% / 25%).

Table S35. Crystal data and structure refinement for K{18c6}[**12**]•2thf.

Identification code	K_18c6_12
Empirical formula	$C_{62}H_{77}Co_2KN_2O_9$
Formula weight	1151.21
Temperature/K	100.0
Crystal system	triclinic
Space group	P-1
a/Å	10.1732(17)
b/Å	12.823(3)
c/Å	23.017(3)
α/°	93.148(7)
β/°	96.286(5)
γ/°	102.551(7)
Volume/Å^3	2903.6(9)
Z	2
ρ_{calc}g/cm^3	1.317
μ/mm^{-1}	0.700
F(000)	1216.0
Crystal size/mm^3	0.463 × 0.158 × 0.149
Radiation	MoKα (λ = 0.71073)
2Θ range for data collection/°	4.294 to 51.998
Index ranges	-12 ≤ h ≤ 12, -15 ≤ k ≤ 15, -28 ≤ l ≤ 28
Reflections collected	54461
Independent reflections	11424 [R_{int} = 0.0387, R_{sigma} = 0.0356]
Data/restraints/parameters	11424/340/782
Goodness-of-fit on F^2	1.034
Final R indexes [I>=2σ (I)]	R_1 = 0.0605, wR_2 = 0.1491
Final R indexes [all data]	R_1 = 0.0768, wR_2 = 0.1561
Largest diff. peak/hole / e Å^{-3}	1.21/-0.92

References

[1] D. F. Evans, *J. Chem. Soc.* **1959**, 2003.
[2] S. K. Sur, *J. Magn. Reson.* **1989**, *82*, 169–173.
[3] H. Bürger, U. Wannagat, *Monatshefte für Chemie* **1963**, *94*, 1007–1012.
[4] C. G. Werncke, P. C. Bunting, C. Duhayon, J. R. Long, S. Bontemps, S. Sabo-Etienne, *Angew. Chem. Int. Ed.* **2015**, *54*, 245–248.
[5] C. G. Werncke, E. Suturina, P. C. Bunting, L. Vendier, J. R. Long, M. Atanasov, F. Neese, S. Sabo-Etienne, S. Bontemps, *Chem. Eur. J.* **2016**, *22*, 1668–1674.
[6] F. Neese, *WIREs Computational Molecular Science* **2012**, *2*, 73–78.
[7] F. Neese, F. Wennmohs, U. Becker, C. Riplinger, *J. Chem. Phys.* **2020**, *152*, 224108.
[8] J. P. Perdew, K. Burke, M. Ernzerhof, *Phys. Rev. Lett.* **1996**, *77*, 3865–3868.
[9] A. D. Becke, *Phys. Rev. A* **1988**, *38*, 3098–3100.
[10] J. Tao, J. P. Perdew, V. N. Staroverov, G. E. Scuseria, *Phys. Rev. Lett.* **2003**, *91*, 146401.
[11] C. Adamo, V. Barone, *J. Chem. Phys.* **1999**, *110*, 6158–6170.
[12] A. D. Becke, *The Journal of Chemical Physics* **1993**, *98*, 5648–5652.
[13] C. Lee, W. Yang, R. G. Parr, *Phys. Rev. B* **1988**, *37*, 785–789.
[14] S. H. Vosko, L. Wilk, M. Nusair, *Canadian Journal of Physics* **2011**, DOI 10.1139/p80-159.
[15] P. J. Stephens, F. J. Devlin, C. F. Chabalowski, M. J. Frisch, *J. Phys. Chem.* **1994**, *98*, 11623–11627.
[16] J. P. Perdew, S. Kurth, A. Zupan, P. Blaha, *Phys. Rev. Lett.* **1999**, *82*, 2544–2547.
[17] J. P. Perdew, J. Tao, V. N. Staroverov, G. E. Scuseria, *J Chem Phys* **2004**, *120*, 6898–6911.
[18] Y. Zhao, D. G. Truhlar, *Theor Chem Account* **2008**, *120*, 215–241.
[19] F. Weigend, R. Ahlrichs, *Phys. Chem. Chem. Phys.* **2005**, *7*, 3297–3305.
[20] D. A. Pantazis, X.-Y. Chen, C. R. Landis, F. Neese, *J. Chem. Theory Comput.* **2008**, *4*, 908–919.
[21] E. van Lenthe, A. Ehlers, E.-J. Baerends, *J. Chem. Phys.* **1999**, *110*, 8943–8953.
[22] E. van Lenthe, E. J. Baerends, J. G. Snijders, *J. Chem. Phys.* **1994**, *101*, 9783–9792.
[23] C. van Wüllen, *J. Chem. Phys.* **1998**, *109*, 392–399.
[24] S. Grimme, S. Ehrlich, L. Goerigk, *Journal of Computational Chemistry* **2011**, *32*, 1456–1465.
[25] S. Grimme, J. Antony, S. Ehrlich, H. Krieg, *J. Chem. Phys.* **2010**, *132*, 154104.
[26] F. Neese, *Journal of Computational Chemistry* **2003**, *24*, 1740–1747.
[27] J. D. Rolfes, F. Neese, D. A. Pantazis, *Journal of Computational Chemistry* **2020**, *41*, 1842–1849.
[28] R. Izsák, F. Neese, *J. Chem. Phys.* **2011**, *135*, 144105.
[29] F. Neese, F. Wennmohs, A. Hansen, U. Becker, *Chemical Physics* **2009**, *356*, 98–109.
[30] C. J. Cramer, D. G. Truhlar, *Acc. Chem. Res.* **2008**, *41*, 760–768.
[31] S. Hirata, M. Head-Gordon, *Chemical Physics Letters* **1999**, *314*, 291–299.
[32] T. Soda, Y. Kitagawa, T. Onishi, Y. Takano, Y. Shigeta, H. Nagao, Y. Yoshioka, K. Yamaguchi, *Chemical Physics Letters* **2000**, *319*, 223–230.
[33] B. O. Roos, P. R. Taylor, P. E. M. Sigbahn, *Chemical Physics* **1980**, *48*, 157–173.
[34] C. Angeli, R. Cimiraglia, S. Evangelisti, T. Leininger, J.-P. Malrieu, *J. Chem. Phys.* **2001**, *114*, 10252–10264.
[35] F. Neese, *J. Am. Chem. Soc.* **2006**, *128*, 10213–10222.
[36] G. Knizia, *J. Chem. Theory Comput.* **2013**, *9*, 4834–4843.
[37] "Chemcraft - Citation," can be found under https://www.chemcraftprog.com/citation.html, **n.d.**
[38] G. Knizia, J. E. M. N. Klein, *Angewandte Chemie International Edition* **2015**, *54*, 5518–5522.
[39] J. P. Perdew, M. Ernzerhof, K. Burke, *J. Chem. Phys.* **1996**, *105*, 9982–9985.
[40] S. Grimme, J. G. Brandenburg, C. Bannwarth, A. Hansen, *J. Chem. Phys.* **2015**, *143*, 054107.
[41] J. G. Brandenburg, C. Bannwarth, A. Hansen, S. Grimme, *J. Chem. Phys.* **2018**, *148*, 064104.
[42] G. M. Sheldrick, *Acta Cryst.* **2015**, *71*, 3.
[43] L. Farrugia, *J. Appl. Crystallogr.* **1999**, *32*, 837.
[44] P. W. Betteridge, J. R. Carruthers, R. I. Cooper, K. Prout, D. J. Watkin, *J. Appl. Crystallogr.* **2003**, *36*, 1487.
[45] *International Tables for X-Ray Crystallography*, Kynoch Press, Birmingham, England, **1974**.
[46] *SADABS-2016/2*, Bruker, **2016**.
[47] *X-Area, X-Red 1.63.1.0*, STOE, **2016**.

3.2 A Diarsene Radical Anion

G. Sieg, M. Fischer, F. Dankert, J.-E. Siewert, C. Hering-Junghans, C. G. Werncke, *Chem. Commun.* **2022**, DOI: 10.1039/D2CC03237F.

Abstract

The isolation of the first diarsene radical anion by reduction of a neutral diarsene is presented. Comprehensive characterization in conjunction with DFT calculations reveal unpaired spin density residing in the antibonding π*-orbital with involvement of the terphenyl ligands. First reactivity studies reveal no pronounced radical but rather reducing properties.

Zusammenfassung

Im Zuge dieser Publikation wurde zunächst das bekannte Diarsen (^{Mes}TerAs)$_2$[138] elektrochemisch untersucht, wobei ein reversibles Redoxpotential bei –2.24 V bestimmt werden konnte. Die chemische Reduktion gelang durch die Zugabe von Kalium zu (^{Mes}TerAs)$_2$ in Gegenwart von 18c6 oder alternativ durch Reaktion mit [K{18c6}][Fe(N(SiMe$_3$)$_2$)$_2$]. Hierdurch konnte das tiefblaue Diarsenradikalanion [K{18c6}][(^{Mes}TerAs)$_2$] (**1**) erhalten werden (Schema 50). Im Gegensatz zu verschiedenen Radikalanionen mit formalen E=E-Doppelbindungen der Gruppe 15 für Stickstoff, Phosphor, Antimon und Bismut ist bisher kein Radikalanion mit einem ungepaarten Elektron an einer Arsen-Arsen-Bindung bekannt.

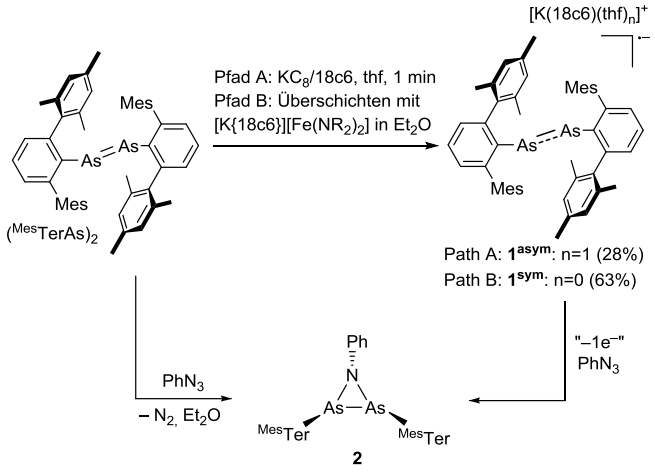

Schema 50. Reduktion von (^{Mes}TerAs)$_2$ zu **1^{sym}** und **1^{asym}** mit zusätzlicher Darstellung von **2** durch Umsetzung von (^{Mes}TerAs)$_2$ oder **1** mit Phenylazid.

Je nach Reaktionspfad und verwendetem Lösungsmittel koordiniert kein oder ein Molekül THF an das Kaliumion, wodurch zwei leicht verschiedene Molekülstrukturen kristallographisch ermittelt werden konnten: Die asymmetrische Verbindung **1^{asym}** mit einem koordinierten Molekül THF und die symmetrische Verbindung **1^{sym}** ohne koordinierendes THF Molekül. Während die As-C und As-As

Bindungen für beide Verbindungen vergleichbar lang ist, zeigt sich der Unterschied vor allem in den As-As-C Bindungswinkeln (**1**^{sym}: 94.57(4)°, **1**^{asym}: 90.7(1)°/106.2(1)°).

Der radikalische Charakter für **1** wurde neben der, im Gegensatz zu (^{Mes}TerAs)$_2$ deutlich längeren As-As Bindung ((^{Mes}TerAs$_2$): 2.276(3) Å, **1**^{sym}: 2.350(4) Å, **1**^{asym}: 2.328(4) Å) vor allem mittels EPR-Spektroskopie nachgewiesen. Hier wurde ein rhombisches Signal mit einem g_{iso}-Wert von 2.04 und einer ^{75}As-^{75}As-Kopplung detektiert werden, was üblich für Radikale mit Element-15-Doppelbindungen ist.[57,58] Zusätzlich konnte durch UV-Vis-Spektroskopie ein Absorptionsmaximum von 610 nm ermittelt werden, was zwischen den Werten für vergleichbare, bekannte Radikalanionen mit Phosphor (λ_{max} = 539 nm) und Antimon (λ_{max} = 812 nm) liegt.[57] Anhand von DFT Rechnungen konnte ermittelt werden, dass **1**^{asym} etwa 10 kcal/mol ärmer ist als **1**^{sym}. In beiden Fällen lässt sich die As-As Bindung als σ-artig (HOMO-1) und π-artig (HOMO) beschreiben, mit dem SOMO als π*-Orbital. In **1**^{sym} beträgt die Mulliken-Spindichte am Arsen 0.468, in **1**^{asym} verteilt sich die ungepaarte Spindichte asymmetrisch auf die Arsenatome (0.477 und 0.279), sowie auf das Aromatengerüst eines der Substituenten. Zusätzlich konnte das experimentell bestimmte Photoabsorptionsmaximum bei λ_{max} = 612 nm mit λ_{max} = 610 nm sehr gut theoretisch bestätigt werden.

Reaktivitätsstudien zeigen, dass **1** ausschließlich als 1e$^-$-Donor fungiert und eine für Radikale typische Reaktivität ausbleibt. So wird keine Umsetzung mit TEMPO-H oder 1,4-Cyclohexadien beobachtet, während die Reaktion von **1** mit [Co^{II}(N(SiMe$_3$)$_2$)$_2$] zum Reduktionsprodukt [Co^{I}(N(SiMe$_3$)$_2$)$_2$]$^-$ und dem neutralen (^{Mes}TerAs)$_2$ führt. Eine unerwartete Reaktivität wurde bei der Zugabe von Phenylazid zu **1** ersichtlich: Hier wurde das Azadiarsacyclopropan cyclo-[(^{Mes}TerAs)$_2$NPh] **2** erhalten, welches vermutlich zunächst durch Abgabe eines Elektrons von **1** und anschließender Reaktion mit (^{Mes}TerAs)$_2$ unter Abspaltung von N_2 zustande kommt. Diese Vermutung konnte durch die direkte Reaktion von (^{Mes}TerAs)$_2$ mit Phenylazid verifiziert werden, bei der **2** in besseren Ausbeuten erhalten wurde.

Eigener Anteil

1^{sym}, **1**^{asym} und **2** wurden von mir dargestellt und durch Röntgenbeugung, UV-Vis-, IR- und NMR-Spektroskopie charakterisiert. Die Röntgenbeugungsexperiemente wurden durch *Dr. Gunnar Werncke* oder durch die Serviceabteilung für Kristallographie der Philipps-Universität-Marburg durchgeführt, die Sturkturlösung und -verfeinerung wurde von mir durchgeführt. Die Elementaranalyse wurde durch die Serviceabteilung Massenspektrometrie und Elementaranalytik der Philipps-Universität-Marburg durchgeführt und von mir ausgewertet. Die EPR-Messungen wurden von *Dr. Andreas Stoy* aus der Arbeitsgruppe von *Prof. Dr. Crispin Lichtenberg* (PUM) durchgeführt und von mir mit der entsprechenden Simulation ausgewertet. Die quantenchemischen Berechnungen wurden von *Dr.*

Christian Hering-Junghans durchgeführt. Die cyclovoltammetrischen Messungen wurden von *Jan-Erik Siewert* durchgeführt und ausgewertet. Das Manuskript wurde in Zusammenarbeit mit *Dr. Gunnar Werncke* von mir verfasst und von den übrigen Autoren überarbeitet.

Please do not adjust margins

View Article Online
DOI: 10.1039/D2CC03237F

COMMUNICATION

A Diarsene Radical Anion

Grégoire Sieg,[1] Malte Fischer,[2,3] Fabian Dankert,[2,4] Jan-Erik Siewert,[2] Christian Hering-Junghans,[2,*] C. Gunnar Werncke[1,*]

Received 00th January 20xx,
Accepted 00th January 20xx

DOI: 10.1039/x0xx00000x

Published on 01 August 2022. Downloaded by University of Marburg on 8/1/2022 9:18:50 AM.

The isolation of the first diarsene radical anion by reduction of a neutral diarsene is presented. Comprehensive characterisation in conjunction with DFT calculations reveal unpaired spin density residing in the antibonding π*-orbital with involvement of the terphenyl ligands. First reactivity studies reveal no pronounced radical but rather reducing properties.

The chemistry of the heavier analogues of diazenes (RE=ER, E = P – Bi) has attracted continuous interest[1] and first attempts to obtain phosphobenzene, PhP=PPh, were reported by Michaelis and Köhler in the 19th century,[2] however only produced the pentaphosphane $(PhP)_5$.[3] The first diphosphene, $(Mes^*P)_2$ (Mes^* = 2,4,6-^{t}Bu$_3$-C$_6$H$_2$) was introduced by Yoshifuji.[4]

Figure 1. Known arsenic containing dipnictene radical cations (top) and heavier dipnictene radical anions $[RE=ER]^{\bullet-}$ (E = P, Sb, Bi) (bottom). (Dipp = 2,6-^{i}Pr$_2$-C$_6$H$_3$, Mes = 2,4,6-Me$_3$-C$_6$H$_2$)

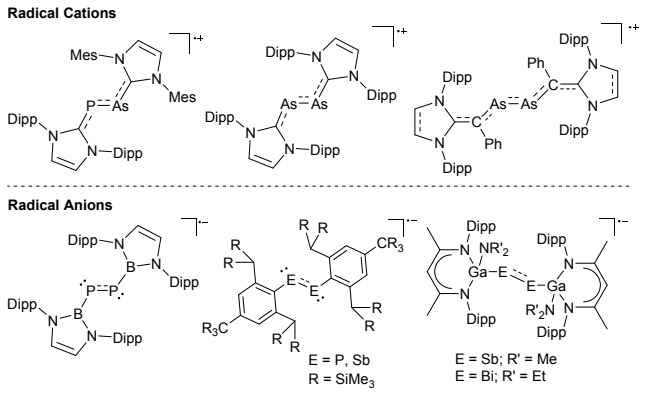

Subsequently this could be extended to diarsenes,[5,6] distibenes[5,7–10,11,12] and dibismuthenes[5,7–10,12,13] using different bulky substituents for their kinetic stabilization. A common feature of these dipnictenes is the presence of an energetically low-lying π*-orbital, which allows in principal for the reduction to a dipnictene radical anion $[RE=ER]^{\bullet-}$ (E = P – Bi). This has been mainly shown for a number of diphosphenes,[14,15,16] but also rare examples of distibenes,[14,15] and a dibismuthene were recently reported (**Figure 1**, bottom).[14] Due to the scarcity of dipnictene radical anions $[RE=ER]^{\bullet-}$, their reactivity is virtually unexplored.[16] Remarkably, isolable diarsene radical anions have not been reported to date, with a related singular phosphaarsene radical anion only being characterized by EPR spectroscopy.[17] This contrasts the few examples of cationic (**Figure 1**, top) and neutral diarsenic[6,18,19] and arsaphosphene[19,20] radicals. Here, we present the first structurally characterized diarsene radical anion and insights into its reactivity. To address the open question of an isolable diarsene radical anion we chose (^{Mes}TerAs)$_2$ (^{Mes}Ter = 2,6-Mes$_2$-C$_6$H$_3$) as a suitable candidate,[5] which was synthesized in here by reducing ^{Mes}TerAsCl$_2$ with Zn and PMe$_3$.[21]

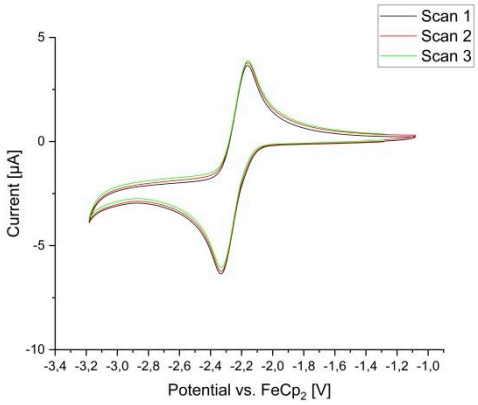

Figure 2. Cyclic voltammogram of (^{Mes}TerAs)$_2$ in THF, 0.1 M $[N^nBu_4][PF_6]$ (3 successive scans at 23 °C, scan rate 100 mV s^{-1}, between −3.2 and −1.0 V vs. $FeCp_2/[FeCp_2]^+$). $E_{1/2red}$ = −2.24 V, E_{ox} = 0.90 V (not shown, see ESI).

[a] *Chemistry Department, Philipps-University, Hans-Meerwein-Str. 4, 35043 Marburg, Germany. E-mail: gunnar.wernecke@chemie.uni-marburg.de*
[b] *Leibniz Institute for Catalysis, Albert-Einstein-Straße 29a, 18059 Rostock, Germany; Email: christian.hering-junghans@catalysis.de*
[c] Chemistry Research Laboratory, Mansfield Road, Oxford OX1 3TA, UK
[d] *Inorganic Chemistry: Coordination Chemistry, Campus C4.1, Saarland University, D-66123 Saarbrücken, Germany*
Electronic Supplementary Information (ESI) available: Experimental and crystallographic details, Cyclovoltametric, IR, EPR-, UV/Vis, NMR-spectroscopic, data. See DOI: 10.1039/x0xx00000x

ChemComm Accepted Manuscript

View Article Online
DOI: 10.1039/D2CC03237F

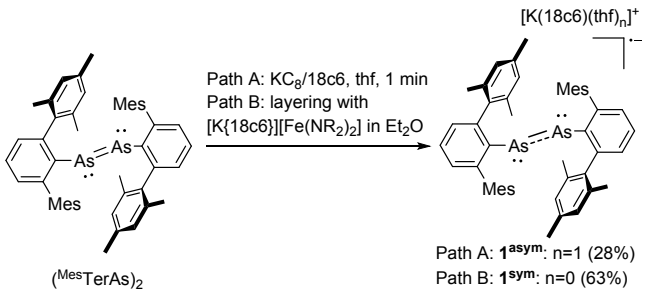

Scheme 1. Synthesis of diarsene radical anion **1**.

CV experiments on (^{Mes}TerAs)$_2$ showed a stable, reversible reduction event at –2.24 V vs Fc/Fc$^+$ (**Figure 2**). Accordingly, (^{Mes}TerAs)$_2$ was treated with KC_8 in THF with added 18-crown-6 (= 18c6 = 1,4,7,10,13,16-hexaoxacyclo-octadecan) to mitigate detrimental cation/anion interactions (**Scheme 1**). This yielded a dark blue solution similar to that of diphosphene radical anions.[15] Upon filtration and layering of the reaction solution with pentane at –40°C, blue crystals of [K(18c6)(thf)][(^{Mes}TerAs)$_2$] (**1^{asym}**, 28% yield) containing a diarsene radical anion were obtained. This salt is highly sensitive and quickly decolorizes (several minutes to hours) under inert conditions in the solid state as well as in THF solution giving (^{Mes}TerAs)$_2$. We suspected the concomitant formation of the corresponding diarsene dianion upon formal disproportionation of the radical anion. However, no evidence for the dianion is found when adding extra equivalents of KC_8 to **1**. This contrasts the observations for the diazene radical anion [ArNNAr]$^{\bullet-}$ (Ar = 4-CN-2,6-iPr$_2$-C$_6$H$_2$), which could be further reduced to give [ArNNAr]$^{2-}$.[22] **1^{asym}** is hardly soluble in Et$_2$O. We therefore used the salt [K(18c6)][Fe^{I}(NR$_2$)$_2$] (R = SiMe$_3$) as an alternative, Et$_2$O-soluble reductant (E_{pc} ≈ –2 V vs. Fc/Fc$^+$)[23] in order to precipitate **1** directly from the reaction mixture. Layering a solution of (^{Mes}TerAs)$_2$ in Et$_2$O with an Et$_2$O solution of the Fe^{I} complex indeed led to the reproducible direct crystallization of pure [K(18c6)][(^{Mes}TerAs)$_2$] (**1^{sym}**) at –35 °C and allowed its isolation in pure form and in an improved yield of 63%.

X-Ray diffraction analysis of **1^{sym}** and **1^{asym}** revealed two slightly different radical anion structures, most likely due to different packing induced by the additional THF coordination towards [K(18c6)]$^+$ in the case of **1^{asym}**. The radical anion in **1^{sym}** (**Figure 3**) is inversion symmetric with an As–As bond length of 2.350(4) Å, an As–C atom distance of 1.976(2) Å and an As–As–C$_{Aryl}$ bond angle of 94.6(0)°. Comparison of the structural parameters with those of (^{Mes}TerAs)$_2$ (As–As 2.276(3) Å; As–C$_{Aryl}$ 1.964(13) Å); As–As–C$_{aryl}$ 98.5(4)°)[5] reveal most notably an elongation of the As–As bond upon reduction. This is ascribed to occupation of the anti-bonding π*-orbital that results in a less pronounced double bond character. In **1^{asym}** the anion exhibits an As–As bond length of 2.328(4) Å with inequivalent As–C$_{aryl}$ bonds (1.991(2), 1.955(2) Å) and As–As–C$_{aryl}$ angles (90.7(1), 106.2(1)°). Thereby, their median values are similar to those of the symmetric anion in **1^{sym}**. In the course of our study we were also able to crystallize a toluene solvate of (^{Mes}TerAs)$_2$, with a non-centrosymmetric structure (see ESI). Here, inequivalent As–C$_{aryl}$ bonds and As– As–C$_{aryl}$ angles comparable to the situ-

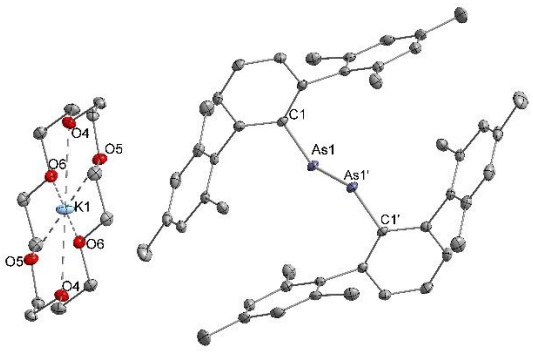

Figure 3. Molecular structure of **1^{sym}**. H atoms are omitted for clarity, thermal ellipsoids are shown with 50% probability. Selected bond lengths (Å) and angles (°) of **1^{sym}** and **1^{asym}** (not depicted, see ESI): **1^{sym}**: As1–As1' 2.350(4), As1–C1 1.976(2); C1–As1–As1' 94.57(4). **1^{asym}**: As1–As2 2.328(4), As1–C1 1.991(2), As2–C2 1.955(2); C1–As1–As2 90.7(1), C2–As2–As2 106.2(1).

ation in **1^{asym}** are observed and the As–As atomic distance is 2.257(2) Å. In any case, side-on coordination of the diarsene to the iron(I) centre is not observed, such as in related alkyne or alkene adducts of the employed iron(I) complex[24] or as in rare examples of iron(0) carbonyls bound to a (RAs)$_2$ unit (R = Ph, IDipCPh, H).[25] In the present case it is thus attributed to steric reasons that no side-on coordination is observed. As expected from its paramagnetic character, the proton NMR spectrum of **1** in THF-d$_8$ was rather uninformative with only two broad and unresolved signals attributable to the [K(18c6)]$^+$ counter-cation at 5.83 and 6.69 ppm. X-Band EPR spectroscopic examination of a solution of **1** in Me-THF at 100 K (**Figure 4** left) gave a signal centred at $g_{1,iso}$ = 2.04, corroborating its radical character, with well resolved hyperfine coupling to ^{57}As (I = 3/2). The observed g-anisotropy (g_{11} = 2.17, g_{12} = 2.01, g_{13} = 1.85) is due to increased spin-orbit contributions that further supports an As-centred radical.[26] The signal could be satisfactorily modelled by coupling of the electron spin to two, yet slightly inequivalent ^{75}As nuclei (A_{11} = 136.31 MHz, A_{12} = 126.34 MHz, A_{13} = 272.73, A_{21} = 86.13 MHz, A_{22} = 130.95 MHz, A_{23} = 105.17 MHz). This reflects an asymmetry of the diarsene radical anion, as indeed observed in **1^{asym}**, and is attributed to partial delocalisation of radical density over the central aromatic ring of the terphenyl substituent (vide infra).

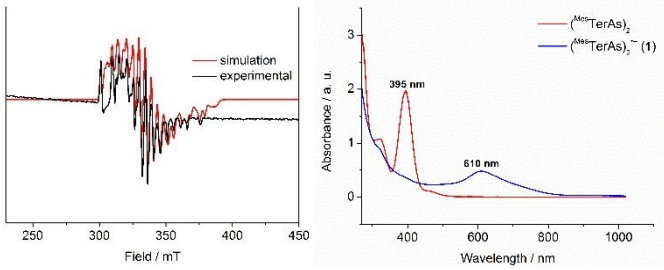

Figure 4. Left: X-band EPR measurement of **1** in frozen ^{Me}THF solution (9.460808 GHz) collected at 100 K (black) and the simulated spectrum (red). The simulation is done for S = ½ with two inequivalent ^{75}As nuclei: g_{iso} = 2.04, g_1 = 2.17, g_2 = 2.01, g_3 = 1.85, A_{11} = 136.31 MHz, A_{12} = 126.34 MHz, A_{13} = 272.73, A_{21} = 86.13 MHz, A_{22} = 130.95 MHz, A_{23} = 105.17 MHz; Right: UV-Vis spectrum of **1** (blue) and ^{Mes}Ter$_2$As$_2$ (red) in THF at 300 K.

Published on 01 August 2022. Downloaded by University of Marburg on 8/1/2022 9:18:50 AM.

ChemComm Accepted Manuscript

This journal is © The Royal Society of Chemistry 20xx

View Article Online
DOI: 10.1039/D2CC03375

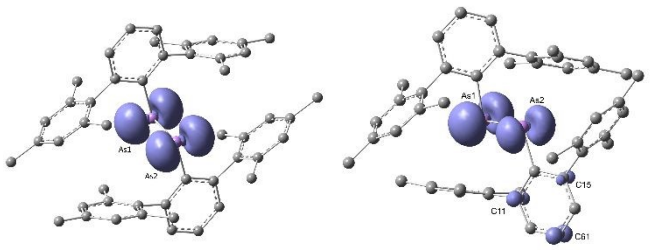

Figure 5. Spin density plots of $\mathbf{As_2^{sym}}$ (left) and $\mathbf{As_2^{asym}}$ (right). Isosurface set at 0.004 a.u.

Comparable radical anions of heavier pnictenes (Sb, Bi) [14,15,16] as well as radical diarsenic cations[6,18,19] show only coupling to two-equivalent pnictogen atoms, which exhbit exclusively symmetric radical anions or cations in the solid state.

UV/Vis spectroscopic examination of **1** (**Figure 4**, right) gave a broad band centred at 610 nm, responsible for its characteristic blue colour. This absorption is red-shifted compared to $(^{Mes}TerAs)_2$ (at 395 nm) and supports weakening of the As–As bond in accordance with the structural changes. The primary absorption band of **1** lies in-between values reported for the diphosphene and distibene radical anions $[(Bbt)E{=}E(Bbt)]^{\bullet-}$ (E = P λ = 539; E = Sb λ = 812 nm; Bbt = 2,6-(CH{$SiMe_3$}$_2$)-4-(C{$SiMe_3$}$_3$)-C_6H_2).

The electronic situation in the symmetric ($[\mathbf{1^{sym}}]^-$) and asymmetric ($[\mathbf{1^{asym}}]^-$) anions, respectively, were investigated by density functional theory (DFT) (for a detailed description of all computations, please refer to the ESI), and confirmed as minima by frequency analyses with the asymmetric $[\mathbf{1^{asym}}]^-$ radical being slightly lower in energy by ca. 10 kJ/mol. In both cases, the As–As bond is mainly described by a σ- (HOMO-1) and a π-type (HOMO) interaction with the SOMO representing the π* orbital. The Mulliken spin density in both radical species is mainly located at the As atoms ($[\mathbf{1^{sym}}]^-$: As 0.468; $[\mathbf{1^{asym}}]^-$: As1 0.477, As2 0.279). In case of $[\mathbf{1^{asym}}]^-$, spin density is further found on the central aryl ring of the ^{Mes}Ter-substituent attached to As2 (C_{ortho}: 0.062, 0.040; C_{para}: 0.080), that consequently bears reduced spin density (**Figure 5**, right). Here, it thus hints to a slight iminyl-like character with the radical character partially dispersed over the aromatic ring, thus explaining the slightly shortened As–C bond as well as the more obtuse As–As–C angle in $[\mathbf{1^{asym}}]^-$. Further, TD-DFT studies reproduced the absorption at 610 nm well (λ_{calc} = 612 nm) and indicate, in agreement with previous reports on diphosphene and distibene radical anions,[15,27] a SOMO to ^{Mes}Ter-π* transition.

We also attempted to obtain the diarsene radical anion void of potassium ion separation, by treating the neutral diarsene with potassium graphite in Et_2O (**Scheme 1**) at −40 °C, which resulted in the rapid precipitation of an insoluble dark blue solid of presumably $K[^{Mes}TerAs]_2$, whose identity and structure could however not be unequivocally authenticated due to inseparable graphite/KC_8. Using the highly reducing yet toluene and Et_2O soluble metal(I) silylamides [KM(N{Dipp}R)$_2$] (M = Mn, Fe)[28] as 18c6-free alternatives of $[K(18c6)][Fe(NR_2)_2]$ as $1e^-$-reductants yielded in no measurable reduction of $(^{Mes}TerAs)_2$ as in case for the formation of **1**.

Given the general absence of reports on the reactivity of dipnictene radical anions, we further probed the reactivity of **1** (**Scheme 2**). No radical-type reactivity could be initiated with substrates bearing susceptible O/C–H bonds (1,4-cyclohexadiene or TEMPO-H). This was theoretically probed with the aid of the hypothetical reaction: $[\mathbf{1^{sym/asym}}]^{\bullet-}$ + TEMPO-H → $[1\text{-}H]^-$ + TEMPO$^{\bullet}$, which was found to be endergonic for $[\mathbf{1^{asym}}]^-$ (11 kJ/mol) and minimally exergonic for $[\mathbf{1^{sym}}]^-$ (−1.5 kJ/mol), in line with no expressed radical reactivity of the diarsene radical anion in **1**.

We further reacted **1** with PhN_3 in THF, which led to an immediate decolourization from blue to yellow. From this an unprecedented, neutral azadiarsacyclopropane, cyclo-$[(^{Mes}TerAs)_2NPh]$ (**2**), was isolated (**Scheme 2**; Figure 6, right).

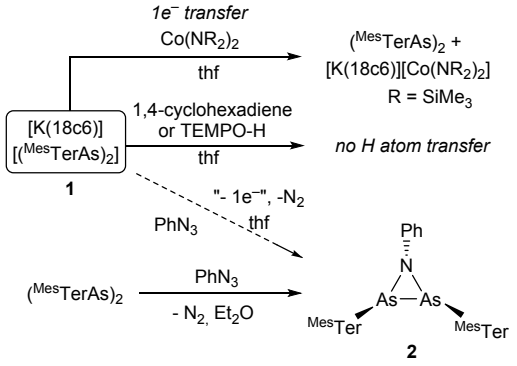

Scheme 2. Reactivity of **1** and of the parent $(^{Mes}TerAs)_2$.

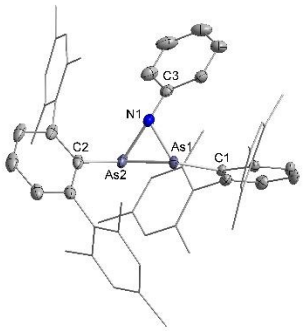

Figure 6. Right: Molecular structure of **2**. Selected bond distances (Å) and angles (°): As1–As2 2.429(1), As1–N1 1.902(2), As2–N1 1.904(2), N1–C3 1.406(2); As1–N1–As2 79.3(1).

In **2**, the nitrogen atom binds symmetrically to both arsenic atoms with N–As atom distances of ca. 1.903 Å and an As–N–As angle of 79.3(1)°. The As–As bond length of 2.429(1) Å is in the range of a single bond.[22] We speculated that the formation of **2** stemmed from an initial electron transfer from **1** to the azide with subsequent further substrate decomposition as an electron sink. Re-formed $(^{Mes}TerAs)_2$ then reacts with a second equivalent of the azide under N_2 extrusion and formal aziridination of the As–As double bond. Indeed, the latter was corroborated by an independent reaction of phenyl azide with $(^{Mes}TerAs)_2$ in Et_2O (**Scheme 2**), analogous to a recent report on an azadistibirane.[29] Diarsene functionalization was already observed for the diarsene $(Mes^*As)_2$ (Mes^* = 2,4,6-C_6H_2) using

Published on 01 August 2022. Downloaded by University of Marburg on 8/1/2022 9:18:50 AM.

ChemComm Accepted Manuscript

View Article Online DOI: 10.1039/D2CC03237F

Published on 01 August 2022. Downloaded by University of Marburg on 8/1/2022 9:18:50 AM.

diazomethane and S_8 which gave the corresponding, yet only spectroscopically characterized diarsacylopropane and thiadiarsirane.[30] This implies that **1** primarily acts as a one-electron reductant. This cascade of electron release and subsequent reaction of the neutral diarsene is likely the pathway in the reaction of a diphosphene radical anion with an excess of sulfur or selenium (affording neutral thia- and selenadiphosphiranes).[16] The potential of **1** to act as a moderate chemical 1e$^-$ -reductant was probed with the reduction of $[Co^{II}(NR_2)_2]$ to $[K(18c6)][Co^{I}(NR_2)_2]$ (**Scheme 2**, **Figure S4**). This reduction was not quantitative and thus implies a reduction potential of ca. –1.5 V vs. Fc/Fc^+.[31]

In conclusion, the isolation of the first diarsene radical anion is reported. This is achieved *via* reduction of $(^{Mes}TerAs)_2$ by KC_8/18c6 in THF or by using the iron(I) silylamide $[K(18c6)][Fe(NR_2)_2]$ (R = $SiMe_3$) as an unconventional, Et_2O-soluble 1e$^-$ reductant. The salts $[K(18c6)(thf)_{0,1}][(^{Mes}TerAs)_2]$ containing diarsene radical anions were comprehensively analysed by X-Ray diffraction analysis, UV/Vis and X-Band EPR spectroscopy as well as computational studies, supporting their As-centered radical character. X-Ray analysis revealed symmetric $[\mathbf{1}^{sym}]^-$ and asymmetric $[\mathbf{1}^{asym}]^-$ radical anions in the solid state, in which spin density is placed on the As_2 unit or is minimally delocalized into one of the ^{Mes}Ter substituents, respectively. First reactivity studies indicate that the diarsene radical anion acts primarily as one-electron reductant. This was exemplified by the reaction with PhN_3, yielding azadiarsacyclopropane **2**, which is also obtained in the reaction of PhN_3 with neutral $(^{Mes}TerAs)_2$.

C. H.-J. thanks the Boehringer Ingelheim Foundation for support through an Exploration Grant. G.W. thanks the Deutsche Forschungsgemeinschaft (DFG, grant WE 5627/4-2 to C. G. W.) for funding. Dr. A. Stoy and Prof. Dr. C. Lichtenberg (Philipps-University Marburg) are kindly acknowledged for acquisition of the EPR data.

Conflicts of interest

There are no conflicts to declare.

Notes and references

1 L. Weber, F. Ebeler and R. S. Ghadwal, *Coord. Chem. Rev.*, 2022, **461**, 214499.
2 H. Köhler and A. Michaelis, *Ber. Dtsch. Chem. Ges.*, 1877, **10**, 807–814.
3 a) J. J. Daly, *J. Chem. Soc.*, 1964, 6147; b) J. J. Daly and L. MAIER, *Nature*, 1964, **203**, 1167–1168;
4 M. Yoshifuji, I. Shima, N. Inamoto, K. Hirotsu and T. Higuchi, *J. Am. Chem. Soc.*, 1981, **103**, 4587–4589.
5 B. Twamley, C. D. Sofield, M. M. Olmstead and P. P. Power, *J. Am. Chem. Soc.*, 1999, **121**, 3357–3367.
6 M. K. Sharma, S. Blomeyer, B. Neumann, H.-G. Stammler and R. S. Ghadwal, *Chem. Eur. J.*, 2019, **25**, 8249–8253.
7 P. K. Majhi, H. Ikeda, T. Sasamori, H. Tsurugi, K. Mashima and N. Tokitoh, *Organometallics*, 2017, **36**, 1224–1226.
8 T. Sasamori, Y. Arai, N. Takeda, R. Okazaki, Y. Furukawa, M. Kimura, S. Nagase and N. Tokitoh, *BCSJ*, 2002, **75**, 661–675.
9 M. Sakagami, T. Sasamori, H. Sakai, Y. Furukawa and N. Tokitoh, *Chem. Asian J.*, 2013, **8**, 690–693.
10 D. Dange, A. Davey, J. A. B. Abdalla, S. Aldridge and C. Jones, *Chem. Commun.*, 2015, **51**, 7128–7131.
11 a) J. Krüger, C. Wölper, A. A. Auer and S. Schulz, *Eur. J. Inorg. Chem.*, 2022, **2022**, DOI: 10.1002/ejic.202100960; b) R. J. Schwamm and M. P. Coles, *Chem. Eur. J.*, 2019, **25**, 14183–14191;
12 N. Tokitoh, Y. Arai, T. Sasamori, R. Okazaki, S. Nagase, H. Uekusa and Y. Ohashi, *J. Am. Chem. Soc.*, 1998, **120**, 433–434.
13 a) N. Tokitoh, Y. Arai, R. Okazaki and S. Nagase, *Science*, 1997, **277**, 78–80; b) C. von Hänisch and D. Nikolova, *Eur. J. Inorg. Chem.*, 2006, **2006**, 4770–4773;
14 H. M. Weinert, C. Wölper, J. Haak, G. E. Cutsail and S. Schulz, *Chem. Sci.*, 2021, **12**, 14024–14032.
15 T. Sasamori, E. Mieda, N. Nagahora, K. Sato, D. Shiomi, T. Takui, Y. Hosoi, Y. Furukawa, N. Takagi, S. Nagase and N. Tokitoh, *J. Am. Chem. Soc.*, 2006, **128**, 12582–12588.
16 N. Nagahora, T. Sasamori, Y. Hosoi, Y. Furukawa and N. Tokitoh, *J. Organomet. Chem.*, 2008, **693**, 625–632.
17 K. Tsuji, Y. Fujii, S. Sasaki and M. Yoshifuji, *Chem. Lett.*, 1997, **26**, 855–856.
18 M. Y. Abraham, Y. Wang, Y. Xie, R. J. Gilliard, P. Wei, B. J. Vaccaro, M. K. Johnson, H. F. Schaefer, P. v. R. Schleyer and G. H. Robinson, *J. Am. Chem. Soc.*, 2013, **135**, 2486–2488.
19 M. K. Sharma, S. Blomeyer, B. Neumann, H.-G. Stammler, M. van Gastel, A. Hinz and R. S. Ghadwal, *Angew. Chem. Int. Ed.*, 2019, **58**, 17599–17603.
20 a) L. P. Ho, M.-K. Zaretzke, T. Bannenberg and M. Tamm, *Chem. Commun.*, 2019, **55**, 10709–10712; b) A. Doddi, D. Bockfeld, M.-K. Zaretzke, T. Bannenberg and M. Tamm, *Chem. Eur. J.*, 2019, **25**, 13119–13123;
21 R. C. Smith, P. Gantzel, A. L. Rheingold and J. D. Protasiewicz, *Organometallics*, 2004, **23**, 5124–5126.
22 W. Wang, G. Tan, R. Feng, Y. Fang, C. Chen, H. Ruan, Y. Zhao and X. Wang, *Chem. Commun.*, 2020, **56**, 3285–3288.
23 C. G. Werncke, P. C. Bunting, C. Duhayon, J. R. Long, S. Bontemps and S. Sabo-Etienne, *Angew. Chem. Int. Ed.*, 2015, **54**, 245–248.
24 a) I. Müller, D. Munz and C. G. Werncke, *Inorg. Chem.*, 2020, **59**, 9521–9537; b) C. G. Werncke and I. Müller, *Chem. Commun.*, 2020, **56**, 2268–2271;
25 a) M. K. Sharma, D. Rottschäfer, B. Neumann, H.-G. Stammler, S. Danés, D. M. Andrada, M. van Gastel, A. Hinz and R. S. Ghadwal, *Chem. Eur. J.*, 2021, **27**, 5803–5809; b) M. Jacob and E. Weiss, *J. Organomet. Chem.*, 1978, **153**, 31–38;
26 G. E. Cutsail, *Dalton Trans.*, 2020, **49**, 12128–12135.
27 S. Asami, S. Ishida, T. Iwamoto, K. Suzuki and M. Yamashita, *Angew. Chem. Int. Ed.*, 2017, **56**, 1658–1662.
28 R. Weller, I. Müller, C. Duhayon, S. Sabo-Etienne, S. Bontemps and C. G. Werncke, *Dalton Trans.*, 2021, **50**, 4890–4903.
29 H. M. Weinert, C. Wölper and S. Schulz, *Chem. Sci.*, 2022, **13**, 3775–3786.
30 L. Weber and U. Sonnenberg, *Chem. Ber.*, 1989, **122**, 1809–1813.
31 C. G. Werncke, E. Suturina, P. C. Bunting, L. Vendier, J. R. Long, M. Atanasov, F. Neese, S. Sabo-Etienne and S. Bontemps, *Chem. Eur. J.*, 2016, **22**, 1668–1674.

ChemComm Accepted Manuscript

 This journal is © The Royal Society of Chemistry 20xx

A Diarsene Radical Anion

Grégoire Sieg,[1] Malte Fischer,[2,3] Fabian Dankert,[2,4] Jan-Erik Siewert,[2] Christian-Hering Junghans,[2,*] C. Gunnar Werncke*[1]

[1] Chemistry Department, Philipps-University, Hans-Meerwein-Str. 4, 35043 Marburg, Germany. E-mail: gunnar.werncke@chemie.uni-marburg.de.

[2]Leibniz Institute for Catalysis, Albert-Einstein-Straße 29a, 18059 Rostock, Germany; E-mail: christian.hering-junghans@catalysis.de

[3]Chemistry Research Laboratory, Mansfield Road, Oxford OX1 3TA, UK

[4]Inorganic Chemistry: Coordination Chemistry, Campus C4.1, Saarland University, D-66123 Saarbrücken, Germany

Table of Contents

1. General Considerations 2
2. Synthesis, Crystallization and Characterization 3
   2.1. Crystallization of (^{Mes}TerAs)$_2^{asym}$ 3
   2.2. Synthesis of 1^{sym} 3
   2.3. Synthesis of 1^{asym} 3
   2.4. Synthesis of 2 5
   2.5. Reaction of 1 with [Co^{II}(N(SiMe$_3$)$_2$)$_2$] 7
   2.6. EPR spectroscopy 8
   2.7. IR spectroscopy 10
   2.8. UV-Vis spectroscopy 12
   2.9. Cyclic voltammetry 13
3. Computational details 14
   3.1. Summary of calculated data 14
   3.1.1. 1^{sym} xyz-coordinates 20
   3.1.2. 1^{asym} xyz-coordinates 22
   3.1.1. 1^{asym} xyz-coordinates 24
   3.1.1. 1^{asym} xyz-coordinates 25
   3.1.1. 1^{asym} xyz-coordinates 25
4. Crystallographic Details 28
5. References 35

1. General Considerations

All manipulations were carried out in a glovebox under a dry argon atmosphere, unless indicated otherwise. Used solvents were either dried by continuous distillation over sodium metal for several days, degassed via three freeze-pump cycles and stored over molecular sieves 4 Å or were purified with the Grubbs-type column system "Pure Solv MD-5" and were freshly distilled prior to use from. Deuterated solvents were used as received, degassed via three freeze-pump cycles and stored over molecular sieves 4 Å. The ^{1}H-NMR spectra were recorded on a BRUKER AV 300 and BRUKER HD 500 NMR spectrometer (Bruker Corporation, Billerica, MA, USA). Chemical shifts are reported in ppm relative to the residual proton signals of the solvent. $w_{1/2}$ is the spectral linewidth of a signal at half its maximum intensity, all using the MestreNova software package (Mestrelab, Version 14.2.0, Santiago de Compostela, Spain). IR measurements were conducted on a Bruker Alpha ATR-IR spectrometer processed with the OPUS Software (Version 7.5) (Bruker Corporation, Billerica, MA, USA). Elemental analyses were performed by the "in-house" service of the Chemistry Department of the Philipps University Marburg, Germany using a CHN(S) analyzer vario MICRO Cube (Elementar Analysensysteme GmbH, Langenselbold, Germany). UV/Vis-spectra were recorded on an AnalytikJena Specord S600 diode array spectrometer (AnalytikJena, Jena, Germany). EPR spectra were recorded on a BRUKER Magnettech ESR5000 spectrometer. EPR simulations were performed using the program EasySpin.[1] Cyclic Voltammetry (CV) were recorded using a Methrom Autolab PGSTAT204 potentiostat at 23 °C in THF containing 0.1 M [N*n*Bu$_4$][PF$_6$] at scan rates of 100 mV·s^{-1}. A standard three-electrode cell configuration was employed using a glassy carbon working electrode, a platinum wire counter electrode, and a silver wire serving as the reference electrode. Formal redox potentials are referenced to the [FeCp$_2$]/[FeCp$_2$]$^+$ redox couple. The measurements were performed with 1 mM compound dissolved in the electrolyte.

^{Mes}Ter$_2$As$_2$,[2] TEMPO-H,[3], Phenylazide,[4] [Co^{II}(N(SiMe$_3$)$_2$)$_2$][5] and [K(18c6)][Fe^{I}(N(SiMe$_3$)$_2$)$_2$][6] were synthesized according to literature procedures. 1,4-Cyclohexadiene was purchased from Acros Organics. KC$_8$ was bought from commercial sources or prepared by mixing respective amounts of graphite (previously dried *in vacuo* via heatgun) with freshly cut potassium metal. The mixture was heated *in vacuo* via heatgun until all potassium metal had reacted.

2. Synthesis, Crystallization and Characterization

2.1. Crystallization of $(^{Mes}TerAs)_2^{asym}$

Single crystals of **$(^{Mes}TerAs)_2^{asym}$** were obtained after recrystallization of $(^{Mes}TerAs)_2$ from a concentrated toluene solution at –32 °C.

2.2. Synthesis of 1^{sym}

$(^{Mes}TerAs)_2$ (15.0 mg, 19 μmol, 1.00 eq.) was dissolved in 2 mL of Et_2O. The yellow solution was layered with a solution of $[K(18c6)][Fe(N(SiMe_3)_2)_2]$ (13.1 mg, 0.019 mmol, 1.00 eq.) at –40 °C to slowly afford $[K(18c6)][(^{Mes}TerAs)_2]$ **1** as a deep blue precipitate (13 mg, 12 μmol , 63%).

Crystals, suitable for X-ray diffraction analysis were obtained by layering a solution of $(^{Mes}TerAs)_2$ in THF with a solution of $[K(18c6)][Fe(N(SiMe_3)_2)_2]$ in Et_2O at –40 °C.

IR (ATR, cm^{-1}): ν = 3016 (vw), 2957 (vw), 2891 (w), 2852 (vw), 1610 (vw), 1560 (vw), 1468 (w), 1433 (w), 1371 (w), 1348 (w), 1284 (w), 1245 (w), 1233 (vw), 1132 (vw), 1101 (s), 1058 (w), 1023 (w), 961 (m), 844 (m), 792 (w), 731 (m), 702 (vw), 654 (vw), 572 (vw), 549 (vw), 531 (vw).

Elemental analysis: calculated ($C_{60}H_{74}As_2KO_6$, 1080.19 g/mol) C 66.72 H 6.91; experimental C 67.13 H 6.50

^{1}H-NMR ([D8]THF, 300 MHz, 300 K, ppm): δ = 3.60 (O-CH_2), 5.83 (br, relative integral = 1), 6.69 (br, relative integral = 1.69).

2.3. Synthesis of 1^{asym}

$(^{Mes}TerAs)_2$ (15.0 mg, 0.019 mmol, 1.00 eq.) was dissolved in 2 mL of THF. The yellow solution was added to a mixture of KC_8 (3 mg, 0.022 mmol, 1.60 eq.) and 18c6 (5 mg, 0.019 mmol, 1.00 eq.). The mixture was filtered and the blue solution was layered with 2 mL of *n*-pentane at –40 °C to afford small amounts of **1^{sym}** as deep blue precipitate (6 mg, 5 μmol, 28%).

Crystals, suitable for X-ray diffraction analysis were obtained by layering a solution **1^{asym}** in THF with 2 mL of *n*-pentane at –40 °C.

IR (ATR, cm^{-1}): $\tilde{\nu}$ = 3016 (vw), 2957 (vw), 2891 (w), 2852 (vw), 1610 (vw), 1560 (vw), 1468 (w), 1433 (w), 1371 (w), 1348 (w), 1284 (w), 1245 (w), 1233 (vw), 1132 (vw), 1101 (s), 1058 (w), 1023 (w), 961 (m), 844 (m), 792 (w), 731 (m), 702 (vw), 654 (vw), 572 (vw), 549 (vw), 531 (vw).

^{1}H-NMR ([D8]THF, 300 MHz, 300 K, ppm): δ = 3.53 (O-CH_2), 5.87 (br, relative integral = 1), 6.69 (br, relative integral = 1.78).

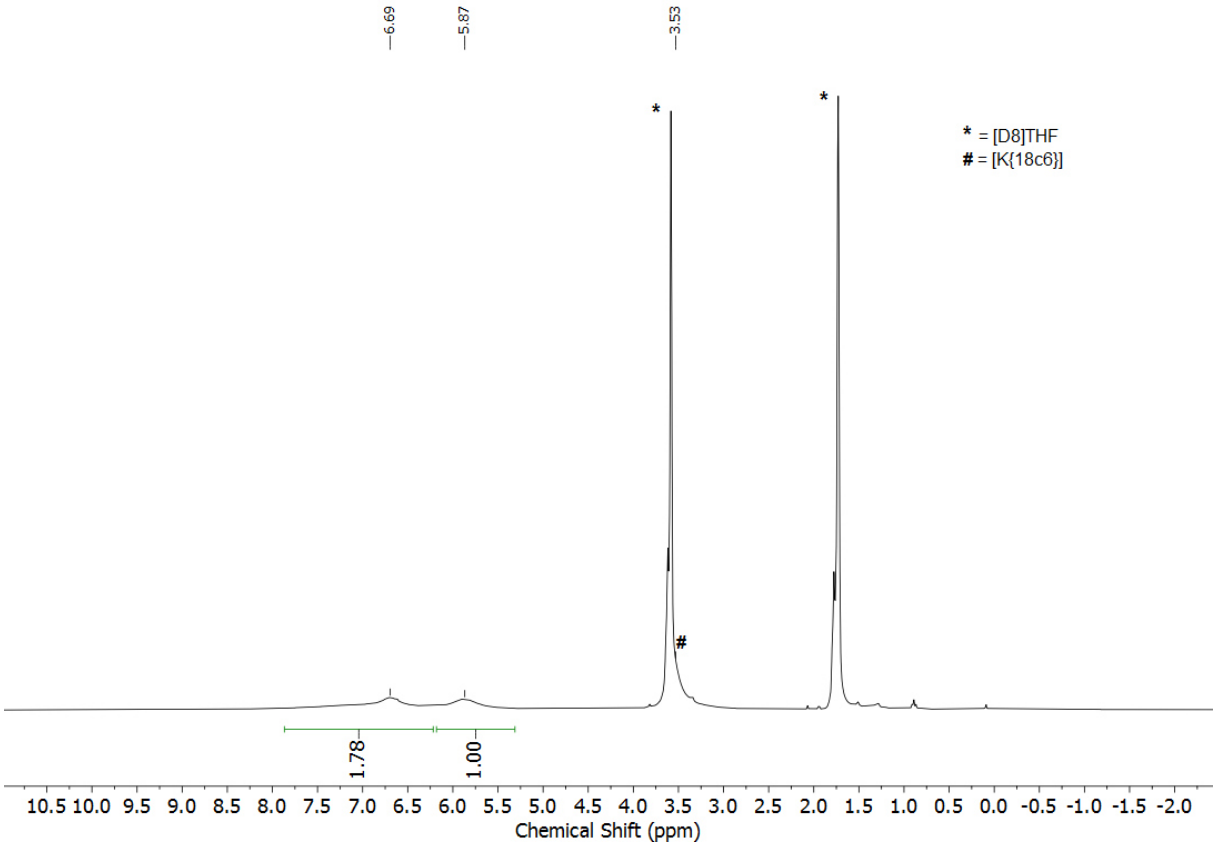

Figure S1. ^{1}H NMR spectrum of **1** in [D8]THF at 300 K, 300 MHz .

2.4. Synthesis of 2

(^{Mes}TerAs)$_2$ (25 mg, 0.032 mmol, 1.00 eq.) and PhN_3 (3.8 mg, 0.032 mmol, 1.00 eq.) were dissolved in 2 mL of Et_2O. After initial gas evolution, the solvent was removed after several minutes under vacuum to afford **3** as an orange solid (19.3 mg, 0.022 mmol, 69%).

^{1}H-NMR ([D8]THF, 300 MHz, 300 K, ppm): δ = 1.67 (s, 12H, *o*-Mes), 1.79 (s, 12H, *o*-Mes), 2.29 (s, 12H, *p*-Mes), 5.82 (d, 2H, $^3J_{HH}$ = 8.6 Hz, *o*-Ph), 6.43 (t, 1H, $^3J_{HH}$ = 6.8 Hz, *p*-Ph), 6.62 (t, 2H, $^3J_{HH}$ = 7.8 Hz, *m*-Ph), 6.69 (d, 4H, $^3J_{HH}$ = 7.5 Hz, *m*-C_6H_3), 6.74 (s, 4H, *m*-Mes), 6.81 (s, 4H, *m*-Mes), 7.18 (t, 2H, $^3J_{HH}$ = 7.5 Hz, *p*-C_6H_3).

^{13}C{^{1}H} ([D8]THF, 75 MHz, 300 K, ppm): δ = 21.5 (*p*-Mes-*C*H$_3$), 21.7 (*o*-Mes-*C*H$_3$), 21.8 (*o*-Mes-*C*H$_3$), 119.4 (*p*-Ph), 122.4 (*o*-Ph), 128.7 (*p*-C_6H_3), 129.3 (*m*-Ph), 129.3 (*m*-Mes), 129.9 (*m*-C_6H_3), 136.8 (*p*-Mes), 137.3 (*o*-Mes), 137.5 (*o*-Mes), 139.8 (*i*-Mes), 144.7 (*i*-C_6H_6), 148.0 (*o*-C_6H_3), 150.5 (*i*-Ph).

IR (ATR, cm^{-1}): $\tilde{\nu}$ = 2938 (w), 2911 (w), 2850 (w), 1610 (w), 1587 (m), 1482 (s), 1443 (m), 1373 (m), 1289 (s), 1167 (w), 1101 (w), 1072 (vw), 1025 (w), 992 (w), 908 (w), 844 (s), 803 (m), 776 (vw), 739 (s), 687 (m), 636 (vw), 588 (w), 574 (w), 547 (vw), 496 (w), 477 (vw).

Elemental analysis: calculated ($C_{54}H_{55}As_2N$, 867.88 g/mol) C 74.73 H 6.39 N 1.61; experimental C 74.56 H 6.32 N 2.10.

Crystals, suitable for X-ray diffraction analysis were obtained by slow evaporation of the solvent from a saturated solution of **2** in Et_2O.

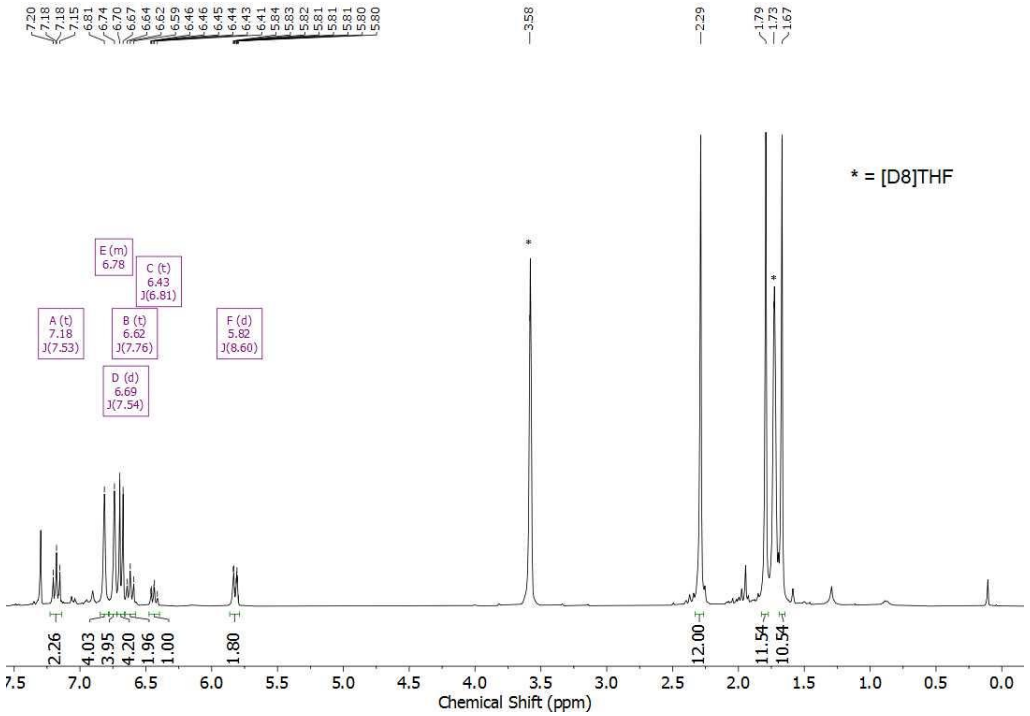

Figure S2. ^{1}H NMR spectrum of **2** in [D8]THF at 300 K, 300 MHz.

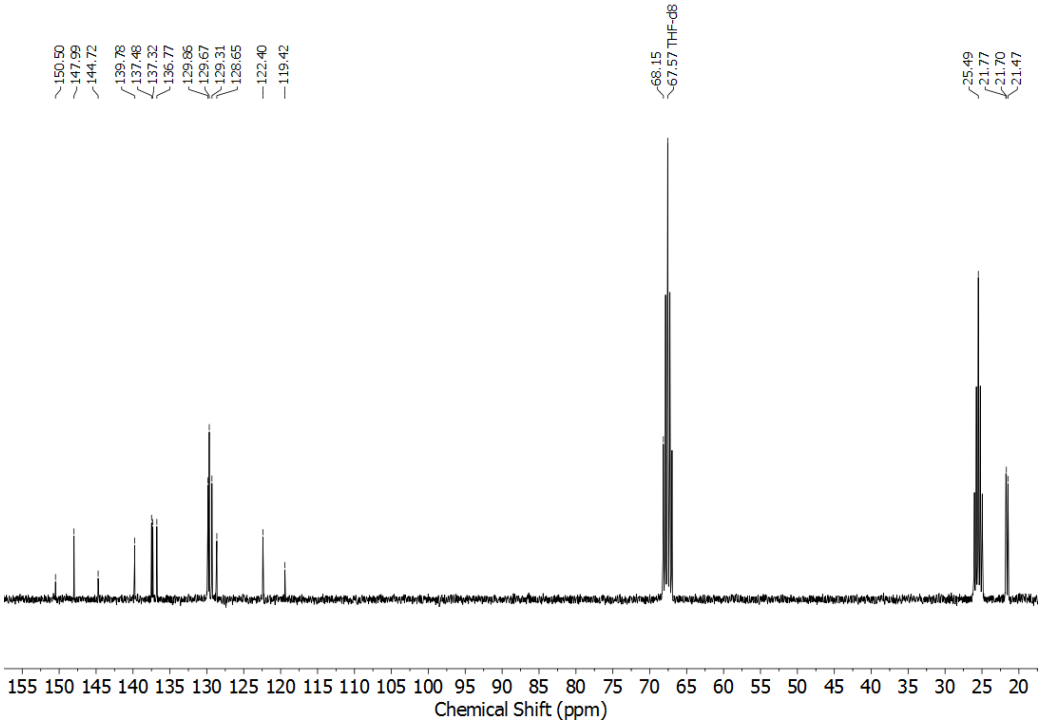

Figure S3. $^{13}C\{^{1}H\}$ NMRspectrum of **2** in [D8]THF at 300 K, 75 MHz.

2.5. Reaction of 1 with $[Co^{II}(N(SiMe_3)_2)_2]$

1 (8.6 mg, 0.008 mmol, 1.00 eq.) was dissolved in 0.3 mL of [D8]THF. The intense blue color immediately changed to green-yellow after the addition of $[Co^{II}(N(SiMe_3)_2)_2]$ (3.1 mg, 0.008 mmol, 1.00 eq.). The partial formation of $^{Mes}Ter_2As_2$ and $[K\{18c6\}][Co^{I}(N(SiMe_3)_2)_2]$ was observed via ^{1}H-NMR spectroscopy. Ratio ($^{Mes}Ter_2As_2$: $[Co^{I}(N(SiMe_3)_2)_2]^-$: $[Co^{II}(N(SiMe_3)_2)_2]$) ≈ 1 : 1 : 2.

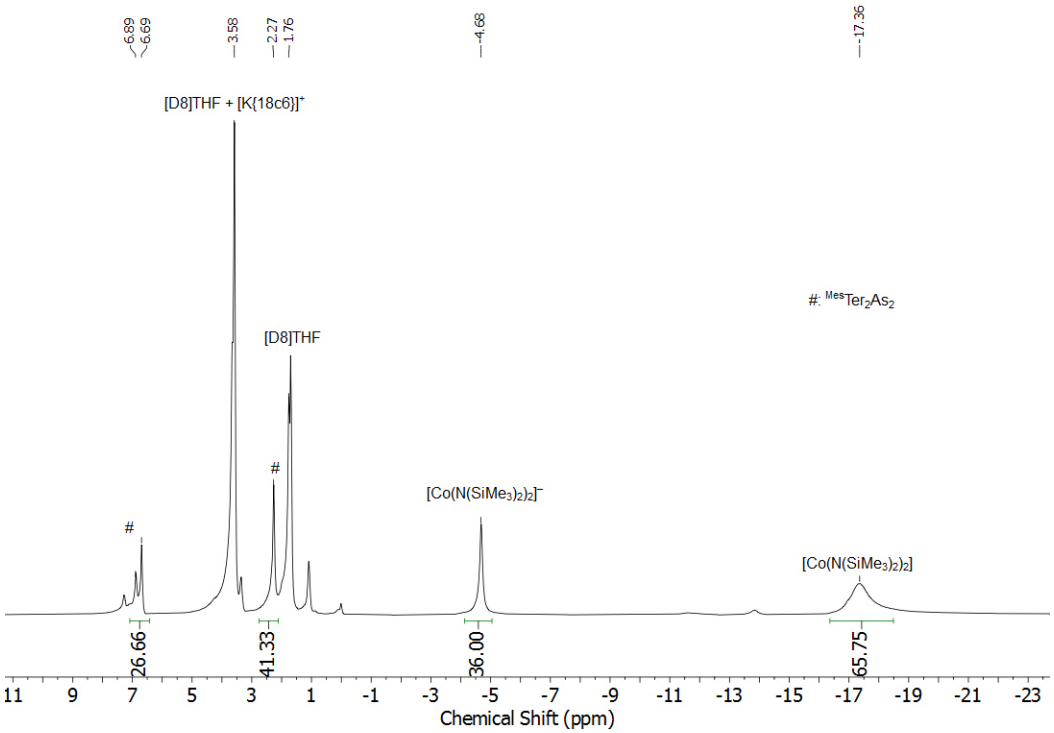

Figure S4. ^{1}H-NMR spectrum of the reaction of **1** with $[Co^{II}(N(SiMe_3)_2)_2]$ in [D8]THF at 300 K.

2.6. EPR spectroscopy

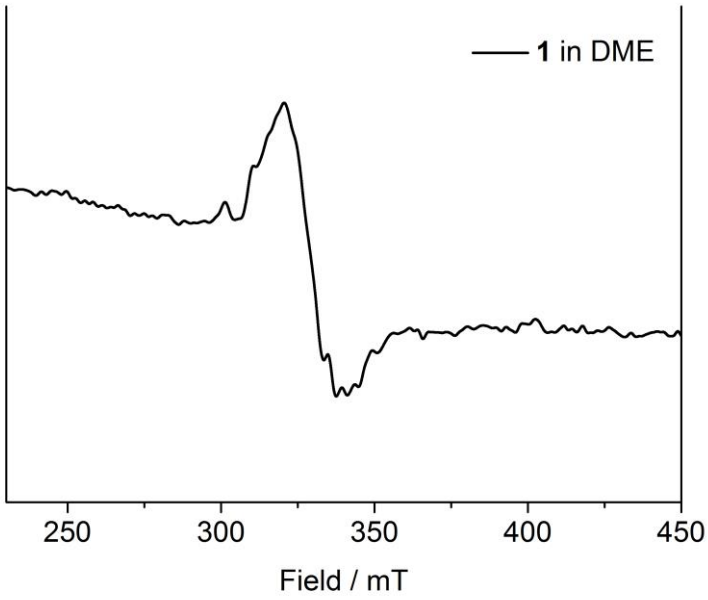

Figure S5. X-band EPR measurement of **1** in frozen Dimethoxyethane (DME) solution at 77 K (9.460808 GHz). The sample was rapidly cooled by liquid N_2 prior measurement.

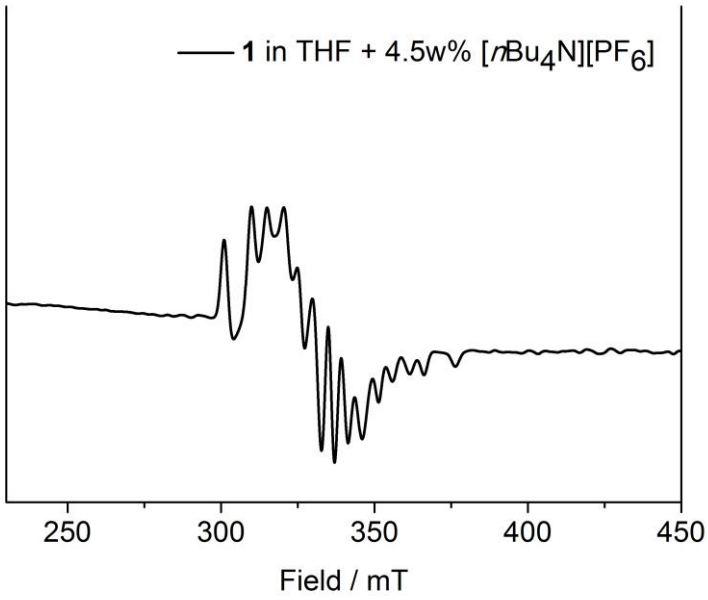

Figure S6. X-band EPR measurement of **1** in frozen THF solution with 4.5w% [nBu$_4$N][PF$_6$] at 77 K (9.460808 GHz). The sample was rapidly cooled by liquid N_2 prior measurement.

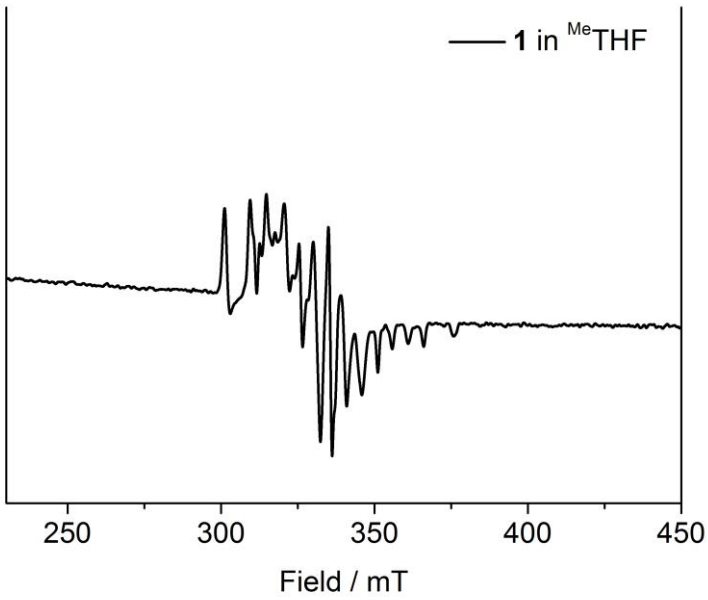

Figure S7. X-band EPR measurement of **1** in frozen 2-Me-THF (^{Me}THF) solution at 77 K (9.460808 GHz). The sample was rapidly cooled by liquid N_2 prior measurement.

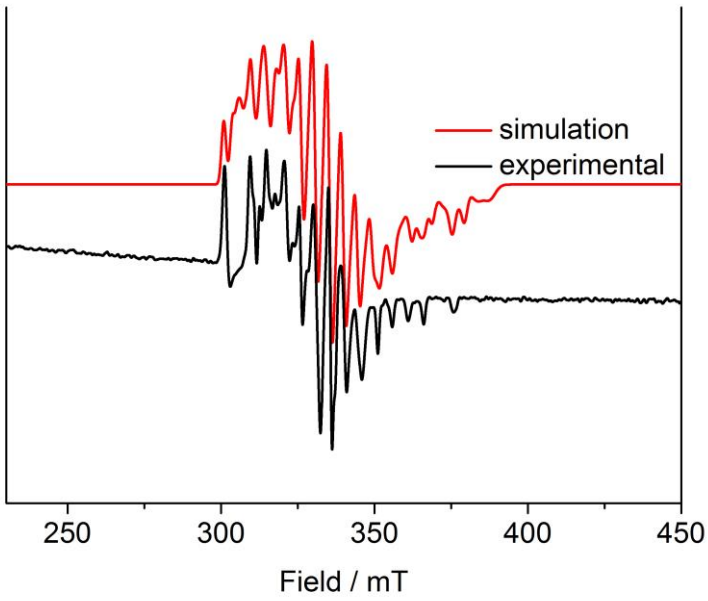

Figure S8. X-band EPR measurement of **1** in frozen 2-Me-THF (^{Me}THF) solution at 77 K (9.460808 GHz). Collected spectrum in black, simulated spectrum in red. $S = ½$ with coupling to two inequivalent ^{75}As nuclei, $g_{iso} = 2.04$, $g_1 = 2.17$, $g_2 = 2.01$, $g_3 = 1.85$, $A_{11} = 136.31$ MHz, $A_{12} = 126.34$ MHz, $A_{13} = 272.73$ MHz, $A_{21} = 86.13$ MHz, $A_{22} = 130.95$ MHz, $A_{23} = 105.17$ MHz.

2.7. IR spectroscopy

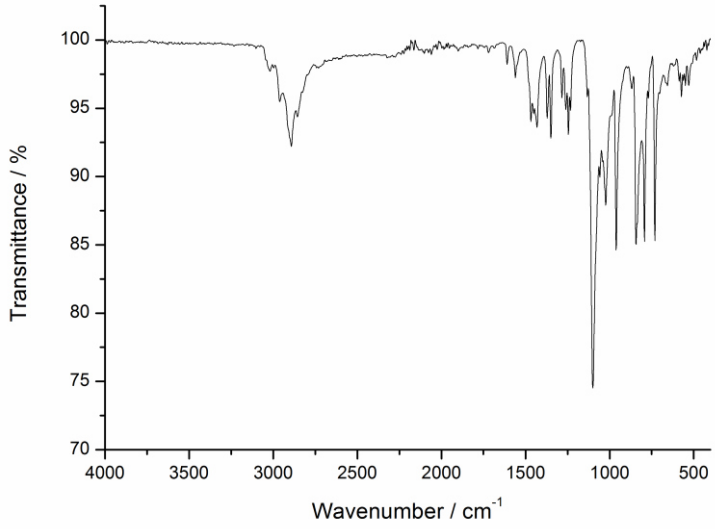

Figure S9. ATR-IR spectrum of **1^{sym}**.

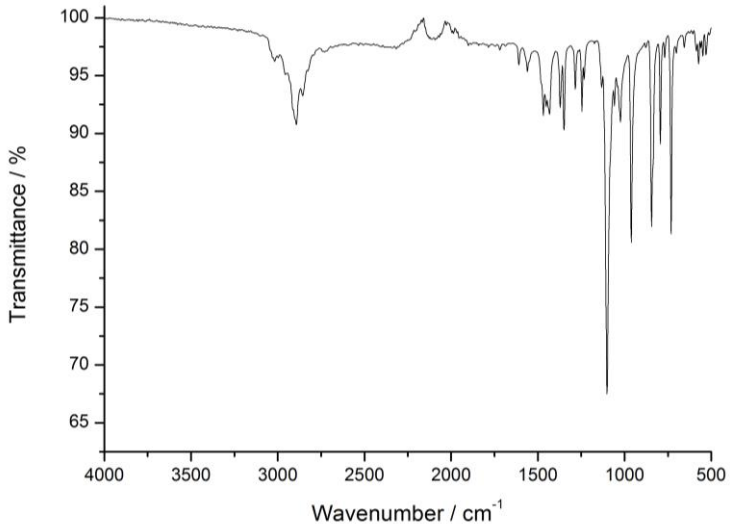

Figure S10. ATR-IR spectrum of **1^{asym}**.

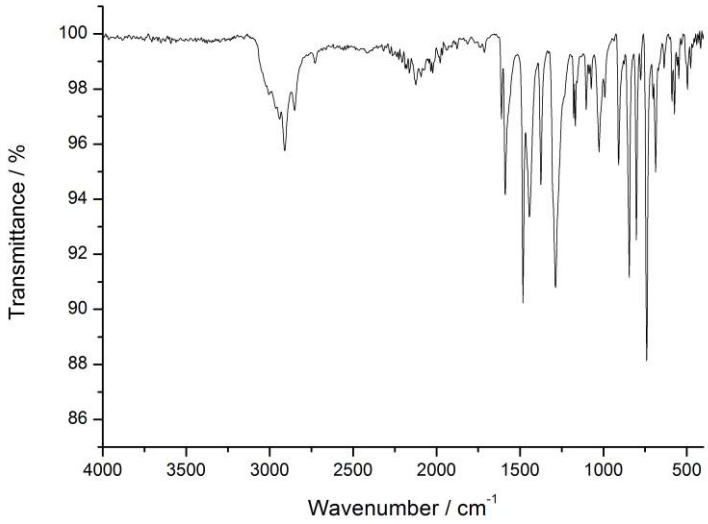

Figure S11. ATR-IR spectrum of **2**.

2.8. UV-Vis spectroscopy

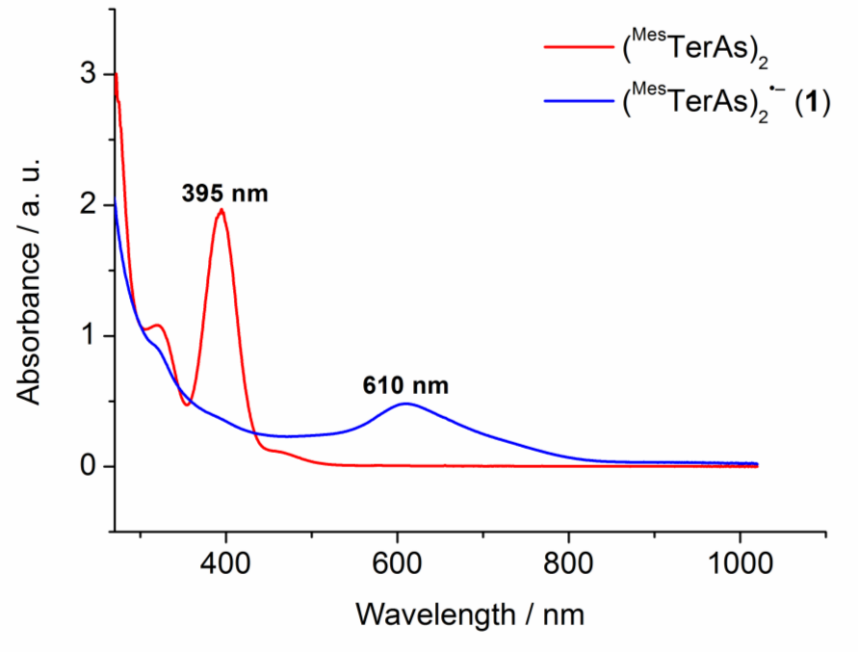

Figure S12. UV-Vis spectrum of (^{Mes}TerAs)$_2$ (red) and [(^{Mes}TerAs)$_2$]$^{\bullet-}$ (**1**, blue) in THF.

2.9. Cyclic voltammetry

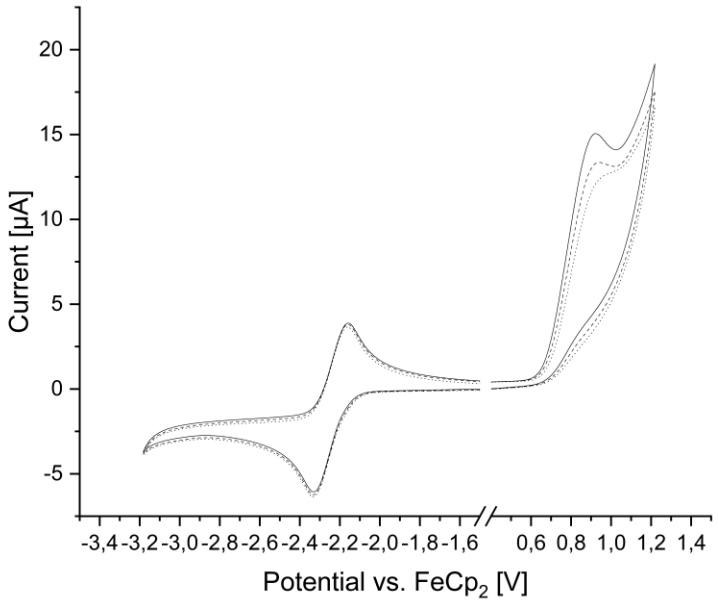

Figure S13. Cyclic voltammogram of (^{Mes}TerAs)$_2$ in THF, 0.1 M [NnBu$_4$][PF$_6$], obtained at 23 °C at a scan rate of 100 mV s^{-1}. $E_{1/2red}$ = −2.24 V, E_{ox} = 0.90 V (vs. FeCp$_2$/[FeCp$_2$]$^+$ redox couple). Multiple scans: blank line first scan, dashed line second scan, dotted line third scan.

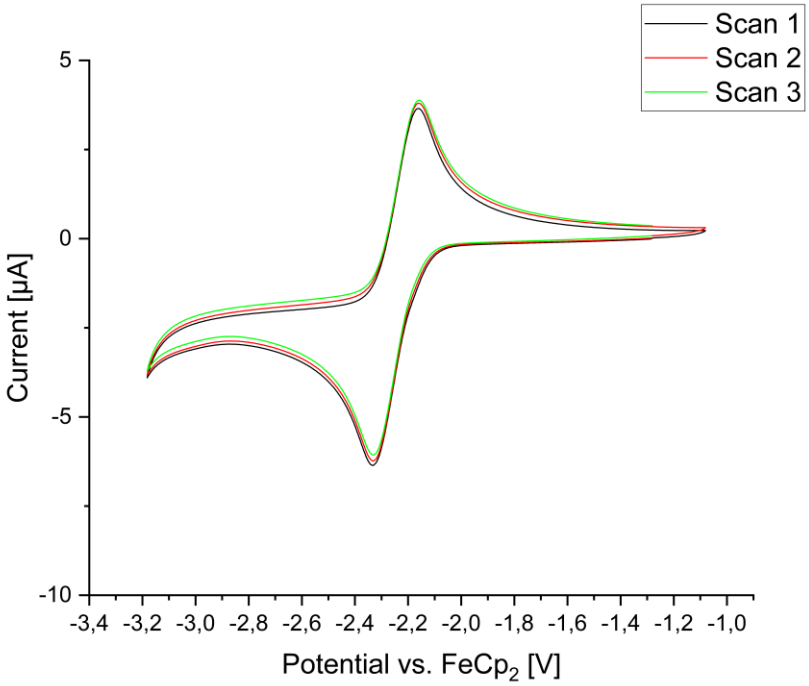

Figure S14. Cyclic voltammogram of (^{Mes}TerAs)$_2$ in THF, 0.1 M [NnBu$_4$]PF$_6$], obtained at 23 °C at a scan rate of 100 mV s^{-1}. $E_{1/2red}$ = −2.24 V (vs. FeCp$_2$/[FeCp$_2$]$^+$ redox couple). Multiple scans at negative potentials between −3.2 and −1.0 V (vs. FeCp$_2$/[FeCp$_2$]$^+$): black line 1st scan, red line 2nd scan, green line 3rd scan.

3. Computational details

3.1. Summary of calculated data

Computations were carried out using Gaussian16[7] or ORCA 4.2.1.[8,9] Multiwfn3.6[10] was used to plot the spin density of the investigated radical species. Structure optimizations employed the DFT functional BP86[11] in conjunction with Grimme's dispersion correction D3(BJ)[12,13] and the def2-SVP basis set[14] (notation BP86-D3/def2-SVP). The resolution of identity (RI) approximation was applied, using Weigend's accurate Coulomb fitting basis.[15] All structures were fully optimized and confirmed as minima by frequency analyses. EPR data were calculated[16–19] using ORCA 4.2.1 at the RI-SOMF(1X)[18,20]/PBE0[9,10,21] - D3/def2-TZVP level of theory, using optimized structures at the BP86-D3/def2-SVP level of theory (vide supra). The Coulomb terms of the hybrid functional as well as the spin-orbit coupling operator were approximated using the RI approximation, while the HF exchange term of the hybrid functional was treated using the Chain of Spheres (COSX) approximation (i.e., RIJCOSX).[20] TD-DFT calculations using optimized structures at the BP86-D3/def2-SVP level of theory (vide supra), were carried out at the B3LYP/def2-TZVP/CPCM(THF) level of theory using ORCA 4.2.1.

Please note that all computations were carried out for single, isolated molecules in the gas phase (ideal gas approximation). There may well be significant differences between gas phase and condensed phase/solution.

Table S1. Summary of calculated data, including electronic energies.

Compound	PG	NIMAG	E_{tot} [a.u][a]	ZPE [kcal/mol]	$G°_{tot}$ [a.u.]	$\Delta G_{solv,THF}$[b]
$[\mathbf{1}^{asym}]^{\cdot-}$	C_1	0	-6330.0199	506.42441	-6329.3034	-0.0744
$[\mathbf{1}^{sym}]^{\cdot-}$	C_i	0	-6330.0147	505.79407	-6329.2986	-0.0733
TEMPOH	*C*1	0	-484.0164	166.18241	-483.7873	-0.0075
TEMPO$^{\cdot}$	C_1	0	-483.4071	159.01274	-483.1905	-0.0087
$\mathbf{[1\text{-}H]^-}$	C_1	0	-6330.6190	510.56520	-6329.8960	-0.0741

[a] Total SCF energy in a.u. [b] $\Delta G_{solv,THF} = E_{tot,THF} - E_{tot}$ (at BP86-D3/def2-SVP; SMD)

Reaction of $[1]^-$ with TEMPO-H:

$[1^{sym/asym}]^{\cdot-}$ + TEMPO-H → $[1\text{-H}]^-$ + TEMPO$^{\cdot}$

Gas Phase (THF-solution) at 298 K

1^{sym}: $\Delta_R G°_{298}$ = -1.5 kJ/mol (-6.6 kJ/mol)

1^{asym}: $\Delta_R G°_{298}$ = 11.1 kJ/mol (9.0 kJ/mol)

Compound	g_{iso}
1^{sym}	2.0390
1^{asym}	2.0437

Euler Rotation of hyperfine tensor to g-tensor (1^{sym})

Atom	Alpha	Beta	Gamma	Ax	Ay	Az
	[degrees]			[MHz]		
As1	-86.0	7.0	83.5	295.50	-131.84	-85.78
As2	-86.0	7.0	83.5	295.50	-131.85	-85.79

Euler Rotation of hyperfine tensor to g-tensor (1^{asym})

Atom	Alpha	Beta	Gamma	Ax	Ay	Az
	[degrees]			[MHz]		
As1	91.1	6.6	-97.8	316.83	-142.99	-90.58
As2	-15.2	1.5	10.0	193.18	-89.11	-46.06

The Mulliken spin density in the radical species **1**^{sym} and **1**^{asym} is mainly located at the As atoms (**1**^{sym}: As1 0.468, As2 0.468; **1**^{asym}: As1 0.477, As2 0.279). In case of the asymmetrical species **1**^{asym} spin density is also located on the central phenyl ring of the ^{Mes}Ter-substituent attached to As2 (C(11,15)$_{ortho}$: 0.062, 0.040; C(61)$_{para}$: 0.080), whereas no spin density > 0.01 is found on the ^{Mes}Ter-substituents in **1**^{sym} (Figure S1).

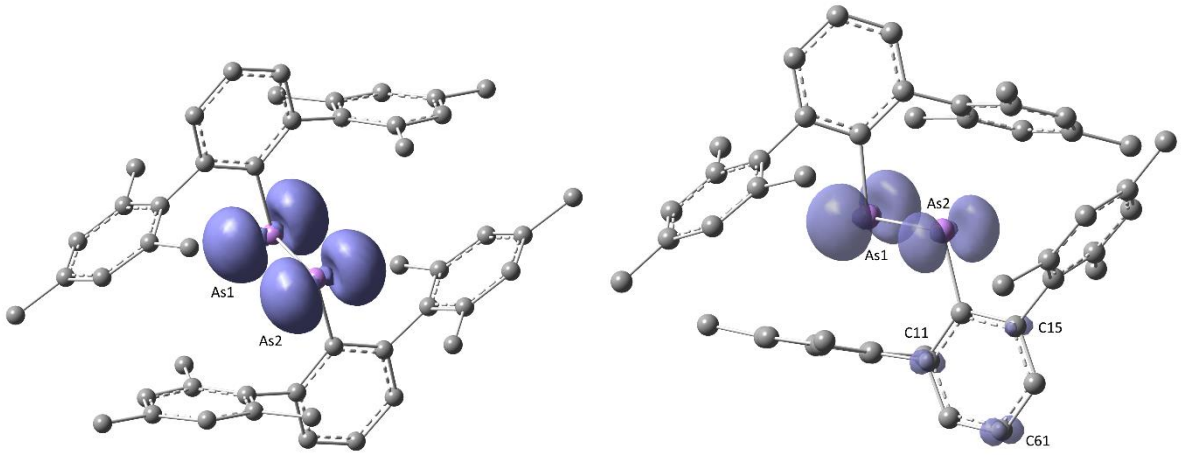

Figure S15: Spin density plot of **1**^{sym} (left) and **1**^{asym} (right). Isosurface set at 0.004 a.u. .

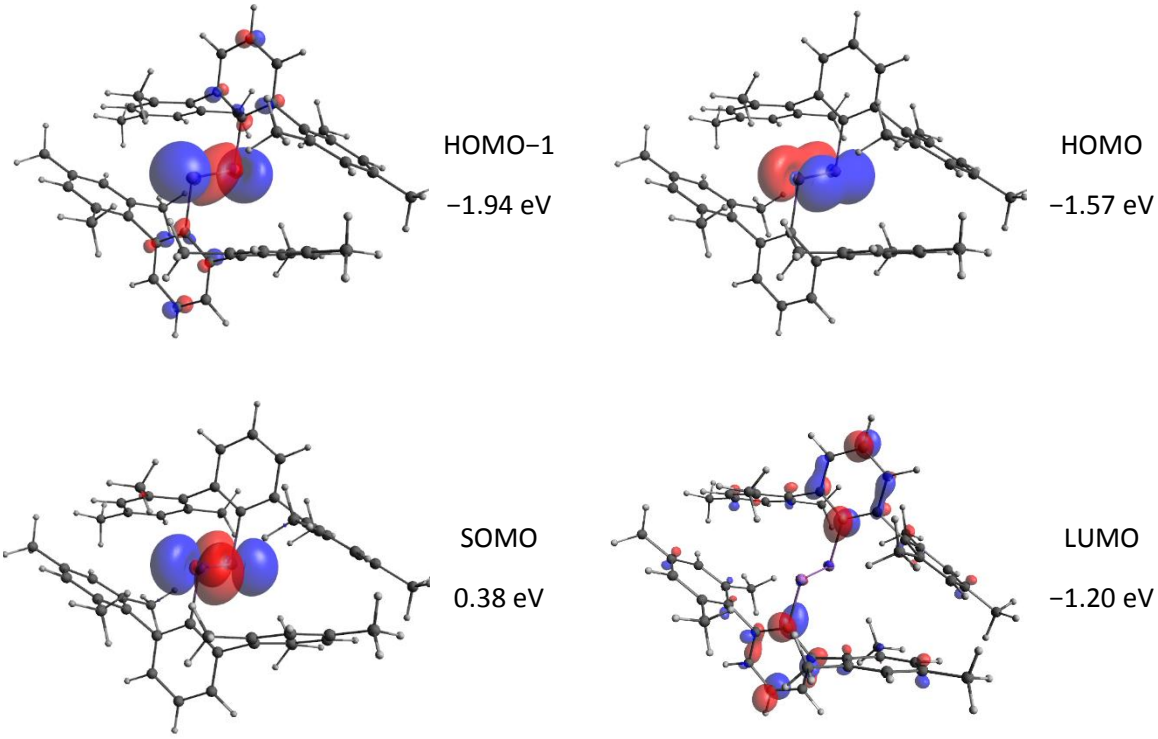

Figure S16. Relevant Kohn-Sham orbitals of **1**^{sym} (BP86-D3/def2-SVP; isosurface value 0.05 a.u.).

TD-DFT/TDA EXCITED STATES for [**1sym**]$^{-}$

---

the weight of the individual excitations are printed if larger than 1.0e-02

STATE 1: E= 0.051817 au 1.410 eV 11372.6 cm**-1

202a -> 203a : 0.965491 (c= -0.98259395)

202a -> 211a : 0.011618 (c= 0.10778804)

STATE 2: E= 0.062417 au 1.698 eV 13698.9 cm**-1

202a -> 204a : 0.979955 (c= -0.98992699)

STATE 3: E= 0.064140 au 1.745 eV 14077.2 cm**-1

202a -> 205a : 0.957603 (c= 0.97857215)

201b -> 202b : 0.033570 (c= -0.18322072)

STATE 4: E= 0.065938 au 1.794 eV 14471.6 cm**-1

202a -> 206a : 0.948243 (c= -0.97377759)

202a -> 207a : 0.015308 (c= -0.12372671)

202a -> 212a : 0.018589 (c= -0.13634122)

STATE 5: E= 0.072688 au 1.978 eV 15953.2 cm**-1

202a -> 208a : 0.800574 (c= 0.89474781)

202a -> 209a : 0.175009 (c= -0.41834038)

STATE 6: E= 0.071976 au 1.959 eV 15796.9 cm**-1

202a -> 206a : 0.018863 (c= 0.13734366)

202a -> 207a : 0.971314 (c= -0.98555248)

STATE 7: E= 0.074471 au 2.026 eV 16344.5 cm**-1

202a -> 208a : 0.159098 (c= 0.39887118)

202a -> 209a : 0.760790 (c= 0.87223290)

202a -> 211a : 0.027742 (c= -0.16656011)

202a -> 215a : 0.015370 (c= 0.12397557)

201b -> 202b : 0.025317 (c= 0.15911397)

STATE 8: E= 0.081416 au 2.215 eV 17868.7 cm**-1

202a -> 203a : 0.018700 (c= 0.13674901)

202a -> 208a : 0.010165 (c= 0.10082252)

202a -> 209a : 0.027903 (c= 0.16704237)

202a -> 211a : 0.802594 (c= 0.89587616)

202a -> 215a : 0.117121 (c= -0.34222877)

STATE 9: E= 0.078807 au 2.144 eV 17296.2 cm**-1

202a -> 210a : 0.985174 (c= -0.99255944)

STATE 10: E= 0.082806 au 2.253 eV 18173.8 cm**-1

202a -> 206a : 0.017778 (c= 0.13333380)

202a -> 212a : 0.965674 (c= -0.98268716)

ABSORPTION SPECTRUM VIA TRANSITION ELECTRIC DIPOLE MOMENTS

State	Energy (cm-1)	Wavelength (nm)	fosc
1	11372.6	879.3	0.003044723
2	13698.9	730.0	0.000000151
3	14077.2	710.4	0.001013183
4	14471.6	691.0	0.000000788
5	15953.2	626.8	0.011686857
6	15796.9	633.0	0.000014845
7	16344.5	611.8	0.003271604
8	17868.7	559.6	0.000788128
9	17296.2	578.2	0.000000138
10	18173.8	550.2	0.000001301

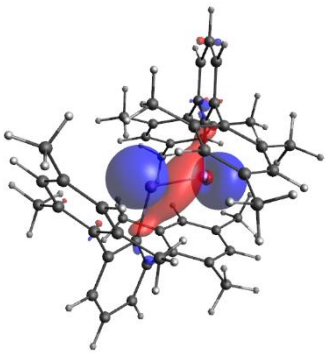

HOMO−1

−1.69 eV

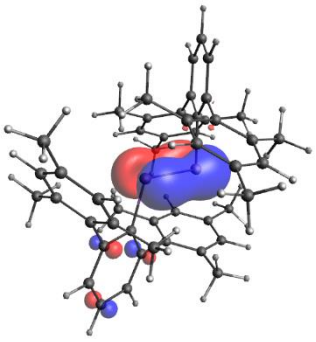

HOMO

−1.47 eV

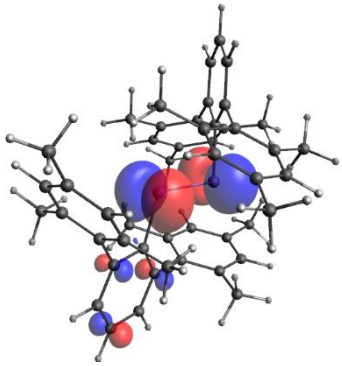

SOMO

0.24 eV

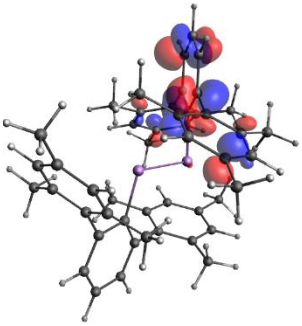

LUMO

−1.36 eV

Figure S17. Relevant Kohn-Sham orbitals of **1**^{asym} (BP86-D3/def2-SVP; isosurface value 0.05 a.u.).

3.2. 1^{sym} xyz-coordinates

1sym @ BP86-D3/def2-SVP

As	8.2986572302	8.6428132896	5.784891648
C	9.4078335594	7.537614695	8.3151864111
C	11.9288960158	8.7690648388	8.0678456193
H	12.9021131533	9.2785485389	7.9712489694
C	11.6881585693	7.8909417974	9.1357950826
H	12.4762330886	7.6912255637	9.8804521631
C	8.0527013348	6.9546203872	8.5867211089
C	9.6672592656	8.3776424683	7.1993804113
C	10.9266459494	9.0273389594	7.1066984617
C	10.425081859	7.2934287234	9.2650466818
H	10.2050747996	6.6346701097	10.1216983331
C	7.2755506276	9.2720042406	9.2949903608
H	8.2612748895	9.4962339952	9.7518454711
H	6.4798775679	9.7491655098	9.9022628273
H	7.2801720941	9.7491047037	8.2892091559
C	12.0624412318	9.7554078457	4.9545422349
C	12.0217802755	12.1221712418	4.2742319376
C	7.0473421447	7.7873346086	9.1528929699
C	12.4616568037	10.7987923629	4.0976061316
H	13.1303026917	10.5610672325	3.2555957965
C	11.2210192045	10.0569857854	6.056141089
C	12.4626543381	8.3330402516	4.6641637916
H	11.5490717435	7.7503519286	4.3919762447
H	12.9063812086	7.8304033117	5.5479791854
H	13.1736889386	8.2759303557	3.8160089011
C	7.8076647709	5.5669686503	8.4241069277
C	11.1514044253	12.3915546155	5.3482233559
H	10.7800584295	13.4199149654	5.5021957244
C	10.7523737478	11.3853864115	6.2459334912
C	5.5799486194	5.8363699967	9.440387648
C	6.5815239365	5.0347900346	8.8682276079
H	6.4037372269	3.9543410966	8.7485268455
C	5.8283595763	7.2176243313	9.5595076935
H	5.0545720974	7.8736500059	9.9954848714
C	8.8054809767	4.6810064188	7.7247311881
H	8.8540860147	4.9736945375	6.6479435362
H	8.507929049	3.6147274111	7.7799011677
H	9.8311676036	4.7943131362	8.1307701588
C	12.4327994164	13.2149225755	3.3138917714
H	12.6142683944	14.1778700538	3.8366936668
H	11.6415005435	13.4070143571	2.5538032521
H	13.3553214181	12.9445192814	2.760136492
C	4.2638484142	5.2446382811	9.8918436743
H	4.2739327248	4.1377819469	9.8273500256
H	3.4184219543	5.6062495614	9.2647805802
H	4.0236780772	5.523749966	10.9408987001

C	9.8097652362	11.7040367937	7.3806710622
H	8.8226025118	11.2237354654	7.1975480197
H	9.6502930852	12.7966067145	7.482867477
H	10.1767370662	11.3019550089	8.34744396
As	9.0138220718	6.7152707104	4.5694672431
C	7.9046457426	7.820469305	2.03917248
C	5.3835832862	6.5890191612	2.2865132718
H	4.4103661487	6.0795354611	2.3831099217
C	5.6243207327	7.4671422026	1.2185638085
H	4.8362462134	7.6668584363	0.473906728
C	9.2597779672	8.4034636128	1.7676377821
C	7.6452200363	6.9804415317	3.1549784798
C	6.3858333526	6.3307450406	3.2476604294
C	6.887397443	8.0646552766	1.0893122093
H	7.1074045024	8.7234138903	0.232660558
C	10.0369286743	6.0860797594	1.0593685303
H	9.0512044124	5.8618500048	0.60251342
H	10.832601734	5.6089184902	0.4520960638
H	10.0323072079	5.6089792963	2.0651497352
C	5.2500380702	5.6026761543	5.3998166562
C	5.2906990265	3.2359127582	6.0801269535
C	10.2651371572	7.5707493914	1.2014659212
C	4.8508224983	4.5592916371	6.2567527595
H	4.1821766103	4.7970167675	7.0987630946
C	6.0914600975	5.3010982146	4.2982178021
C	4.8498249639	7.0250437484	5.6901950994
H	5.7634075584	7.6077320714	5.9623826464
H	4.4060980934	7.5276806883	4.8063797057
H	4.1387903634	7.0821536443	6.53834999
C	9.5048145311	9.7911153497	1.9302519634
C	6.1610748767	2.9665293845	5.0061355352
H	6.5324208725	1.9381690346	4.8521631667
C	6.5601055541	3.9726975885	4.1084253999
C	11.7325306826	9.5217140033	0.9139712431
C	10.7309553655	10.3232939654	1.4861312832
H	10.9087420751	11.4037429034	1.6058320456
C	11.4841197257	8.1404596687	0.7948511976
H	12.2579072046	7.4844339941	0.3588740197
C	8.5069983253	10.6770775812	2.629627703
H	8.4583932873	10.3843894625	3.7064153548
H	8.804550253	11.7433565889	2.5744577234
H	7.4813116983	10.5637708638	2.2235887323
C	4.8796798856	2.1431614245	7.0404671197
H	4.6982109076	1.1802139462	6.5176652243
H	5.6709787585	1.9510696429	7.800555639
H	3.9571578839	2.4135647186	7.5942223991
C	13.0486308878	10.1134457189	0.4625152168
H	13.0385465772	11.2203020531	0.5270088655

H	13.8940573477	9.7518344386	1.0895783109
H	13.2888012247	9.834334034	-0.586539809
C	7.5027140657	3.6540472063	2.9736878289
H	8.4898767902	4.1343485346	3.1568108713
H	7.6621862168	2.5614772855	2.8714914141
H	7.1357422358	4.0561289911	2.0069149311

3.3. 1^{asym} xyz-coordinates

1asym @ BP86-D3/def2-SVP

As	7.9225619341	10.0583634496	4.1134187887
As	9.8855832323	8.7674556493	4.4208787141
C	7.6459945197	9.3203370147	2.2865424568
C	7.3638387467	7.9563178982	1.9808296563
C	7.679627012	10.2614568693	1.2197347707
C	7.0235279807	12.6604586784	1.7050399219
C	8.0664687137	11.4499620993	7.1113784844
C	8.0379696214	11.6953537464	1.4821983466
C	9.7055127416	12.4626276229	5.5876211107
C	10.637195585	9.2792236344	6.1544460061
C	10.3744118141	10.4435108421	6.9465025398
C	13.2339774033	5.8382490066	4.2703233913
H	14.0388119253	5.811102881	3.5151614391
C	7.4498538803	13.4192432736	5.7749371401
C	11.6320461699	8.3649382501	6.6404620092
C	9.4013692571	12.0954843845	1.4369870554
C	9.3659163157	11.4709624837	6.5428919285
C	12.9639446599	7.0503820347	4.9348943465
C	11.4688349168	4.735156284	5.494992428
H	10.8815875183	3.8290098345	5.7230726334
C	9.71764412	13.4563132852	1.6042301203
H	10.7780142765	13.7610098204	1.5721866603
C	7.3822881028	14.012675122	1.8599485665
H	6.5878232737	14.75853955	2.0339858927
C	12.5010702516	4.6669244755	4.5382815367
C	7.1259210148	7.5716912673	0.6430715368
H	6.9101099934	6.51152581	0.4290260586
C	11.0848489645	10.6637271045	8.1443978725
H	10.8569752938	11.574708178	8.7239390316
C	7.1327764159	12.4293488661	6.7240773445
H	6.1142645129	12.3916488537	7.1482060261
C	7.423432533	9.8571368615	-0.1065583279
H	7.4620880399	10.6099407568	-0.9118933529
C	8.7239975281	14.433657635	1.8114725298
C	8.7435537438	13.4217394892	5.2238885933
H	9.0002244234	14.1620114459	4.4511391586
C	7.2937245487	6.9018338563	3.042520451
C	11.1521416839	5.931462969	6.1634343218
C	12.3328190646	8.6157282906	7.832277006

H 13.0870311368 7.8830421207 8.1666034209
C 11.9182975255 7.0964160595 5.8920506544
C 13.7294014754 8.308295262 4.5976228572
H 14.1989406068 8.7576618972 5.4970525294
H 13.0330086772 9.0736371375 4.1901859807
H 14.518098883 8.1143349372 3.8427539751
C 7.6728768444 10.3307835651 8.0465716145
H 7.7536879047 9.3554555418 7.5197816729
H 6.6288859168 10.4484583191 8.401237121
H 8.3444131594 10.2679767392 8.9277918686
C 5.5859368717 12.2215228441 1.845690062
H 5.2547287926 11.5989962745 0.989113855
H 4.9020117404 13.0893201446 1.9409305728
H 5.4755975994 11.5877102831 2.7534156598
C 11.0542514434 12.4299868557 4.9174278152
H 11.8813163015 12.3853491914 5.6561728325
H 11.1993148972 13.3051459322 4.2540260567
H 11.1294875837 11.50620102 4.2999245782
C 7.1454898224 8.511729462 -0.399350544
H 6.950464092 8.1955414924 -1.4372131971
C 6.1708982687 6.843851827 3.9123896989
C 12.0680585755 9.7677113401 8.5965565975
H 12.6162685832 9.9604859266 9.5327105353
C 6.1169648268 5.8420394786 4.8975215242
H 5.2476136023 5.8129212093 5.5776532892
C 8.2239437581 4.9396174185 4.1493307632
H 9.0397041885 4.2050839504 4.2428141237
C 10.4841183636 11.0629528513 1.2614664841
H 10.5008192289 10.375437553 2.1416890739
H 11.4837027538 11.5331148186 1.1685060169
H 10.3025473246 10.4235209497 0.3729065615
C 5.0588054927 7.8579097758 3.8010852142
H 5.4173083348 8.8473043858 4.1692134387
H 4.1757862462 7.5580876776 4.40149492
H 4.7438233064 8.0067250012 2.7475541582
C 9.0958884811 15.8824418428 2.0318570962
H 9.9278745227 16.2004165822 1.3686877674
H 9.4356274459 16.0576057111 3.0783128143
H 8.2343511736 16.5578996414 1.8518715802
C 8.3278126725 5.9376448674 3.1593023045
C 7.1365527578 4.8789945757 5.0352317239
C 9.9740314179 6.0032315737 7.1010919922
H 9.5855823923 4.9944708413 7.3440789749
H 9.1576217081 6.5821415999 6.6126274031
H 10.2269596424 6.5342660432 8.0410738159
C 12.7759574376 3.3802315839 3.7923191284
H 12.0055381547 3.1965285618 3.0101491287
H 12.7605325537 2.5005699035 4.4704923853

H 13.7615413674 3.4040670351 3.2838352739
C 9.5387205968 5.9565038696 2.2544926304
H 9.362717427 5.3693433292 1.3248569208
H 10.4176622824 5.5272114294 2.7765826955
H 9.7987816506 6.9883555352 1.9506170205
C 6.4041234794 14.4001823986 5.2989165865
H 5.8029223298 13.9573423301 4.4746676472
H 6.8639492317 15.3271669427 4.8997025429
H 5.6990258779 14.6798939672 6.1099289042
C 7.0620398714 3.824893483 6.1167167224
H 7.0997008065 4.2825314753 7.129426846
H 7.9054979911 3.1085227366 6.0437810185
H 6.1155908663 3.2436123233 6.0618920971

3.4. TEMPO xyz-coordinates

TEMPO @ BP86-D3/def2-SVP
C -3.9951352714 -1.6549558323 -0.0989772697
C -1.8227089157 -0.1217573463 -0.0759456973
C -2.4356748731 0.5806393735 1.153751449
C -3.9649450596 0.589240795 1.1482996644
C -4.4688523964 -0.8545433822 1.1322904243
H -2.0861024137 0.0568346698 2.0710436128
H -2.0233703452 1.61100754 1.2026984251
H -4.3485566376 1.1193163296 2.0453184006
H -4.3519216564 1.1506213331 0.2699841803
H -4.105092179 -1.368553044 2.0496142629
H -5.5783724076 -0.8984511051 1.1654467058
N -2.522546782 -1.432144113 -0.3338222025
O -1.9684537529 -2.2043017842 -1.1934108559
C -1.9320476167 0.7528875094 -1.3451973341
H -1.265701797 1.6357983056 -1.2622942331
H -1.6239102802 0.1546996435 -2.2253715333
H -2.9639454685 1.1187086365 -1.5148399934
C -0.3450606401 -0.4520293854 0.1941883621
H 0.2181267382 0.4819314052 0.394663836
H -0.2510398709 -1.1166270816 1.0771622969
H 0.0996943924 -0.9685843721 -0.6764548297
C -4.764667969 -1.2461970465 -1.3751630948
H -4.2919255937 -1.7282890475 -2.2535624343
H -5.8208250877 -1.5790702171 -1.3104262122
H -4.7615398019 -0.1497479757 -1.5338636482
C -4.1827844835 -3.1605160247 0.1534472043
H -3.6002707982 -3.4807004786 1.0413265251
H -5.2541371981 -3.3799712394 0.3370202413
H -3.8331987046 -3.7440230455 -0.7183038322

3.5. TEMPO-H xyz-coordinates

TEMPO-H @ BP86-D3/def2-SVP

C	-3.9491396019	-1.6597282831	-0.0785224748
C	-1.8360203774	-0.1705679065	-0.0570595531
C	-2.4264689827	0.5731187102	1.164111255
C	-3.9566334719	0.576809469	1.1790616658
C	-4.4673567519	-0.8652108473	1.143468398
H	-2.0596405644	0.0714674321	2.0866593093
H	-2.0184214574	1.606426897	1.1747920319
H	-4.3314588626	1.0956107315	2.0868876752
H	-4.3523215373	1.1507413654	0.3129086142
H	-4.1304377154	-1.3882543628	2.0655463783
H	-5.577742325	-0.9021080134	1.139049579
N	-2.464275257	-1.522610578	-0.0926625905
O	-1.9624620456	-2.2180154472	-1.25841125
H	-1.4513353837	-2.9468217518	-0.8583290056
C	-2.008747596	0.6535616647	-1.3555700047
H	-1.3103026607	1.5157241049	-1.3551171031
H	-1.777000673	0.0207234524	-2.2340944028
H	-3.0321390098	1.0557256048	-1.4765480961
C	-0.3293936389	-0.3963035258	0.1818369579
H	0.186007551	0.5708949608	0.3539678866
H	-0.1776182984	-1.0420558973	1.0710911775
H	0.1386098947	-0.8854574213	-0.6949843136
C	-4.6495762151	-1.2074348518	-1.3823480118
H	-4.1200200268	-1.6305241466	-2.2578946815
H	-5.6964162914	-1.574810504	-1.3993539631
H	-4.6822766094	-0.1072806342	-1.49355576
C	-4.2465463713	-3.156681204	0.1420631676
H	-3.7015342997	-3.5253180065	1.0352957843
H	-5.332976704	-3.318235932	0.2979761463
H	-3.9312831671	-3.7535559293	-0.7362571261

3.6. $[1\text{-H}]^-$ xyz-coordinates

$[1\text{-H}]^-$ @ BP86-D3/def2-SVP

As	0.0691254009	1.101674703	0.3610491525
C	1.2800765324	-0.0604369198	2.9040038139
C	2.8344271513	2.2589238285	3.3166385197
H	3.4424632918	3.1698083763	3.4534319946
C	2.8859004184	1.217392105	4.2631163481
H	3.5168628518	1.302773011	5.16238382
C	0.4518018498	-1.3045019716	2.8084650535
C	1.2248937198	0.9868979399	1.9264959896
C	2.0371608572	2.1474527186	2.1662242193
C	2.1152632604	0.0656494779	4.0347208238
H	2.1296677509	-0.7613422396	4.7656900701
C	-1.5992107284	0.0274276386	3.4813317491

H	-1.0685644116	0.5606214986	4.2978344283
H	-2.6595415395	-0.1203520485	3.7684109711
H	-1.5514407572	0.6959904329	2.5873388341
C	3.0021566478	3.1480964387	0.0648495031
C	2.1903838388	5.2985565649	-0.8125131498
C	-0.9295301362	-1.2780490328	3.1466473811
C	3.0489715058	4.1833900784	-0.88501526
H	3.7728415382	4.1112614708	-1.7153369211
C	2.0774903558	3.2390038422	1.1401695783
C	3.8663163846	1.9218329582	-0.0751921594
H	3.2201916382	1.0559178258	-0.3438749802
H	4.3691401683	1.6642180753	0.8790735615
H	4.6290086529	2.0475071014	-0.8687358795
C	1.0607977907	-2.5353566952	2.4429368275
C	1.280439735	5.3666414737	0.2587352953
H	0.5939063965	6.228434348	0.3309018762
C	1.2123769412	4.3571265227	1.2392576316
C	-1.0793178679	-3.7056472514	2.7666018645
C	0.2862563175	-3.7118368843	2.4286315455
H	0.7623674863	-4.6589627281	2.1207213099
C	-1.6673389453	-2.4754850658	3.1173694791
H	-2.7417084642	-2.437826118	3.3604892106
C	2.5047878045	-2.5635389032	1.9988584947
H	2.6451161728	-1.8906631073	1.1253889845
H	2.8140192108	-3.5862602967	1.7020599872
H	3.1928517291	-2.1988294373	2.7889101993
C	2.2174748084	6.363313686	-1.8861202062
H	1.7489412007	7.307572082	-1.5397194957
H	1.6615986041	6.0341521062	-2.7928736203
H	3.2543760481	6.5933455185	-2.2111969044
C	-1.9104209215	-4.9648155753	2.7006642086
H	-1.2779472767	-5.869554886	2.5916686349
H	-2.6047128907	-4.9280078813	1.8330051054
H	-2.5370717723	-5.0922898614	3.6097249399
C	0.2017413526	4.4280303494	2.3615711846
H	-0.4624801743	3.5376471413	2.3333428065
H	-0.4272364672	5.338139977	2.2838293002
H	0.6937053661	4.4224231994	3.3567138709
As	-0.1189854341	-1.2470991628	-0.3099414735
C	-0.5784348695	-0.2623775242	-3.0572942893
C	-3.3731523701	-0.6020572072	-3.0681871973
H	-4.4664020489	-0.7456596692	-3.057593324
C	-2.7354601636	-0.0869919848	-4.2063085381
H	-3.3211115068	0.1798700334	-5.1010847146
C	0.9103474794	-0.10725289	-3.1364851646
C	-1.2217632837	-0.7735845859	-1.8937403278
C	-2.6343240348	-0.9512922326	-1.9166846844
C	-1.3419929009	0.073206198	-4.196146695

H	-0.8184836703	0.4564553668	-5.0875652576
C	1.1069766437	-2.6442580123	-3.3502023885
H	0.2186995005	-2.665081793	-4.0145128214
H	1.8404409289	-3.3939843955	-3.7101442009
H	0.7583335283	-2.9562852163	-2.340053909
C	-3.9386123988	-0.699555497	0.2414790525
C	-4.8582015512	-2.6804172144	1.3824333299
C	1.7223349298	-1.2656211315	-3.2870286714
C	-4.6596941534	-1.2905622486	1.2989054665
H	-5.0735940285	-0.6378817041	2.0865112496
C	-3.3899877334	-1.5378410137	-0.7621758392
C	-3.7014870074	0.7866867865	0.2053029124
H	-2.6211692594	1.0100144102	0.3955141932
H	-3.9349946659	1.2165842103	-0.7902771943
H	-4.3011224762	1.3130780459	0.9748160036
C	1.5081581298	1.1831696669	-3.1494669779
C	-4.3123870634	-3.4904563941	0.3675221815
H	-4.4628280324	-4.5834227768	0.4055253004
C	-3.5728478716	-2.9426115442	-0.6964780288
C	3.7335327867	0.1474654207	-3.3684792017
C	2.9074493572	1.2807642898	-3.2722174302
H	3.3637631244	2.2842353628	-3.270966725
C	3.1184524442	-1.1178614541	-3.3853935057
H	3.7423537504	-2.0226184127	-3.4896962031
C	0.6950864373	2.4391926833	-2.9681125437
H	0.4504806537	2.5412826138	-1.8846384431
H	1.267337873	3.3361069315	-3.2769260441
H	-0.265544303	2.4102956282	-3.5179037929
C	-5.5971835592	-3.2998959042	2.5464375101
H	-6.3398802278	-4.0541260986	2.2091395914
H	-4.8941967798	-3.826033311	3.230118193
H	-6.131532674	-2.5347475262	3.1452573893
C	5.2379789818	0.2838053343	-3.4151022976
H	5.5477839721	1.2564316279	-3.8502724302
H	5.6726876545	0.2326349116	-2.3916415058
H	5.7083283093	-0.5274863841	-4.0092847596
C	-2.9237116385	-3.8362992149	-1.7264154252
H	-1.8168662014	-3.7510562496	-1.664893733
H	-3.197946824	-4.8995442496	-1.5727665679
H	-3.1979584631	-3.5420600941	-2.760642996
H	-1.3433773565	-1.7354486011	0.4850726871

4. Crystallographic Details

Data for **(^{Mes}TerAs)$_2^{asym}$** (CCDC 2174953) was collected at 293 K on a STOE IPDS II diffractometer using Mo-Kα radiation. Data for **1^{sym}** (CCDC 2174952), **1^{asym}** (CCDC 2174950) and **2** (CCDC 2174951) were collected at 100 K on a BRUKER Quest D8 diffractometer using Mo-Kα radiation. The structures have been solved using the SHELXT V2014/1 algorithm[21] employed in the Olex2 platform and refined by means of least-squares procedures on a F2 with the aid of the program SHELXL-2016/6, included in the software package WinGX version 1.63[22] or using CRYSTALS.[23] The Atomic Scattering Factors were taken from International Tables for X-Ray Crystallography.[24] All non-hydrogen atoms were refined anisotropically. All hydrogen atoms were refined by using a riding model. Absorption corrections were introduced by using the MULTISCAN[25] and X-Red program[26]. Drawings of molecules were performed with the program DIAMOND with 50% probability displacement ellipsoids for non-H atoms. H atoms are generally omitted for clarity.

Table S2. Overview of bond metrics of neutral and anionic diarsenes $[(^{Mes}TerAs)_2]^{0,\cdot-}$.

	symmetric		asymmetric	
Bond lengths (Å) & angles (°)	$[(^{Mes}TerAs)_2]^{\cdot-}$	$(^{Mes}TerAs)_2$[27]	$[(^{Mes}TerAs)_2]^{\cdot-}$	$(^{Mes}TerAs)$
As1–As2	2.350(4)	2.276(3)	2.328(4)	2.257(2) Å
As1–C1	1.976(2)	1.964(13)	1.955(2)	1.979(7) Å
As2–C2	1.976(2)	1.964(13)	1.991(2)	1.963(8) Å
As1–As2–C2	94.57(4)	98.5(4)	90.7(1)	94.3(2)°
As2–As1–C1	94.57(4)	98.5(4)	106.2(1)	107.2(2)°

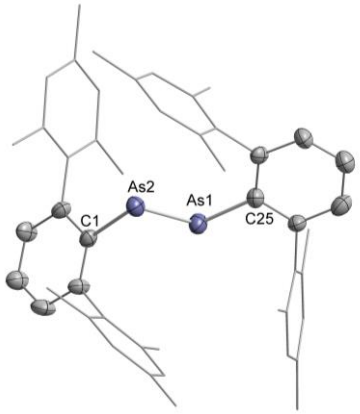

Figure S18. Molecular structure of **(^{Mes}TerAs)$_2^{asym}$** within the crystal. Hydrogen atoms are omitted for clarity, thermal ellipsoids are shown with 50% probability. Co-crystalline toluene molecules are omitted for clarity.

Bond	Length / Angle
C1–As2	1.979(7) Å
C25–As1	1.963(8) Å
As1–As2	2.257(2) Å
C1–As2–As1	94.3(2)°
C25–As1–As2	107.2(2)°

Table S3. Crystal data and structure refinement for **(^{Mes}TerAs)$_2^{asym}$**

Identification code	MesTer2As2asym
Empirical formula	$C_{48}H_{50}As_2$
Formula weight	960.98
Temperature/K	150(2)
Crystal system	triclinic
Space group	*P*-1
a/Å	10.701(6)
b/Å	11.234(7)
c/Å	22.349(14)
α/°	97.97(5)
β/°	102.80(5)
γ/°	94.98(5)
Volume/Å^3	2575(3)
Z	2
ρ_{calc}g/cm^3	1.239
μ/mm^{-1}	1.335
F(000)	1008
Crystal size/mm^3	0.26 × 0.19 × 0.1
Radiation	MoKα (λ = 0.71073)
2Θ range for data collection/°	3.688 to 50.996
Index ranges	-12 ≤ h ≤ 12, -13 ≤ k ≤ 13, -27 ≤ l ≤ 27
Reflections collected	18831
Independent reflections	9186 [R_{int} = 0.0921, R_{sigma} = 0.1528]
Data/restraints/parameters	9186/0/463
Goodness-of-fit on F^2	0.862
Final R indexes [I>=2σ (I)]	R_1 = 0.0739, wR_2 = 0. 1678
Final R indexes [all data]	R_1 = 0. 1468, wR_2 = 0. 1887
Largest diff. peak/hole / e Å^{-3}	1.48/-0.60

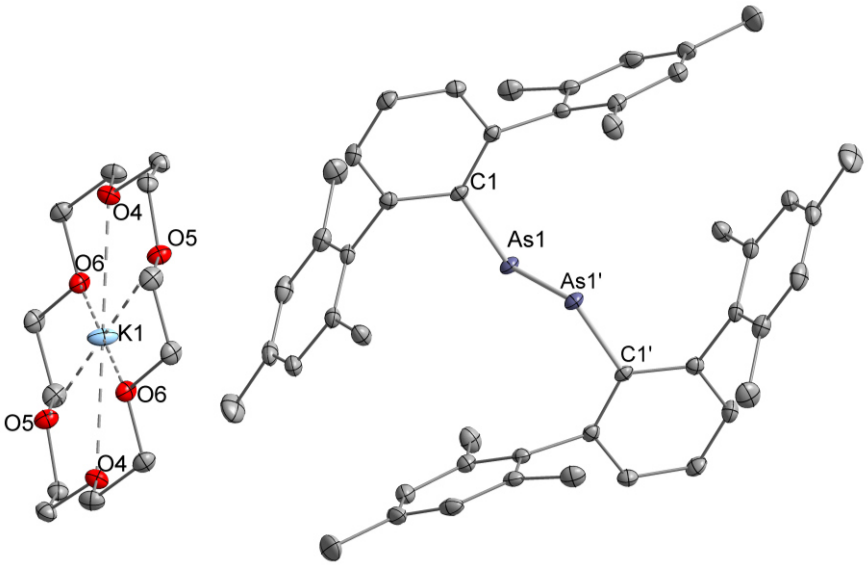

Figure S19. Molecular structure of **1^{sym}** within the crystal. Hydrogen atoms are omitted for clarity, thermal ellipsoids are shown with 50% probability.

Table S4. Crystal data and structure refinement for **1^{sym}**.

Identification code	1sym
Empirical formula	$C_{60}H_{74}As_2KO_6$
Formula weight	1080.13
Temperature/K	100.0
Crystal system	triclinic
Space group	P-1
a/Å	11.2440(5)
b/Å	11.7593(6)
c/Å	11.8985(6)
α/°	69.008(2)
β/°	67.573(2)
γ/°	82.513(2)
Volume/Å^3	1357.69(12)
Z	1
ρ_{calc}g/cm^3	1.321
μ/mm^{-1}	1.357
F(000)	567.0
Crystal size/mm^3	0.411 × 0.169 × 0.156
Radiation	MoKα (λ = 0.71073)
2Θ range for data collection/°	3.918 to 57.356
Index ranges	-15 ≤ h ≤ 15, -15 ≤ k ≤ 15, -16 ≤ l ≤ 16
Reflections collected	81354
Independent reflections	6960 [R_{int} = 0.0419, R_{sigma} = 0.0204]
Data/restraints/parameters	6960/0/319
Goodness-of-fit on F^2	1.044
Final R indexes [I>=2σ (I)]	R_1 = 0.0253, wR_2 = 0.0576
Final R indexes [all data]	R_1 = 0.0317, wR_2 = 0.0592
Largest diff. peak/hole / e Å^{-3}	0.36/-0.34

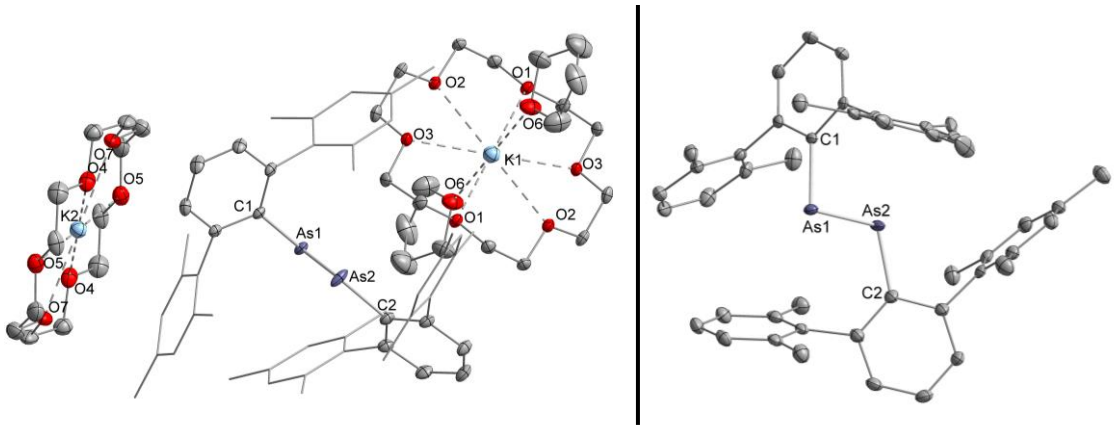

Figure S20. Molecular structure of **1**^{asym} within the crystal (left) and anion from another perspective (right). Both fragments of [K{18c6}]$^+$ are half present in the unit cell with the other halves depicted being symmetry-generated. Statistically, the unit cell contains one molecule of coordinating THF. Two non-coordinating molecules of THF are not depicted. Hydrogen atoms are omitted for clarity. Thermal ellipsoids are shown with 50% probability.

Table S5. Crystal data and structure refinement for **1**^{asym}.

Identification code	1asym
Empirical formula	$C_{72}H_{98}As_2KO_9$
Formula weight	1296.44
Temperature/K	100.0
Crystal system	triclinic
Space group	*P*-1
a/Å	12.6616(6)
b/Å	13.6573(7)
c/Å	20.3961(9)
α/°	91.769(2)
β/°	92.237(2)
γ/°	98.385(2)
Volume/Å^3	3484.2(3)
Z	2
ρ_{calc}g/cm^3	1.236
μ/mm^{-1}	1.072
F(000)	1374.0
Crystal size/mm^3	0.357 × 0.304 × 0.152
Radiation	MoKα (λ = 0.71073)
2Θ range for data collection/°	4 to 57.516
Index ranges	-17 ≤ h ≤ 16, -18 ≤ k ≤ 18, -27 ≤ l ≤ 27
Reflections collected	65832
Independent reflections	17337 [R_{int} = 0.0599, R_{sigma} = 0.0657]
Data/restraints/parameters	17337/12/772
Goodness-of-fit on F^2	1.042
Final R indexes [I>=2σ (I)]	R_1 = 0.0515, wR_2 = 0.1002
Final R indexes [all data]	R_1 = 0.0879, wR_2 = 0.1086
Largest diff. peak/hole / e Å^{-3}	1.13/-0.66

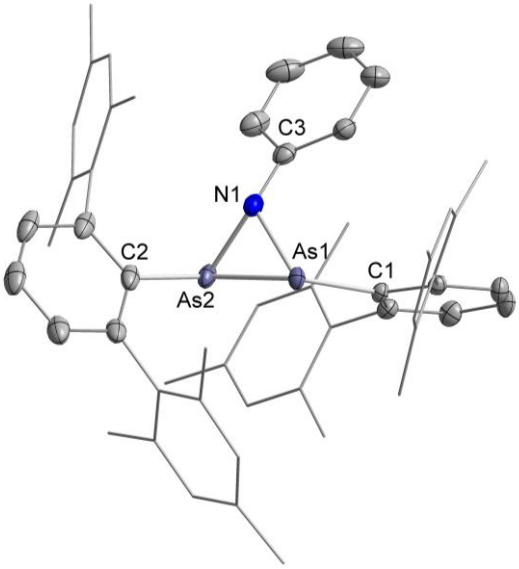

Figure S21. Molecular structure of **2** within the crystal. Hydrogen atoms are omitted for clarity, thermal ellipsoids are shown with 50% probability.

Table S6. Selected bond lengths and angles of **2**.

Bond	Length / Angle
As1-As2	2.429(1) Å
As1-N1	1.902(2) Å
As2-N1	1.904(2) Å
As1-C1	2.000(2) Å
As2-C2	1.983(2) Å
N1-C3	1.406(2) Å
As1-N1-As2	79.3 (1)°
N1-As1-As2	50.4(1)°
N1-As2-As1	50.3(1)°
As1-N1-C3	125.3(1)°
As2-N1-C3	124.8(1)°
C1-As1-N1	106.7(1)°
C1-As1-As2	107.4(0)°
C2-As2-N1	97.8(1)°
C2-As2-As1	100.4(1)°

Table S7. Crystal data and structure refinement for **2**.

Identification code	3
Empirical formula	$C_{54}H_{55}As_2N$
Formula weight	867.83
Temperature/K	100.0
Crystal system	triclinic
Space group	P-1
a/Å	11.2536(14)
b/Å	11.3183(14)
c/Å	20.673(2)
α/°	98.509(3)
β/°	99.330(4)
γ/°	102.359(3)
Volume/Å^3	2492.1(5)
Z	2
ρ_{calc}g/cm^3	1.157
μ/mm^{-1}	1.374
F(000)	904.0
Crystal size/mm^3	0.436 × 0.206 × 0.156
Radiation	MoKα (λ = 0.71073)
2Θ range for data collection/°	3.782 to 54.55
Index ranges	-14 ≤ h ≤ 14, -14 ≤ k ≤ 14, -26 ≤ l ≤ 26
Reflections collected	77651
Independent reflections	11181 [R_{int} = 0.0542, R_{sigma} = 0.0339]
Data/restraints/parameters	11181/0/526
Goodness-of-fit on F^2	1.055
Final R indexes [I>=2σ (I)]	R_1 = 0.0305, wR_2 = 0.0794
Final R indexes [all data]	R_1 = 0.0395, wR_2 = 0.0828
Largest diff. peak/hole / e Å^{-3}	0.56/-0.52

5. References

[1] S. Stoll, A. Schweiger, *Journal of Magnetic Resonance* **2006**, *178*, 42–55.
[2] R. C. Smith, P. Gantzel, A. L. Rheingold, J. D. Protasiewicz, *Organometallics* **2004**, *23*, 5124–5126.
[3] E. A. Mader, E. R. Davidson, J. M. Mayer, *J. Am. Chem. Soc.* **2007**, *129*, 5153–5166.
[4] R. O. Lindsay, C. F. H. Allen, in *Organic Syntheses* (Ed.: John Wiley & Sons, Inc.), John Wiley & Sons, Inc., Hoboken, NJ, USA, **2003**, pp. 96–96.
[5] H. Bürger, U. Wannagat, *Monatshefte für Chemie* **1963**, *94*, 1007–1012.
[6] C. G. Werncke, P. C. Bunting, C. Duhayon, J. R. Long, S. Bontemps, S. Sabo-Etienne, *Angew. Chem. Int. Ed.* **2015**, *54*, 245–248.
[7] M. J. Frisch, G. W. Tricks, H. B. Schlegel, G. E. Scuseria, M. A. Robb, J. R. Cheeseman, G. Scalmani, V. Barone, G. A. Petersson, H. Nakatsuji, X. Li, M. Caricato, A. V. Marenich, J. Bloino, B. G. Janesko, R. Gomperts, B. Mennucci, H. P. Hratchian, J. V. Ortiz, A. F. Izmaylov, J. L. Sonnenberg, D. Williams-Young, F. Ding, F. Lipparini, F. Egidi, J. Goings, B. Peng, A. Petrone, T. Henderson, D. Ranasinghe, V. G. Zakrewski, J. Gao, N. Rega, G. Zheng, W. Liang, M. Hada, M. Ehara, K. Toyota, R. Fukuda, J. Hasegawa, M. Ishida, T. Nakajima, Y. Honda, O. Kitao, H. Nakai, T. Vreven, K. Throssel, J. A. Montgomery Jr., J. E. Peralta, F. Ogliaro, M. J. Bearpark, J. J. Heyd, E. N. Brothers, K. N. Kudin, V. N. Staroverov, T. A. Keith, R. Kobayashi, J. Normand, K. Raghavachrai, A. P. Rendell, J. C. Burant, S. S. Iyengar, J. Tomasi, M. Cossi, J. M. Millam, M. Klene, C. Adamo, R. Cammi, J. W. Ochterski, R. L. Martin, K. Morokuma, O. Farkas, J. B. Foresman, D. J. Fox, *Gaussian 16, Revision C.01*, Gaussian Inc., Wallingford CT, **2016**.
[8] F. Neese, *WIREs Comput Mol Sci* **2018**, *8*, DOI 10.1002/wcms.1327.
[9] F. Neese, F. Wennmohs, U. Becker, C. Riplinger, *J. Chem. Phys.* **2020**, *152*, 224108.
[10] T. Lu, F. Chen, *J. Comput. Chem.* **2012**, *33*, 580–592.
[11] J. P. Perdew, *Phys. Rev. B* **1986**, *33*, 8822–8824.
[12] S. Grimme, J. Antony, S. Ehrlich, H. Krieg, *The Journal of Chemical Physics* **2010**, *132*, 154104.
[13] S. Grimme, S. Ehrlich, L. Goerigk, *J. Comput. Chem.* **2011**, *32*, 1456–1465.
[14] F. Weigend, R. Ahlrichs, *Phys. Chem. Chem. Phys.* **2005**, *7*, 3297.
[15] F. Weigend, *Phys. Chem. Chem. Phys.* **2006**, *8*, 1057.
[16] F. Neese, *The Journal of Chemical Physics* **2001**, *115*, 11080–11096.
[17] F. Neese, *The Journal of Chemical Physics* **2003**, *118*, 3939–3948.
[18] F. Neese, *The Journal of Chemical Physics* **2005**, *122*, 034107.
[19] F. Neese, *EMagRes*, John Wiley & Sons Ltd, Chichester, UK, **2017**.
[20] F. Neese, F. Wennmohs, A. Hansen, U. Becker, *Chemical Physics* **2009**, *356*, 98–109.
[21] G. M. Sheldrick, *Acta Crystallogr., Sect. A: Found. Crystallogr.* **2015**, *71*, 3–8.
[22] L. Farrugia, *J. Appl. Crystallogr.* **1999**, *32*, 837.
[23] P. W. Betteridge, J. R. Carruthers, R. I. Cooper, K. Prout, D. J. Watkin, *J. Appl. Crystallogr.* **2003**, *36*, 1487.
[24] *International Tables for X-Ray Crystallography*, Kynoch Press, Birmingham, England, **1974**.
[25] *SADABS-2016/2*, Bruker, **2016**.
[26] *X-Area, X-Red 1.63.1.0*, STOE, **2016**.
[27] B. Twamley, C. D. Sofield, M. M. Olmstead, P. P. Power, *J. Am. Chem. Soc.* **1999**, *121*, 3357–3367.

3.3 Taming the Stilbene Radical Anion

G. Sieg, I. Müller. K. Weißer, C. G. Werncke, *submitted.*

Abstract

Radical anions appear as intermediates in a variety of organic reductions and have recently garnered interest for their role as mediators for electron-driven catalysis as well as for organic electron conductor materials. Due to their unstable nature, the isolation of such organic radical anions is usually only possible by using extended aromatic systems, whereas non-aromatic unsaturated hydrocarbons have so far only been observed in-situ. We herein report the first isolation, structure and spectroscopic characterization a simple aryl substituted alkene radical anion, namely that of stilbene (1,2-diphenyl ethylene), achieved by encapsulation between two [K{18c6}] cations. The formation of the radical anion is accompanied by Z→E isomerization of the involved double bond, also on a catalytic scale. Employing the linear iron(I) complex $[Fe(NR_2)_2]^-$ as a reductant and coordination site also allows for this transformation, via formation of an iron(II) bound radical anion. The use of the iron complex now also allows for Z->E isomerization of electron richer, simple alkenes bearing either mixed alkyl/aryl or even bis(alkyl) substitution.

Zusammenfassung

Im Zuge dieser Publikation wurde erstmals das bisher nur spektroskopisch beschriebene Stilben-Radikalanion (in **1**) durch Stabilisierung mit zwei [K{18c6}]-Kationen isoliert (Schema 51).[46,139–142] Dies konnte durch die Reduktion von *E*-Stilben mit KC_8 unter Zugabe von $[K\{18c6\}][Fe(N(SiMe_3)_2)_2]$ und einem Äquivalent 18-Krone-6 (18c6) erreicht werden. Die hohe Reduktionskraft von **1** konnte durch Zugabe von Benzophenon gezeigt werden, wobei durch einen Elektronentransfer der analoge Ketyl-Komplex **2** erhalten wurde.

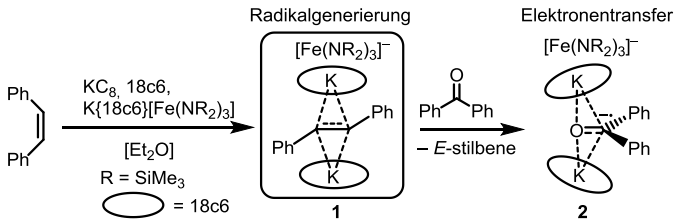

Schema 51. Generierung des Z-Stilben-Radikalanions in **1** durch Reduktion mit KC_8 und Stabilisierung durch zwei [K{18c6}]-Kationen und weiterer Elektronentransfer zum stabilisierten Ketyl-Radikalanion in **2**.

Aufgrund einer vorliegenden Fehlordnung der Stilbeneinheit innerhalb der, durch Röntgenbeugung am Einkristall erhaltenen, Molekülstruktur konnte die zentrale C-C-Bindungslänge in **1** nicht präzise bestimmt werden, jedoch wurde der radikalische Charakter des Stilben-Fragmentes durch EPR-Spektroskopie eindeutig nachgewiesen. Zudem wurde eine Photoabsorption bei λ = 485 nm bestimmt,

was in Einklang mit nicht isolierten Na^+(*E*-Stilben)$^{\bullet-}$ (λ = 494 nm) steht.[140] Ferner lässt sich durch den Elektronentransfer auf Benzophenon zu **2** und auf $[Co^{II}(NR_2)_2]$ zu $[Co^{I}(NR_2)_2]^-$ die erwartete Redoxreaktivität beobachten.

Die beobachtete *Z*- zu *E*-Isomerisierung in **1** wurde weiter untersucht (Schema 52). Dabei konnte eine katalytische Aktivität bei Zugabe von überschüssigen *Z*-Stilben zu **1** beobachtet werden, allerdings scheint **1** unter diesen Bedingungen schnell zu zerfallen. Um dieser Problematik zu entgehen, wurde stattdessen der stark reduzierende Komplex $[Fe^{I}(N(SiMe_3)_2)_2]^-$ (**[Fe^{I}]**) verwendet. Hier konnte bei niedrigen Beladungen (4 mol%) eine katalytische Transformation von *Z*- zu *E*-Stilben mit einer Ausbeute von 95% innerhalb von 45 min beobachtet werden. Auch die elektronenreicheren Substrate *E*-β-Methylstyrol und *E*-3-Hexen konnten so isomerisiert werden, allerdings nur bei deutlich höheren Reaktionszeiten. Auch der Einsatz des sterisch anspruchsvolleren $[Fe^{I}(N(Dipp)(SiMe_3))_2]^-$als Katalysator resultierte in langsameren Reaktionen.

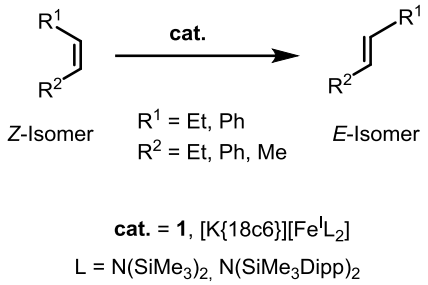

Schema 52. Katalytische *E*- nach *Z*-Isomerisierung von Stilben, β-Methylstyrol und 3-Hexen.

Um diesen Prozess genauer zu verstehen, wurden stöchiometrische Reaktionen der oben genannten Substrate mit **[Fe^{I}]** durchgeführt. Während die Reaktion mit *Z*-3-Hexen ausblieb, konnte im Falle von *E*-β-Methylstyrol ein Gleichgewicht auf der Seite der Edukte mit dem *side-on* Komplex $[Fe(N(SiMe_3)_2)_2$(*E*-β-Methylstyrol)$]^-$ (**4**) beobachtet werden (Schema 53). Die Reaktion von **[Fe^{I}]** mit *Z*-Stilben liefert analog zu **4** den *side-on* Komplex $[Fe(N(SiMe_3)_2)_2$(*E*-Stilben)$]^-$ (**3**), welcher isoliert und vollständig charakterisiert wurde. Die Oxidationsstufe des Eisenions in **3** konnte mit Hilfe von ^{57}Fe-Mößbauer-Spektroskopie auf +II bestimmt werden, wodurch **3** als Eisen(II)Komplex mit einem gebundenen Radikalanion als Liganden beschrieben werden kann, im Gegensatz zu einer möglichen Koordination des neutralen Substrates an ein Eisen(I)ion.

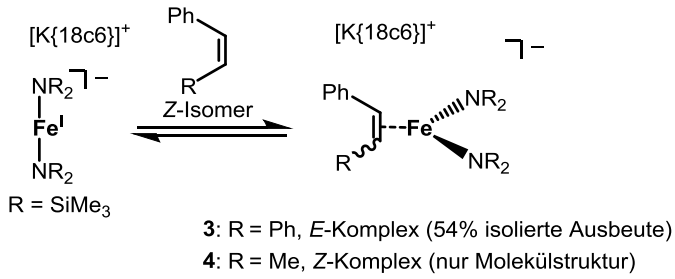

Schema 53. Reversible Koordination von *E*-Stilben und *E*-β-Methylstyrol an **[Fe^{I}]**.

Durch die gesammelten Erkenntnisse kann davon ausgegangen werden, dass im Zuge der katalytischen *Z*- zu *E*-Isomerisierung zunächst das Substrat über seine Doppelbindung an das Eisen(I)ion koordiniert und dabei zum Radikalanion reduziert wird. Durch die Verringerung der Bindungsordnung kann nun der Substituent um die zentrale C-C-Bindungsachse rotieren und in die thermodynamisch günstigere *E*-Konformation übergehen. Der gebildete Komplex überträgt im Gleichgewicht sein Elektron an das Eisen(II)ion und verlässt die Koordinationssphäre, wodurch ein neues *Z*-Stilben Molekül koordinieren kann.

Eigener Anteil

Die Synthese und strukturelle Charakterisierung von **1** und **2**, alle und Katalyse-Experimente, sowie damit zusammenhängende Experimente, sowie die Charakterisierung aller Verbindungen durch IR-, NMR- und UV-Vis-Spektroskopie wurde von mir durchgeführt und ausgewertet. Verbindung **3** und **4** wurden erstmals von *Dr. Igor Müller* synthetisiert und strukturell charakterisiert. Die Röntgenbeugungsexperiemente wurden durch *Dr. Gunnar Werncke* oder durch die Serviceabteilung für Kristallographie der Philipps-Universität-Marburg durchgeführt, die Sturkturlösung und -verfeinerung wurde von mir durchgeführt. Die Elementaranalyse wurde durch die Serviceabteilung Massenspektrometrie und Elementaranalytik der PUM durchgeführt und von mir ausgewertet. Die EPR-Messungen wurden von *Dr. Andreas Stoy* aus der Arbeitsgruppe von *Prof. Dr. Crispin Lichtenberg* (PUM) durchgeführt und von mir mit der entsprechenden Simulation ausgewertet. ^{57}Fe-Mössbauer Messungen wurden von *Kilian Weißer* aus der Arbeitsgruppe von *Prof. Dr. Christian Limberg* (Humbold-Universität zu Berlin) durchgeführt und ausgewertet. Das Manuscript wurde von mir und *Dr. Gunnar Werncke* in Zusammenarbeit verfasst.

ARTICLE

Taming the Stilbene Radical Anion

Grégoire Sieg, [a] Igor Müller,[a] Kilian Weißer[b] and C. Gunnar Werncke*,[a]

Received 00th January 20xx,
Accepted 00th January 20xx

DOI: 10.1039/x0xx00000x

Radical anions appear as intermediates in a variety of organic reductions and have recently garnered interest for their role as mediators for electron-driven catalysis as well as for organic electron conductor materials. Due to their unstable nature, the isolation of such organic radical anions is usualy only possible by using extended aromatic systems, whereas non-aromatic unsaturated hydrocarbons have so far only been observed *in-situ*. We herein report the first isolation, structure and spectroscopic characterization a simple aryl substituted alkene radical anion, namely that of stilbene (1,2-diphenyl ethylene), achieved by encapsulation between two [K{18c6}] cations. The formation of the radical anion is accompanied by *Z*→*E* isomerization of the involved double bond, also on a catalytic scale. Employing the linear iron(I) complex $[Fe(NR_2)_2]^-$ as a reductant and coordination site also allows for this transformation, via formation of an iron(II) bound radical anion. The use of the iron complex now also allows for *Z*→*E* isomerization of electron richer, simple alkenes bearing either mixed alkyl/aryl or even bis(alkyl) substitution.

Introduction

Organic radicals are known to play key roles in many well-established organic reactions. Radical anions, in particular, appear as intermediates in a variety of organic reductions.[1–3] They are intrinsically unstable due to their ability to react subsequently in a multitude of reaction pathways, such as dimerization which is exploited for example in pinacol-type coupling reactions.[1] In recent years, organic radical anions have garnered further importance due to the surge of photoredox catalysis.[4–6] In this context, radical anions are mediators for bond transformations whereas the transmitted electron itself is sometimes considered as a catalyst in analogy to proton-catalysed reactions.[7–9]

As such the understanding of the behaviour of simple radical anions is of longstanding interest, whereas common methods to stabilize such compounds rely on the use of extended aromatic systems or electron withdrawing functional groups, such as carbonyl units, to lower the energy of the involved π* orbitals as well as to disperse of the radical character over an extended π-system.[10–14] In this instance respective radical anions play an important role in organic functional materials such as electric conductors, transistors or magnetic devices.[15–19] Isolable examples of pure carbon-based radical anions are still scarce and concern only aromatic compounds with energetically accessible π*-orbitals, most prominently alkali metal anthracenes and naphthalenes.

In contrast, radical anions of alkene based compounds were so far only observed *in-situ*,[20–23] but are of fundamental interest for nearly a century.[24] Of those, the stilbene radical anion $[S]^{\bullet-}$ (S = stilbene/1,2-diphenylethylene) has been particular subject of extensive EPR[25] and electronic absorption spectroscopic[26–28] as well as cyclovoltammetric[29] analyses. Thereby, the radical anion could only be generated in-situ, either via (electro)chemical reduction,[25,30,31] photolysis[32] or/and radiolysis.[33] It also showed, that Z-stilbene is subject to *Z*->*E* isomerisation, as was extensively examined by Szwarc and others.[25,30,34–36] Kinetic studies indicate that the isomerisation does probably not occur via the initially formed stilbene radical anion (*Z*-$[S]^{\bullet-}$), but the dianion (*Z*-$[S]^{2-}$). The latter stems from reversible disproportionation of $[S]^{\bullet-}$ (into $[S]^{2-}$ and $[S]^0$), and isomerises more rapidly than the radical anion *Z*-$[S]^{\bullet-}$.[36–40]

Herein we report now on the isolation, structure and spectroscopic characterization of the stilbene radical anion, only achieved by its encapsulation between two [K{18c6}] cations. The radical anion readily undergoes electron transfer with excess of stilbene, for which accordingly catalytic *Z*→*E* isomerisation can be observed. Using the linear iron(I) silylamide $[Fe(NR_2)_2]^-$ the catalytic *Z*→*E* isomerisation can conceptionally be extended to 1,2-alkyl/aryl and -dialkyl alkenes, not achievable by the "free" stilbene radical anion, and proceeds via a metal(II) bound radical anion.

Results and discussion

Isolation of the stilbene radical anion

Z-stilbene was reacted with 18-crown-6 and KC_8 in Et_2O in the presence of $[K\{18c6\}][Fe(NR_2)_3]$[41] (R = $SiMe_3$). This resulted in an immediate colour change from light yellow to dark red and ultimately yielded $[(K\{18c6\})_2(E\text{-stilbene})][Fe(NR_2)_3]$ (**1**) in 61% yield (Scheme 1). The use of $[K\{18c6\}][Fe(NR_2)_3]$ is of essence as

[a] *Fachbereich Chemie, Philipps-Universität Marburg, Hans-Meerwein-Straße 4, 35037 Marburg, Germany*
[b] *Institut für Chemie, Humboldt-Universität zu Berlin, Brook-Taylor-Str. 2, 12489 Berlin, Germany.*
† Footnotes relating to the title and/or authors should appear here.
Electronic Supplementary Information (ESI) available: [details of any supplementary information available should be included here]. See DOI: 10.1039/x0xx00000x

in the absence of the additional [K{18c6}] cation no reduction of stilbene was observed, while the trisamide serves as a reductively stable non-coordinating anion. Similar observations were already done during the isolation of a pyridine radical anion.[42] The [K{18c6}] cation is equally important moiety as the use of crypt.222 as potassium masking agent resulted in undefined decomposition. **1** is stable at room temperature under inert conditions for several hours in solution and for months in solid state at –30 °C. Attempts for the isolation of a *Z*-conformer of the radical anion were not successful, in agreement with the observed rapid isomerisation to the thermodynamically more stable *E*-conformer.[25,30,34–36]

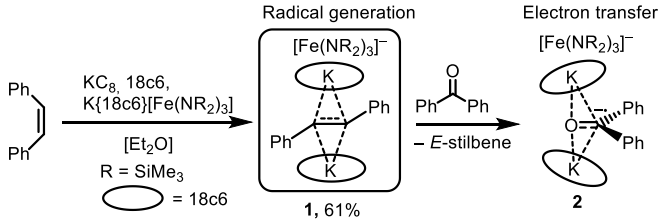

Scheme 1 Synthesis of the bis(cation) stabilized stilbene radical anion **1** and formation of the ketyl complex **2**.

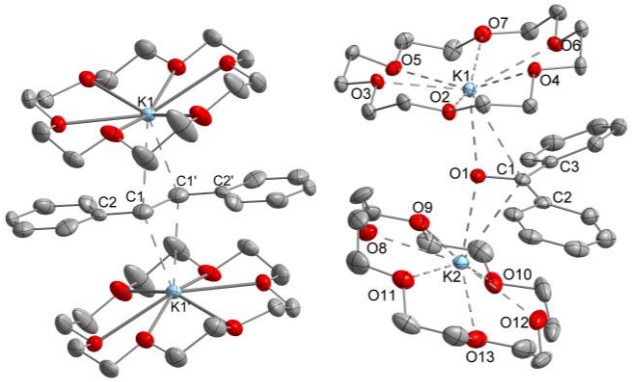

Figure 1. Molecular structure of **1** (left) and **2** (right). Hydrogen atoms and the[Fe(N(SiMe$_3$)$_2$)$_3$]$^-$ anions are omitted for clarity. Selected bond lengths (Å) and angles (°): **1**) C1–C1' 1.415(5) [1.350(7)], C1–C2 1.389(7) [1.488(7)], C2–C1–C1' 127.6(4) [125.7(4)]. Bond metrics of the second disordered part are given in square brackets. **2**) O1–C1 1.299(2), C1–C2 1.452(2), C1–C3 1.473(2), O1–K1 2.724(1), O1–K2 2.701(1), C1–K1 3.172(1), C1–K2 3.134(2), C2–C1–C3 123.3(1), O1–C1–C2 119.1(1), O1–C1–C3 117.5(1).

X-Ray diffraction analysis on suitable crystals revealed the formed E-stilbene unit being encapsulated between two [K{18c6}] cations (Figure 1 left). The potassium atoms are situated above and below the central alkene, which is indicative of charge localisation on the double bond. Due to an intrinsic persistent crystallographic problem, unchanged upon variation of the crystallisation process, the whole stilbene unit is heavily disordered lengthwise over two positions (1:1). Accordingly, this prohibits so far an in-depths discussion of the structural metrics. For example both crystallographic parts exhibit highly different C–C bonds (1.35 Å and 1.41 Å), which are thus only in part elongated in comparison with the free stilbene (1.34 Å).[43]

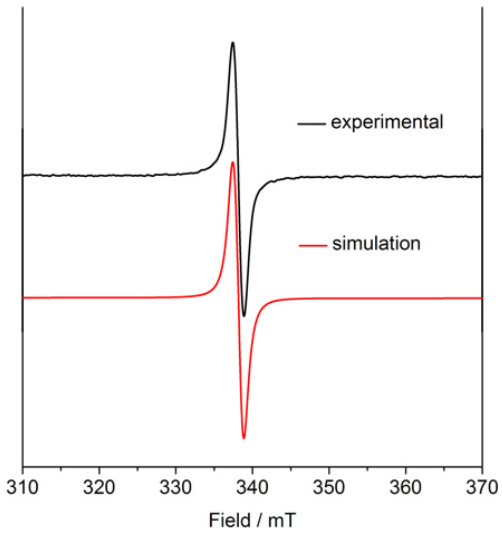

Figure 2. X-band EPR measurement of **1** in frozen toluene solution (9.476718 GHz) collected at 100 K (black) and simulated spectrum (red). S = ½, g = 2.002396.

To support the notion of a stilbene radical anion, X-Band EPR spectroscopy was performed on a frozen solution of **1** (Figure 2) at 100 K. This resulted in a sharp isotropic singlet signal at g = 2.002396, in agreement with the presence of an organic radical anion. No resolved hyperfine coupling was observed, as expected on the basis of previous reports on *in-situ* formed stilbene radical anions.[25,35] This indicated partial delocalisation of the electron over the whole stilbene molecule, favoured by its enforced planar structure. According to the paramagnetic character, the proton NMR spectrum of **1** showed no features beyond the signals attributed to the [K{18c6}] moieties as well as the [Fe(NR$_2$)$_3$]$^-$ anion (Figure S1). UV-Vis spectroscopic examination of **1** in solution (Figure 3) revealed a single absorption band at 485 nm which is in good agreement with *in-situ* generated Na$^+$(*E*-stilbene)$^{\bullet-}$ in THF (494 nm).[39]

The radical anionic nature of **1** was also chemically substantiated as it (incompletely) reduces [Co^{II}(NR$_2$)$_2$] to the corresponding linear cobalt(I) complex [Co^{I}(NR$_2$)$_2$]$^-$ (Figure S8) whose reduction potential (E_{red} = –1.45 V vs Fc/Fc$^+$) is less than of the stilbene ($E_{1/2}$ (*Z*-stilbene) = –2.67 V; $E_{1/2}$ (*E*-stilbene) = –2.70 V vs Fc/Fc$^+$).[29,44,45] Further, if **1** is subjected to benzophenone ($E_{1/2}$ = –2.13 V vs Fc/Fc$^+$) it resulted in intensely blue [(K{18c6})$_2$(Ph$_2$CO)]$_2$[Fe(NR$_2$)$_3$] (**2**), with a characteristic absorption at 685 nm for the ketyl radical anion.[14] **2** can also be independently obtained by reducing Ph$_2$CO with KC$_8$ in the presence of 18-crown-6 and [K{18c6}][Fe(NR$_2$)$_2$]. Having displaced the stilbene unit in **1**, the ketyl radical anion of **2** is now sandwiched between the [K{18c6}] cations (Figure 1 right). These are tilted towards each other by approximately 42.5° to account for the non-planarity of the ketyl unit. The C–O bond length of the ketyl unit in **2** amounts to 1.299(2) Å, which is typical for ketyl radical anions with a reduced C=O bond order by population of the antibonding π^* orbital[44,46] (for benzophenone: d(C-O) = 1.23(1) Å).[47] Interestingly, besides interactions with the ketyl oxygen (d(K1/2–O1) = 2.724(1) / 2.701(1) Å), the potassium cations also exhibit close contacts to the ketyl carbon (d(K1/2–C1) = 3.172(1) / 3.134(2) Å), thus

This journal is © The Royal Society of Chemistry 20xx

Please do not adjust margins

overall coordinating in an asymmetric side-on fashion to the C=O unit. It contrasts the typical end-on coordination of alkali metal ketyl or fluorenyl salts in solid state[14,48] and is likely due to the repulsion of the opposing crown-ethers. Attempts to acquire radical anions of a more electron rich 1,2-alkyl/aryl-substituted ethylene (β-methyl styrene) or even a 1,2-dialkyl ethylene (3-hexene) were not successful.

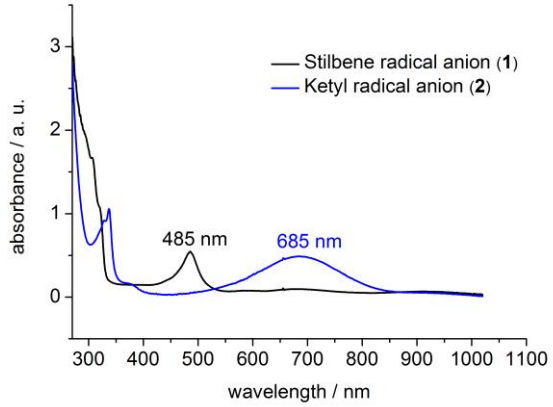

Figure 3. UV-Vis spectrum of **1** and **2** in THF at 300 K.

Behaviour of the radical anion 1 towards ethylene derivatives

The unequivocal isolation of the cation stabilized stilbene radical anion **1** now offered the opportunity to study its behaviour in solution towards further stilbene and other, more electron rich derivatives (namely β-methyl styrene and 3-hexene). First, quenching **1** with D_2O yielded purely E-stilbene with no evidence of either bisbenzyl, stemming from disproportionation of the radical anion into stilbene and the stilbene dianion, or tetraphenylbutane from possible dimerisation of the radical anion under these conditions, as well as deuterium incorporation.

Treatment of **1** with an equimolar amount of *E*-stilbene in THF-d_8 yielded no signs of the added stilbene by proton NMR spectroscopy at room temperature or at –80 °C (Figure S6). Only upon increasing the amount of *E*-stilbene to up to 10 equivalents a very broad signal centred at the median signal position of *E*-stilbene (7.39 ppm) emerged (Figure S7). This speaks to rapid electron transfer between **1** and the added stilbene, that effectuates paramagnetic line broadening. Interestingly, the stilbene addition is accompanied by the appearance of a minor set of signals at around 7.05 ppm as well as at 2.93 ppm, whose amount (approx. 10% with regards to employed **1**) is unaffected by quenching of the reaction mixture with D_2O. We tentatively attributed this to the formation of 1,2,3,4-tetraphenyl butane due to stilbene radical anion dimerisation. Given that such a behaviour is absent for **1** itself, it implicates that the presence of additional stilbene leads to minor amounts of free, unstabilised radical anions lacking [K{18c6}] in solution, thus allowing for C–C coupling.

Upon addition of an excess of *Z*-stilbene (Table 1) to a solution of **1** (4 mol%) in [D8]THF substrate conversion to *E*-stilbene is observed within the first 2.5 h (27% E-product) after which the reaction stops, visible by a colour change from deep yellow to colourless. This is likely due to degradation of the stilbene radical anion, such as before mentioned unproductive dissociation into stilbene and its dianion, or radical anion dimerisation.[37,39] Given the involvement of the stilbene radical anion in this transformation, unsurprisingly KC_8 itself catalyses also its *Z*→*E* transformation in THF. In Et_2O no isomerisation is observed, showing the importance of potassium cation complexation. Analogous isomerisation reactions of an 1,2-alkyl/aryl-substituted *Z*-ethylene (*Z*-β-methyl styrene) or Z-1,2-dialkyl ethylene derivatives (*Z*-3-hexene) by **1**, or KC_8 were not observed.

Iron mediated Z->E isomerisation of alkenes

To overcome these shortcomings in terms of *Z*→*E* isomerisation of alkylated ethylene derivatives we contemplated on formation and isomerisation of such species in the coordination sphere of a highly reducing metal complex (Scheme 2). For that we chose the iron(I) silylamide $[Fe^{I}(NR_2)_2]^-$ (E_{red} –2.07 V),[49] which was already proven for the formation of iron(II) bound radical anions of ketones and related nitrogen derivatives (imines and aldimines).[44] Further, distinct yet slow *Z*→*E* isomerisation was observed for an ethylene bridged bisphosphine (cis-1,2-bis(diphosphino)ethylene).[41] Indeed, by using 4 mol% of $[K\{18c6\}][Fe^{I}(NR_2)_2]$ *Z*-stilbene is converted by 95% within 45 minutes. Intriguingly, *Z*-β-methylstyrene as well as even *Z*-3-hexene are now also transformed, however needing higher catalyst loadings (10 mol%) and substantially longer reaction times (Figure 4). The slower reaction is to be expected due to the general increase of the π*-orbital energy in case of alkyl substituents.

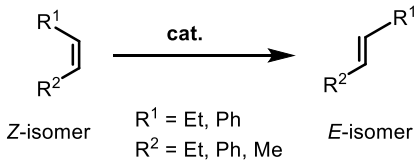

cat. = **1**, $[K\{18c6\}][Fe^{I}L_2]$

L = $N(SiMe_3)_2$, $N(SiMe_3Dipp)_2$

Scheme 2. Catalytic *Z* to *E* conversion of alkenes with $[Fe^{I}]$ as catalyst.

Table 1 Catalytic isomerization of *Z* alkenes in [D8]THF. (R = $SiMe_3$)

catalyst	R^1	R^2	cat. (mol%)	reaction time	conversion (%)
1	Ph	Ph	4	2h30	27%
	Ph	Me	5	20h	0%
KC_8	Ph	Ph	4	5 min	100%
$K\{18c6\}[Fe^{I}(NR_2)_2]$	Ph	Ph	4	45 min	**95%**
	Ph	Me	10	6h30	**82%**
	Et	Et	10	7d	**75%**
K{18c6} $[Fe^{I}(NR\{Dipp\})_2]$	Ph	Ph	10	3h45	5,4%
	Ph	Ph	10	24h	12%
$K\{18c6\}[Fe^{II}(NR_2)_3]$	Ph	Ph	10	3h45	0%

Mechanistic examination of these catalytic reactions gave pseudo-first order kinetics for these transformations, with no

Please do not adjust margins

Please do not adjust margins

signs of an induction phase. To further substantiate the direct involvement of [K{18c6}][Fe^{I}(NR$_2$)$_2$] we conducted poisoning experiments, to rule out the involvement of *in-situ* formed iron nanoparticles or similar decomposition species. Addition of stoichiometric amounts of 2,2'-bipyridine to the reaction mixture, proven to bind tightly to [Fe(NR$_2$)$_2$]$^-$,[50] stopped the reaction. Upon addition of further [Fe(NR$_2$)$_2$]$^-$ the reaction resumed (Figure 4, bottom right). Conversely, the reaction is unaffected by the addition of an excess of PCy$_3$ which does not interact with [Fe(NR$_2$)$_2$]$^-$,[49] but influences the activity of nanoparticles.[51,52] Further, the divalent complex [K{18c6}][Fe^{II}(NR$_2$)$_3$] (R = SiMe$_3$), a possible degradation product, was also not catalytically active. To explore the steric effect of the iron(I) catalyst, the same reactions were conducted with the sterically more demanding complex [K{18c6}][Fe^{I}(NR{Dipp})$_2$][53] (Table 1). While a *Z* to *E* isomerization is observable for stilbene, the reaction proceeds considerably slower.

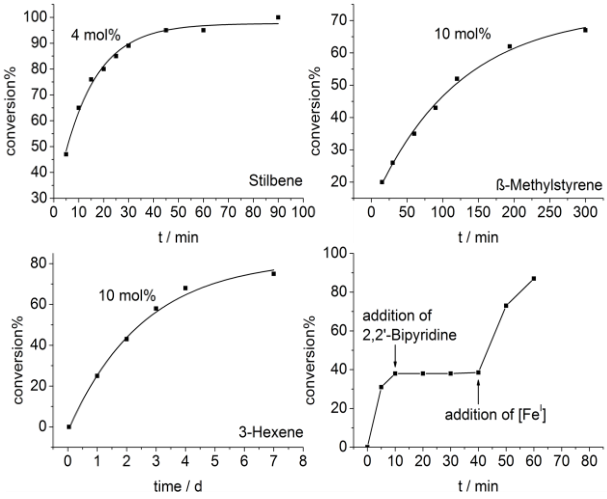

Figure 4. Catalytic *Z* to *E* conversion for stilbene (top left), ß-methylstyrene (top right), 3-hexene (bottom left) using [Fe^{I}] as catalyst and poisoning experiment with 2,2'-bipyridine (bottom right).

Stoichiometric treatment of [K{18c6}][Fe(NR$_2$)$_2$] with the substrates in Et$_2$O resulted in an instantaneous change of colour of the solution from green to red/brown in case of Z-stilbene. Crystallisation from the pentane layered Et$_2$O filtrate gave the *side-on* complex [K{18c6}][Fe(NR$_3$)$_2$(*E*-stilbene)] (**3**) in good yields (54) and purity (Scheme 3). For *Z-ß*-methyl styrene the colour change upon substrate addition was less pronounced, whereas only few crystals of the π-alkene complex **4** were obtained besides mostly unreacted [K{18c6}][Fe(NR$_2$)$_2$]. Unsurprisingly, in case of the even more electron rich Z-3-hexene no direct evidence of π-alkene complex formation was evident. Within **3** the substrate coordinates to the iron ion in a η^2 fashion (Figure 5, left). The central C–C bond (1.438(10) Å) is significantly elongated in comparison with free stilbene (1.338 Å)[43], yet similar to other iron(I) alkene complexes.[54] The Fe-N distances (1.99 Å) are bigger than in the iron(I) precursor (1.92 Å)[49] and three coordinate iron(II) halide complexes (1.95 – 1.97 Å)[55] but comparable to previously reported π-alkyne iron complexes (1.97 – 2.00 Å).[56] No evidence of the formation of a *Z*-alkene complex (e.g. by in-situ proton NMR spectroscopy) was found, hinting to rapid bond isomerisation.

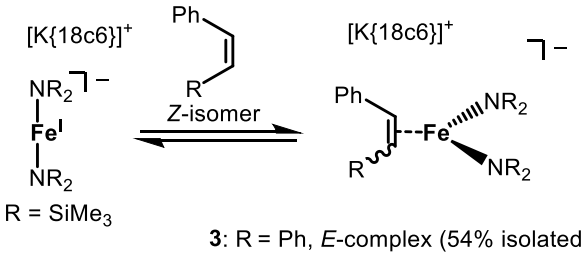

3: R = Ph, *E*-complex (54% isolated yield)
4: R = Me, *Z*-complex (X-ray structure only)

Scheme 3. Synthesis of the side-on alkene complexes **3** and **4** (top).

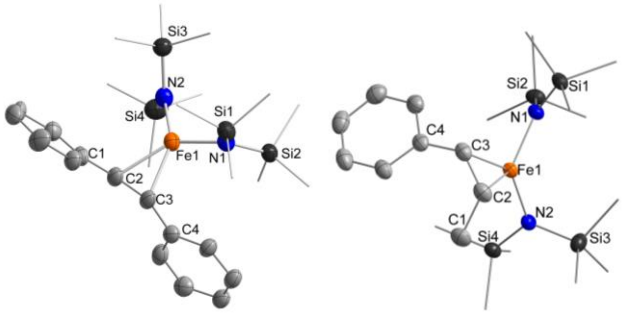

Figure 5. Molecular structure of the complex anion in **3** (left) and **4** (right). H atoms and [K{18c6}]$^+$ are omitted for clarity. Selected bond lengths (Å) and angles (°): **3**) Fe1–N1 1.994(5), Fe1–N2 1.990(3), Fe1–C2 2.157(5), Fe1–C3 2.142(8), C2–C3 1.438(10), N1–Fe1–N2 116.7(2). **4**) Fe1–N1 1.997(1), Fe1–N2 1.981(1), Fe1–C2 2.066(2), Fe1–C3 2.091(2), C2–C3 1.416(3), N1–Fe1–N2 118.3(1).

The structure of the anion in **4** is similar to the one found for **3** with a slightly shorter C2–C3 distance (1.416(3) Å) but otherwise comparable bond metrics. ^{1}H-NMR spectroscopic examination of isolated **3** gave a resonance for their SiMe$_3$-groups at –6.01 ppm (Figure S3). This signal position exhibit a light high-field shift in comparison to comparable π-alkyne iron or three-coordinate- iron(II) compounds (–1.88 to –4.05 ppm).[44,55,57] Additional resonances at 92.7 ppm, 91.2 ppm and –25.3 ppm are attributed to substrate protons. Importantly, dissolution of pristine **3** gives rise to a signal belonging to the initially employed [Fe(NR$_2$)$_2$]$^-$ as well as E-stilbene. This implicated a dissociation equilibrium of **3** in solution, corroborated by measuring a 1:1 mixture of *Z*-stilbene and [K{18c6}][Fe(NR$_2$)$_2$]. Similar observations are made for mixing the iron(I) precursor with *Z-ß*-methyl styrene that resulted in a signal at –5.36 ppm attributed to the SiMe$_3$ groups of **4** (Figure S4). Here the equilibrium is situated mostly on the educt side, which explains the absence of any paramagnetic signals of the bound substrate as well as overwhelming recrystallization of the starting materials. For the even more electron rich *Z*-3-hexene no signs of a π-complex are observed in solution. In all cases however, complete transformation of the employed *Z* alkene to the E-isomer is observed. In view of isolation of the *Z*-conformer of *ß*-methyl styrene in **4**, it thus indicates a very weak binding of *Z-ß*-methyl styrene to [Fe(NR$_2$)$_2$]$^-$.

This journal is © The Royal Society of Chemistry 20xx

Please do not adjust margins

Please do not adjust margins

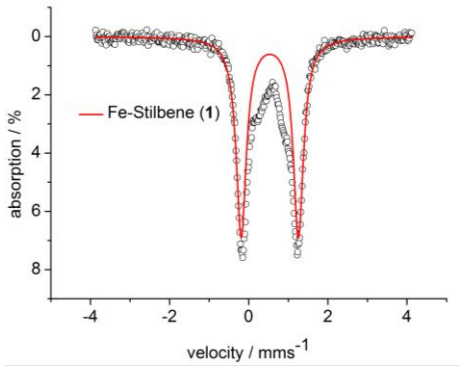

Figure 6. Zero-field ^{57}Fe-Mössbauer spectrum of **3** at 13 K. δ = 0.53 mms^{-1}, ΔQ = 1.44 mms^{-1}.

To gain insights into the electronic situation of the formed π-complexes, zero-field ^{57}Mößbauer spectroscopy was employed. The spectrum of **3** at 13 K shows a doublet signal for the main species with an isomer shift of δ = 0.53 mms^{-1} and a quadrupole splitting of ΔQ = 1.44 mms^{-1}. The isomer shift corresponds very well with low coordinate iron(II) complexes ([Fe(NR$_2$)$_3$]$^-$: δ = 0.59 mms^{-1}, ΔQ = 0.60 mms^{-1} ; [Fe(NR$_2$)$_2$I]$^-$: δ = 0.63 mms^{-1}, ΔQ = 0.60 mms^{-1}; [Fe(NR$_2$)$_2$OCPh$_2$$^{(\bullet)}$]$^{(-)}$: δ = 0.62 mms^{-1}, ΔQ = 1.20/1.83 mms^{-1})[44,49,58]. As such, the Mössbauer data implicates the formulation of **3** as an iron(II) bound alkene radical anion. Such a description is plausible in view of DFT and CASSCF studies on the interaction of alkynes with [Fe(NR$_2$)$_2$]$^-$ [57] and a T-shaped iron(I) complex[59] which were best described as metal(II) bound alkyne radical anions. X-band EPR spectroscopic measurements at 100 K performed on **3** in THF gave no pronounced features, as expected for a non-Kramers iron(II) ion (S = 2), with only a very weak absorption at g = 2.002224 (Figure S13). The latter likely corresponds to decomposition of **3**, or possibly minimal dissociation into the neutral iron(II) amide and the free radical anion. To elaborate on the latter possibility, **3** was treated with KNR$_2$ and 18c6 which however did not lead to extrusion of stilbene as a radical anion and formation of **1** (Scheme 4, top). Similarly, the inverse reaction of **1** with an excess of [Fe^{II}(NR$_2$)$_2$] - to recoordinate the radical anion under formation of **3** - was not successful. As such the isomerisation of the ethylene derivative in **3** likely proceeds in the coordination sphere of the iron ion, and substrate dissociation occurs not as a free radical anion but as a neutral species. Overall, we thus propose for iron a catalytic cycle that starts with Z-alkene binding to the linear iron(I) silylamide (Scheme 4, bottom). The formed a π-complex (**A**, as in complex **4**) can also be described as an iron(II) bound Z-alkene radical anion (**A'**). Subsequently, weakening of one of the Fe–C would allow for rotation along the C–C bond (**B**). Such an asymmetric substrate binding was found as a stable and energetically feasible state in case of related alkyne chromium complexes.[57] This yields in an *E*-alkene complex (**C/C'**, as complex **3**). Subsequently, the formed *E*-alkene is replaced by the next *Z*-alkene.

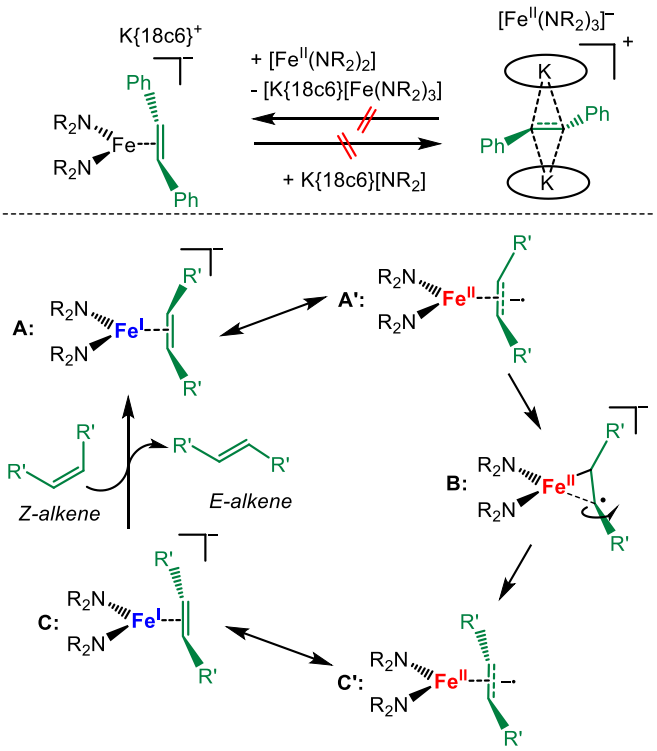

Scheme 4. Top: Attempted interconversion of 3 and 1. Bottom: Proposed mechanism for the *Z* to *E* isomerization of alkenes with [Fe^{I}] as catalyst. Coordination of the *Z*-alkene to the metal ion as π- (**A**) or radical anion (**A'**) complex ; **B**: Rotation along the C–C bond; **C/C'** *E*-alkene complex.

Conclusions

In conclusion, we presented the isolation and characterisation of a long time elusive simple alkene radical anion, namely in form of the *E*–stilbene radical anion. This otherwise fleeting species is stabilized by encapsulation between two [K{18c6}] units. Similarly, coordination of stilbene to the highly reducing iron(I) complex [Fe(NR$_2$)$_2$]$^-$ (R = SiMe$_3$) leads to a situation best described as a metal(II) bound alkene radical anion. In both cases, the radical anion formation can be used for catalytic *Z*→*E* isomerisation of C=C double bonds. Whereas the stilbene radical anion can only isomerize itself. In case of iron the isomerisation can be conceptionally extended to harder to reduce 1,2-alkyl/aryl and dialkyl ethylene. This study thus gives new avenues to obtain very simple organic radical anions either by direct isolation or in the coordination sphere of a highly one-electron reducing metal centre, which is under current scrutiny.

Author Contributions

G. S. and I. M. carried out the synthetic work and analytical characterization, including the crystallographic studies. K. W. performed the ^{57}Fe Mössbauer analysis. G. S. and C. G. W. wrote the manuscript.

This journal is © The Royal Society of Chemistry 20xx

Please do not adjust margins

Please do not adjust margins

Conflicts of interest

There are no conflicts to declare.

Acknowledgements

We thank Prof. Dr. Christian Limberg (HU Berlin) for access to the Mössbauer spectrometer as well as Dr. Andreas Stoy and Prof. Dr. Crispin Lichtenberg for the acquisition of EPR-spectroscopic data. The Deutsche Forschungsgemeinschaft is acknowledged for funding (grant WE5627/4-2).

Notes and references

1 T. Wirth, *Angew. Chem. Int. Ed. Engl.*, 1996, **35**, 61–63.
2 M. L. Di Vona and V. Rosnati, *J. Org. Chem.*, 1991, **56**, 4269–4273.
3 M. Ephritikhine, *Chem. Commun.*, 1998, 2549–2554.
4 M. Zhang, W. D. Rouch and R. D. McCully, *Eur. J. Org. Chem.*, 2012, 6187–6196.
5 S. Okamoto, K. Kojiyama, H. Tsujioka and A. Sudo, *Chem. Commun.*, 2016, **52**, 11339–11342.
6 S. Okamoto, R. Ariki, H. Tsujioka and A. Sudo, *J. Org. Chem.*, 2017, **82**, 9731–9736.
7 A. Studer and D. P. Curran, *Nat. Chem.*, 2014, **6**, 765–773.
8 D. W. Borhani and F. D. Greene, *J. Org. Chem.*, 1986, **51**, 1563–1570.
9 D. Leifert, C. G. Daniliuc and A. Studer, *Org. Lett.*, 2013, **15**, 6286–6289.
10 K. Kato and A. Osuka, *Angew. Chem. Int. Ed.*, 2019, **131**, 9074–9082.
11 M. Irwin, R. K. Jenkins, M. S. Denning, T. Krämer, F. Grandjean, G. J. Long, R. Herchel, J. E. McGrady and J. M. Goicoechea, *Inorg. Chem.*, 2010, **49**, 6160–6171.
12 M. Irwin, T. Krämer, J. E. McGrady and J. M. Goicoechea, *Inorg. Chem.*, 2011, **50**, 5006–5014.
13 M. Irwin, L. R. Doyle, T. Krämer, R. Herchel, J. E. McGrady and J. M. Goicoechea, *Inorg. Chem.*, 2012, **51**, 12301–12312.
14 T. A. Scott, B. A. Ooro, D. J. Collins, M. Shatruk, A. Yakovenko, K. R. Dunbar and H.-C. Zhou, *Chem. Commun.*, 2009, 65–67.
15 C. S. Sevov, R. E. M. Brooner, E. Chénard, R. S. Assary, J. S. Moore, J. Rodríguez-López and M. S. Sanford, *J. Am. Chem. Soc.*, 2015, **137**, 14465–14472.
16 Y. Che, A. Datar, X. Yang, T. Naddo, J. Zhao and L. Zang, *J. Am. Chem. Soc.*, 2007, **129**, 6354–6355.
17 X. Zhan, A. Facchetti, S. Barlow, T. J. Marks, M. A. Ratner, M. R. Wasielewski and S. R. Marder, *Adv. Mater.*, 2011, **23**, 268–284.
18 H. Iwamura, *Polyhedron*, 2013, **66**, 3–14.
19 S. Kumar, Y. Kumar, S. Keshri and P. Mukhopadhyay, *Magnetochemistry*, 2016, **2**, 42.
20 G. J. Hoijtink and P. H. Van der Meij, *Z. physik. Chem. Neue Folge*, 1959, **20**, 1–14.
21 M. Szwarc, in *Application of Spectroscopic and Electrochemical Techniques in Studies of Chemistry of Radical Anions and Dianions. In: Mamantov, G. (eds) Characterization of Solutes in Nonaqueous Solvents.*, Springer, Boston, MA, 1978.
22 J. Matsuda, J. Jagur-Grodzinski and M. Szwarc, *Proc. R. Soc. Lond. A*, 1965, **288**, 212–223.
23 H. Muto, K. Nunome and K. Matsuura, *J. Am. Chem. Soc.*, 1991, **113**, 1840–1841.
24 W. Schlenk and E. Bergmann, *Justus Liebigs Ann. Chem.*, 1928, **463**, 1–97.
25 F. Gerson, H. Ohya-Nishiguchi, M. Szwarc and G. Levin, *Chem. Phys. Lett.*, 1977, **52**, 587–589.
26 H. Suzuki, K. Koyano, T. Shida and A. Kira, *Bull. Chem. Soc. Jpn.*, 1982, **55**, 3690–3701.
27 H. Suzuki, K. Ogawa, T. Shida and A. Kira, *Bull. Chem. Soc. Jpn.*, 1983, **56**, 66–74.
28 C. N. R. Rao, V. Kalyanaraman and M. V. George, *Appl. Spectrosc. Rev.*, 1970, **3**, 153–228.
29 O. Abdul-Rahim, A. N. Simonov, J. F. Boas, T. Rüther, D. J. Collins, P. Perlmutter and A. M. Bond, *J. Phys. Chem. B*, 2014, **118**, 3183–3191.
30 K. Nozaki, A. Naito, T.-I. Ho, H. Hatano and S. OKazaki, *Chem. Lett.*, 1989, 511–514.
31 G. F. Wright, *J. Am. Chem. Soc.*, 1939, **61**, 2106–2110.
32 T. Majima, M. Fukui, A. Ishida and S. Takamuku, *J. Phys. Chem.*, 1996, **100**, 8913–8919.
33 J. R. Langan and G. A. Salmon, *J. Chem. Soc., Faraday Trans. 1*, 1982, **78**, 3645.
34 C. S. Johnson and R. Chang, *J. Chem. Phys.*, 1965, **43**, 3183–3192.
35 R. Chang and C. S. Johnson, *J. Chem. Phys.*, 1967, **46**, 2314–2316.
36 S. Sorensen, G. Levin and M. Szwarc, *J. Am. Chem. Soc.*, 1975, **97**, 2341–2345.
37 T. A. Ward, G. Levin and M. Szwarc, *J. Am. Chem. Soc.*, 1975, **97**, 258–261.
38 G. Levin, T. A. Ward and M. Szwarc, *J. Am. Chem. Soc.*, **96**, 270–272.
39 H. C. Wang, G. Levin and M. Szwarc, *J. Am. Chem. Soc.*, 1977, **99**, 2642–2647.
40 L. R. Dosser, J. B. Pallix, G. H. Atkinson, H. C. Wang, G. Levin and M. Szwarc, *Chem. Phys. Lett.*, 1979, **62**, 555–561.
41 C. G. Werncke and I. Müller, *Chem. Commun.*, 2020, **56**, 2268–2271.
42 I. Müller and C. G. Werncke, *Chem. Eur. J.*, 2021, **27**, 4932–4938.
43 A. Hoekstra, P. Meertens and A. Vos, *Acta Crystallogr. B: Struct. Sci. Cryst. Eng. Mater.*, 1975, **31**, 2813–2817.
44 G. Sieg, Q. Pessemesse, S. Reith, S. Yelin, C. Limberg, D. Munz and C. G. Werncke, *Chem. Eur. J.*, 2021, **27**, 16760–16767.
45 O. Abdul-Rahim, A. N. Simonov, T. Rüther, J. F. Boas, A. A. J. Torriero, D. J. Collins, P. Perlmutter and A. M. Bond, *Anal. Chem.*, 2013, **85**, 6113–6120.
46 K. C. MacLeod, I. M. DiMucci, E. P. Zovinka, S. F. McWilliams, B. Q. Mercado, K. M. Lancaster and P. L. Holland, *Organometallics*, 2019, **38**, 4224–4232.
47 E. B. Fleischer, N. Sung and S. Hawkinson, *J. Phys. Chem.*, 1968, **72**, 4311–4312.
48 Z. Hou, A. Fujita, T. Koizumi, H. Yamazaki and Y. Wakatsuki, *Organometallics*, 1999, **18**, 1979–1985.
49 C. G. Werncke, P. C. Bunting, C. Duhayon, J. R. Long, S. Bontemps and S. Sabo-Etienne, *Angew. Chem. Int. Ed.*, 2015, **54**, 245–248.
50 I. Müller, C. Schneider, C. Pietzonka, F. Kraus and C. G. Werncke, *Inorganics*, 2019, 117.
51 D. Gärtner, S. Sandl and A. Jacobi von Wangelin, *Catal. Sci. Technol.*, 2020, **10**, 3502–3514.
52 J. F. Sonnenberg and R. H. Morris, *Catal. Sci. Technol.*, 2014, **4**, 3426–3438.
53 C.-Y. Lin, J. C. Fettinger, F. Grandjean, G. J. Long and P. P. Power, *Inorg. Chem.*, 2014, **53**, 9400–9406.
54 Y. Yu, J. M. Smith, C. J. Flaschenriem and P. L. Holland, *Inorg. Chem.*, 2006, **45**, 5742–5751.
55 C. G. Werncke, J. Pfeiffer, I. Müller, L. Vendier, S. Sabo-Etienne and S. Bontemps, *Dalton Trans.*, 2019, **48**, 1757–1765.
56 R. Weller, I. Müller, C. Duhayon, S. Sabo-Etienne, S. Bontemps and C. G. Werncke, *Dalton Trans.*, 2021, **50**, 4890–4903.
57 I. Müller, D. Munz and C. G. Werncke, *Inorg. Chem.*, 2020, **59**, 9521–9537.

 This journal is © The Royal Society of Chemistry 20xx

Please do not adjust margins

Please do not adjust margins

58 A. Eichhöfer, Y. Lan, V. Mereacre, T. Bodenstein and F. Weigend, *Inorg. Chem.*, 2014, **53**, 1962–1974.
59 J. C. Ott, H. Wadepohl and L. H. Gade, *Inorg. Chem.*, 2021, **60**, 3927–3938.

This journal is © The Royal Society of Chemistry 20xx

Please do not adjust margins

Taming the Stilbene Radical Anion

Grégoire Sieg,[1] Igor Müller[1], Kilian Weißer[2] and C. Gunnar Werncke[1]

[1] Chemistry Department, Philipps-University, Hans-Meerwein-Str. 4, 35043 Marburg, Germany. E-mail: gunnar.werncke@chemie.uni-marburg.de.

[2] Institut für Chemie, Humboldt-Universität zu Berlin, Brook-Taylor-Str. 2, 12489 Berlin, Germany.

Table of Content

1. General considerations 3
2. Synthesis and Analysis 4
2.1. Synthesis of $[K\{18c6\}]_2[C_{14}H_{12}][Fe^{II}(N(SiMe_3)_2)_3]$ (1) 4
2.2. Synthesis of $[K\{18c6\}]_2[Ph_2CO][Fe^{II}(N(SiMe_3)_2)_3]$ (2) 5
2.3. Synthesis of $[K\{18c6\}][Fe(N(SiMe_3)_2)_2((E)$-stilbene)] (3) 6
2.4. Synthesis of $[K\{18c6\}]_2[Fe(N(SiMe_3)_2)_2((Z)$-ß-methylstyrene)] (4) 7
2.5. Reaction of 1 with *E*-stilbene (1 equivalent) 8
2.6. Reaction of 1 with *E*-stilbene (1, 5, 10 equivalents) 9
2.7. Reaction of 1 with $[Co^{II}(N(SiMe_3)_2)_2]$ 9
2.8. IR Spetroscopy 11
2.9. ^{57}Mössbauer spectroscopy 12
2.10. EPR spectroscopy 13
2.11. UV Vis spectroscopy 14
3. Catalysis 17
3.1. General procedure 17
3.2. Z to E isomerization of stilbene with KC8 as catalyst 17
3.1. *Z* to *E* isomerization of stilbene with 1 as catalyst 17
3.2. *Z* to *E* isomerization of stilbene with $[K\{18c6\}][Fe^{I}(N(SiMe_3)_2)_2]$ as catalyst 18
3.3. *Z* to *E* isomerization of stilbene with $[K\{18c6\}][Fe^{I}(N(Dipp)(SiMe_3))_2]$ as catalyst 22
3.4. *Z* to *E* isomerization of ß-methylstyrene with $[K\{18c6\}][Fe^{I}(N(SiMe_3)_2)_2]$ as catalyst 22
3.5. *Z* to *E* isomerization of 3-hexene with $[K\{18c6\}][Fe^{I}(N(SiMe_3)_2)_2]$ as catalyst 24
3.6. Poisoning experiment 27
4. Crystallography 29
5. References 34

1. General considerations

All manipulations were carried out in a glovebox under a dry argon atmosphere, unless indicated otherwise. Used solvents were dried by continuous distillation over sodium metal for several days, degassed via three freeze-pump cycles and stored over molecular sieves 4 Å. Deuterated solvents were used as received, degassed via three freeze-pump cycles and stored over molecular sieves 4 Å. The ^{1}H-NMR spectra were recorded on a BRUKER AV 300 and BRUKER HD 500 NMR spectrometer (Bruker Corporation, Billerica, MA, USA). Chemical shifts are reported in ppm relative to the residual proton signals of the solvent. $w_{1/2}$ is the line width of a signal at half its maximum intensity. Integrals of the broad signals of the hmds units were obtained directly or by peak fitting (in case of overlapping signals) using the MestreNova software package (Mestrelab, Santiago de Compostela, Spain). IR measurements were conducted on a Bruker Alpha ATR-IR spectrometer (Bruker Corporation, Billerica, MA, USA). Elemental analyses were performed by the "in-house" service of the Chemistry Department of the Philipps University Marburg, Germany using a CHN(S) analyzer vario MICRO Cube (Elementar Analysensysteme GmbH, Langenselbold, Germany). UV/Vis-spectra were recorded on an AnalytikJena Specord S600 diode array spectrometer (AnalytikJena, Jena, Germany). EPR spectra were recorded on a BRUKER Magnettech ESR5000 spectrometer. EPR simulations were performed using the program EasySpin.[1]

Mößbauer spectra were recorded on a SeeCo MS6 spectrometer. The spectrometer comprises the following instruments: A Janis CCS-850 cryostat, including a CTI-Cryogenics closed cycle 10K refrigerator and a CTI-Cryogenics 8200 helium compressor. Temperature was controlled by a LakeShore 335 temperature controller. Spectra were recorded using a LND45431 Kr gas proportional counter with beryllium window connected to the SeeCo W204 gamma-ray spectrometer. The W204 includes high voltage supply, a 10 bit and 5 µs ADC and two single channel analyzers. Motor control and recording of spectra was taken care of by the W304 resonant gamma-ray spectrometer. For the reported spectra a Rivertec MCo7.114 source (57Co in Rh matrix) with an activity of about 1 GBq was used. Spectra were recorded in plastic sample holders with about 30 mg of sample at 13 K and data was accumulated for about 48 hours each. Mößbauer data was processed and simulated using the WMOSS4 program ver. F (www.wmoss.org). Isomeric shifts are referenced to alpha-iron at room temperature.

(*Z*)-Stilbene, (*Z*)-propenylbenzene and (*Z*)-3-hexene were purchased from commercial sources. [Fe(N(SiMe$_3$)$_2$)$_2$], [Co(N(SiMe$_3$)$_2$)$_2$], K{18c6}[M(N(SiMe$_3$)$_2$)$_2$] (Fe and Co), were prepared according to literature procedures.[2–4] KC_8 was prepared by mixing respective amounts of graphite (previously dried in vacuo via heatgun) with freshly cut potassium metal. The mixture was heated in vacuo via heat gun until all potassium metal had reacted.

2. Synthesis and Analysis

2.1. Synthesis of $[K\{18c6\}]_2[C_{14}H_{12}][Fe^{II}(N(SiMe_3)_2)_3]$ (1)

$[K\{18c6\}][Fe(N(SiMe_3)_2)_3]$ (297 mg, 0.35 mmol, 1.00 eq.), 18c6 (93 mg, 0.35 mmol, 1.00 eq.) and KC_8 (50 mg, 0.37 mmol, 1.05 eq.) were suspended in 2 mL of Et_2O. (*Z*)-stilbene (64 mg, 0.35 mmol, 1.00 eq.) was added. The mixture was filtered and the resulting dark brown solution was layered with 2 mL of *n*-pentane to afford **1**•(18c6)($[K\{18c6\}][Fe(N(SiMe_3)_2)_3]$) as dark brown-yellow single crystals (260 mg, 0.19 mmol, 61%).

^{1}H-NMR ([D8]THF, 300 MHz, 300 K, ppm): 3.47 (s, 48H, O-CH_2), –2.54 (br, 54H, $SiMe_3$)

Notes:

Due to paramagnetically induced signal broadening, the proton signals for the stilbene radical anion could not be detected.

The signal integral for $[K\{18c6\}]^+$ is determined by subtracting the amount of solvent residue signal from the overlapping singals at 3.47 ppm.

Elemental analysis: calculated ($C_{98}H_{216}Fe_2K_3N_6O_{24}Si_{12}$) C 48.46 H 8.96 N 3.46; experimental C 48.99 H 8.42 N 3.91
IR (ATR, cm^{-1}): 2942 (w), 2887 (w), 1560 (w), 1472 (w), 1453 (w), 1352 (w), 1280 (w), 1233 (m), 1105 (s), 976 (s), 864 (m), 823 (s), 780 (m), 749 (m), 7088 (w), 658 (m), 609 (w), 529 (w), 502 (w).

Crystals, suitable for X-ray diffraction analysis were obtained by layering a solution of **1** in Et_2O with *n*-pentane at –40 °C.

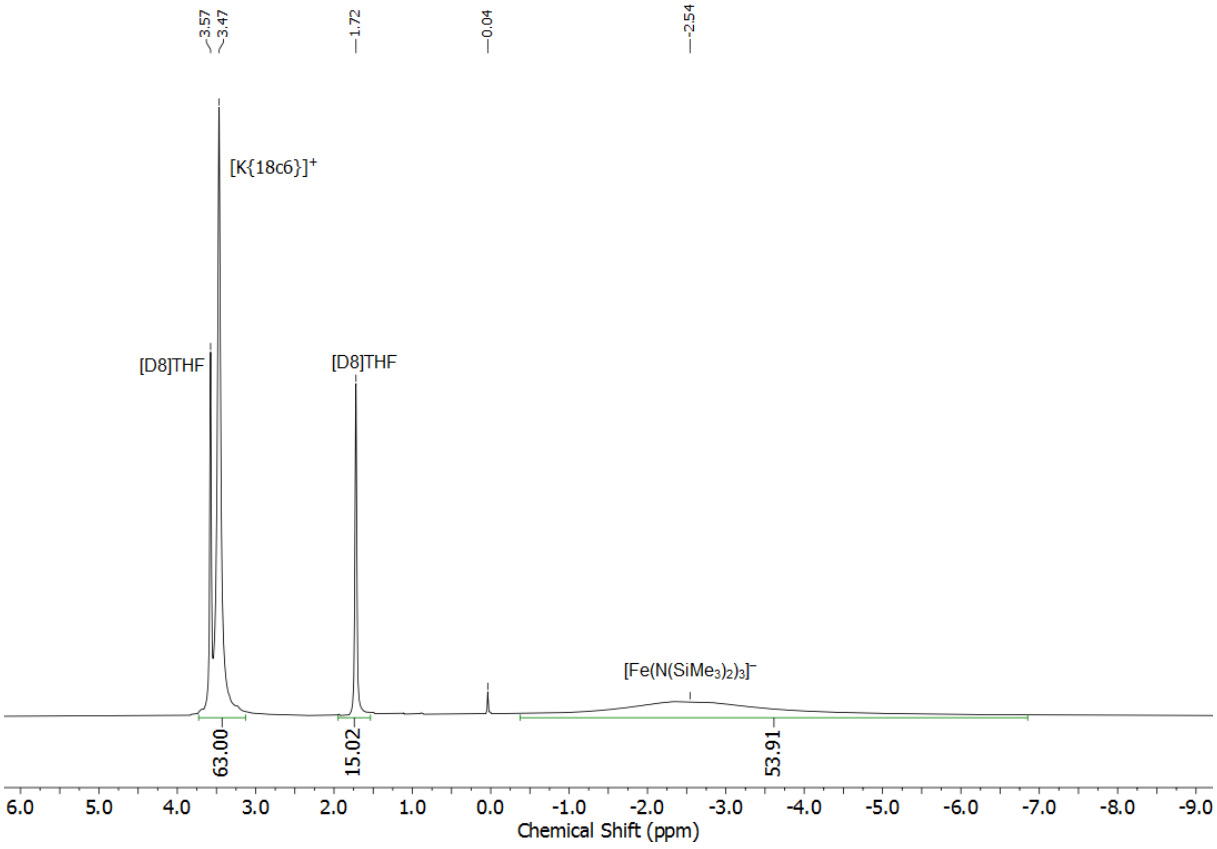

Figure S1. ^{1}H NMR spectrum of **1** in [D8]THF at 300 K, 300 MHz.

2.2. Synthesis of $[K\{18c6\}]_2[Ph_2CO][Fe^{II}(N(SiMe_3)_2)_3]$ (2)

$[K\{18c6\}][Fe(N(SiMe_3)_2)_3]$ (50 mg, 0.08 mmol, 1.00 eq.), 18c6 (21 mg, 0.08 mmol, 1.00 eq.) and KC_8 (12 mg, 0.09 mmol, 1.12 eq.) were suspended in 2 mL of Et_2O. Benzophenone (16 mg, 0.08 mmol, 1.00 eq.) was added. The mixture was filtered and the resulting dark blue solution was layered with 2 mL of *n*-pentane to afford **2** as blue single crystals (56 mg, 0.04 mmol, 52%).

Alternative Synthesis:

1•(18c6)([K{18c6}][Fe(N(SiMe$_3$)$_2$)$_3$]) (63 mg, 0.026 mmol, 1.00 eq.) and benzophenone (5 mg, 0.026 mmol, 1.00 eq) were dissolved in 2 mL of Et_2O. The solution immediately turned into deep blue and was layered with 2 ml of *n*-pentane to afford a mixture of **2** and *E*-stilbene as crystalline solid.

^{1}H-NMR ([D8]THF, 300 MHz, 300 K, ppm): 3.45 (s, 48H, O-CH_2), –2.42 (br, 54H, $SiMe_3$)

Notes:

Due to paramagnetically induced signal broadening, the proton signals for the ketyl radical anion could not be detected.

Elemental analysis: calculated ($C_{55}H_{112}FeK_2N_3O_{13}Si_6$) C 49.82 H 8.51 N 3.17; experimental C 47.81 H 8.67 N 3.42; low C-values can be attributed to the formation of siliconcarbide during the combustion process.
IR (ATR, cm^{-1}): 2942 (w), 2885 (m), 1602 (vw), 1579 (vw), 1554 (vw), 1451 (w), 1389 (vw), 1352 (m), 1284 (vw), 1233 (m), 1105 (s), 978 (s), 864 (s), 823 (s), 778 (m), 749 (m), 706 (m), 658 (m), 609 (w), 529 (vw)

Crystals, suitable for X-ray diffraction analysis were obtained by layering a solution of **2** in Et_2O with *n*-pentane at –40 °C.

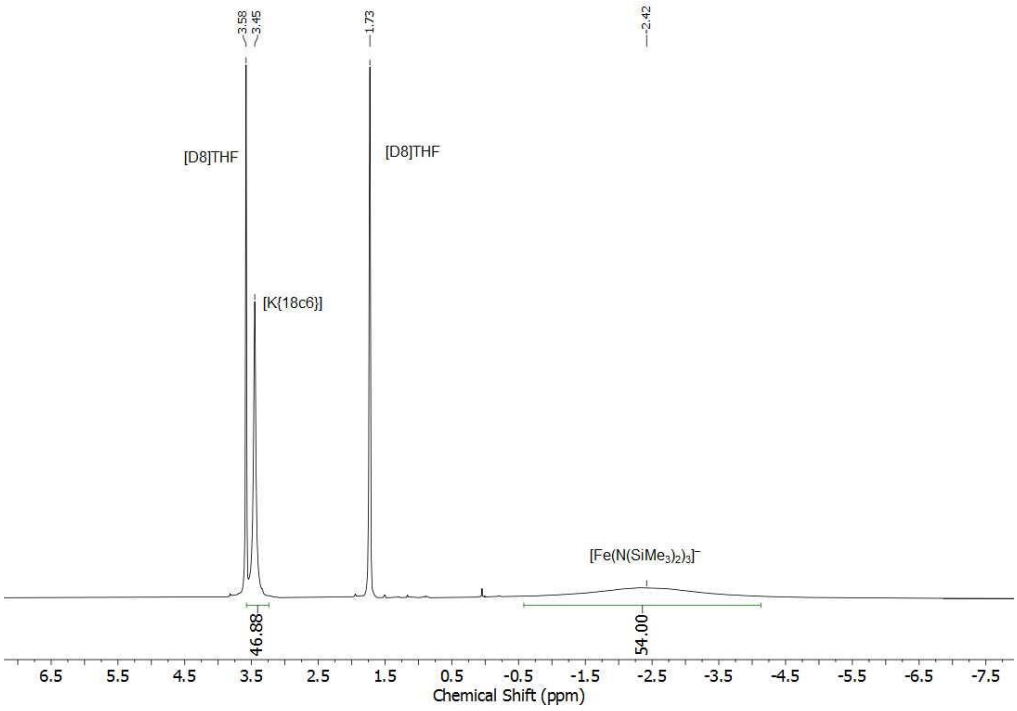

Figure S2. ^{1}H NMR spectrum of **2** in [D8]THF at 300 K, 300 MHz.

2.3. Synthesis of [K{18c6}][Fe(N(SiMe$_3$)$_2$)$_2$((*E*)-stilbene)] (3)

[K(18c6)][Fe((N(SiMe$_3$)$_2$)$_2$] (150 mg, 0.22 mmol. 1.00 eq) and (*Z*)-stilbene (40 mg, 0.22 mmol, 1.00 eq.) were dissolved in 2 mL of Et_2O. The resulting red solution was layered with 2 mL of *n*-pentane. The resulting red solid was filtered off and dried under vaccum to afford **3** (102 mg, 0.12 mmol, 54%).

^{1}H-NMR ([D8]THF, 300 MHz, 300 K, ppm): 92.69 (br, 1H), 91.24 (br, 0.5H), 1.94 (48H, O-CH_2), –6.01 (br, 36H, -$SiMe_3$), –25.29 (br, 3H).

Elemental analysis: calculated ($C_{42}H_{80}FeKN_2O_7Si_4$; **3** + E_2O) C 54.10 H 8.65 N 3.00; experimental C 54.03 H 8.23 N 3.05

IR (ATR, cm^{-1}): 2940 (w), 2885 (w), 1587 (w), 1486 (w), 1470 (w), 1350 (w), 1282 (w), 1233 (m), 1173 (w), 1103 (s), 980 (s), 961 (s), 885 (m), 866 (m), 821 (s), 776 (m), 749 (m), 702 (m), 691 (m), 661 (m), 611 (m), 520 (w).

Crystals, suitable for X-ray diffraction analysis were obtained by layering a solution of **3** in Et_2O with *n*-pentane at –40 °C.

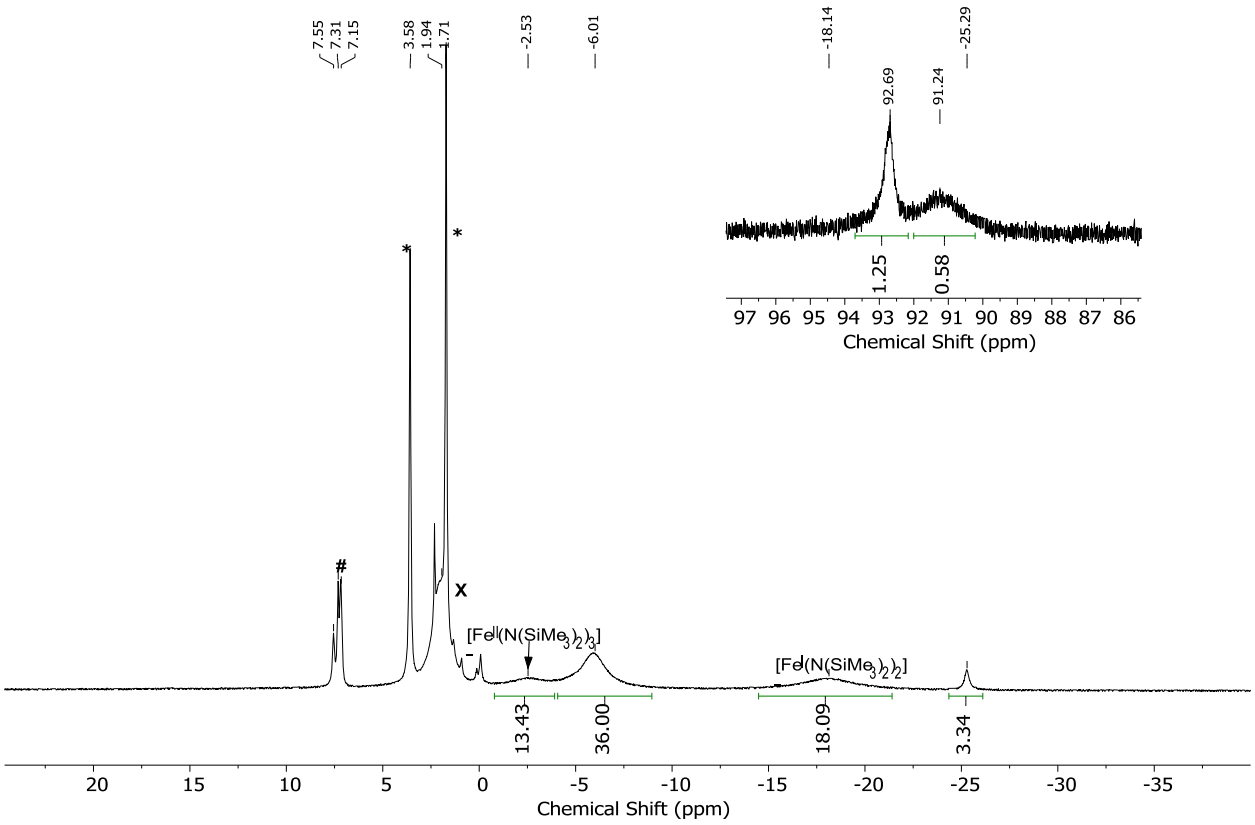

Figure S3. ^{1}H NMR spectrum of **3** in [D8]THF at 300 K, 300 MHz. *: [D8]THF, #: *E*-stilbene, X: [K{18c6}]+[D8]THF

2.4. Synthesis of $[K\{18c6\}]_2[Fe(N(SiMe_3)_2)_2((Z)$-ß-methylstyrene)] (4)

$[K(18c6)][Fe((N(SiMe_3)_2)_2]$ (68.0 mg, 0.10 mmol, 1.00 eq.) and (*Z*)-ß-methylstyrene (11.8 mg, 0.10 mmol, 1.00 eq.) were dissolved in 3 mL of Et_2O. After several hours, the reaction solution turned from green-yellow to brown. The solution was layered with 2 mL of *n*-pentane. The resulting red solid was filtered off and dried under vacuum to afford a mixture of **4,** $[K(18c6)][Fe((N(SiMe_3)_2)_2]$ and *E*-ß-methylstyrene.

^{1}H-NMR ([D8]THF, 300 MHz, 300 K, ppm): –0.35 (br, O-CH_2, 36 H), –5.36 (br, -$SiMe_3$, 4.4 H), –18.36 (br, -$SiMe_3$, 36 H)

Crystals, suitable for X-ray diffraction analysis were obtained by layering a solution of **4** in Et_2O with *n*-pentane at –40 °C.

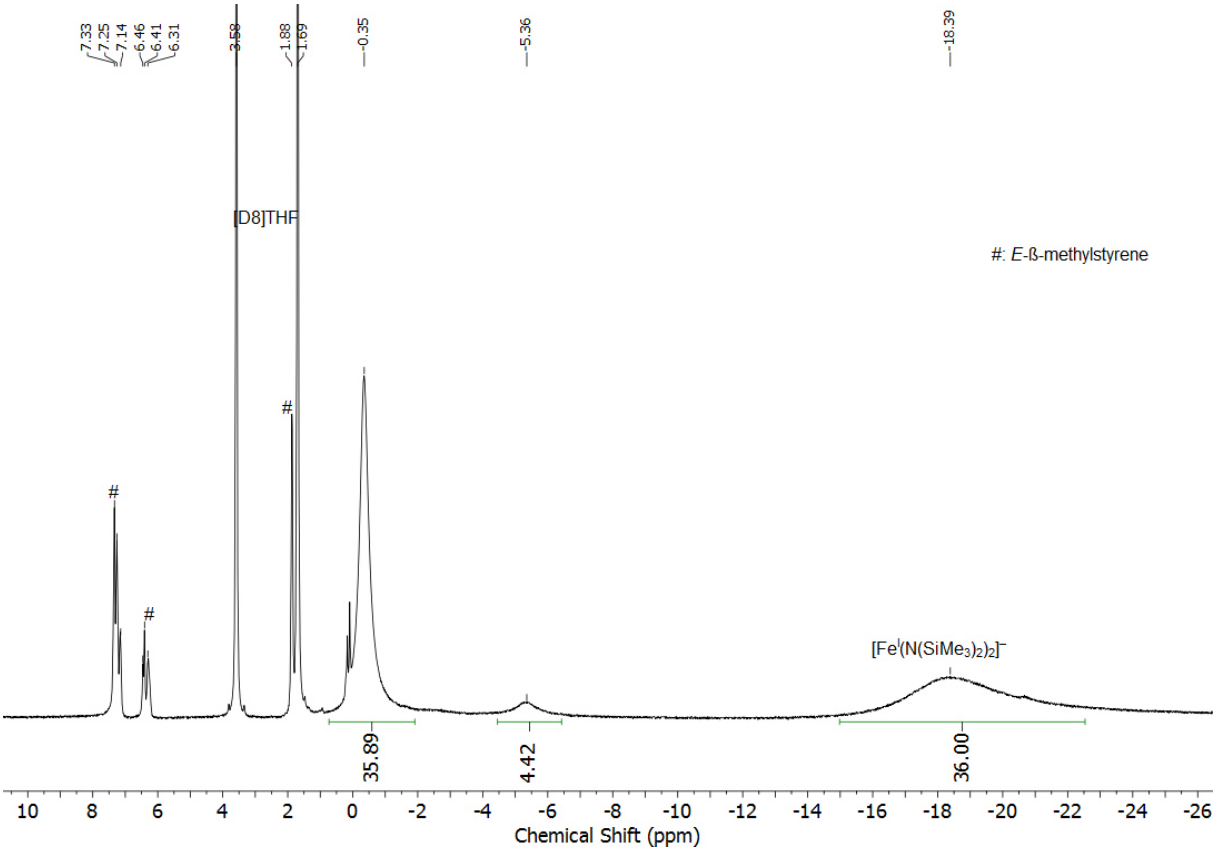

Figure S4. ^{1}H NMR spectrum of **4** in [D8]THF at 300 K, 300 MHz. #: *E*-ß-methylstyrene.

2.5. Reaction of 1 with *E*-stilbene (1 equivalent)

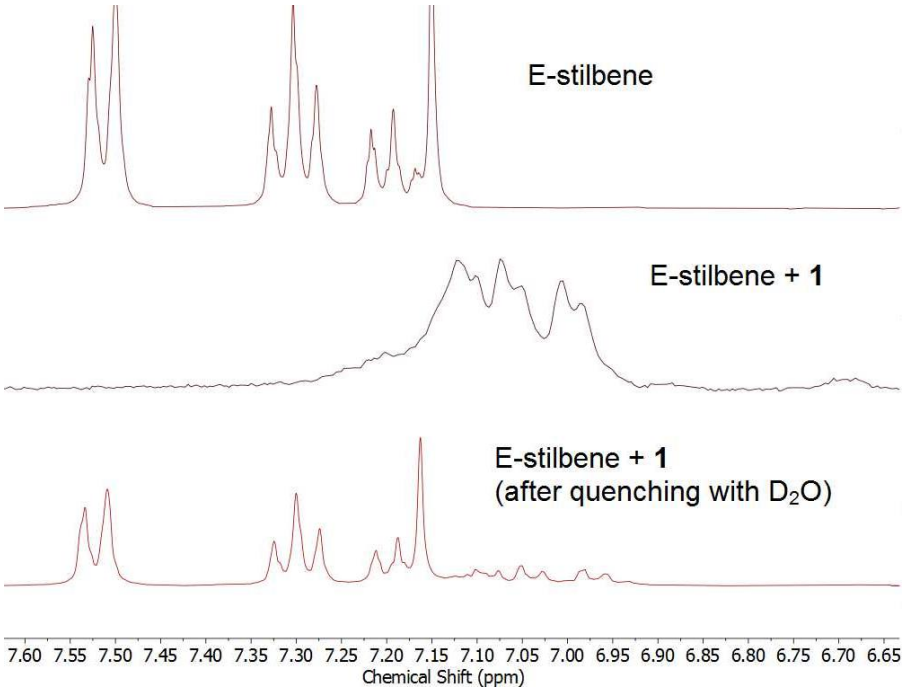

Figure S5. Top: ^{1}H NMR spectrum of *E*-stilbene. Middle: ^{1}H-NMR spectrum of *E*-stilbene with one equivalent of **1**. Bottom: ^{1}H-NMR spectrum of *E*-stilbene and one equivalent of **1** after quenching with D_2O. All spectra in [D8]THF at 300 K, 300 MHz in the range of 6.65 to 7.60 ppm.

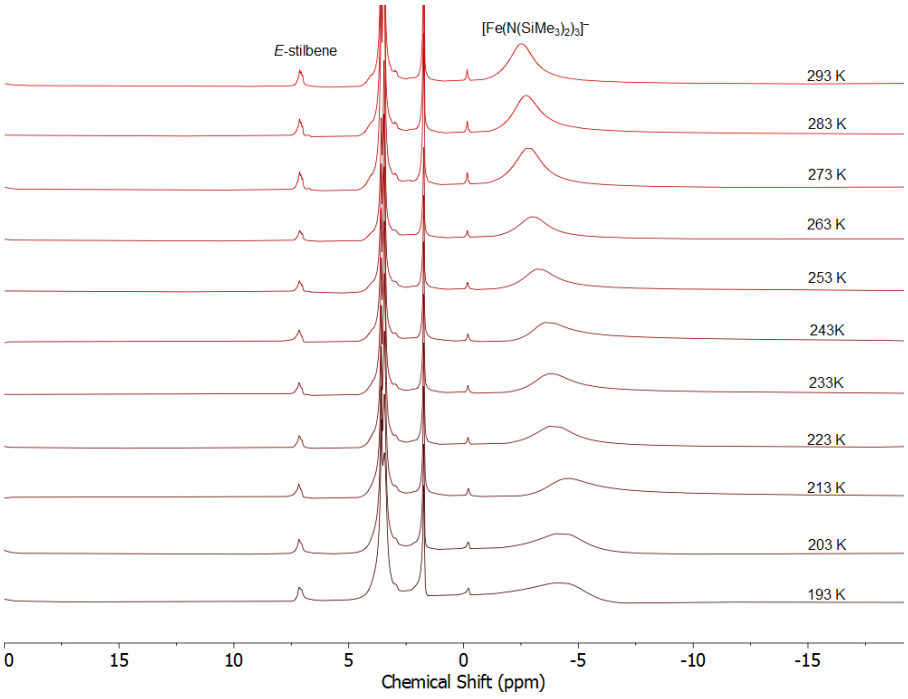

Figure S6. Temperature variable ^{1}H-NMR spectra of **1** with one equivalent of *E*-stilbene from 193 K to 293 K in [D8]THF, 500 MHz.

2.6. Reaction of 1 with *E*-stilbene (1, 5, 10 equivalents)

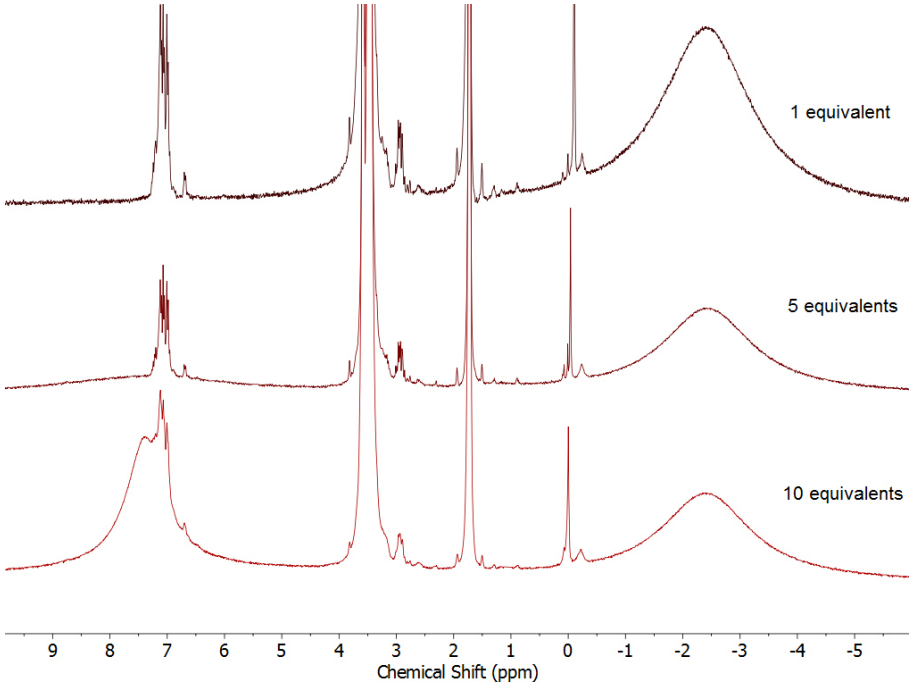

Figure S7. ^{1}H-NMR spectra of the mixture of **1** with *E*-stilbene: 1 equivalent (top), 5 equivalents (middle), 10 equivalents (bottom). All spectra in [D8]THF at 300 K, 300 MHz.

2.7. Reaction of 1 with $[Co^{II}(N(SiMe_3)_2)_2]$

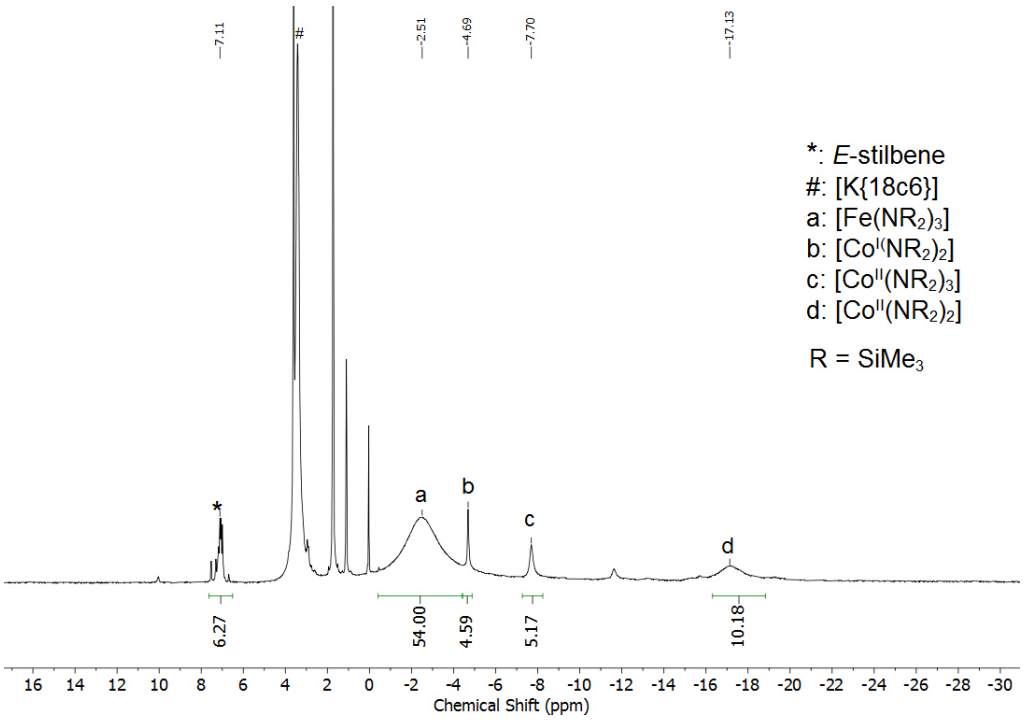

Figure S8. ^{1}H-NMR spectrum of the reaction of **1** with $[Co^{II}(N(SiMe_3)_2)_2]$ in [D8]THF at 300 K, 300 MHz.

2.8. Attempted reaction of [K{18c6}][Fe^{I}(N(SiMe$_3$)$_2$)$_2$] with *Z*-3-hexene

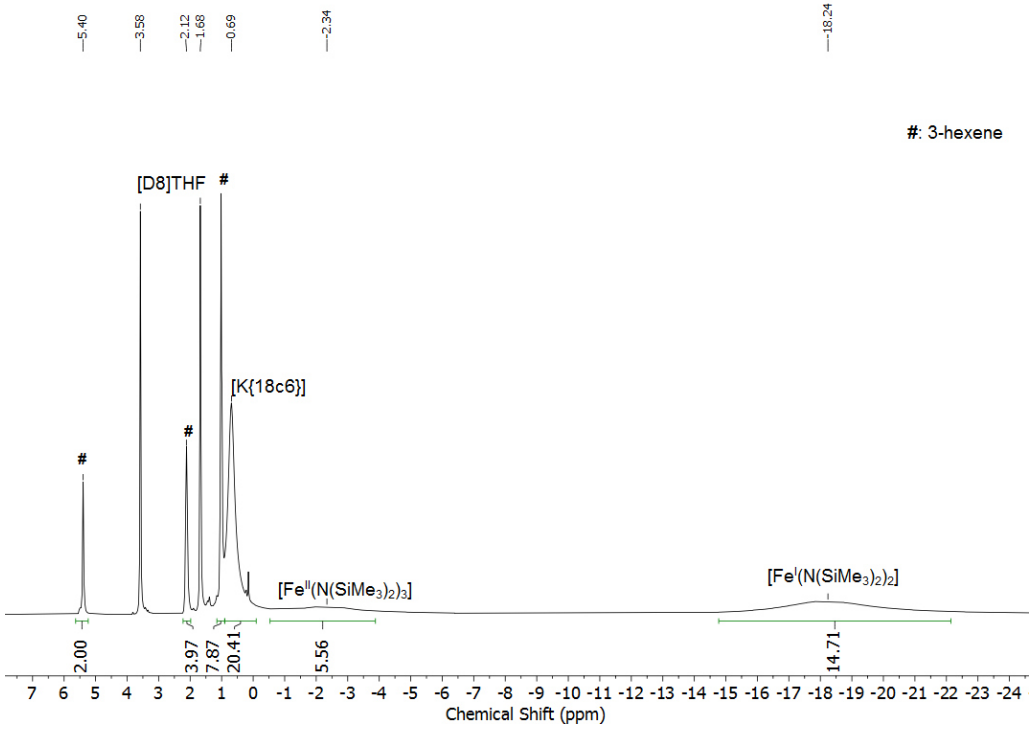

Figure S9. 1H-NMR spectrum of an equimolar mixture of [K{18c6}][Fe^{I}(N(SiMe$_3$)$_2$)$_2$] with *Z*-3-hexene. Spectrum collected in [D8]THF at 300 K, 300 MHz. No signal for an Fe-hexene complex can be detected. **#**: 3-hexene (*E*/*Z*).

2.9. IR Spetroscopy

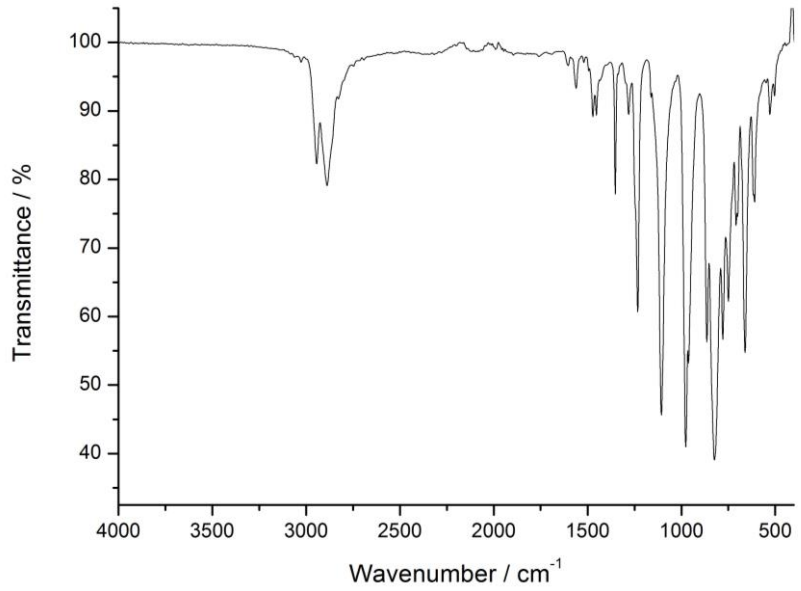

Figure S10. ATR-IR spectrum of **1**.

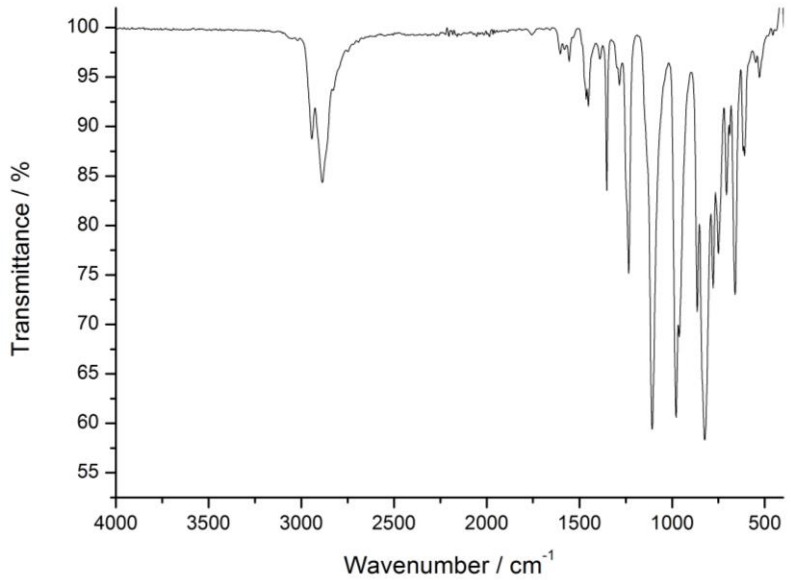

Figure S11. ATR-IR spectrum of **2**.

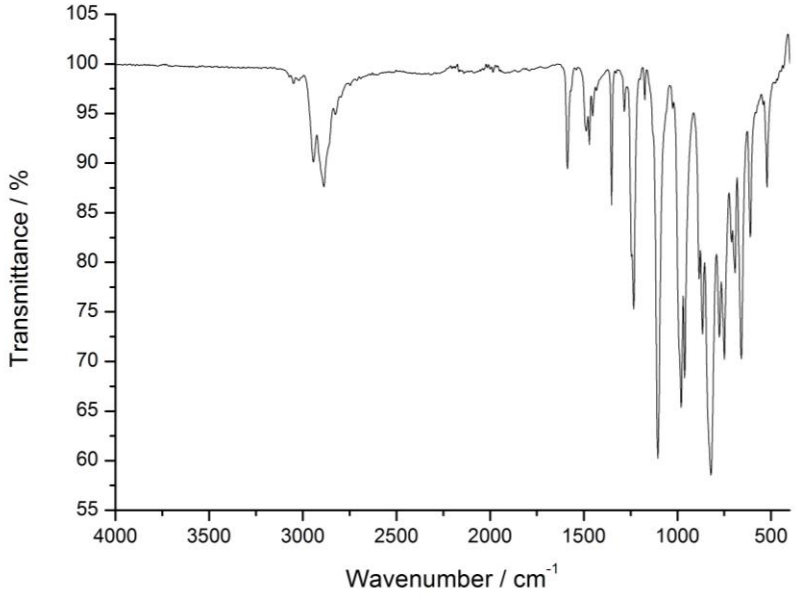

Figure S12. ATR-IR spectrum of **3**.

2.10. ^{57}Mössbauer spectroscopy

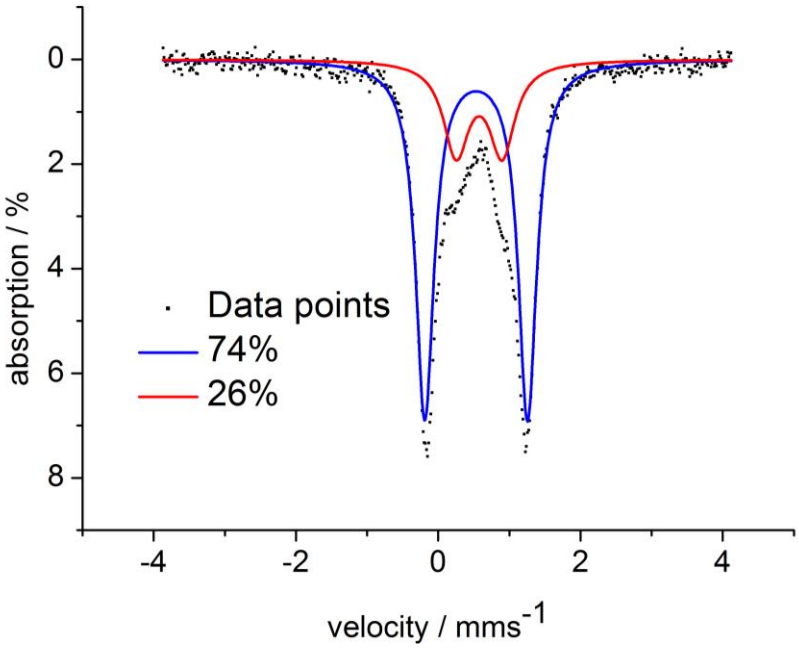

Figure S13. Zero-field ^{57}Mössbauer spectrum of **3** at 13 K. The blue line represents a fit with δ = 0.53 mms^{-1}, δQ = 1.44 mms^{-1} which can be assigned to **3** (74%). The red line represents a fit with δ = 0.57 mms^{-1}, δQ = 0.65 mms^{-1} which can be attributed to the decomposition product $[Fe(N(SiMe_3)_2)_3]^-$ (26%).[5]

2.11. EPR spectroscopy

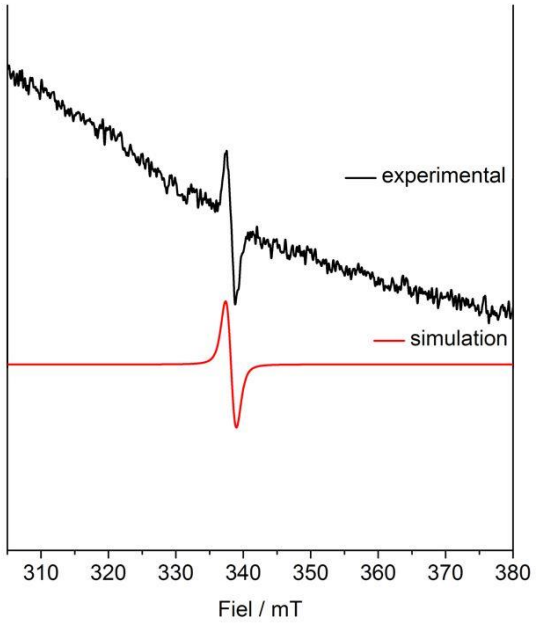

Figure S14. X-band EPR measurement of **3** in frozen toluene solution (9.476718 GHz) collected at 100 K (black) and simulated spectrum (red). g = 2.002224.

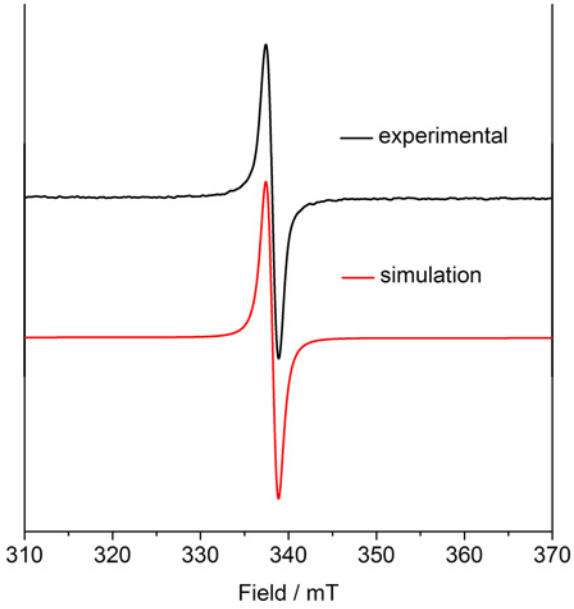

Figure S15. X-band EPR measurement of **1** in frozen toluene solution (9.476718 GHz) collected at 100 K (black) and simulated spectrum (red). g = 2.002396.

2.12. UV Vis spectroscopy

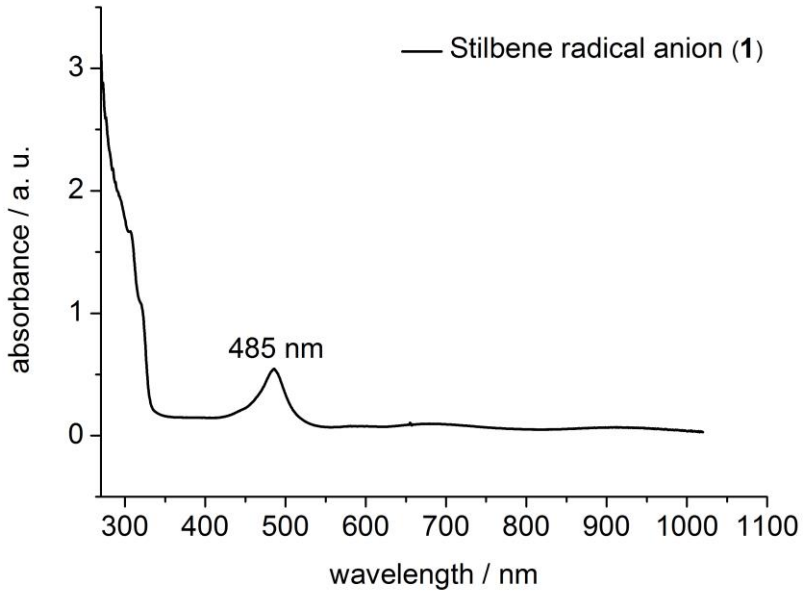

Figure S16. UV Vis spectrum of **1** in Et_2O at 300 K.

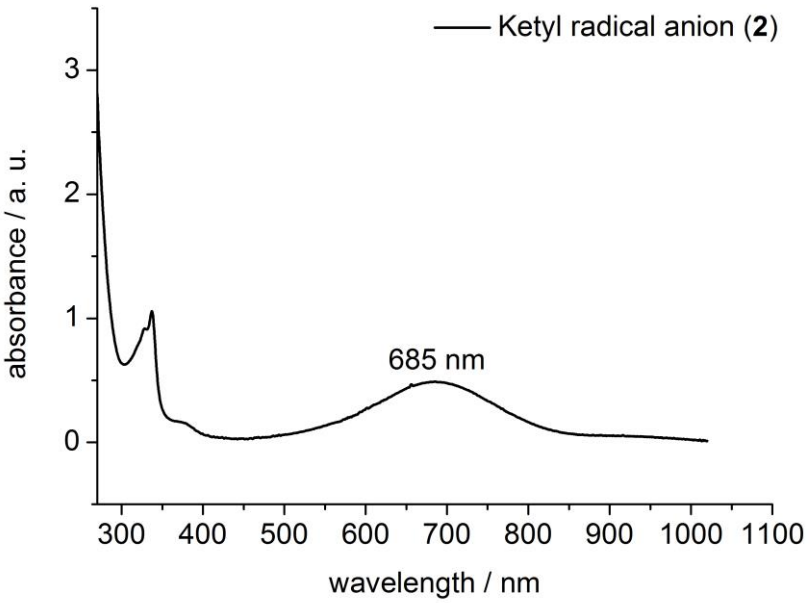

Figure S17. UV Vis spectrum of **2** in Et_2O at 300 K.

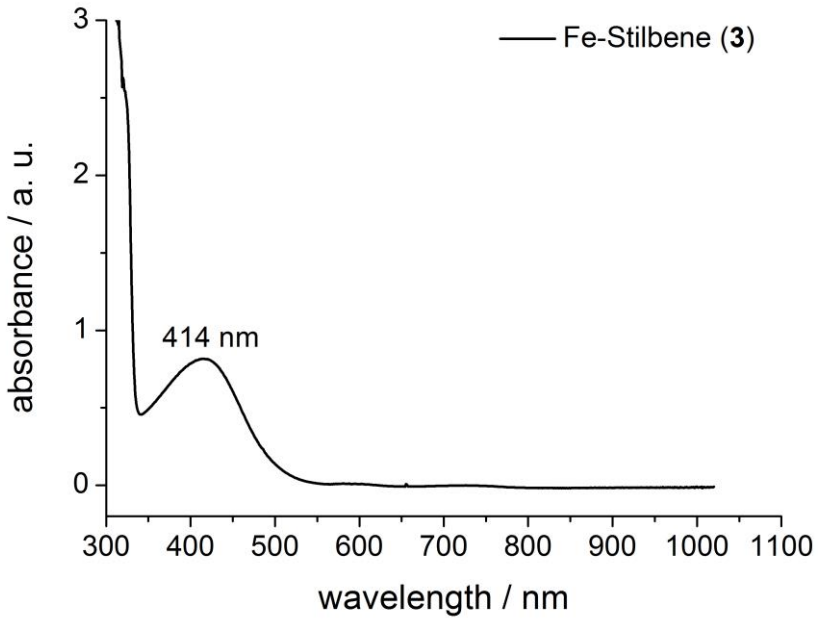

Figure S18. UV Vis spectrum of **3** in THF at 300 K.

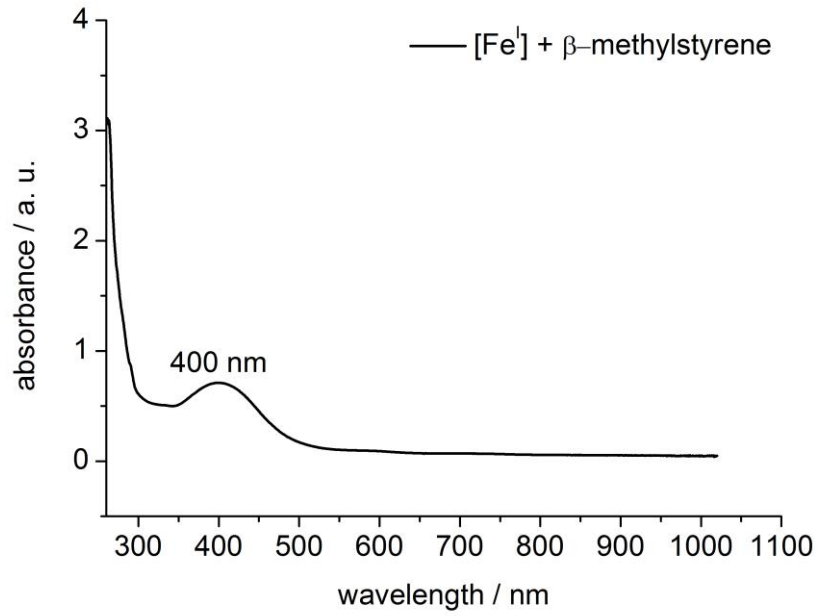

Figure S19. UV Vis spectrum of an equimolar mixture of [Fe^{I}] (= [K{18c6}][Fe(N(SiMe$_3$)$_2$)$_2$]) with ß-methylstyrene in Et$_2$O at 300 K.

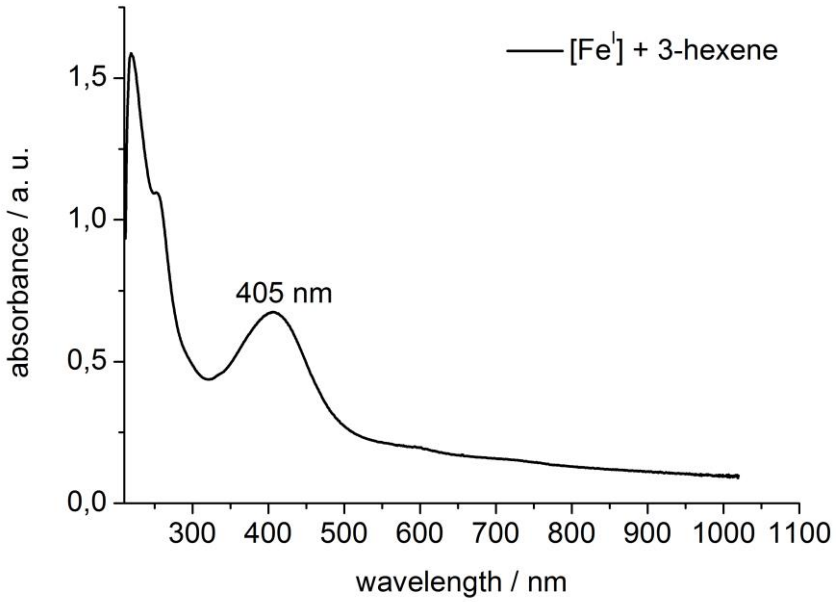

Figure S20. UV Vis spectrum of an equimolar mixture of [Fe^{I}] (= [K{18c6}][Fe(N(SiMe$_3$)$_2$)$_2$]) with 3-hexene in Et$_2$O at 300 K.

3. Catalysis

3.1. General procedure

The substrate and the catalyst were dissolved in [D8]THF under the exclusion of light. A fraction from the reaction mixture for the given reaction time was removed and quenched with a few drops of D_2O. The precipitate was filtered off and the filtrate was used as ^1H NMR sample. The conversion amount was determined as following:

$$conversion\% = \frac{\%E}{\%E + \%Z}$$

Relative amounts of *E* and *Z* isomers were determined via size of isomer-specific integrals in the ^1H NMR spectrum. An example of an ^1H NMR spectrum is given for each substrate.

3.2. Z to E isomerization of stilbene with KC8 as catalyst

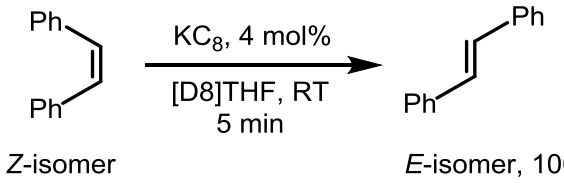

Scheme S1. Conversion of *Z*-stilbene into *E*-stilbene in [D8]THF using KC_8 as catalyst.

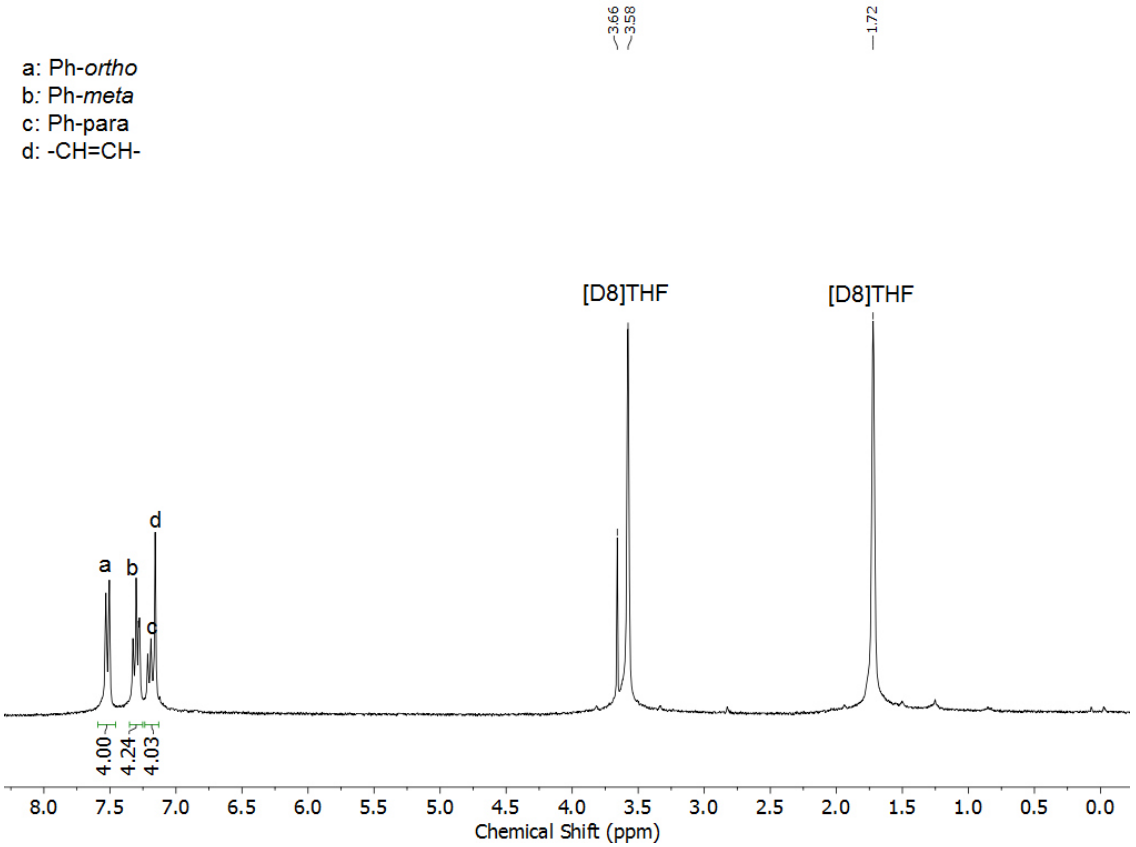

Figure S21. ^1H NMR spectrum of the conversion of Z-stilbene to E-stilbene in [D8]THF at 300K, 300 MHz using KC_8 as catalyst with 4 mol% catalyst load after 5 min. E isomer (100 %) can be detected. The spectrum was collected after quenching the reaction with D_2O.

3.3. Z to E isomerization of stilbene with 1 as catalyst

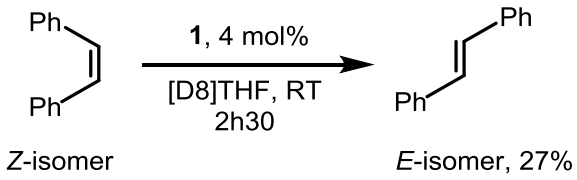

Scheme S2. Conversion of *Z*-stilbene into *E*-stilbene in [D8]THF using **1** as catalyst.

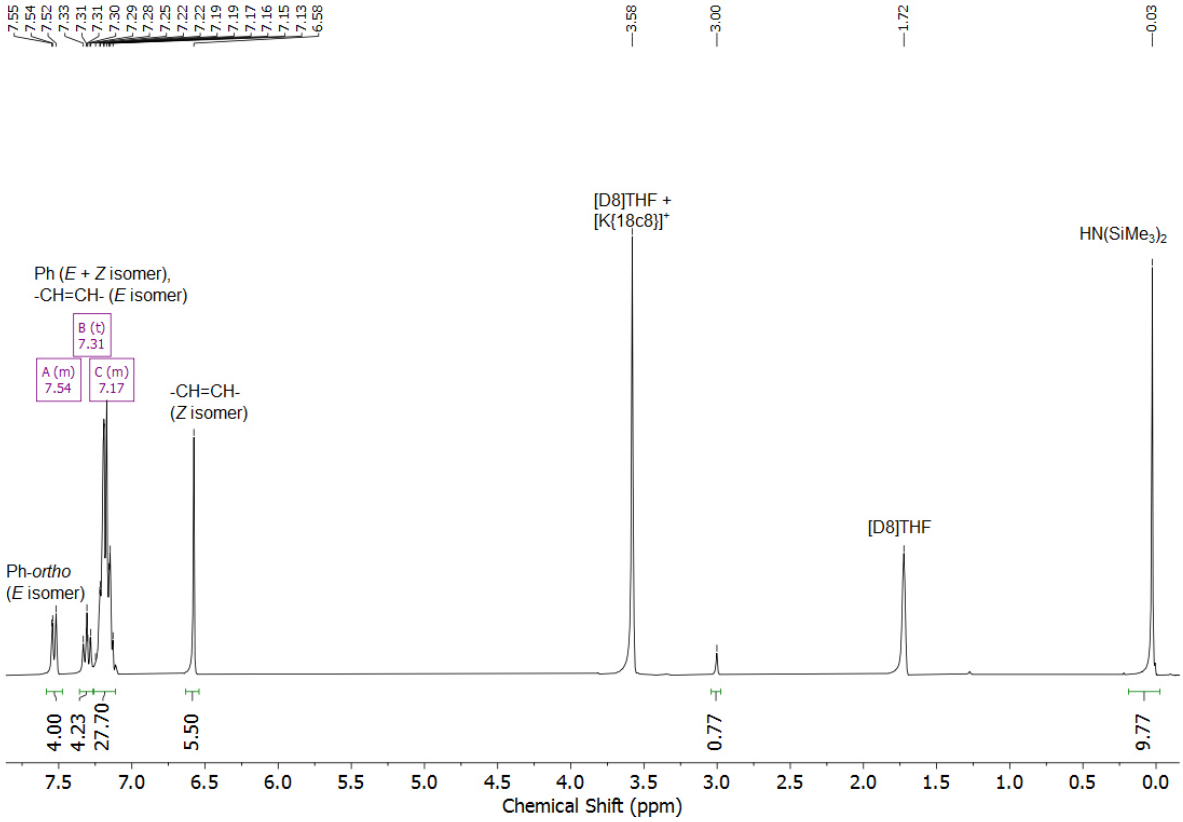

Figure S22. ^{1}H NMR spectrum of the conversion of Z-stilbene to E-stilbene in [D8]THF at 300K, 300 MHz using **1** as catalyst with 4 mol% catalyst load after 2h30. Z isomer (73 %) and E isomer (27 %) can be detected. The spectrum was collected after quenching the reaction with D_2O.

3.4. *Z* to *E* isomerization of stilbene with [K{18c6}][Fe^{I}(N(SiMe$_3$)$_2$)$_2$] as catalyst

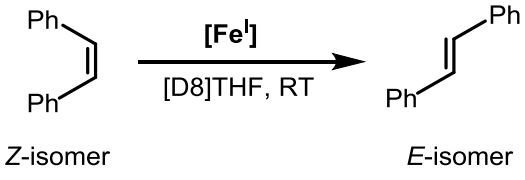

[Fe^{I}] = [K{18c$_6$}][Fe^{I}(N(SiMe$_3$)$_2$)$_2$]

Scheme S3. Conversion of Z-stilbene into E-stilbene in [D8]THF using [K{18c6}][Fe^{I}(N(SiMe$_3$)$_2$)$_2$] as catalyst.

Table S1. Conversion of Z-stilbene into E-stilbene in [D8]THF using [K{18c6}][$Fe^{I}(N(SiMe_3)_2)_2$] as catalyst.

cat. load	reaction time / min	conversion (%)
3mol%	5	51
3mol%	10	63
3mol%	15	71
3mol%	20	75
3mol%	30	83
3mol%	45	86
3mol%	60	90
3mol%	90	84
4mol%	5	47
4mol%	10	65
4mol%	15	76
4mol%	20	80
4mol%	25	85
4mol%	30	89
4mol%	45	95
4mol%	60	95
4mol%	90	100

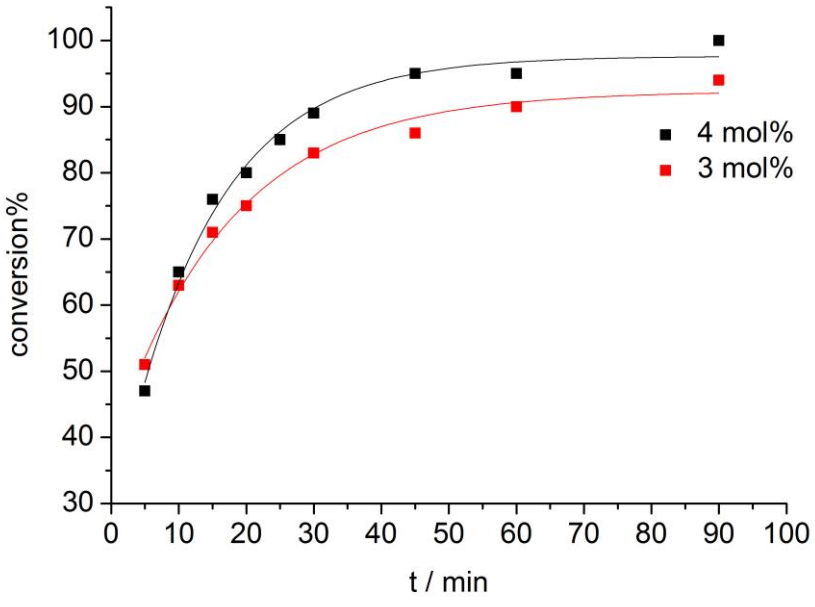

Figure S23. Conversion of Z-stilbene into E-stilbene in [D8]THF using [K{18c6}][$Fe^{I}(N(SiMe_3)_2)_2$] as catalyst with 3mol% catalyst

load (red) and 4mol% catalyst load (black). Data points are represented as dots and the corresponding data fitting is represented as line.

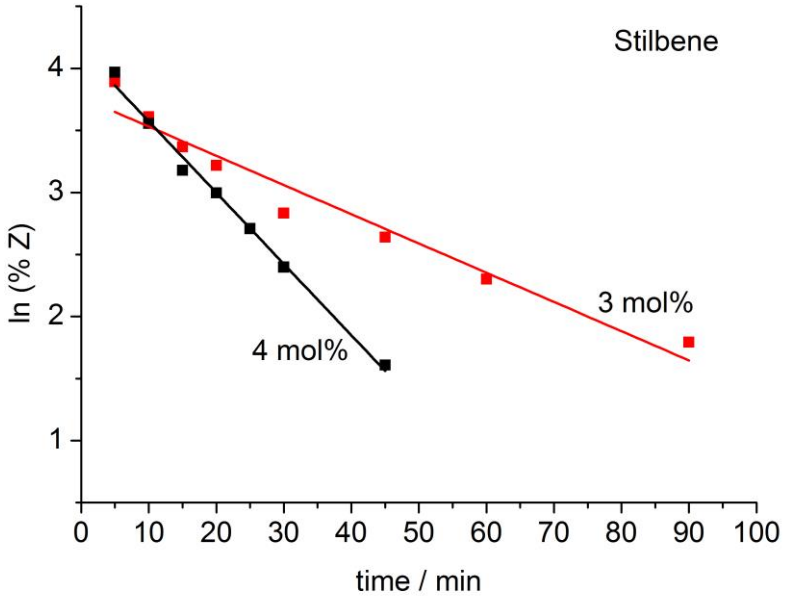

Figure S24. Conversion of Z-stilbene into E-stilbene in [D8]THF using [K{18c6}][$Fe^{I}(N(SiMe_3)_2)_2$] as catalyst with 3mol% catalyst load (red) and 4mol% catalyst load (black). Data points are represented as dots and the corresponding data fitting is represented as line. Logarithmic scale of %*Z*.

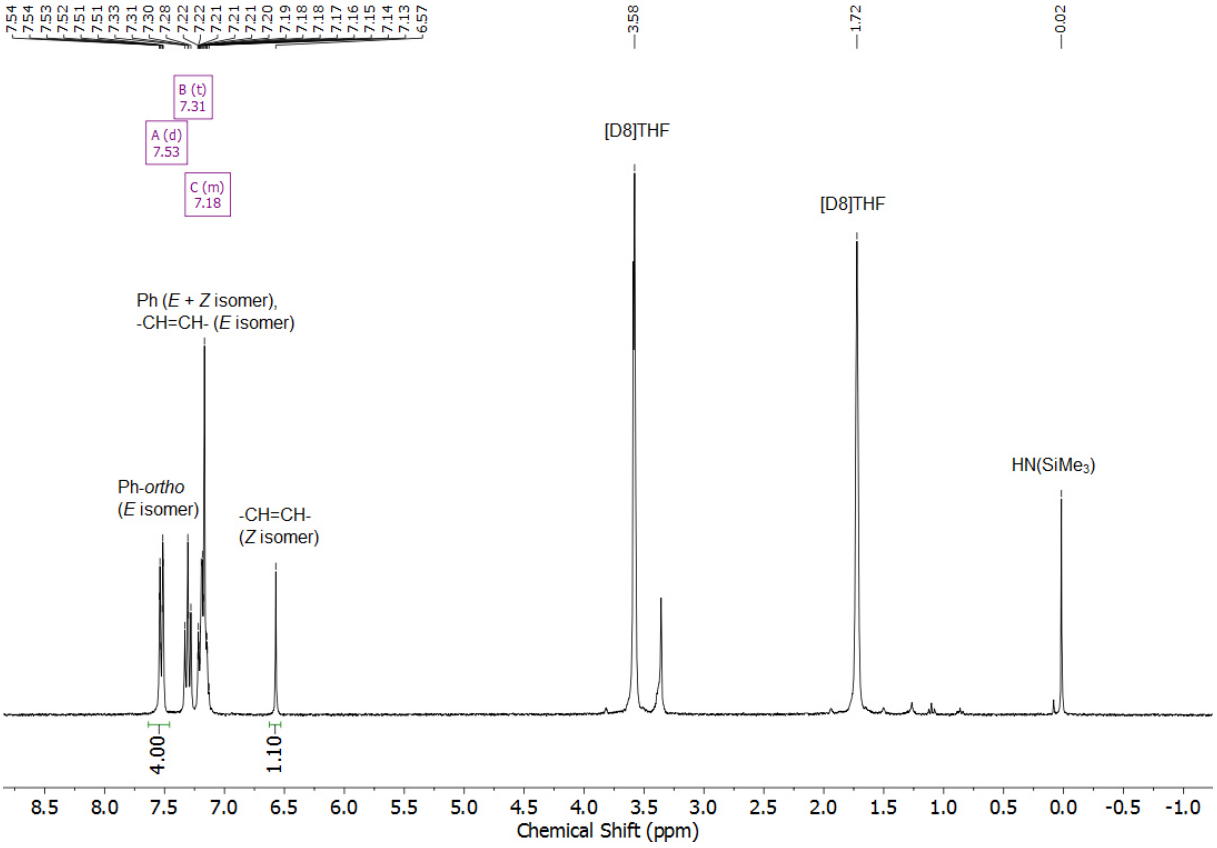

Figure S25. ^{1}H NMR spectrum of the conversion of *Z*-stilbene to *E*-stilbene in [D8]THF at 300K, 300 MHz using [K{18c6}][Fe^{I}(N(SiMe$_3$)$_2$)$_2$] as catalyst with 10 mol% catalyst load after 10 min. *Z* isomer (35 %) and *E* isomer (65 %) can be detected. The spectrum was collected after quenching the reaction with D_2O.

3.5. *Z* to *E* isomerization of stilbene with [K{18c6}][Fe^{I}(N(Dipp)(SiMe$_3$))$_2$] as catalyst

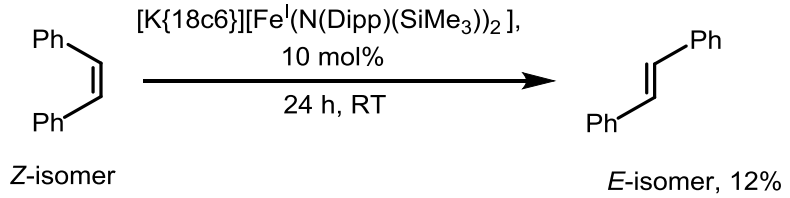

Scheme S4. Conversion of *Z*-stilbene into *E*-stilbene in [D8]THF using [K{18c6}][Fe^{I}(N(Dipp)(SiMe$_3$))$_2$] as catalyst.

Table S2. Conversion of *Z*-stilbene into *E*-stilbene in [D8]THF using [K{18c6}][Fe^{I}(N(Dipp)(SiMe$_3$))$_2$] as catalyst.

cat. load	reaction time	conversion (%)
10 mol%	3h45	5,4%
10 mol%	24h	12%

3.6. *Z* to *E* isomerization of ß-methylstyrene with [K{18c6}][Fe^{I}(N(SiMe$_3$)$_2$)$_2$] as catalyst

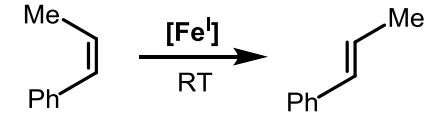

Scheme S5. Conversion of *Z*-ß-methylstyrene into *E*-ß-methylstyrene in [D8]THF using [K{18c6}][Fe^{I}(N(SiMe$_3$)$_2$)$_2$] as catalyst.

Table S3. Conversion of *Z*-ß-methylstyrene into *E*-ß-methylstyrene in [D8]THF using [K{18c6}][Fe^{I}(N(SiMe$_3$)$_2$)$_2$] as catalyst.

cat. load	reaction time / min	Amount of conversion (%)
10mol%	15	20
10mol%	30	26
10mol%	60	35
10mol%	90	43
10mol%	120	52
10mol%	194	62
10mol%	300	67

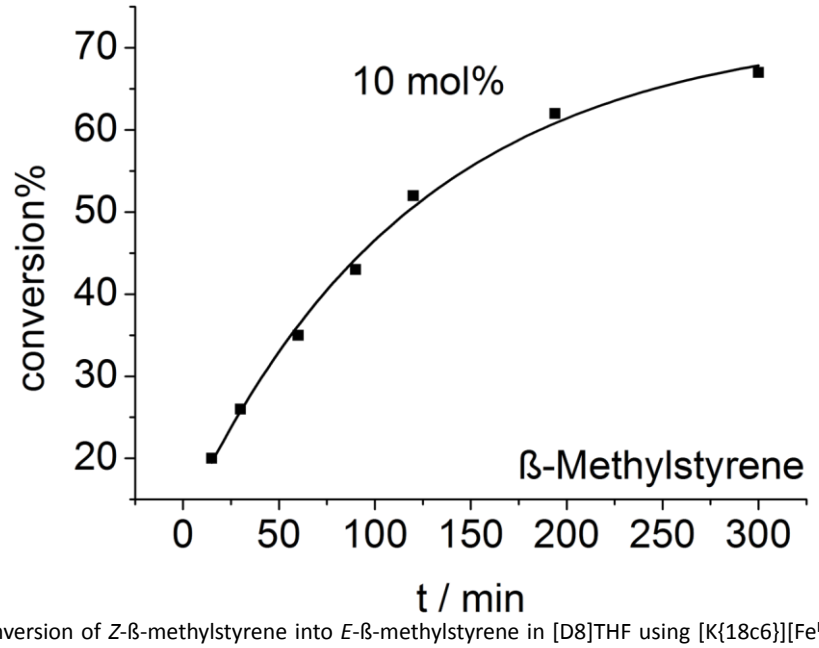

Figure S26. Conversion of *Z*-ß-methylstyrene into *E*-ß-methylstyrene in [D8]THF using [K{18c6}][Fe^{I}(N(SiMe$_3$)$_2$)$_2$] as catalyst with 10 mol% catalyst load. Data points are represented as dots and the corresponding data fitting is represented as line.

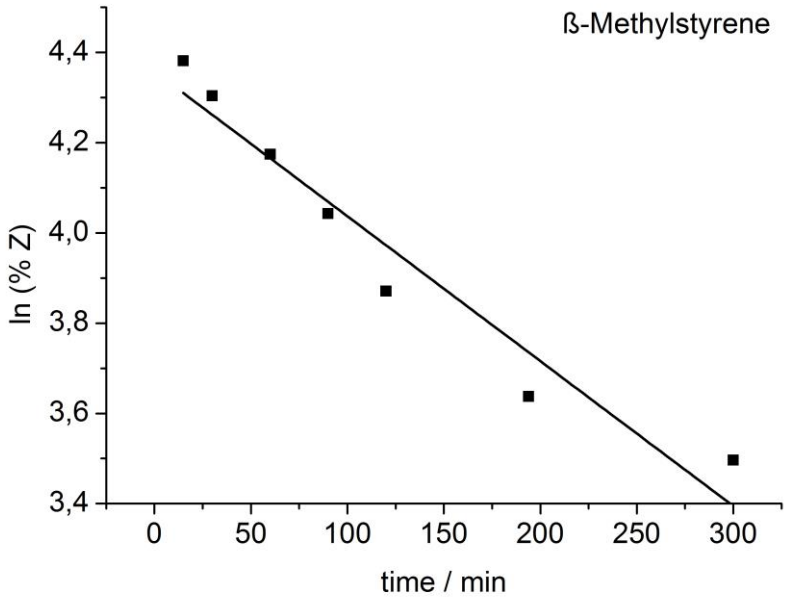

Figure S27. Conversion of *Z*-ß-methylstyrene into *E*-ß-methylstyrene in [D8]THF using [K{18c6}][Fe^{I}(N(SiMe$_3$)$_2$)$_2$] as catalyst with 10 mol% catalyst load. Data points are represented as dots and the corresponding data fitting is represented as line. Logarithmic scale of %*Z*

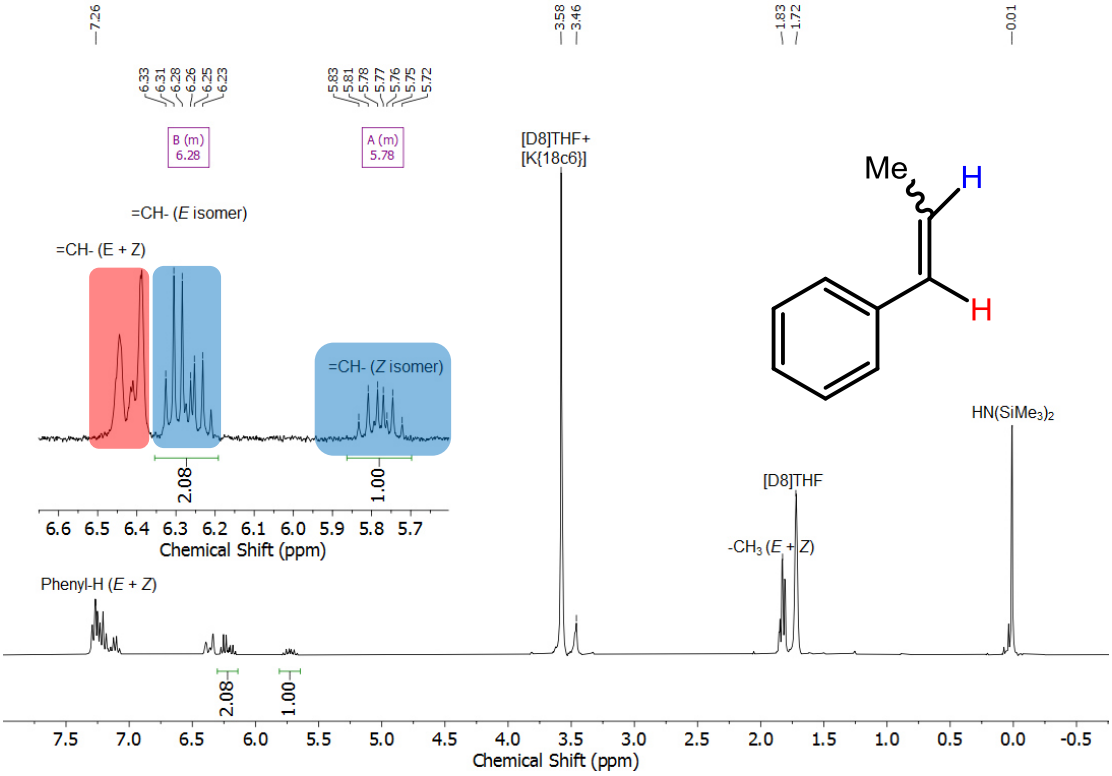

Figure S28. ^{1}H NMR spectrum of the conversion of *Z*-ß-methylstyrene to *E*-ß-methylstyrene in [D8]THF at 300 K, 300 MHz using [K{18c6}][Fe^{I}(N(SiMe$_3$)$_2$)$_2$] as catalyst with 10mol% catalyst load after 5 h. *Z* isomer (33 %) and *E* isomer (67 %) can be detected. The spectrum was collected after quenching the reaction with D_2O.

3.7. *Z* to *E* isomerization of 3-hexene with [K{18c6}][Fe^{I}(N(SiMe$_3$)$_2$)$_2$] as catalyst

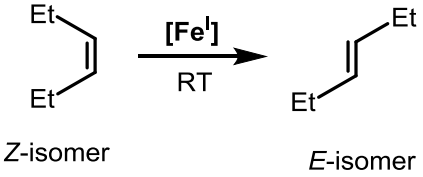

Scheme S6. Conversion of Z-3-hexene into E-3-hexene in [D8]THF using [K{18c6}][Fe^{I}(N(SiMe$_3$)$_2$)$_2$] as catalyst.

Table S4. Conversion of Z-3-hexene into E-3-hexene in [D8]THF using [K{18c6}][Fe^{I}(N(SiMe$_3$)$_2$)$_2$] as catalyst.

cat. load	reaction time	conversion (%)
10mol%	1 h	0
10mol%	1 d	25
10mol%	2 d	43
10mol%	3 d	58

10mol%	4 d	68
10mol%	7 d	75

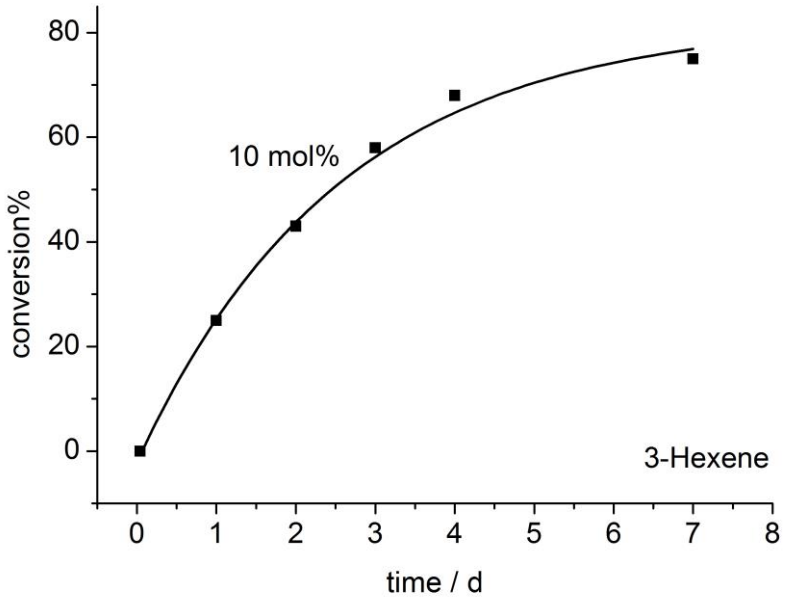

Figure S29. Conversion of *Z*-3-hexene into *E*-3-hexene in [D8]THF using [K{18c6}][Fe^{I}(N(SiMe$_3$)$_2$)$_2$] as catalyst with 10 mol% catalyst load. Data points are represented as dots and the corresponding data fitting is represented as line.

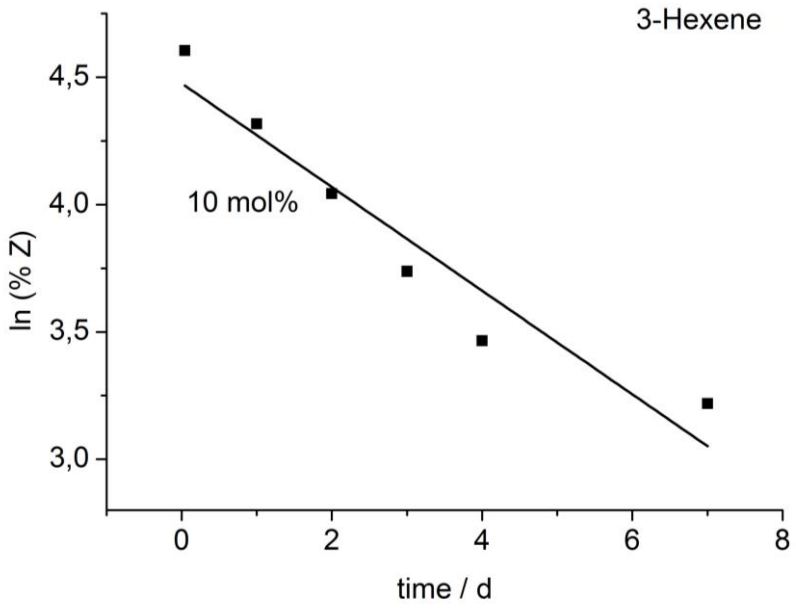

Figure S30. Conversion of *Z*-3-hexene into *E*-3-hexene in [D8]THF using [K{18c6}][Fe^{I}(N(SiMe$_3$)$_2$)$_2$] as catalyst with 10 mol% catalyst load. Data points are represented as dots and the corresponding data fitting is represented as line. Logarithmic scale of %*Z*.

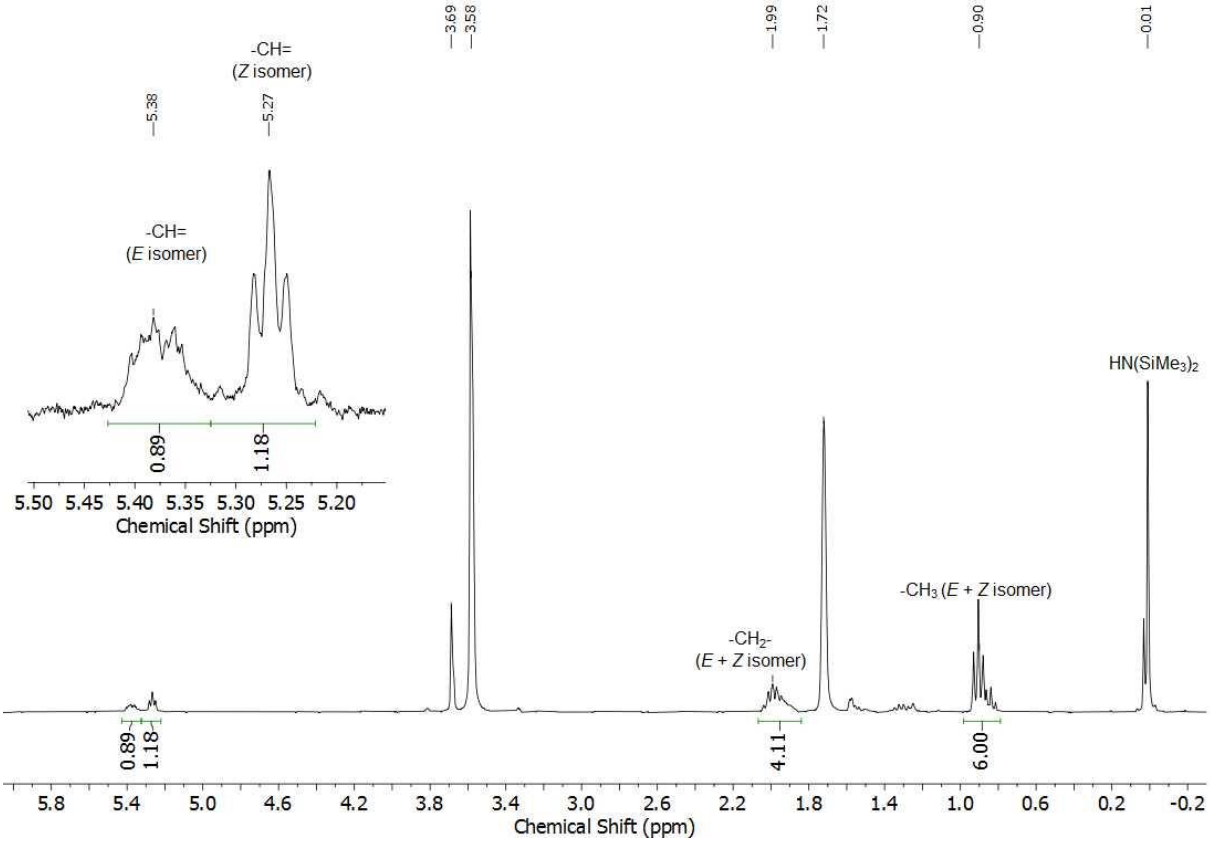

Figure S31. ^{1}H NMR spectrum of the conversion of *Z*-3-hexene to *E*-3-hexene in [D8]THF at 300 K, 300 MHz using [K{18c6}][Fe^{I}(N(SiMe$_3$)$_2$)$_2$] as catalyst with 10mol% catalyst load after 2 d. *Z* isomer (57 %) and *E* isomer (43 %) can be detected. The spectrum was collected after quenching the reaction with D_2O.

3.8. Poisoning experiment

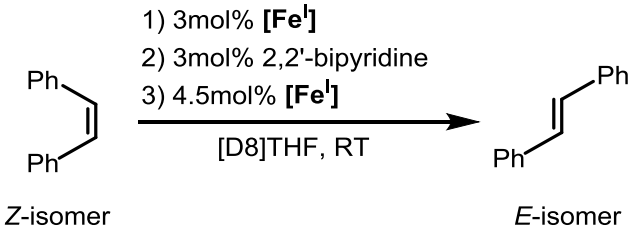

Scheme S7. Poisoning experiment for the isomerization of stilbene in [D8]THF with [Fe^{I}] as catalyst and 2,2'-bipyridine as poisoning reagent.

Table S5. Poisoning experiment for the isomerization of stilbene. 3mol% of 2,2'-bipyridine were added to a mixture of Z-stilbene and 3mol% [**Fe^{I}**] in [D8]THF after 10 min. 4.5mol% [**Fe^{I}**] were added after 40 min.

cat. load	reaction time / min	conversion (%)
3mol%	5	31
3mol%	10	38
0mol%	20	38
0mol%	30	38
0mol%	40	38.5
4.5mol%	50	73
4.5mol%	60	87

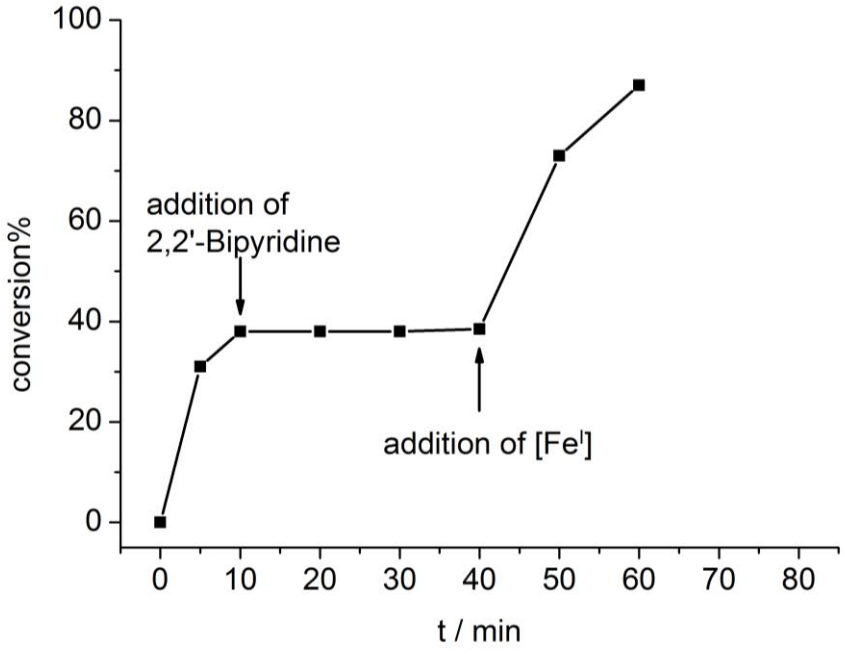

Figure S32. Poisoning experiment for the isomerization of stilbene. 3mol% of 2,2'-bipyridine were added to a mixture of Z-stilbene and 3mol% [**Fe^{I}**] in [D8]THF after 10 min. 4.5mol% [**Fe^{I}**] were added after 40 min.

4. Crystallography

Data for **1** (CCDC 2178650) and **2** (CCDC 2178649) were collected at 100 K on a BRUKER Quest D8 diffractometer using a graphite-monochromated Mo-Kα radiation and equipped with an Oxford Cryosystems Cryostream Coolder Device. Data for **3** (CCDC 2178648) and **4** (CCDC 2178651) were collected at 100 K on a STOE IPDS2 diffractometer, using a graphite-monochromated Mo-Kα radiation and equipped with an Oxford Cryosystems Cryostream Coolder Device. The structures have been solved using OLEX SHELXT V2014/1[6] and refinded by means of least-squares procedures on a F2 with the aid of the program SHELXL-2016/6, included in the software package WinGX version 1.63[7] or using CRYSTALS.[8] The Atomic Scattering Factors were taken from International Tables for X-Ray Crystallography.[9] All non-hydrogen atoms were refinded anisotropically. All hydrogen atoms were refinded by using a riding model. Absorption corrections were introduced by using the MULTISCAN[10] and X-Red program[11]. Drawings of molecules were performed with the program DIAMOND with 50% probability displacement ellipsoids for non-H atoms. H atoms are generally omitted for clarity.

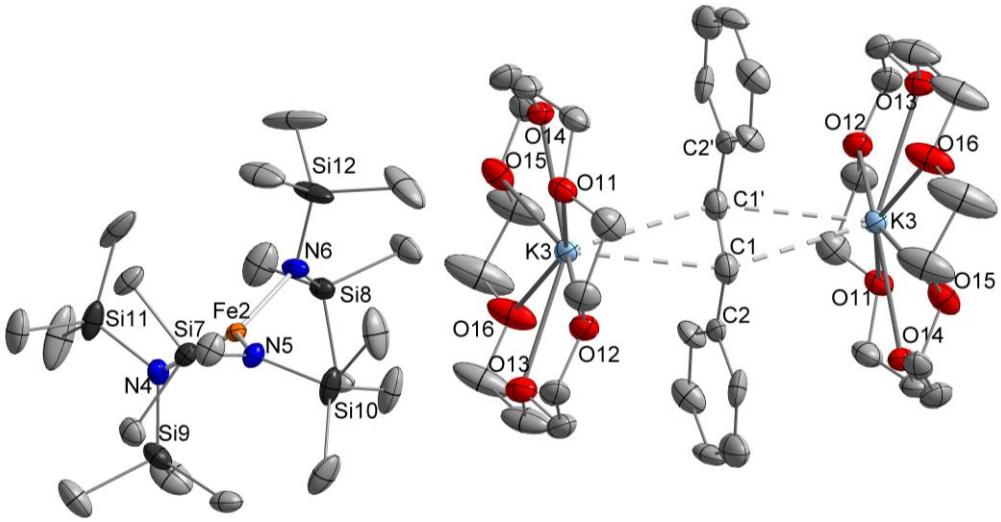

Figure S33. Molecular structure of **1**•(18c6)([K{18c6}][Fe(N(SiMe$_3$)$_2$)$_3$]) within the crystal. Hydrogen atoms, one molecule of [K(18c6)][Fe(N(SiMe$_3$)$_2$)$_3$] as well as one molecule of 18c6 have been omitted for clarity. Thermal ellipsoids are shown with 50% probability. An inversion-symmetrical disorder has been found for the stilbene fragment (50% / 50%).

Table S6. Crystal data and structure refinement of **1**•(18c6)([K{18c6}][Fe(N(SiMe$_3$)$_2$)$_3$]).

Identification code	**1**
Empirical formula	$C_{98}H_{216}Fe_2K_3N_6O_{24}Si_{12}$
Formula weight	2428.84
Temperature/K	100.0
Crystal system	monoclinic
Space group	$P2_1/n$
a/Å	16.0976(10)
b/Å	15.8981(8)
c/Å	26.7651(15)
α/°	90
β/°	93.037(2)
γ/°	90
Volume/Å^3	6840.1(7)
Z	2
ρ_{calc}g/cm^3	1.179
μ/mm^{-1}	0.468
F(000)	2630.0
Crystal size/mm^3	0.3 × 0.2 × 0.1
Radiation	MoKα (λ = 0.71073)
2Θ range for data collection/°	3.86 to 60.13
Index ranges	-22 ≤ h ≤ 22, -22 ≤ k ≤ 22, -37 ≤ l ≤ 36
Reflections collected	182148
Independent reflections	20029 [R_{int} = 0.0474, R_{sigma} = 0.0328]
Data/restraints/parameters	20029/149/889
Goodness-of-fit on F^2	1.026
Final R indexes [I>=2σ (I)]	R_1 = 0.0439, wR_2 = 0.1047
Final R indexes [all data]	R_1 = 0.0646, wR_2 = 0.1144
Largest diff. peak/hole / e Å^{-3}	0.67/-0.84

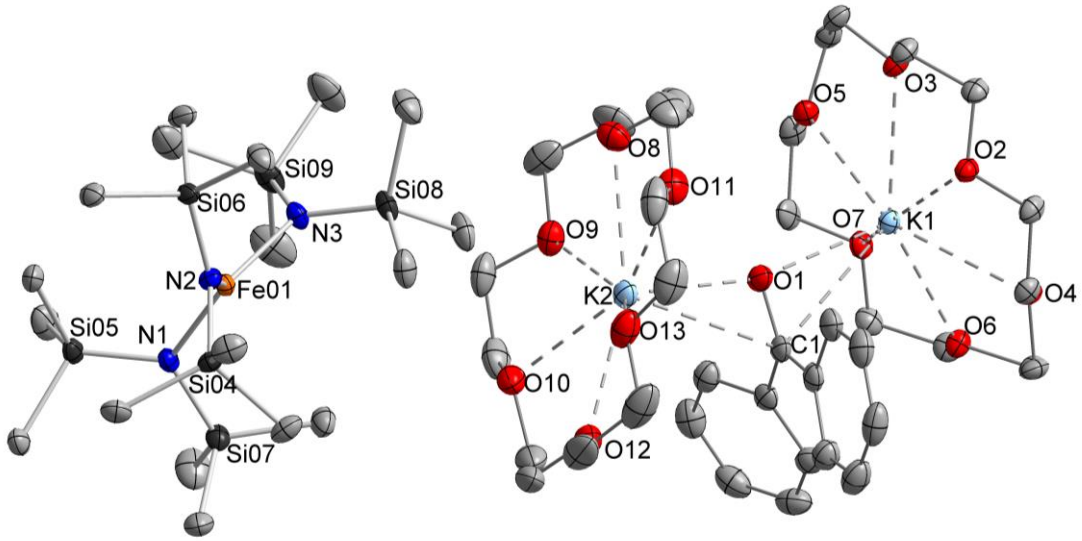

Figure S34. Molecular structure of **2** within the crystal. Hydrogen atoms are omitted for clarity, thermal ellipsoids are shown with 50% probability.

Table S7. Crystal data and structure refinment for **2**.

Identification code	**2**
Empirical formula	$C_{55}H_{112}FeK_2N_3O_{13}Si_6$
Formula weight	1326.06
Temperature/K	100.0
Crystal system	triclinic
Space group	P-1
a/Å	10.7165(3)
b/Å	17.9760(4)
c/Å	19.6298(4)
α/°	80.4780(10)
β/°	84.3760(10)
γ/°	84.0040(10)
Volume/Å^3	3696.40(15)
Z	2
ρ_{calc}g/cm^3	1.191
μ/mm^{-1}	0.467
F(000)	1430.0
Crystal size/mm^3	0.519 × 0.15 × 0.13
Radiation	MoKα (λ = 0.71073)
2Θ range for data collection/°	3.834 to 64.726
Index ranges	-16 ≤ h ≤ 16, -26 ≤ k ≤ 27, -28 ≤ l ≤ 29
Reflections collected	87985
Independent reflections	22101 [R_{int} = 0.0392, R_{sigma} = 0.0521]
Data/restraints/parameters	22101/60/902
Goodness-of-fit on F^2	1.075
Final R indexes [I>=2σ (I)]	R_1 = 0.0345, wR_2 = 0.0868
Final R indexes [all data]	R_1 = 0.0584, wR_2 = 0.0918
Largest diff. peak/hole / e Å^{-3}	0.66/-0.40

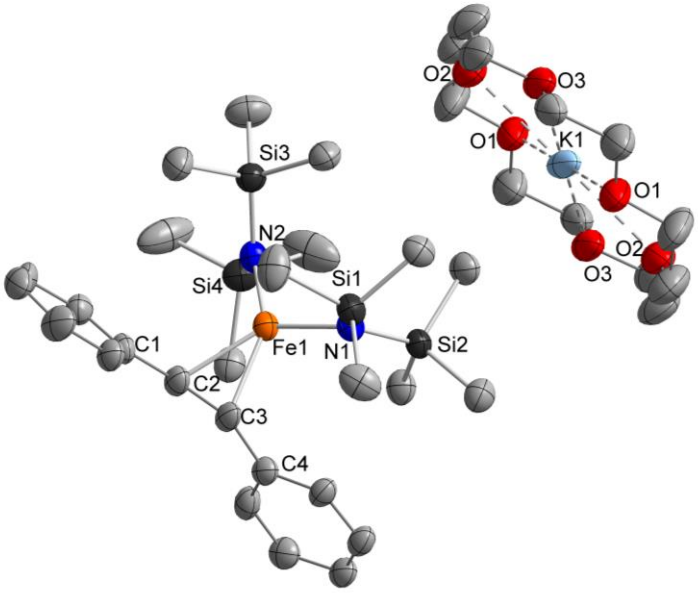

Figure S35. Molecular structure of **3**•0.5Et_2O within the crystal. Hydrogen atoms are omitted for clarity, thermal ellipsoids are shown with 50 % probability. Et_2O is not depicted. An inversion-symmetrical disorder has been found for the stilbene fragment (67% / 33%).

Table S8. Crystal data and structure refinment for **3**.

Identification code	**3**
Empirical formula	$C_{40}H_{77}FeKN_2O_{6.5}Si_4$
Formula weight	897.34
Temperature/K	100.0
Crystal system	monoclinic
Space group	*C*2/*c*
a/Å	37.416(5)
b/Å	13.2067(15)
c/Å	28.584(4)
α/°	90
β/°	133.663(7)
γ/°	90
Volume/Å^3	10218(2)
Z	8
ρ_{calc}g/cm^3	1.167
μ/mm^{-1}	0.512
F(000)	3872.0
Crystal size/mm^3	0.438 × 0.419 × 0.285
Radiation	MoKα (λ = 0.71073)
2Θ range for data collection/°	2.864 to 53.62
Index ranges	-47 ≤ h ≤ 46, -15 ≤ k ≤ 16, -35 ≤ l ≤ 36
Reflections collected	24901
Independent reflections	10544 [R_{int} = 0.0663, R_{sigma} = 0.0586]
Data/restraints/parameters	10544/387/675
Goodness-of-fit on F^2	1.108
Final R indexes [I>=2σ (I)]	R_1 = 0.0712, wR_2 = 0.1722
Final R indexes [all data]	R_1 = 0.0934, wR_2 = 0.1808
Largest diff. peak/hole / e Å^{-3}	0.50/-0.51

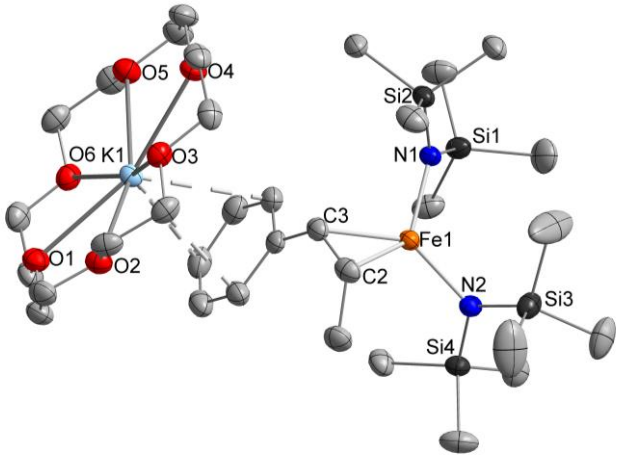

Figure S36. Molecular structure of **4** within the crystal. Hydrogen atoms are omitted for clarity, thermal ellipsoids are shown with 50% probability.

Table S9. Crystal data and structure refinement for **4**.

Identification code	**4**
Empirical formula	$C_{33}H_{70}FeKN_2O_6Si_4$
Formula weight	798.22
Temperature/K	100.0
Crystal system	monoclinic
Space group	$P2_1/c$
a/Å	12.1227(8)
b/Å	18.3502(12)
c/Å	21.0291(14)
α/°	90
β/°	104.641(5)
γ/°	90
Volume/Å^3	4526.1(5)
Z	4
ρ_{calc}g/cm^3	1.171
μ/mm^{-1}	0.569
F(000)	1724.0
Crystal size/mm^3	0.984 × 0.524 × 0.412
Radiation	MoKα (λ = 0.71073)
2Θ range for data collection/°	2.988 to 58.508
Index ranges	-16 ≤ h ≤ 16, -22 ≤ k ≤ 25, -28 ≤ l ≤ 26
Reflections collected	30974
Independent reflections	12149 [R_{int} = 0.0459, R_{sigma} = 0.0488]
Data/restraints/parameters	12149/0/437
Goodness-of-fit on F^2	0.951
Final R indexes [I>=2σ (I)]	R_1 = 0.0372, wR_2 = 0.0944
Final R indexes [all data]	R_1 = 0.0607, wR_2 = 0.1008
Largest diff. peak/hole / e Å^{-3}	0.74/-0.37

5. References

[1] S. Stoll, A. Schweiger, *J. Magn. Reson.* **2006**, *178*, 42–55.

[2] H. Bürger, U. Wannagat, *Monatsh. Chem.* **1963**, *94*, 1007–1012.

[3] C. G. Werncke, P. C. Bunting, C. Duhayon, J. R. Long, S. Bontemps, S. Sabo-Etienne, *Angew. Chem. Int. Ed.* **2015**, *54*, 245–248.

[4] C. G. Werncke, E. Suturina, P. C. Bunting, L. Vendier, J. R. Long, M. Atanasov, F. Neese, S. Sabo-Etienne, S. Bontemps, *Chem. Eur. J.* **2016**, *22*, 1668–1674.

[5] A. Eichhöfer, Y. Lan, V. Mereacre, T. Bodenstein, F. Weigend, *Inorg. Chem.* **2014**, *53*, 1962–1974.

[6] G. M. Sheldrick, *Acta Crystallogr., Sect. A: Found. Crystallogr.* **2015**, *71*, 3–8.

[7] L. Farrugia, *J. Appl. Crystallogr.* **1999**, *32*, 837.

[8] P. W. Betteridge, J. R. Carruthers, R. I. Cooper, K. Prout, D. J. Watkin, *J. Appl. Crystallogr.* **2003**, *36*, 1487.

[9] *International Tables for X-Ray Crystallography*, Kynoch Press, Birmingham, England, **1974**.

[10] *SADABS-2016/2*, Bruker, **2016**.

[11] *X-Area, X-Red 1.63.1.0*, STOE, **2016**.

3.4 Bond activation by bent, formally manganese(I), iron(I) and cobalt(I) di(silylamides)

G. Sieg, T. Vaupel, K. Dollberg, C. G. Werncke, *manuscript in preparation.*

Abstract

Activation of small organic molecules and bonds is of key interest to modern coordination chemistry. Specifically the reduction of organic double bonds with metals is a crucial step in many organic reaction mechanisms. With several known instances of low-coordinate, monovalent bond activation, we intended the investigation in an alternate ligand system with a strained geometry. While the direct reduction of the anionic metal(II)-halide precursors of manganese, iron and cobalt was not possible, we herein present the activation of a variety of molecules with C-C-, C-O and N-N-double bonds, C-C-triple bonds as well as azide-functions with the reaction of the precursor in presence of the substrate under reducing conditions. The resulting complexes have been characterized structurally and spectroscopically and show different coordination behaviour dependent of the used metal.

Zusammenfassung

Im Rahmen dieser Publikation sollte die bereits für monovalente Silyl(aryl)amidokomplexe $[M^{I}(L_2)]^-$ (M = Fe, Co, L = $N(SiMe_3)_2$, $N(SiMe_3)(Dipp)$) untersuchte Aktivierung kleiner Moleküle und Mehrfachbindungssysteme[123,135,143–148] auf ein, in diesem Kontext neues, gespanntes Ligandensystem übertragen werden. Dafür wurde der bereits für Hauptgruppenelemente bewährte N,N-Aryl-1,1,3,3-tetramethyldisiloxan-1,3-diamido-Ligand („NON“) mit Mesitylsubstituenten verwendet.[149–152] Da die Reduktion der neutralen Dimerkomplexe **1 – 3** nicht gelang, wurden diese in einem ersten Schritt mit Alkylammoniumhalogeniden umgesetzt, um die anionischen, mononuklearen Halogenidokomplexe **4 – 6** zu erhalten (Schema 54).

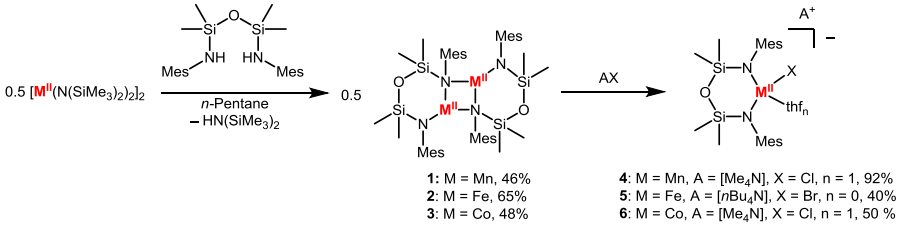

Schema 54. Synthese der anionischen Metall(II)komplexe **4 – 6**.

Die Bildung der anvisierten Spezies $[M^{I}(Mes_2NON)]^-$ (M = Mn – Fe) durch Umsetzung der Vorläuferkomplexe mit KC_8 konnte aufgrund von Zersetzung nicht beobachtet werden. Aus diesem Grunde wurde die Reduktion dieser unter Anwesenheit von zu aktivierenden Substraten durchgeführt wurde. Ausgehend des Mangankomplexes **4** konnten so die Komplexe **7 – 10** erhalten werden, in

denen verschiedene simple organische Moleküle aktiviert werden konnten, wie Olefine oder Azide oder Azobenzol (Schema 55).

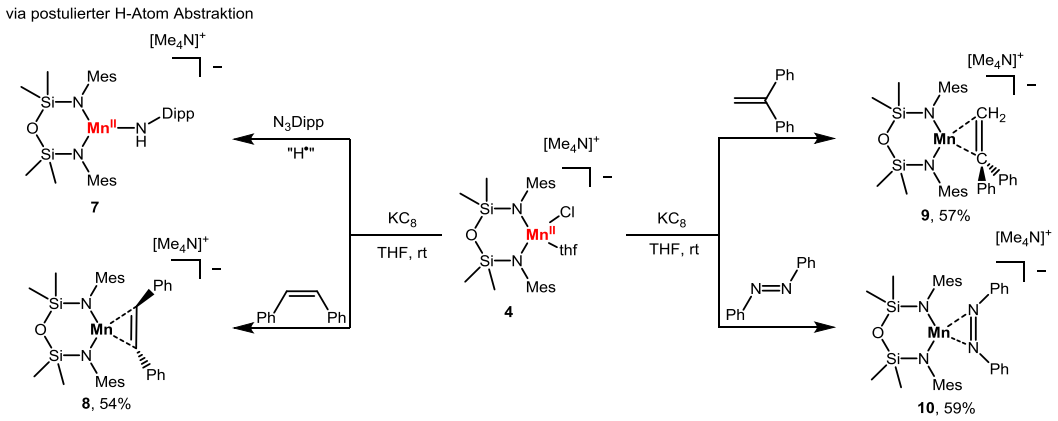

Schema 55. Substrataktivierung ausgehend von **4** unter reduzierenden Bedingungen.

Bei Reaktion von **4** mit Dipp-Azid (Dipp: Di*iso*propyl) unter Zugabe von KC_8 konnte der Amidokomplex **7** erhalten werden, welcher vermutlich durch einen HAT vom eingesetzten THF auf einen intermediär gebildeten Imidokomplex entstand. Ähnliche Reaktivitäten wurden bereits für Imidokomplexe beobachtet.[123,145] Bei Zugabe von C=C-Doppelbindungen zu **4** mit KC_8 konnte für die Komplexe **8** und **9** eine *side-on* Koordination an das Manganion unter Aufweitung der C-C-Bindung beobachtet werden. Für den Stilbenkomplex **8** wird eine *Z*- zu *E*-Isomerisierung beobachtet, welche wahrscheinlich analog zu der in Kapitel 3.3 beschriebenen Komplexen über ein Mangan(II)-stabilisiertes Radikalanion stattfindet.[148] Im Falle von **10** konnte erstmalig eine Manganverbindung mit *side-on* Koordination einer N-N-Bindung erhalten werden, die bei Vergleich mit einem strukturell verwandten Eisenkomplex[153] als Mangan(II)-gebundener Radikalanionenkomplex begriffen werden kann.

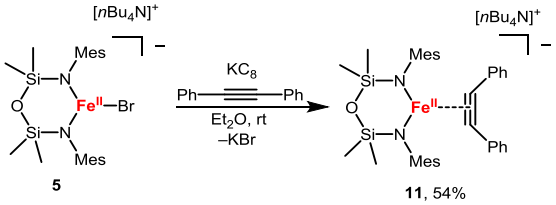

Bei Einsatz des Eisenkomplexes **5** als Vorläufer konnte durch Aktivierung von Diphenylacetylen Verbindung **11** erhalten werden, dessen Anion strukturell mit dem bekannten Komplexanionen $[Fe(N(SiMe_3)_2)_2(PhCCPh)]^-$ und $[Mn(N(SiMe_3)_2)(Dipp)(PhCCPh)]^-$ verwandt ist.[135] Diese wurden durch quantenchemische Untersuchungen als Metall(II)-Radikalkomplexe beschrieben, was dementsprechend auch für **11** plausibel ist.

Zuletzt konnten ausgehend von **6** verschiedene Cobaltkomplexe mit einer Reihe an Substraten erhalten werden (Schema 56). Bei Reaktion von **6** mit KC_8 und Dipp-Azid konnte wie bei **7** die Bildung eines Amidokomplexes beobachtet werden. Verringert man jedoch den sterischen Anspruch der

Substituenten und setzt das *tert*-Butyl-Azid ein, so bildet sich vermutlich intermediär ein Imidokomplex aus, der durch eine 2+3 Cycloaddition mit einem weiterem Equivalent Azid zum Tetrazenkomplex **13** reagiert. Diese Reaktivität konnte beim Cobaltsilylamidokomplex $[Co(N(SiMe_3)_2)_2]^-$ nicht beobachtet werden[145] und zeugt von einer Änderung der Reaktivität durch einen vergleichbar kleinen N-Co-N-Bisswinkel.

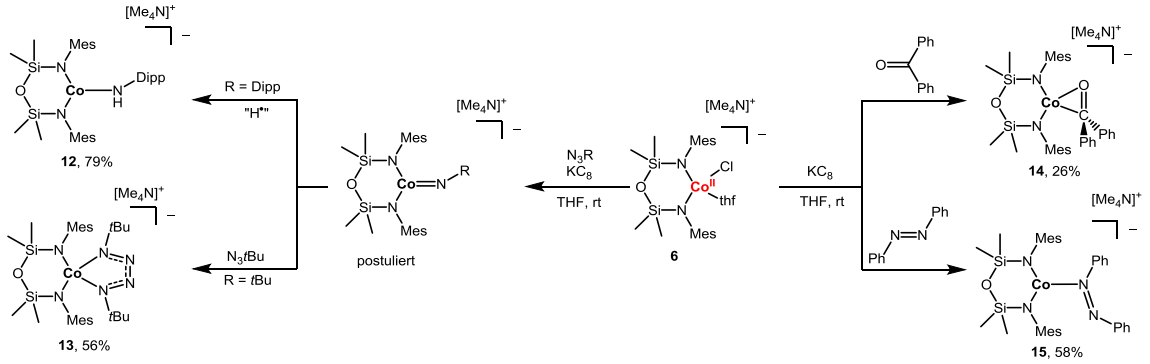

Schema 56. Substrataktivierung ausgehend von **6** unter reduzierenden Bedingungen.

Bei Reaktion von **6** mit Benzophenon und KC_8 wurde der *side-on* Komplex **14** erhalten. Dieser weist strukturelle Ähnlichkeit zu einem als „maskiertes Radikal“ beschriebenen Eisen-Benzophenonkomplex [(NacNac)Fe(bp)] auf, bei dem kein ligandbasierter Radikalcharakter beobachtet werden konnte.[69] Das Fehlen einer, für Ketylradikale üblichen Photoabsorption in **14**, ebenso wie die *side-on* Koordination (im Gegensatz zu *end-on* Koordination der Cobalt-Benzophenonkomplexe in Kapitel 3.1) deutet auf eine Koordination eines neutralen Benzophenon-Moleküls hin.[146] Setzt man stattdessen als Substrat Azobenzol ein, wird im Gegensatz zu **10** asymmetrisch-koordinierter Cobaltkomplex **15** erhalten, welcher im Vergleich zu Cobaltkomplexen mit gleichem Koordinationsmodus eine ungewöhnlich lange N-N-Bindung (1.348(2) Å vs. 1.243 Å für Azobenzol) aufweist.[154–157]

Eigener Anteil

Die Synthesen von **4 – 6**, **11**, sowie die Charakterisierung durch IR- und NMR-Spektroskopie wurde von *Kevin Dollberg* unter meiner Aufsicht durchgeführt. Die Synthesen von **7**, **9**, **10**, **12**, **13** und **15**, sowie deren Untersuchung durch NMR-Spektroskopie wurde von *Theresa Vaupel* unter meiner Aufsicht durchgeführt. Alle übrigen Verbindungen wurden von mir synthetisiert. Deren Untersuchung mittels IR-, NMR- und UV-Vis-Spektroskopie, sowie die ausstehenden Analysen der vorher aufgezählten Verbindungen wurde von mir durchgeführt und ausgewertet. Die Röntgenbeugungsexperiemente wurden durch *Dr. Gunnar Werncke* oder durch die Serviceabteilung für Kristallographie der Philipps-Universität-Marburg durchgeführt, die Sturkturlösung und -verfeinerung wurde von mir durchgeführt. Die Elementaranalyse, sowie die massenspektrometrischen Untersuchungen wurden durch die

Serviceabteilung Massenspektrometrie und Elementaranalytik der PUM durchgeführt und von mir ausgewertet. Das Manuscript wurde von mir verfasst und von *Dr. Gunnar Werncke* überarbeitet.

ARTICLE

Bond activation by bent, formally manganese(I), iron(I) and cobalt(I) di(silylamides)

Received 00th January 20xx,
Accepted 00th January 20xx

DOI: 10.1039/x0xx00000x

Grégoire Sieg[a], Theresa Vaupel[a], Kevin Dollberg[a], and C. Gunnar Werncke*[a]

Bond activation of small organic molecules is of key interest to modern coordination chemistry. Specifically the reduction of organic double bonds with metals is a crucial step in many organic reaction mechanisms. With several known instances of low-coordinate, monovalent bond activation, we intended the investigation in an alternate ligand system with a strained geometry. While the direct reduction of the anionic metal(II)-halide precursors of manganese, iron and cobalt was not possible, we herein present the activation of a variety of molecules with C-C-, C-O and N-N-double bonds, C-C-triple bonds as well as azide-functions with the reaction of the precursor in presence of the substrate under reducing conditions. The resulting complexes have been characterized structurally and spectroscopically and show different coordination behaviour dependent of the used metal.

Introduction

Bond activation of small organic molecules is of key interest to modern coordination chemistry. Specifically the reduction of organic double bonds with metals is a crucial step in many well-established reaction mechanisms, such as the reductive coupling of carbonyles[1–4], imines[5–7], anionic polymerization[8] and azo-cleavage.[9] In this regard low-coordinate (coordination number and low-valent open shell 3d-transition metal complexes are under intense scrutiny, as they provide the electrons as well as free coordination sites for substrate activation and conversion, such as in the very prominent chelating ß-diketiminato[10–14] or diminopyridine[15–19] complexes. In this context linear complexes bearing non-chelating neutral N-heterocyclic carbenes (NHC), cyclic alkyl amino carbenes (cAAC) as well as anionic silylamides have received increasing attention.[20,21] Hereby linear homoleptic metal(I) silylamides of the type $[M(NR_2)_2]^-$, revealed a large variety of substrate activation patterns as well as served as a platform for the stabilisation of reactive imido metal complexes in higher spin states. Substrate coordination is thereby accompanied by bending of the N–M–M angle to 120–140°, thus resembling the situation of said NacNac complexes.

Building on these observations work we contemplated about the impact of enforcing deviations of the near linear N–M–N bond angle of said linear metal(I) silylamides towards the electronic properties and reactivity of such compounds. For that we chose the N,N-dimesityl-1,1,3,3-tetramethyldisiloxane-1,3-diamido (^{Mes}NON) ligand, as it is structurally related to the well-established aryl(silyl)amido ligands $N(SiMe_3)(R)$ (R = Ph, Dipp, Mes)[22]. This NON ligand, with different substituents, had already been employed in coordination chemistry of transition metals and group 13 elements.[23–29] and was initially introduced by Roesky[30,31] and later Leznoff[23–25] for 3d-metal complexes.

Herein we present now our endeavours concerning elusive bent metal(I) silylamido complexes with two-coordinate metal(I) ion as well their reactivity towards substrates. If applicable, reactivity differences between these complexes as well their strictly linear counterparts are discussed.

Results and discussion

Synthesis of anionic metal(II)halide-complexes

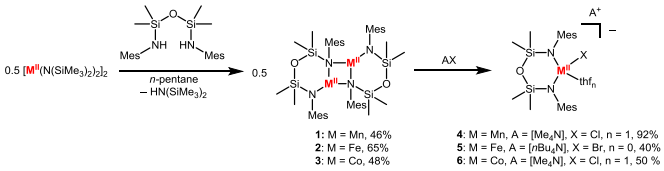

Schema 1. Synthesis of the neutral, dimeric $[M^{II}(^{Mes}NON)]_2$ complexes **1** – **3,** and the anionic metal(II) halide complexes **4** – **6**.

In a first step, we prepared the dimeric $[M^{II}(^{Mes}NON)]_2$ complexes **1** – **3** by transmetallation from the respective $[M^{II}(N(SiMe_3)_2)_2]$ complexes by addition of $^{Mes}NONH_2$. Whereas **2** and **3** have previously been synthesized by the group of Leznoff through salt metathesis out of $^{Mes}NONLi_2$ and $M^{II}Cl$,[23,24] we found our route to be more efficient in regards to reaction times and purity. **1** crystallizes isostructurally to **2** with slightly longer bonds to the N-atoms but otherwise comparable bond metrics. **1** shows no detectable signals in the ^{1}H-NMR spectrum, as expected for a measured magnetic moment of 7.58 μ_B.

[a] Fachbereich Chemie, Philipps-Universität Marburg, Hans-Meerwein-Straße 4, 35037 Marburg, Germany

Electronic Supplementary Information (ESI) available: Experimental and crystallographic details, IR, UV-Vis, NMR-spectroscopic data.
See DOI: 10.1039/x0xx00000x

Please do not adjust margins

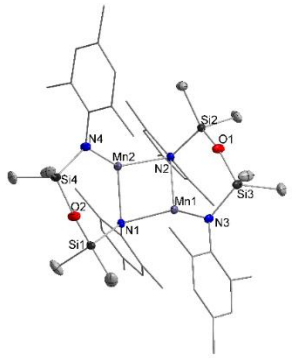

Figure 1. Molecular structures of **1**. Hydrogen atoms are omitted for clarity, thermal ellipsoids are shown with 50% probability. Selected bond lengths (Å) and angles: Mn1-N1 2.115(1), Mn1-N2 2.165(2), Mn1-N3 1.967(1), Mn2-N1 2.168(1), Mn2-N2 2.111(1), Mn2-N4 1.968(1), N2-Mn1-N3 119.36(6)°, N1-Mn2-N4 119.69(5).

Subsequently we pursuit the reduction of these complexes with KC_8 in the presence or absence of crypt.222 or 18c6, in Et_2O or THF. In all cases colour changes were observed however despite numerous attempts, no clear reaction products emerged. In a few cases insights into reaction pathways became evident via X-Ray diffraction analysis on singular crystals. Obtained polynuclear structures indicated complex reaction pathways that included consecutive redox and/or ligand rearrangement processes, which we attributed to the use of the dimeric starting materials.

Synthesis of anionic halide complexes

To enforce a monomeric form of complexes **1** – **3**, we then prepared the ionic halido metal complexes $[(^{Mes}NON)M(X)]^-$ as starting point for reduction studies. As such the tetraalkyl ammonium salts $[Me_4N]Cl$ and $[^nBu_4N]Br$ were added to the neutral dimeric complexes **1** – **3** in THF. For iron, we obtained the trigonal-planar complex **5** with a three coordinate iron(II) center. In contrast, for manganese and cobalt we isolated the complexes **4** and **6** with four coordinated metal(II) centers bearing an additional THF ligand. The manganese complex **4** shows larger Mn-Cl (2.393(1) Å) and Mn-O (2.216(2) Å) bond lengths than similar reported four-coordinate Mn^{II} complexes but slightly shorter Mn-N bonds (2.063(2) Å, 2.046(2) Å).[32,33] The coordination geometry is nearly tetragonal with τ_4 = 0.89. In case of **5**, the Fe-N bond lengths (1.926(3) Å, 1.930(2) Å) and the Fe-Br bond length (2.378(1) Å) correspond well to the previously reported complexes iron(II)-bromido-silylamido complexes $[L_2Fe^{II}Br]^-$ (L = $N(SiMe_3)_2$, N(Dipp)($SiMe_3$)).[34,35] As expected, the N1-Fe1-N2 bond angle of 114.57(9)° is significantly smaller in comparison (130.90(7)° and 138.52(9)° respectively) due to the geometrically constrained ligand. For the cobalt complex **6**, all bond lengths are well comparable to those of similar coordinated Co^{II} complexes[36,37] with a nearly tetrahedral coordination geometry around the Co ion with τ_4 = 0.86.

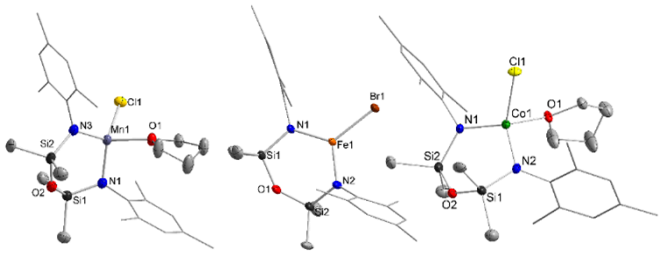

Figure 2. Molecular structures of **4** (left), **5** (middle) and **6** (right). Hydrogen atoms are omitted for clarity, thermal ellipsoids are shown with 50% probability. Selected bond lengths (Å) and angles (deg.): **4**: Mn1-N1 2.063(2), Mn1-N3 2.046(2), Mn1-Cl1 2.393(6), Mn1-O1 2.216(1), N1-Mn1-N3 109.95(7); **5**: Fe1-N1 1.930(2), Fe1-N2 1.926(2), Fe1-Br1 2.378(0), N1-Fe1-N2 114.56(8); **6**: Co1-N1 1.963(3), Co1-N2 1.968(3), Co1-Cl1 2.316(1), Co1-O1 2.123(3), N1-Co1-N2 107.98(14).

As for **1**, **4** shows no detectable signals in the ^{1}H-NMR spectrum, whereas **5** and **6** show a set of signals in the paramagnetic range (**5**: 62 ppm, 54 ppm, 38 ppm; **6**: 53 ppm, 43 ppm, 36 ppm). While these cannot be unambiguously assigned, they serve as a good spectroscopic reference for further reactions.

With the isolation of the ionic compounds **4** – **6** we once again tried to isolate reduced metal(I) complexes by reduction of the metal(II) precursors with potassium graphite. Unfortunately, this synthetic route proved to be unsuccessful with an initial colour change but immediate precipitation of black, insoluble solids. It thus showed so far that compared to the linear metal(I) silylamides, the herein envisioned metal(I) derivatives with a strongly bent N–M–N axis are too unstable by themselves.

Synthesis of manganese complexes

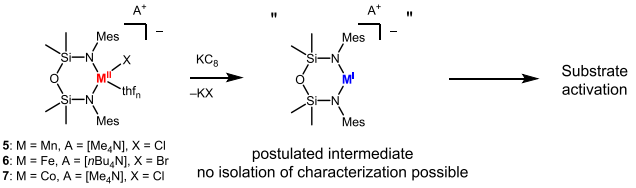

5: M = Mn, A = $[Me_4N]$, X = Cl
6: M = Fe, A = $[nBu_4N]$, X = Br
7: M = Co, A = $[Me_4N]$, X = Cl

Schema 2. Synthetic route for substrate activation by a postulated monovalent intermediate.

In order to investigate nonetheless their potential in substrate activation chemistry, we tried to trap them chemically by performing the metal(II) complex reduction in presence of different substrates. For that we chose primarily substrates that are prone to interaction with electron rich metal centres, namely act a π-acceptors, yet do not react with the divalent precursors themselves as well as potassium graphite.

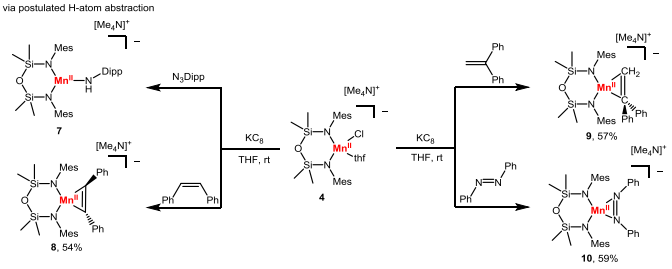

Schema 3. Synthesis of **7** – **10** through substrate activation with $[(^{Mes}NON)Mn^{II}(thf)Cl]^-$ (**4**) under reducing conditions

This journal is © The Royal Society of Chemistry 20xx

Please do not adjust margins

Please do not adjust margins

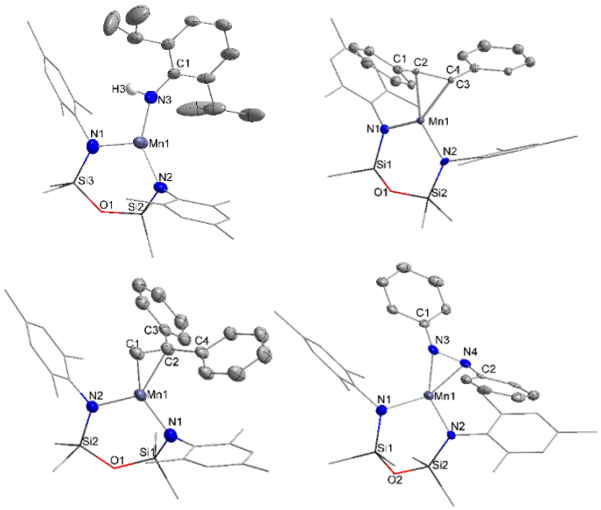

Figure 3. Molecular structures of the anions in **7** (top left), **8** (top right), **9** (bottom left), **10** (bottom right). Hydrogen atoms are omitted for clarity, thermal ellipsoids are shown with 50% probability.

The addition of KC_8 to **4** in presence of Dipp-azide led to immediate gas evolution. Instead of a trigonal arylimido manganese complexes, the arylamido complex $[Me_4N][(^{Mes}NON)Mn(NHDipp)]$ (**7**) was obtained in moderate yields. Its formation is likely result of H atom abstraction (HAT) from the solvent by the initial formed imido manganese complex. This behaviour is in line with analogous reactions of trigonal imido cobalt silylamides from our group.[38] To our knowledge, **7** is one of only few examples of three-coordinate Mn complexes with a primary organo amide –N(H)R as a ligand with the other ones being reported from Power.[39] The Mn1-N1 (2.003(7) Å) and N1-C1 (1.356(9) Å) bond lengths are similar to those in the mentioned complexes $[(ArylN(H))_2Mn^{II}thf]$ (d(Mn-N) = 1.986(1) Å, d(N-C) = 1.371(2) Å) and $[(ArylN(H))_2Mn^{II}py]$ (d(Mn-N) = 1.996(2) Å, d(N-C) = 1.368(2) Å).

Reduction of **4** in presence of *Z*-1,2-diphenylethene (*Z*-stilbene) led to the formation of $[Me_4N][(^{Mes}NON)Mn^{II}(E\text{-stilbene})]$ (**8**). In this case a *Z* to *E* isomerization occurred, which was recently investigated by our group for the Fe^{I}-silyl(aryl)amido complexes $[L_2Fe^{I}]^-$ (L = $N(SiMe_3)_2$, N(Dipp)($SiMe_3$)).[40] For **8**, two different C2-C3 bond lengths of 1.464(11) Å and 1.364(15) Å could be determined.[§] The former is slightly larger than in the reported Fe^{II} complex $[((SiMe_3)_2N)_2Fe^{II}(E\text{-stilbene})]^-$ (d = 1.416(3) Å), as well as other low coordinate iron-alkene complexes L^1FeL^2 (L^1 = *ß*-diketiminate ligand) (L^2 = EtCH=CHEt: d = 1.401(8)/1.420(4) Å; L^2 = H_2C=CHPh: d = 1.396(5) Å).[11] In comparison with free *E*-stilbene, a clear elongation from 1.311 Å to 1.464(11) Å is noticeable, indicating a reduced C-C bond order. The latter bond length is in the range of the free substrate and shorter than known complexes. In contrast, the bond angles around C2 and C3 are almost identical in all cases.[40] The solid-state IR spectrum of **9** shows a no absorption in the expected double bond range of 1600 – 1750 cm^{-1}, with the only distinct stretching frequency at 1583 cm^{-1}, stemming from the phenyl groups. Further investigation by means of UV-Vis spectroscopy revealed for **8** an absorption band at 476 nm. This is comparable with the isolated stilbene radical anion (485 nm) and the spectroscopically observed $Na^+(E\text{-stilbene})^{\bullet-}$ (494 nm).[40,41]

Similarly, reduction of **4** with KC_8 in presence of the terminal alkene 1,1-diphenylethen resulted in the formation of primarily $[Me_4N][(^{Mes}NON)Mn(\eta^2\text{-}Ph_2C{=}C)]$ (**9**). Additionally, presence of the manganese complex $(^{Mes}NON)Mn(CH_2NMe_3)(thf)]$, **9b**, (see Figure S33 for structure) was observed as a co-crystallizing compounds by X-Ray diffraction analysis. The ammonium ylide ligand likely stems from activation of the tetramethylammonium counter cation by the presumably formed $[Mn(MesNON)]^-$, and underscores its high reactivity. The 1,1-diphenylethene substrate in **9** coordinates in a slightly asymmetric side-on η^2-fashion with Mn-C bond lengths of 2.082(4) and 2.157(3) Å. Only a few manganese compounds with side-on C-C double bond interaction are known to date[42–45] but metal complexes of 1,1-diphenylethene are known or iron, nickel and rhodium. [46–48] The C1-C2 bond length in **9** is larger than those reported (Mn: 1.451(4) Å, Fe: 1.412(3) Å, Ni: 1.391(6) Å, Rh: 1.421(4) Å) with similar C2-C3/4 bond lengths and C3-C2-C4 bond angles. In comparison with the structurally close 1,1-di-*p*-tolylethene, the C1-C2 bond length is elongated from 1.338 Å, while other bonds and angles show no significant deviation.[49]

Table 1. Selected bond lengths (Å) and angles (deg.) for **7** – **10** and comparison with the corresponding substrate: [a]: E-azobenzene ,[d]: 1,1-Di-*p*-tolylethene, [s]: E-stilbene.[49–51]

Bond	**7**	**8**	**9**	**10**	Free
substrate	NHDipp	stilbene	dpe	ab	substrate
Mn1-N1	2.003(7)	2.022(6)	2.028(3)	1.977(6)	
Mn1-N2	2.045(5)	2.010(5)	2.034(2)	1.994(6)	
Mn1-N3	2.015(5)			2.006(7)	
Mn1-N4				1.997(7)	
Mn1-C1			2.082(4)		
Mn1-C2		2.162(8)	2.157(3)		
Mn1-C3		2.166(9)			
N3-N4				1.418(9)	1.243[ab]
C1-C2		1.512(12)/ 1.464(11)[§]	1.451(4)		1.338[dpe], 1.472[s]
C2-C3		1.364(15) 1.468(12)[§]	1.490(4)		1.499[dpe], 1.331[s]
C3-C4		1.540(13) 1.483(10)[§]			1.474[s]
C2-C4			1.489(4)		1.474[dpe]
N3-C1	1.356(9)			1.421(10)	1.433[a]
N4-C2				1.432(10)	1.433[a]
N1-Mn1-N2	109.1(2)	111.3(2)	106.5(1)	103.7(3)	
Mn1-N3-C1	147.7(5)				
C3-C2-C4			119.0(3)		117.60[dpe]
C1-C2-C3		124.9(8)/ 123.7(1)[§]			126.1[s]
C2-C3-C4		127.0(8)/ 123.5(1)[§]			
C1-N3-N4				111.6(6)	113.6[ab]
N3-N4-C2				110.3(6)	113.6[ab]

Finally, the reduction of **4** in presence of azobenzene (ab) provides $[Me_4N][(^{Mes}NON)Mn(PhN{=}NPh)]$ (**10**) with the ab ligand coordinating in a side-on fashion to the manganese ion, similarly to **8** and **9**. In general, the R-N=N-R ligand is described as dianionic hydrazido ligands for early transition metals and

Please do not adjust margins

Please do not adjust margins

neutral azo-ligand for late transition metals.[52] To our knowledge, this is the first reported instance of a manganese-bound N-N double bond, with only few examples of such coordination for 3d metal ions.[53–58]

Comparison of **10** with a structurally similar iron-azobenzene complex[12] (d_{N-N} = 1.398(2) Å), described as metal bound radical anion, shows a similarly elongated N-N bond, especially with regards to the free ab with no significant deviations from the original bond C-N-N bond angles.[51] For **10** an IR absorption of 1470 cm^{-1} for the N-N stretching as well as an UV-Vis absorption at 417 nm and 474 nm could be detected.

For all complexes **7** – **10**, the Mn-N_{NON} bond lengths (1.994(6) Å – 2.045(5) Å) lie in the range of similar, three coordinate Mn^{II} silyl(aryl)amido complexes and **4** (d_{Mn-N} = 2.05±0.1 Å) .[59,60]

Due to the high paramagnetic character of the manganese ions, no additional information could be gathered by means of ^{1}H-NMR spectroscopy. However, given the elongation of the central element-element double bond of the substrate in all cases and computational description of related manganese alkyne complexes as Mn(II) bound radical anions it is tempting to ascribe a similar situation for the herein shown manganese π-complexes compounds.

Synthesis of iron complexes

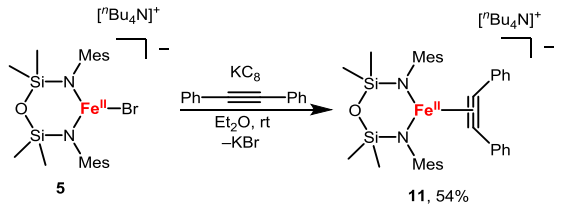

Schema 4. Synthesis of **11** by reduction of **5** in presence of diphenylacetylene.

Reduction of **5** with KC_8 in presence of diphenylacetylene resulted in the formation of the iron(II) complex [^{n}Bu$_4$N][(^{Mes}NON)Fe^{II}(PhCCPh)] (**11**). A related side-on coordination of alkynes to two-coordinate low-valent iron complexes was observed before.[10,11,15,61,62] Comparison of the N-Fe-N bond angle in **11** (109.87(6)°) with Fe-α-Diimine (80.83(3)°), Fe-NacNac (93.75(8)°) and Fe-diamide (117.74(15)°) complexes coordinating to an internal C-C triple bond shows that the bond angle is mainly dictated by the ligand geometry with bidentate ligands resulting in overall sharper angles. The length of the C-C bond (1.263 – 1.296 Å) however does not correlate with the bond angle in these compounds but is clearly elongated in comparison to the free diphenylacetylene (~1.20 Å). The Fe-N (1.955(2) – 1.986(2) Å) and Fe-C (1.929 – 1.966 Å) bond lengths are of similar length in all cases.

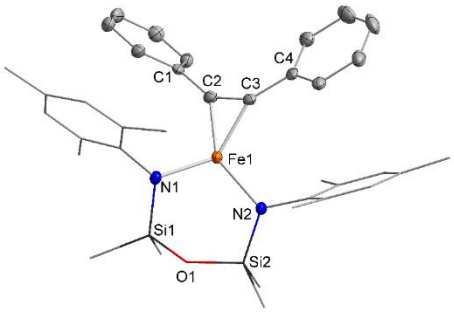

Figure 4. Molecular structure of the anion in **11**. Hydrogen atoms are omitted for clarity, thermal ellipsoids are shown with 50% probability. Selected bond lengths (Å) and angles (deg): Fe1-N1 1.955(2), Fe1-N2 1.976(1), Fe1-C2 1.966(2), Fe1-C3 1.958(2), C1-C2 1.461(2), C2-C3 1.287(2), C3-C4 1.463(2), N1-Fe1-N2 109.87(6), C1-C2-C3 146.90(17), 143.13(17).

Spectroscopic investigation by means of ^{1}H-NMR spectroscopy shows a clear change in comparison to **5**: The formerly low-shifted signals now appear below 21 ppm with signals at 20.45 ppm, 13.86 ppm, 12.93 ppm, 11.63 ppm, 8.92 ppm and –4.23 ppm (Figure SXX), with the counter-ion showing resonances between 0 and 4 ppm. This implicates a change in the electronic situation of the Fe-NON fragment. Overall the structural and spectroscopic data indicates an activation of the C-C triple bond, similar to [Fe(N(SiMe$_3$)$_2$)$_2$(PhCCPh)], which was described as a Fe^{II} bound radical anion by means of computational bond analysis. Interestingly, the geometry of the ligand does not seem to impact the coordination mode.

Synthesis of cobalt complexes

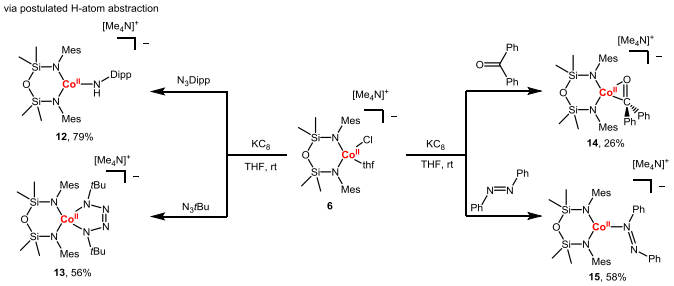

Schema 5. Synthesis of **13** – **16** through substrate activation with [(^{Mes}NON)Co^{II}(thf)Cl]$^-$ (**6**) under reducing conditions.

The reduction of **6** in presence of Dipp-N_3lead to the formation of the primary arylamido complex **12**, analogous to observations made for manganese (**7**). Accordingly it is presumably product of C-H abstraction through an intermediary imido cobalt species, as observed for trigonal imido cobalt complexes bearing monodentate silylamide ligands.[38,63] Comparison of **12** with [$L_2Co^{II}NHDipp]^-$ (L = N(DippSiMe$_3$)) reveals similar Co-N bond lengths, as well as N(H)-C bond lengths with an expectedly sharper N_{NON}-Co-N_{NON} bond angle for **12**. The ^{1}H-NMR spectrum of the compound in [D8]THF (Figure S4) shows a series of mostly weak signals ranging from -6.33 to 47.56 ppm.

Employing the sterically less demanding *tert*-butylazide leads to the formation of the tetrazene complex **13**, result of a [2+3] dipolar addition of a second equivalent of the azide to an initially formed *tert*-butyl imido complex. This contrasts the

This journal is © The Royal Society of Chemistry 20xx

Please do not adjust margins

Please do not adjust margins

reaction of $[Co^{I}L_2]^-$ (L = $N(SiMe_3)_2$) that stops at the imido complex $[Co^{III}(N^tBu)L_2]^-$. In comparison to $[Co^{III}(N^tBu)L_2]^-$ this indicates an overall increased space around the cobalt ion in **13** due to the less obtuse N-M-N angle of the ^{Mes}NON ligand. So far, only a few cobalt-tetrazene complexes have been reported, mostly with an additional Cp-ligand.[64,65] More structurally related compounds have been reported in the group of Betley with the use of a dipyrromethene ligand system.[66,67] Comparison of **13** with $[LCo^{II}(N_4(CMe_2{}^nBu)_2]$ (L = 5-mesityl-1,9-(2,4,6-$Ph_3C_6H_2$)dipyrrin) shows similar N_{NON}-Co-N_{NON} and N-N bond lengths but longer Co-N3/6 bond lengths (1.966/1.967 Å vs. 1.924/1.945 Å). The Co ion in **13** is coordinated in a slightly distorted tetrahedral fashion with τ_4 = 0.84. The rather uniform N-N bond lengths within the tetrazene, as well as bond metrics around the cobalt ion strongly indicate a cobalt(II) bound tetrazene radical anion. The ^{1}H-NMR spectrum (Figure S5) displays sharp signals at 14.18 and 13.20 ppm, most likely stemming from the mesityl substituents, and broader resonances at 11.87, 9.58, 6.99 and –2.48. The latter can be assigned to the $SiMe_3$-protons, while the other signals are probably originating from the *tert*-butyl groups and the counter-ion. The rapid formation of **12** from the imido complex [(^{Mes}NON)Co(NDipp)] is stable, leading to **12** via HAT from the solvent.

Reduction of **6** in presence of benzophenone (bp) yields the Co-benzophenone complex **14** with a side-on coordination of the substrate to the metal ion. This behaviour has been observed for an iron(II) *ß*-diketiminate (= L^1) complex $[L^1Fe^{II}(\eta^2\text{-}OCPh_2)]$.[14] In both cases the C-O bond length exhibits an increase from 1.23 Å to 1.331(7) Å (in **14**) and 1.358(5) Å (in $[L^1Fe^{II}(\eta^2\text{-}OCPh_2)]$), indicating a reduced C-O bond order, which is in good comparison to an end on cobalt(II) bound ketyl radical anion $[Co^{II}(N(SiMe_3)_2)_2(OCPh_2)]$ ($d_{C\text{-}O}$ = 1.324(2) Å).[68] Investigations via UV-Vis spectroscopy reveal an absorption shoulder at 370 nm, showing a strong blue shift in comparison with $[LFe^{II}(\eta^2\text{-}OCPh_2)]$ (520 nm) and no visible feature in the region of expected ketyl radicals.[69–71] The ^{1}H-NMR spectrum shows a total of seven resonances in the paramagnetic range (Figure S6) in different intensities. While no traces of **6** could be detected, a clear assignment of the signals is not possible. Comparison of **14** with $[Co^{II}(N(SiMe_3)_2)_2(OCPh_2)]$ gives no common resonances for the ketyl ligand.

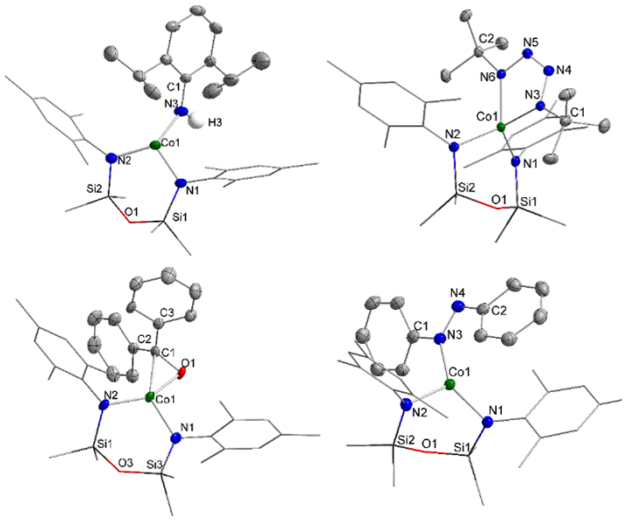

Figure 5. Molecular structures of **12** (top left), **13** (top right), **14** (bottom left), **15** (bottom right). Hydrogen atoms are omitted for clarity, thermal ellipsoids are shown with 50% probability.

Reaction of **6** with KC_8 in the presence of ab does not lead to a side-on coordination as in **10**, but rather an asymmetric coordination of the substrate to the Co ion in **15** via one nitrogen atom. This motif has not yet been reported for three-coordinate cobalt complexes but is present in higher coordinate Co complexes, as shown in recent years,[72–78] with N-N bond lengths between 1.261 and 1.330 Å, though mostly on the lower end. **15** exhibits a significantly longer N-N bond (1.348(2) Å), indicating a different bonding situation. A similar bond length has been described for a non-coordinated azo-radical anion (d = 1.326(7) Å).[79] The Co-N3 bond length in **15** however lies in the range of before mentioned asymmetrically coordinated azo complexes. The ^{1}H-NMR spectrum reveals a variety of signals in the paramagnetic range between -25.48 and 72.49 ppm (Figure S7). The strong paramagnetic shift prohibits a clear assignment of these signals.

This journal is © The Royal Society of Chemistry 20xx

Please do not adjust margins

Please do not adjust margins

Table 2. Selected bond lengths (Å) and angles (deg.) for **7** – **10** and comparison with the corresponding substrate: [ab]: *E*-azobenzene ,[bp]: benzophenone.[51,80]

Bond	**12**	**13**	**14**	**15**	Free
substrate	NHDipp	$^{t}Bu_2N_4$	bp	ab	substrate
Co1-N1	1.943(2)	1.973(3)	1.930(5)	1.951(2)	
Co1-N2	1.917(2)	1.981(3)	1.899(5)	1.938(2)	
Co1-N3	1.910(3)	1.966(3)		1.929(1)	
Co1-N6		1.967(3)			
Co1-C1			2.027(6)		
Co1-O1			1.882(4)		
N3-N4		1.314(4)		1.348(2)	1.243[ab]
C1-C2			1.491(8)		1.48[bp]
C2-C3			1.479(8)		1.50[bp]
C1-O1			1.331(7)		1.23[bp]
N4-N5		1.338(4)			
N5-N6		1.306(4)			
N3-C1	1.364(3)	1.504(5)		1.410(2)	1.433[ab]
N4-C2				1.380(2)	1.433[ab]
N6-C2		1.495(4)			
N1-Co1-N2	110.08(9)	106.36(11)	109.71(20)	112.82(6)	
Co1-N3-C1	138.50(19)			122.39(11)	
C2-C1-C3			122.86(59)		122[bp]
C1-N3-N4				113.57(14)	113.6[ab]
N3-N4-C2				111.81(14)	113.6[ab]

Conclusions

Building on our work on linear homoleptic 3d-metal(I) silylamides of the type $[ML_2]^-$ (L = $N(SiMe_3)_2$, N(Dipp)$SiMe_3$) in bond activation, we now showed the consequences of using a chelating bis(silylamid) ligand set ($[(N\{Mes\}SiMe_2)_2O]^{2-}$ = $^{Mes}NON^{2-}$) set with an enforced bent N–M–N angle. Reduction of in part known neutral dimeric compounds of the type $[(^{Mes}NON)M]_2$ as well as novel monomeric anionic complexes $[NR_4][(^{Mes}NON)MX]$ (R = Me or ^{n}Bu; X = Br or Cl) of Mn, Fe and Co resulted in unproductive decomposition, attributed to an increased reactivity of the presumed strongly bent two-coordinate metal(I) species $[(^{Mes}NON)M]^-$. The presence of such a low-valent complex was substantiated by trapping with a variety of π-acceptor substrates, such as alkenes, alkynes, diazobenzene and ketones. Isolation and analysis of respective π-complexes allowed for mapping out consequences of a strongly bent N–M–N axis, in comparison with the more obtuse bis(mono-silylamide) ligand set. For example, in case of manganese coordination of Z-stilbene leads to *Z*→*E* isomerisation of the substrates. This hints to the presence of a metal(II) bound radical anion, as in the related a linear iron(I) silylamide system. For benzophenone (bp) the side-on cobalt complex $[Co(^{Mes}NON)(\eta^2\text{-bp}]^-$ shows no substantial radical anion behaviour, opposed to the terminal cobalt(II) ketyl complex $[Co^{II}(bp^-)(N(SiMe_3)_2)_2]^-$. Activation of different organo azides resulted not in the expected trigonal imido complexes but either subequent H atom abstraction and amide formation, or [2+3] cycloaddition with a second organo azide to give a tetrazene complex. It thus shows, that it is possible to tune the reactivity of a two-coordinate open-shell 3d-metal(I) silylamide by changing and/or fixing the N–M–N angle of the ancillary ligand set.

Author Contributions

K. D. performed the synthesis and analysis of **4** – **6**, **11**. T. V. performed the synthesis and characterization **7**, **9**, **10**, **12**, **13**, **15**. G. S. synthesised the remaining compounds, did all remaining analyses and wrote the manuscript. C. G. W. supervised the project and contributed to the manuscript.

Conflicts of interest

There are no conflicts to declare.

Acknowledgements

The Deutsche Forschungsgemeinschaft is gratefully acknowledged for funding (grant WE 5627/4-1).

Notes and references

§ Due to a disorder, two different bond lengths were determined.

1 M. L. Di Vona and V. Rosnati, *J. Org. Chem.*, 1991, **56**, 4269–4273.
2 T. Wirth, *Angew. Chem. Int. Ed.*, 1996, **35**, 61–63.
3 M. Ephritikhine, *Chem. Commun.*, 1998, 2549–2554.
4 A. Fuerstner and A. Hupperts, *J. Am. Chem. Soc.*, 1995, **117**, 4468–4475.
5 R. D. Rieke and S.-H. Kim, *J. Org. Chem.*, 1998, **63**, 5235–5239.
6 T. Imamoto and S. Nishimura, *Chem. Lett.*, 1990, 1141–1142.
7 E. J. Roskamp and S. F. Pedersen, *J. Am. Chem. Soc.*, 1987, **109**, 3152–3154.
8 M. Szwarc, M. Levy and R. Milkovich, *J. Am. Chem. Soc.*, 1956, **78**, 2656–2657.
9 G. Lunn and E. B. Sansonne, *Synthesis*, 1985, 1104–1108.
10 S. A. Stoian, Y. Yu, J. M. Smith, P. L. Holland, E. L. Bominaar and E. Münck, *Inorg. Chem.*, 2005, **44**, 4915–4922.
11 Y. Yu, J. M. Smith, C. J. Flaschenriem and P. L. Holland, *Inorg. Chem.*, 2006, **45**, 5742–5751.
12 A. R. Sadique, E. A. Gregory, W. W. Brennessel and P. L. Holland, *J. Am. Chem. Soc.*, 2007, **129**, 8112–8121.
13 T. R. Dugan, E. Bill, K. C. MacLeod, G. J. Christian, R. E. Cowley, W. W. Brennessel, S. Ye, F. Neese and P. L. Holland, *J. Am. Chem. Soc.*, 2012, **134**, 20352–20364.
14 K. C. MacLeod, I. M. DiMucci, E. P. Zovinka, S. F. McWilliams, B. Q. Mercado, K. M. Lancaster and P. L. Holland, *Organometallics*, 2019, **38**, 4224–4232.
15 S. C. Bart, E. J. Hawrelak, E. Lobkovsky and P. J. Chirik, *Organometallics*, 2005, **24**, 5518–5527.
16 S. C. Bart, E. Lobkovsky, E. Bill and P. J. Chirik, *J. Am. Chem. Soc.*, 2006, **128**, 5302–5303.
17 Y. Chen, R. Chen, C. Qian, X. Dong and J. Sun, *Organometallics*, 2003, **22**, 4312–4321.
18 I. S. Paulino and U. Schuchardt, *Catal. Commun.*, 2004, **5**, 5–7.
19 W. Zhang, W. Chai, W.-H. Sun, X. Hu, C. Redshaw and X. Hao, *Organometallics*, 2012, **31**, 5039–5048.
20 C.-Y. Lin and P. P. Power, *Chem. Soc. Rev.*, 2017, **46**, 5347–5399.
21 S. Roy, K. C. Mondal and H. W. Roesky, *Acc. Chem. Res.*, 2016, **49**, 357–369.
22 R. Weller, I. Müller, C. Duhayon, S. Sabo-Etienne, S. Bontemps and C. G. Werncke, *Dalton Trans.*, 2021, **50**, 4890–4903.
23 G. Mund, A. J. Gabert, R. J. Batchelor, J. F. Britten and D. B. Leznoff, *Chem. Commun.*, 2002, 2990–2991.

 This journal is © The Royal Society of Chemistry 20xx

Please do not adjust margins

Please do not adjust margins

24 A. K. Das, Z. Moatazedi, G. Mund, A. J. Bennet, R. J. Batchelor and D. B. Leznoff, *Inorg. Chem.*, 2007, **46**, 366–368.
25 G. Mund, D. Vidovic, R. J. Batchelor, J. F. Britten, R. D. Sharma, C. H. W. Jones and D. B. Leznoff, *Chem. Eur. J.*, 2003, **9**, 4757–4763.
26 R. J. Schwamm, M. P. Coles and C. M. Fitchett, *Dalton Trans.*, 2017, **46**, 4066–4074.
27 R. Schwamm, M. Anker, M. Lein and M. P. Coles, *Angew. Chem. Int. Ed.*, 2018, 1503–1507.
28 M. J. Evans, M. D. Anker, A. Mouchfiq, M. Lein and J. R. Fulton, *Chem. Eur. J.*, 2020, **26**, 2606–2609.
29 R. J. Schwamm, C. A. von Randow, A. Mouchfiq, M. J. Evans, M. P. Coles and J. R. Fulton, *Eur. J. Inorg. Chem.*, 2021, 3466–3473.
30 A. J. Elias, H. G. Schmidt, M. Noltemeyer and H. W. Roesky, *Eur. J. Solid State Inorg. Chem.*, 1992, **29**, 23.
31 A. J. Elias, H. W. Roesky, W. T. Robinson and G. M. Sheldrick, *J. Chem. Soc., Dalton Trans.*, 1993, 6.
32 A. J. Blake, N. L. Gillibrand, G. J. Moxey and D. L. Kays, *Inorg. Chem.*, 2009, **48**, 10837–10844.
33 A. B. Scharf, S.-L. Zheng and T. A. Betley, *Dalton Trans.*, 2021, **50**, 6418–6422.
34 C. G. Werncke, J. Pfeiffer, I. Müller, L. Vendier, S. Sabo-Etienne and S. Bontemps, *Dalton Trans.*, 2019, **48**, 1757–1765.
35 R. Weller, L. Völlinger and C. G. Werncke, *Eur. J. Inorg. Chem.*, 2021, **2021**, 4383–4392.
36 E. R. King and T. A. Betley, *J. Am. Chem. Soc.*, 2009, **131**, 14374–14380.
37 J. Camacho-Bunquin, M. J. Ferguson and J. M. Stryker, *J. Am. Chem. Soc.*, 2013, **135**, 5537–5540.
38 A. Reckziegel, C. Pietzonka, F. Kraus and C. G. Werncke, *Angew. Chem. Int. Ed.*, 2020, **59**, 8527–8531.
39 C. Ni, B. Rekken, J. C. Fettinger, G. J. Long and P. P. Power, *Dalton Trans.*, 2009, 8349.
40 G. Sieg, I. Müller, K. Weißer and C. G. Werncke, *submitted*.
41 H. C. Wang, G. Levin and M. Szwarc, *J. Am. Chem. Soc.*, 1977, **99**, 2642–2647.
42 H. G. Alt and H. E. Engelhardt, *J. Organomet. Chem.*, 1989, **362**, 117–124.
43 G. S. Girolami, C. G. Howard and G. Wilkinson, *J. Chem. Soc., Dalton Trans.*, 1985, 921–929.
44 R. Weller, L. Ruppach, A. Shlyaykher, F. Tambornino and C. G. Werncke, *Dalton Trans.*, 2021, **50**, 10947–10963.
45 W. Chen, Q. Chen, Y. Ma, X. Leng, S.-D. Bai and L. Deng, *Chin. Chem. Lett.*, 2020, **31**, 1342–1344.
46 G. Bai, P. Wei, A. K. Das and D. W. Stephan, *Dalton Trans.*, 2006, 1141–1146.
47 G. Bai, P. Wei and D. W. Stephan, *Organometallics*, 2005, **24**, 5901–5908.
48 H. Wadepohl, A. Metz and H. Pritzkow, *Chem. Eur. J.*, 2002, **8**, 1591–1602.
49 G. Casalone, A. Gavezzotti, C. Mariani, A. Mugnoli and M. Simonetta, *Acta Cryst.*, 1970, **B26**, 1–8.
50 A. Hoekstra, P. Meertens and A. Vos, *Acta Crystallogr. B: Struct. Sci. Cryst. Eng. Mater.*, 1975, **31**, 2813–2817.
51 C. J. Brown, *Acta Cryst*, 1966, **21**, 146–152.
52 M. Retboell and K. A. Joergensen, *Inorg. Chem.*, 1994, **33**, 6403–6405.
53 Z. W. Gilbert, R. J. Hue and I. A. Tonks, *Nat. Chem.*, 2016, **8**, 63–68.
54 L. D. Durfee, J. E. Hill, P. E. Fanwick and I. P. Rothwell, *Organometallics*, 1990, **9**, 75–80.
55 S. D. Ittel and J. A. Ibers, *J. Organomet. Chem.*, 1973, **57**, 389–402.
56 Y. Fedotova, A. Kornev, V. Sushev, Y. Kursky, T. Mushtina, N. Makarenko, G. Fukin, G. Abakumov, L. Zakharov and A. Rheingold, *J. Organomet. Chem.*, 2004, **689**, 3060–3074.
57 Y. Gao, G. Li and L. Deng, *J. Am. Chem. Soc.*, 2018, **140**, 2239–2250.
58 N. S. Labrum, A. C. Cabelof and K. G. Caulton, *Chem. Eur. J.*, 2020, **26**, 13915–13926.
59 C. G. Werncke, E. Suturina, P. C. Bunting, L. Vendier, J. R. Long, M. Atanasov, F. Neese, S. Sabo-Etienne and S. Bontemps, *Chem. Eur. J.*, 2016, **22**, 1668–1674.
60 P. Mastroplerro, A. R. Kennedy and E. Hevia, *Eur. J. Inorg. Chem.*, 1016–1022.
61 J. Cheng, Q. Chen, X. Leng, S. Ye and L. Deng, *Inorg. Chem.*, 2019, **58**, 13129–13141.
62 I. Müller, D. Munz and C. G. Werncke, *Inorg. Chem.*, 2020, **59**, 9521–9537.
63 A. Reckziegel, M. Kour, B. Battistella, S. Mebs, K. Beuthert, R. Berger and C. G. Werncke, *Angew. Chem. Int. Ed.*, 2021, **60**, 15376–15380.
64 W. Zhong, Q. Yang, Y. Shang, G. Liu, H. Zhao, Y. Li and H. Yan, *Organometallics*, 2012, **31**, 6658–6668.
65 S. Vanicek, M. Jochriem, C. Hassenrück, S. Roy, H. Kopacka, K. Wurst, T. Müller, R. F. Winter, E. Reisner and B. Bildstein, *Organometallics*, 2019, **38**, 1361–1371.
66 E. R. King, G. T. Sazama and T. A. Betley, *J. Am. Chem. Soc.*, 2012, **134**, 17858–17861.
67 Y. Baek and T. A. Betley, *J. Am. Chem. Soc.*, 2019, **141**, 7797–7806.
68 G. Sieg, Q. Pessemesse, S. Reith, S. Yelin, C. Limberg, D. Munz and C. G. Werncke, *Chem. Eur. J.*, 2021, **27**, 16760–16767.
69 O. P. Lam, C. Anthon, F. W. Heinemann, J. M. O'Connor and K. Meyer, *J. Am. Chem. Soc.*, 2008, **130**, 6567–6576.
70 Z. Hou, T. Miyano, H. Yamazaki and Y. Wakatsuki, *J. Am. Chem. Soc.*, 1995, **117**, 4421–4422.
71 T. A. Scott, B. A. Ooro, D. J. Collins, M. Shatruk, A. Yakovenko, K. R. Dunbar and H.-C. Zhou, *Chem. Commun.*, 2009, 65–67.
72 P. Ghosh, S. Samanta, S. K. Roy, S. Joy, T. Krämer, J. E. McGrady and S. Goswami, *Inorg. Chem.*, 2013, **52**, 14040–14049.
73 N. Leconte, B. Baptiste, C. Philouze and F. Thomas, *Dalton Trans.*, 2018, **47**, 11303–11307.
74 R. Rakshit, S. Ghorai, A. Sarmah, A. Tiwari, R. K. Roy and C. Mukherjee, *Dalton Trans.*, 2015, **44**, 3724–3727.
75 Y.-F. Qiao, L. Du, J. Zhou, Y. Hu, L. Li, B. Li and Q.-H. Zhao, *J. Coord. Chem.*, 2014, **67**, 2615–2629.
76 S. Sinha, S. Das, R. Mondal, S. Mandal and N. D. Paul, *Dalton Trans.*, 2020, **49**, 8448–8459.
77 H. O. Oloyede, J. A. O. Woods, H. Görls, W. Plass and A. O. Eseola, *New J. Chem.*, 2019, **43**, 18322–18330.
78 H. O. Oloyede, J. A. O. Woods, H. Görls, W. Plass and A. O. Eseola, *New J. Chem.*, 2020, **44**, 14849–14858.
79 W. Wang, G. Tan, R. Feng, Y. Fang, C. Chen, H. Ruan, Y. Zhao and X. Wang, *Chem. Commun.*, 2020, **56**, 3285–3288.
80 E. B. Fleischer, N. Sung and S. Hawkinson, *J. Phys. Chem.*, 1968, **72**, 4311–4312.

Please do not adjust margins

Bond activation by bent, formally manganese(I), iron(I) and cobalt(I) di(silylamides)

Grégoire Sieg, Theres Vaupel, Kevin Dollberg, C. Gunnar Werncke*

Chemistry Department, Philipps-University, Hans-Meerwein-Str. 4, 35043 Marburg, Germany. E-mail: gunnar.werncke@chemie.uni-marburg.de.

Table of Contents

1. General Considerations 3
2. Synthesis, Crystallization and Charakterization 4
1.1. Synthesis of [Mn(^{Mes}NON)]$_2$ (1) 4
1.2. Synthesis of [Me$_4$N][Mn(^{Mes}NON)Cl)(thf)] (4) 4
1.3. Synthesis of [^{n}Bu$_4$N][Fe(^{Mes}NON)Br)] (5) 4
1.4. Synthesis of [Me$_4$N][Co(^{Mes}NON)Cl(thf)] (6) 5
1.5. Synthsis of [Me$_4$N][Mn(^{Mes}NON)(NHDipp)] (7) 5
1.6. Synthesis of [Me$_4$N][Mn(^{Mes}NON)(trans-stilbene)] (8) 5
1.7. Synthesis of [Me4N][Mn(^{Mes}NON)(Ph$_2$C=CH$_2$)] (9) 6
1.8. Synthesis of [Me$_4$N][Mn(^{Mes}NON)(PhN=NPh)] (10) 6
1.9. Synthesis of [Me$_4$N][Fe(^{Mes}NON)(PhCCPh)] (11) 6
1.10. Synthesis of [Me$_4$N][Co(^{Mes}NON)(NHDipp)] (12) 7
1.11. Synthesis of [Me4N][Co(^{Mes}NON)(N$_4$^{t}Bu$_2$)] (13) 7
1.12. Synthesis of [Me$_4$N][Co(^{Mes}NON)(Ph$_2$CO)] (14) 7
1.13. Synthesis of [Me4N][Co(^{Mes}NON)(PhN=NPh)] (15) 7
1.14. NMR spectroscopy 9
1.15. Mass spectrometry 13
1.16. IR spectroscopy 14
1.17. UV-Vis spectroscopy 18
3. Crystallographic Details 23
4. References 37

1. General Considerations

All manipulations were carried out in a glovebox under a dry argon atmosphere, unless indicated otherwise. Used solvents were either dried by continuous distillation over sodium metal for several days, degassed via three freeze-pump cycles and stored over molecular sieves 4 Å. Deuterated solvents were used as received, degassed via three freeze-pump cycles and stored over molecular sieves 4 Å. The ^{1}H-NMR spectra were recorded on a BRUKER AV 300 spectrometer (Bruker Corporation, Billerica, MA, USA). Chemical shifts are reported in ppm relative to the residual proton signals of the solvent. $w_{1/2}$ is the spectral linewidth of a signal at half its maximum intensity, all using the MestreNova software package (Mestrelab, Version 14.2.0, Santiago de Compostela, Spain). IR measurements were conducted on a Bruker Alpha ATR-IR spectrometer processed with the OPUS Software (Version 7.5) (Bruker Corporation, Billerica, MA, USA). Elemental analyses were performed by the "in-house" service of the Chemistry Department of the Philipps University Marburg, Germany using a CHN(S) analyzer vario MICRO Cube (Elementar Analysensysteme GmbH, Langenselbold, Germany). UV/Vis-spectra were recorded on an AnalytikJena Specord S600 diode array spectrometer (AnalytikJena, Jena, Germany). EPR spectra were recorded on a BRUKER Magnettech ESR5000 spectrometer. EPR simulations were performed using the program EasySpin.[1]

$[M^{II}(N(SiMe_3)_2)_2]^2$ (M = Mn, Fe, Co), [Fe(^{Mes}NON)][3], [Co(^{Mes}NON)][4], $^{Mes}NONH_2$,[5] N_3Dipp[6] and $N_3{}^tBu$[7] were synthesized according to literature procedures. $[Me_4N]Cl$, $[^nBu_4N]Br$, 1,1-diphenylethylene, *trans*-1,2-diphenylethylene, azobenzene, diphenylacetylene and benzophenone were purchased from commercial sources. KC_8 was prepared by mixing respective amounts of graphite (previously dried in vacuo via heatgun) with freshly cut potassium metal. The mixture was heated in vacuo via heatgun until all potassium metal had reacted.

2. Synthesis, Crystallization and Charakterization

1.1. Synthesis of [Mn(^{Mes}NON)]$_2$ (1)

^{Mes}NONH$_2$ (401 mg, 1.00 mmol, 1.00 Aq.) and [Mn(N(SiMe$_3$)$_2$)$_2$] (376 mg, 1.00 mmol, 1.00 eq.) were dissolved in 10 mL of *n*-pentane. The solution was stored at room temperature overnight to afford **1** as a crystalline violet solid (209 mg, 0.23 mmol, 46%).

^{1}H-NMR: Due to strong signal-broadening, only solvent residue signals can be assigned.

IR (ATR, cm^{-1}): 2952 (w), 2901 (w), 2856 (w), 1462 (w), 1295 (w), 1256 (m), 1227 (m), 1196 (m), 1155 (w), 1140 (w), 1041 (s), 953 (m), 912 (s), 858 (m), 850 (s), 807 (s), 782 (s), 718 (m), 702 (m), 671 (w), 646 (w), 591 (w), 568(w), 539 (w), 525 (w), 502 (w), 459 (w)

Elemental analysis: calculated ($C_{44}H_{68}Mn_2N_4O_2Si_4$ 907.27 g/mol) C 58.25 H 7.55 N 6.18; experimental C 57.89 H 7.69 N 6.08

μ_{eff} (Evans) = 7.58 μ_B.

MS: LIFDI(+): Mn(^{Mes}NON)]$_2^+$ *m/z* = 906.31685 (100%) (experimental), 906.31803 (calculated)

Crystals, suitable for X-ray diffraction analysis were obtained directly from the reaction mixture.

1.2. Synthesis of [Me$_4$N][Mn(^{Mes}NON)Cl)(thf)] (4)

[Mn(^{Mes}NON)]$_2$ (200 mg, 0.22 mmol, 1.00 eq.) and [Me$_4$N]Cl (48 mg, 0.44 mmol, 2.00 eq.) were dissolved in 4 mL of THF and stirred for 30 min. The resulting clear, light-yellow solution was layered with 10 mL of *n*-pentane to afford **4** as a colorless crystalline solid (260 mg, 0.40 mmol, 92%).

^{1}H-NMR: Due to strong signal-broadening, only solvent residue signals can be assigned.

IR (ATR, cm^{-1}): 2944 (w), 2895 (w), 1468 (m), 1416 (m), 1367 (w), 1297 (m), 1231 (s), 1155 (w), 1000 (s), 961 (s), 932 (s), 879 (m), 856 (m), 794 (s), 763 (s), 712 (m), 665 (m), 584 (w), 514 (m), 453 (w)

Elemental analysis: calculated ($C_{30}H_{54}ClMnN_3O_2Si_2$ 635.33 g/mol) C 56.71 H 8.57 N 6.61; experimental C 55.64 H 8.46 N 6.55; low C-values can be attributed to the formation of siliconcarbide during the combustion process.

Crystals, suitable for X-ray diffraction analysis were obtained by layering a solution of **4** in THF with Et$_2$O at –40 °C.

1.3. Synthesis of [^{n}Bu$_4$N][Fe(^{Mes}NON)Br)] (5)

[Fe(^{Mes}NON)]$_2$ (90.1 mg, 0.10 mmol, 1.00 eq.) and [^{n}Bu$_4$N]Br (64.5 mg, 0.20 mmol, 2.00 eq.) were dissolved in 2 mL of Et$_2$O and the mixture was stirred overnight. The resulting solution was filtered and then layered with 2 mL of *n*-pentane at –40 °C to afford **5** as crystalline white solid (62 mg, 0.08 mmol, 40%).

^{1}H NMR (300 MHz, 300 K, [D8]THF, ppm): δ = 61.94 (br, 6H, *p*-Mes), 53.66 (br, 4H, *m*-Mes), 37.75 (br, 12H, *o*-Mes), 9.75 (br, 12H, SiMe$_2$).

Elemental analysis: calculated ($C_{38}H_{70}FeBrN_3OSi_2$ 776.92 g/mol) C 58.75 H 9.08 N 5.64; experimental C 58.57 H 9.06 N 5.64.

IR: (ATR, cm-1): $\tilde{\nu}$ = 2959 (w), 2903 (w), 2870 (w), 2160 (vw), 1466 (m), 1418 (w), 1381 (w), 1297 (w), 1229 (s), 1155 (m), 1004 (s), 959 (m), 918 (s), 858 (m), 807 (s), 759 (s), 714 (m), 667 (w), 644 (w), 586 (w), 531 (m).

Crystals, suitable for X-ray diffraction analysis were obtained by layering a solution of **5** in Et_2O with *n*-pentane at –40 °C.

1.4. Synthesis of [Me$_4$N][Co(^{Mes}NON)Cl(thf)] (6)

[Co(^{Mes}NON)]$_2$ (50.0 mg, 0.055 mmol, 1.00 eq.) and [Me$_4$N]Cl (12 mg, 0.11 mmol, 1.00 eq.) were dissolved in 2 mL of THF. The mixture was stirred overnight. The resulting dark solution was layered with 2 mL of Et_2O to afford **6** as crystalline blue solid (32 mg, 0.05 mmol, 45%).

^{1}H-NMR (300 MHz, 298 K, [D8]THF, ppm) δ: 53.08 (s, 3H, Me-para), 42.49 (s, 6H, 2 x Me-ortho), 36.20 (s, 2H, 2 x HAr), 4.48 (s, 6H, 2 x Si-Me).

Elemental analysis: calculated ($C_{30}H_{54}CoClN_3O_2Si_2$ 639.33 g/mol) C 56.36 H 8.51 N 6.57; experimental C 55.59 H 8.27 N 6.58.

IR: (ATR, cm-1): $\tilde{\nu}$ = 3025 (w), 2955 (m), 2899 (m), 1468 (m), 1416 (m), 1367 (w), 1297 (m), 1237 (s), 1219 (s), 1153 (m), 1120 (w), 1064 (w), 998 (s), 965 (s), 939 (s), 910 (s), 858 (m), 798 (s), 757 (s), 722 (m), 706 (m), 667 (m), 638 (m), 591 (m), 518 (s), 457 (w), 401 (w).

Crystals, suitable for X-ray diffraction analysis were obtained by layering a solution of **6** in THF with *n*-pentane at –40 °C.

1.5. Synthsis of [Me$_4$N][Mn(^{Mes}NON)(NHDipp)] (7)

Me$_4$N][Mn(^{Mes}NON)Cl)(thf)] (50 mg, 0.079 mmol, 1.00 eq.), KC_8 (12.1 mg, 0.089 mg, 1.13 eq.) and 2,6-di*iso*propylazide (18.2 mg, 0.089 mmol, 1.13 eq) were dissolved in 2 mL of THF. Gas evolution was immediately observed. The resulting dark solution was filtered and the solvent was removed. The resulting dark residue was dissolved in 2 mL of Et_2O and layered with 2 mL of *n*-pentane to afford **7** as crystalline red solid.

Crystals, suitable for X-ray diffraction analysis were obtained by layering a solution of **7** in Et_2O with *n*-pentane at –40 °C.

1.6. Synthesis of [Me$_4$N][Mn(^{Mes}NON)(trans-stilbene)] (8)

[Me$_4$N][Mn(^{Mes}NON)Cl)(thf)] (100 mg, 0.15 mmol, 1.00 eq.), KC_8 (23 mg, 0.17 mmol, 1.13 eq.) and (*Z*)-stilbene (27 mg , 0.15 mmol, 1.00 eq.) were dissolved in 2 mL of THF and stirred for 30 min. The mixture was then filtered and the resulting dark brown solution was layered with 1.5 mL of *n*-pentane to afford **8** as a crystalline dark brown solid (57 mg, 0.081 mmol, 54%).

^{1}H-NMR: Due to strong signal-broadening, only solvent residue signals can be assigned.

IR (ATR, cm^{-1}): 2942 (w), 2901 (w), 1583 (m), 1480 (m), 1416 (m), 1367 (w), 1293 (m), 1229 (s), 1173 (w), 1157 (w), 1000 (m), 963 (s), 930 (s), 893 (m), 860 (m), 792 (s), 791 (s), 714 (s), 696 (s), 656 (m), 582 (w), 514 (s)

Elemental analysis: calculated ($C_{40}H_{58}MnN_3OSi_2$ 708.03 g/mol) C 67.86 H 8.26 N 5.93; experimental C 67.12 H 7.91 N 5.56 low C-values can be attributed to the formation of siliconcarbide during the combustion process.

Crystals, suitable for X-ray diffraction analysis were obtained by layering a solution of **8** in THF with *n*-pentane at –40 °C.

1.7. Synthesis of [Me4N][Mn(^{Mes}NON)($Ph_2C=CH_2$)] (9)

[Me_4N][Mn(^{Mes}NON)Cl)(thf)] (100 mg, 0.168 mmol, 1.00 eq.), KC_8 (23 mg, 0.170 mmol, 1.00 eq.) and 1,1-diphenylethene (28.5 mg, 0.158/ mmol, 0.94 eq.) were dissolved in 2 mL of THF. The reaction mixture immediately turned dark yellow and was filtered. The fitrate was layered with 2 mL of *n*-pentane to afford (2x **9 + 9b**) as dark yellow crystalline solid (64 mg, 0.031 mmol, 57%).

^{1}H-NMR: Due to strong signal-broadening, only solvent residue signals can be assigned.

IR (ATR, cm^{-1}): 2946 (br, m), 2899 (m, br), 1585 (w), 1466 (m), 1418 (m), 1369 (w), 1297 (m), 1229 (s), 1153 (m), 1000 (m), 963 (m), 930 (s), 877 (m), 856 (m), 792 (s), 757 (s), 698 (m), 570 (m), 512 (m)

Elemental analysis: calculated (2 x **9** + **9b**; $C_{110}H_{169}Mn_3N_9O_4Si_6$ 2014.34 g/mol) C 65.57 H 8.45 N 6.26; experimental C 61.55 H 7.44 N 6.21

Crystals, suitable for X-ray diffraction analysis were obtained by layering a solution of **9** in THF with *n*-pentane at –40 °C.

1.8. Synthesis of [Me_4N][Mn(^{Mes}NON)(PhN=NPh)] (10)

[Me_4N][Mn(^{Mes}NON)Cl)(thf)] (100 mg, 0.15 mmol, 1.00 eq.), KC_8 (23.0 mg, 0.17 mmol, 1.13 eq.) and *E*-azobenzene (29.0 mg, 0.15 mmol, 1.00 eq) were dissolved in 2 mL of THF. The resulting dark red solution was filtered and the solvent was removed from the filtrate. The residue was dissolved in 2 mL of Et_2O and layered with 2 mL of *n*-pentane at –40 °C to afford **10** as crystalline red solid (63 mg, 0.088 mmol, 59%).

^{1}H-NMR: Due to strong signal-broadening, only solvent residue signals can be assigned.

IR (ATR, cm^{-1}): 2946 (w), 2893 (w), 1583 (w), 1470 (m), 1416 (w), 1367 (w), 1301 (w), 1219 (s), 1151 (m), 1068 (w), 1009 (s), 963 (m), 922 (s), 897 (m), 860 (m), 798 (s), 778 (m), 759 (s), 718 (m), 700 (s), 669 (w), 640 (w), 595 (w), 560 (w), 518 (s), 405 (w)

Elemental analysis: calculated ($C_{38}H_{56}MnN_5OSi_2$ 710.01 g/mol) C 64.28 H 7.95 N 9.86; experimental C 63.30 H 7.64 N 10.04 low C-values can be attributed to the formation of siliconcarbide during the combustion process.

Crystals, suitable for x-ray diffraction analysis were obtained by cooling a saturated solution of 10 in Et_2O to –40 °C.

1.9. Synthesis of [Me_4N][Fe(^{Mes}NON)(PhCCPh)] (11)

[^{n}Bu_4N][Fe(^{Mes}NON)Br)] (62 mg, 0.079 mmol, 1.00 eq.), Diphenylacetylene (14 mg, 0.079 mmol, 1.00 eq.) and KC_8 (12 mg, 0.087 mmol, 1.10 eq.) were dissolved in 2 mL of Et_2O. The mixture was stirred for

1 h and then filtered. The deep brown filtrate was layered with 2 mL of *n*-pentane to afford XX as deep red solid (37 mg, 0.042 mmol, 54%)

Elemental analysis: calculated ($C_{52}H_{80}FeN_3OSi_2$ 875.25.92 g/mol) C 71.36 H 9.21 N 4.80; experimental C 71.22 H 9.16 N 4.82 .

Crystals, suitable for x-ray diffraction analysis were obtained by cooling a saturated solution of **11** in Et_2O to –40 °C.

1.10. Synthesis of [Me$_4$N][Co(^{Mes}NON)(NHDipp)] (12)

[Me$_4$N][Co(^{Mes}NON)Cl)(thf)] (50 mg, 0.078 mmol, 1.00 eq.), KC_8 (12 mg, 0.089 mmol, 1.14 eq.) and 2,6-di*iso*propylazide (18 mg, 0.088 mmol, 1.14 eq) were dissolved in 2 mL of THF. Gas evolution was immediately observed. The resulting dark green solution was filtered and the solvent was removed. The resulting dark residue was dissolved in 2 mL of Et_2O and layered with 2 mL of *n*-pentane to afford **12** as crystalline green solid (44 mg, 0.062 mmol, 79%).

Elemental analysis: calculated ($C_{39}H_{67}CoN_4OSi_2$ 723.10 g/mol) C 64.46 H 9.11 N 7.91;

Crystals, suitable for X-ray diffraction analysis were obtained by layering a solution of **12** in Et_2O with *n*-pentane at –40 °C.

1.11. Synthesis of [Me4N][Co(^{Mes}NON)(N$_4$^{t}Bu$_2$)] (13)

[Me$_4$N][Co(^{Mes}NON)Cl)(thf)] (50 mg, 0.078 mmol, 1.00 eq.), KC_8 (12 mg, 0.088 mg, 1.13 eq.) and *tert*-butylazide (16 mg, 0.16 mmol, 2.00 eq.) were dissolved in 2 mL of THF. The resulting dark green mixture was filtered and the filtrate was layered with 2 mL of *n*-pentane to afford **13** as green crystalline solid (31 mg, 0.044 mmol, 56%).

Elemental analysis: calculated ($C_{34}H_{64}CoN_7OSi_2$ 702.04 g/mol) C 58.17 H 9.19 N 13.97;

Crystals, suitable for X-ray diffraction analysis were obtained by layering a solution of **13** in THF with *n*-pentane at –40 °C.

1.12. Synthesis of [Me$_4$N][Co(^{Mes}NON)(Ph$_2$CO)] (14)

[Me$_4$N][Co(^{Mes}NON)Cl)(thf)] (77 mg, 0.12 mmol, 1.00 eq.), KC_8 (18 mg, 0.13 mmol, 1.01 eq.) and benzophenone (22 mg, 0.12 mmol, 1.00 eq.) were dissolved in 2 mL of THF. The resulting dark brown mixture was filtered and the solvent was removed from the filtrate. The residue was dissolved in 2 mL of Et_2O and layered with 2 mL of *n*-pentane to afford **14** as brown crystalline solid (22 mg, 0.03 mmol, 26%).

Elemental analysis: calculated ($C_{39}H_{56}CoN_3O_2Si_2$ 714.00 g/mol) C 65.61 H 8.25 N 5.89; experimental C 64.21 H 7.73 N 5.68

Crystals, suitable for X-ray diffraction analysis were obtained by layering a solution of **14** in Et_2O with *n*-pentane at –40 °C.

1.13. Synthesis of [Me4N][Co(^{Mes}NON)(PhN=NPh)] (15)

[Me$_4$N][Co(^{Mes}NON)Cl)(thf)] (50 mg, 0.078 mmol, 1.00 eq.), KC_8 (14 mg, 0.089 mmol, 1.13 eq.) and *E*-azobenzene (15 mg, 0.082 mmol, 1.05 eq) were dissolved in 2 mL of THF. The resulting dark red solution was filtered and the solvent was removed from the filtrate. The residue was dissolved in 2 mL of Et_2O

and layered with 2 mL of *n*-pentane at –40 °C to afford **15** as crystalline red solid (32 mg, 0.045 mmol, 58%).

^{1}H-NMR:

IR (ATR, cm^{-1}): 2950 (w, br), 2899 (w, br), 1583 (w), 1470 (m), 1416 (w), 1367 (vw), 1299 (m), 1254 (m), 1235 (s), 1159 (m), 1072 (vw), 990 (s), 963 (m), 852 (m), 813 (s), 796 (s), 782 (s), 757 (s), 700 (s), 667 (m), 578 (w), 525 (m), 405 (w)

Elemental analysis: calculated ($C_{38}H_{56}CoN_5OSi_2$ 714.00 g/mol) C 63.92 H 7.91 N 9.81; experimental C 58.33 H 6.85 N 9.12

Crystals, suitable for x-ray diffraction analysis were obtained by layering a solution of **15** in 2 mL of Et_2O with 2 ml of *n*-pentane at –40 °C.

1.14. NMR spectroscopy

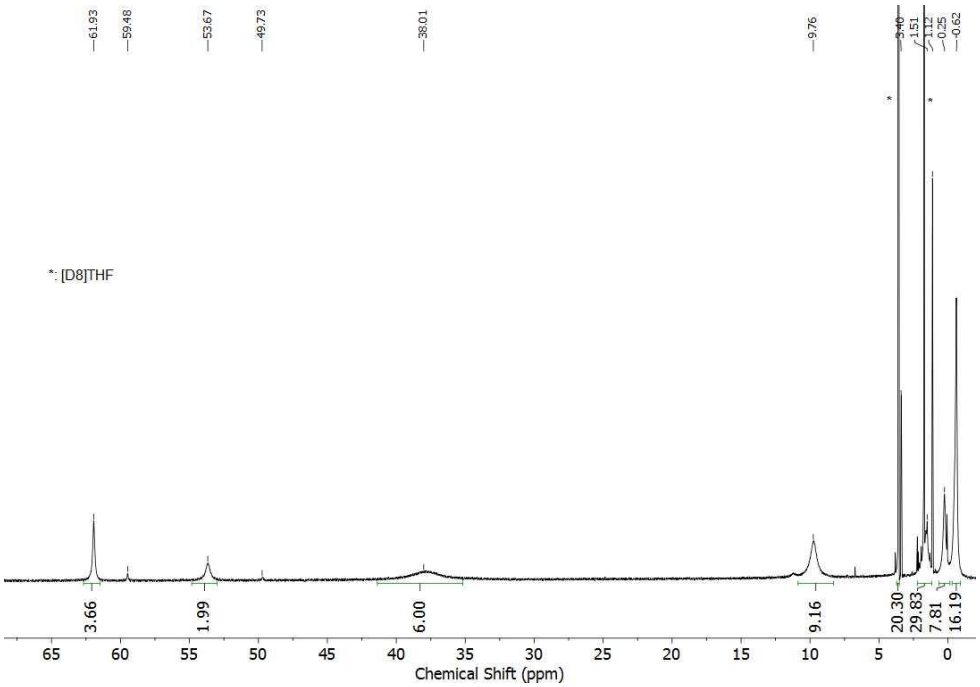

Figure S1. ^{1}H-NMR spectrum of **5** in [D8]THF at 300 K and 300 MHz. *: [D8]THF.

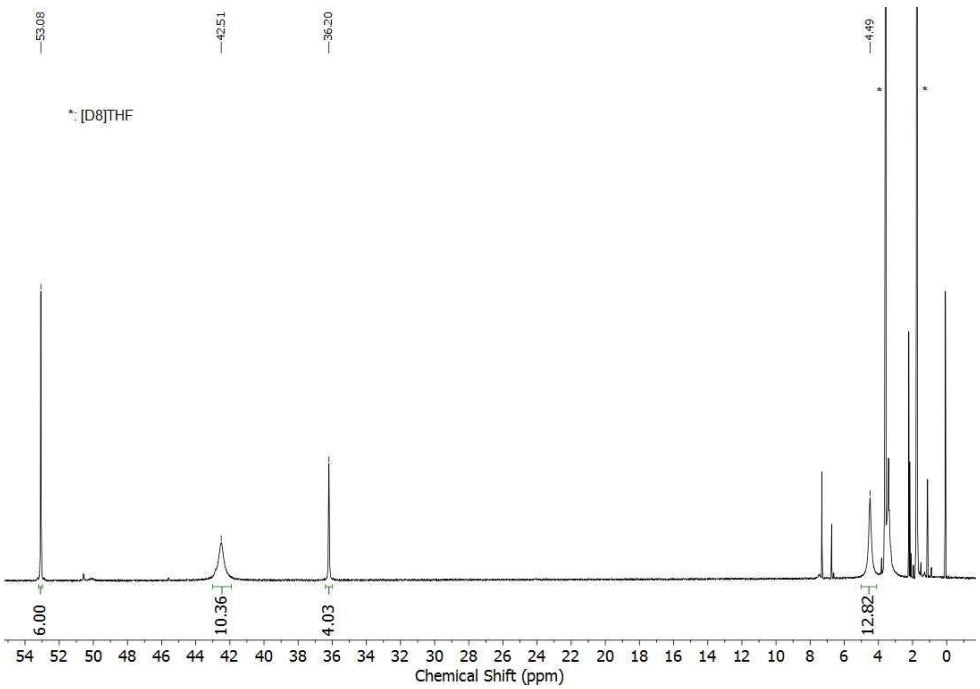

Figure S2. ^{1}H-NMR spectrum of **6** in [D8]THF at 300 K and 300 MHz.

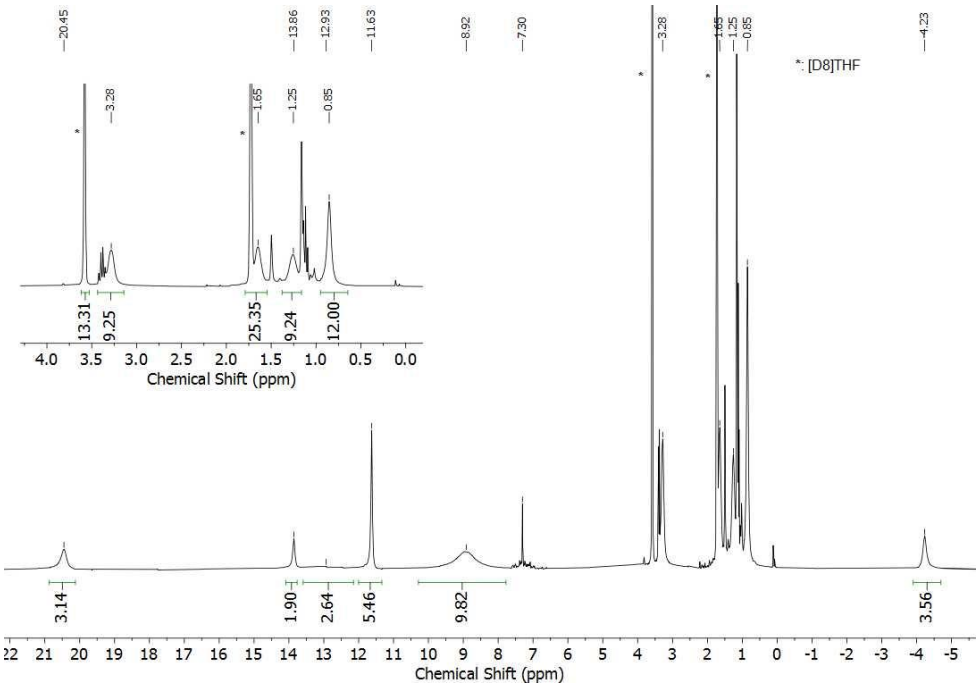

Figure S3. ^{1}H-NMR spectrum of **11** in [D8]THF at 300 K and 300 MHz. *: [D8]THF.

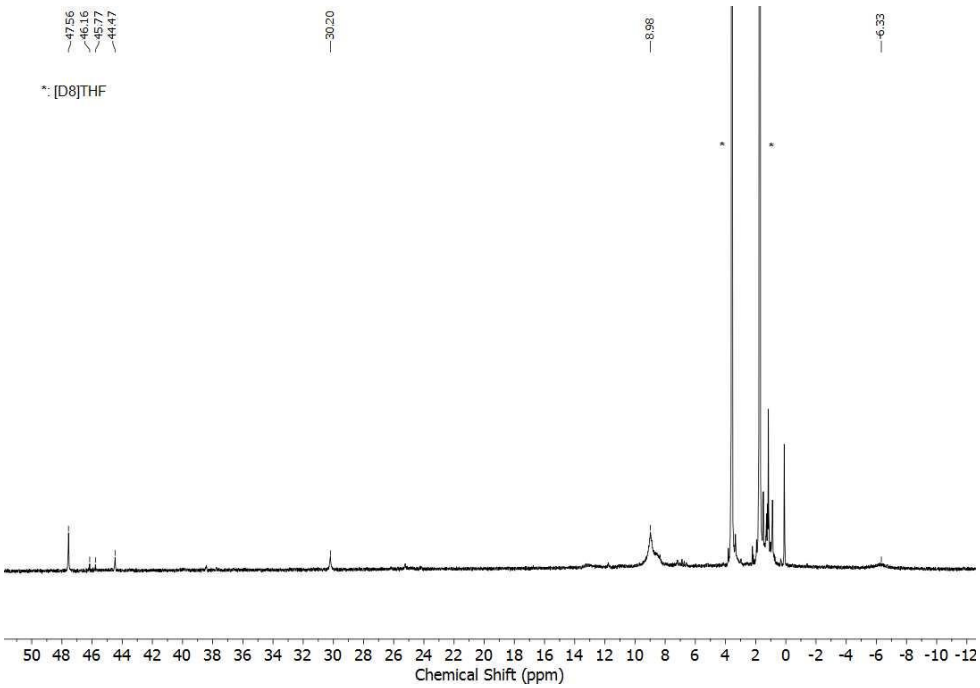

Figure S4. ^{1}H-NMR of **12** in [D8]THF at 300 K and 300 MHz. *: [D8]THF.

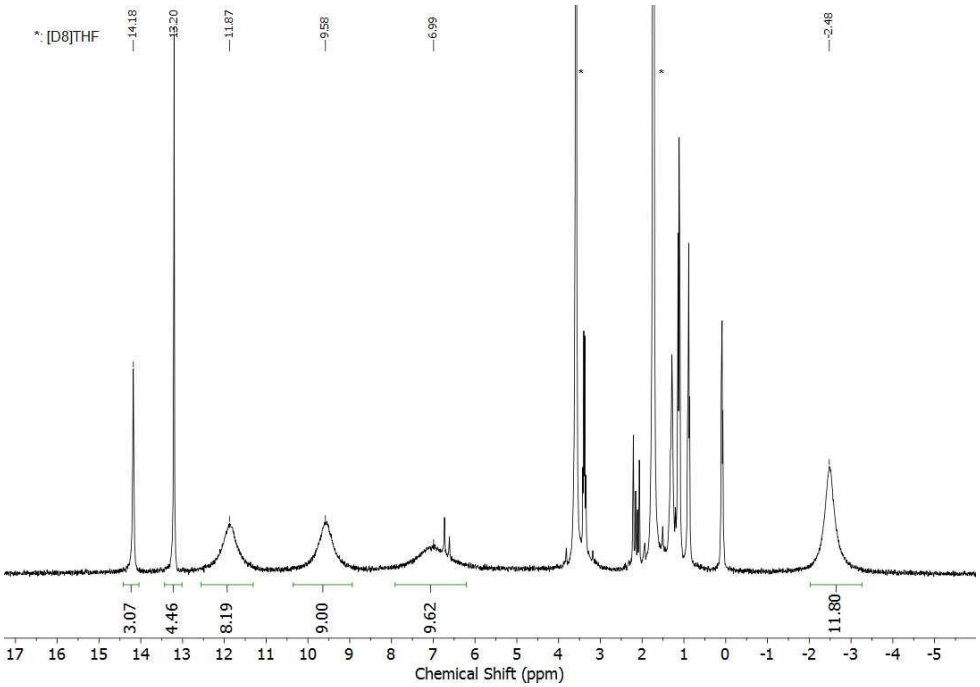

Figure S5. ^{1}H-NMR spectrum of **13** in [D8]THF at 300 K and 300 MHz. *: [D8]THF.

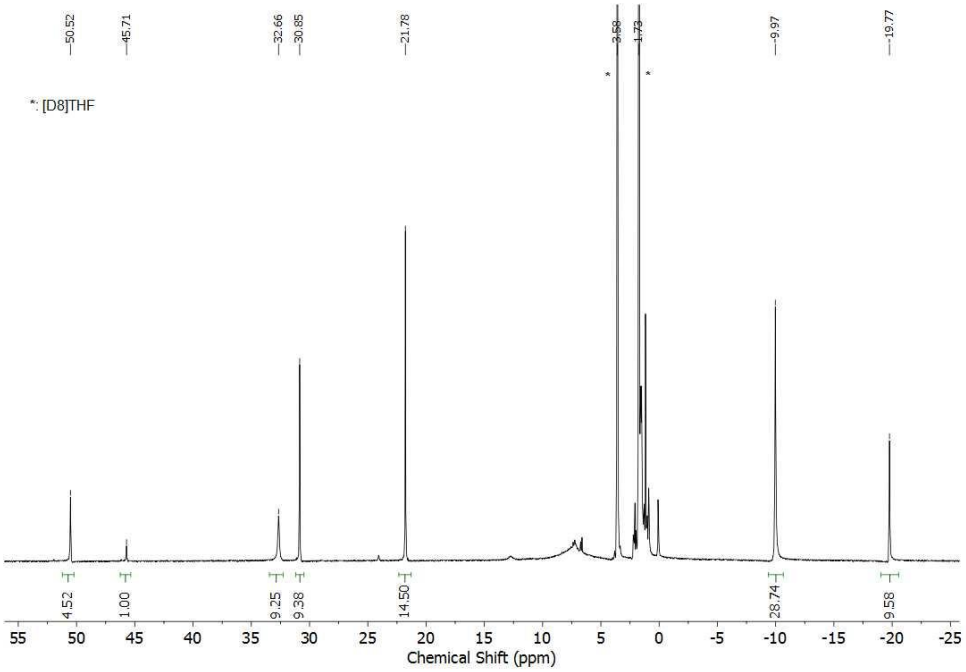

Figure S6. ^{1}H-NMR spectrum of **14** in [D8]THF at 300 K and 300 MHz. *: [D8]THF.

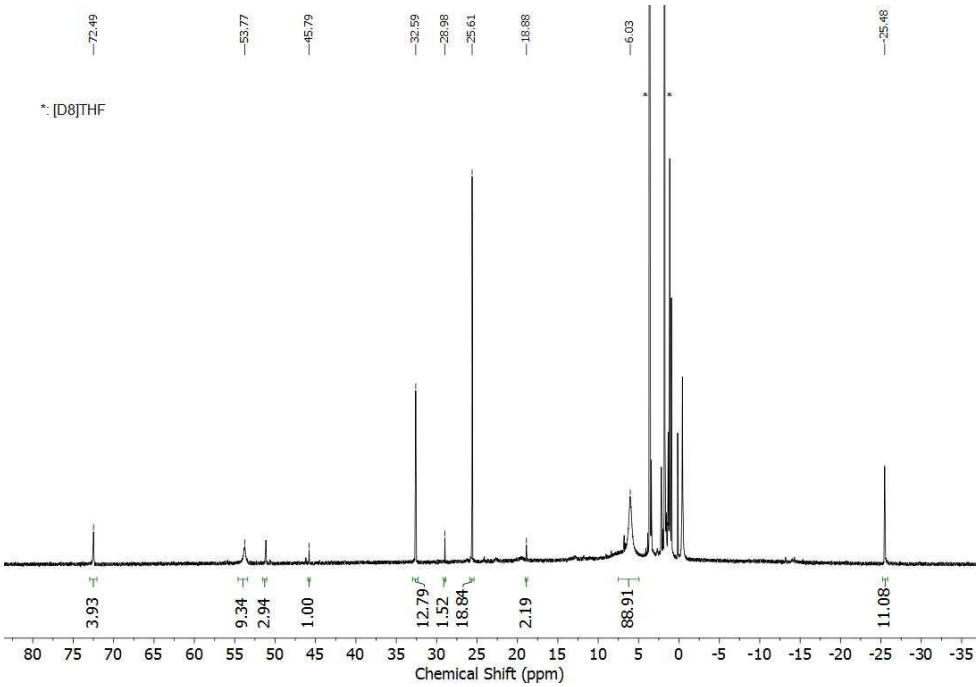

Figure S7. ^{1}H-NMR spectrum of **15** in [D8]THF at 300 K and 300 MHz. *: [D8]THF.

1.15. Mass spectrometry

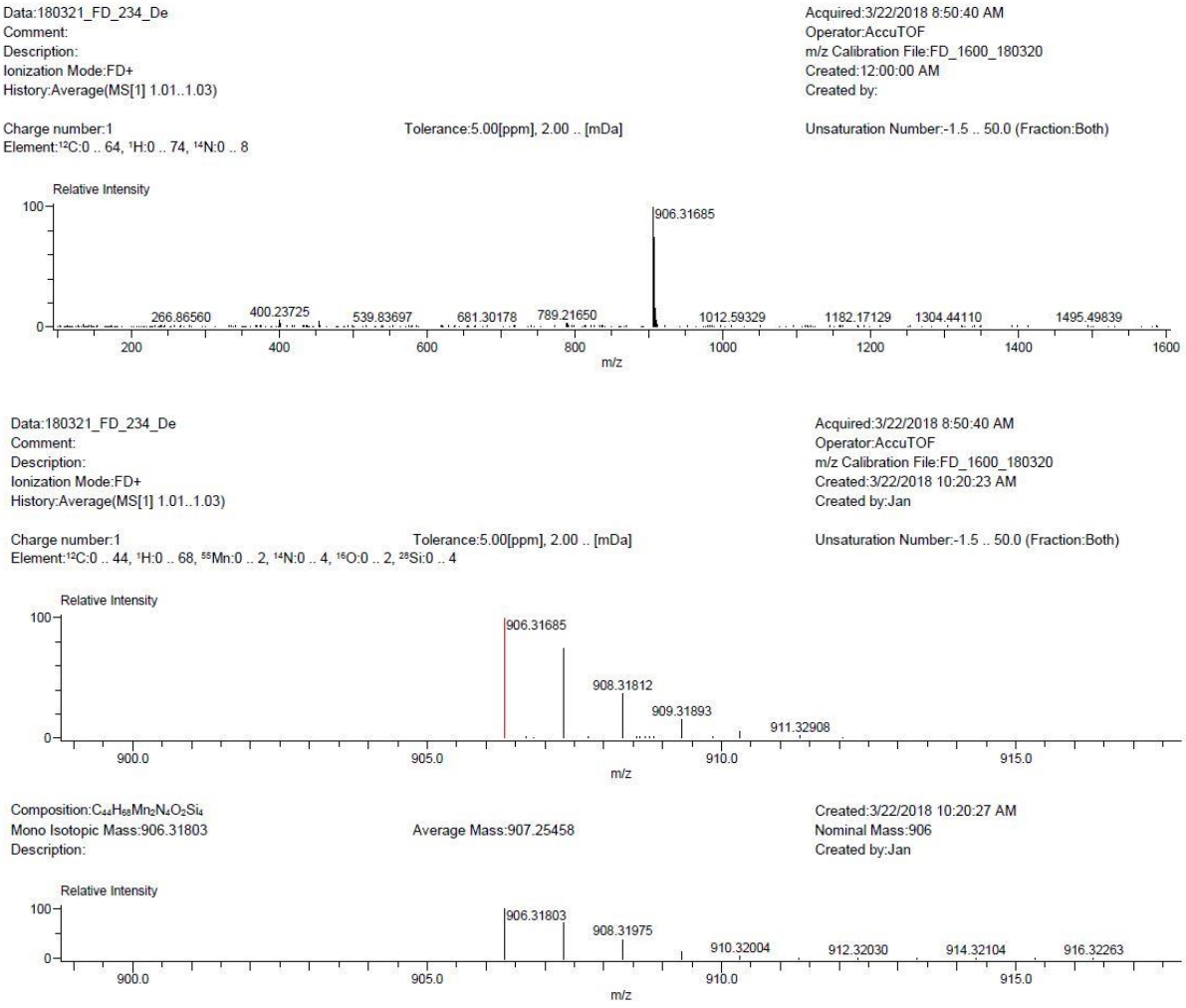

Mass	Intensity	Relative Intensity	Calc. Mass	Mass Difference [mDa]	Mass Difference [ppm]	Possible Formula	Unsaturation Number
906.31685	45982.64	100.00	906.31803	-1.18	-1.30	$^{12}C_{44}{}^{1}H_{68}{}^{55}Mn_2{}^{14}N_4{}^{16}O_2{}^{28}Si_4$	19.0

Figure S8. LIFDI-MS spectrum of **1** with overview spectrum (top) and high-resolution spectrums (middle, bottom).

1.16. IR spectroscopy

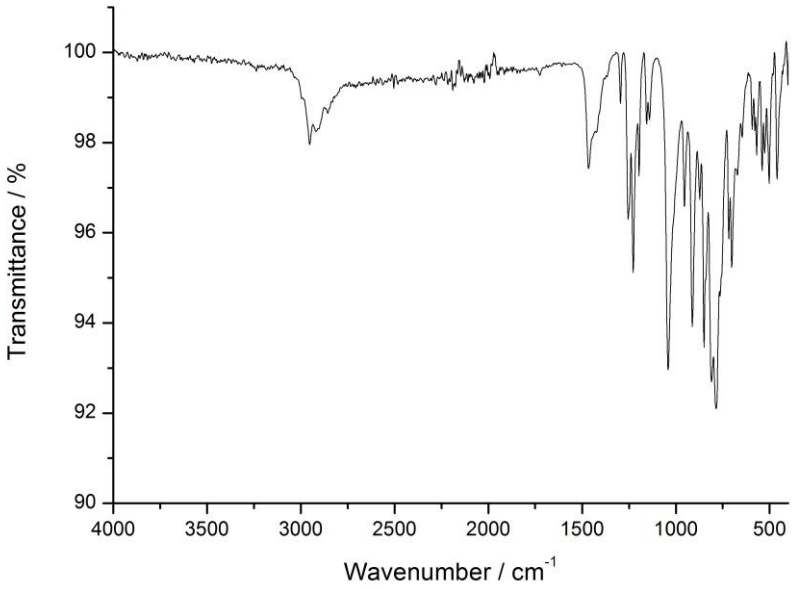

Figure S9. ATR-IR spectrum of **1**.

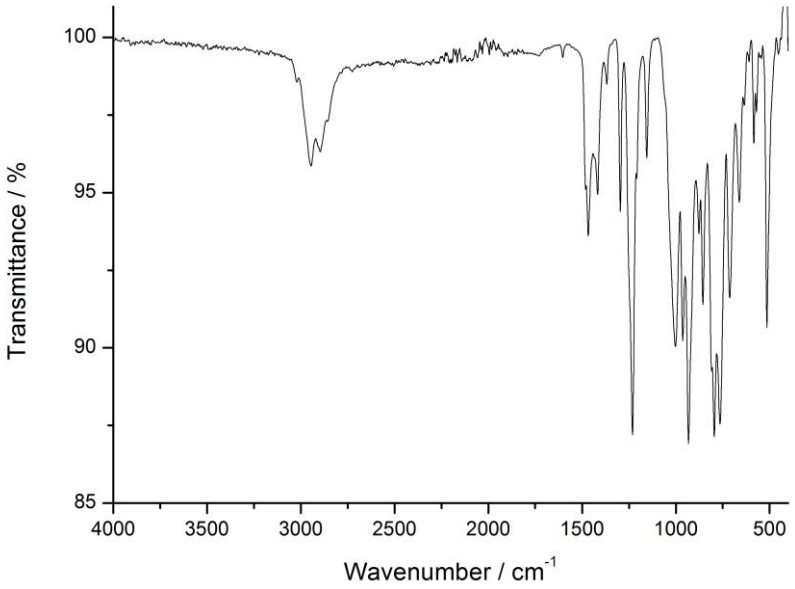

Figure S10. ATR-IR spectrum of **4**.

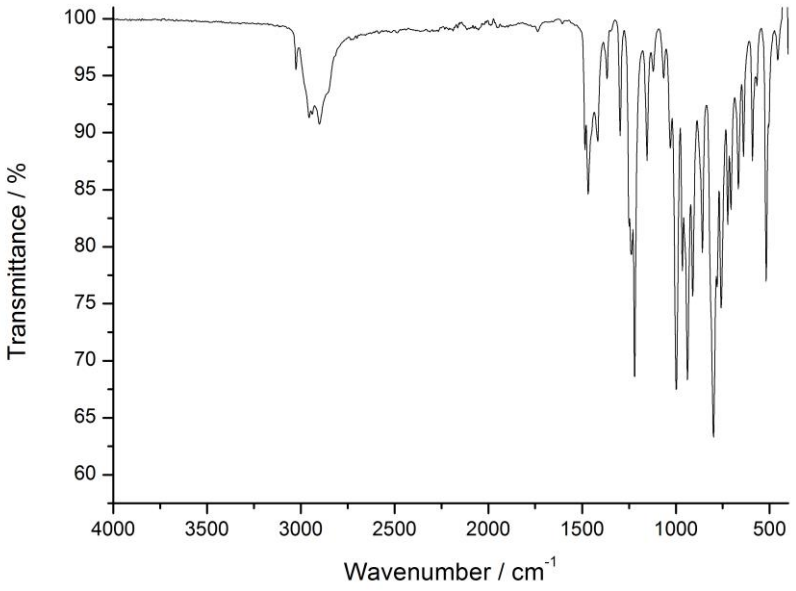

Figure S11. ATR-IR spectrum of **6**.

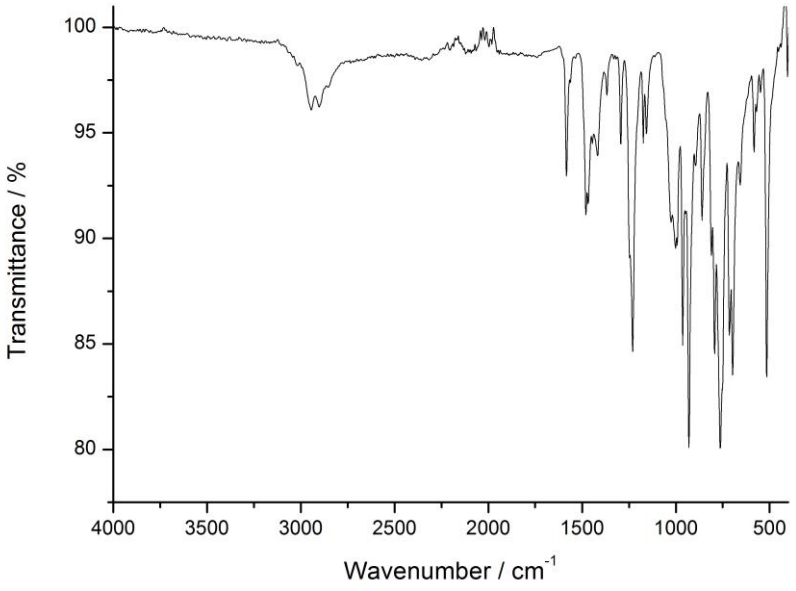

Figure S12. ATR-IR spectrum of **8**.

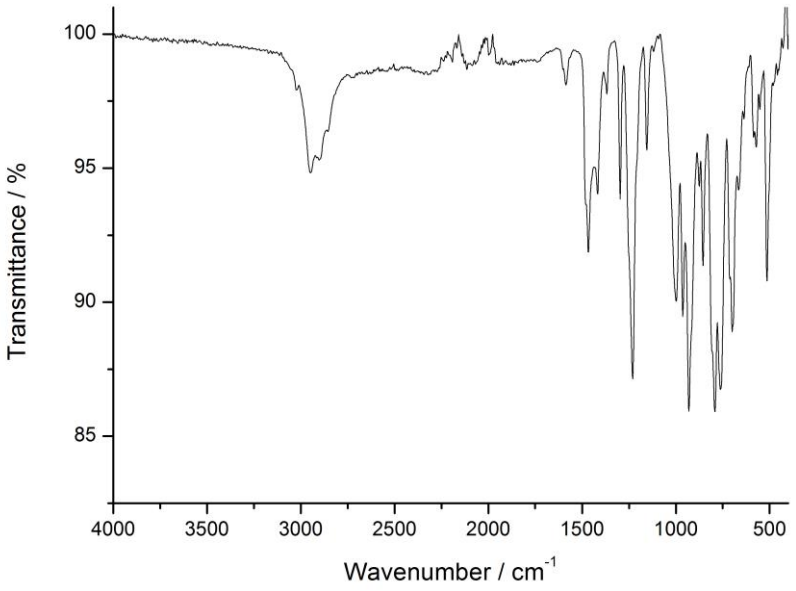

Figure S13. ATR-IR spectrum of **9**.

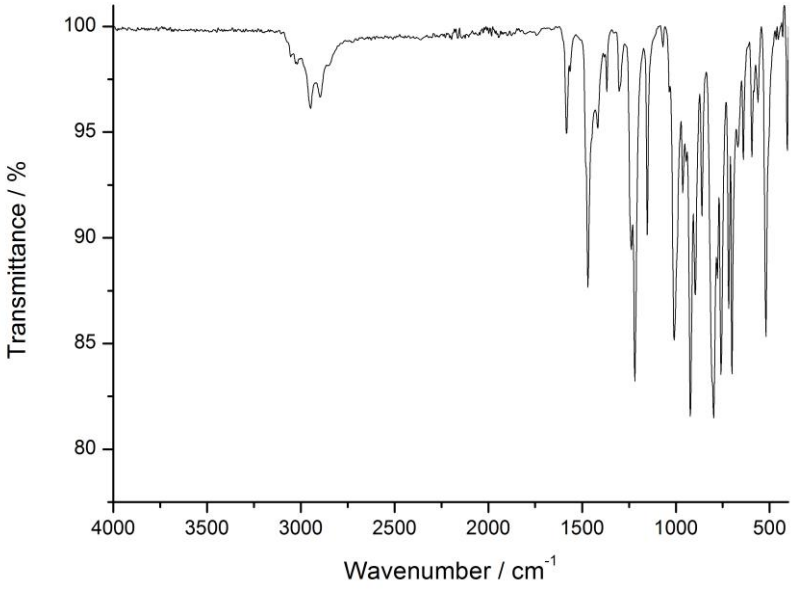

Figure S14. ATR-IR spectrum of **10**.

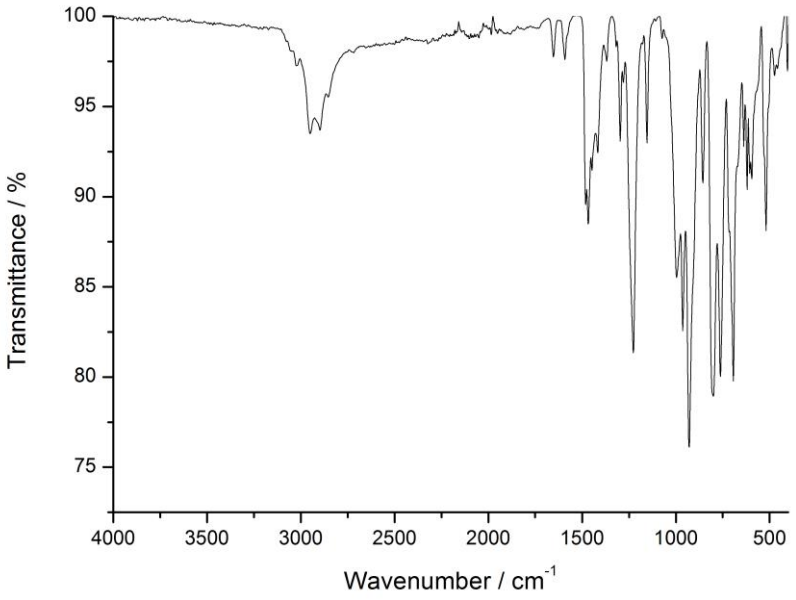

Figure S15. ATR-IR spectrum of **14**.

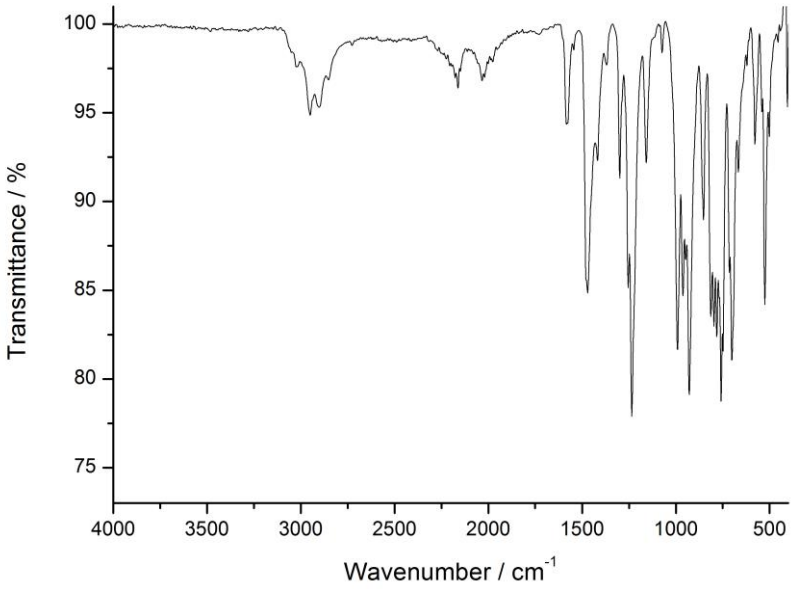

Figure S16. ATR-IR spectrum of **15**.

1.17. UV-Vis spectroscopy

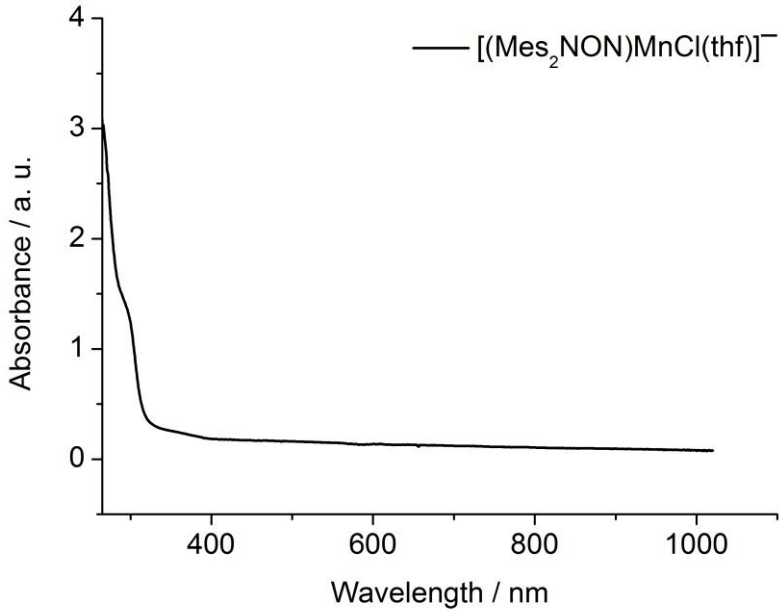

Figure S17. UV-Vis spectrum of **4** in THF at 300 K.

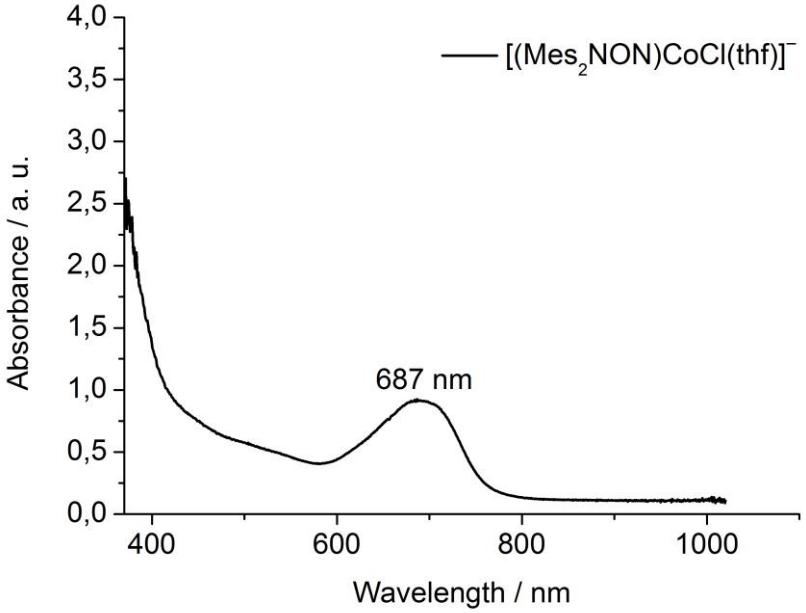

Figure S18. UV-Vis spectrum of **6** in Et_2O at 300 K.

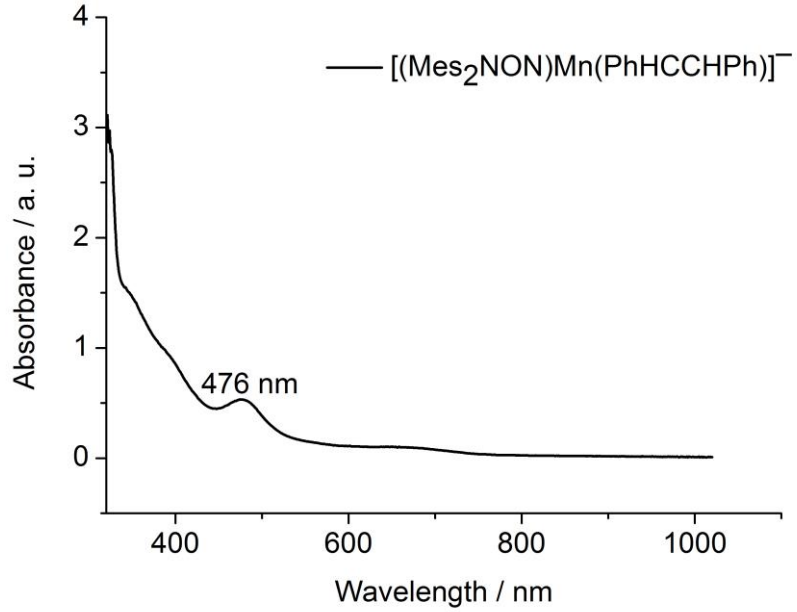

Figure S19. UV-Vis spectrum of **8** in THF at 300 K.

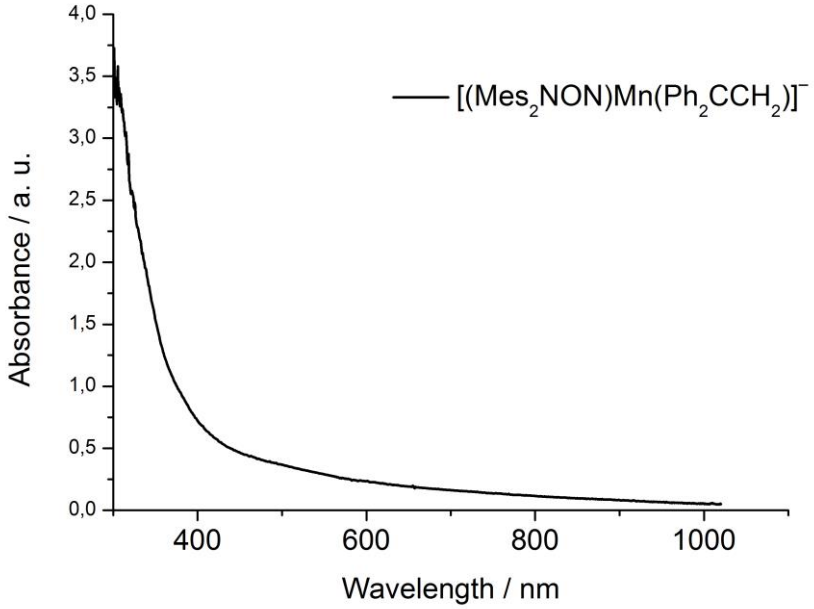

Figure S20. UV-Vis spectrum of **9** in Et_2O at 300 K.

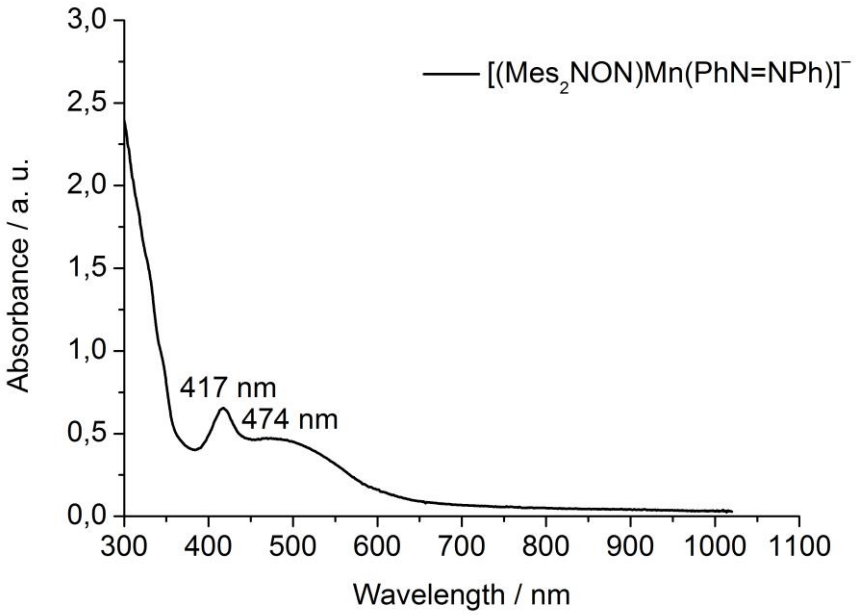

Figure S21. UV-Vis spectrum of **10** in Et_2O at 300 K.

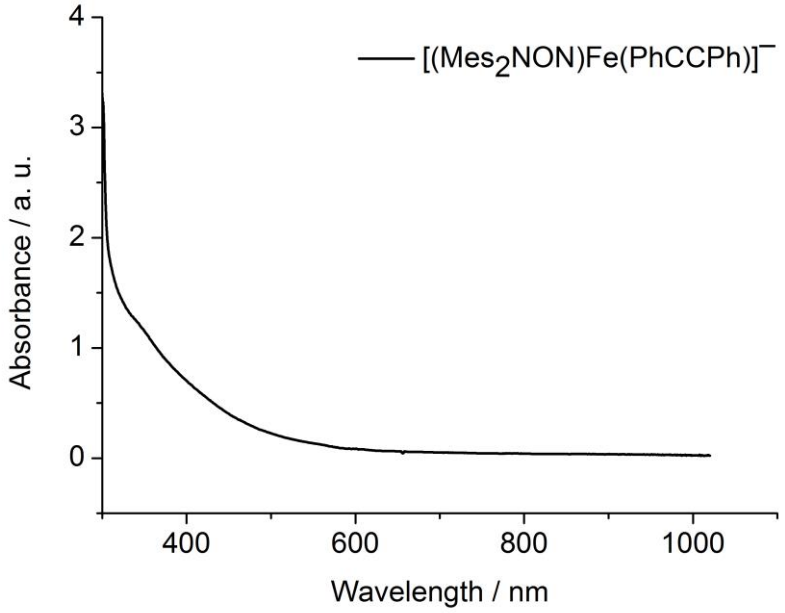

Figure S22. UV-Vis spectrum of **11** in THF at 300 K.

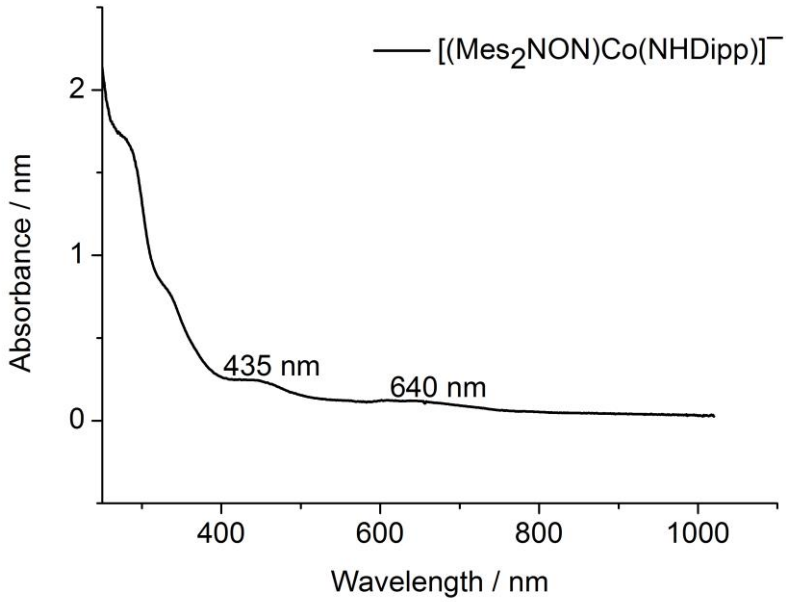

Figure S23. UV-Vis spectrum of **12** in THF at 300 K.

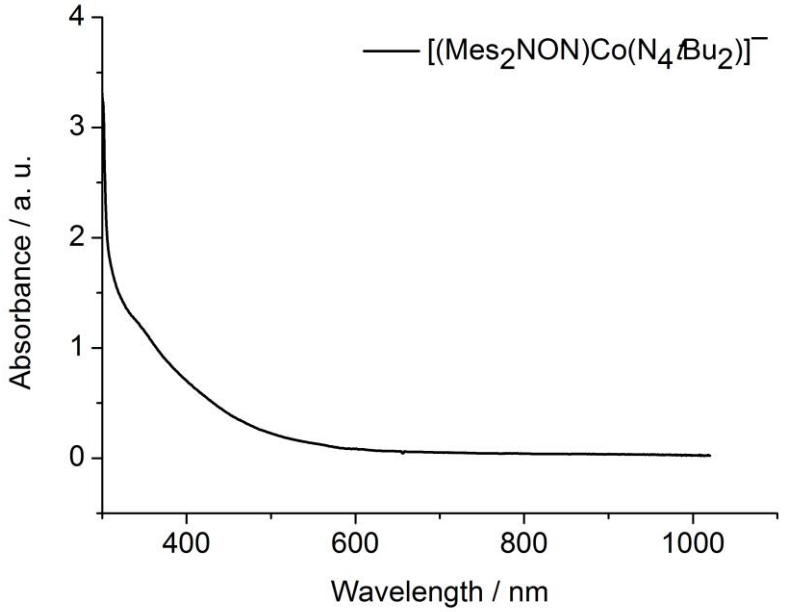

Figure S24. UV-Vis spectrum of **13** in THF at 300 K.

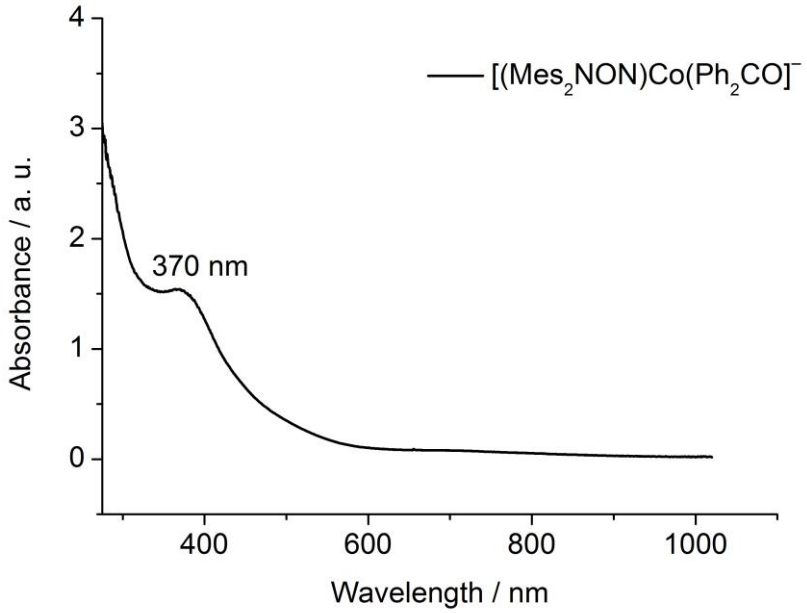

Figure S25. UV-Vis spectrum of **14** in Et_2O at 300 K.

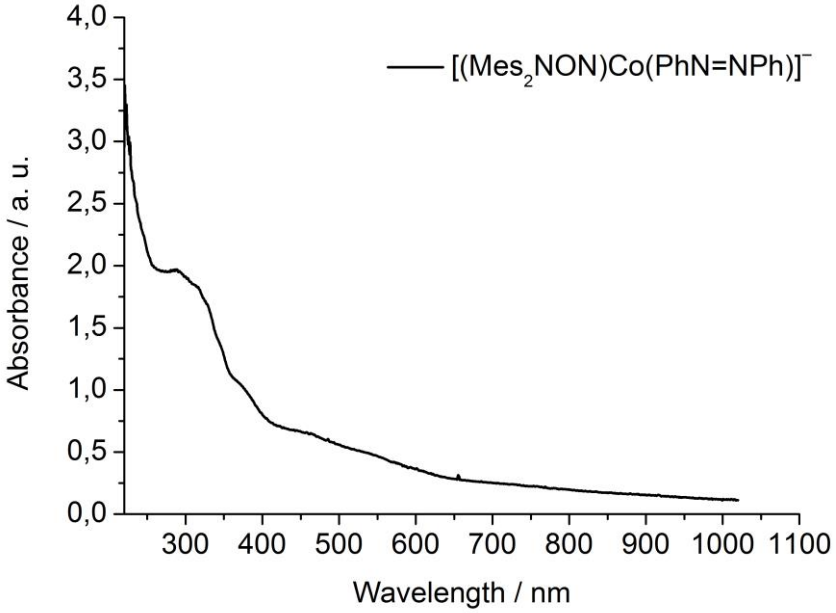

Figure S26. UV-Vis spectrum of **15** in Et_2O at 300 K.

3. Crystallographic Details

Data for **1, 4 – 15** were collected at 100 K on a BRUKER Quest D8 diffractometer using Mo-Kα radiation. The structures have been solved using the SHELXT V2014/1 algorithm[8] employed in the Olex2 platform and refined by means of least-squares procedures on a F2 with the aid of the program SHELXL-2016/6, included in the software package WinGX version 1.63[9] or using CRYSTALS.[10] The Atomic Scattering Factors were taken from International Tables for X-Ray Crystallography.[11] All non-hydrogen atoms were refined anisotropically. All hydrogen atoms were refined by using a riding model. Absorption corrections were introduced by using the MULTISCAN[12] and X-Red program[13]. Drawings of molecules were performed with the program DIAMOND with 50% probability displacement ellipsoids for non-H atoms. H atoms are generally omitted for clarity.

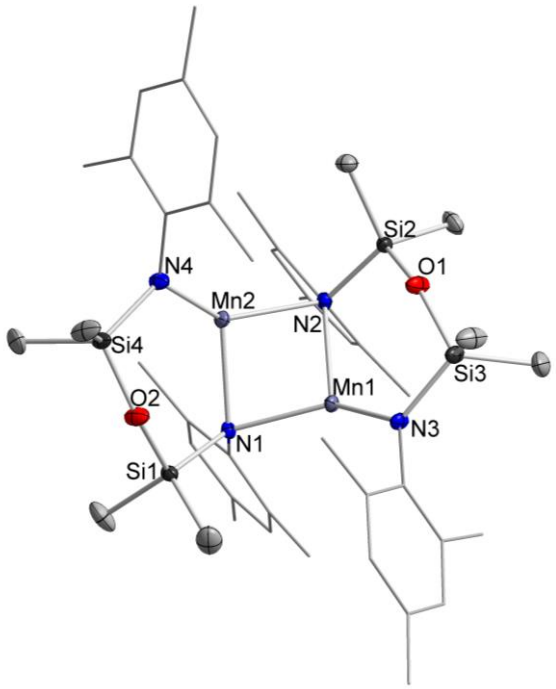

Figure S27. Molecular structure of **1** within the crystal. Hydrogen atoms are omitted for clarity, thermal ellipsoids are shown with 50% probability.

Table S1. Crystal data and structural refinement for **1**.

Identification code	**1**
Empirical formula	$C_{44}H_{68}Mn_2N_4O_2Si_4$
Formula weight	907.26
Temperature/K	100.1
Crystal system	Triclinic
Space group	*P*-1
a/Å	11.3540(5)
b/Å	11.4462(5)
c/Å	19.7987(9)
α/°	75.089(2)
β/°	77.245(2)
γ/°	75.235(2)
Volume/Å^3	2370.90(19)
Z	2
ρ_{calc}g/cm^3	1.271
μ/mm^{-1}	0.672
F(000)	964.0
Crystal size/mm^3	0.381 × 0.316 × 0.24
Radiation	MoKα (λ = 0.71073)
2Θ range for data collection/°	4.57 to 60
Index ranges	-15 ≤ h ≤ 15, -16 ≤ k ≤ 16, -27 ≤ l ≤ 27
Reflections collected	103445
Independent reflections	13812 [R_{int} = 0.0341, R_{sigma} = 0.0203]
Data/restraints/parameters	13812/6/565
Goodness-of-fit on F^2	1.114
Final R indexes [I>=2σ (I)]	R_1 = 0.0369, wR_2 = 0.0958
Final R indexes [all data]	R_1 = 0.0412, wR_2 = 0.0975
Largest diff. peak/hole / e Å^{-3}	1.02/-0.57

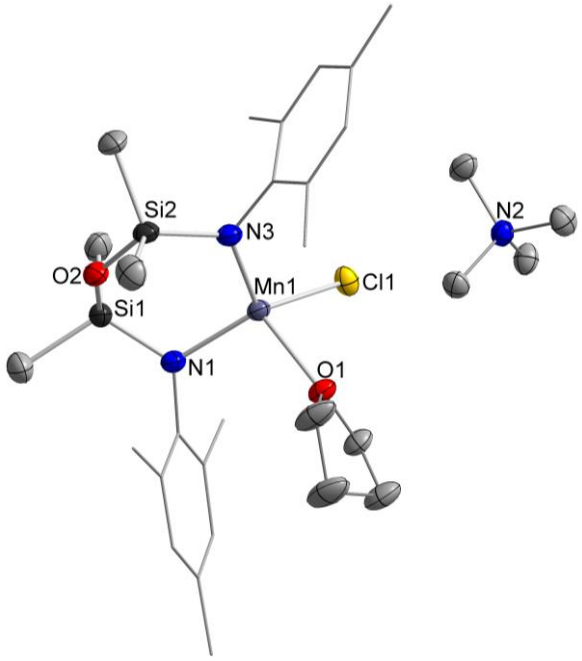

Figure S28. Molecular structure of **4** within the crystal. Hydrogen atoms are omitted for clarity, thermal ellipsoids are shown with 50% probability.

Table 2. Crystal data and structural refinement for **4**.

Identification code	GWX155_0m
Empirical formula	$C_{30}H_{54}ClMnN_3O_2Si_2$
Formula weight	635.33
Temperature/K	100.0
Crystal system	monoclinic
Space group	$P2_1/c$
a/Å	18.0545(12)
b/Å	12.3041(8)
c/Å	18.9949(11)
α/°	90
β/°	114.784(2)
γ/°	90
Volume/Å^3	3831.0(4)
Z	4
ρ_{calc}g/cm^3	1.102
μ/mm^{-1}	0.503
F(000)	1364.0
Crystal size/mm^3	0.734 × 0.097 × 0.081
Radiation	MoKα (λ = 0.71073)
2Θ range for data collection/°	4.066 to 60.154
Index ranges	-25 ≤ h ≤ 25, -16 ≤ k ≤ 16, -26 ≤ l ≤ 25
Reflections collected	84507
Independent reflections	10877 [R_{int} = 0.0813, R_{sigma} = 0.0716]
Data/restraints/parameters	10877/0/366
Goodness-of-fit on F^2	1.038
Final R indexes [I>=2σ (I)]	R_1 = 0.0499, wR_2 = 0.1213
Final R indexes [all data]	R_1 = 0.0842, wR_2 = 0.1331
Largest diff. peak/hole / e Å^{-3}	0.44/-0.45

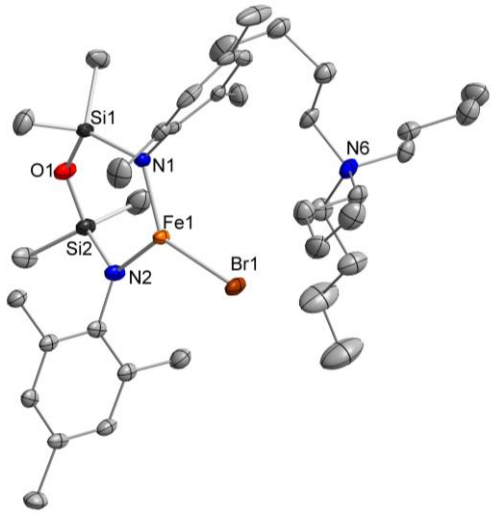

Figure S29. Molecular structure of **5**•0.5Et_2O, within the crystal. One molecule of Et_2O is not depicted. Hydrogen atoms are omitted for clarity, thermal ellipsoids are shown with 50% probability.

Table S3. Crystal data and structural refinement for **5**.

Identification code	SGPX15_0m
Empirical formula	$C_{40}H_{75}BrFeN_3O_{1.5}Si_2$
Formula weight	813.97
Temperature/K	99.99
Crystal system	triclinic
Space group	P-1
a/Å	12.3953(6)
b/Å	19.8080(10)
c/Å	20.7515(9)
α/°	100.697(2)
β/°	101.255(2)
γ/°	105.465(2)
Volume/Å^3	4661.4(4)
Z	2
ρ_{calc}g/cm^3	1.160
μ/mm^{-1}	1.264
F(000)	1748.0
Crystal size/mm^3	0.5 × 0.117 × 0.077
Radiation	MoKα (λ = 0.71073)
2Θ range for data collection/°	4.264 to 53.998
Index ranges	-15 ≤ h ≤ 15, -23 ≤ k ≤ 25, -26 ≤ l ≤ 26
Reflections collected	84343
Independent reflections	20333 [R_{int} = 0.0708, R_{sigma} = 0.0719]
Data/restraints/parameters	20333/0/904
Goodness-of-fit on F^2	1.029
Final R indexes [I>=2σ (I)]	R_1 = 0.0487, wR_2 = 0.0873
Final R indexes [all data]	R_1 = 0.0892, wR_2 = 0.0941
Largest diff. peak/hole / e Å^{-3}	0.71/-0.38

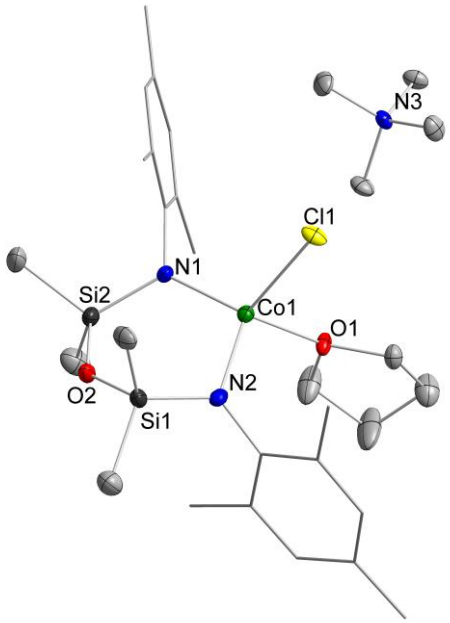

Figure 30. Molecular structure of **6** within the crystal. Hydrogen atoms are omitted for clarity and thermal ellipsoids are shown with 50% probability.

Table S4. Crystal data and structural refinement for **6**.

Identification code	SGPX23_0m
Empirical formula	$C_{30}H_{54}ClCoN_3O_2Si_2$
Formula weight	639.32
Temperature/K	100.0
Crystal system	monoclinic
Space group	$P2_1/c$
a/Å	18.0153(12)
b/Å	12.0531(9)
c/Å	18.9229(13)
α/°	90
β/°	114.467(2)
γ/°	90
Volume/Å^3	3739.9(5)
Z	4
ρ_{calc}g/cm^3	1.135
μ/mm^{-1}	0.621
F(000)	1372.0
Crystal size/mm^3	0.396 × 0.066 × 0.044
Radiation	MoKα (λ = 0.71073)
2Θ range for data collection/°	4.194 to 50
Index ranges	-21 ≤ h ≤ 21, -14 ≤ k ≤ 14, -22 ≤ l ≤ 20
Reflections collected	47679
Independent reflections	6596 [R_{int} = 0.1655, R_{sigma} = 0.0963]
Data/restraints/parameters	6596/2/380
Goodness-of-fit on F^2	1.060
Final R indexes [I>=2σ (I)]	R_1 = 0.0678, wR_2 = 0.1236
Final R indexes [all data]	R_1 = 0.1091, wR_2 = 0.1323
Largest diff. peak/hole / e Å^{-3}	0.46/-0.44

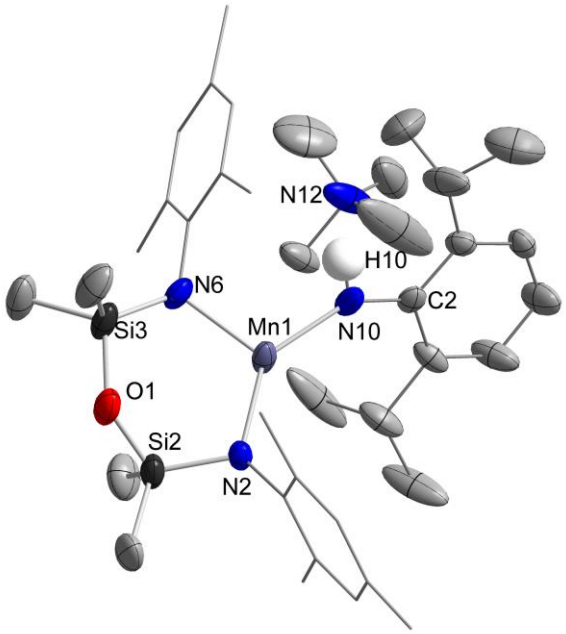

Figure 31. Molecular structure of **7**, within the crystal. Hydrogen atoms are omitted for clarity, thermal ellipsoids are shown with 50% probability.

Table 5. Crystal data and structural refinement for **7**.

Identification code	SGPX66_0ma
Empirical formula	$C_{38}H_{65}MnN_4OSi_2$
Formula weight	705.06
Temperature/K	100.0
Crystal system	monoclinic
Space group	$P2_1/n$
a/Å	11.7151(5)
b/Å	70.184(3)
c/Å	15.1177(6)
α/°	90
β/°	100.0090(10)
γ/°	90
Volume/Å^3	12240.8(9)
Z	12
ρ_{calc}g/cm^3	1.148
μ/mm^{-1}	0.415
F(000)	4584.0
Crystal size/mm^3	0.223 × 0.151 × 0.097
Radiation	MoKα (λ = 0.71073)
2Θ range for data collection/°	3.716 to 49.998
Index ranges	-13 ≤ h ≤ 13, -83 ≤ k ≤ 83, -17 ≤ l ≤ 17
Reflections collected	119891
Independent reflections	21526 [R_{int} = 0.1284, R_{sigma} = 0.0892]
Data/restraints/parameters	21526/260/1421
Goodness-of-fit on F^2	1.245
Final R indexes [I>=2σ (I)]	R_1 = 0.1155, wR_2 = 0.2359
Final R indexes [all data]	R_1 = 0.1457, wR_2 = 0.2457
Largest diff. peak/hole / e Å^{-3}	0.54/-0.59

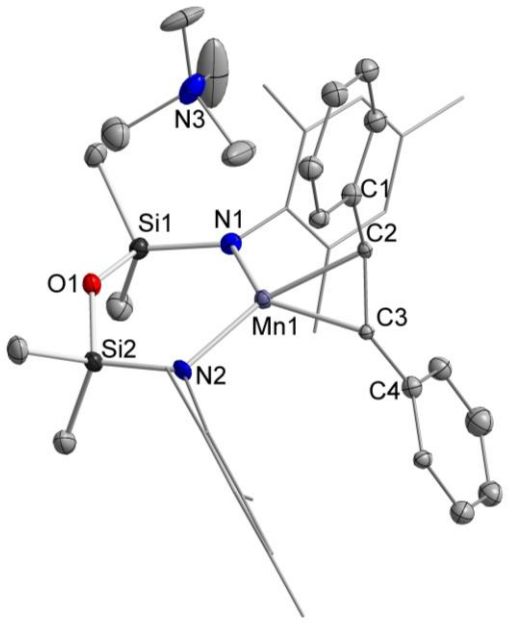

Figure S32. Molecular structure of **8**, within the crystal. Hydrogen atoms are omitted for clarity, thermal ellipsoids are shown with 50% probability. Molecules of THF and *n*-pentane are not depicted. An inversion-symmetrical disorder has been found for the stilbene fragment (50% / 50%).

Table S6. Crystal data and structural refinement for **8**.

Identification code	SGPX61_0m
Empirical formula	$C_{44}H_{66}MnN_3O_2Si_2$
Formula weight	780.11
Temperature/K	100.0
Crystal system	monoclinic
Space group	Cc
a/Å	26.982(2)
b/Å	11.8545(10)
c/Å	16.9301(14)
α/°	90
β/°	127.433(2)
γ/°	90
Volume/Å^3	4300.1(6)
Z	4
ρ_{calc}g/cm^3	1.205
μ/mm^{-1}	0.401
F(000)	1680.0
Crystal size/mm^3	0.93 × 0.174 × 0.118
Radiation	MoKα (λ = 0.71073)
2Θ range for data collection/°	3.926 to 51.998
Index ranges	-33 ≤ h ≤ 33, -14 ≤ k ≤ 14, -20 ≤ l ≤ 20
Reflections collected	43493
Independent reflections	8419 [R_{int} = 0.0806, R_{sigma} = 0.0749]
Data/restraints/parameters	8419/733/592
Goodness-of-fit on F^2	1.039
Final R indexes [I>=2σ (I)]	R_1 = 0.0478, wR_2 = 0.0888
Final R indexes [all data]	R_1 = 0.0653, wR_2 = 0.0926
Largest diff. peak/hole / e Å^{-3}	0.34/-0.32

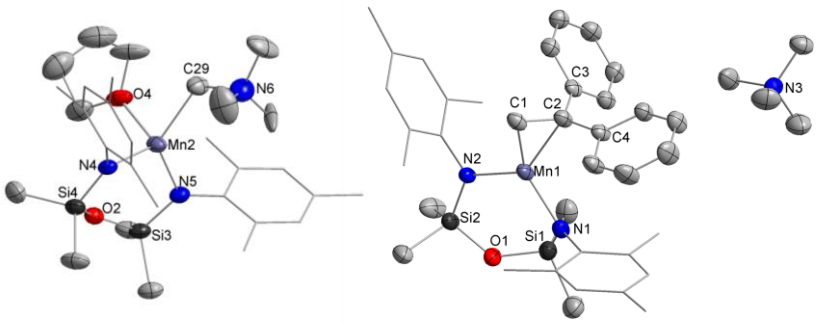

Figure S33. Molecular structure of **9** (right) and **9b** (left) within the crystal. The unit cell contains one additional molecule of **9** (not depicted). Hydrogen atoms are omitted for clarity, thermal ellipsoids are shown with 50% probability. Disorders were found for the C atoms around N6 (67% / 33%) and around N7 (50% / 50%). One free molecule of Et_2O was disordered over multiple positions and thus squeezed.

Table S7. Crystal data and structure refinement for **9** + **9b**.

Identification code	sgpx87_0m
Empirical formula	$C_{110}H_{169}Mn_3N_9O_4Si_6$
Formula weight	2015.10
Temperature/K	100.00
Crystal system	monoclinic
Space group	$P2_1/c$
a/Å	18.3185(10)
b/Å	18.0547(9)
c/Å	39.081(2)
α/°	90
β/°	101.418(2)
γ/°	90
Volume/Å^3	12669.6(12)
Z	4
ρ_{calc}g/cm^3	1.056
μ/mm^{-1}	0.398
F(000)	4332.0
Crystal size/mm^3	0.389 × 0.224 × 0.156
Radiation	MoKα (λ = 0.71073)
2Θ range for data collection/°	4.082 to 50.084
Index ranges	-21 ≤ h ≤ 21, -21 ≤ k ≤ 21, -46 ≤ l ≤ 46
Reflections collected	177486
Independent reflections	22364 [R_{int} = 0.0637, R_{sigma} = 0.0476]
Data/restraints/parameters	22364/93/1695
Goodness-of-fit on F^2	1.079
Final R indexes [I>=2σ (I)]	R_1 = 0.0551, wR_2 = 0.1542
Final R indexes [all data]	R_1 = 0.0789, wR_2 = 0.1625
Largest diff. peak/hole / e Å^{-3}	0.90/-0.47

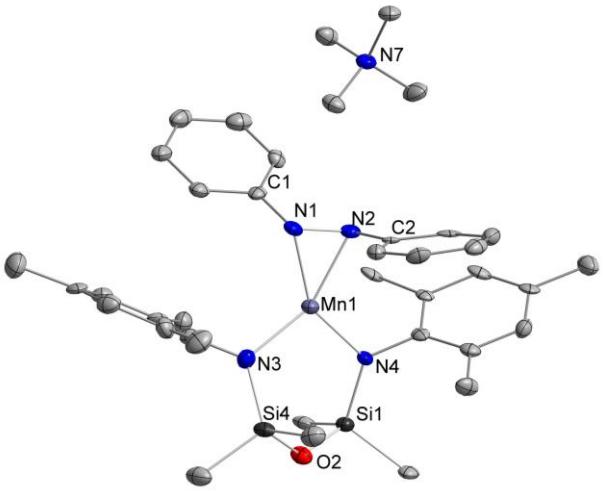

Figure S34. Molecular structure of **10**, within the crystal. Hydrogen atoms are omitted for clarity, thermal ellipsoids are shown with 50% probability.

Table S8. Crystal data and structural refinement for **10**.

Identification code	SGPX86_0m
Empirical formula	$C_{42}H_{66}MnN_5O_2Si_2$
Formula weight	784.11
Temperature/K	100.0
Crystal system	orthorhombic
Space group	$Pca2_1$
a/Å	16.2459(11)
b/Å	33.706(2)
c/Å	16.1373(11)
α/°	90
β/°	90
γ/°	90
Volume/Å^3	8836.4(10)
Z	8
ρ_{calc}g/cm^3	1.179
μ/mm^{-1}	0.392
F(000)	3376.0
Crystal size/mm^3	0.176 × 0.174 × 0.105
Radiation	MoKα (λ = 0.71073)
2Θ range for data collection/°	4.3 to 50.078
Index ranges	-19 ≤ h ≤ 19, -40 ≤ k ≤ 40, -19 ≤ l ≤ 19
Reflections collected	110350
Independent reflections	15583 [R_{int} = 0.1591, R_{sigma} = 0.1221]
Data/restraints/parameters	15583/13/970
Goodness-of-fit on F^2	1.022
Final R indexes [I>=2σ (I)]	R_1 = 0.0623, wR_2 = 0.1180
Final R indexes [all data]	R_1 = 0.1060, wR_2 = 0.1312
Largest diff. peak/hole / e Å^{-3}	0.36/-0.58

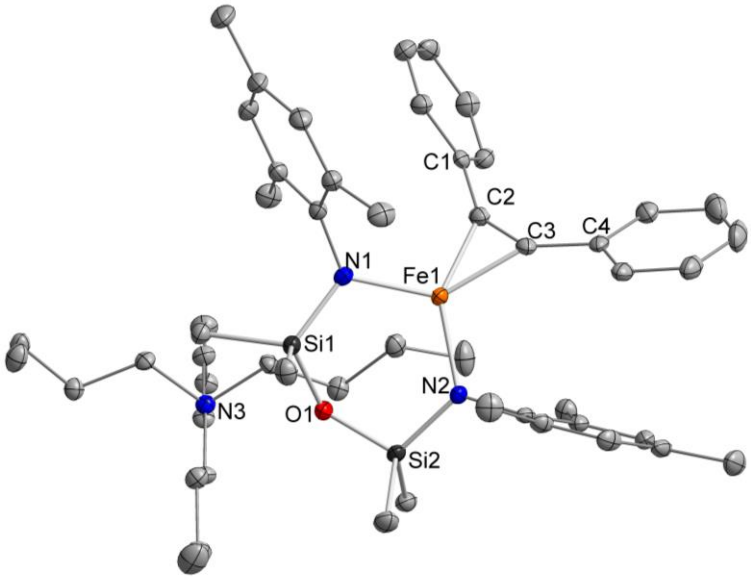

Figure S35. Molecular structure of **11** within the crystal. Hydrogen atoms are omitted for clarity and thermal ellipsoids are shown with 50% probability.

Table S9. Crystal data and structural refinement for **11**.

Identification code	SGPX22_0m
Empirical formula	$C_{51}H_{80}FeN_4OSi_2$
Formula weight	877.22
Temperature/K	100.0
Crystal system	monoclinic
Space group	C2/c
a/Å	21.080(3)
b/Å	12.5710(14)
c/Å	38.890(4)
α/°	90
β/°	97.635(5)
γ/°	90
Volume/Å^3	10215(2)
Z	8
ρ_{calc}g/cm^3	1.141
μ/mm^{-1}	0.380
F(000)	3808.0
Crystal size/mm^3	0.326 × 0.224 × 0.152
Radiation	MoKα (λ = 0.71073)
2Θ range for data collection/°	4.456 to 60.182
Index ranges	-20 ≤ h ≤ 29, -17 ≤ k ≤ 17, -46 ≤ l ≤ 49
Reflections collected	51481
Independent reflections	13923 [R_{int} = 0.0443, R_{sigma} = 0.0593]
Data/restraints/parameters	13923/0/546
Goodness-of-fit on F^2	1.023
Final R indexes [I>=2σ (I)]	R_1 = 0.0465, wR_2 = 0.0886
Final R indexes [all data]	R_1 = 0.0816, wR_2 = 0.0989
Largest diff. peak/hole / e Å^{-3}	0.38/-0.34

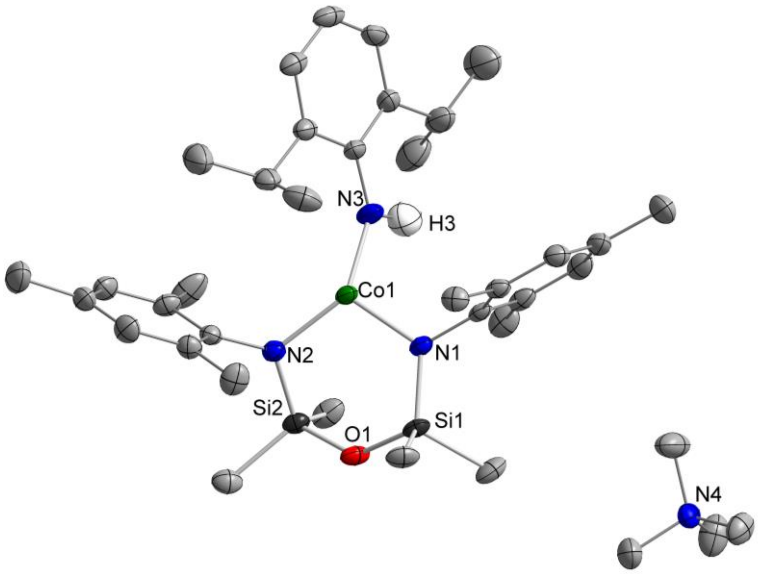

Figure S36. Molecular structure of **12**•THF within the crystal. One molecule of THF is not depicted. Hydrogen atoms (except H3) are omitted for clarity and thermal ellipsoids are shown with 50% probability.

Table S10. Crystal data and structural refinement for **12**.

Identification code	SGPX58_0m
Empirical formula	$C_{42}H_{72}CoN_4O_2Si_2$
Formula weight	780.14
Temperature/K	99.98
Crystal system	monoclinic
Space group	$P2_1/n$
a/Å	10.9002(7)
b/Å	14.7670(9)
c/Å	27.4303(17)
α/°	90
β/°	90.534(2)
γ/°	90
Volume/Å^3	4415.1(5)
Z	4
ρ_{calc}g/cm^3	1.174
μ/mm^{-1}	0.480
F(000)	1692.0
Crystal size/mm^3	0.368 × 0.179 × 0.094
Radiation	MoKα (λ = 0.71073)
2Θ range for data collection/°	4.008 to 53.568
Index ranges	-13 ≤ h ≤ 13, -18 ≤ k ≤ 18, -34 ≤ l ≤ 34
Reflections collected	62388
Independent reflections	9406 [R_{int} = 0.0410, R_{sigma} = 0.0324]
Data/restraints/parameters	9406/2/502
Goodness-of-fit on F^2	1.056
Final R indexes [I>=2σ (I)]	R_1 = 0.0528, wR_2 = 0.1324
Final R indexes [all data]	R_1 = 0.0703, wR_2 = 0.1412
Largest diff. peak/hole / e Å^{-3}	1.33/-0.47

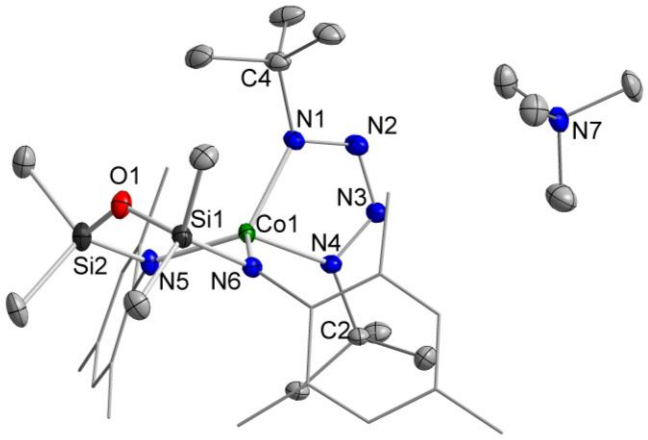

Figure S37. Molecular structure of **13**•2Et_2O within the crystal. Two molecules of Et_2O are not depicted. Hydrogen atoms are omitted for clarity and thermal ellipsoids are shown with 50% probability.

Table S11. Crystal data and structure refinement for **13**.

Identification code	SGPX63_0m
Empirical formula	$C_{42}H_{82}CoN_7O_3Si_2$
Formula weight	848.25
Temperature/K	100.0
Crystal system	orthorhombic
Space group	$P2_12_12_1$
a/Å	10.2023(4)
b/Å	19.5963(9)
c/Å	24.6589(11)
α/°	90
β/°	90
γ/°	90
Volume/Å^3	4930.0(4)
Z	4
ρ_{calc}g/cm^3	1.143
μ/mm^{-1}	0.438
F(000)	1848.0
Crystal size/mm^3	0.3 × 0.2 × 0.1
Radiation	MoKα (λ = 0.71073)
2Θ range for data collection/°	3.902 to 53.592
Index ranges	-12 ≤ h ≤ 12, -24 ≤ k ≤ 24, -31 ≤ l ≤ 31
Reflections collected	118612
Independent reflections	10503 [R_{int} = 0.0411, R_{sigma} = 0.0214]
Data/restraints/parameters	10503/0/521
Goodness-of-fit on F^2	1.109
Final R indexes [I>=2σ (I)]	R_1 = 0.0438, wR_2 = 0.1134
Final R indexes [all data]	R_1 = 0.0474, wR_2 = 0.1158
Largest diff. peak/hole / e Å^{-3}	1.03/-0.33

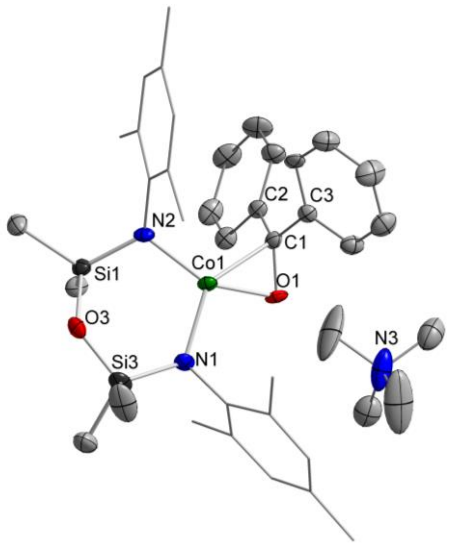

Figure S38. Molecular structure of **14**•2THF within the crystal. Two molecules of THF are not depicted. Hydrogen atoms are omitted for clarity and thermal ellipsoids are shown with 50% probability.

Table S12. Crystal data and structure refinement for **14**.

Identification code	SGPX56_0ma
Empirical formula	$C_{47}H_{71}CoN_3O_4Si_2$
Formula weight	857.17
Temperature/K	100.01
Crystal system	orthorhombic
Space group	Pbca
a/Å	12.1337(14)
b/Å	45.913(5)
c/Å	33.918(4)
α/°	90
β/°	90
γ/°	90
Volume/Å^3	18896(4)
Z	16
ρ_{calc}g/cm^3	1.205
μ/mm^{-1}	0.458
F(000)	7376.0
Crystal size/mm^3	0.462 × 0.138 × 0.104
Radiation	MoKα (λ = 0.71073)
2Θ range for data collection/°	3.982 to 50.104
Index ranges	-14 ≤ h ≤ 14, -54 ≤ k ≤ 41, -39 ≤ l ≤ 40
Reflections collected	121112
Independent reflections	16694 [R_{int} = 0.1943, R_{sigma} = 0.1086]
Data/restraints/parameters	16694/228/1059
Goodness-of-fit on F^2	1.170
Final R indexes [I>=2σ (I)]	R_1 = 0.0986, wR_2 = 0.1915
Final R indexes [all data]	R_1 = 0.1524, wR_2 = 0.2058
Largest diff. peak/hole / e Å^{-3}	0.45/-0.65

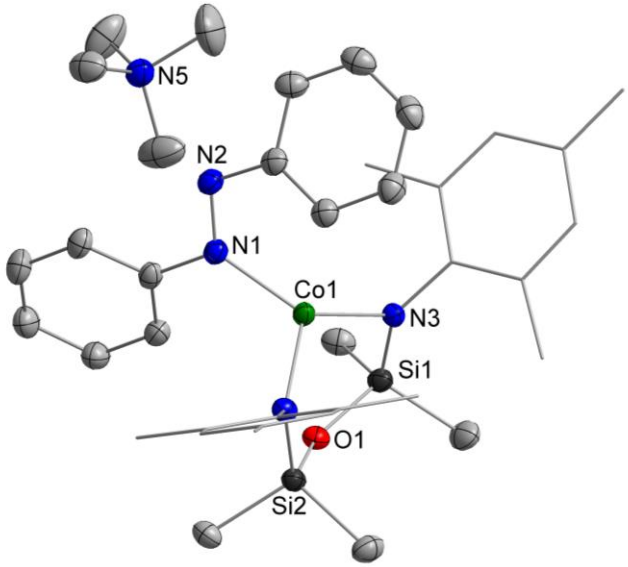

Figure S39. Molecular structure of **15** within the crystal. Hydrogen atoms are omitted for clarity and thermal ellipsoids are shown with 50% probability.

Table S13. Crystal data and structure refinement for **15**.

Identification code	SGPX71_0m
Empirical formula	$C_{38}H_{56}CoN_5OSi_2$
Formula weight	713.98
Temperature/K	100.0
Crystal system	monoclinic
Space group	P21/c
a/Å	11.7178(5)
b/Å	14.3128(7)
c/Å	23.4200(11)
α/°	90
β/°	98.077(2)
γ/°	90
Volume/Å^3	3888.9(3)
Z	4
ρcalcg/cm^3	1.219
μ/mm^{-1}	0.538
F(000)	1528.0
Crystal size/mm^3	0.279 × 0.204 × 0.189
Radiation	MoKα (λ = 0.71073)
2Θ range for data collection/°	4.52 to 57.496
Index ranges	-15 ≤ h ≤ 15, -19 ≤ k ≤ 19, -31 ≤ l ≤ 31
Reflections collected	63107
Independent reflections	10057 [R_{int} = 0.0346, R_{sigma} = 0.0277]
Data/restraints/parameters	10057/0/442
Goodness-of-fit on F^2	1.021
Final R indexes [I>=2σ (I)]	R1 = 0.0383, wR2 = 0.0947
Final R indexes [all data]	R1 = 0.0533, wR2 = 0.1024
Largest diff. peak/hole / e Å^{-3}	1.34/-0.68

4. References

1 S. Stoll and A. Schweiger, *J. Magn. Reson.*, 2006, **178**, 42–55.
2 H. Bürger and U. Wannagat, *Monatsh. Chem.*, 1963, **94**, 1007–1012.
3 A. K. Das, Z. Moatazedi, G. Mund, A. J. Bennet, R. J. Batchelor and D. B. Leznoff, *Inorg. Chem.*, 2007, **46**, 366–368.
4 G. Mund, A. J. Gabert, R. J. Batchelor, J. F. Britten and D. B. Leznoff, *Chem. Commun.*, 2002, 2990–2991.
5 D. B. Leznoff, G. Mund, K. C. Jantunen, P. H. Bhatia, A. J. Gabert and R. J. Batchelor, *Journal of Nuclear Science and Technology*, 2002, **39**, 406–409.
6 L. P. Spencer, R. Altwer, P. Wei, L. Gelmini, J. Gauld and D. W. Stephan, *Organometallics*, 2003, **22**, 3841–3854.
7 J. C. Bottaro, P. E. Penwell and R. J. Schmitt, *Synthetic Communications*, 1997, **27**, 1465–1467.
8 G. M. Sheldrick, *Acta Crystallogr., Sect. A: Found. Crystallogr.*, 2015, **71**, 3–8.
9 L. Farrugia, *J. Appl. Crystallogr.*, 1999, **32**, 837.
10 P. W. Betteridge, J. R. Carruthers, R. I. Cooper, K. Prout and D. J. Watkin, *J. Appl. Crystallogr.*, 2003, **36**, 1487.
11 *International Tables for X-ray crystallography*, Kynoch Press, Birmingham, England, IV., 1974, vol. IV.
12 *SADABS-2016/2*, Bruker, 2016.
13 *X-Area, X-Red 1.63.1.0*, STOE, 2016.

4. Zusammenfassung

Im Rahmen dieser Arbeit wurden Beiträge zum Verständnis der Ein-Elektronen-Reduktion von C=C-, C=N-, C=O-, N=N- und As=As-Doppelbindungen geliefert (Schema 57). Hierzu wurden verschiedene Syntheseansätze zu Isolierung der erhaltenen Radikalanionen gewählt: Das Einführen der Substrate in der Ligandensphäre eines hochreduzierenden Metallions (Fe^{I}, Co^{I}), durch starke sterische Abschirmung des Radikalzentrums oder durch Stabilisierung durch zwei Kationen im Sandwich-Motiv. Im letzten Projekt wurden verschiedene Substrate mit E=E- Bindungen der Elemente Kohlenstoff, Sauerstoff und Stickstoff (zusätzlich zu weiteren Substraten) durch Zugabe der gespannten Silylarylamido-Komplexe [(Mes_2NON)M^{II}Cl(thf)] (M = Mn, Co) aktiviert und untersucht. Alle erhaltenen Verbindungen wurden durch NMR-, IR-, UV-Vis-Spektroskopie und untersucht. Bei ausgewählten Verbindungen kamen weiterführende analytische Methoden wie ^{57}Fe-Mößbauer und EPR-Spektroskopie zu Einsatz, um genauere Einblicke in die elektronische Situation dieser Verbindungen zu erhalten. Diese Erkenntnisse wurden ergänzend durch quantenchemische Berechnungen nachvollzogen. Für eine Vielzahl an Verbindungen konnten ferner Zerfallswege und Reaktivitäten ermittelt werden, was ein weitergehendes Verständnis zur Chemie der neu erhaltenen Moleküle und Komplexe liefert.

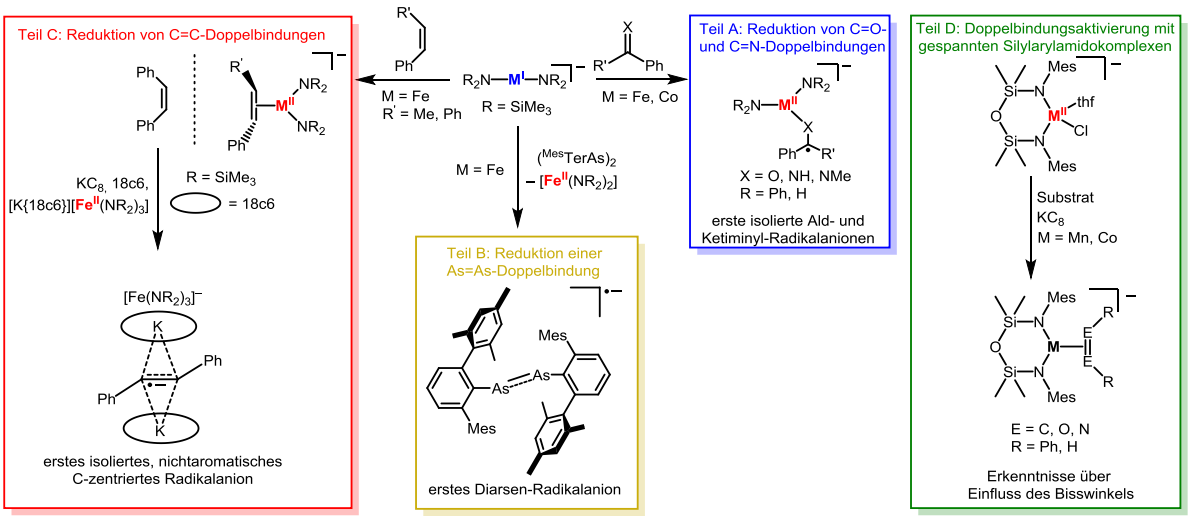

Schema 57. Übersicht der Teilprojekte A – D und der wichtigsten, im Rahmen dieser Arbeit entstandenen Verbindungen

Zunächst wurde die Reduktion von C=O- und C=N-Doppelbindungen untersucht (Teil A), wobei eine Reihe an *end-on* metallgebundenen Radikalanionen [**I**]$^-$ – [**V**]$^-$ durch die Reaktion von [M^{I}($N(SiMe_3)_2$)$_2$]$^-$ (M = Fe, Co) mit Benzophenon (bp), Benzophenonimin (bpi) und Benzaldehydmethylamin (bama) isoliert werden konnte. [**I**]$^-$, [**II**]$^-$ und [**V**]$^-$ lassen sich alternativ durch die Reduktion der zuvor dargestellten neutralen Adduktkomplexe aus [M^{II}($N(SiMe_3)_2$)$_2$] (M = Fe, Co) und bp bzw. bama (**I**, **II** und **V**) mit KC_8 gewinnen. Die Reaktion von [M^{II}($N(SiMe_3)_2$)$_2$] mit bpi hingegen führt zu den dimeren Ketimidokomplexen **VII** und **VIII**.

Durch spektroskopische Untersuchungen (v. a. EPR- und ^{57}Fe-Mößbauerspektroskopie) wurde die Oxidationsstufe der Metallionen in [**I**]$^-$ – [**V**]$^-$ als +II identifiziert und Carbonylkohlenstoff-zentrierte radikalische Charakter der gebundenen Substrate durch quantenchemische Rechnungen bestätigt.

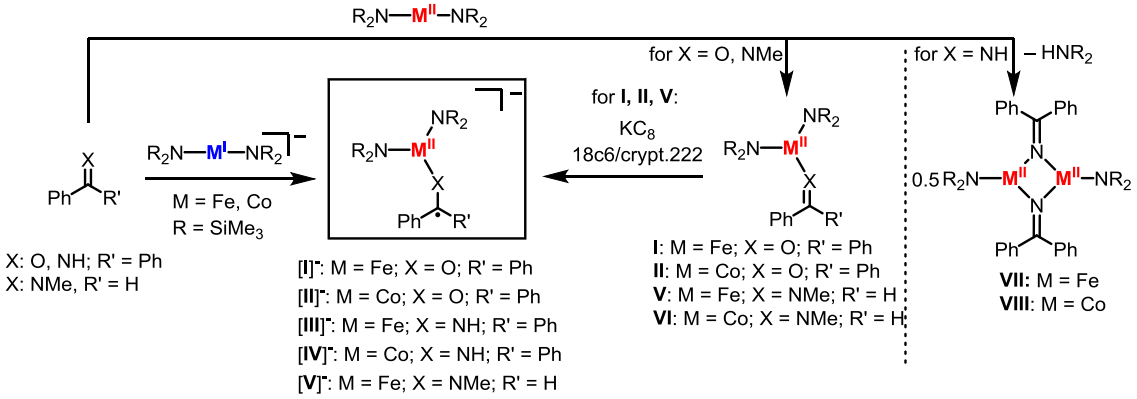

Schema 58. Synthese der Radikalanionen-Komplexe [**I**]$^-$ - [**V**]$^-$, sowie der Neutralkomplexe **I**, **II**, **V** – **VIII**.

Setzt man anstatt polarer Carbonyle und Imine, das sterische anspruchsvolle Diarsen (^{Mes}TerAs)$_2$ ein, erfolgt bei der Reaktion mit [Fe(N(SiMe$_3$)$_2$)$_2$]$^-$ keine Koordination sondern ein Elektronentransfer statt. Dabei wird das "freie" Diarsenradikalanion **IX** erhalten, welches in Abhängigkeit der Kristallisationsbedingungen eine symmetrische (**IX^{sym}**) oder asymmetrische (**IX^{asym}**) Struktur des Anions aufweist (Schema 59 links). Der Radikalcharakter von **IX** konnte mittels EPR-Spektroskopie nachgewiesen werden (Schema 59 rechts). Die beobachtete Asymmetrie wird hier durch unterschiedliche Kopplungskonstanten des ungepaarten Elektrons zu den einzelnen ^{75}As-Kernen sichtbar. Quantenchemische Rechnungen beschreiben die Bindungssituation der As-As-Bindung als Kombination einer σ- (HOMO-1) und π -Bindung (HOMO), mit dem SOMO als π*-Orbital.

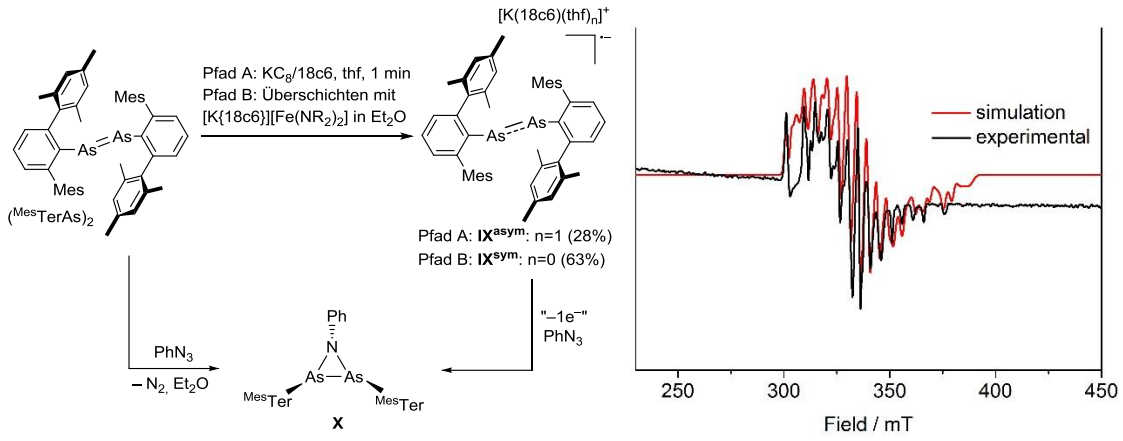

Schema 59. Darstellung des Diarsen-Radikalanions **IX** (links) mit dessen EPR-Spektrum bei 77 K in ^{Me}THF (rechts).

Zusätzlich wurde die Reaktivität von **IX** untersucht, wodurch gezeigt werden konnte, dass dieses ausschließlich als Ein-Elektronen-Donor fungiert und keine radikalbasierte Reaktivität aufweist. Im Zuge dieser Untersuchungen wurde mit **X** das erste Azadiarsacyclopropan synthetisiert.

Im Teil C wurde Fokus auf die Reduktion von C=C-Doppelbindungen gelegt, wodurch die erstmalige Isolation und strukturelle Charakterisierung des Stilben-Radikalanions (in **XI**) gelang (Schema 60). Dies konnte durch die Stabilisierung mit zwei [K{18c6}]-Kationen und einem schwach koordinierenden Anion $[Fe^{II}(N(SiMe_3)_2)_2]$ ermöglicht werden. Auch hier konnte das Vorliegen eines ungepaarten Elektrons auf dem Stilbenanion anhand von EPR-Spektroskopie nachgewiesen werden. Die Reduktionskraft von **XI** konnte durch einen Elektronentransfer auf Benzophenon gezeigt werden, wodurch die analoge Ketylradikal-Spezies (in **XII**) entsteht. Im Zuge dessen wird eine *Z*- zu *E*-Isomerisierung beobachtet. Dies ist auch katalytisch möglich, ist jedoch auf Stilben als Substrat, sowie durch die Labilität von **XI** begrenzt.

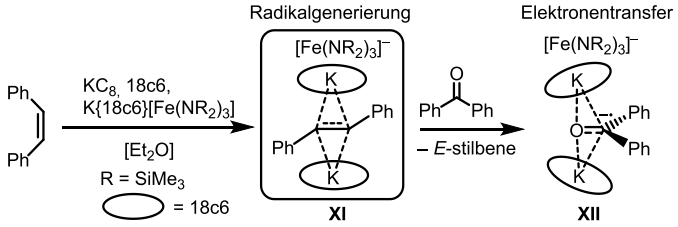

Schema 60. Darstellung des Stilben-Radikalanions in **XI** und Elektronentransfer auf Benzophenon zum Ketyl-Radikal **XII**.

Die Einschränkung hinsichtlich der Katalysatorstabilität kann durch die Verwendung von $[K\{18c6\}][Fe^{I}(N(SiMe_3)_2)_2]$ überwunden werden, wobei hier auch die Isomerisierung von β-Methylstyrol und 3-Hexen möglich ist (Schema 61 links). Mechanistische Untersuchungen deuten auf das Vorliegen eines Eisen(II)-gebundenen Radikalanions hin, welches infolge in der Koordinationssphäre des Eisenions isomerisiert. Zum Verständnis hiervon wurden die Eisen-Alkenkomplexe **XIII** und **XIV** mit der Oxidationszahl +II synthetisiert (Schema 61 rechts).

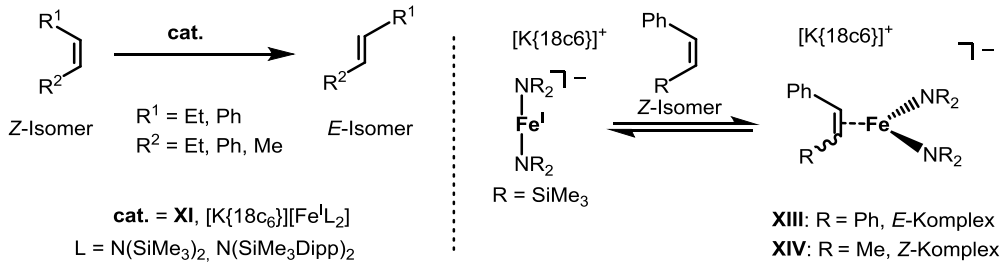

Schema 61. Katalytische *Z*- zu *E*-Isomerisierung (links) und Darstellung der Eisen-Alkenkomplexe **XIII** und **XIV** (rechts).

Zuletzt (Teil D) wurde basierend auf Reaktionsuntersuchungen an linearen Metall(I)silylamiden (wie z. B. $[Fe^{I}(N(SiMe_3)_2)_2]^-$) der Effekt einer erzwungenen Abwinkelung der N-M-N Bindungsachse auf die

Stabilität des zweifach-koordinierten Metall(I)ions untersucht (Schema 62). Dies wurde über einen bis(silylamid)-Chelatliganden erreicht. Angestrebte Metall(I)komplexe erwiesen sich jedoch als zu reaktiv, konnten dennoch zur Umsetzung mit Substraten genutzt und somit indirekt nachgewiesen werden. So zeigt sich eine erhöhte Reaktivität entsprechender Imidokomplexe, welche über die H-Atom-Abstraktion vom Lösungsmittel direkt zum Amid weiterreagierten (**XVI-Mn/Co**). Alternativ führt der kleinere Bisswinkel des Liganden (ca. 105° für die Chelatliganden im Vergleich zu ca. 120° für zwei Silylamide) zu einer geringeren sterischen Abschirmung des intermediären Metallimids und erlaubt eine 2 + 3 Cycloaddition unter Bildung eines Tetrazenkomplexes **XVII**. Zuletzt zeigt sich im Falle von Cobalt und Benzophenon nun eine *side-on* Koordination des Substrates, im Gegensatz zur beobachteten terminalen Koordination als Radikalanion im Falle linearer Metall(I)komplexe.

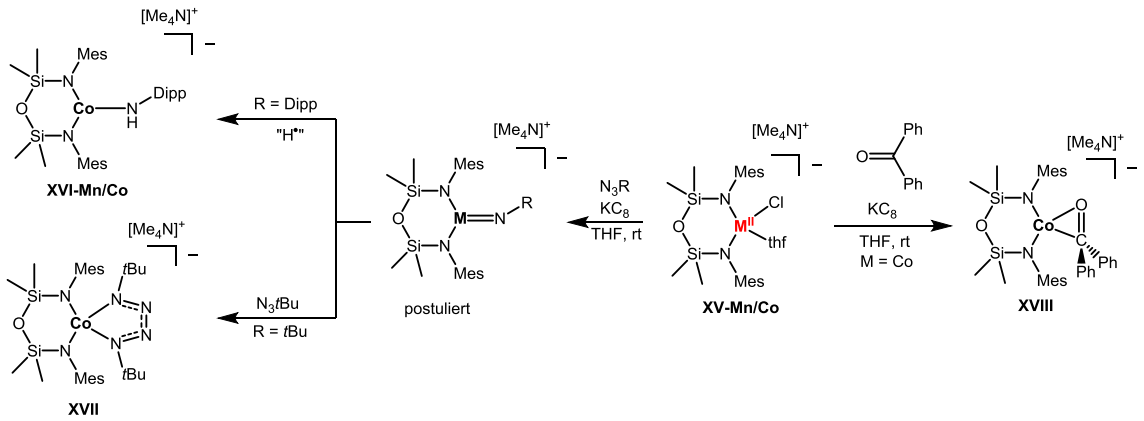

Schema 62. Ausgewählte Substrataktivierungen unter reduzierenden Bedingungen ausgehend von Mangan- und Cobalthalogenidokomplexen **XV-Mn/Co**.

Zusammenfassen kann gesagt werden, dass im Rahmen dieser Arbeit eine Vielzahl an Verbindungen bislang nicht beobachteter Radikalanionen dargestellt wurden. Diese wurden durch einen SET auf die neutralen Substrate erhalten und konnten durch passenden Methoden strukturell und spektroskopisch untersucht werden. Die erhaltenen Einblicke über die Reaktivität solcher Verbindungen trug zum Verständnis der Chemie dieser besonderen Verbindungsklasse bei.

5. English Summary

Within this thesis, contributions to the understanding in the field of one-electron reductions of C=C, C=N, C=O, N=N and As=As double bonds were gathered (Scheme 1). Different synthetic strategies were chosen, such as reduction of substrates within the coordination-sphere of highly reducing metal ions (Fe^{I}, Co^{I}), through sterical shielding or via the stabilization in a sandwich-type structure. In the last part, different substrates with E=E double bonds of carbon, oxygen and nitrogen (and other substrates) were activated with strained silylarylamido complexes [$(Mes_2NON)M^{II}Cl(thf)$] (M = Mn, Co). All compounds were investigated by means of NMR, IR and UV-Vis spectroscopy. Selected compounds were further investigated with ^{57}Fe-Mössbauer (for iron compounds) and EPR spectroscopy to gain insights into their electronic situation. This was clarified with use of quantum calculations. For many compounds, an understanding for the decomposition and reactivity was given, providing insights to the chemistry of the newly gained molecules and complexes.

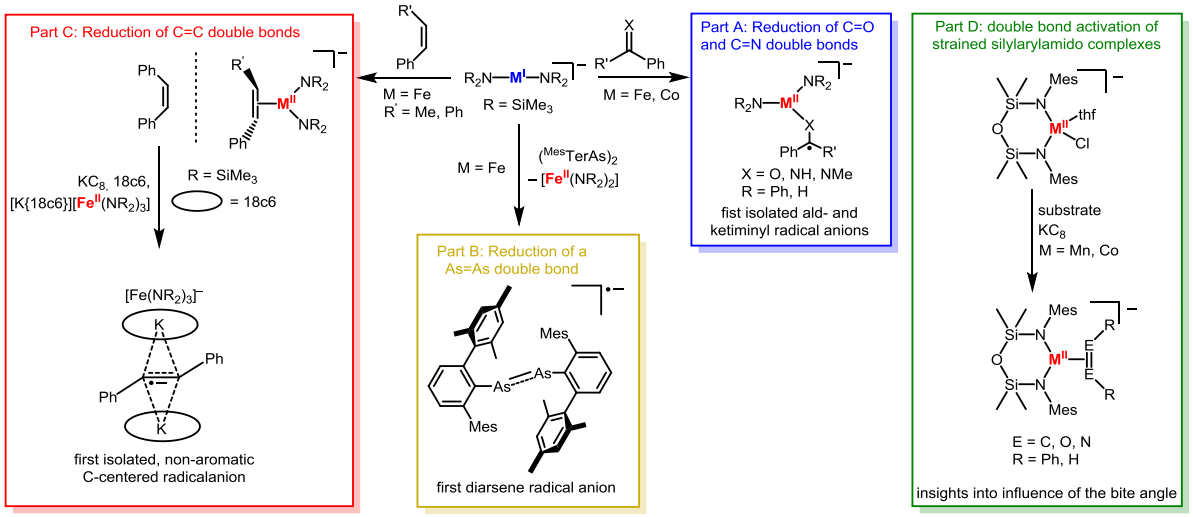

Scheme 1. Overview of the different projects A – D and most important compounds that were isolated during this thesis.

In part A the reduction of C=O and C=N double bonds was investigated, were a range of *end-on* coordinating metal-bound radical anions [**I**]$^-$ – [**V**]$^-$ were obtained and isolated by the reaction of [$M^{I}(N(SiMe_3)_2)_2]^-$ (M = Fe, Co) with benzophenone (bp), benzophenoneimine (bpi) and benzaldehydemethylamine (bama). [**I**]$^-$, [**II**]$^-$ and [**V**]$^-$ could alternatively be prepared by reduction of the neutral adduct complexes of [$M^{II}(N(SiMe_3)_2)_2$] (M = Fe, Co) and bp or bama (**I**, **II** und **V**) with KC_8. However, the reaction of [$M^{II}(N(SiMe_3)_2)_2$] with bpi leads to the dimeric ketimido complexes **VII** and **VIII**.

By means of EPR and ^{57}Fe-Mößbauer spectroscopy the oxidation state of [**I**]$^-$ – [**V**]$^-$ could be unequivocally established as +II, denoting the radical character, which was solidified with quantum calculations.

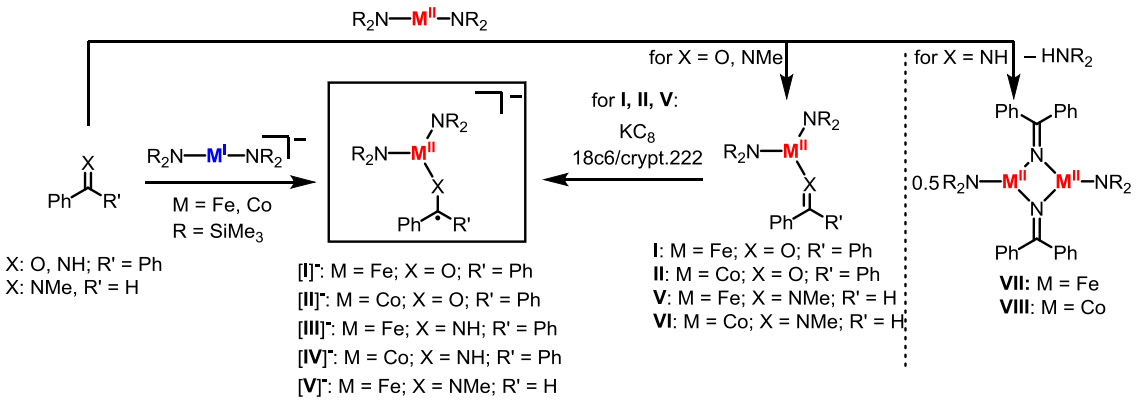

Scheme 2. Synthesis of the radical anion complexes [**I**]$^{-}$ – [**V**]$^{-}$, as well as the neutral complexes **I**, **II**, **V** – **VIII**.

By employing the sterically demanding diarsene (^{Mes}TerAs)$_2$ instead of polar carbonyls and imines, the reaction with [Fe(N(SiMe$_3$)$_2$)$_2$]$^{-}$ does not lead to a coordination but an electron transfer. The "free" diarsene radical anion **IX** is obtained with a symmetric (**IX^{sym}**) or asymmetric (**IX^{asym}**) anion structure, depending on the crystallization conditions (Scheme 3 left).

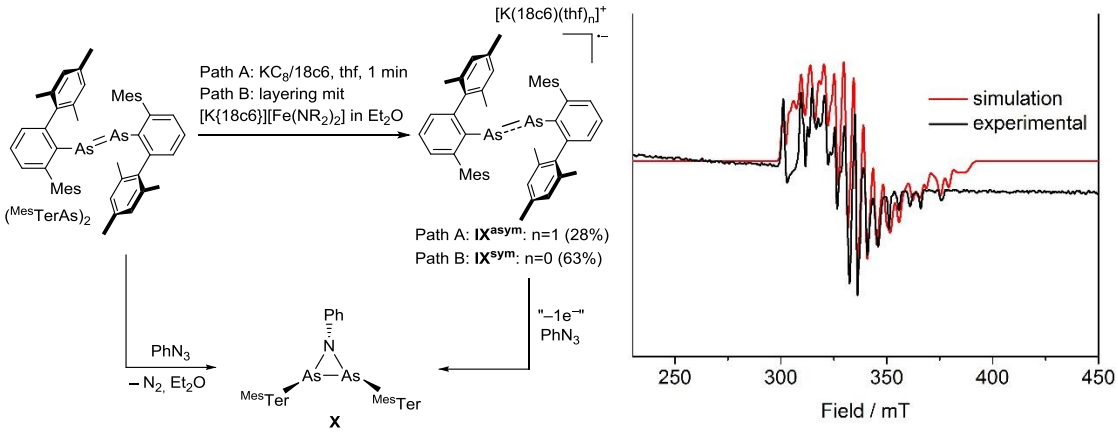

Scheme 3. Synthesis of the diarsene radical anion **IX** (left) and its EPR spectrum at 77 K in ^{Me}THF (right).

The radical character of **IX** could be determined by means of EPR spectroscopy (Scheme 3 right). Here the observed asymmetry is noticeable through the different coupling constants of the unpaired electron to the ^{75}As nuclei. With the help of quantum calculations, the bonding situation of the As-As bond could be described as a σ- (HOMO-1) and π -bond (HOMO), with the SOMO as π* orbital. With the investigation of the reactivity of **IX**, it was shown that it only reacts as a one-electron donor with no apparent radical reactivity. Within the scope of the reactivity studies the first azadiarsacyclopropane was synthesized in form of **X**.

In part C the focus was shifted towards the reduction of C=C double bonds, where the first isolation and structural characterization of the stilbene radical anion (in **XI**) was achieved (Scheme 4). This was done by encapsulation of the radical anion between to [K{18c6}] cations and a weakly-coordinating

anion in the form of $[Fe^{II}(N(SiMe_3)_2)_2]$. Again, the proof of the unpaired electron on the stilbene moiety was provided by EPR measurements. The reducing properties of **XI** were demonstrated by electron transfer to benzophenone, which afforded the ketyl radical in **XII**. The formation of **IX** was further accompanied by *Z*→*E* isomerization. This could be also be done catalytically with stilbene as substrate yet is restricted by the lability of **XI**.

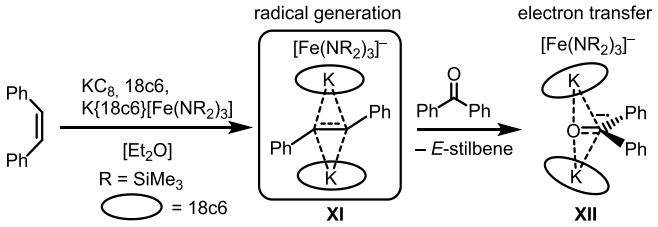

Scheme 4. Synthesis of the stilbene radical anion in **XI** and electron transfer to benzophenone to form the ketyl radical **XII**.

These restrictions were overcome by use of $[K\{18c6\}][Fe^{I}(N(SiMe_3)_2)_2]$ as catalyst, where the isomerization of β-methylstyrene and 3-hexene was additionally possible (Scheme 5 left). Mechanistic investigations hint to the existence of an iron(II)-bound radical anion which undergoes subsequent isomerization in the coordination sphere of the iron ion. For further insights, the iron alkene complexes **XIII** and **XIV** with the oxidation state +II were synthesized (Scheme 5 right).

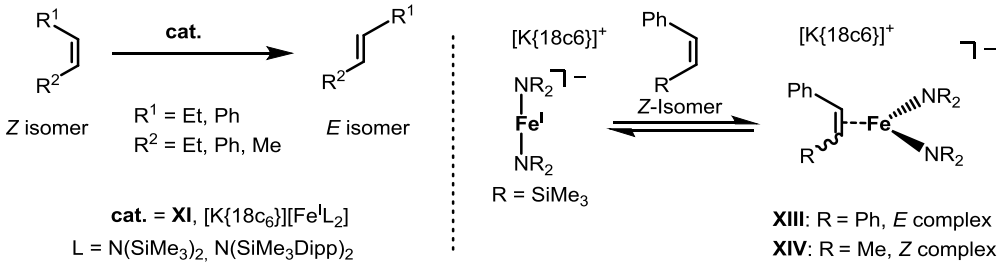

Scheme 5. Catalytic *Z* to *E* isomerization (left) and synthesis of the iron alkene complexes **XIII** and **XIV** (right).

Based on the findings for the reactivity of linear metal(I) silylamides (e. g. $[Fe^{I}(N(SiMe_3)_2)_2]^-$), the effect of a forcefully bent N-M-N bond axis was investigated (Scheme 6). This was done by use of a chelating bis(silylamide) ligand. Envisioned metal(I)complexes proved to be too reactive but could be reacted with substrates to give indirect proof of existence. The increased reactivity led to the formation of corresponding imido complexes which then reacted to amide complexes via H atom transfer from the solvent (**XVI-Mn/Co**). Alternatively, the smaller bite angle if the ligand led to a smaller sterical shielding of the metal imide and allowed for a 2 + 3 cycloaddition with generation of the tetrazene complex **XVII**. Lastly, in case of cobalt and benzophenone a *side-on* coordination was observed, showing alternative binding modes (in **XVIII**) in comparison with the linear silyl amide complexes.

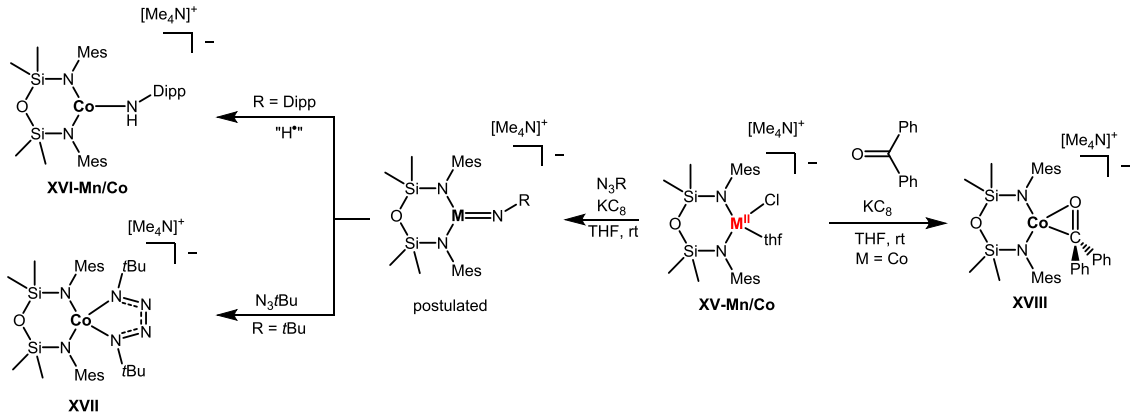

Scheme 6. Selected substrate activations under reducing conditions starting from the manganese and cobalt complexes **XV-Mn/Co.**

In summary, a variety of new compounds with so far no not observed radical anions could be synthesized. These were formed by a SET to the neutral substrates and were investigated structurally and spectroscopically. The newly gained insights into the reactivity of such complexes and molecules contributed to the broader understanding of the chemistry of this unique type of compounds.

6. Anhang

6.1 Wissenschaftlicher Werdegang

-entfernt-

6.2 Publikationsliste

Die in dieser Arbeit enthaltenen Publikationen sind durch fett gedruckte Titel gekennzeichnet.

[5] **Bond activation by bent, formally manganese(I), iron(I) and cobalt(I) di(silylamides)**

G. Sieg, T. Vaupel, K. Dollberg, C. G. Werncke, *manuscript in preparation*.

[4] **Taming the Stilbene Radical Anion**

G. Sieg, I. Müller, K. Weißer, C. G. Werncke, *submitted*.

[3] **A Diarsene Radical Anion**

G. Sieg, M. Fischer, F. Dankert, J.-E. Siewert, C. Hering-Junghans, C. G. Werncke, *Chem. Commun.* **2022**, DOI: 10.1039/D2CC03237F.

[2] **Cobalt and Iron Stabilized Ketyl, Ketiminyl and Aldiminyl Radical Anions**

G. Sieg, Q. Pessemesse, S. Reith, S. Yelin, C. Limberg, D. Munz, C. G. Werncke, *Chem. Eur. J.* **2021**, *27*, 16760–16767.

[1] Cationic group 1 carbodiphosphorane complexes

J. E. Münzer, G. H. R. Sieg, R. Vehlies, P. A. Fuzon, X. Xie, B. Neumüller, I. Kuzu, *Polyhedron* **2021**, *196*, 115014.

6.3 Dewar-Chatt-Duncanson-Modell

Das DEWAR-CHATT-DUNCANSON-Modell beschreibt Wechselwirkungen zwischen Übergansmetallen und Mehrfachbindungen (u. a. Alkene und Alkine).[158–160] Hierbei existiert eine σ-Hinbindung, bei der Elektronen aus dem HOMO des Liganden in ein leeres d-Orbital des Metalls mit passender Symmetrie doniert werden. Zudem werden in der π-Rückbindung Elektronen aus besetzten d-Orbitalen des Metalls in das unbesetzte π*−Orbital des Liganden doniert. Diese Wechselwirkungen resultieren in einer Stabilisierung der Metall-Ligand-Bindung bei gleichzeitiger Schwächung (verbunden mit einer Verlängerung) der Mehrfachbindung. Im Falle von Dreifachbindungen können weitere, zu den hier gezeigten Orbitalen orthogonal stehende, π−Orbitale mit d-Orbitalen des Metalls mit passender Symmetrie wechselwirken.

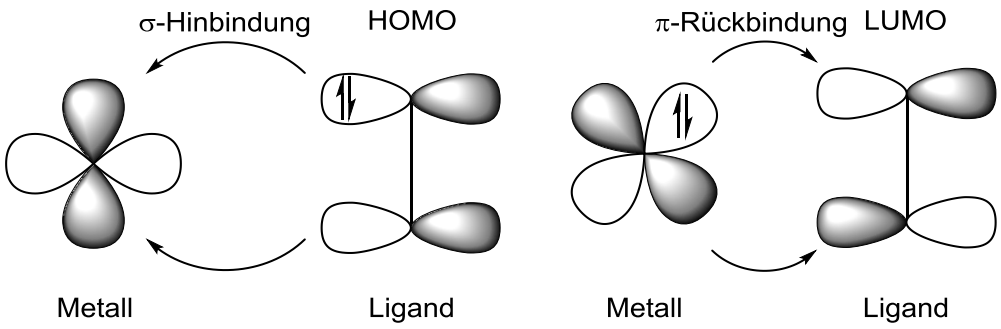

Abbildung 3. Elektronische Wechselwirkungen nach dem DEWAR-CHATT-DUNCANSON-Modell. Links die σ-Hinbindung aus dem HOMO des Liganden in ein freies d-Orbital des Metalls, rechts die π-Rückbindung von einem besetzten d-Orbital in das LUMO des Liganden.[158–160]

Bei steigender Elektronegativität der Metalle schwindet der π-Rückbindungscharakter, weshalb sich die resultierenden Komplexe am besten als π-Komplexe beschreiben lassen. Für frühe Übergangsmetalle hingegen entspricht die Bindungssituation der eines Metallacyclopropan- bzw. Metallacyclopropen-Komplexes (siehe Schema 46).[124,125]

6.4 Molekularer Magnetismus

6.4.1 Magnetische Suszeptibilität

Wird Materie einem äußeren Magnetfeld mit der Feldstärke *H* und der Flussdichte *B* ausgesetzt, wobei *B* im materiefreien Raum zu H proportional ist (Gleichung 1),

$$B = \mu_0 H \qquad (1)$$

Mit μ_0 = Vakuumpermeabilität

so ändert sich die Flussdichte *B* innerhalb der Materie entsprechend der Magnetisierung *M* (Gleichung 2).

$$B = \mu_0(H + M) \tag{2}$$

Entsprechend kann die Magnetisierung beschrieben werden als:

$$M = \frac{B - \mu_0 H}{\mu_0} \tag{3}$$

Für den Fall magnetisch isotroper Stoffe gilt, dass die Magnetisierung proportional zur Feldstärke ist. Der Proportionalitätsfaktor ist die dimensionslosen magnetischen Suszeptibilität χ:

$$M = \chi H \tag{4}$$

χ setzt sich aus einem diamagnetischen Anteil χ_{dia} und einem paramagnetischen Anteil χ_{para} zusammen (Gleichung 5), wobei im Falle von diamagnetischen Substanzen χ_{para} = 0 ist. Diamagnetische Stoffe besitzen üblicherweise eine negative Suszeptibilität von -10^{-4} bis -10^{-6}, während paramagnetische Stoffe eine Suszeptibilität von 10^{-2} bis 10^{-5} besitzen. Letztere besitzen zwar auch einen diamagnetischen Anteil, dieser wird allerdings vom paramagnetischen Anteil überwogen.[161]

$$\chi = \chi_{dia} + \chi_{para} \tag{5}$$

6.4.2 Paramagnetismus

Verbindungen, welche über freie Elektronen verfügen, weisen beim Anlegen eines äußeren Magnetfeldes eine positive magnetische Suszeptibilität χ auf. Dieser wird auch als CURIE-Paramagnetismus bezeichnet und nimmt bei niedrigen Temperaturen stark zu. Grund für dieses Phänomen ist die Anordnung der magnetischen Dipole in Feldrichtung (sofern ein Feld vorhanden ist) unter Ausbildung eines energetisch günstigeren Zustandes. Durch die makroskopische Anordnung der magnetischen Momente in Feldrichtung lässt sich ein positiver Beitrag für χ messen. Bei steigender Temperatur wird diese Ordnung unterbunden und χ nimmt ab. Dieser Effekt wird durch das CURIE-Gesetz mit der stoffspezifischen CURIE-Konstanten C beschrieben (Gleichung 6):

$$\chi_{mol} = \frac{C}{T} \tag{6}$$

Mit χ_{mol} = molare Suszeptibilität und T = Temperatur

Bei der Auftragung der reziproken Suszeptibilität gegen die Temperatur erhält wird für diesen Fall eine Gerade mit der Steigung von $1/C$ (Abbildung 4) erhalten.

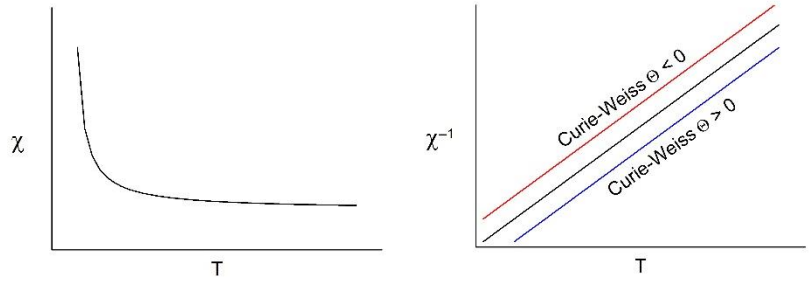

Abbildung 4. Verlauf der Suszeptibilität bei CURIE-Paramagnetismus (links) und reziproke Auftragung (rechts) für CURIE-Verhalten (schwarz) und CURIE-WEISS-Verhalten mit positiver (blau) und negativer (rot) WEISS-Konstante.

Dieser Fall des Paramagnetismus liegt in Verbindungen mit magnetisch isolierten Zentren, kombiniert mit *spin-only*-Paramagnetismus vor. Für viele Fälle lassen sich besser mit dem CURIE-WEISS-Paramagnetismus beschreiben, bei dem die Temperatur durch den Parameter Θ, der sogenannten WEISS-Konstante, korrigiert wird (Gleichung 7).

$$\chi_{mol} = \frac{C}{T - \Theta} \tag{7}$$

Das CURIE-WEISS-Gesetz erlaubt die Beschreibung für kooperative Effekte, beispielsweise die Wechselwirkung von Metallionen über verbrückende Liganden. In der Realität gilt das Gesetz nur für Temperaturen oberhalb der CURIE-Temperatur T_C, während darunter Nahordnungsphänomene dominieren. Θ ist positiv für Stoffe, die unterhalb von T_C Ferromagnetismus aufweisen. Tritt hingegen unterhalb der NÉEL-Temperatur T_N Antiferromagnetismus oder Ferrimagnetismus auf, ist Θ negativ (Abbildung 4 rechts).

Auf Grundlage der BOLTZMANN-Statistik konnte LANGEVIN die theoretische Erklärung für dieses Verhalten geben. Zudem wurde von ihm eine Zusammenhang zwischen C und dem effektiven magnetischen Moment μ_{eff} gefunden, welches auf ein einzelnes Zentrum bezogen ist (Gleichung 8).

$$\chi_{mol} = \mu_0 \frac{N_A \mu_{eff}^2}{3k_B T} = \frac{C}{T} \qquad \text{mit} \qquad C = m_0 \frac{N_A \mu_{eff}^2}{3k_B} \tag{8), (9}$$

Mit N_A = Avogadro-Konstante und k_B = Boltzmann-Konstante

Bei Elektronen, die vereinfach beschrieben um einen Kern rotieren, tritt sowohl ein Eigendrehimpuls (Spin, *s*), wie auch ein Bahndrehimpuls *l* auf. Aufgrund der Wechselwirkung des magnetischen Spinmomentes μ_s mit dem Magnetfeld der Bahnbewegung koppeln beide Drehimpulse miteinander zu einem Gesamtdrehimpuls *j*:

$$j = l + s \tag{10}$$

Mit Einbeziehung des RUSSEL-SAUNDERS-Kopplungsschemas für Ionen mit schwacher Spin-Bahn-Wechselwirkung ergibt sich für *C* mit dem LANDÉ-Faktor g_j:

$$C = \frac{\overbrace{\mu_0 N_A g_j^2 J(J+1)\mu_B^2}^{\mu^2}}{3k_B} \qquad \text{mit} \qquad g_j = 1 + \frac{J(J+1)+S(S+1)-L(L+1)}{2J(J+1)} \qquad (11), (12)$$

Mit *J* = Gesamtdrehimpulsquantenzahl, *L* = Bahndrehimpulsquantenzahl, *S* = Spinquantenzahl

μ_B = BOHR-Magneton

Für reinen Spin-Paramagnetismus ergibt sich aufgrund von *L* = 0 und *J* = *S*:

$$\mu^2 = g^2 S(S+1)\mu_B^2 \quad \text{bzw.} \quad \frac{\mu_{S.O.}}{\mu_B} = g\sqrt{S(S+1)} \qquad (13), (14)$$

Mit *g* = 2 (für einzelne Elektronen) und dem *spin-only*-Wert $\mu_{S.O.}$ für das magnetische Moment

Durch Umstellen von Gleichung (8) lässt sich für n_{eff} eine vereinfachte Abhängigkeit von χ und *T* herleiten (Gleichung 15). n_{eff} ist hier eine empirische Zahl, und entspricht der Magnetonenzahl des magnetischen Momentes.

$$n_{eff} = \frac{\mu_{eff}}{\mu_B} = \sqrt{\frac{3k_B}{\mu_0 N_A \mu_B^2}}\sqrt{\chi T} = 2{,}827\sqrt{\chi T} \qquad (15)$$

Während $\mu_{S.O.}$ keine Spin-Bahn-Wechselwirkungen berücksichtigt, kann sich der real gemessene Wert μ_{eff} abhängig der Elektronenkonfiguration des betrachteten Metallions davon unterscheiden.[161]

7. Danksagung

An erster Stelle möchte ich Dr. Gunnar Werncke für die Übernahme des Erstgutachtens und vor allem für die langjährige Betreuung dieser Arbeit danken. Trotz eines schwierigen Starts haben wir im Endeffekt einen sehr fruchtbaren Modus der Zusammenarbeit gefunden und das Thema zu einem erfolgreichen Abschluss gebracht. Die Zeit hat mir über alle Maße Spaß bereitet und ich bin froh, den Weg in deine Arbeitsgruppe gefunden zu haben.

Mein Dank geht natürlich auch an Prof. Dr. Stefanie Dehnen, die ohne zu zögern der Erstellung des Zweitgutachtens zugestimmt hat. Auch für die Aufnahme in die erweiterte Arbeitsgruppe und die vielen Grillfeste, Weihnachtsfeiern oder sonstige Anlässe, welche ohne sie nicht möglich gewesen wären, möchte ich mich bedanken.

Prof. Dr. Andreas Seubert und Prof. Dr. Wolf-Christian Pilgrim möchte ich an der Stelle für die Teilnahme an der Prüfungskommission danken.

An dieser Stelle erwähnt werden müssen auch alle jetzigen und ehemaligen Mitarbeiter der AGs Dehnen, Heine, Kuzu und Tambornino. Der tägliche Gang in die Mensa, gemeinsame Kuchenessen, Grillen, Biertrinken und sonstige Aktivitäten werden mit immer in positiver Erinnerung bleiben. Auch die Jährlichen Fahrten zum Edersee mit der AG vön Hänisch werde ich sicher vermissen.

Den größten Anteil zum erfolgreichen Gelingen meiner Promotion haben mit Sicherheit meine (ehemaligen) Kollegen der AG Werncke, Alexander Reckziegel, Andres Gonzalez-Gomez, Sascha Reith, Dr. Ruth Weller, Dr. Christian Schneider, Dr. Igor Müller und allen Studenten, die in der Zeit das Labor bevölkert haben.

Meinen Bachelorstudenten Kevin Dollberg und Leonard Briefs, sowie meinen Vertiefern Yannick Lohse, Sascha Reith, Robert Vehlies und Theresa Vaupel möchte ich für die schönen Momente im Labor und die Beiträge zu meiner Forschung danken.

Selbstverständlich sollen auch meine Kooperationspartner nicht unerwähnt bleiben: Prof. Dr. Dominik Munz und Quentin Pessemesse für die quantenchemischen Rechnungen, Dr. Stefan Yelin und Kilian Weißer für die Mößbauer-Messungen und Dr. Christian Hering-Junghans und seiner Arbeitsgruppe für die Mitarbeit an den Arsen-Verbindungen. Besonders erwähnt sei hier auch Dr. Andreas Stoy, der mit mir oft sehr spontan EPR-Messungen aufnehmen durfte und sich deswegen nie beschwert hat.

Zu guter Letzt auch die Mitarbeiter der Serviceabteilungen, vor allem Cornelia Mischke für die NMR-Messungen, sowie Dr. Sergei Ivlev und Radostan Riedel für die Messungen meiner Einkristalle.

Außerhalb der Uni gibt es eine ganze Reihe an Menschen, die mich in der Zeit begleitet haben. Namentlich erwähnt sein sollen vor allem meine Kollegen und Freunde Yannick, Mirko, Simon, Jonathan, Chloé, Andi, Paula, Hannah, Sascha und Julia (letzteren beiden soll auch nochmal ausdrücklich für das Korrekturlesen der Arbeit gedankt sein). Die Zeit nach der Arbeit wäre ohne euch nur halb so witzig gewesen und die vielen Unternehmungen (Sushi-Essen, Sudhaus-Schnitzel, Kanufahren, Grillen, Poolparties, …) waren mir immer eine riesen Freude.

Neben der Uni waren es vor allem die Jungs und Mädels vom VDSt Marburg, die für ein gemütliches Gespräch immer zu haben waren und auch sonst für einigen Spaß gesorgt haben. An der Stelle seien Lukas (beide), Luca (auch beide), Leon, Jack, Marcel, Sebastian, Chris, Marie, Anna, Jörn (auch als langjähriger Sportpartner), Eric, Rasmus und Timo namentlich, sowie die Homberger Gruppe um Yannik, Kay, Alex und Manu genannt.

Auch die Nature-Crew um Anton, Olaf, Chris, Domi, Timur, Luca und Steffi seien an dieser Stelle erwähnt. Ich hoffe, wir werden noch genug Gelegenheiten für gemeinsame Feiern finden.

Immer wieder schön sind auch die Treffen mit meinen Schulkameraden Jonas, Patrick und Yassin, welche regelmäßig für besondere Erinnerungen sorgen.

Ein ganz besonderer Dank geht an dieser Stelle an meine Freunde Pascal und Selina, welche mich, neben allen schönen Momenten, auch durch die weniger schönen Zeiten begleitet haben. Vor allem fürs Zuhören, wenn mal wieder gar nichts lief, und dafür, dass ihr mir auch ehrlich gesagt habt, was euch an mir stört. Ohne eure Motivation wäre vieles nicht so einfach gewesen!

Das Wichtigste kommt bekanntlich zum Schluss und das ist meine Familie mit Viviane, Camille und meinen Eltern Horst und Yolande. Ohne eure Geduld und Unterstützung seit meinen jüngsten Jahren wäre dies alles nicht möglich gewesen.

8. Literaturverzeichnis

[1] M. Gomberg, *J. Am. Chem. Soc.* **1900**, *22*, 757–771.

[2] T. Wirth, *Angew. Chem. Int. Ed.* **1996**, *35*, 61–63.

[3] M. L. Di Vona, V. Rosnati, *J. Org. Chem.* **1991**, *56*, 4269–4273.

[4] A. Y. Chan, I. B. Perry, N. B. Bissonnette, B. F. Buksh, G. A. Edwards, L. I. Frye, O. L. Garry, M. N. Lavagnino, B. X. Li, Y. Liang, E. Mao, A. Millet, J. V. Oakley, N. L. Reed, H. A. Sakai, C. P. Seath, D. W. C. MacMillan, *Chem. Rev.* **2022**, *122*, 1485–1542.

[5] N. E. S. Tay, D. Lehnherr, T. Rovis, *Chem. Rev.* **2022**, *122*, 2487–2649.

[6] N. Holmberg-Douglas, D. A. Nicewicz, *Chem. Rev.* **2022**, *122*, 1925–2016.

[7] A. D. McNaught, A. Wilkinson, *IUPAC. Compendium of Chemical Terminology, 2nd Ed. (the "Gold Book")*, Blackwell Scientific Publications, Oxford, **1997**.

[8] H. Lankamp, W. T. Nauta, C. MacLean, *Tetrahedron Lett.* **1968**, *2*, 249–254.

[9] D. J. Brown, *J. Am. Chem. Soc.* **1948**, *70*, 1208–1209.

[10] Y. Zakon, L. Halicz, F. Gelman, *Environ. Sci. Technol.* **2013**, *47*, 14147–14153.

[11] J. Clayden, N. Greeves, S. Warren, P. Wothers, *Organic Chemistry*, Oxford University Press, Oxford, **2001**.

[12] W. P. Neumann, Wolfram. Uzick, A. K. Zarkadis, *J. Am. Chem. Soc.* **1986**, *108*, 3762–3770.

[13] J. Frank, M. Elewa, M. M. Said, H. A. El Shihawy, M. El-Sadek, D. Müller, A. Meister, G. Hause, S. Drescher, H. Metz, P. Imming, K. Mäder, *J. Org. Chem.* **2015**, *80*, 6754–6766.

[14] I. Dhimitruka, A. A. Bobko, C. M. Hadad, J. L. Zweier, V. V. Khramtsov, *J. Am. Chem. Soc.* **2008**, *130*, 10780–10787.

[15] W. Rundel, K. Scheffler, *Tetrahedron Lett.* **1963**, *15*, 993–995.

[16] E. Beckmann, T. Paul, *Justus Liebigs Ann. Chem.* **1891**, *266*, 1–28.

[17] T. A. Scott, B. A. Ooro, D. J. Collins, M. Shatruk, A. Yakovenko, K. R. Dunbar, H.-C. Zhou, *Chem. Commun.* **2009**, 65–67.

[18] F. Seel, *Sulfur in Artwork: Lapis Lazuli and Ultramarine Pigments*, Elsevier, **1984**.

[19] "Bild eines Lapislazuli-Gesteinsblocks," can be found under https://de.wikipedia.org/wiki/Lapislazuli#/media/Datei:Lapis_lazuli_block.jpg (abgerufen am 21.07.2022), **2022**.

[20] B. Kalyanaraman, C. C. Felix, R. C. Sealy, *Environ. Health Perspect.* **1985**, *64*, 185–198.

[21] P. Pacher, J. S. Beckman, L. Liaudet, *Physiol. Rev.* **2007**, *87*, 315–424.

[22] M. Bhattacharya, S. Chakraborty, *Res. rev.: j. pharmacogn. phytochem.* **2015**, *3*, 8.

[23] G. Barja, *Ann. N. Y. Acad. Sci.* **1998**, *854*, 224–238.

[24] B. Chance, H. Sies, A. Boveris, *Physiol. Rev.* **1979**, *59*, 527–605.

[25] J. F. Turrens, *J. Physiol.* **2003**, *552*, 335–344.

[26] L. Deguillaume, M. Leriche, K. Desboeufs, G. Mailhot, C. George, N. Chaumerliac, *Chem. Rev.* **2005**, *105*, 3388–3431.

[27] E. M. White, P. P. Vaughan, R. G. Zepp, *Aquat. Sci.* **2003**, *65*, 402–414.

[28] K. P. Kepp, *Chem. Rev.* **2012**, *112*, 5193–5239.

[29] C. S. Sevov, R. E. M. Brooner, E. Chénard, R. S. Assary, J. S. Moore, J. Rodríguez-López, M. S. Sanford, *J. Am. Chem. Soc.* **2015**, *137*, 14465–14472.

[30] Y. Che, A. Datar, X. Yang, T. Naddo, J. Zhao, L. Zang, *J. Am. Chem. Soc.* **2007**, *129*, 6354–6355.

[31] X. Zhan, A. Facchetti, S. Barlow, T. J. Marks, M. A. Ratner, M. R. Wasielewski, S. R. Marder, *Adv. Mater.* **2011**, *23*, 268–284.

[32] A. Rananaware, M. Samanta, R. S. Bhosale, M. A. Kobaisi, B. Roy, V. Bheemireddy, S. V. Bhosale, S. Bandyopadhyay, S. V. Bhosale, *Sci. Rep.* **2016**, *6*, 22928.

[33] G. Odian, *Principles of Polymerization, 4th Edition*, Wiley Interscience, New York, **2004**.

[34] A. H. E. Müller, K. Matyjaszewski, Eds. , *Controlled and Living Polymerizations: From Mechanisms to Applications*, Wiley-VCH, Weinheim, **2009**.

[35] M. Szwarc, *Nature* **1956**, *178*, 1168.

[36] R. G. Hicks, *Stable Radicals - Fundamentals and Applied Aspects of Odd-Electron Compounds*, John Wiley & Sons, Hoboken, **2011**.

[37] L. Ji, A. Friedrich, I. Krummenacher, A. Eichhorn, H. Braunschweig, M. Moos, S. Hahn, F. L. Geyer, O. Tverskoy, J. Han, C. Lambert, A. Dreuw, T. B. Marder, U. H. F. Bunz, *J. Am. Chem. Soc.* **2017**, *139*, 15968–15976.

[38] F. Otón, V. Lloveras, M. Mas-Torrent, J. Vidal-Gancedo, J. Veciana, C. Rovira, *Angew. Chem. Int. Ed.* **2011**, *123*, 11094–11098.

[39] Y. Kumar, S. Kumar, K. Mandal, P. Mukhopadhyay, *Angew. Chem. Int. Ed.* **2018**, *130*, 16556–16560.

[40] P. B. Hitchcock, M. F. Lappert, A. V. Protchenko, *J. Am. Chem. Soc.* **2001**, *123*, 189–190.

[41] N. D. Scott, J. F. Walker, V. L. Hansley, *J. Am. Chem. Soc.* **1936**, *58*, 2442.

[42] H. Bock, C. Arad, C. Näther, Z. Havlas, *J. Chem. Soc., Chem. Commun.* **1995**, 2393–2394.

[43] N. G. Connelly, W. E. Geiger, *Chem. Rev.* **1996**, *96*, 877–910.

[44] E. M. Kaiser, R. A. Benkeser, *Δ ^{9,10} -Octalin: Naphthalene, 1,2,3,4,5,6,7,8-Octahydro-*, John Wiley & Sons, Inc., Hoboken, NJ, USA, **2003**.

[45] F. Gerson, H. Ohya-Nishiguchi, M. Szwarc, G. Levin, *Chem. Phys. Lett.* **1977**, *52*, 587–589.

[46] G. Levin, T. A. Ward, M. Szwarc, *J. Am. Chem. Soc.* **1974**, *96*, 270–272.

[47] J. E. Gano, E. J. Jacob, P. Sekher, G. Subramaniam, L. A. Eriksson, D. Lenoir, *J. Org. Chem.* **1996**, *61*, 6739–6743.

[48] L. R. Dosser, J. B. Pallix, G. H. Atkinson, H. C. Wang, G. Levin, M. Szwarc, *Chem. Phys. Lett.* **1979**, *62*, 555–561.

[49] J. Matsuda, J. Jagur-Grodzinski, M. Szwarc, *Proc. R. Soc. Lond. A* **1965**, *288*, 212–223.

[50] H. Bock, H.-F. Herrmann, D. Fenske, H. Goesmann, *Angew. Chem. Int. Ed.* **1988**, *27*, 1067–1069.

[51] M. M. Olmstead, P. P. Power, *J. Am. Chem. Soc.* **1986**, *108*, 4235–4236.

[52] S. Inoue, M. Ichinohe, A. Sekiguchi, *J. Am. Chem. Soc.* **2007**, *129*, 6096–6097.

[53] X. Pan, X. Wang, Y. Zhao, Y. Sui, X. Wang, *J. Am. Chem. Soc.* **2014**, *136*, 9834–9837.

[54] M. K. Mondal, L. Zhang, Z. Feng, S. Tang, R. Feng, Y. Zhao, G. Tan, H. Ruan, X. Wang, *Angew. Chem. Int. Ed.* **2019**, *131*, 15976–15980.

[55] W. Wang, G. Tan, R. Feng, Y. Fang, C. Chen, H. Ruan, Y. Zhao, X. Wang, *Chem. Commun.* **2020**, *56*, 3285–3288.

[56] S. Asami, S. Ishida, T. Iwamoto, K. Suzuki, M. Yamashita, *Angew. Chem. Int. Ed.* **2017**, *129*, 1680–1684.

[57] T. Sasamori, E. Mieda, N. Nagahora, K. Sato, D. Shiomi, T. Takui, Y. Hosoi, Y. Furukawa, N. Takagi, S. Nagase, N. Tokitoh, *J. Am. Chem. Soc.* **2006**, *128*, 12582–12588.

[58] H. M. Weinert, C. Wölper, J. Haak, G. E. Cutsail, S. Schulz, *Chem. Sci.* **2021**, *12*, 14024–14032.

[59] F. Benner, S. Demir, *Chem. Sci.* **2022**, *13*, 5818–5829.

[60] Z. Hou, A. Fujita, T. Koizumi, H. Yamazaki, Y. Wakatsuki, *Organometallics* **1999**, *18*, 1979–1985.

[61] W. Kaim, *Chem. Ber.* **1981**, *114*, 3789–3800.

[62] W. Kaim, *J. Am. Chem. Soc.* **1982**, *104*, 3833–3837.

[63] A. Sokolowski, J. Müller, T. Weyhermüller, R. Schnepf, P. Hildebrandt, K. Hildenbrand, E. Bothe, K. Wieghardt, *J. Am. Chem. Soc.* **1997**, *119*, 8889–8900.

[64] S. Kimura, E. Bill, E. Bothe, T. Weyhermüller, K. Wieghardt, *J. Am. Chem. Soc.* **2001**, *123*, 6025–6039.

[65] W. Kaim, B. Schwederski, *Coord. Chem. Rev.* **2010**, *254*, 1580–1588.

[66] Z. Hou, T. Miyano, H. Yamazaki, Y. Wakatsuki, *J. Am. Chem. Soc.* **1995**, *117*, 4421–4422.

[67] O. P. Lam, C. Anthon, F. W. Heinemann, J. M. O'Connor, K. Meyer, *J. Am. Chem. Soc.* **2008**, *130*, 6567–6576.

[68] J. C. Ott, H. Wadepohl, L. H. Gade, *Angew. Chem. Int. Ed.* **2020**, *59*, 9448–9452.

[69] K. C. MacLeod, I. M. DiMucci, E. P. Zovinka, S. F. McWilliams, B. Q. Mercado, K. M. Lancaster, P. L. Holland, *Organometallics* **2019**, *38*, 4224–4232.

[70] K. Kaleta, P. Arndt, T. Beweries, A. Spannenberg, O. Theilmann, U. Rosenthal, *Organometallics* **2010**, *29*, 2604–2609.

[71] S. S. Sen, D. Kratzert, D. Stern, H. W. Roesky, D. Stalke, *Inorg. Chem.* **2010**, *49*, 5786–5788.

[72] W. Ren, D. Gu, *Inorg. Chem.* **2016**, *55*, 11962–11970.

[73] N. Doslik, T. Sixt, W. Kaim, *Angew. Chem. Int. Ed.* **1998**, *37*, 2403–2404.

[74] N. D. Paul, U. Rana, S. Goswami, T. K. Mondal, S. Goswami, *J. Am. Chem. Soc.* **2012**, *134*, 6520–6523.

[75] W. J. Evans, D. K. Drummond, L. R. Chamberlain, R. J. Doedens, S. G. Bott, Hongming. Zhang, J. L. Atwood, *J. Am. Chem. Soc.* **1988**, *110*, 4983–4994.

[76] K. A. Kreisel, G. P. A. Yap, K. H. Theopold, *Inorg. Chem.* **2008**, *47*, 5293–5303.

[77] W. Zhou, L. Chiang, B. O. Patrick, T. Storr, K. M. Smith, *Dalton Trans.* **2012**, *41*, 7920.

[78] C. Römelt, T. Weyhermüller, K. Wieghardt, *Coord. Chem. Rev.* **2019**, *380*, 287–317.

[79] B. de Bruin, E. Bill, E. Bothe, T. Weyhermüller, K. Wieghardt, *Inorg. Chem.* **2000**, *39*, 2936–2947.

[80] P. J. Chirik, K. Wieghardt, *Science* **2010**, *327*, 794–795.

[81] M. V. Joannou, J. M. Hoyt, P. J. Chirik, *J. Am. Chem. Soc.* **2020**, *142*, 5314–5330.

[82] G. J. P. Britovsek, V. C. Gibson, D. F. Wass, *Angew. Chem. Int. Ed.* **1999**, *38*, 428–447.

[83] B. L. Small, *Acc. Chem. Res.* **2015**, *48*, 2599–2611.

[84] E. Clemmensen, *Ber. Dtsch. Chem. Ges.* **1913**, *46*, 1837–1843.

[85] R. Fittig, *Ann. Chem. Pharm.* **1859**, *110*, 23–45.

[86] A. P. Schreibmann, *Tetrahedron Lett.* **1970**, *11*, 4271–4272.

[87] J. L. Namy, J. Souppe, H. B. Kagan, *Tetrahedron Lett.* **1983**, *24*, 765–766.

[88] J. E. McMurry, M. P. Fleming, *J. Am. Chem. Soc.* **1974**, *96*, 4708–4709.

[89] M. Ephritikhine, *Chem. Commun.* **1998**, 2549–2554.

[90] E. J. Roskamp, S. F. Pedersen, *J. Am. Chem. Soc.* **1987**, *109*, 3152–3154.

[91] M. Nakajima, E. Fava, S. Loescher, Z. Jiang, M. Rueping, *Angew. Chem. Int. Ed.* **2015**, *54*, 8825–8832.

[92] S. Okamoto, K. Kojiyama, H. Tsujioka, A. Sudo, *Chem. Commun.* **2016**, *52*, 11339–11342.

[93] S. Okamoto, R. Ariki, H. Tsujioka, A. Sudo, *J. Org. Chem.* **2017**, *82*, 9731–9736.

[94] R. R. Landolt, H. W. Berk, H. T. Russell, *Toxicol. Appl. Pharmacol.* **1972**, *21*, 589–590.

[95] H. Kruszyna, R. Kruszyna, J. Hurst, R. P. Smith, *J. Toxicol. Environ. Health* **1980**, *6*, 757–773.

[96] M.-J. Hosseini, I. Jafarian, S. Farahani, R. Khodadadi, S. H. Tagavi, P. Naserzadeh, A. Mohammadi-Bardbori, N. Arghavanifard, *Metallomics* **2016**, *8*, 252–259.

[97] H. H. Binder, *Lexikon Der Chemischen Elemente*, S. Hirzel Verlag, Stuttgart, **1999**.

[98] D. R. Lide (Hrsg.), *CRC Handbook of Chemistry and Physics. Section 14, Geophysics, Astronomy, and Acoustics; Abundance of Elements in the Earth's Crust and in the Sea.*, CRC Press, Boca Raton, Florida, **2005**.

[99] H. Bürger, U. Wannagat, *Monatsh. Chem.* **1963**, *94*, 1007–1012.

[100] R. A. Andersen, A. Haaland, K. Rypdal, H. V. Volden, *J. Chem. Soc., Chem. Commun.* **1985**, 1807–1808.

[101] R. A. Bartlett, P. P. Power, *J. Am. Chem. Soc.* **1987**, *109*, 7563–7564.

[102] R. A. Andersen, K. Faegri, J. C. Green, A. Haaland, M. F. Lappert, W. P. Leung, K. Rypdal, *Inorg. Chem.* **1988**, *27*, 1782–1786.

[103] M. M. Olmstead, P. P. Power, S. C. Shoner, *Inorg. Chem.* **1991**, *30*, 2547–2551.

[104] T. Hatakeyama, R. Imayoshi, Y. Yoshimoto, S. K. Ghorai, M. Jin, H. Takaya, K. Norisuye, Y. Sohrin, M. Nakamura, *J. Am. Chem. Soc.* **2012**, *134*, 20262–20265.

[105] R. Wolf, M. Brynda, C. Ni, G. J. Long, P. P. Power, *J. Am. Chem. Soc.* **2007**, *129*, 6076–6077.

[106] C. A. Laskowski, G. L. Hillhouse, *J. Am. Chem. Soc.* **2008**, *130*, 13846–13847.

[107] A. A. Danopoulos, P. Braunstein, K. Yu. Monakhov, J. van Leusen, P. Kögerler, M. Clémancey, J.-M. Latour, A. Benayad, M. Tromp, E. Rezabal, G. Frison, *Dalton Trans.* **2017**, *46*, 1163–1171.

[108] Y. Liu, L. Deng, *J. Am. Chem. Soc.* **2017**, *139*, 1798–1801.

[109] Z. Mo, Z. Ouyang, L. Wang, K. L. Fillman, M. L. Neidig, L. Deng, *Org. Chem. Front.* **2014**, *1*, 1040–1044.

[110] Z. Mo, D. Chen, X. Leng, L. Deng, *Organometallics* **2012**, *31*, 7040–7043.

[111] C. G. Werncke, P. C. Bunting, C. Duhayon, J. R. Long, S. Bontemps, S. Sabo-Etienne, *Angew. Chem. Int. Ed.* **2015**, *54*, 245–248.

[112] C. G. Werncke, E. Suturina, P. C. Bunting, L. Vendier, J. R. Long, M. Atanasov, F. Neese, S. Sabo-Etienne, S. Bontemps, *Chem. Eur. J.* **2016**, *22*, 1668–1674.

[113] M. I. Lipschutz, X. Yang, R. Chatterjee, T. D. Tilley, *J. Am. Chem. Soc.* **2013**, *135*, 15298–15301.

[114] R. Weller, I. Müller, C. Duhayon, S. Sabo-Etienne, S. Bontemps, C. G. Werncke, *Dalton Trans.* **2021**, *50*, 4890–4903.

[115] A. M. Bryan, G. J. Long, F. Grandjean, P. P. Power, *Inorg. Chem.* **2013**, *52*, 12152–12160.

[116] I. C. Cai, M. I. Lipschutz, T. D. Tilley, *Chem. Commun.* **2014**, *50*, 13062–13065.

[117] R. Weller, L. Ruppach, A. Shlyaykher, F. Tambornino, C. G. Werncke, *Dalton Trans.* **2021**, *50*, 10947–10963.

[118] I. Müller, C. Schneider, C. Pietzonka, F. Kraus, C. G. Werncke, *Inorganics* **2019**, *7*, 117.

[119] T. R. Dugan, E. Bill, K. C. MacLeod, G. J. Christian, R. E. Cowley, W. W. Brennessel, S. Ye, F. Neese, P. L. Holland, *J. Am. Chem. Soc.* **2012**, *134*, 20352–20364.

[120] I. Müller, C. G. Werncke, *Chem. Eur. J.* **2021**, *27*, 4932–4938.

[121] D. A. Iovan, T. A. Betley, *J. Am. Chem. Soc.* **2016**, *138*, 1983–1993.

[122] Y. Dong, J. T. Lukens, R. M. Clarke, S.-L. Zheng, K. M. Lancaster, T. A. Betley, *Chem. Sci.* **2020**, *11*, 1260–1268.

[123] A. Reckziegel, M. Kour, B. Battistella, S. Mebs, K. Beuthert, R. Berger, C. G. Werncke, *Angew. Chem. Int. Ed.* **2021**, *60*, 15376–15380.

[124] V. Varga, K. Mach, M. Polásek, P. Sedmera, J. Hiller, U. Thewalt, S. I. Troyanov, *J. Organomet. Chem.* **1996**, *506*, 241–251.

[125] G. B. Wijeratne, E. M. Zolnhofer, S. Fortier, L. N. Grant, P. J. Carroll, C.-H. Chen, K. Meyer, J. Krzystek, A. Ozarowski, T. A. Jackson, D. J. Mindiola, J. Telser, *Inorg. Chem.* **2015**, *54*, 10380–10397.

[126] C. Martín, M. Sierra, E. Alvarez, T. R. Belderrain, P. J. Pérez, *Dalton Trans.* **2012**, *41*, 5319.

[127] M. S. Nechaev, V. M. Rayón, G. Frenking, *J. Phys. Chem. A* **2004**, *108*, 3134–3142.

[128] F. Dai, G. P. A. Yap, K. H. Theopold, *J. Am. Chem. Soc.* **2013**, *135*, 16774–16776.

[129] S. A. Stoian, Y. Yu, J. M. Smith, P. L. Holland, E. L. Bominaar, E. Münck, *Inorg. Chem.* **2005**, *44*, 4915–4922.

[130] Y. Yu, J. M. Smith, C. J. Flaschenriem, P. L. Holland, *Inorg. Chem.* **2006**, *45*, 5742–5751.

[131] S. C. Bart, E. J. Hawrelak, E. Lobkovsky, P. J. Chirik, *Organometallics* **2005**, *24*, 5518–5527.

[132] J. Cheng, Q. Chen, X. Leng, S. Ye, L. Deng, *Inorg. Chem.* **2019**, *58*, 13129–13141.

[133] A. Enachi, D. Baabe, M.-K. Zaretzke, P. Schweyen, M. Freytag, J. Raeder, M. D. Walter, *Chem. Commun.* **2018**, *54*, 13798–13801.

[134] J. Du, W. Chen, Q. Chen, X. Leng, Y.-S. Meng, S. Gao, L. Deng, *Organometallics* **2020**, *39*, 729–739.

[135] I. Müller, D. Munz, C. G. Werncke, *Inorg. Chem.* **2020**, *59*, 9521–9537.

[136] W. H. Monillas, G. P. A. Yap, L. A. MacAdams, K. H. Theopold, *J. Am. Chem. Soc.* **2007**, *129*, 8090–8091.

[137] O. P. Lam, P. L. Feng, F. W. Heinemann, J. M. O'Connor, K. Meyer, *J. Am. Chem. Soc.* **2008**, *130*, 2806–2816.

[138] B. Twamley, C. D. Sofield, M. M. Olmstead, P. P. Power, *J. Am. Chem. Soc.* **1999**, *121*, 3357–3367.

[139] T. A. Ward, G. Levin, M. Szwarc, *J. Am. Chem. Soc.* **1975**, *97*, 258–261.

[140] H. C. Wang, G. Levin, M. Szwarc, *J. Am. Chem. Soc.* **1977**, *99*, 2642–2647.

[141] T. L. Staples, J. Jagur-Grodzinski, M. Szwarc, *J. Am. Chem. Soc.* **1969**, *91*, 3721–3723.

[142] S. Sorensen, G. Levin, M. Szwarc, *J. Am. Chem. Soc.* **1975**, *97*, 2341–2345.

[143] C. G. Werncke, J. Pfeiffer, I. Müller, L. Vendier, S. Sabo-Etienne, S. Bontemps, *Dalton Trans.* **2019**, *48*, 1757–1765.

[144] C. G. Werncke, I. Müller, *Chem. Commun.* **2020**, *56*, 2268–2271.

[145] A. Reckziegel, C. Pietzonka, F. Kraus, C. G. Werncke, *Angew. Chem. Int. Ed.* **2020**, *59*, 8527–8531.

[146] G. Sieg, Q. Pessemesse, S. Reith, S. Yelin, C. Limberg, D. Munz, C. G. Werncke, *Chem. Eur. J.* **2021**, *27*, 16760–16767.

[147] C. Schneider, L. Guggolz, C. G. Werncke, *Dalton Trans.* **2022**, *51*, 179–184.

[148] G. Sieg, I. Müller, K. Weißer, C. G. Werncke, *in pereparation* **2022**.

[149] R. J. Schwamm, M. P. Coles, C. M. Fitchett, *Dalton Trans.* **2017**, *46*, 4066–4074.

[150] R. Schwamm, M. Anker, M. Lein, M. P. Coles, *Angew. Chem. Int. Ed.* **2018**, 1503–1507.

[151] M. J. Evans, M. D. Anker, A. Mouchfiq, M. Lein, J. R. Fulton, *Chem. Eur. J.* **2020**, *26*, 2606–2609.

[152] R. J. Schwamm, C. A. von Randow, A. Mouchfiq, M. J. Evans, M. P. Coles, J. R. Fulton, *Eur. J. Inorg. Chem.* **2021**, 3466–3473.

[153] A. R. Sadique, E. A. Gregory, W. W. Brennessel, P. L. Holland, *J. Am. Chem. Soc.* **2007**, *129*, 8112–8121.

[154] C. J. Brown, *Acta Cryst* **1966**, *21*, 146–152.

[155] P. Ghosh, S. Samanta, S. K. Roy, S. Joy, T. Krämer, J. E. McGrady, S. Goswami, *Inorg. Chem.* **2013**, *52*, 14040–14049.

[156] N. Leconte, B. Baptiste, C. Philouze, F. Thomas, *Dalton Trans.* **2018**, *47*, 11303–11307.

[157] S. Sinha, S. Das, R. Mondal, S. Mandal, N. D. Paul, *Dalton Trans.* **2020**, *49*, 8448–8459.

[158] M. Dewar, *Bull. Soc. chim. Fr.* **1951**, *18*, C78.

[159] J. Chatt, L. A. Duncanson, L. M. Venanzi, *J. Chem. Soc.* **1955**, 4456–4460.

[160] A. Duncanson, J. Chatt, *J. Chem. Soc.* **1953**, 2939–2947.

[161] H. Luecken, *Magnetochemie*, B. G. Teubner, Stuttgart, **1999**.